Lecture Notes in Physics

Volume 864

For further volumes:
www.springer.com/series/5304

The Lecture Notes in Physics

The series Lecture Notes in Physics (LNP), founded in 1969, reports new developments in physics research and teaching—quickly and informally, but with a high quality and the explicit aim to summarize and communicate current knowledge in an accessible way. Books published in this series are conceived as bridging material between advanced graduate textbooks and the forefront of research and to serve three purposes:

- to be a compact and modern up-to-date source of reference on a well-defined topic
- to serve as an accessible introduction to the field to postgraduate students and nonspecialist researchers from related areas
- to be a source of advanced teaching material for specialized seminars, courses and schools

Both monographs and multi-author volumes will be considered for publication. Edited volumes should, however, consist of a very limited number of contributions only. Proceedings will not be considered for LNP.

Volumes published in LNP are disseminated both in print and in electronic formats, the electronic archive being available at springerlink.com. The series content is indexed, abstracted and referenced by many abstracting and information services, bibliographic networks, subscription agencies, library networks, and consortia.

Proposals should be sent to a member of the Editorial Board, or directly to the managing editor at Springer:

Christian Caron
Springer Heidelberg
Physics Editorial Department I
Tiergartenstrasse 17
69121 Heidelberg/Germany
christian.caron@springer.com

Andreas Wipf

Statistical Approach to Quantum Field Theory

An Introduction

Springer

Andreas Wipf
Theoretisch-Physikalisches-Institut
Friedrich-Schiller-Universität Jena
Jena, Germany

ISSN 0075-8450 ISSN 1616-6361 (electronic)
Lecture Notes in Physics
ISBN 978-3-642-33104-6 ISBN 978-3-642-33105-3 (eBook)
DOI 10.1007/978-3-642-33105-3
Springer Heidelberg New York Dordrecht London

Library of Congress Control Number: 2012951838

Printed on acid-free paper

Springer is part of Springer Science+Business Media (www.springer.com)

To Ingrid, Leonie, Severin, and Valentin

Preface

Statistical field theory deals with the behavior of classical or quantum systems consisting of an enormous number of degrees of freedom in and out of equilibrium. Quantum field theory provides a theoretical framework for constructing quantum mechanical models of systems with an infinite number of degrees of freedom. It is the natural language of particle physics and condensed matter physics. In the past decades the powerful methods in statistical physics and Euclidean quantum field theory have come closer and closer, with common tools based on the use of path integrals. The interpretation of Euclidean field theories as particular systems of statistical physics opened up new avenues to understand strongly coupled quantum systems or quantum field theories at zero or finite temperature. The powerful methods of statistical physics and stochastics can be applied to study for example the vacuum sector, effective action, thermodynamic potentials, correlation functions, finite size effects, nature of phase transitions or critical behavior of quantum systems.

The first chapters of this book contain a self contained introduction to path integrals in Euclidean quantum mechanics and statistical mechanics. The resulting high-dimensional integrals can be estimated with the help of Monte Carlo simulations based on Markov processes. The method is first introduced and then applied to ordinary integrals and to quantum mechanical systems. Thereby the most commonly used algorithms are explained in detail. Equipped with theses stochastic methods we may use high performance computers as an "experimental" tool for a new brand of theoretical physics.

The book contains several chapters devoted to an introduction into simple lattice field theories and a variety of spin systems with discrete and continuous spins. An ideal guide to the fascinating area of phase transitions is provided by the ubiquitous Ising model. Despite its simplicity the model is often used to illustrate the key features of statistical systems and the methods available to understand these features. The Ising model has always played an important role in statistical physics, both at pedagogical and methodological levels. Almost all chapters in the middle part of the book begin with introducing methods, approximations, expansions or rigorous results by first considering the Ising model. In a next step we generalize from the Ising model to other lattice systems, for example Potts models, $O(N)$ models, scalar

field theories, gauge theories, and fermionic theories. For spin models and field theories on a lattice it is often possible to derive rigorous results or bounds. Important examples are the bounds provided by the mean field approximation, inequalities between correlation functions of ferromagnetic systems, and the proofs that there exist spontaneously broken phases at low temperature or the duality transformations for Abelian models which relate the weak coupling and strong coupling regions or the low temperature and high temperature phases. All these interesting results are derived and discussed with great care.

As an alternative to the lattice formulation of quantum field theories one may use a variant of the flexible renormalization group methods. For example, implementing (spacetime) symmetries is not so much an issue for a functional renormalization group method as it sometimes is for a lattice regularization and hence the method is somehow complementary to the ab initio lattice approach. In cases where a lattice regularization based on a positive Boltzmann factor fails, for example for gauge theories at finite density, the functional method may work. Thus it is often a good strategy to consider both methods when it comes to properties of strongly coupled systems under extreme conditions. Knowledge of the renormalization group method and in particular the flow of scale dependent functionals from the microscopic to the macroscopic world is a key part of modern physics and thus we have devoted two chapters to this method.

According to present day knowledge all fundamental interactions in nature are described by gauge theories. Gauge theories can be formulated on a finite spacetime lattice without spoiling the important local gauge invariance. Thereby the functional integral turns into a finite-dimensional integral which can be handled by stochastic means. Problems arise when one considers gauge fields in interaction with fermions at finite temperature and non-zero baryon density. A lot of efforts have gone into solving or at least circumventing these problems to simulate quantum chromodynamics, the microscopic gauge theory underlying the strong interaction between quarks and gluons. The last chapters of the book deal with gauge theories without and with matter.

This book is based on an elaboration of lecture notes of the course Quantum Field Theory II given by the author at the Friedrich-Schiller-University Jena. It is designed for advanced undergraduate and beginning graduate students in physics and applied mathematics. For this reason, its style is greatly pedagogical; it assumes only some basics of mathematics, statistical physics, and quantum field theory. But the book contains some more sophisticated concepts which may be useful to researchers in the field as well. Although many textbooks on statistic physics and quantum field theory are already available, they largely differ in contents from the present book. Beginning with the path integral in quantum mechanics and with numerical methods to calculate ordinary integrals we bridge the gap to lattice gauge theories with dynamical fermions. Each chapter ends with some problems which should be useful for a better understanding of the material presented in the main text. At the end of many chapters you also find listings of computer programs, either written in C or in the freely available Matlab-clone Octave. Not only because of the restricted size of the book I did not want to include lengthy simulation programs for gauge theories.

Acknowledgments Over the years I have had the pleasure of collaborating and discussing many of the themes of this book with several of my teachers, colleagues and friends. First of all, I would like especially to thank the late Lochlain O'Raifeartaigh for the long and profitable collaboration on effective potentials, anomalies, and two-dimensional field theories, and for sharing his deep understanding of many aspects of symmetries and field theories. I would like to use this opportunity to warmly thank the academic teachers who have influenced me most—Jürg Fröhlich, Res Jost, John Lewis, Konrad Osterwalder, Eduard Stiefel, and especially Norbert Straumann. I assume that their influence on my way of thinking about quantum field theory and statistical physics might be visible in some parts of this book.

I have been fortunate in having the benefit of collaborations and discussions with many colleagues and friends and in particular with Manuel Asorey, Pierre van Baal, Janos Balog, Steven Blau, Jens Braun, Fred Cooper, Stefan Durr, Chris Ford, Lazlo Feher, Thomas Filk, Peter Forgacs, Christof Gattringer, Holger Gies, Tom Heinzl, Karl Jansen, Claus Kiefer, Kurt Langfeld, Axel Maas, Emil Mottola, Renato Musto, Jan Pawlowski, Ivo Sachs, Lorenz von Smekal, Thomas Strobl, Torsten Tok, Izumi Tsutsui, Sebastian Uhlmann, Matt Visser, Christian Wiesendanger, and Hiroshi Yoneyma. On several topics covered in the second and more advanced part of the book I collaborated intensively with my present and former Ph.D. students Georg Bergner, Falk Bruckmann, Leander Dittman, Marianne Heilmann, Tobias Kästner, Andreas Kirchberg, Daniel Körner, Dominque Länge, Franziska Synatschke-Czerwonka, Bjoern Wellegehausen and Christian Wozar. Last but not least I am indebted to Holger Gies and Kurt Langfeld for a critical reading of parts of the manuscript and Marianne Heilmann for translating the German lecture notes into English.

Jena, Germany Andreas Wipf

Contents

Notations

A_μ	Gauge potential
$A(\omega, \omega')$	Acceptance rate for $\omega \to \omega'$
β, β_T	Inverse gauge coupling $\sim 1/g^2$ or inverse temperature $1/k_B T$
$\not{D}, \not{\partial}$	Dirac operator and free Dirac operator
$\mathscr{C}$	Closed path or loop
χ	Susceptibility
$\mathscr{D}\phi$	Formal path integral measure
D_μ	Covariant derivative in μ-direction
F, f	Free energy and free energy density
$F_{\mu\nu}$	Field strength tensor
ϕ_x, φ_x	Microscopic and macroscopic lattice field at lattice site x
$\hat{\phi}(x)$	Field operator at spacetime point x
$\hat{\phi}_{\mathrm{E}}(x)$	Euclidian field operator at spacetime point x
Γ, Γ_k	Effective action, scale dependent effective action
$j(x), j_x$	External source at spacetime point x and at lattice site x
$\mathscr{L}$	Lagrangian density or Legendre transformation
Λ	Spacetime lattice
$H(\omega)$	Energy of spin configuration ω
$\hat{H}$	Hamiltonian operator of quantum system
$K(t), K(\tau)$	Propagator at real time t and imaginary time τ
N_t, N_s	Number of lattice points in time and space direction
$O, \hat{O}$	Observable in a classical statistical system and in quantum theory
$\mathscr{P}, P$	Polyakov loop and its gauge invariant trace
P_ω	Equilibrium probability for configuration ω
$\psi(x), \psi_x$	Fermionic field in continuum and on the lattice
$\hat{q}(t)$	Position operator at time t
s_x	Value of spin variable at lattice site x
S, S_{E}	Action and Euclidean action
$S_{\mathrm{B}}, S_{\mathrm{F}}$	Action for bosons and fermions
S_{B}	Shannon–Boltzmann entropy
T_c	Critical temperature

$T(\omega, \omega')$	Probability to test transition $\omega \to \omega'$
$U(\beta)$	Inner energy
$U_\ell, U_{x,\mu}$	Group valued link variable
$U_p, U_{x,\mu\nu}$	Plaquette variable
u, u_k	Effective potential and scale dependent effective potential
ω	Path, spin or field configuration
Ω	Set of path, spin or field configurations
$\Omega(x)$	Gauge transformation at lattice point x
R_k	Regulator function in flow equation
$W(\omega, \omega')$	Transition probability $\omega \to \omega'$
W, W_k	Schwinger functional, scale dependent Schwinger functional
$W[\mathscr{C}]$	Wilson loop around closed path $\mathscr{C}$
$w(j)$	Schwinger function for constant j
$Z(\beta)$	Partition function
$\zeta_A(s)$	Zeta function of operator A

Chapter 1
Introduction

A quantum field theory (QFT) is an extension of the principles of quantum mechanics to fields based on the wave properties of matter. It is generally accepted that QFT is an appropriate framework for describing the interaction between infinitely many degrees of freedom. It is the natural language of particle physics and condensed matter physics with applications ranging from the Standard Model of elementary particles and their interactions to the description of critical phenomena and phase transitions, such as in the theory of superconductivity.

A relativistic quantum field theory unifies the basic principles of quantum theory and special relativity in a consistent manner. The quantization of the electromagnetic field was outlined by M. BORN and P. JORDAN back in 1925 [1] and just a year later with HEISENBERG they showed how to quantize general systems with an infinite number of degrees of freedom [2]. The theory was further developed and applied to the photon–atom interactions by P. DIRAC who studied the quantized photon field in interaction with atoms and calculated emission and absorption rates [3]. In a next step P. JORDAN, W. PAULI and W. HEISENBERG [4–6] completed the quantization of electrodynamics, compatible with special relativity. This was achieved by quantizing the Dirac and Maxwell fields in interaction. In particular, Heisenberg and Pauli emphasized the importance of the Lagrangian formulation in field theory and developed the quantization procedure which nowadays is called *canonical quantization*. To this day, their approach to QFT remains a popular one and is presented in textbooks.

In a perturbative approach one first quantizes the non-interacting field and subsequently includes the interaction by a local interaction density. The direct application of this method leads to divergent expressions for physical quantities, e.g. an infinitely large self-energy. The solution of this problem has led to the renormalization method which originated in the early work and has been completed by TOMONAGA, SCHWINGER, FEYNMAN and DYSON. The latter outlined a proof of renormalizablity of QED [7], which was complemented by other authors in the 1950s and 1960s. For a renormalizable QFT there exists a method consisting of a regularization and subsequent renormalization that gives finite and physically sensible results by absorbing the divergences into redefinitions of only a few coupling

A. Wipf, *Statistical Approach to Quantum Field Theory*, Lecture Notes in Physics 864,
DOI 10.1007/978-3-642-33105-3_1,

constants and the field. QED is the most studied and successful prototype of a renormalizable quantum field theory with a (local) gauge symmetry. The high precision of QED-calculations is based upon the applicability of perturbation theory, where the dimensionless fine-structure constant $\alpha \sim 1/137$ serves as expansion parameter. The following years were dedicated to the formal improvement of field theory in general. The connection between spin and statistics was found, the CPT-theorem was formulated, the representation theory of the (anti)commutation rules was developed, the Euclidean formulation of QFT' was investigated [8, 9] and symmetry principles came to the fore.

An exciting period followed which began with the advent of *non-Abelian gauge theories*, formulated by YANG and MILLS to extend the concept of a local gauge symmetry from Abelian groups to non-Abelian groups [10], in order to describe the interactions between elementary particles. The efforts culminated in the model of S. GLASHOW, S. WEINBERG and A. SALAM [11–13] for the electro-weak interaction. In particular after G. 'T HOOFT proved the renormalizability of spontaneously broken gauge theories [14]—the weak interaction is described by such a theory—the interest in Yang–Mills theories continued to increase. Shortly after these developments it became clear that the forces between strongly interacting particles is described by yet another non-Abelian gauge theory, namely *quantum chromodynamics* (QCD) [15]. However, it is not easy to compare QCD with experiment. This is not only because the coupling is strong and not weak as in electrodynamics, but also because of the related fact that the fundamental constituents of the theory, the quarks and force-carrying gluons have never been seen directly, and are generally believed to be unattainable because of the phenomenon of confinement. To prove confinement or related properties as chiral symmetry breaking in strongly coupled field theories we must leave the realm of perturbation theory.

New insights into the renormalization procedure beyond perturbation theory are obtained with the path integral quantization of physical systems [16]. After a rotation of time to imaginary values one obtains the Euclidean functional integral formulation of QFT. The integrand contains the exponential of the negative action of the classical field theory. When one approximates the continuous (Euclidean) spacetime by a finite lattice the functional integral of a QFT turns into a well-defined finite dimensional integral. This means that the discretization regularizes the QFT without reference to perturbation theory. In a second step one may renormalize the theory by performing the continuum limit in which the lattice spacing tends to zero. Equally important, the finite dimensional integral is an ensemble average in classical equilibrium statistical mechanics. Thereby the classical action of the field theory discretized on a spacetime lattice becomes the energy function of a particular classical spin model. This far-reaching observation bridges the gap between two apparently unrelated branches of physics: quantum (field) theory and classical statistical physics. Actually, any QFT at finite temperature is described by an Euclidean functional integral on a cylinder with the imaginary time as periodic variable. It follows that after discretization the functional integral for the finite temperature QFT turns into an ensemble average of a classical spin model with periodic boundary conditions in one direction. In this context the formulation of gauge theories on a space

time lattice was of utmost importance. Lattice gauge theories with discrete gauge groups have been investigated by F. WEGNER [17] and three years later K. WILSON succeeded in putting non-Abelian gauge theories on a spacetime lattice [18]. Many recent non-perturbative results on gauge theories at zero and finite temperatures are based on this pioneering work.

The interrelation between quantum field theories at zero or finite temperature and classical spin models is extremely beneficial both for QFT and statistical physics. For example, many non-perturbative problems of interest in QFT can be handled with the powerful and well-established methods of classical statistical physics. For example, on may address difficult problems like mass generation, decay widths, symmetry breaking, phase transitions or condensates, to name a few. Thereby many rigorous results, inequalities, dualities and approximation methods in statistical physics can be put to use in lattice field theory. Shortly after the seminal work of K. Wilson, the first numerical simulations of lattice gauge theories were performed [19, 20]. Today observable quantities as for example particle masses, decay widths, condensates, thermodynamical potentials, and finite temperature phase diagrams can be calculated with the powerful Monte Carlo method. The following chapters contain an introduction into this exciting and active fields of research in theoretical physics. For a further reading I included primary and secondary literature, including textbooks, at the end of each chapter.

References

1. M. Born, P. Jordan, Zur Quantenmechanik. Z. Phys. **34**, 858 (1925)
2. M. Born, W. Heisenberg, P. Jordan, Zur Quantenmechanik II. Z. Phys. **35**, 557 (1926)
3. P.A.M. Dirac, The quantum theory of emission and absorption of radiation. Proc. R. Soc. Lond. A **114**, 243 (1927)
4. P. Jordan, W. Pauli, Zur Quantenelektrodynamik. Z. Phys. **47**, 151 (1928)
5. W. Heisenberg, W. Pauli, Zur Quantendynamik der Wellenfelder I. Z. Phys. **56**, 1 (1929)
6. W. Heisenberg, W. Pauli, Zur Quantendynamik der Wellenfelder II. Z. Phys. **59**, 168 (1930)
7. F.J. Dyson, The S-matrix in quantum electrodynamics. Phys. Rev. **75**, 1736 (1949)
8. J. Schwinger, On the Euclidean structure of relativistic field theory. Proc. Natl. Acad. Sci. USA **44**, 956 (1958)
9. K. Symanzik, Euclidean quantum field theory, I. Equations for a scalar model. J. Math. Phys. **7**, 510 (1966)
10. C.N. Yang, R.L. Mills, Conservation of isotopic spin and isotopic gauge invariance. Phys. Rev. **96**, 191 (1954)
11. S.L. Glashow, Partial-symmetries of weak interaction. Nucl. Phys. **22**, 579 (1961)
12. S. Weinberg, A model of leptons. Phys. Rev. Lett. **19**, 1264 (1964)
13. A. Salam, Weak and electromagnetic interactions, in *Elementary Particle Theory* (Almquist and Wiksell, Stockholm, 1968)
14. G. 't Hooft, Renormalizable Lagrangians for massive Yang–Mills fields. Nucl. Phys. B **35**, 167 (1971)
15. H. Fritzsch, M. Gell-Mann, H. Leutwyler, Advantages of the color octet cluon picture. Phys. Lett. B **47**, 365 (1973)
16. R. Feynman, Spacetime approach to non-relativistic quantum mechanic. Rev. Mod. Phys. **20**, 267 (1948)

17. F.J. Wegner, Duality in generalized Ising models and phase transitions without local order parameters. J. Math. Phys. **10**, 2259 (1971)
18. K.G. Wilson, Confinement of quarks. Phys. Rev. D **10**, 2445 (1974)
19. M. Creutz, Confinement and the critical dimensionality of spacetime. Phys. Rev. Lett. **43**, 553 (1979)
20. M. Creutz, Monte Carlo simulations in lattice gauge theories. Phys. Rep. **95**, 201 (1983)

Chapter 2
Path Integrals in Quantum and Statistical Mechanics

There exist three apparently different formulations of quantum mechanics: HEISENBERG's matrix mechanics, SCHRÖDINGER's wave mechanics and FEYNMAN's path integral approach. In contrast to matrix and wave mechanics, which are based on the Hamiltonian approach the latter is based on the Lagrangian approach.

2.1 Summing Over All Paths

Already back in 1933 DIRAC asked himself, whether the classical Lagrangian and action are as significant in quantum mechanics as they are in classical mechanics [1, 2]. He observed that the probability amplitude

$$K(t, q', q) = \langle q' | \mathrm{e}^{-\mathrm{i}\hat{H}t/\hbar} | q \rangle \tag{2.1}$$

for the propagation of a system from a point with coordinate q to another point with coordinate q' in time t is given by

$$K(t, q', p) \propto \mathrm{e}^{\mathrm{i}S[q_{\mathrm{cl}}]/\hbar}, \tag{2.2}$$

where q_{cl} denotes the classical trajectory from q to q'. In the exponent the action of this trajectory enters as a multiple of Planck's reduced constant $\hbar$. For a free particle with Lagrangian

$$L_0 = \frac{m}{2}\dot{q}^2 \tag{2.3}$$

the formula (2.2) is verified easily: A free particle moves with constant velocity $(q' - q)/t$ from q to q' and the action of the classical trajectory is

$$S[q_{\mathrm{cl}}] = \int_0^t \mathrm{d}s\, L_0\big[q_{\mathrm{cl}}(s)\big] = \frac{m}{2t}(q' - q)^2.$$

The factor of proportionality in (2.2) is then uniquely fixed by the condition $\mathrm{e}^{-\mathrm{i}\hat{H}t/\hbar} \to \mathbb{1}$ for $t \to 0$, which in position space reads

$$\lim_{t\to 0} K(t, q', q) = \delta(q', q). \tag{2.4}$$

A. Wipf, *Statistical Approach to Quantum Field Theory*, Lecture Notes in Physics 864,
DOI 10.1007/978-3-642-33105-3_2, © Springer-Verlag Berlin Heidelberg 2013

Alternatively, it is fixed by the property $\mathrm{e}^{-\mathrm{i}\hat{H}t/\hbar}\mathrm{e}^{-\mathrm{i}\hat{H}s/\hbar} = \mathrm{e}^{-\mathrm{i}\hat{H}(t+s)/\hbar}$ that takes the form

$$\int \mathrm{d}u\, K\left(t, q', u\right) K\left(s, u, q\right) = K\left(t+s, q', q\right) \tag{2.5}$$

in position space. Thus, the correct free-particle propagator on a line is given by

$$K_0\left(t, q', q\right) = \left(\frac{m}{2\pi\mathrm{i}\hbar t}\right)^{1/2} \mathrm{e}^{\mathrm{i}m(q'-q)^2/2\hbar t}. \tag{2.6}$$

Similar results hold for the harmonic oscillator or systems for which $\langle\hat{q}(t)\rangle$ fulfills the classical equation of motion. For such systems $\langle V'(\hat{q})\rangle = V'(\langle\hat{q}\rangle)$ holds true. However, for general systems the simple formula (2.2) must be extended and it was FEYNMAN who discovered this extension back in 1948. He realized that *all paths* from q to q' (and not only the classical path) contribute to the propagator. This means that in quantum mechanics a particle can potentially move on any path $q(s)$ from the initial to the final destination,

$$q(0) = q \quad \text{and} \quad q(t) = q'. \tag{2.7}$$

The probability amplitude emerges as the superposition of contributions from all trajectories,

$$K\left(t, q', q\right) \sim \sum_{\text{all paths}} \mathrm{e}^{\mathrm{i}S[\text{path}]/\hbar}, \tag{2.8}$$

where a single path contributes a term $\sim\exp(\mathrm{i}S[\text{path}]/\hbar)$.

In passing we note that already in 1923 WIENER introduced the sum over all paths in his studies of stochastic processes [3]. Thereby a single path was weighted with a real and positive probability and *not* with a complex amplitude as in (2.8). Wiener's path integral corresponds to Feynman's path integral for imaginary time and describes quantum systems in thermal equilibrium with a heat bath at fixed temperature. In this book we will explain this extraordinary result and apply it to interesting physical systems. Moreover, the path integral method allows for a uniform treatment of quantum mechanics, quantum field theory and statistical mechanics and can be regarded as a basic tool in modern theoretical physics. It represents an alternative approach to the canonical quantization of classical systems and earned its first success in the 1950s. The path integral method is very beautifully and intelligibly presented in Feynman's original work [4] as well as in his book with HIBBS [5]. The latter reference contains many applications and is still recognized as a standard reference. Functional integrals have been developed further by outstanding mathematicians and physicists, especially by KAC [9]. An adequate reference for these developments is contained in the review article by GELFAND and YAGLOM [10]. In the present chapter we can only give a short *introduction* to path integrals. For a deeper understanding the reader should consult more specialized books and review articles. Some of them are listed in the bibliography at the end of this chapter.

2.2 Recalling Quantum Mechanics

There are two well-established ways to quantize a classical system: *canonical quantization* and *path integral quantization*. For completeness and later use we recall the main steps of canonical quantization both in Schrödinger's wave mechanics and Heisenberg's matrix mechanics.

A classical system is described by its coordinates $\{q^i\}$ and momenta $\{p_i\}$ on *phase space* Γ. An observable O is a real-valued function on Γ. Examples are the coordinates on phase space and the energy $H(q, p)$ of the system under consideration. We assume that phase space comes along with a symplectic structure and has local coordinates with Poisson brackets

$$\left\{q^i, p_j\right\} = \delta^i_j. \tag{2.9}$$

The brackets are extended to observables through antisymmetry and the derivation rule $\{OP, Q\} = O\{P, Q\} + \{O, Q\}P$. The evolution in time of an observable is determined by

$$\dot{O} = \{O, H\}, \quad \text{e.g.} \quad \dot{q}^i = \left\{q^i, H\right\} \quad \text{and} \quad \dot{p}_i = \{p_i, H\}. \tag{2.10}$$

In the canonical quantization the function on phase space are mapped to operators and the Poisson brackets of two functions become commutators of the associated operators:

$$O(q, p) \to \hat{O}(\hat{q}, \hat{p}) \quad \text{and} \quad \{O, P\} \to \frac{1}{\mathrm{i}\hbar}[\hat{O}, \hat{P}]. \tag{2.11}$$

The time evolution of an (not explicitly time-dependent) observable is determined by *Heisenberg's equation*

$$\frac{\mathrm{d}\hat{O}}{\mathrm{d}t} = \frac{\mathrm{i}}{\hbar}[\hat{H}, \hat{O}]. \tag{2.12}$$

In particular the phase space coordinates (q^i, p_i) become operators with commutation relations $[\hat{q}^i, \hat{p}_j] = \mathrm{i}\hbar\delta^i_j$ and time evolution given by

$$\frac{\mathrm{d}\hat{q}^i}{\mathrm{d}t} = \frac{\mathrm{i}}{\hbar}\left[\hat{H}, \hat{q}^i\right] \quad \text{and} \quad \frac{\mathrm{d}\hat{p}_i}{\mathrm{d}t} = \frac{\mathrm{i}}{\hbar}[\hat{H}, \hat{p}_i].$$

For a system of non-relativistic and spinless particles the Hamiltonian reads

$$\hat{H} = \hat{H}_0 + \hat{V} \quad \text{with } \hat{H}_0 = \frac{1}{2m}\sum \hat{p}_i^2, \tag{2.13}$$

and one arrives at Heisenberg's equations of motion,

$$\frac{\mathrm{d}\hat{q}^i}{\mathrm{d}t} = \frac{\hat{p}_i}{2m} \quad \text{and} \quad \frac{\mathrm{d}\hat{p}_i}{\mathrm{d}t} = -\hat{V}_{,i}\,. \tag{2.14}$$

Observables are represented by hermitian operators on a Hilbert space $\mathscr{H}$, whose elements characterize the states of the system:

$$\hat{O}(\hat{q}, \hat{p}) : \mathscr{H} \to \mathscr{H}. \tag{2.15}$$

Consider a particle confined to an endless wire. Its Hilbert space is $\mathscr{H} = L_2(\mathbb{R})$ and its position and momentum operator are represented in position space as

$$(\hat{q}\psi)(q) = q\psi(q) \quad \text{and} \quad (\hat{p}\psi)(q) = \frac{\hbar}{i}\partial_q \psi(q). \tag{2.16}$$

In experiments we can measure matrix elements of observables, represented by hermitian operators, and in particular expectation values of hermitian operators in a state of the system. The time dependence of an expectation value $\langle\psi|\hat{O}(t)|\psi\rangle$ is determined by the Heisenberg equation (2.12).

The transition from the *Heisenberg picture* to the *Schrödinger picture* involves a time-dependent similarity transformation,

$$\hat{O}_\mathrm{s} = \mathrm{e}^{-\mathrm{i}t\hat{H}/\hbar}\hat{O}\mathrm{e}^{\mathrm{i}t\hat{H}/\hbar} \quad \text{and} \quad |\psi_\mathrm{s}\rangle = \mathrm{e}^{-\mathrm{i}t\hat{H}/\hbar}|\psi\rangle, \tag{2.17}$$

and leads to time-independent observables in the Schrödinger picture,

$$\frac{\mathrm{d}}{\mathrm{d}t}\hat{O}_\mathrm{s} = \mathrm{e}^{-\mathrm{i}t\hat{H}/\hbar}\left(-\frac{\mathrm{i}}{\hbar}[\hat{H},\hat{O}] + \frac{\mathrm{d}}{\mathrm{d}t}\hat{O}\right)\mathrm{e}^{\mathrm{i}t\hat{H}/\hbar} = 0.$$

Note that the Hamiltonian operator is the same in both pictures, $\hat{H}_s = \hat{H}$ and that all expectation values are left invariant by the similarity transformation,

$$\langle\psi|\hat{O}(t)|\psi\rangle = \big\langle\psi_\mathrm{s}(t)\big|\hat{O}_\mathrm{s}\big|\psi_\mathrm{s}(t)\big\rangle. \tag{2.18}$$

A state vector in the Schrödinger picture $|\psi_\mathrm{s}(t)\rangle$ fulfills the *Schrödinger equation*

$$\mathrm{i}\hbar\frac{\mathrm{d}}{\mathrm{d}t}|\psi_\mathrm{s}\rangle = \hat{H}|\psi_\mathrm{s}\rangle \quad \Longleftrightarrow \quad \big|\psi_\mathrm{s}(t)\big\rangle = \mathrm{e}^{-\mathrm{i}t\hat{H}/\hbar}\big|\psi_\mathrm{s}(0)\big\rangle. \tag{2.19}$$

In position space this formal solution of the evolution equation has the form

$$\begin{aligned}\psi_\mathrm{s}\big(t,q'\big) \equiv \big\langle q'|\psi_\mathrm{s}(t)\big\rangle &= \int \big\langle q'\big|\mathrm{e}^{-\mathrm{i}t\hat{H}/\hbar}|q\big\rangle\big\langle q|\psi_\mathrm{s}(0)\big\rangle\,\mathrm{d}q \\ &\equiv \int K\big(t,q',q\big)\psi_\mathrm{s}(0,q)\,\mathrm{d}q,\end{aligned} \tag{2.20}$$

where we inserted the resolution of the identity with $\hat{q}$-eigenstates,

$$\int \mathrm{d}q|q\rangle\langle q| = \mathbb{1}, \tag{2.21}$$

and introduced the kernel of the unitary time evolution operator

$$K\big(t,q',q\big) = \big\langle q'\big|\hat{K}(t)|q\big\rangle, \qquad \hat{K}(t) = \mathrm{e}^{-\mathrm{i}t\hat{H}/\hbar}. \tag{2.22}$$

The *propagator* $K(t,q',q)$ is interpreted as the probability amplitude for the propagation from q at time 0 to q' at time t. This is emphasized by the notation

$$K\big(t,q',q\big) \equiv \big\langle q',t|q,0\big\rangle. \tag{2.23}$$

The amplitude solves the time-dependent Schrödinger equation

$$\mathrm{i}\hbar\frac{\mathrm{d}}{\mathrm{d}t}K\big(t,q',q\big) = \hat{H}K\big(t,q',q\big), \tag{2.24}$$

where $\hat{H}$ acts on q', and fulfills the initial condition

$$\lim_{t\to 0} K(t,q',q) = \delta(q'-q). \tag{2.25}$$

The conditions (2.24) and (2.25) uniquely define the propagator. In particular for a non-relativistic particle with Hamiltonian (2.13) in d dimensions the solution reads

$$K_0(t,q',q) = \langle q'|\mathrm{e}^{-\mathrm{i}t\hat{H}_0/\hbar}|q\rangle = \left(\frac{m}{2\pi\mathrm{i}\hbar t}\right)^{d/2} \mathrm{e}^{\mathrm{i}m(q'-q)^2/2\hbar t}, \quad q,q' \in \mathbb{R}^d. \tag{2.26}$$

In one dimension we recover the result (2.6). After this preliminaries we now turn to the path integral representation of the propagator.

2.3 Feynman–Kac Formula

We shall derive Feynman's path integral representation for the unitary time evolution operator $\exp(-\mathrm{i}\hat{H}t)$ as well as Kac's path integral representation for the positive operator $\exp(-\hat{H}\tau)$. Thereby we shall utilize the product formula of TROTTER. In case of matrices this formula was already verified by LIE and has the form:

Theorem 2.1 (Lie's theorem) *For two matrices* A *and* B

$$\mathrm{e}^{\mathsf{A}+\mathsf{B}} = \lim_{n\to\infty} \left(\mathrm{e}^{\mathsf{A}/n}\mathrm{e}^{\mathsf{B}/n}\right)^n.$$

To prove this theorem we define for each n the two matrices $\mathsf{S}_n := \exp(\mathsf{A}/n + \mathsf{B}/n)$ and $\mathsf{T}_n := \exp(\mathsf{A}/n)\exp(\mathsf{B}/n)$ and telescope the difference of their nth powers,

$$\left\|\mathsf{S}_n^n - \mathsf{T}_n^n\right\| = \left\|\mathsf{S}_n^{n-1}(\mathsf{S}_n - \mathsf{T}_n) + \mathsf{S}_n^{n-2}(\mathsf{S}_n - \mathsf{T}_n)\mathsf{T}_n + \cdots + (\mathsf{S}_n - \mathsf{T}_n)\mathsf{T}_n^{n-1}\right\|.$$

Since the norm of a product is less or equal than the product of the norms we have $\|\exp(X)\| \le \exp(\|X\|)$. Using the triangle inequality we have

$$\|\mathsf{S}_n\|, \|\mathsf{T}_n\| \le a^{1/n} \quad \text{with } a = \mathrm{e}^{\|\mathsf{A}\|+\|\mathsf{B}\|}$$

and therefore

$$\left\|\mathsf{S}_n^n - \mathsf{T}_n^n\right\| \equiv \left\|\mathrm{e}^{\mathsf{A}+B} - \left(\mathrm{e}^{\mathsf{A}/n}\mathrm{e}^{B/n}\right)^n\right\| \le n \times a^{(n-1)/n}\|\mathsf{S}_n - \mathsf{T}_n\|.$$

Finally, using $\mathsf{S}_n - \mathsf{T}_n = -[\mathsf{A},\mathsf{B}]/2n^2 + O(1/n^3)$, the product formula is verified for matrices. But the theorem also holds for unbounded self-adjoint operators.

Theorem 2.2 (Trotter's theorem) *If* $\hat{A}$ *and* $\hat{B}$ *are self-adjoint operators and* $\hat{A}+\hat{B}$ *is essentially self-adjoint on the intersection* $\mathscr{D}$ *of their domains, then*

$$\mathrm{e}^{-\mathrm{i}t(\hat{A}+\hat{B})} = s\text{-}\lim_{n\to\infty} \left(\mathrm{e}^{-\mathrm{i}t\hat{A}/n}\mathrm{e}^{-\mathrm{i}t\hat{B}/n}\right)^n. \tag{2.27}$$

If in addition $\hat{A}$ *and* $\hat{B}$ *are bounded from below, then*

$$\mathrm{e}^{-\tau(\hat{A}+\hat{B})} = s\text{-}\lim_{n\to\infty} \left(\mathrm{e}^{-\tau\hat{A}/n}\mathrm{e}^{-\tau\hat{B}/n}\right)^n. \tag{2.28}$$

The convergence here is in the sense of the strong operator topology. For operators $\hat{A}_n$ and $\hat{A}$ on a common domain $\mathscr{D}$ in the Hilbert space we have s-$\lim_{n\to\infty} \hat{A}_n = \hat{A}$ iff $\|\hat{A}_n\psi - \hat{A}\psi\| \to 0$ for all $\psi \in \mathscr{D}$. Formula (2.27) is used in quantum mechanics and formula (2.28) finds its application in statistical physics and the Euclidean formulation of quantum mechanics [7, 8].

Let us assume that $\hat{H}$ can be written as $\hat{H} = \hat{H}_0 + \hat{V}$ and apply the product formula to the evolution kernel in (2.22). With $\varepsilon = t/n$ and $\hbar = 1$ we obtain

$$\begin{aligned} K(t, q', q) &= \lim_{n\to\infty} \langle q' | \left(\mathrm{e}^{-\mathrm{i}\varepsilon\hat{H}_0}\mathrm{e}^{-\mathrm{i}\varepsilon\hat{V}}\right)^n |q\rangle \\ &= \lim_{n\to\infty} \int \mathrm{d}q_1 \cdots \mathrm{d}q_{n-1} \prod_{j=0}^{j=n-1} \langle q_{j+1}|\mathrm{e}^{-\mathrm{i}\varepsilon\hat{H}_0}\mathrm{e}^{-i\varepsilon\hat{V}}|q_j\rangle, \end{aligned} \tag{2.29}$$

where we repeatedly inserted the resolution of the identity (2.21) and denoted the initial and final point by $q_0 = q$ and $q_n = q'$, respectively. The potential $\hat{V}$ is diagonal in position space such that

$$\langle q_{j+1}|\mathrm{e}^{-\mathrm{i}\varepsilon\hat{H}_0}\mathrm{e}^{-\mathrm{i}\varepsilon\hat{V}}|q_j\rangle = \langle q_{j+1}|\mathrm{e}^{-\mathrm{i}\varepsilon\hat{H}_0}|q_j\rangle \mathrm{e}^{-\mathrm{i}\varepsilon V(q_j)}. \tag{2.30}$$

Here we insert the result (2.26) for the propagator of the free particle with Hamiltonian $\hat{H}_0$ and obtain

$$\begin{aligned} K(t, q', q) = \lim_{n\to\infty} \int \mathrm{d}q_1 \cdots \mathrm{d}q_{n-1} &\left(\frac{m}{2\pi\mathrm{i}\varepsilon}\right)^{n/2} \\ &\times \exp\left\{\mathrm{i}\varepsilon \sum_{j=0}^{j=n-1} \left(\frac{m}{2}\left(\frac{q_{j+1}-q_j}{\varepsilon}\right)^2 - V(q_j)\right)\right\}. \end{aligned} \tag{2.31}$$

This is the celebrated *Feynman–Kac formula,* which provides the path integral representation for the propagator. To make clear why it is called path integral, we divide the time interval $[0, t]$ into n subintervals of equal length $\varepsilon = t/n$ and identify q_k with $q(s = k\varepsilon)$. Now we connect the points

$$(0, q_0), (\varepsilon, q_1), \ldots, (t-\varepsilon, q_{n-1}), (t, q_n)$$

by straight line segments, which give rise to a broken-line path as depicted in Fig. 2.1. The exponent in (2.31) is just the Riemann integral for the action of a particle moving along the broken-line path,

$$\sum_{j=0}^{j=n-1} \varepsilon \left\{\frac{m}{2}\left(\frac{q_{j+1}-q_j}{\varepsilon}\right)^2 - V(q_j)\right\} = \int_0^t \mathrm{d}s \left\{\frac{m}{2}\left(\frac{\mathrm{d}q}{\mathrm{d}s}\right)^2 - V\big(q(s)\big)\right\}. \tag{2.32}$$

The integral $\int \mathrm{d}q_1 \cdots \mathrm{d}q_{n-1}$ represents the sum over all broken-line paths from q to q'. Every continuous path can be approximated by a broken-line path if only ε is small enough. Next we perform the so-called continuum limit $\varepsilon \to 0$ or equivalently $n \to \infty$. In this limit the finite-dimensional integral (2.31) turns into an infinite-dimensional (formal) integral over all paths from q to q'. With the definition

$$\left(\frac{m}{2\pi\mathrm{i}\varepsilon}\right)^{n/2} =: C \tag{2.33}$$

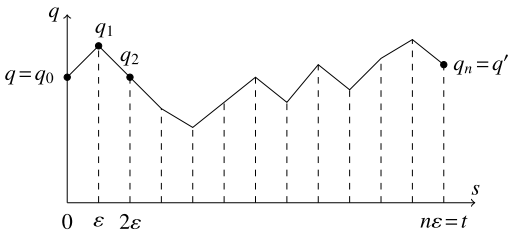

Fig. 2.1 Broken-line path entering the discretized path integral (2.31)

we arrive at the formal result

$$K\left(t, q', q\right) = C \int_{q(0)=q}^{q(t)=q'} \mathscr{D}q \mathrm{e}^{\mathrm{i}S[q]/\hbar}. \tag{2.34}$$

The 'measure' $\mathscr{D}q$ is defined via the limiting process $n \to \infty$ in (2.31). Since the infinite product of Lebesgue measures does not exist, $\mathscr{D}$ has no precise mathematical meaning. Only after a continuation to imaginary time a measure on all paths can be rigorously defined.

The formula (2.34) holds true for more general systems, for example interacting particles moving in more than one dimension and in the presence of external fields. It also applies to mechanical systems with generalized coordinates $q^1, \ldots, q^N$. The formula is also correct in quantum field theories where one integrates over all fields instead of all paths. Further properties of the path integral as well as many examples and applications can be found in the reference given at the end of this chapter.

2.4 Euclidean Path Integral

The oscillating integrand $\exp(\mathrm{i}S)$ entering the path integral (2.34) leads to distributions. If only we could suppress these oscillations, then it may be possible to construct a well-defined path integral. This may explain why most rigorous work on path integrals is based on imaginary time. For imaginary time it is indeed possible to construct a measure on all paths: the Wiener measure. The continuation from real to imaginary time is achieved by a *Wick rotation* and the continuation from imaginary time back to real time by an inverse Wick rotation. In practice, one replaces t by $-\mathrm{i}\tau$ in the path integral (2.34), works with the resulting Euclidean path integral, and replaces τ by $\mathrm{i}t$ in the final expressions.

2.4.1 Quantum Mechanics in Imaginary Time

The unitary time evolution operator has the spectral representation

$$\hat{K}(t) = \mathrm{e}^{-\mathrm{i}\hat{H}t} = \int \mathrm{e}^{-\mathrm{i}Et} \, \mathrm{d}\hat{P}_{\mathrm{E}}, \tag{2.35}$$

where $\hat{P}_{\mathrm{E}}$ is the spectral family of the Hamiltonian operator $\hat{H}$. If $\hat{H}$ has discrete spectrum then $\hat{P}_{\mathrm{E}}$ is the orthogonal projector onto the subspace of $\mathscr{H}$ spanned by all eigenfunctions with energies less than E. In the following we assume that the Hamiltonian operator is bounded from below. Then we can subtract its ground state energy to obtain a non-negative $\hat{H}$ for which the integration limits in (2.35) are 0 and ∞. With the substitution $t \to t - \mathrm{i}\tau$ we obtain

$$\mathrm{e}^{-(\tau+\mathrm{i}t)\hat{H}} = \int_0^\infty \mathrm{e}^{-E(\tau+\mathrm{i}t)}\,\mathrm{d}\hat{P}_{\mathrm{E}}. \tag{2.36}$$

This defines a holomorphic semigroup in the lower complex half-plane

$$\{t - \mathrm{i}\tau \in \mathbb{C}, \tau \geq 0\}. \tag{2.37}$$

If the operator (2.36) is known on the lower imaginary axis ($t = 0, \tau \geq 0$), then one can perform an analytic continuation to the real axis ($t, \tau = 0$). The analytic continuation to complex time $t \to -\mathrm{i}\tau$ corresponds to a transition from the Minkowski metric $\mathrm{d}s^2 = \mathrm{d}t^2 - \mathrm{d}x^2 - \mathrm{d}y^2 - \mathrm{d}z^2$ to a metric with Euclidean signature. Hence a theory with imaginary time is called *Euclidean theory*.

The time evolution operator $\hat{K}(t)$ exists for real time and defines a *one-parametric unitary group*. It fulfills the Schrödinger equation

$$\mathrm{i}\frac{\mathrm{d}}{\mathrm{d}t}\hat{K}(t) = \hat{H}\hat{K}(t)$$

with a complex and oscillating kernel $K(t, q', q) = \langle q'|\hat{K}(t)|q\rangle$. For imaginary time we have a hermitian (and not unitary) evolution operator

$$\hat{K}(\tau) = \mathrm{e}^{-\tau\hat{H}} \tag{2.38}$$

with positive spectrum. $\hat{K}(\tau)$ exists for positive τ and form a *semigroup* only. For almost all initial data evolution back into the 'imaginary past' is impossible.

The evolution operator for imaginary time satisfies the *heat equation*

$$\frac{\mathrm{d}}{\mathrm{d}\tau}\hat{K}(\tau) = -\hat{H}\hat{K}(\tau), \tag{2.39}$$

instead of the Schrödinger equation and has kernel

$$K(\tau, q', q) = \langle q'|\mathrm{e}^{-\tau\hat{H}}|q\rangle, \qquad K(0, q', q) = \delta(q', q). \tag{2.40}$$

This kernel is real[1] for a real Hamiltonian. Furthermore it is strictly positive:

Theorem 2.3 *Let the potential V be continuous and bounded from below and $\hat{H} = -\Delta + \hat{V}$ be an essentially self-adjoint operator. Then*

$$\langle q'|\mathrm{e}^{-\tau\hat{H}}|q\rangle > 0. \tag{2.41}$$

[1] If we couple the system to a magnetic field, $\hat{H}$ and $\hat{K}(\tau)$ become complex quantities.

The reader may consult the textbook [6] for a proof of this theorem. As examples we consider the kernel of the *free particle* with mass m,

$$K_0(\tau, q', q) = \left(\frac{m}{2\pi\tau}\right)^{d/2} \mathrm{e}^{-m(q'-q)^2/2\tau}, \tag{2.42}$$

and of the *harmonic oscillator* with frequency ω,

$$K_\omega(\tau, q', q) = \left(\frac{m\omega/(2\pi)}{\sinh\omega\tau}\right)^{d/2} \exp\left\{-\frac{m\omega}{2}\left(\left(q'^2 + q^2\right)\coth\omega\tau - \frac{2q'q}{\sinh\omega\tau}\right)\right\}, \tag{2.43}$$

both for imaginary time and in d dimensions. Both kernels are strictly positive. This positivity is essential for the far-reaching relation of Euclidean quantum theory and probability theory: The quantity

$$P_\tau(q) \equiv C\,K(\tau, q, 0) \tag{2.44}$$

can be interpreted as probability for the transition from point 0 to point q during the time interval τ.[2] The probability of ending somewhere should be 1,

$$\int \mathrm{d}q\, P_\tau(q) = 1, \tag{2.45}$$

and this requirement determines the constant C. For a free particle we obtain

$$P_\tau(q) = \left(\frac{m}{2\pi\tau}\right)^{d/2} \mathrm{e}^{-mq^2/2\tau}.$$

It represents the probability density for *Brownian motion* with diffusion coefficient inversely proportional to the mass, $D = 1/2m$.

In quantum field theory vacuum expectation values of products of field operators at different spacetime points encode all information about the theory. They determine scattering amplitudes and spectral properties of the particles and hence play a distinguished role. In quantum mechanics these expectation values are given by

$$W^{(n)}(t_1, \ldots, t_n) = \langle 0|\hat{q}(t_1)\cdots\hat{q}(t_n)|0\rangle, \qquad \hat{q}(t) = \mathrm{e}^{\mathrm{i}t\hat{H}}\hat{q}\,\mathrm{e}^{-\mathrm{i}t\hat{H}}. \tag{2.46}$$

These *Wightman functions* are not symmetric in their arguments $t_1, \ldots, t_n$ since the position operators at different times do not commute. Again we normalize the Hamiltonian such that the energy of the ground state $|0\rangle$ vanishes and perform an analytic continuation of the Wightman functions to complex times $z_i = t_i - \mathrm{i}\tau_i$:

$$W^{(n)}(z_1, \ldots, z_n) = \langle 0|\hat{q}\,\mathrm{e}^{-\mathrm{i}(z_1-z_2)\hat{H}}\hat{q}\,\mathrm{e}^{-\mathrm{i}(z_2-z_3)\hat{H}}\hat{q}\cdots\hat{q}\,\mathrm{e}^{-\mathrm{i}(z_{n-1}-z_n)\hat{H}}\hat{q}|0\rangle. \tag{2.47}$$

We used that $\hat{H}$ annihilates the ground state or that $\exp(\mathrm{i}\zeta\hat{H})|0\rangle = |0\rangle$. The functions $W^{(n)}$ are well-defined if the imaginary parts of their arguments z_k are ordered according to

$$\Im(z_k - z_{k+1}) \le 0.$$

[2] To keep the notation simple, we use q as the final point.

With $z_i = t_i - \mathrm{i}\tau_i$ one ends up with analytic functions $W^{(n)}$ in the region

$$\tau_1 > \tau_2 > \cdots > \tau_n. \tag{2.48}$$

The Wightman distributions for real time represent boundary values of the analytic Wightman functions with complex arguments:

$$W^{(n)}(t_1, \ldots, t_n) = \lim_{\substack{\Im z_i \to 0 \\ \Im(z_{k+1} - z_k) > 0}} W^{(n)}(z_1, \ldots, z_n). \tag{2.49}$$

On the other hand, if the arguments are purely imaginary then we obtain the *Schwinger functions*. For $\tau_1 > \tau_2 > \cdots > \tau_n$ they are given by

$$\begin{aligned} S^{(n)}(\tau_1, \ldots, \tau_n) &= W^{(n)}(-\mathrm{i}\tau_1, \ldots, -\mathrm{i}\tau_n) \\ &= \langle 0|\hat{q}\mathrm{e}^{-(\tau_1-\tau_2)\hat{H}}\hat{q}\mathrm{e}^{-(\tau_2-\tau_3)\hat{H}}\hat{q}\cdots\hat{q}\mathrm{e}^{-(\tau_{n-1}-\tau_n)\hat{H}}\hat{q}|0\rangle. \end{aligned} \tag{2.50}$$

As an example we consider the harmonic oscillator with Hamiltonian

$$\hat{H} = \omega\hat{a}^\dagger\hat{a},$$

expressed in terms of the step operators $\hat{a}, \hat{a}^\dagger$, which obey the commutation relation $[\hat{a}, \hat{a}^\dagger] = 1$. The ground state $|0\rangle$ in annihilated by $\hat{a}$ and hence has zero energy. The first excited state $|1\rangle = \hat{a}^\dagger|0\rangle$ has energy ω. The two-point Wightman function depends on the time difference only,

$$\begin{aligned} W^{(2)}(t_1 - t_2) &= \langle 0|\hat{q}(t_1)\hat{q}(t_2)|0\rangle = \frac{1}{2m\omega}\langle 0|\big(\hat{a} + \hat{a}^\dagger\big)\mathrm{e}^{-\mathrm{i}(t_1-t_2)\hat{H}}\big(\hat{a} + \hat{a}^\dagger\big)|0\rangle \\ &= \frac{1}{2m\omega}\langle 1|\mathrm{e}^{-\mathrm{i}t\omega\hat{a}^\dagger\hat{a}}|1\rangle = \frac{\mathrm{e}^{-\mathrm{i}\omega(t_1-t_2)}}{2m\omega}. \end{aligned}$$

The corresponding Schwinger function is given by

$$S^{(2)}(\tau_1 - \tau_2) = \frac{\mathrm{e}^{-\omega(\tau_1-\tau_2)}}{2m\omega} \quad (\tau_1 > \tau_2). \tag{2.51}$$

In a relativistic quantum field theory the Schwinger functions $S^{(n)}(x_1, \ldots, x_n)$ are invariant under Euclidean Lorentz transformation from the group $SO(4)$. This invariance together with locality imply that the $S^{(n)}$ are symmetric functions of their arguments $x_i \in \mathbb{R}^4$. This is not necessarily true for the Schwinger functions in quantum mechanics.

2.4.2 Imaginary-Time Path Integral

To formulate the path integral for imaginary time we employ the product formula (2.28), which follows from the product formula (2.27) through the substitution of it

by τ. For such systems the analogue of (2.31) for Euclidean time τ is obtained by the substitution of $i\varepsilon$ by ε. Thus we find

$$\begin{aligned} K(\tau, q', q) &= \langle \hat{q}' | \mathrm{e}^{-\tau \hat{H}/\hbar} | \hat{q} \rangle \\ &= \lim_{n\to\infty} \int \mathrm{d}q_1 \cdots \mathrm{d}q_{n-1} \left(\frac{m}{2\pi\hbar\varepsilon} \right)^{n/2} \mathrm{e}^{-S_{\mathrm{E}}(q_0, q_1, \ldots, q_n)/\hbar}, \\ S_{\mathrm{E}}(\ldots) &= \varepsilon \sum_{j=0}^{n-1} \left\{ \frac{m}{2} \left(\frac{q_{j+1} - q_j}{\varepsilon} \right)^2 + V(q_j) \right\}, \end{aligned} \tag{2.52}$$

where $q_0 = q$ and $q_n = q'$. The multi-dimensional integral represents the sum over all broken-line paths from q to q'. Interpreting S_{E} as Hamiltonian of a classical lattice model and $\hbar$ as temperature, it is (up to the fixed endpoints) the partition function of a one-dimensional lattice model on a lattice with $n+1$ sites. The real-valued variable q_j defined on site j enters the action S_{E}, which contains interactions between the variables q_j and q_{j+1} at neighboring sites. The values of the lattice field

$$\{0, 1, \ldots, n-1, n\} \to \{q_0, q_1, \ldots, q_{n-1}, q_n\}$$

are prescribed at the end points $q_0 = q$ and $q_n = q'$. Note that the classical limit $\hbar \to 0$ corresponds to the low-temperature limit of the lattice-system.

The multi-dimensional integral (2.52) corresponds to the summation over all lattice fields. What happens to the finite-dimensional integral when we take the *continuum limit* $n \to \infty$? Then we obtain the Euclidean path integral representation for the positive kernel

$$K(\tau, q', q) = \langle q' | \mathrm{e}^{-\tau \hat{H}/\hbar} | q \rangle = C \int_{q(0)=q}^{q(\tau)=q'} \mathscr{D}q \, \mathrm{e}^{-S_{\mathrm{E}}[q]/\hbar}. \tag{2.53}$$

The integrand contains the Euclidean action

$$S_{\mathrm{E}}[q] = \int_0^\tau d\sigma \left\{ \frac{m}{2} \dot{q}^2 + V(q(\sigma)) \right\}, \tag{2.54}$$

which for many physical systems is bounded from below.

2.5 Path Integral in Quantum Statistics

The Euclidean path integral formulation immediately leads to an interesting connection between quantum statistical mechanics and classical statistical physics. Indeed, if we set $\tau/\hbar \equiv \beta$ and integrate over $q = q'$ in (2.53), then we end up with the path integral representation for the canonical *partition function* of a quantum system with Hamiltonian $\hat{H}$ at inverse temperature $\beta = 1/k_B T$. More precisely, setting $q = q'$ and $\tau = \hbar\beta$ in the left-hand side of this formula, then the integral over q yields the trace of $\exp(-\beta\hat{H})$, which is just the canonical *partition function*,

$$\int \mathrm{d}q \, K(\hbar\beta, q, q) = \mathrm{tr}\, \mathrm{e}^{-\beta\hat{H}} = Z(\beta) = \sum \mathrm{e}^{-\beta E_n} \quad \text{with } \beta = \frac{1}{k_B T}. \tag{2.55}$$

Setting $q = q'$ in the Euclidean path integral in (2.53) means that we integrate over paths beginning and ending at q during the imaginary-time interval $[0, \hbar\beta]$. The final integral over q leads to the path integral over *all periodic paths* with period $\hbar\beta$,

$$Z(\beta) = C \oint \mathscr{D}q \mathrm{e}^{-S_{\mathrm{E}}[q]/\hbar}, \qquad q(\hbar\beta) = q(0). \tag{2.56}$$

For example, the kernel of the harmonic oscillator in (2.43) on the diagonal is

$$K_\omega(\beta, q, q) = \sqrt{\frac{m\omega}{2\pi \sinh(\omega\beta)}} \exp\{-m\omega \tanh(\omega\beta/2) q^2\}, \tag{2.57}$$

where we used units with $\hbar = 1$. The integral over q yields the partition function

$$\begin{aligned} Z(\beta) &= \sqrt{\frac{m\omega}{2\pi \sinh(\omega\beta)}} \int \mathrm{d}q \exp\{-m\omega \tanh(\omega\beta/2) q^2\} \\ &= \frac{1}{2\sinh(\omega\beta/2)} = \frac{\mathrm{e}^{-\omega\beta/2}}{1 - \mathrm{e}^{-\omega\beta}} = \mathrm{e}^{-\omega\beta/2} \sum_{n=0}^{\infty} \mathrm{e}^{-n\omega\beta}, \end{aligned} \tag{2.58}$$

where we used $\sinh x = 2\sinh x/2 \cosh x/2$. A comparison with the spectral sum over all energies in (2.55) yields the energies of the oscillator with (angular) frequency ω,

$$E_n = \omega\left(n + \frac{1}{2}\right), \quad n = 0, 1, 2, \ldots. \tag{2.59}$$

For large values of $\omega\beta$, i.e. for very low temperature, the spectral sum is dominated by the contribution of the ground state energy. Thus for cold systems the *free energy* converges to the ground state energy

$$F(\beta) \equiv -\frac{1}{\beta} \log Z(\beta) \overset{\omega\beta\to\infty}{\to} E_0. \tag{2.60}$$

One often is interested in the energies and wave functions of excited states. We now discuss an elegant method to extract this information from the path integral.

2.5.1 Thermal Correlation Functions

The energies of excited states are encoded in the *thermal correlation functions*. These functions are expectation values of products of the position operator

$$\hat{q}_{\mathrm{E}}(\tau) = \mathrm{e}^{\tau \hat{H}/\hbar} \hat{q} \mathrm{e}^{-\tau \hat{H}/\hbar}, \qquad \hat{q}_{\mathrm{E}}(0) = \hat{q}(0), \tag{2.61}$$

at different imaginary times in the canonical ensemble,

$$\left\langle \hat{q}_{\mathrm{E}}(\tau_1) \cdots \hat{q}_{\mathrm{E}}(\tau_n) \right\rangle_\beta \equiv \frac{1}{Z(\beta)} \mathrm{tr}\left(\mathrm{e}^{-\beta \hat{H}} \hat{q}_{\mathrm{E}}(\tau_1) \cdots \hat{q}_{\mathrm{E}}(\tau_n)\right). \tag{2.62}$$

The normalizing function $Z(\beta)$ is the partition function (2.56). From the thermal two-point function

$$\begin{aligned}\left\langle \hat{q}_{\mathrm{E}}(\tau_1)\hat{q}_{\mathrm{E}}(\tau_2)\right\rangle_\beta &= \frac{1}{Z(\beta)}\,\mathrm{tr}\big(\mathrm{e}^{-\beta\hat{H}}\hat{q}_{\mathrm{E}}(\tau_1)\hat{q}_{\mathrm{E}}(\tau_2)\big)\\ &= \frac{1}{Z(\beta)}\,\mathrm{tr}\big(\mathrm{e}^{-(\beta-\tau_1)\hat{H}}\hat{q}\,\mathrm{e}^{-(\tau_1-\tau_2)\hat{H}}\hat{q}\,\mathrm{e}^{-\tau_2\hat{H}}\big)\end{aligned} \tag{2.63}$$

we can extract the *energy gap* between the ground state and the first excited state. For this purpose we use orthonormal energy eigenstates $|n\rangle$ to calculate the trace and in addition insert the resolution of the identity-operator $\mathbb{1} = \sum |m\rangle\langle m|$. This yields

$$\langle \ldots \rangle_\beta = \frac{1}{Z(\beta)} \sum_{n,m} \mathrm{e}^{-(\beta-\tau_1+\tau_2)E_n}\mathrm{e}^{-(\tau_1-\tau_2)E_m}\langle n|\hat{q}|m\rangle\langle m|\hat{q}|n\rangle. \tag{2.64}$$

Note that in the sum over n the contributions from the excited states are exponentially suppressed at low temperatures $\beta \to \infty$, implying that the thermal two-point function converges to the Schwinger function in this limit:

$$\left\langle \hat{q}_{\mathrm{E}}(\tau_1)\hat{q}_{\mathrm{E}}(\tau_2)\right\rangle_\beta \overset{\beta\to\infty}{\to} \sum_{m\geq 0} \mathrm{e}^{-(\tau_1-\tau_2)(E_m-E_0)}\left|\langle 0|\hat{q}|m\rangle\right|^2 = \langle 0|\hat{q}_{\mathrm{E}}(\tau_1)\hat{q}_{\mathrm{E}}(\tau_2)|0\rangle. \tag{2.65}$$

In the first step we used that for low temperature the partition function tends to $\exp(-\beta E_0)$. Likewise, we find for the one-point function the result

$$\lim_{\beta\to\infty}\left\langle \hat{q}_{\mathrm{E}}(\tau)\right\rangle_\beta = \langle 0|\hat{q}|0\rangle. \tag{2.66}$$

In the *connected two-point function*

$$\left\langle \hat{q}_{\mathrm{E}}(\tau_1)\hat{q}_{\mathrm{E}}(\tau_2)\right\rangle_{c,\beta} \equiv \left\langle \hat{q}_{\mathrm{E}}(\tau_1)\hat{q}_{\mathrm{E}}(\tau_2)\right\rangle_\beta - \left\langle \hat{q}_{\mathrm{E}}(\tau_1)\right\rangle_\beta\left\langle \hat{q}_{\mathrm{E}}(\tau_2)\right\rangle_\beta \tag{2.67}$$

the term with $m = 0$ in the sum (2.65) is absent and this leads to an exponential decaying function for large time-differences,

$$\lim_{\beta\to\infty}\left\langle \hat{q}_{\mathrm{E}}(\tau_1)\hat{q}_{\mathrm{E}}(\tau_2)\right\rangle_{c,\beta} = \sum_{m>0} \mathrm{e}^{-(\tau_1-\tau_2)(E_m-E_0)}\left|\langle 0|\hat{q}|m\rangle\right|^2. \tag{2.68}$$

For large time-differences $\tau_1 - \tau_2$ the term with $m = 1$ dominates the sum such that

$$\left\langle \hat{q}_{\mathrm{E}}(\tau_1)\hat{q}_{\mathrm{E}}(\tau_2)\right\rangle_{c,\beta\to\infty} \to \mathrm{e}^{-(E_1-E_0)(\tau_1-\tau_2)}\left|\langle 0|\hat{q}|1\rangle\right|^2, \quad \tau_1-\tau_2\to\infty. \tag{2.69}$$

It follows that we can read off the energy gap $E_1 - E_0$ as well as the transition probability $|\langle 0|q|1\rangle|^2$ from the asymptotics of the connected two-point function.

To arrive at the path integral representation for the thermal two-point correlation function we consider the matrix elements

$$\left\langle q'\right|\hat{K}(\beta)\hat{q}_{\mathrm{E}}(\tau_1)\hat{q}_{\mathrm{E}}(\tau_2)\left|q\right\rangle, \quad \text{with } \hat{q}_{\mathrm{E}}(\tau) = \hat{K}(-\tau)\hat{q}\,\hat{K}(\tau). \tag{2.70}$$

Here $\hat{K}(\tau) = \exp(-\tau\hat{H})$ denotes the evolution operator for imaginary time with path integral representation given in (2.53). Now we insert twice the resolution of the identity and obtain

$$\langle \ldots \rangle = \int \mathrm{d}v\,\mathrm{d}u\left\langle q'\right|\hat{K}(\beta-\tau_1)\left|v\right\rangle v\langle v|\hat{K}(\tau_1-\tau_2)|u\rangle u\langle u|\hat{K}(\tau_2)|q\rangle.$$

In this result we make use of the path integral representations for the three propagators to find the path integral representation: Firstly, we sum over all paths from $q \to u$ in the time interval τ_2 and multiply the result with the coordinate u at time τ_2. Next we sum over all paths $u \to v$ in the time interval $\tau_1 - \tau_2$ and multiply with the coordinate v at time τ_1. The last step includes the summation over all paths $v \to q'$ in the time interval $\beta - \tau_1$. The integration over the intermediate positions u and v means that the summation extends over *all* paths $q \to q'$ and not only over paths going through u at time τ_2 and v at time τ_1. Besides $\exp(-S_\mathrm{E})$, the integrand includes the multiplicative factor $vu = q(\tau_1)q(\tau_2)$. Since the entire propagation time is β we end up with

$$\left\langle q' \middle| \mathrm{e}^{-\beta\hat{H}} \hat{q}_\mathrm{E}(\tau_1)\hat{q}_\mathrm{E}(\tau_2) \middle| q \right\rangle = C \int_{q(0)=q}^{q(\beta)=q'} \mathscr{D}q \mathrm{e}^{-S_\mathrm{E}[q]} q(\tau_1)q(\tau_2), \quad \tau_1 > \tau_2. \tag{2.71}$$

The thermal expectation value is given by the trace. Thus we set $q = q'$, integrate over q and divide the result by the partition function $Z(\beta)$. Integrating over q is equivalent to summing over all periodic paths with period β. Hence, we obtain

$$\left\langle \hat{q}_\mathrm{E}(\tau_1)\hat{q}_\mathrm{E}(\tau_2) \right\rangle_\beta = \frac{1}{Z(\beta)} \oint \mathscr{D}q \mathrm{e}^{-S_\mathrm{E}[q]} q(\tau_1)q(\tau_2) \tag{2.72}$$

with partition function given in (2.56). In the derivation we assumed the time-order $\tau_1 > \tau_2$ when applying the Trotter formula.

The path integral representation of higher time-ordered correlation functions are obtained in a similar fashion. They are all generated by the kernel

$$Z\big(\beta, j, q', q\big) = C \int_{q(0)=q}^{q(\beta)=q'} \mathscr{D}q \mathrm{e}^{-S_\mathrm{E}[q] + \int \mathrm{d}\tau j(\tau) q(\tau)}, \tag{2.73}$$

in which one integrates over all paths from q to q', or by the partition function in presence of an external source,

$$Z(\beta, j) = \int \mathrm{d}q\, Z(\beta, j, q, q) = C \oint_{q(0)=q(\beta)} \mathscr{D}q \mathrm{e}^{-S_\mathrm{E}[q] + \int \mathrm{d}\tau j(\tau) q(\tau)}. \tag{2.74}$$

The object in (2.73) generates matrix elements similarly as in (2.71) but with an arbitrary number of insertions of position operators. The function $Z(\beta, j)$ generates all time-ordered thermal correlation functions. For example, the thermal two-point function follows by differentiating the generating function (2.74) twice:

$$\left\langle T \hat{q}_\mathrm{E}(\tau_1)\hat{q}_\mathrm{E}(\tau_2) \right\rangle_\beta = \frac{1}{Z(\beta, 0)} \frac{\delta^2}{\delta j(\tau_1)\delta j(\tau_2)} Z(\beta, j)\bigg|_{j=0}, \tag{2.75}$$

wherein T indicates the time ordering. Since the right-hand side is symmetric in its arguments τ_1, τ_2 and both sides are identical for $\tau_1 > \tau_2$, we must include the time-ordering on the left-hand side. The ordering also results from a repeated calculation for $\tau_2 > \tau_1$.

The *connected correlation functions* are generated by the logarithm of the partition function, called *Schwinger functional*

$$W(\beta, j) \equiv \log Z(\beta, j), \tag{2.76}$$

by repeated differentiations with respect to the external source,

$$\left\langle T\,\hat{q}_{\mathrm{E}}(\tau_1)\hat{q}_{\mathrm{E}}(\tau_2)\cdots\hat{q}_{\mathrm{E}}(\tau_n)\right\rangle_{c,\beta} = \frac{\delta^n}{\delta j(\tau_1)\cdots\delta j(\tau_n)} W(\beta, j)\bigg|_{j=0}. \tag{2.77}$$

If we consider conservative systems and a time-independent source j, then the Schwinger functional is proportional to the free energy in the presence of the source.

2.6 The Harmonic Oscillator

We wish to study the path integral for the Euclidean oscillator with discretized time. The results are instructive particularly with regard to lattice field theories considered later in this book. So let us discretize the Euclidean time interval $[0, \tau]$ with n sampling points separated by a lattice constant $\varepsilon = \tau/n$. For the Lagrangian

$$L = \frac{m}{2}\dot{q}^2 + \mu q^2 \tag{2.78}$$

the discretized path integral over periodic paths reads

$$\begin{aligned} Z &= \int \mathrm{d}q_1\cdots\mathrm{d}q_n \left(\frac{m}{2\pi\varepsilon}\right)^{n/2} \exp\left\{-\varepsilon\sum_{j=0}^{n-1}\left(\frac{m}{2}\left(\frac{q_{j+1}-q_j}{\varepsilon}\right)^2 + \mu q_j^2\right)\right\} \\ &= \left(\frac{m}{2\pi\varepsilon}\right)^{n/2} \int \mathrm{d}q_1\cdots\mathrm{d}q_n \exp\left(-\frac{1}{2}(\mathbf{q}, \mathsf{A}\mathbf{q})\right), \end{aligned} \tag{2.79}$$

where we assumed $q_0 = q_n$ and introduced the symmetric matrix

$$\mathsf{A} = \frac{m}{\varepsilon}\begin{pmatrix} \alpha & -1 & 0 & \cdots & 0 & -1 \\ -1 & \alpha & -1 & \cdots & 0 & 0 \\ & & \ddots & & & \\ & & & \ddots & & \\ 0 & 0 & \cdots & -1 & \alpha & -1 \\ -1 & 0 & \cdots & 0 & -1 & \alpha \end{pmatrix}, \quad \alpha = 2\left(1 + \frac{\mu}{m}\varepsilon^2\right). \tag{2.80}$$

This is a *Toeplitz matrix,* in which each descending diagonal from left to right is constant. This property results from the invariance of the action under lattice translations. For the explicit calculation of Z we consider the *generating function*

$$\begin{aligned} Z[j] &= \left(\frac{m}{2\pi\varepsilon}\right)^{n/2} \int \mathrm{d}^n q \exp\left\{-\frac{1}{2}(\mathbf{q}, \mathsf{A}\mathbf{q}) + (\mathbf{j}, \mathbf{q})\right\} \\ &= \frac{(m/\varepsilon)^{n/2}}{\sqrt{\det \mathsf{A}}} \exp\left\{\frac{1}{2}\left(\mathbf{j}, \mathsf{A}^{-1}\mathbf{j}\right)\right\}. \end{aligned} \tag{2.81}$$

Here we applied the known result for Gaussian integrals. The n eigenvalues of A are

$$\lambda_k = \frac{m}{\varepsilon}\left(\alpha - 2\cos\frac{2\pi}{n}k\right) = \frac{2}{\varepsilon}\left(\mu\varepsilon^2 + 2m\sin^2\frac{\pi k}{n}\right), \quad k = 1, \ldots, n \tag{2.82}$$

and the corresponding orthonormal eigenvectors have the form

$$\psi(k) = \frac{1}{\sqrt{n}}\left(z^k, z^{2k}, \ldots, z^{nk}\right)^T \quad \text{with } z = \mathrm{e}^{2\pi \mathrm{i}/n}. \tag{2.83}$$

With the spectral resolution for the inverse matrix $\mathsf{A}^{-1} = \sum_k \lambda_k^{-1} \psi^\dagger(k)\psi(k)$ we obtain

$$\left(\mathsf{A}^{-1}\right)_{pq} = \frac{\varepsilon}{2n} \sum_{k=1}^{n} \frac{\mathrm{e}^{2\pi \mathrm{i} k(p-q)/n}}{\mu\varepsilon^2 + 2m \sin^2 \frac{\pi k}{n}}. \tag{2.84}$$

Note that the connected correlation function

$$\langle q_{i_1} \cdots q_{i_m} \rangle = \frac{\partial^m}{\partial j_{i_1} \cdots \partial q_{i_m}} \log Z[j] \bigg|_{j=0} \tag{2.85}$$

of the harmonic oscillator vanishes for $m > 2$. This means that all correlation functions are given in terms of the two-point function

$$\langle q_i q_j \rangle_c = \langle q_i q_j \rangle = \frac{\partial^2}{\partial j_i \partial j_j} \left(\mathbf{j}, \mathsf{A}^{-1}\mathbf{j}\right) = \left(\mathsf{A}^{-1}\right)_{ij}. \tag{2.86}$$

As a consequence of time-translation invariance the expectation value

$$\left\langle q_i^2 \right\rangle = \frac{\varepsilon}{2n} \sum_{k=1}^{n} \frac{1}{\mu\varepsilon^2 + 2m \sin^2 \frac{\pi k}{n}} \tag{2.87}$$

is independent of i. This and similar expectation values, together with the virial theorem, yield the ground state energies of Hamiltonians discretized on finite lattices. More details and numerical results are found in the chapter on simulations.

2.7 Problems

2.1 (Gaussian integral) Show that

$$\int \mathrm{d}z_1 \, \mathrm{d}\bar{z}_1 \cdots \mathrm{d}z_n \, \mathrm{d}\bar{z}_n \exp\left(- \sum_{ij} \bar{z}_i A_{ij} z_j \right) = \pi^n (\det \mathsf{A})^{-1}$$

with A being a positive Hermitian $n \times n$ matrix and z_i complex integration variables.

2.2 (Harmonic oscillator) In (2.43) we quoted the result for the kernel $K_\omega(\tau, q', q)$ of the d-dimensional harmonic oscillator with Hamiltonian

$$\hat{H} = \frac{1}{2m}\hat{p}^2 + \frac{m\omega^2}{2}\hat{q}^2$$

at imaginary time τ. Derive this formula.

Hint: Express the kernel in terms of the eigenfunctions of $\hat{H}$, which for $\hbar = m = \omega = 1$ are given by

$$\exp\bigl(-\xi^2 - \eta^2\bigr) \sum_{n=0}^{\infty} \frac{\zeta^n}{2^n n!} H_n(\xi) H_n(\eta) = \frac{1}{\sqrt{1-\zeta^2}} \exp\left(\frac{-(\xi^2 + \eta^2 - 2\xi\eta\zeta)}{1-\zeta^2} \right).$$

The functions H_n denote the Hermite polynomials.

Comment This result also follows from the direct evaluation of the path integral.

2.3 (Free particle on a circle) A free particle moves on an interval and obeys periodic boundary conditions. Compute the time evolution kernel $K(t_b - t_a, q_b, q_a) = \langle q_b, t_b | q_a, t_a \rangle$. Use the familiar formula for the kernel of the free particle (2.26) and enforce the periodic boundary conditions by a suitable sum over the evolution kernel for the particle on $\mathbb{R}$.

2.4 (Connected and unconnected correlation function) The unconnected thermal correlation functions are given by

$$\bigl\langle T\, \hat{q}_{\mathrm{E}}(\tau_1) \cdots \hat{q}_{\mathrm{E}}(\tau_n) \bigr\rangle_\beta = \frac{1}{Z(\beta)} \frac{\delta^n}{\delta j(\tau_1) \cdots \delta j(\tau_n)} Z(\beta, j) \Big|_{j=0}$$

with generating functional

$$Z(\beta, j) = \oint \mathcal{D}q \exp\left(-S_{\mathrm{E}}[q] + \int_0^\beta j(\tau) q(\tau) \right),$$

wherein one integrates over all β-periodic paths. Assume that the Euclidean Lagrangian density

$$\mathscr{L}_E(q, \dot{q}) = \frac{1}{2}\dot{q}^2 + V(q)$$

contains an even potential, i.e. $V(-q) = V(q)$.

(a) Show that $\langle \hat{q}_{\mathrm{E}}(\tau) \rangle_\beta = 0$.
(b) Express the unconnected 4-point function $\langle T\, \hat{q}_{\mathrm{E}}(\tau_1) \cdots \hat{q}_{\mathrm{E}}(\tau_4) \rangle_\beta$ via connected correlation functions.

2.5 (Semi-classical expansion of the partition function) In Chap. 2.5 we discussed the path integral representation of the thermal partition function, given by

$$Z(\beta) = C \int \mathrm{d}q \int_{q(0)=q}^{q(\hbar\beta)=q} \mathscr{D}q\, \mathrm{e}^{-S_{\mathrm{E}}[q]/\hbar}.$$

We rescale the imaginary time and the amplitude according to

$$\tau \to \hbar\tau \quad \text{and} \quad q(.) \to \hbar q(.).$$

After rescaling the 'time interval' is of length β instead of $\hbar\beta$ and

$$Z(\beta) = C \int \mathrm{d}q \int_{q(0)=q/\hbar}^{q(\beta)=q/\hbar} \mathscr{D}q \exp\left\{ -\int_0^\beta \left(\frac{1}{2} m \dot{q}^2 + V\bigl(\hbar q(.)\bigr) \right) \mathrm{d}\tau \right\}.$$

For a moving particle the kinetic energy dominates the potential energy for small $\hbar$. Thus we decompose each path into its constant part and the fluctuations about the constant part: $q(.) = q/\hbar + \xi(.)$. Show that

$$Z(\beta) = \frac{C}{\hbar} \int \mathrm{d}q \int_{\xi(0)=0}^{\xi(\beta)=0} \mathscr{D}\xi \exp\left\{ - \int_0^\beta \left(\frac{1}{2} m \dot{\xi}^2 + V(q + \hbar\xi) \right) \mathrm{d}\tau \right\}.$$

Determine the constant C by considering the limiting case $V = 0$ with the well-known result $Z(\beta, q, q) = (m/2\pi\beta\hbar^2)^{1/2}$. Then expand the integrand in powers of $\hbar$ and prove the intermediate result

$$Z = \frac{C}{\hbar} \int \mathrm{d}q \mathrm{e}^{-\beta V(q)} \int_{\xi(0)=0}^{\xi(\beta)=0} \mathscr{D}\xi \mathrm{e}^{-\frac{1}{2}m \int \mathrm{d}\tau \dot{\xi}^2} \left\{ 1 - \hbar V'(q) \int \xi(\tau) - \frac{1}{2}\hbar^2 \left(V''(q) \int \xi^2(\tau) - V'^2(q) \int \xi(\tau) \int \xi(s) \right) + \cdots \right\}.$$

Conditional expectation values as

$$\left\langle \xi(\tau_1)\xi(\tau_2) \right\rangle = \left\langle \xi(\tau_2)\xi(\tau_1) \right\rangle = C \int_{\xi(0)=0}^{\xi(\beta)=0} \mathscr{D}\xi \mathrm{e}^{-\frac{1}{2}m \int \mathrm{d}\tau \dot{\xi}^2} \xi(\tau_1)\xi(\tau_2)$$

are computed by differentiating the generating functional

$$C \int_{\xi(0)=0}^{\xi(\beta)=0} \mathscr{D}\xi \mathrm{e}^{-\frac{1}{2}m \int \mathrm{d}\tau \dot{\xi}^2 + \int \mathrm{d}\tau j\xi} = \frac{m}{2\pi\beta} \exp\left(\frac{1}{m\beta} \int_0^\beta \mathrm{d}\tau \int_0^\tau \mathrm{d}\tau' (\beta - \tau)\tau' j(\tau) j(\tau') \right).$$

Prove this formula for the generating functional and compute the leading and sub-leading contributions in the semi-classical expansion.

2.6 (High-temperature expansion of the partition function) Analyze the temperature dependence of the partition function (set $\hbar = 1$). Repeat the calculation in problem 2.5 but this time with the rescalings

$$\tau \to \beta\tau \quad \text{and} \quad \xi \to \sqrt{\beta}\xi,$$

and show that

$$Z(\beta) = \frac{C}{\sqrt{\beta}} \int \mathrm{d}q \int_{\xi(0)=0}^{\xi(1)=0} \mathscr{D}\xi \exp\left\{ - \int_0^1 \left(\frac{m}{2} \dot{\xi}^2 + \beta V(q + \sqrt{\beta}\xi) \right) \mathrm{d}\tau \right\}.$$

Expand $Z(\beta)$ in powers of the inverse temperature and use the generating functional in problem 2.5 (with $\beta = 1$) to compute the correlation functions. The remaining integrals over correlation functions are easily calculated. Determine the contributions of order $T^{1/2}$, $T^{-1/2}$ and $T^{-3/2}$ in the high-temperature expansion of $Z(\beta)$.

References

1. P.A.M. Dirac, The Lagrangian in quantum mechanics. Phys. Z. Sowjetunion **3**, 64 (1933)
2. P.A.M. Dirac, *The Principles of Quantum Mechanics* (Oxford University Press, London, 1947)
3. N. Wiener, Differential space. J. Math. Phys. Sci. **2**, 132 (1923)
4. R. Feynman, Spacetime approach to non-relativistic quantum mechanic. Rev. Mod. Phys. **20**, 267 (1948)
5. R. Feynman, A. Hibbs, *Quantum Mechanics and Path Integrals* (McGraw-Hill, New York, 1965)
6. J. Glimm, A. Jaffe, *Quantum Physics: A Functional Integral Point of View* (Springer, Berlin, 1981)
7. P.R. Chernoff, Note on product formulas for operator semigroups. J. Funct. Anal. **2**, 238 (1968)
8. M. Reed, B. Simon, *Methods of Modern Mathematical Physics I* (Academic Press, New York, 1972)
9. M. Kac, Random walk and the theory of Brownian motion. Am. Math. Mon. **54**, 369 (1947)
10. I.M. Gel'fand, A.M. Yaglom, Integration in functional spaces and its applications in quantum physics. J. Math. Phys. **1**, 48 (1960)
11. G. Roepstorff, *Path Integral Approach to Quantum Physics* (Springer, Berlin, 1996)
12. L.S. Schulman, *Techniques and Applications of Path Integration* (Wiley, New York, 1981)
13. E. Nelson, Feynman integrals and the Schrödinger equation. J. Math. Phys. **5**, 332 (1964)
14. S.G. Brush, Functional integrals and statistical physics. Rev. Mod. Phys. **33**, 79 (1961)
15. J. Zinn-Justin, *Path Integrals in Quantum Mechanics* (Oxford University Press, London, 2004)
16. H. Kleinert, *Path Integral, in Quantum Mechanics, Statistics, Polymer Physics and Financial Markets* (World Scientific, Singapore, 2006)
17. U. Mosel, *Path Integrals in Field Theory: An Introduction* (Springer, Berlin, 2004)

Chapter 3
High-Dimensional Integrals

Unfortunately, path integrals can be evaluated only for very simple systems like the harmonic oscillator, free particle or topological field theories. More complicated systems are analyzed via perturbation theory (e.g. semi-classical expansion, perturbative expansion in powers of the interaction, strong-coupling expansion, high- and low-temperature expansions) or numerical methods. In Chap. 2 we have demonstrated that path integrals for imaginary time or systems in thermal equilibrium may be approximated by finite-dimensional integrals. We discretized time as $s \in \{0, \varepsilon, \ldots, n\varepsilon = \tau\}$ and approximated the Euclidean action by a Riemann sum. The latter depends on the values

$$\mathbf{q} = \{q_0, q_1, \ldots, q_n\} = \big\{q(0), q(\varepsilon), \ldots, q(n\varepsilon)\big\}$$

of the path at the lattice points $s_k = k\varepsilon$. In this lattice approximation every expectation value is given by a finite-dimensional integral,

$$\langle O\rangle = \frac{\int \mathscr{D}\mathbf{q}\, O(\mathbf{q}) \mathrm{e}^{-S_\mathrm{E}(\mathbf{q})}}{\int \mathscr{D}\mathbf{q} \mathrm{e}^{-S_\mathrm{E}(\mathbf{q})}} \quad \text{with} \int \mathscr{D}\mathbf{q} = \int_{-\infty}^{\infty} \prod_1^n \mathrm{d}q_j. \tag{3.1}$$

The function $S_\mathrm{E}(\mathbf{q}) = S_\mathrm{E}(q_1, \ldots, q_n)$ in the exponents is the Euclidean lattice action. For a particle on a line it is given in Eq. (2.52). In this chapter we shall only consider Euclidean path integrals and thus skip the index E.

3.1 Numerical Algorithms

We are confronted with high-dimensional integrals in quantum statistics, solid-state physics, Euclidean quantum field theory, high-energy physics and numerous other branches in natural sciences or even the financial market. For example, consider the expectation value of interest derivatives, which can be written as a high-dimensional integral. Assuming a duration of 30×12 months and a separate interest rate each month one is confronted with a 360-dimensional integral. Thus we are in need of efficient algorithms to compute these integrals with a controllable error.

A. Wipf, *Statistical Approach to Quantum Field Theory*, Lecture Notes in Physics 864,
DOI 10.1007/978-3-642-33105-3_3,

RICHARD BELLMAN coined the phrase *the curse of dimensionality* to describe the rapid growth in the difficulty as the number of integration variables increases [1].

3.1.1 Newton–Cotes Integration Method

We distinguish between two classes of numerical algorithms, depending on whether we evaluate the integrand at equidistant sampling points (Newton–Cotes integration method) or at carefully chosen, but not equidistant sampling points (Gaussian integration method). For particular integrands the Gaussian method may be much more efficient. For example, the maximum degree of exactness is obtained for the *Gauss-Legendre formula*, the sampling points of which are given by zeros of Legendre polynomials. A lucid representation of the Gaussian integration method is found in [2]. Other textbooks are [3–6].

Numerical algorithms are based on Riemann's definition of integrals. To see whether a given function $f : [a, b] \to \mathbb{R}$ is Riemann-integrable, we choose a partition of the interval

$$\gamma: \quad a = x_0 < x_1 < x_2 < \cdots < x_{n-2} < x_{n-1} < x_n = b \tag{3.2}$$

and consider the associated lower and upper Riemann sum

$$U(f,\gamma) = \sum_{i=0}^{n-1} (x_{i+1} - x_i) \cdot \inf\{f(x) | x_i \le x \le x_{i+1}\}$$
$$O(f,\gamma) = \sum_{i=0}^{n-1} (x_{i+1} - x_i) \cdot \sup\{f(x) | x_i \le x \le x_{i+1}\},$$

with $O(f,\gamma) \ge U(f,\gamma)$. The function f is called Riemann-integrable, if

$$\sup_\gamma U(f,\gamma) = \inf_\gamma O(f,\gamma)$$

and we denote by

$$\int_a^b f(x)\,\mathrm{d}x \equiv \sup_\gamma U(f,\gamma) \tag{3.3}$$

the *Riemann integral* of f. This definition is easily extended to multi-dimensional integrals and serves as point of departure for numerical algorithms.

Many algorithms are based on the approximation of arbitrary smooth functions by *polynomial interpolations*. We remind the reader that there is a unique polynomial P_m of degree $\le m$, which assumes the values $f_i = f(x_i)$ of a given function f at $(m+1)$ sampling points $x_0, x_1, \ldots, x_{m-1}, x_m$. The construction of this interpolating polynomial makes use of the $m+1$ *Lagrange polynomials* of degree m:

$$L_p^{(m)}(x) = \prod_{\substack{i=0 \\ i \ne p}}^{m} \frac{x - x_i}{x_p - x_i}, \quad p = 0, \ldots, m \text{ with } L_p^{(m)}(x_q) = \delta_{pq}. \tag{3.4}$$

The interpolating polynomial of degree m is given by

$$P_m(x) = \sum_{p=0}^{m} f(x_p) L_p^{(m)}(x). \tag{3.5}$$

The error of the polynomial approximation is bounded by the following result:

Theorem 3.1 *Let f be a $(m+1)$-times continuous differentiable function and P_m the interpolating polynomial of degree $\leq m$ with sampling points $x_0, \ldots, x_m \in \Delta$. Then there exists for every $x \in \Delta$ a point ξ_x (which lies in the smallest interval containing all sampling points) such that*

$$f(x) - P_m(x) = \frac{f^{(m+1)}(\xi_x)}{(m+1)!} L^{(m)}(x), \quad L^{(m)}(x) = \prod_{i=0}^{m} (x - x_i). \tag{3.6}$$

This theorem leads to the following representation of the integral from the smallest to the largest sampling point:

$$\int_{x_0}^{x_m} \mathrm{d}x\, f(x) = \sum_{p=0}^{m} f(x_p) \underbrace{\int \mathrm{d}x L_p^{(m)}(x)}_{\gamma_p^{(m)}} + \int \mathrm{d}x \frac{f^{(m+1)}(\xi_x)}{(m+1)!} L^{(m)}(x). \tag{3.7}$$

We call $\gamma_p^{(m)}$ the *weights* and x_p the *nodes* of the integration formula. For equidistant nodes at points

$$x_0, x_1 = x_0 + \varepsilon, x_2 = x_0 + 2\varepsilon, \ldots, x_m = x_0 + m\varepsilon \tag{3.8}$$

we find, after setting $x = x_0 + \varepsilon t$ with $t \in [0, m]$ in (3.7), the weights

$$\gamma_p^{(m)} = \varepsilon \int_0^m \mathrm{d}t \prod_{\substack{i=0 \\ i \neq p}}^{m} \frac{t-i}{p-i} \equiv \varepsilon w_p^{(m)} = \varepsilon w_{m-p}^{(m)}, \quad p = 0, 1, \ldots, m. \tag{3.9}$$

Applying the formula (3.7) to constant functions yields the simple sum rule $\sum_p \gamma_p^{(m)} = m\varepsilon$ or equivalently

$$w_0^{(m)} + w_1^{(m)} + \cdots + w_m^{(m)} = m. \tag{3.10}$$

Hence the Newton–Cotes formulas can be written as

$$\int_{x_0}^{x_m} \mathrm{d}x\, f(x) \sim \sum_{p=0}^{m} \varepsilon w_p^{(m)} f(x_0 + \varepsilon p). \tag{3.11}$$

The corresponding weights $w_p^{(m)}$ for $m = 0, \ldots, 6$ are listed in Table 3.1.

The integration step-length ε can be chosen sufficiently small in order to ensure that the quadrature error is less than a prescribed tolerance. We illustrate how one can estimate the error for the Simpson formula. Thus we consider the difference

Table 3.1 Weights for the Newton–Cotes formulas

m	name	$p=$	0	1	2	3	4	5	6
0	rectangle rule	$w_p^{(0)} =$	1						
1	trapezoidal rule	$2 \times w_p^{(1)} =$	1	1					
2	Simpson's rule	$3 \times w_p^{(2)} =$	1	4	1				
3	3/8-rule	$8 \times w_p^{(3)} =$	3	9	9	3			
4	Milne's rule	$45 \times w_p^{(4)} =$	14	64	24	64	14		
5	6-point rule	$288 \times w_p^{(5)} =$	95	375	250	250	288	95	
6	Weddle's rule	$140 \times w_p^{(6)} =$	41	216	27	272	27	216	41

between the integral of f from $-\varepsilon$ to ε and the corresponding approximation (3.11) with $m = 2$,

$$E_2(\varepsilon) = \int_{-\varepsilon}^{\varepsilon} \mathrm{d}x\, f(x) - \frac{\varepsilon}{3}\big(f(-\varepsilon) + 4f(0) + f(\varepsilon)\big).$$

Differentiating the error $E_2(\varepsilon)$ three times with respect to ε leads to

$$E_2'''(\varepsilon) = -\frac{\varepsilon}{3}\big(-f'''(-\varepsilon) + f'''(\varepsilon)\big).$$

The absolute value of this expression can be bounded as follows:

$$\big|E_2'''(\varepsilon)\big| = \frac{\varepsilon}{3}\big|f'''(\varepsilon) - f'''(-\varepsilon)\big| \le \frac{2\varepsilon}{3} M_3 \quad \text{with } M_3 = \sup_{t\in[-\varepsilon,\varepsilon]} \big|f'''(t)\big|.$$

Integrating three times provides the error estimation

$$\big|E_2(\varepsilon)\big| \le M_3 \cdot \frac{\varepsilon^4}{36}. \tag{3.12}$$

If the function f is at least four times differentiable, then the we may apply the mean value theorem to E_2''' and obtain

$$E_2'''(\varepsilon) = \frac{2\varepsilon}{3}\varepsilon \cdot f^{(4)}(\xi).$$

This results in an improved error bound,

$$\big|E_2(\varepsilon)\big| \le M_4 \cdot \frac{\varepsilon^5}{90} \quad \text{with } M_4 = \sup_{t\in[-\varepsilon,\varepsilon]} \big|f^{(4)}(t)\big|. \tag{3.13}$$

Hence with *Simpson's rule* (Kepler's rule for the calculation of wine casks) even cubic polynomials are integrated in an exact manner. Analogous error bounds for approximations based on interpolating polynomials of degree $m \le 6$ with equidistant nodes are listed in Table 3.2. They bound the errors for integrals from the smallest to the largest sampling point and contain as factors $M_m = \sup_{[x_0,x_m]} |f^{(m)}|$.

With increasing degree m the coefficients of the Newton–Cotes formulas grow rapidly and have alternating signs. This leads to integration formulas containing

Table 3.2 Error estimation of the integration over the interval $[x_0, x_m]$ with $x_m = x_0 + m\varepsilon$

m	name	$E_m(\varepsilon)$	m	name	$E_m(\varepsilon)$
0	rectangle rule	$\varepsilon^2 M_1/2$	4	Milne's rule	$8\varepsilon^7 M_6/945$
1	trapezoidal rule	$\varepsilon^3 M_2/12$	5	6-point rule	$275\varepsilon^7 M_6/12096$
2	Simpson's rule	$\varepsilon^5 M_4/90$	6	Weddle's rule	$9\varepsilon^9 M_8/1400$
3	3/8-rule	$3\varepsilon^5 M_4/80$			

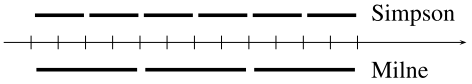

Fig. 3.1 In the composite formulas the interval is divided into subintervals or length ε. We cluster m neighboring subintervals and apply the previous integration rules to each cluster

differences of large numbers. Largely for this reason higher-order Newton–Cotes formulas are rarely used in practice. In passing we also note that any method based on polynomial interpolation may lead to wrong results in case the function is not sufficiently often differentiable.

Composite Integration Formulas

By partitioning the integration interval into smaller subintervals of equal length we arrive at the *composite* rectangle, trapezoidal and Simpson rule or one of the higher-order composite integration formulas. Thereby the number of intervals should be a multiple of m. For the Simpson rule the situation is depicted in Fig. 3.1. Let us study the composite Simpson rule in more detail. First we partition the interval $[a, b]$ into $2n$ subintervals of length ε such that $b - a = 2n\varepsilon$. The $2n + 1$ sampling points are $x_j = a + \varepsilon j$ with $j = 0, 1, \ldots, 2n$. The integral is approximated by

$$\begin{aligned} S_2(f) \approx \frac{\varepsilon}{3}\big(\big\{f(x_0) + 4f(x_1) + f(x_2)\big\} + \big\{f(x_2) + 4f(x_3) + f(x_4)\big\} + \cdots \\ + \big\{f(x_{2n-2}) + 4f(x_{2n-1}) + f\big(x_{2n}\big)\big\}\big). \end{aligned}$$

The resulting formula is called *composite Simpson quadrature formula*, and reads

$$S_2(f) = \frac{\varepsilon}{3}\left(f(x_0) + 4\sum_{j=0}^{n-1} f(x_{2j+1}) + 2\sum_{j=1}^{n-1} f(x_{2j}) + f(x_{2n})\right). \tag{3.14}$$

We can bound the error of the composite Simpson formula as follows:

$$\left|\int_a^b f(x)\,\mathrm{d}x - S_2(f)\right| \le \frac{1}{90}\varepsilon^5 \cdot n \underbrace{\sup_{t\in[a,b]} \left|f^{(4)}(t)\right|}_{M_4} = \frac{b-a}{180}\varepsilon^4 M_4. \tag{3.15}$$

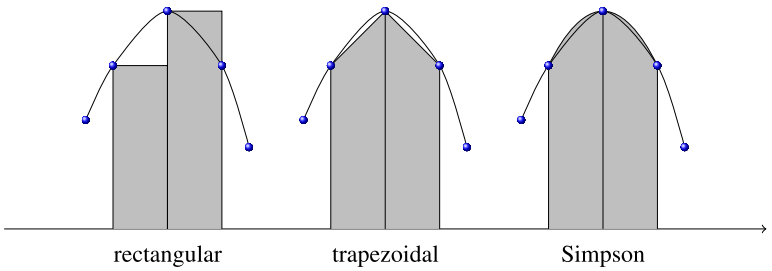

Fig. 3.2 Numerical integration via the rectangle rule, the trapezoidal rule and Simpson's rule

Similar bounds can be derived for other composite quadrature formulas. For the partition of $[a, b]$ into $m \times n$ subintervals of length $\varepsilon = (b-a)/mn$ we find

$$\left| \int_a^b f(x)\,\mathrm{d}x - S_m(f) \right| \le \frac{b-a}{m\varepsilon} E_m(\varepsilon), \tag{3.16}$$

where the numbers $E_m(\varepsilon)$ are listed in Table 3.2. But now M_m in this table denotes the supremum of $|f^{(m)}|$ on the integration interval. Let us calculate and compare four approximations to the integral of $\exp(x)$ from 0 to 1: with the rectangle rule, the trapezoidal rule, the Simpson rule and the Monte Carlo method. The latter will be explained in Sect. 3.2. For the numerical approximations we applied the following composite quadrature formulas:

$$\begin{aligned}
&\text{rectangle rule:} && \sum_{i=0,1,2}^{n-1} \varepsilon f(x_i), \\
&\text{trapezoidal rule:} && \sum_{i=0,1,2}^{n-1} \frac{\varepsilon}{2}\big(f(x_i) + f(x_{i+1})\big), \\
&\text{Simpson's rule:} && \sum_{i=0,2,4}^{n-2} \frac{\varepsilon}{3}\big(f(x_i) + 4f(x_{i+1}) + f(x_{i+2})\big).
\end{aligned} \tag{3.17}$$

Recall that in the last formula n must be even. The interpolations used in these approximations are sketched in Fig. 3.2. With the program `1dintegral.c` on p. 42 one can estimate the definite integral

$$\int_0^1 \mathrm{d}x\, \mathrm{e}^x \quad \text{with } \varepsilon \in \{10^{-n} | n = 1, 2, \ldots, 6\} \tag{3.18}$$

with the help of Simpson's rule. With a slight modification of the code we are able to integrate with the other quadrature formulas as well. The following table compares the results obtained with the piecewise constant, linear or quadratic interpolations. For Simpson's rule we observe a rapid convergence to the exact value 1.7182818.

Table 3.3 Convergence of different methods. The integer n is defined in (3.18)

n, $\log M$	Rectangle	Trapezoidal	Simpson	Monte Carlo
1	1.633799	1.719713	1.718283	1.853195
2	1.709705	1.718296	1.718282	1.793378
3	1.717423	1.718282	1.718282	1.720990
4	1.718196	1.718282	1.718282	1.711849
5	1.718273	1.718282	1.718282	1.719329
6	1.718281	1.718282	1.718282	1.718257

3.2 Monte Carlo Integration

The Monte Carlo method was presumably invented by STANISLAW ULAM. He developed this method in 1946 while he was thinking about the probability of profit for solitaire:

> The first thoughts and attempts I made to practice [the Monte Carlo Method] were suggested by a question which occurred to me in 1946 as I was convalescing from an illness and playing solitaires. The question was what are the chances that a Canfield solitaire laid out with 52 cards will come out successfully? After spending a lot of time trying to estimate them by pure combinatorial calculations, I wondered whether a more practical method than "abstract thinking" might not be to lay it out say one hundred times and simply observe and count the number of successful plays. ...

A few years later the method was applied to the problem of neutron diffusion which could not be solved analytically [7]. Of utmost importance in physics is the application of the Monte Carlo method to estimate high-dimensional integrals. For an nice introduction to this method see the review [8].

A basic algorithm to estimate the integral of a function $f : G \to \mathbb{R}$ could be:

- generate M uniformly distributed points $\{x_1, \ldots, x_M\}$ in G,
- compute the function value $f(x_i)$ for every point $x_i, i = 1, \ldots, M$,
- compute the mean value

$$I(M) = \frac{\mathrm{Vol}(G)}{M} \sum_{i=1}^{M} f(x_i). \tag{3.19}$$

For any Riemann integrable function the mean $I(M)$ converges for large M to the integral. For the exponential integral in (3.18) we calculated the mean for $M = 10, 100, \ldots$ and the results are contained in the last column of Table 3.3. We used the simple Monte Carlo program listed on p. 42. In line 38 of the code the random number generator is called to generate a random number in $[0, 1]$.

Figure 3.3 compares the convergence behavior of the rectangle and Simpson quadrature formulas and of the simple Monte Carlo integration. Simpson's integration rule, applied to the exponential function, agrees with the exact result in 1 ppm already for a partitioning of $[0, 1]$ in ten subintervals. When we consider the problem of numerical integration over n-dimensional domains,

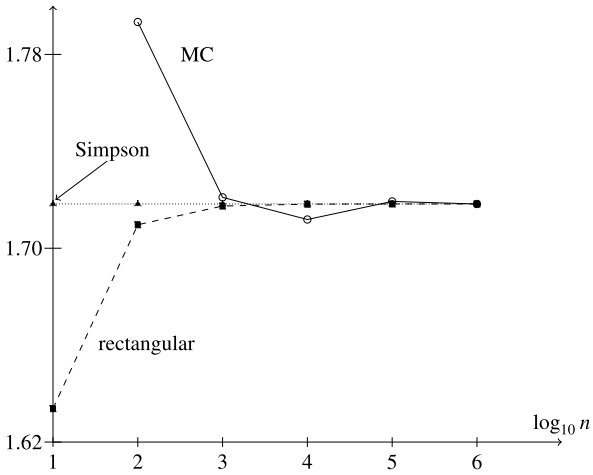

Fig. 3.3 Convergence of different integration methods: rectangle rule, trapezoidal rule and Monte Carlo integration

$$I = \int_G \mathrm{d}q_1 \cdots \mathrm{d}q_n \, f(q_1, \ldots, q_n) \equiv \int_G \mathrm{d}^n q \, f(\mathbf{q}) \tag{3.20}$$

then an obvious strategy is to apply a rule such as Simpson's rule in each dimension, creating what is called a product rule. But any product rule is prohibitively time-consuming when n is large. As an example, consider fixed integration limits 0 and 1 as well as a fixed distance ε between the sampling points for variable dimension n of the integral. Then the number of nodes is equal to ε^{-n} and the computing time is proportional to this number. To estimate this time we choose a coarse partition of the interval $[0, 1]$ with $\varepsilon = 0.1$ for which the number of sampling points is $\sim 10^n$. Calculating the contribution of one node takes approximately 10^{-7} seconds of CPU-time such that the numerical integration of a 12-dimensional integral takes approximately a whole day. Nevertheless, there are other ways of tackling high-dimensional integrals, as demonstrated by TRAUB and PASKOV when they treated a mathematical finance problem from Wall Street as an integration problem over the 360-dimensional unit cube [9]. They used what nowadays is called quasi-Monte Carlo method, a deterministic algorithm which is widely used in the financial sector to estimate financial derivatives. For reviews on this potentially interesting development see [10, 11].

3.2.1 Hit-or-Miss Monte Carlo Method and Binomial Distribution

We wish to estimate the value of a definite integral $I = \int \mathrm{d}^n x \, f(x)$ with stochastic means. First we transform both the coordinates and function such we are dealing with an integration problem of a function $0 \leq f \leq 1$ over the n-dimensional unit cube. We are not touching the problem of how best to transform a given problem to the unit cube. Let us first consider a one-dimensional integral of a function on the unit interval. The integral is equal to the area below the graph of f, see Fig. 3.4.

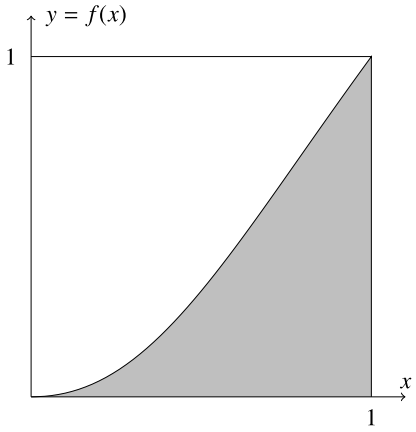

Fig. 3.4 The *gray area* underneath the graph of f is proportional to the relative frequency of hits when shooting on the unit square

How can we calculate this area with probabilistic means? From a random number generator which generates uniformly distributed numbers on the unit interval we take two random numbers x and y. Now we shoot on the unit square in Fig. 3.4. A hit of the shaded area is then identified with $y \leq f(x)$. The *probability* for a hit is

$$p = \frac{\text{number of hits}}{\text{number of trials}} = \frac{\text{gray area}}{\text{total area}} = \frac{I}{1} = I. \tag{3.21}$$

Let us repeat shooting M times such that the number of hits is in $\{0, \ldots, M\}$. For statistically independent shots the probability for k hits is given by the *binomial distribution*

$$P(M,k) = \binom{M}{k} p^k (1-p)^{M-k} \quad \text{with} \sum_{k=0}^{M} P(M,k) = 1. \tag{3.22}$$

The binomial coefficient in this distribution function counts the number of ways of picking k hits from M shots. The distribution (3.22) describes a bell-shaped curve, localized at pM. The *generating function* for the moments of the binomial distribution can be computed easily:

$$Z(t) = \left\langle \mathrm{e}^{tk} \right\rangle = \sum_{k=0}^{M} \mathrm{e}^{kt} P(M,k) = \left(\mathrm{e}^t p + (1-p) \right)^M. \tag{3.23}$$

Being the sum of all probabilities $Z(0) = \langle 1 \rangle = 1$. The expectation values of arbitrary powers of k are obtained by differentiating the generating function with respect to t.

For example, for a very large number of shots the *relative frequency of hits* is

$$\left\langle \frac{k}{M} \right\rangle = \frac{1}{M} \sum_{k=0}^{M} k P(M,k) = \frac{1}{M} \frac{\mathrm{d}Z}{\mathrm{d}t}\bigg|_{t=0} = p, \tag{3.24}$$

Table 3.4 Convergence behavior of different methods. M is defined as stated in (3.19)

$\log_{10} M$	p	$I-p$	σ	p_{impr}	$I-p_{\text{impr}}$	σ_{impr}
1	0.500000	−0.123630	0.158114	0.333333	0.043037	0.000000
2	0.330000	0.046370	0.047021	0.363333	0.013037	0.017059
3	0.399000	−0.022630	0.015485	0.377333	−0.000963	0.006486
4	0.378900	−0.002530	0.004851	0.376833	−0.000463	0.002040
5	0.376570	−0.000200	0.001532	0.377693	−0.001323	0.000651
6	0.374857	0.001513	0.000484	0.376305	0.000065	0.000203
7	0.376273	0.000097	0.000153	0.376303	0.000067	0.000064

as expected. The relative frequency has mean square

$$\left\langle \frac{k^2}{M^2} \right\rangle = \frac{1}{M^2} \frac{\mathrm{d}^2 Z}{\mathrm{d}t^2}\bigg|_{t=0} = \frac{p}{M} + \left(1 - \frac{1}{M}\right) p^2. \tag{3.25}$$

More interesting is the variance of the relative frequency,

$$\sigma^2 = \frac{1}{M^2} \left\langle \big(k - \langle k \rangle\big)^2 \right\rangle = \frac{1}{M^2} \frac{\mathrm{d}^2 \log Z}{\mathrm{d}t^2}\bigg|_{t=0} = \frac{p(1-p)}{M}. \tag{3.26}$$

Note that the standard deviation σ decreases only slowly with the number of trials, $\sigma \sim M^{-1/2}$ and this slow decrease is typical for probabilistic methods.

Numerical Experiment

An estimation of the probability p is given by the relative frequency of hits in M trials. Table 3.4 contains estimations p of the definite integral

$$I = \int_0^1 f(x) \approx 0.376370, \quad f(x) = \frac{x^2 \mathrm{e}^x}{1 - x + x\mathrm{e}^x}, \tag{3.27}$$

for an increasing number of trials M and of the corresponding spreads σ around the estimated values. The numbers in columns 2, 3 and 4 were calculated with the program `hitandmissarea.c`, listed on p. 43.

The simple hit-or-miss method can be improved with little effort. Observe that the variance decreases when p approaches 0 or 1. As a warning we mention that at the same time the relative error increases. Now we choose an analytically integrable function $g \le f$, which approximates f rather well. Thus the first integral in

$$I = \underbrace{\int \big(f(x) - g(x)\big)\,\mathrm{d}x}_{\text{small}} + \underbrace{\int g(x)\,\mathrm{d}x}_{\text{known}} \tag{3.28}$$

is small and the integrand lies between 0 and 1. It is estimated by means of the hit-or-miss method with reduced variance. For the function f in (3.27) we may choose

$$g(x) = x^2 \quad \text{with} \int g(x)\,\mathrm{d}x = 1/3.$$

With this reweighing technique we obtain improved estimates and smaller variances for integrals of interest. The last three columns in Table 3.4 contain the estimates and standard deviations for the improved method for various values of trials M. These values were computed with the program `hitandmissarea.c` on p. 43.

3.2.2 Sum of Random Numbers and Gaussian Distribution

The program `gaussdistr.c` on p. 44 generates the sum $s = x_1 + x_2 + \cdots + x_n$ of n equally distributed and independent random numbers on the unit interval. The sum itself is a random number with values in $[0, n]$ and generating function

$$Z(t) = \left\langle \mathrm{e}^{ts} \right\rangle = \int_{I^n} \mathrm{d}^n x\, \mathrm{e}^{t(x_1+\cdots+x_n)} = \left(\int_0^1 \mathrm{d}x\, \mathrm{e}^{tx} \right)^n = t^{-n} \left(\mathrm{e}^t - 1 \right)^n. \quad (3.29)$$

We find the expected result for the mean value of s

$$m = \langle s \rangle = \left. \frac{dZ}{\mathrm{d}t} \right|_{t=0} = \int_{I^n} \mathrm{d}^n x (x_1 + \cdots + x_n) = \frac{n}{2}. \quad (3.30)$$

Similarly, we obtain for the square of the statistical spread

$$\left. \frac{\mathrm{d}^2 \log Z}{\mathrm{d}t^2} \right|_{t=0} = \sigma^2 = \left\langle s^2 \right\rangle - m^2 = \frac{n}{12}. \quad (3.31)$$

According to the law of large numbers[1] we obtain the Gaussian distribution

$$P_s = \frac{1}{\sqrt{2\pi}\sigma} \mathrm{e}^{-(s-m)^2/2\sigma^2}. \quad (3.32)$$

The program calculates the distribution of s for $n = 10, 50, 100$. For each n a histogram is generated from one million trials. Rescaling s with n leads to a maximum of the distribution at $s/n = 1/2$ and a variance of $1/12n$. Figure 3.5 compares the distributions obtained by Monte Carlo simulation and the Gaussian distributions (3.32).

The inequality (3.57) describes the probability that the random number s/n deviates more than δ from its mean value. In the present case it reads

$$P\left[\left| \frac{s}{n} - \frac{1}{2} \right| \geq \delta \right] \leq \frac{1}{12n\delta^2}. \quad (3.33)$$

[1] For a discussion and proof of this law see p. 40.

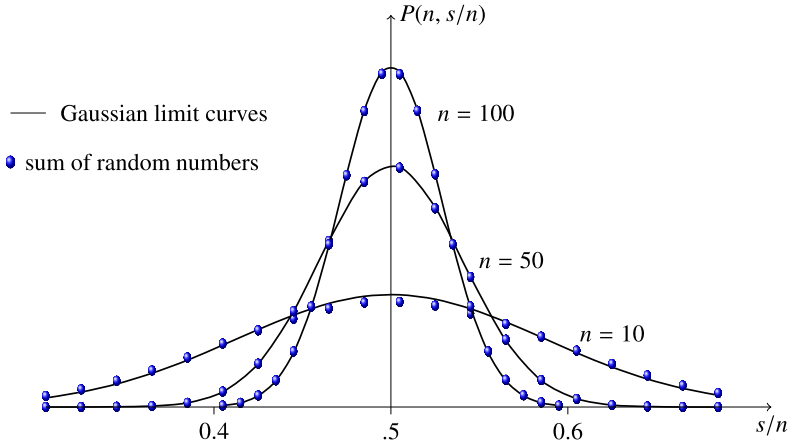

Fig. 3.5 The sum s of n random numbers forms a Gaussian distribution for large n. The limit distribution of the rescaled random variable s/n has the mean value $1/2$. Furthermore the square of the statistical spread is $1/12n$

3.3 Importance Sampling

Numerical algorithms approximate integrals by finite sums,

$$\int \mathrm{d}^n q\, f(\mathbf{q}) \sim \sum_{\mu=1}^{M} f(\mathbf{q}_\mu) \Delta \mathbf{q}_\mu .$$

In case of high-dimensional integrals and slowly varying functions f it may be advantageous to choose the sampling points $\mathbf{q}_\mu$ randomly. But in physical problems we are often confronted with integrands that vary by several orders of magnitude for different points in which case we may waste computing time at sampling points with small integrands. The idea of *importance sampling*, according to which one preferably samples points with large integrands, is incorporated in many stochastic algorithms for calculating high-dimensional integrals. The best-known examples are based on the Metropolis algorithm. Since the sampling points lie primarily in regions with high values of f, the variance of the estimate of the integral decreases.

To implement this idea we choose a function $g(\mathbf{q})$ for which the integral is known analytically and which represents a good approximation of the function $f(\mathbf{q})$. We write

$$\int_0^1 f(\mathbf{q})\, \mathrm{d}^n q = \int_0^1 \mathrm{d}^n q\, g(\mathbf{q}) \frac{f(\mathbf{q})}{g(\mathbf{q})}. \tag{3.34}$$

Through the generation of random points $\mathbf{q}_\mu$ distributed according to $g(\mathbf{q})\, \mathrm{d}^n q$ we come to the estimation

$$\int f(\mathbf{q})\, \mathrm{d}^n q \approx \bar{f} = \frac{1}{M} \sum_{\mu=1}^{M} \frac{f(\mathbf{q}_\mu)}{g(\mathbf{q}_\mu)}, \tag{3.35}$$

whereupon we performed M "measurements". Note that the reweighed summands vary only little. But keep in mind that the integral of $g(\mathbf{q})$ must be known in order to extract g-distributed random numbers.

Now let us consider expectation values in lattice field theories,

$$\langle O \rangle \approx \frac{1}{Z} \int \mathscr{D}\mathbf{q} O(\mathbf{q}) \mathrm{e}^{-S(\mathbf{q})}, \qquad \mathscr{D}\mathbf{q} = \mathrm{d}q_1 \cdots \mathrm{d}q_n, \qquad Z = \int \mathscr{D}\mathbf{q} \mathrm{e}^{-S(\mathbf{q})}, \tag{3.36}$$

for which we would like to choose the Boltzmann distribution

$$P(\mathbf{q}) = \frac{1}{Z} \mathrm{e}^{-S(\mathbf{q})} \tag{3.37}$$

as function g. Then we only need to average over the in many cases slowly varying (in contrast to P) observables $O(\mathbf{q})$:

$$\langle O \rangle \approx \bar{O} = \frac{1}{M} \sum_{\mu=1}^{M} O(\mathbf{q}_\mu). \tag{3.38}$$

Here M denotes the number of generated points $\mathbf{q}_\mu$ in configuration space. Thus the Monte Carlo estimation $\bar{O}$ of the mean value of O represents an arithmetic average.

We are confronted with the following algorithmic problem: The n-dimensional integrals

$$\langle O \rangle = \int \mathscr{D}\mathbf{q} O(\mathbf{q}) P(\mathbf{q}), \qquad \int \mathscr{D}\mathbf{q} P(\mathbf{q}) = 1, \tag{3.39}$$

with fixed probability density P should be approximated for varying observables O. We therefore need algorithms which generate P-distributed points $\mathbf{q}_1, \mathbf{q}_2, \ldots$ in the n-dimensional domain of integration. The following *Metropolis algorithm* [7] generates a series of such points:

1. Start with $\mu = 0$ and an arbitrary initial point $\mathbf{q}_\mu$.
2. Choose a point $\mathbf{q}'$ at random and in addition a random number $r \in [0, 1]$.
3. If $P(\mathbf{q}')/P(\mathbf{q}_\mu) > r$, set $\mathbf{q}_{\mu+1} = \mathbf{q}'$. Otherwise set $\mathbf{q}_{\mu+1} = \mathbf{q}_\mu$.
4. Increase μ by one and repeat steps 2, 3 and 4.

The resulting points $\{\mathbf{q}_\mu\}$ are distributed according to $P(\mathbf{q})$ and

$$\bar{O} = \frac{1}{M} \sum_{\mu=1}^{M} O(\mathbf{q}_\mu) \tag{3.40}$$

represents an estimate of $\langle O \rangle$ which converges to $\langle O \rangle$ for large values of M. In lattice field theories the points $\mathbf{q}_\mu$ are called *lattice configurations*.

The program `samplingarea.c` on p. 45 estimates the definite integral

$$I = 128 \cdot \frac{\int_0^1 \mathrm{d}x\, \mathrm{d}y\, \mathrm{d}z\, x^3 y^2 z \exp(-x^2 - y^2 - z^2)}{\int_0^1 \mathrm{d}x\, \mathrm{d}y\, \mathrm{d}z \exp(-x^2 - y^2 - z^2)} = 128 \cdot \left\langle x^3 y^2 z \right\rangle \approx 2.4313142$$

Table 3.5 Calculation of the three-dimensional integral via the Metropolis algorithm

M	5 000	1 0000	15 000	20 000	25 000	30 000	35 000
$\bar{I}$	2.33113	2.31536	2.33432	2.38934	2.3568	2.34805	2.35253
E	0.10018	0.11595	0.09699	0.04197	0.07449	0.08327	0.07878
M	40 000	45 000	50 000	55 000	60 000	65 000	70 000
$\bar{I}$	2.34528	2.34193	2.35193	2.35089	2.35659	2.35952	2.36130
E	0.08603	0.08939	0.07938	0.08043	0.07473	0.07179	0.07001
M	75 000	80 000	85 000	90 000	95 000	100 000	1 000 000
$\bar{I}$	2.36969	2.37196	2.36937	2.38248	2.38742	2.38448	2.43686
E	0.06162	0.05935	0.06194	0.04884	0.04390	0.04683	−0.00555

via the Metropolis algorithm with the exponential function, normalized by the integral in the denominator, as distribution P. We observe a slow convergence to the exact result with errors of the order $1/\sqrt{M}$. Table 3.5 contains the computed estimates for various M. The last entry results from 10^6 Monte Carlo iterations and has an error of 0.00555.

3.4 Some Basic Facts in Probability Theory

Knowing the basic facts about probability theory is of course useful in any statistical approach to physical problems. Thus it is worth summarizing the main concepts of probability and statistics. The axiomatic approach to this theory was developed by KOLMOGOROW in the 1930's. See [12] for an introduction to probability, and [13] for an introduction to measure theory.

The set of elementary events, the *sample space*, is denoted by Ω. A general event is a subset of Ω and the set of events is the *event space* Σ. The measure $P : \Sigma \to [0, 1]$ is a *probability measure* in case $P(\Omega) = 1$. The triple (Ω, Σ, P) consisting of a sample space, an event space and a probability measure form a probability space.

The probability measure should fulfill the following axioms:

- The probability $P(A)$ of an event $A \subset \Omega$ is in $[0, 1]$.
- The probability of some elementary event occurring in Ω is $P(\Omega) = 1$.
- The probability of the union of countably many disjoint events is equal to the sum of the probabilities of the individual events (σ additivity):

$$P(A_1 \cup A_2 \cup \cdots) = \sum P(A_i) \quad \text{if } A_i \cap A_j = \emptyset.$$

From Kolmogorov axioms one concludes

$$P(\Omega \backslash A) = 1 - P(A) \quad \text{and} \quad P(A_1 \cup A_2) = P(A_1) + P(A_2) - P(A_1 \cap A_2).$$

The incidental result $X : \Omega \to \mathbb{R}$ is called *random variable* with expectation value (mean value)

$$\langle X \rangle = \sum_{w \in \Omega} X(w) P[w] = \sum_{x \in X(\Omega)} x \sum_{\substack{w \in \Omega \\ X(w)=x}} P[w] = \sum_{x \in X(\Omega)} x P_X(x), \quad (3.41)$$

wherein $P[w]$ denotes the probability for the event w and

$$P_X(x) = P\big(X^{-1}(x)\big) \quad (3.42)$$

represents the probability for the random variable X to assume the value x. The mean value of repeated measurements of X is simply $\langle X \rangle$ and the expression

$$P_X(\Delta) = \sum_{x \in \Delta} P_X(x). \quad (3.43)$$

is interpreted as probability for finding an event for which X has a value in Δ. If X is a real-valued random variable, then P_X is the probability density and we have

$$P_X(\Delta) = \int_\Delta P_X(x)\,\mathrm{d}x. \quad (3.44)$$

For a continuous function f the expectation value of the random variable $f(X)$ is

$$\big\langle f(X) \big\rangle = \sum_{w \in \Omega} f\big(X(w)\big) = \sum_{x \in X(\Omega)} f(x) P_X(x). \quad (3.45)$$

The average value of any linear combination of random variables is the corresponding linear combination of individual averages,

$$\langle X \rangle = \langle X_1 \rangle + \cdots + \langle X_N \rangle. \quad (3.46)$$

The random variables are called *independent* if the probability of the events w with $X_i(w) = x_i$ factorizes for arbitrary $x_1, \ldots, x_N$:

$$P\big(\{w | X_1(w) = x_1, \ldots, X_N(x) = x_N\}\big) = P_{X_1}(x_1) \cdots P_{X_N}(x_N). \quad (3.47)$$

The generating function of independent random variables factorizes,

$$\begin{aligned} \big\langle \mathrm{e}^{\mathrm{i}(t_1 X_1 + \cdots + t_N X_N)} \big\rangle &= \sum_w \mathrm{e}^{\mathrm{i}(t_1 x_1 + \cdots + t_N x_N)} P\big(\{w | X_1(w) = x_1, \ldots, X_N(x) = x_N\}\big) \\ &= \sum_{x_1, \ldots, x_N} \prod_{k=1}^{N} \mathrm{e}^{\mathrm{i}t_k x_k} P_{X_k}(x_k) = \big\langle \mathrm{e}^{\mathrm{i}t_1 X_1} \big\rangle \cdots \big\langle \mathrm{e}^{\mathrm{i}t_N X_N} \big\rangle. \end{aligned} \quad (3.48)$$

For $t = t_1 = \cdots = t_N$ we obtain the following useful relation for the generating function of the connected correlations of independent random variables,

$$\log\big\langle \mathrm{e}^{\mathrm{i}t(X_1 + \cdots + X_N)} \big\rangle = \sum_{i=1}^{N} \log\big\langle \mathrm{e}^{\mathrm{i}t X_i} \big\rangle. \quad (3.49)$$

Differentiating twice with respect to t at $t = 0$ we conclude that the variance of the sum of independent random variables X_i is equal the sum of the variance of X_i,

$$\mathrm{Var}[X] = \sum_{i=1}^{N} \mathrm{Var}[X_i], \qquad \mathrm{Var}[X] \equiv \left\langle X^2 \right\rangle - \langle X \rangle^2 = \left\langle (\Delta X)^2 \right\rangle, \tag{3.50}$$

where ΔX denotes the random variable $X - \langle X \rangle$.

Theorem 3.2 (Markov's theorem) *Let X be a random variable which assumes non-negative values only. Then for all $t \in \mathbb{R}^+$*

$$P[X \geq t] \leq \frac{1}{t} \langle X \rangle. \tag{3.51}$$

The proof of Markov's theorem is quite simple:

$$\begin{aligned} \langle X \rangle &= \sum_{x \geq 0} x \cdot P_X(x) \geq \sum_{x \geq t} x \cdot P_X(x) \geq \sum_{x \geq t} t \cdot P_X(x) \\ &= t \sum_{x \geq t} P_X(x) = t \cdot P[X \geq t]. \end{aligned}$$

This result leads to the useful Chebyshev inequality for the average deviation of a real-valued random number from its average value.

Theorem 3.3 (Chebyshev's theorem) *Let X be a random variable and $t \in \mathbb{R}^+$. Then*

$$P\big[|\Delta X| \geq t\big] \leq \frac{1}{t^2} \mathrm{Var}[X]. \tag{3.52}$$

Proof

$$P\big[|\Delta X| \geq t\big] = P\big[(\Delta X)^2 \geq t^2\big] \overset{(3.51)}{\leq} \frac{\mathrm{Var}[X]}{t^2}.$$

Another very important theorem (we already mentioned it) is the □

Theorem 3.4 (Law of large numbers) *Given a random variable X and arbitrary, but fixed numbers $\varepsilon, \delta > 0$. Define*

$$K := \frac{\mathrm{Var}[X]}{\varepsilon \cdot \delta^2} = const., \tag{3.53}$$

let $X_1, \ldots, X_N$ be independent random variables with the same distribution as X and define $Z := (X_1 + \cdots + X_N)/N$. Then the following bound holds:

$$P\big[|\Delta Z| \geq \delta\big] \leq \varepsilon. \tag{3.54}$$

Proof Linearity of expectation values and (3.50) imply

$$\langle Z \rangle = \frac{1}{N} \sum \langle X_i \rangle = \langle X \rangle \quad \text{and} \quad \mathrm{Var}[Z] = \frac{1}{N^2} \sum \mathrm{Var}[X_i] = \frac{\mathrm{Var}[X]}{N}. \tag{3.55}$$

The latter inequality is interesting in its own. It is the well known *square root law* for the relative fluctuations

$$\frac{\sqrt{\mathrm{Var}[Z]}}{\langle Z \rangle} \leq \frac{1}{N} \frac{\sqrt{\mathrm{Var}[X]}}{\langle X \rangle} \tag{3.56}$$

and it means that the scale of the relative fluctuations of Z is of order $O(N^{-1/2})$. It implies that for a large number of random variables X_i (trials) we may neglect the fluctuations. In other words, the accuracy of a statistics tends to improve with the number of trials.

Combining Chebyshev's inequality with the result (3.55) leads to the bound

$$P\big[|\Delta Z| \geq \delta\big] \leq \frac{\mathrm{Var}[Z]}{\delta^2} = \frac{\mathrm{Var}[X]}{N \cdot \delta^2} \leq \varepsilon. \tag{3.57}$$

Now let $X_1, \ldots, X_N$ be a series of independent and identically distributed random variables with vanishing mean and covariance matrix $\langle X_i X_j \rangle = \delta_{ij}\sigma^2$. Furthermore we define the random variable

$$Y_N := \frac{1}{\sqrt{N}} \sum_{i=1}^{N} X_i. \tag{3.58}$$

The generating function for Y_N is given by

$$\begin{aligned}\left\langle \mathrm{e}^{\mathrm{i}tY_N} \right\rangle &= \prod_{i=1}^{N} \left\langle \exp\left(\mathrm{i}\frac{t}{\sqrt{N}} X_i\right)\right\rangle \\ &= \left\langle 1 + \mathrm{i}\frac{t}{\sqrt{N}} X_1 - \frac{1}{2}\frac{t^2}{N} X_1^2 + \frac{1}{O(N^{3/2})}\right\rangle^N \overset{N\to\infty}{\longrightarrow} \exp\left(-\frac{1}{2}t^2\sigma^2\right).\end{aligned}$$

On the other hand the generating function of a Gaussian random variable with mean m and variance σ^2 is given by

$$\frac{1}{\sqrt{2\pi}\sigma} \int \mathrm{d}x\, \mathrm{e}^{-(x-m)^2/2\sigma^2} \mathrm{e}^{\mathrm{i}tx} = \exp\left(\mathrm{i}mt - \frac{1}{2}t^2\sigma^2\right).$$

It follows at once that for large N the random variables Y_N are Gaussian with mean 0 and variance σ^2. □

3.5 Programs for Chap. 3

The C-programs

- `1dintegral.c`
- `hitandmissarea.c`
- `gaussdistr.c`
- `samplingarea.c`

were mentioned and used in Chap. 3. They are listed and explained in this section. The first program `1dintegral.c` in Listing 3.1 calculates the definite integral of a function on the unit interval with Simpson's rule for lattice constants

$$\varepsilon \in \left\{10^{-n} | n = 1, 2, \ldots, 6\right\}$$

and with the Monte Carlo method. The function is defined in line 10 of the listing.

The C-program in Listing 3.2 computes the area below a given function with the help of the hit-or-miss Monte Carlo method in a rather simple way. The function is defined in line 9 of the listing.

Listing 3.1 1-dimensional integrals

```
/*program 1dintegral.c
/*numerical integration of f(x) from alpha to beta
/*with Simpson algorithm and Monte Carlo method*/
#include <stdio.h>
#include <stdlib.h>
#include <math.h>
#include <time.h>

/*function to be integrated*/
double f(double x)
{return exp(x);}
/*random number between 0 and 1*/
double randa(void)
{return (double)rand()/((double)RAND_MAX);}
int main(void)
{
   double eps,sum,int_simpson,int_monte_carlo,x0,x1,x2;
   double alpha=0,beta=1; /*limits of integration*/
   long i,N;
   srand ( time(NULL) );
     printf("log_10(N)\t int_simpson\t int_monte_carlo\n");
for (N=10;N<1000001;N*=10)
   {
     eps=(beta-alpha)/N;
/*simpson rule*/
     sum=0;
     for (i=0;i<N-1;i=i+2)
       {x0=alpha+eps*i;x1=x0+eps;x2=x1+eps;
         sum=sum+(f(x0)+4.0*f(x1)+f(x2))/3.0;}
     int_simpson=sum*eps;
/*Monte Carlo method*/
     sum=0;
     for (i=0;i<N;i++)
       {x0=randa();sum=sum+f(x0);}
     int_monte_carlo=eps*sum;
     printf("%8.0f \t%f \t%f \n",
     log10(N),int_simpson,int_monte_carlo);
     }
  return 0;
}
```

The program in Listing 3.3 computes the distribution of the sum s of 10, 50 and 100 random numbers $r \in [0, 1]$. Each time we perform one million trials. The values of the stochastic variable s form a histogram, which is saved in the array *mean[100]*. Furthermore we rescale the random variable s with $2m$ such that the maximum of the distribution lies at $s/(2m) = 1/2$.

The program in Listing 3.4 applies the technique of *importance sampling*. There we only consider points associated with *large* integrands. Thus the variance of a single estimate is reduced. The program `samplingarea.c` computes the proper integral

Listing 3.2 hit_or_miss

```
/*program hitormissarea.c
/*integration of f(x) with hit-or miss method*/
#include <stdio.h>
#include <stdlib.h>
#include <math.h>
#include <time.h>
#define M 10000001 /*number of attempts*/
double f(double x) /*function to be integrated*/
{return x*x*exp(x)/(1-x+x*exp(x));}
double g(double x) /*function for improved method*/
{return x*x*exp(x)/(1-x+x*exp(x))-x*x;}
int main(void)
{
double sum1,sum2,I1,I2,sig1,sig2,x,y;
   long n,m;
   srand48(time(NULL));
   printf("attemps\t\t p\t\t integ-p\t sigma_1\t");
   printf("p_imp\t\t integ-p_imp\t sigma_2\n");
   for (m=10;m<M;m*=10)
     {sum1=0;sum2=0;
       for (n=1;n<m+1;n++)
         {x=drand48();y=drand48();
           if (y<f(x)) sum1=sum1+1;
           if (y<g(x)) sum2=sum2+1;
         };
       I1=sum1/m;I2=sum2/m;
       sig1=sqrt(I1*(1-I1)/m);sig2=sqrt(I2*(1-I2)/m);
       n=(int)log10(m);
       printf("%8ld\t%8.5f\t%8.5f\t%8.5f\t%8.5f\t%8.5f\
              t%8.5f\n",
       m,I1,0.376370-I1,sig1,1/3.0+I2,0.043037-I2,sig2);
     };
   return 0;
}
```

$$128 \cdot \frac{\int_0^1 \mathrm{d}x\,\mathrm{d}y\,\mathrm{d}z\,x^3y^2z\exp(-x^2-y^2-z^2)}{\int_0^1 \mathrm{d}x\,\mathrm{d}y\,\mathrm{d}z\exp(-x^2-y^2-z^2)} \approx 2.4313142$$

with the help of the Metropolis algorithm.

3.6 Problems

3.1 (Numerical calculation of integrals) Calculate the exponential integral

$$\int_0^1 \mathrm{d}x\mathrm{e}^x$$

with the help of Simpson's rule. Compare your result with the exact one.

Listing 3.3 Gauss distribution

```
/*Programm gaussdistr.c
/*sum of random numbers from the interval [0,1]*/
#include <stdio.h>
#include <stdlib.h>
#include <math.h>
#include <time.h>
#define PI 3.1415926
#define numbersadded 50 /*number of added random numbers*/
#define M 1000000 /*number of MC iterations*/
int main(void)
{ double sum,aux=6.0*numbersadded,mean[100];
   double dM=100.0/(double)M; /*scaling factor 100*/
   long i,j,sumi;
   /*initial values*/
   for (i=0;i<numbersadded;i++) mean[i]=0;
     sum=0;srand48(time(NULL));
   /*repeat experiment M times*/
   for (i=0;i<M;i++)
     {sum=0;
       /*sum of random numbers in each experiment*/
       for (j=0;j<numbersadded;j++)
                 sum=sum+drand48();
       /*100 bins for histogram*/
       sumi=(int)(0.5+100*sum/numbersadded);
       ++mean[sumi];
     };
   printf("maximum at bin = 49.5\n");
   printf("bin\t estimate\t Gaussian dist\n");
   for (i=30;i<71;i=i+2)
           {sum=i-50;
           printf("%li\t%8.5f\t%8.5f\n",
           i,mean[i]*dM,sqrt(aux/PI)*exp(-aux*sum*sum*dM));
           };
   return 0;
}
```

3.2 (Error of Simpson formula) For the function

$$f(x) = e^x \cos(x) \quad \text{in } [0, \pi]$$

compute the minimum number of intervals such that the error of the composite Simpson formula is less than 10^{-4}.

3.3 (Volume of n-dimensional unit ball) Write a program to find the volume of an n-dimensional ball using the Monte Carlo technique. The volume will be the number of points with the sum,

$$\sum_{j=1}^{n} x_j^2 < 1$$

Listing 3.4 sampling area

```
/*pogram samplingarea.c
/*three-dimensional integral with importance sampling.*/
#include <stdio.h>
#include <stdlib.h>
#include <math.h>
#include <time.h>
#define M 100000 /*number of measured MC-iterationen*/
#define MA 1000 /*every MA'th configuration is measured*/
/*distribution*/
double P(double *x)
{return exp(-x[0]*x[0]-x[1]*x[1]-x[2]*x[2]);}
/*function to be integrated*/
double f(double *x)
{return 128.0*x[0]*x[0]*x[0]*x[1]*x[1]*x[2];}
int main(void)
{ double integral,sum,x[3],y[3];
   long i,j;
   srand48(time(NULL));
   sum=0; x[0]=drand48();x[1]=drand48();x[2]=drand48();
   for (i=1;i<M+1;i++)
     { for(j=0;j<MA;j++)
         { y[0]=drand48(); y[1]=drand48(); y[2]=drand48();
           if (P(y)>P(x)*drand48() )
             { x[0]=y[0];x[1]=y[1];x[2]=y[2];};
         };
       sum=sum+f(x);integral=sum/i;
       if (i%5000==0)
       printf("i = %ld\t integral = %.5f\t error = %8.5f\n",
       i,integral,2.4313142-integral);
     };
   return 0;
}
```

divided by the total number of points in the region from which the x_i are selected. A convenient region is the n-cube defined by

$$-1 < x_j < 1, \quad j = 1, \ldots, n$$

having volume 2^n.

3.4 (Particle diffusion) A particle starts at the origin in two dimensions and after each time-intervals jumps with equal probability $1/4$ to one of the neighboring points. After the first jump the particle is at one of the points $(\pm 1, 0)$ or $(0, \pm 1)$. Write a program to jump a large number of times, and print out the distance r of the particle from its starting point after all jumps are completed. Theory predicts that the expected value of r is $K \times \sqrt{n}$ after n jumps. Start the program sufficiently many times so that you get an'experimental' value for the constant K.

References

1. R. Bellman, *Dynamic Programming* (Princeton University Press, Princeton, 1957)
2. F.B. Hildebrand, *Introduction to Numerical Analysis* (McGraw-Hill, New York, 1956)
3. W.H. Press, S.A. Teukolsky, W.T. Vetterling, B.P. Flannery, *Numerical Recipes: The Art of Scientific Computing*, 3rd edn. (Cambridge University Press, Cambridge, 2007)
4. A. Quarteroni, R. Sacco, F. Saleri, *Numerical Mathematics*. Text in Applied Mathematics, vol. 37 (Springer, New York, 2006)
5. A. Quarteroni, F. Saleri, *Scientific Computing with Matlab and Octave* (Springer, Berlin, 2006)
6. R.H. Landau, M.J. Páez, C.C. Bordeianu, *Computational Physics* (Wiley-VCH, New York, 2007)
7. N. Metropolis, S. Ulam, The Monte Carlo method. J. Am. Stat. Assoc. **44**, 335 (1949)
8. S. Weinzierl, Introduction to Monte Carlo methods. Preprint arXiv:hep-ph/0006269v1
9. S.H. Paskov, J.F. Traub, Faster evaluation of financial derivatives. J. Portf. Manag. **22**, 113 (1995)
10. F.Y. Kuo, I.H. Sloan, Lifting the curse of dimensionality. Not. Am. Math. Soc. **52**, 1320 (2005)
11. E. Novak, H. Wozniakovski, in *When Are Integration and Discrepancy Tractable?* ed. by R.A. DeVore, A. Iserles, E. Süli. Found. of Comp. Math. (Cambridge University Press, Cambridge, 2001)
12. J. Pitman, *Probability*. Springer Texts in Statistics (Springer, Berlin, 1993)
13. P.R. Halmos, *Measure Theory*. Graduate Texts in Mathematics (Springer, Berlin, 1976)

Chapter 4
Monte Carlo Simulations in Quantum Mechanics

This chapter provides an introduction to particular Markov processes which obey the detailed balance condition. We explain the Metropolis algorithm—still the workhorse in many simulations—the heat bath algorithm and the hybrid Monte Carlo algorithm. We will apply these algorithms to simulate the anharmonic oscillator. Later in this book we shall use these algorithms to analyze nonperturbative aspects of spin-systems and quantum field theories.

4.1 Markov Chains

We begin our discussion with a particular realization of the method of "importance sampling" as introduced in Chap. 3. For simplicity we first consider a system with a discrete set of configurations $\{\omega\}$. With an appropriate Markov chain we generate configurations distributed according to a prescribed probability distribution $P(\omega)$. Later on P will be an equilibrium distribution of a statistical system. A Markov chain shows one important property: it is a discrete-time process for which the future behavior, given the past and the present, only depends on the present and not on the past. Hence the system has a short-term memory. A Markov chain is characterized by transition probabilities $W(\omega, \omega') = W(\omega \to \omega')$, which are interpreted as probabilities for a given configuration ω to make a transition to ω' in one time-step. In passing we note that a Markov process is a continuous-time version of a Markov chain.

Stochastic Matrices and Stochastic Vectors We consider $W(\omega, \omega')$ as matrix elements of a *'stochastic matrix' W*. If the number of configurations is not finite, then W is a linear operator. Clearly, the matrix elements of a *stochastic matrix* must be positive and normalized:

$$W\big(\omega, \omega'\big) \geq 0 \quad \text{and} \quad \sum_{\omega'} W\big(\omega, \omega'\big) = 1. \tag{4.1}$$

A. Wipf, *Statistical Approach to Quantum Field Theory*, Lecture Notes in Physics 864,
DOI 10.1007/978-3-642-33105-3_4,

The probability for jumping from ω to ω' during two time-steps is given by the sum of probabilities of all realizations of this two-step process. This means that the probability for the transition $\omega \to \omega'$ after two time-steps is given by

$$W^{(2)}(\omega, \omega') = \sum_{\omega_1} W(\omega, \omega_1) W(\omega_1, \omega'), \tag{4.2}$$

where one sums over all intermediate configurations which could have been visited after one time-step. Similarly, we obtain the probabilities

$$W^{(n)}(\omega, \omega') = \sum_{\omega_1 \cdots \omega_{n-1}} W(\omega, \omega_1) W(\omega_1, \omega_2) \cdots W(\omega_{n-1}, \omega') \tag{4.3}$$

for the transitions from ω to ω' after n steps and conclude that the long-time behavior of the chain is determined by high powers of the stochastic matrix.

A *stochastic vector* $\mathbf{p}$ has non-negative entries p_ω which add up to 1:

$$\sum_{\omega} p_\omega = 1. \tag{4.4}$$

The entry p_ω represents the probability of finding the system in configurations ω. In statistical mechanics $\mathbf{p}$ is identified with a (mixed) state. In order not to confuse ω with p_ω we call ω a configuration and not a state as it is called in textbooks on Markov chains. A stochastic matrix transforms stochastic vectors into stochastic vectors:

$$\sum_{\omega'} (\mathbf{p}W)(\omega') = \sum_{\omega\omega'} p_\omega W(\omega, \omega') = \sum_{\omega} p_\omega = 1.$$

Let us consider the following stochastic matrix of a system with two configurations:

$$W = \begin{pmatrix} a & 1-a \\ 0 & 1 \end{pmatrix}, \quad 0 \le a \le 1. \tag{4.5}$$

Its eigenvalues are $\{1, a\}$ and its powers converge exponentially fast to a stochastic matrix with identical rows,

$$W^n = \begin{pmatrix} a^n & 1-a^n \\ 0 & 1 \end{pmatrix} \overset{n\to\infty}{\to} \begin{pmatrix} 0 & 1 \\ 0 & 1 \end{pmatrix}.$$

Later we will prove that for most stochastic matrices the powers W^n converge to a stochastic matrix with *identical rows*. A counterexample is given by

$$W = \begin{pmatrix} a & \frac{1}{2}(1-a) & \frac{1}{2}(1-a) \\ 0 & 0 & 1 \\ 0 & 1 & 0 \end{pmatrix} \quad \text{with } 0 \le a < 1. \tag{4.6}$$

The even powers are

$$W^n = \begin{pmatrix} a^n & \frac{1}{2}(1-a^n) & \frac{1}{2}(1-a^n) \\ 0 & 1 & 0 \\ 0 & 0 & 1 \end{pmatrix} \to \begin{pmatrix} 0 & \frac{1}{2} & \frac{1}{2} \\ 0 & 1 & 0 \\ 0 & 0 & 1 \end{pmatrix}, \quad n \text{ even},$$

and the odd powers read

$$W^n = \begin{pmatrix} a^n & \frac{1}{2}(1-a^n) & \frac{1}{2}(1-a^n) \\ 0 & 0 & 1 \\ 0 & 1 & 0 \end{pmatrix} \to \begin{pmatrix} 0 & \frac{1}{2} & \frac{1}{2} \\ 0 & 0 & 1 \\ 0 & 1 & 0 \end{pmatrix}, \quad n \text{ odd}.$$

Any stochastic vector $\mathbf{p}$ is mapped into

$$\mathbf{p}W^{2n} \overset{n\to\infty}{\to} \left(0, p_2 + \frac{p_1}{2}, p_3 + \frac{p_1}{2}\right),$$
$$\mathbf{p}W^{2n+1} \overset{n\to\infty}{\to} \left(0, p_3 + \frac{p_1}{2}, p_2 + \frac{p_1}{2}\right).$$

For a generic $\mathbf{p}$ the series $\mathbf{p}W^n$ approaches exponentially fast a periodic orbit with period 2. This lack of convergence to a stochastic vector is only possible since every column of W contains at least one zero. Note that W has the fixed point $(0, 0.5, 0.5)$ and that for exceptional stochastic vectors with $p_2 = p_3$ the series $W^n\mathbf{p}$ converges to this fixed point.

4.1.1 Fixed Points of Markov Chains

Every stochastic matrix has the eigenvalue 1. The corresponding right-eigenvector is given by $\sim(1, 1, \ldots, 1)^T$. But since W acts from the right we are interested in the left-eigenvector with eigenvalue 1. We follow [1] and consider the series

$$\mathbf{p}_n = \frac{1}{n}\sum_{j=0}^{n-1} \mathbf{p}\, W^j. \tag{4.7}$$

Since stochastic vectors form a compact set, the series has a convergent subsequence

$$\frac{1}{n_k}\sum_{0}^{n_k-1} \mathbf{p}\, W^j \to \mathbf{P}.$$

We multiply this subsequence by W from the right,

$$\frac{1}{n_k}\sum_{1}^{n_k} \mathbf{p}\, W^j \to \mathbf{P}W.$$

In the difference of the last two formulas only two terms in the left-hand sides remain and we obtain in the limit $n_k \to \infty$

$$\frac{1}{n_k}\left(\mathbf{p} - \mathbf{p}\, W^{n_k}\right) \to \mathbf{P} - \mathbf{P}W.$$

This leads to the eigenvalue equation

$$\mathbf{P}W = \mathbf{P}, \tag{4.8}$$

which means that every stochastic matrix W has at least one *fixed point* $\mathbf{P}$, i.e. a left-eigenvector with eigenvalue 1.

We now assume that W has at least one column with minimal element greater than a positive number δ. This means that *all configurations* can jump with non-vanishing probability to any given configuration. Stochastic matrices with this property are called *attractive* and for an attractive matrix the series $W^n\mathbf{p}$ converges for any stochastic vector $\mathbf{p}$. Note that W in (4.6) is not attractive and this explains why the associated Markov chain does not converge. For the proof of convergence we first note that for two real numbers p and p' we have

$$\big|p - p'\big| = p + p' - 2\min\big(p, p'\big),$$

and this relation implies

$$\big\|\mathbf{p} - \mathbf{p}'\big\| = 2 - 2\sum_{\omega} \min\big(p_\omega, p'_\omega\big) \tag{4.9}$$

for two stochastic vectors. We used the ℓ_1-norm $\|\mathbf{p}\| = \sum_\omega |p_\omega|$.

Next we wish to prove that an attractive W acts on vectors $\boldsymbol{\Delta} = (\Delta_1, \Delta_2, \ldots)$ with

$$\|\boldsymbol{\Delta}\| \equiv \sum |\Delta_\omega| = 2 \quad \text{and} \quad \sum \Delta_\omega = 0 \tag{4.10}$$

in a contractive way. Let us assign the stochastic vector $\mathbf{e}_\omega$ to each ω which represents the probability distribution for finding ω with probability one. This means that all entries of $\mathbf{e}_\omega$ vanish with the exception of entry ω, which is 1. The stochastic vectors $\{\mathbf{e}_\omega\}$ form an orthonormal basis. In a first step we prove that W is contractive for difference vectors $\mathbf{e}_\omega - \mathbf{e}_{\omega'}$. Thus we apply the identity (4.9) to the stochastic vectors $\mathbf{e}_\omega W$ and $\mathbf{e}_{\omega'} W$, i.e. to rows of W belonging to ω and ω'. In case of an attractive W we find for $\omega \neq \omega'$

$$\begin{aligned}\|\mathbf{e}_\omega W - \mathbf{e}_{\omega'} W\| &= 2 - 2\sum_{\omega''} \min\big\{W\big(\omega, \omega''\big), W\big(\omega', \omega''\big)\big\} \\ &\leq 2 - 2\delta = (1-\delta)\underbrace{\|\mathbf{e}_\omega - \mathbf{e}_{\omega'}\|}_{=2} \quad \text{with } 0 < \delta < 1. \end{aligned} \tag{4.11}$$

This already proves that W is contractive on difference vectors $\mathbf{e}_\omega - \mathbf{e}_{\omega'}$. We used the inequality

$$\min_{\omega''}\big\{W\big(\omega, \omega''\big) W\big(\omega', \omega''\big)\big\} \geq \min\big\{W\big(\omega, \omega^*\big)(W\big(\omega', \omega^*\big)\big\} \geq \delta,$$

where ω^* belongs to the particular column of W with elements greater than or equal to δ. Now we shall prove the contraction property for all vectors $\boldsymbol{\Delta}$ in (4.10). Adding and subtracting the relations

$$\|\boldsymbol{\Delta}\| = \sum_{\omega:\Delta_\omega \geq 0} \Delta_\omega - \sum_{\omega:\Delta_\omega < 0} \Delta_\omega = 2 \quad \text{and} \quad \sum_{\omega:\Delta_\omega \geq 0} \Delta_\omega + \sum_{\omega:\Delta_\omega < 0} \Delta_\omega = 0,$$

we extract the values of the individual sums,

$$\sum_{\Delta_\omega \geq 0} \Delta_\omega = 1 \quad \text{and} \quad \sum_{\Delta_\omega < 0} \Delta_\omega = -1. \tag{4.12}$$

To keep the notation simple we denote in the following formulas the non-negative elements of $\boldsymbol{\Delta}$ by Δ_ω and the negative elements by $\Delta_{\omega'}$. Note that the index sets $\{\omega\}$ and $\{\omega'\}$ are disjunct. With (4.12) we obtain

$$\|\boldsymbol{\Delta}\| = 2 = -2\sum \Delta_\omega \sum \Delta_{\omega'} = -\sum \Delta_\omega \Delta_{\omega'} \underbrace{\|\mathbf{e}_\omega - \mathbf{e}_{\omega'}\|}_{=2}, \tag{4.13}$$

where in the last step we took into account $\omega \neq \omega'$. Now we use the simple relations

$$\sum \Delta_\omega \mathbf{e}_\omega = -\sum \Delta_{\omega'} \sum \Delta_\omega \mathbf{e}_\omega,$$
$$\sum \Delta_{\omega'} \mathbf{e}_{\omega'} = +\sum \Delta_\omega \sum \Delta_{\omega'} \mathbf{e}_{\omega'},$$

which follow from (4.12), to bound the norm of $\boldsymbol{\Delta} W$:

$$\begin{aligned} \|\boldsymbol{\Delta} W\| &= \Big\| \sum \Delta_\omega \mathbf{e}_\omega W + \sum \Delta_{\omega'} \mathbf{e}_{\omega'} W \Big\| = \Big\| -\sum \Delta_{\omega'} \Delta_\omega (\mathbf{e}_\omega - \mathbf{e}_{\omega'}) W \Big\| \\ &\leq -\sum \Delta_\omega \Delta_{\omega'} \big\| (\mathbf{e}_\omega - \mathbf{e}_{\omega'}) W \big\| \leq -\sum \Delta_\omega \Delta_{\omega'} \|\mathbf{e}_\omega - \mathbf{e}_{\omega'}\| (1-\delta), \end{aligned} \tag{4.14}$$

where in the last step we applied the inequality (4.11). A comparison with formula (4.13) proves the desired inequality

$$\|\boldsymbol{\Delta} W\| \leq (1-\delta)\|\boldsymbol{\Delta}\|, \tag{4.15}$$

for vectors which satisfy the conditions (4.10). Since this inequality is linear in $\boldsymbol{\Delta}$ it also holds for vectors which do not fulfill the condition $\|\boldsymbol{\Delta}\| = 2$. This shows that a stochastic matrix W is contractive on all vectors the elements of which add up to zero and especially on differences of any two stochastic vectors.

Iterating the inequality (4.15) yields

$$\big\| \boldsymbol{\Delta} W^n \big\| \leq (1-\delta)^n \|\boldsymbol{\Delta}\|. \tag{4.16}$$

Let us apply this estimate to the difference vector $\mathbf{p} - \mathbf{P}$, where $\mathbf{P}$ is a fixed point of the Markov chain and $\mathbf{p}$ is an arbitrary stochastic vector. The elements of $\mathbf{p} - \mathbf{P}$ add up to zero such that the bound in (4.16) applies,

$$\big\| (\mathbf{p} - \mathbf{P}) W^n \big\| = \big\| \mathbf{p}\, W^n - \mathbf{P} \big\| \overset{n\to\infty}{\to} 0,$$

or, equivalently

$$\mathbf{p}\, W^n \overset{n\to\infty}{\to} \mathbf{P}. \tag{4.17}$$

For the particular stochastic vectors $\mathbf{e}_\omega$ the left-hand side is the row of $\lim_{n\to\infty} W^n = W^{\mathrm{eq}}$ belonging to ω and we conclude that W^{eq} has identical rows,

$$W^{\mathrm{eq}}(\omega, \omega') = \lim_{n\to\infty} W^n(\omega, \omega') = P_{\omega'}. \tag{4.18}$$

To summarize, for an attractive W the situation is similar to that for the stochastic matrix in (4.5): the series $W^n \mathbf{p}$ converges to a fixed point and all elements in one single column of $W^{\mathrm{eq}} = \lim_{n\to\infty} W^n$ are equal.

It is easy to show that for an attractive W the fixed point $\mathbf{P}$ is *unique*. Indeed, if there would exist a second fixed point $\mathbf{P}'$, then

$$P'_{\omega'} = \sum_{\omega} P'_{\omega} W(\omega, \omega') = \lim_{n\to\infty} \sum_{\omega} P'_{\omega} W^n(\omega, \omega') \overset{(4.18)}{=} \sum_{\omega} P'_{\omega} P_{\omega'} = P_{\omega'}$$

would hold and this proves the uniqueness of the fixed point. With (4.18) we also conclude that for an attractive W the stochastic matrix W^{eq} is unique.

The generalization of these results to continuous systems with infinitely many configurations should be self-evident. As an example, consider a mechanical system, the pure states of which correspond to the points $\mathbf{q} \in \mathbb{R}^n$. We now have to deal with *probability densities* $p(\mathbf{q})$ instead of stochastic vectors. The sums over discrete indices ω turn into integrals over the continuous variables $\mathbf{q}$. The conditions (4.1) now read

$$W(\mathbf{q}, \mathbf{q}') \geq 0 \quad \text{and} \quad \int \mathscr{D}\mathbf{q}'\, W(\mathbf{q}, \mathbf{q}') = 1, \tag{4.19}$$

and the fixed point condition (4.8) takes the form

$$P(\mathbf{q}') = \int \mathscr{D}\mathbf{q}\, P(\mathbf{q})\, W(\mathbf{q}, \mathbf{q}'). \tag{4.20}$$

In statistical physics and quantum field theory at finite temperature the fixed point $P(\mathbf{q})$ corresponds to the canonical ensemble and we look out for Markov chains with this equilibrium distribution as fixed point.

4.2 Detailed Balance

The *condition of detailed balance* is a simple and physically well-founded constraint on a Markov chain which implies the fixed point equation (4.8). Detailed balance means a balance between any two configurations: the equilibrium probability for ω, multiplied by the jump probability from ω to ω' is equal to the equilibrium probability of ω' multiplied by the jump probability from ω' to ω,

$$P_{\omega} W(\omega, \omega') = P_{\omega'} W(\omega', \omega). \tag{4.21}$$

If in equilibrium the configuration ω is more likely occupied than the configuration ω', then the transition amplitude from ω to ω' is less than the amplitude for the reverse transition.

The condition of detailed balance guarantees that $\mathbf{P}$ is a fixed point of the chain,

$$\sum_{\omega} P_{\omega} W(\omega, \omega') = \sum_{\omega} P_{\omega'} W(\omega', \omega) = P_{\omega'}, \tag{4.22}$$

but it does not fix W uniquely. We may use the residual freedom to choose simple and efficient algorithms. In particular the fast *Metropolis* and *heat bath algorithms* are universally applicable and are often used. For statistical systems which can be dualized there exist the more efficient *cluster algorithms*, which do not suffer from the problem of the so-called "critical slowing down". These and other Monte Carlo algorithms will be introduced and applied in this book. More material can be found in the textbooks [2–4].

4.2.1 Acceptance Rate

The probabilities $W(\omega, \omega)$ of not jumping are not constrained by the condition of detailed balance. Thus we may change the probabilities $W(\omega, \omega')$ for the transition between different configurations without violating the sum rule (4.1) if we only readjust the unconstrained $W(\omega, \omega)$.

We factorize the transition probability into the product of a test probability and an acceptance rate

$$W\big(\omega, \omega'\big) = T\big(\omega, \omega'\big)\, A\big(\omega, \omega'\big), \tag{4.23}$$

where $T(\omega, \omega')$ is the probability of testing the new configuration ω' with given initial configuration ω. If ω' is tested then the quantity $0 \leq A(\omega, \omega') \leq 1$ corresponds to the probability that the transition to ω' is accepted. Note that the conditions

$$\frac{T(\omega, \omega')A(\omega, \omega')}{T(\omega', \omega)A(\omega', \omega)} = \frac{P_{\omega'}}{P_{\omega}} \tag{4.24}$$

do not fix the ratios of acceptance rates. A good Monte Carlo algorithm requires the best possible choice for these rates. For too small rates only a tiny fraction of jumps is accepted and the system is stuck in its initial configuration. We waste valuable computing time without passing through the configuration space. Thus, in many cases one sets the greater of two acceptance rates $A(\omega, \omega')$ and $A(\omega', \omega)$ equal to 1. The smaller rate is chosen such that the condition (4.24) is satisfied.

4.2.2 Metropolis Algorithm

In this simple algorithm the test probability is the same for all configurations ω' that can be *reached* from ω [5]. The test probability of the remaining configurations is set to zero. Thus, if N is the number of accessible configurations then

$$T\big(\omega, \omega'\big) = \begin{cases} 1/N, & \text{if } \omega \to \omega' \text{ is possible,} \\ 0, & \text{otherwise.} \end{cases} \tag{4.25}$$

We choose the acceptance rate

$$A\big(\omega, \omega'\big) = \min\left(\frac{P_{\omega'}T(\omega', \omega)}{P_{\omega}T(\omega, \omega')}, 1\right) \tag{4.26}$$

for which W in (4.23) fulfills the condition for detailed balance. In fact, the condition

$$P_{\omega}T\big(\omega, \omega'\big) \times \min\left(\frac{P_{\omega'}T(\omega', \omega)}{P_{\omega}T(\omega, \omega')}, 1\right) = P_{\omega'}T\big(\omega', \omega\big) \times \min\left(\frac{P_{\omega}T(\omega, \omega')}{P_{\omega'}T(\omega', \omega)}, 1\right)$$

is fulfilled both for $P_{\omega'}T(\omega', \omega)$ larger and smaller $P_{\omega}T(\omega, \omega')$. A generalization of this straightforward algorithm is due to Hastings [6]. As compared to the universally applicable Metropolis algorithm one may achieve a considerable improvement.

A good choice of the initial configuration ω may save computing time. For example, at high temperatures the degrees of freedom are uncorrelated and we choose the variables at random in contrast to low temperatures where they are strongly correlated.

We now discuss a particular implementation of the algorithm for the simulation of lattice systems, here a discrete quantum mechanical system over n lattice points. We choose an initial configuration $\mathbf{q} = (q_1, \ldots, q_n)$. The first lattice-variable q_1 is altered or remains unchanged according to the following rules:

1. Suggest a provisional change of q_1 in a randomly chosen q_1'.
2. If the action decreases, that is, $\Delta S < 0$, then permanently replace q_1 by q_1'.
3. If the action increases, choose an uniformly distributed random number $r \in [0, 1]$. The suggestion q_1' is accepted if $\exp(-\Delta S) > r$. Otherwise the lattice-variable q_1 remains unaltered.
4. Proceed with the variables $q_2, q_3, \ldots$ in the same way till all variables have been tested.
5. If the last lattice point is reached, a "sweep through the lattice" or a *Monte Carlo iteration* is finished and one starts again with the first lattice point.

A realistic simulation includes thousands of sweeps through the lattice in order to reduce statistical errors. Depending on the initial configuration it may take some sweeps to generate configurations distributed according to the equilibrium distribution. In order to check whether the Markov chain is close to "equilibrium", one measures selected expectation values as function of the Monte Carlo time with a MC-iteration as unit of time. After equilibrium is reached only statistical fluctuations remain and we measure expectation values according to (3.38).

2-State System Consider a system with two energy eigenstates

$$H|\ell\rangle = E_\ell|\ell\rangle \quad (\ell = 1, 2) \quad \text{with } \Delta E = E_2 - E_1 > 0. \tag{4.27}$$

The transition $|2\rangle \to |1\rangle$ reduces the energy and therefore $W(2, 1) = 1$. On the other hand the excitation probability $W(1, 2)$ is equal to the Boltzmann factor

$$B_{21} = \mathrm{e}^{-\beta(E_2 - E_1)} < 1.$$

Since the elements in any row add up to 1, the stochastic matrix has the form

$$W = \begin{pmatrix} 1 - B_{21} & B_{21} \\ 1 & 0 \end{pmatrix}. \tag{4.28}$$

Its powers

$$W^n = \frac{1}{1 + B_{21}} \left\{ \begin{pmatrix} 1 & B_{21} \\ 1 & B_{21} \end{pmatrix} + (-B_{21})^n \begin{pmatrix} B_{21} & -B_{21} \\ -1 & 1 \end{pmatrix} \right\}$$

converge exponentially fast to the stochastic matrix

$$W^{\mathrm{eq}} = \frac{1}{1 + B_{21}} \begin{pmatrix} 1 & B_{21} \\ 1 & B_{21} \end{pmatrix} = \frac{1}{Z} \begin{pmatrix} \mathrm{e}^{-\beta E_1} & \mathrm{e}^{-\beta E_2} \\ \mathrm{e}^{-\beta E_1} & \mathrm{e}^{-\beta E_2} \end{pmatrix}, \tag{4.29}$$

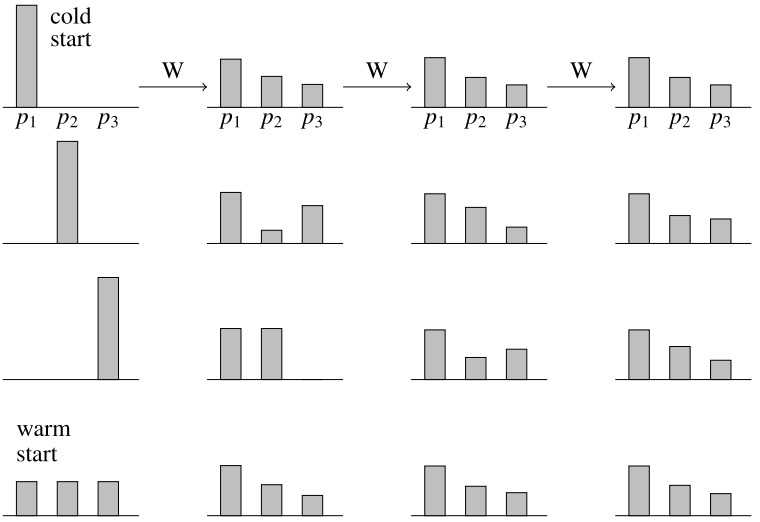

Fig. 4.1 Convergence to equilibrium for a system with 3 states, depending on the initial distribution

where $Z = \exp(-\beta E_1) + \exp(-\beta E_2)$ is the partition function of the two-state system. It follows that every initial probability distribution converges to the Boltzmann distribution

$$\mathbf{p} \to \mathbf{P} = \frac{1}{Z}\left(\mathrm{e}^{-\beta E_1}, \mathrm{e}^{-\beta E_2}\right). \tag{4.30}$$

3-State System Let $|1\rangle, |2\rangle, |3\rangle$ be the energy eigenstates with energies $E_1 < E_2 < E_3$. The stochastic matrix takes the form

$$W = \frac{1}{2}\begin{pmatrix} 2 - B_{21} - B_{31} & B_{21} & B_{31} \\ 1 & 1 - B_{32} & B_{32} \\ 1 & 1 & 0 \end{pmatrix}, \quad B_{pq} = \mathrm{e}^{-\beta(E_p - E_q)}, \tag{4.31}$$

and its powers converge to

$$W^{\mathrm{eq}} = \frac{1}{Z}\begin{pmatrix} \mathrm{e}^{-\beta E_1} & \mathrm{e}^{-\beta E_2} & \mathrm{e}^{-\beta E_3} \\ \mathrm{e}^{-\beta E_1} & \mathrm{e}^{-\beta E_2} & \mathrm{e}^{-\beta E_3} \\ \mathrm{e}^{-\beta E_1} & \mathrm{e}^{-\beta E_2} & \mathrm{e}^{-\beta E_3} \end{pmatrix}. \tag{4.32}$$

Thus every initial distribution converges to the Boltzmann distribution

$$\mathbf{P} = \frac{1}{Z}\left(\mathrm{e}^{-\beta E_1}, \mathrm{e}^{-\beta E_2}, \mathrm{e}^{-\beta E_3}\right). \tag{4.33}$$

Figure 4.1 demonstrates the approach to equilibrium for different initial distributions. The energy differences are $\beta E_2 - \beta E_1 = 0.5$ and $\beta E_3 - \beta E_2 = 0.3$. The convergence to equilibrium is best for a "cold start" with initial state given by the ground state and a "warm start" with uniformly distributed initial probabilities. The convergence is worst when the system starts in the state with the highest energy.

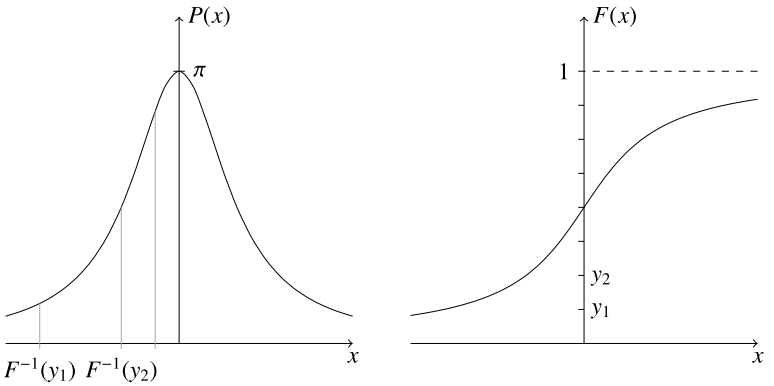

Fig. 4.2 A uniform distribution is mapped to a P-distribution by the inverse of F, where F denotes the anti-derivative of P

4.2.3 Heat Bath Algorithm

For the heat bath algorithm the transition probability $W(\omega, \omega')$ depends only on the final state ω' such that the condition of detailed balance (4.21) implies $W(\omega, \omega') \propto P_{\omega'}$. The normalization conditions for P and W lead to

$$W\left(\omega, \omega'\right) = P_{\omega'}. \tag{4.34}$$

The algorithm is particularly useful when the equilibrium distribution P can be integrated or summed up easily. Let us first apply the heat bath algorithm to estimate one-dimensional integrals of the form $\langle O \rangle = \int O(x) P(x)\, \mathrm{d}x$ with fixed P and varying O. Thus we need random numbers distributed according to $P(x)$. To this end we first generate uniformly distributed random numbers y_i on the unit interval and consider the preimages $\{F^{-1}(y_i)\}$ of these numbers. Here F denotes the monotonically increasing anti-derivative of the probability density,

$$F(x) = \int_{-\infty}^{x} P(u)\, \mathrm{d}u \in [0, 1].$$

Because of the identity

$$y_2 - y_1 = \int_{F^{-1}(y_1)}^{F^{-1}(y_2)} P(u)\, \mathrm{d}u,$$

these preimages are distributed according to P. This is made clear in Fig. 4.2.

For systems with a finite number of configurations the anti-derivative is simply a step function. Let us order the n configuration $\omega = \{1, 2, \ldots, n\}$ according to their probabilities, such that $P_1 \geq P_2 \geq \cdots \geq P_n$ as shown in Fig. 4.3. Then a possible implementation of the direct *heat bath algorithm* proceeds as follows:

1. Select an uniformly distributed random number $r \in [0, 1]$.
2. If $r < P_1$, choose the first configuration $\omega = 1$ and go to 1.

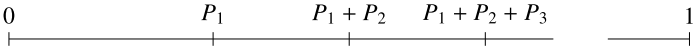

Fig. 4.3 The configurations are ordered such that $P_1 \geq P_2 \geq \cdots \geq P_n$

3. Otherwise, if $r < P_1 + P_2$, select the second configuration $\omega = 2$ and go to 1.
4. ... and so on.

The stochastic matrix corresponding to this algorithm is ideal,

$$W = \begin{pmatrix} P_1 & P_2 & \dots & P_n \\ P_1 & P_2 & \dots & P_n \\ \vdots & \vdots & \dots & \vdots \\ P_1 & P_2 & \dots & P_n \end{pmatrix} = W^{\mathrm{eq}} \quad \Longrightarrow \quad W^2 = W. \tag{4.35}$$

This simple algorithm has an obvious disadvantage: it is only applicable to systems with a relatively small number of configurations and slows down when this number increases. Also note that for a Boltzmann equilibrium distribution one needs to know the partition function in order to compute the probabilities.

So let us modify the simple algorithm such that it applies to systems with continuous variables. The modification uses a Metropolis algorithm for the conditional probabilities of the joint distribution $P(\mathbf{q})$. For example, $P(q_1|q_2, \dots, q_n)$ denotes the probability of q_1 for given $q_2, \dots, q_n$. If $\mathbf{q}$ denotes the configuration at a given time, then a configuration $\mathbf{q}'$ at the subsequent time is chosen according to

$$\begin{aligned} q_1' &\sim P(q_1|q_2, q_3, \dots, q_n), \\ q_2' &\sim P\big(q_2|q_1', q_3, \dots, q_n\big), \\ q_3' &\sim P\big(q_3|q_1', q_2', \dots, q_n\big), \\ &\vdots \qquad\qquad \vdots \\ q_n' &\sim P\big(q_n|q_1', q_2', \dots, q_{n-1}'\big), \end{aligned}$$

where $q_1' \sim P(q_1|q_2, q_3, \dots, q_n)$ means that the new q_1' has to be chosen according to the conditional probability $P(\dots)$. Later on we will discuss an implementation of this algorithm for spin systems.

4.3 The Anharmonic Oscillator

In this section we analyse quantum mechanical systems at imaginary time and discretized on a one-dimensional lattice. They are characterized by their Euclidean lattice action

$$S(\mathbf{q}) = \varepsilon \sum_{j=0}^{n-1} \left\{ \frac{m}{2} \frac{(q_{j+1} - q_j)^2}{\varepsilon^2} + V(q_j) \right\}. \tag{4.36}$$

In particular we shall consider the anharmonic oscillator with quartic potential

$$V(q) = \mu q^2 + \lambda q^4 \tag{4.37}$$

in more detail. The choice of the number n of lattice points and of the lattice constant ε is limited mainly by two aspects:

- ε should be sufficiently small to be near the continuum limit $\varepsilon \to 0$.
- The quantities of interest should fit into the interval $n\varepsilon$. For instance, the width of the ground state should be less than $n\varepsilon$.

If λ_0 is a typical length scale of the system at hand then the quantities n and ε should satisfy constraints of the type

$$\varepsilon \lessapprox \frac{\lambda_0}{10} \quad \text{and} \quad n\varepsilon \gtrapprox 10\lambda_0. \tag{4.38}$$

Another problem concerns the size of *statistical fluctuations* in any Monte Carlo simulation. The relative standard deviation of a random variable O is

$$\Delta_O = \sqrt{\frac{\langle O^2\rangle - \langle O\rangle^2}{\langle O\rangle^2}} \propto (\text{number of lattice points})^{-1/2}. \tag{4.39}$$

As an estimate for the expectation value $\langle O\rangle$ we take

$$\bar{O} = \frac{1}{M}\sum_{\mu=1}^{M} O(\mathbf{q}_\mu) \tag{4.40}$$

with Boltzmann-distributed configurations $\mathbf{q}_\mu$. Depending on the initial configuration the Markov chain may need some "time" to equilibrate. In the simulations of the anharmonic oscillator presented below equilibrium is reached after approximately 10–100 sweeps through the lattice. In addition, since configurations of successive sweeps are correlated, only every MAth sweep is used to estimate expectation values. The number MA should be larger than the relevant *autocorrelation time*—the time over which the values $O(\mathbf{q}_\mu)$ are correlated. Different random variables may have vastly different autocorrelation times. As a general rule they are large for spatially averaged quantities.

Hence we must generate $M \times MA$ configurations to obtain the Monte Carlo estimate (4.40). For the particular simulations of the anharmonic oscillator presented below we take one in five configurations to estimate the correlation functions

$$\langle q_i^2\rangle, \qquad \langle q_i^4\rangle \quad \text{and} \quad \langle q_i q_{i+m}\rangle. \tag{4.41}$$

Here we follow [7] and apply the well-known *virial theorem*

$$\frac{1}{2m}\langle 0|\hat{p}^2|0\rangle = \frac{1}{2}\langle 0|\hat{q}\,V'(\hat{q})|0\rangle \tag{4.42}$$

to relate the correlation functions (4.41) to the ground state energy of the oscillator. This theorem yields the following path integral representation for this energy:

$$E_0 = \langle 0|\frac{1}{2}\hat{q}\,V'(\hat{q}) + V(\hat{q})|0\rangle = \frac{1}{Z}\int \mathscr{D}q\, \mathrm{e}^{-S[q]}\left(\frac{1}{2}qV'(q) + V(q)\right). \tag{4.43}$$

Similarly, using (2.65) we can relate the energy of the first excited state to vacuum expectation values as follows:

$$E_1 = -\frac{1}{\Delta\tau} \lim_{\tau\to\infty} \log \frac{\langle 0|\hat{q}_E(\tau+\Delta\tau)\,\hat{q}(0)|0\rangle}{\langle 0|\hat{q}_E(\tau)\,\hat{q}_E(0)|0\rangle} + E_0. \tag{4.44}$$

Finally, to extract information about the ground state wave function we recall

$$K(\tau, q', q) = \sum_n \mathrm{e}^{-\tau E_n} \psi_n(q')\psi_n(q), \tag{4.45}$$

where the ψ_n denote the normalized energy-eigenfunctions in position space. Thus we may compute the probability density for finding the particle (in its ground state) at q by setting $q' = q$ and assuming large Euclidean times,

$$\lim_{\tau\to\infty} \frac{K(\tau, q, q)}{\int \mathrm{d}q\, K(\tau, q, q)} = \left|\psi_0(q)\right|^2. \tag{4.46}$$

The left-hand side is given by an imaginary-time path integral and hence is accessible to Monto Carlo simulations. In fact, the simulation program `anharmonic.c` on p. 68 counts for all MC-configuration the number of coordinates that lie in each bin of a binning of coordinate space to calculate the left-hand side of (4.46).

4.3.1 Simulating the Anharmonic Oscillator

Since a CPU only knows numbers, we rescale the dimensionful constants and coordinates in the action (4.36) with powers of the dimensionful lattice constant ε to arrive at dimensionless lattice quantities $(m_L, \mu_L, \lambda_L, q_L)$:

$$q_L = q/\varepsilon, \qquad m_L = \varepsilon m, \qquad \mu_L = \varepsilon^3\mu \quad \text{and} \quad \lambda_L = \varepsilon^5\lambda. \tag{4.47}$$

In terms of these dimensionless quantities the lattice action takes the simple form

$$S(\mathbf{q}) = \sum_{j=0}^{n-1} \left\{ \frac{m_L}{2}(q_{j+1} - q_j)_L^2 + \mu_L q_{j,L}^2 + \lambda_L q_{j,L}^4 \right\}. \tag{4.48}$$

In a local Metropolis algorithm we test a new configuration $\mathbf{q}'$ which differs from the old configuration $\mathbf{q}$ only on one lattice point, say lattice point j. Then the difference of the two actions is

$$\begin{aligned} S(\mathbf{q}') - S(\mathbf{q}) \approx (q_j' - q_j)_L \{ & -m_L(q_{j+1} + q_{j-1})_L \\ & + (q_j' + q_j)_L \{ m_L + \mu_L + \lambda_L (q_j'^2 + q_j^2)_L \} \}. \end{aligned} \tag{4.49}$$

Here the problem arises how to determine energies or lengths in physical units. They are only given in terms of the unknown lattice constant ε which does not even enter the lattice action $S(\mathbf{q})$. Thus one first calculates some observable (for example an energy), which is then compared to the experimentally known value to set the scale.

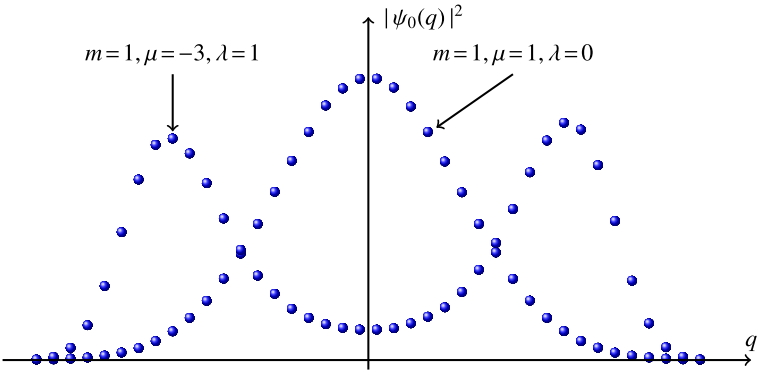

Fig. 4.4 Square of the ground state wave function for the harmonic and anharmonic oscillators as obtained with the Monte Carlo program `anharmonic1.c` listed on p. 68. The dimensionless parameters are given in the plot. More details are explained in the main text

Alternatively one may express all dimensionful quantities in units of a known and fixed unit of length ℓ,

$$\varepsilon = a\ell, \qquad q = \tilde{q}\ell, \qquad m = \tilde{m}/\ell, \qquad \mu = \tilde{\mu}/\ell^3 \quad \text{and} \quad \lambda = \tilde{\lambda}/\ell^5. \tag{4.50}$$

In this system of units

$$S(\mathbf{q}') - S(\mathbf{q}) = (\tilde{q}_j' - \tilde{q}_j)\left\{-\frac{\tilde{m}}{a}(\tilde{q}_{j+1} + \tilde{q}_{j-1}) + (\tilde{q}_j' + \tilde{q}_j)\left\{\frac{\tilde{m}}{a} + a\tilde{\mu} + a\tilde{\lambda}(\tilde{q}_j'^2 + \tilde{q}_j^2)\right\}\right\}. \tag{4.51}$$

This formula is used in the header-file `stdanho.h` on p. 71 which is called by the program `anharmonic1.c` listed on p. 68. The parameters m, μ, λ, the number of lattice points N (in the C-program n is renamed N) and the lattice constant a are all defined in another header-file `constants.h` on p. 70. In order to have uncorrelated configurations only one out of MA configuration is measured. In addition, since a Markov chain needs some time to reach equilibrium, we start measuring configurations only after $MA \times ME$ sweeps through the lattice have been done.

To measure the square of $\psi_0(q)$ on the interval $[-INTERV, INTERV]$ with the help of (4.46) we divide the interval into BIN bins. With the parameter $DELTA$ we adjust the amplitude of a tentative coordinate change during a local update according to $q' = q + DELTA \times (1 - 2r)$, where r is a uniform random number on $[0, 1]$. The program `anharmonic1.c` generates the histogram of the probability distribution. In Fig. 4.4 we plotted the so obtained density $|\psi_0(q)|^2$, both for the harmonic and the anharmonic oscillator.

The similar program `anharmonic2.c` listed on p. 69 calculates the ground state energy from the formula (4.43). We fix the size Na of the interval in units of ℓ and increase the number of lattice point N or equivalently decrease the lattice constant a. Table 4.1 shows how the ground state energies of the oscillators vary

Table 4.1 Ground state energies for the harmonic oscillator with $(m, \mu) = (1, 0.5)$ and the anharmonic oscillator with $(m, \mu, \lambda) = (1, -3, 1)$. The entries in the third column measure the violation of the Wick-relation (4.52). The exact lattice values E_0(exact) are computed numerically

a	$E_0(1, 0.5)$	Wick	E_0(exact)	$E_0(1, -3, 1)$
1	0.4477	−0.0008	0.4473	−1.4624
1/2	0.4851	0.0010	0.4851	−1.1339
1/3	0.4928	0.0016	0.4932	−1.0177
1/4	0.4926	0.0014	0.4962	−0.9758
1/5	0.4970	0.0040	0.4976	−0.9466
1/6	0.4948	0.0006	0.4983	−0.9369
1/7	0.5016	0.0003	0.4988	−0.9173
1/8	0.4989	0.0067	0.4991	−0.9144
1/9	0.4992	0.0012	0.4993	−0.9160
1/10	0.4985	0.0009	0.4994	−0.9097

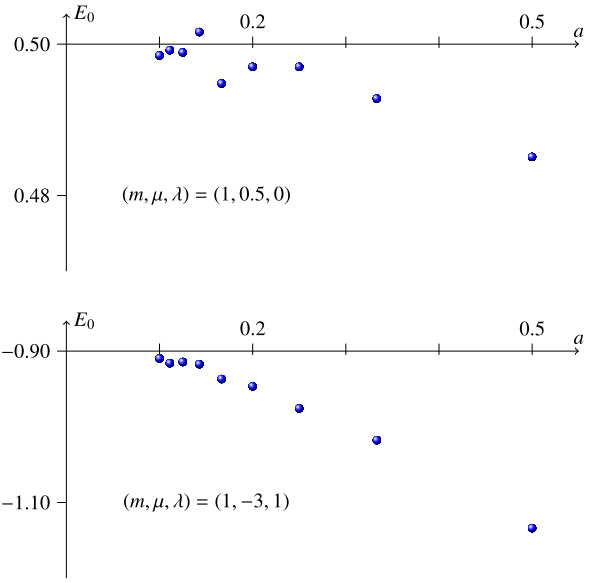

Fig. 4.5 Convergence of the MC-results for the ground state energies of the harmonic oscillator (*top panel*) and anharmonic oscillator (*bottom panel*) with decreasing lattice constant a. In both cases $m = 1$ may be used to set the scale

with the lattice constant a. We see that for $a \lessapprox 0.2$ the system is already close to its continuum limit. All simulations have been performed on the fixed interval $aN = 10$. How fast the ground state energies converge to their continuum values is plotted in Fig. 4.5. An extrapolation of the lattice results to the continuum limit yield the following Monte Carlo estimates:

$$E_0(\text{harmonic oscillator}) \approx 0.50, \qquad E_0(\text{anharmonic oscillator}) \approx -0.91.$$

Thus we reproduced the exact ground state energy of the harmonic oscillator in the continuum limit. Finally we note that for the harmonic oscillator

$$\langle 0|\hat{q}^4|0\rangle - 3\langle 0|\hat{q}^2|0\rangle^2 = 0. \tag{4.52}$$

The column labeled "Wick" in Table 4.1 contains estimates for the left-hand side of this identity. The deviations from zero are due to statistical errors in our simulations.

4.4 Hybrid-Monte Carlo Algorithm

The powerful hybrid-Monte Carlo algorithm has been developed by S. DUANE ET AL. [8]. A pedagogical description can be found in [9] and in our presentation we follow in part the reviews [10, 11]. The algorithm represents a combination of molecular dynamics (see [12]) and Metropolis algorithm. It aims at global updates of whole configurations with reasonable large acceptance rates, in order to minimize the time required to generate independent configurations.

Molecular dynamics (MD) simulations are frequently and successfully used to study (classical) many-body systems and are applied to problems in material science, astrophysics and biophysics. In molecular dynamics simulations one solves the equations of motion numerically and makes use of the property that statistical ensemble averages are equal to time averages of the system, known as the ergodic hypothesis.

From an initial configuration, represented by a point $(\mathbf{q}_0, \mathbf{p}_0)$ in phase space, one obtains a unique solution of Hamilton's equations of motion,

$$\dot{q}_i = \frac{\partial H}{\partial p_i}, \qquad \dot{p}_i = -\frac{\partial H}{\partial q_i}. \tag{4.53}$$

Without any numerical errors the energy is a constant of motion and this simple observation will be relevant in what follows.

In Euclidean quantum mechanics discretized on an imaginary-time lattice Λ with n points $\{x\}$ we introduce an extended phase space with dimension $2n$. Each point in extended phase space consists of a broken-line path characterized by variables $\{q_x\}$ and their canonically conjugated momenta $\{p_x\}$. To construct a Markov process with *global updates* and high acceptance rate we introduce the following auxiliary Hamiltonian in extended phase space:

$$H(\mathbf{q}, \mathbf{p}) = \frac{\mathbf{p}^2}{2} + S(\mathbf{q}), \quad \mathbf{p}^2 = \sum_{x \in \Lambda} p_x^2, \tag{4.54}$$

where $\mathbf{q} = (q_1, \ldots, q_n)$ and $\mathbf{p} = (p_1, \ldots, p_n)$. This Hamiltonian generates a dynamics with respect to a fictitious time—it will be the time of the associated Markov process. Integrating the equations of motion over a certain "period of time" maps a point $(\mathbf{q}, \mathbf{p})$ in extended phase space to another point $(\mathbf{q}', \mathbf{p}')$. This mapping is used to suggest the image point as new configuration in a Markov chain in which the pair $(\mathbf{q}', \mathbf{p}')$ is accepted with probability

$$A\big(\mathbf{q}, \mathbf{p} \to \mathbf{q}', \mathbf{p}'\big) = \min\big\{1, \exp\big(H(\mathbf{q}, \mathbf{p}) - H\big(\mathbf{q}', \mathbf{p}'\big)\big)\big\}. \tag{4.55}$$

For an exact solution of the equations of motion (4.53) energy is conserved and the acceptance probability would be one. But any numerical integration comes along

with rounding errors such that H is only conserved up to discretization errors in which case the acceptance of the new configuration is not guaranteed. By tuning the period of integration one can ensure that the acceptance rate stays close to 1. In almost all algorithms the fictitious momenta are drawn from a Gaussian distribution,

$$P_G(\mathbf{p}) = \mathcal{N} \mathrm{e}^{-\mathbf{p}^2/2}. \tag{4.56}$$

Now we show that the corresponding Markov process obeys the condition of detailed balance if the integrator is time-reversible. Let us first calculate the transition probability from $\mathbf{q}$ to $\mathbf{q}'$. Under time-reversal a point $(\mathbf{q}, \mathbf{p})$ in phase space is mapped to $(\mathbf{q}, -\mathbf{p})$. Since the equations of motion and the integrator are both time-reversible we conclude that the probability to move from an initial to a final point is invariant under time-reversal,

$$T\big(\mathbf{q}, \mathbf{p} \to \mathbf{q}', \mathbf{p}'\big) = T\big(\mathbf{q}', -\mathbf{p}' \to \mathbf{q}, -\mathbf{p}\big). \tag{4.57}$$

With the known acceptance rate in (4.55) and the Gaussian distribution of momenta we can calculate the transition probability $W(\mathbf{q}, \mathbf{q}')$ as follows:

$$W\big(\mathbf{q}, \mathbf{q}'\big) = \int \mathscr{D}\mathbf{p} \mathscr{D}\mathbf{p}' P_G(\mathbf{p})\, T\big(\mathbf{q}, \mathbf{p} \to \mathbf{q}', \mathbf{p}'\big) A\big(\mathbf{q}, \mathbf{p} \to \mathbf{q}', \mathbf{p}'\big), \tag{4.58}$$

where one averages and sums over initial and final momenta, respectively. Thus the left-hand side of the condition of detailed balance,

$$\mathrm{e}^{-S(\mathbf{q})}\, W\big(\mathbf{q}, \mathbf{q}'\big) = \mathrm{e}^{-S(\mathbf{q}')}\, W\big(\mathbf{q}', \mathbf{q}\big), \tag{4.59}$$

can be written as

$$\mathrm{e}^{-S(\mathbf{q})}\, W\big(\mathbf{q}, \mathbf{q}'\big) = \mathcal{N} \int \mathscr{D}\mathbf{p} \mathscr{D}\mathbf{p}' \mathrm{e}^{-H(\mathbf{q},\mathbf{p})}\, T\big(\mathbf{q}, \mathbf{p} \to \mathbf{q}', \mathbf{p}'\big) A\big(\mathbf{q}, \mathbf{p} \to \mathbf{q}', \mathbf{p}'\big). \tag{4.60}$$

Similarly as in the proof of detailed balance for the Metropolis algorithm on p. 53 we can show that

$$\mathrm{e}^{-H(\mathbf{q},\mathbf{p})}\, A\big(\mathbf{q}, \mathbf{p} \to \mathbf{q}', \mathbf{p}'\big) = \mathrm{e}^{-H(\mathbf{q}',\mathbf{p}')}\, A\big(\mathbf{q}', \mathbf{p}' \to \mathbf{q}, \mathbf{p}\big). \tag{4.61}$$

Inserting this relation into (4.60) and using that H and A are even functions of the momenta, we conclude

$$\begin{aligned} \mathrm{e}^{-S(\mathbf{q})}\, W\big(\mathbf{q}, \mathbf{q}'\big) &= \mathcal{N} \int \mathscr{D}\mathbf{p} \mathscr{D}\mathbf{p}' \mathrm{e}^{-H(\mathbf{q}',\mathbf{p}')}\, T\big(\mathbf{q}, \mathbf{p} \to \mathbf{q}', \mathbf{p}'\big) A\big(\mathbf{q}', \mathbf{p}' \to \mathbf{q}, \mathbf{p}\big) \\ &= \mathcal{N} \int \mathscr{D}\mathbf{p} \mathscr{D}\mathbf{p}' \mathrm{e}^{-H(\mathbf{q}',\mathbf{p}')}\, T\big(\mathbf{q}', \mathbf{p}' \to \mathbf{q}, \mathbf{p}\big) A\big(\mathbf{q}', \mathbf{p}' \to \mathbf{q}, \mathbf{p}\big) \\ &= \mathrm{e}^{-S(\mathbf{q}')} W\big(\mathbf{q}', \mathbf{q}\big). \end{aligned}$$

The proof makes clear that the distribution of momenta cannot be arbitrary. We must impose that the product $P_G \exp(-S)$ is proportional to $\exp(-H)$ and for the Hamiltonian (4.54) this means that the distribution must be Gaussian. The described HMC scheme leaves room for improvement. In particular, one has considerable freedom

in defining the auxiliary Hamiltonian that governs the molecular dynamics evolution. One method of speeding up the evolution is Fourier acceleration, in which the different Fourier modes are assigned different step sizes or masses. This techniques was introduced for Langevin simulations of field theories [13] and can be applied to HMC simulations as well [14]. Note that the proof of detailed balance also assumes that the molecular dynamics evolution defines a volume preserving symplectic map in phase space.

4.4.1 Implementing the HMC-Algorithm

To fulfil the condition of detailed balance we need a time-reversible and symplectic integrator to numerically solve the fictitious Hamiltonian dynamics. Using the naive forward difference operator $\dot{f}(\tau)h \approx f(\tau+h) - f(\tau)$ in the discretized equations of motion leads to the *time-irreversible* prescription

$$\begin{aligned} \mathbf{q}(\tau+h) &= \mathbf{q}(\tau) + h\mathbf{p}(\tau), \\ \mathbf{p}(\tau+h) &= \mathbf{p}(\tau) + h\mathbf{F}\big(\mathbf{q}(\tau)\big), \end{aligned} \tag{4.62}$$

with force $\mathbf{F} = -\nabla_{\mathbf{q}} S$. This prescription must not be used in any HMC-algorithm. In most simulation the time-reversible leapfrog integration is used instead. Here one first moves forward with the momenta a half step in fictitious time. Then one moves forward several time-steps alternately with coordinates $\mathbf{q}$ and momenta $\mathbf{p}$. The last move of the momenta is again a half step in fictitious time.

One sweep amounts to an integration over a fictitious time-interval $\tau = ph$. We denote the position and momentum at fictitious time kh by $\mathbf{q}_{(k)}$ and $\mathbf{p}_{(k)}$. In particular $\mathbf{q}_{(p)}$ and $\mathbf{p}_{(p)}$ are the final position and momentum. From an initial configuration we determine the final configuration as follows:

1. Begin with a initial lattice field $\mathbf{q}_{(0)}$. Depending on the parameters (couplings, temperature) one chooses a cold or warm start.
2. Generate Gauss-distributed momenta $\mathbf{p}_{(0)}$ with variance 1 and mean 0.
3. Move a half step forward with the momenta,

$$\mathbf{p}_{(1/2)} = \mathbf{p}_{(0)} + \frac{h}{2}\mathbf{F}(\mathbf{q}_{(0)}). \tag{4.63}$$

4. Iterate the following two steps:

$$\begin{aligned} &\text{(a)} \quad \mathbf{q}_{(k)} = \mathbf{q}_{(k-1)} + h\mathbf{p}_{(k-1/2)}, && k = 1, 2, \ldots, p, \\ &\text{(b)} \quad \mathbf{p}_{(k+1/2)} = \mathbf{p}_{(k-1/2)} + h\mathbf{F}(\mathbf{q}_{(k)}), && k = 1, \ldots, p-1. \end{aligned} \tag{4.64}$$

5. Finally move a half step forward with the momenta,

$$\mathbf{p}_{(N)} = \mathbf{p}_{(p-1/2)} + \frac{h}{2}\mathbf{F}(\mathbf{q}_{(p)}). \tag{4.65}$$

6. Accept the newly generated configuration $(\mathbf{q}', \mathbf{p}') = (\mathbf{q}_{(p)}, \mathbf{p}_{(p)})$ with probability given in (4.55).

7. Start over again with the old or the new configuration at point 2.

The so obtained Markov chain converges to the Boltzmann distribution corresponding to the action S.

The leapfrog integrator used in the steps 3, 4, and 5 is time-reversible and defines a symplectic and therefore volume preserving map in phase space. This *second-order symplectic integrator* maps the initial point $\mathbf{q}_{(0)}, \mathbf{p}_{(0)}$ to the final point $\mathbf{q}_{(p)}, \mathbf{p}_{(p)}$. To test for a correct implementation of the algorithm one observes that for any symplectic map $\mathbf{q}, \mathbf{p} \to \mathbf{q}', \mathbf{p}'$

$$\int \mathscr{D}\mathbf{q}'\mathscr{D}\mathbf{p}' \mathrm{e}^{-H(\mathbf{q}',\mathbf{p}')} = \int \mathscr{D}\mathbf{q}\mathscr{D}\mathbf{p}\, \mathrm{e}^{-H(\mathbf{q},\mathbf{p})-\Delta H(\mathbf{q},\mathbf{p})}, \tag{4.66}$$

where $\Delta H(\mathbf{q}, \mathbf{p}) = H(\mathbf{q}', \mathbf{p}') - H(\mathbf{q}, \mathbf{p})$ denotes the increase in energy along the trajectory. With the help of the *Jensen inequality*, which expresses the convexity of the exponential function, one concludes that the inequality

$$1 = \left\langle \mathrm{e}^{-\Delta H} \right\rangle \geq \mathrm{e}^{-\langle \Delta H \rangle} \tag{4.67}$$

must hold in the simulations.

There are two parameters which must be adjusted to increase speed and efficiency of the algorithm. These are the step size h of the discretization of fictitious time and the interval $\tau = ph$ over which one follows a trajectory. In the leapfrog integration one violates the conservation of energy due to discretization errors. According to [15]

$$\Delta H \propto h^3 + O\left(h^4\right). \tag{4.68}$$

For fixed integration time τ the expectation value of ΔH shows the following dependency on the lattice-volume V and the step size:

$$\langle \Delta H \rangle \propto V h^4. \tag{4.69}$$

Thus, for fixed volume we can adjust the acceptance rate by tuning the step size h. Note that with increasing τ we spend more time to generate new configurations but at the same time these configurations are less correlated. As always one must find a good compromise to end up with an efficient algorithm. Also note that due to the unavoidable rounding errors the leapfrog integration is not exactly time-reversible and one should check that this does not screw up the results. For example, on can integrate first forward and then again backward in fictitious time to estimate the violation of time-reversibility. For more details you may consult [11].

4.4.2 HMC-Algorithm for Harmonic Oscillator

The explicit form of the HMC-algorithm for the one-dimensional oscillator follows from the auxiliary Hamiltonian,

$$H = \frac{\mathbf{p}^2}{2} + S(\mathbf{q}), \quad S(\mathbf{q}) = \sum_x \left(\frac{1}{2}(\partial q)_x^2 + \frac{\omega^2}{2} q_x^2 + \frac{\lambda}{4} q_x^4 \right), \tag{4.70}$$

where ∂ is a discretization of the differential operator on the lattice with lattice constant one. The non-linear equations of motion read

$$\begin{aligned} \dot{q}_x &= +\frac{\partial H}{\partial p_x} = p_x, \\ \dot{p}_x &= -\frac{\partial H}{\partial q_x} = \left(\partial^2 q\right)_x - \omega^2 q_x - \lambda q_x^3. \end{aligned} \tag{4.71}$$

For the harmonic oscillator with $\lambda = 0$ we obtain a system of coupled linear differential equations

$$\dot{\mathbf{q}} = \mathbf{p} \quad \text{and} \quad \dot{\mathbf{p}} = -\mathsf{A}\mathbf{q} \tag{4.72}$$

with the positive matrix $\mathsf{A} = -\partial^2 + \omega^2$. For the most naive discretization the matrix ∂^2 is a tridiagonal Toeplitz matrix with -2 on the main-diagonal and 1 on the upper and lower bidiagonals—it is just the matrix in (2.80) with particular parameters. The explicit solution of the HMC-implementation on p. 64 reads

$$\begin{pmatrix} q_{(p)} \\ p_{(p)} \end{pmatrix} = \mathsf{M} \begin{pmatrix} q_{(0)} \\ p_{0)} \end{pmatrix} \tag{4.73}$$

with *symplectic matrix*

$$\mathsf{M} = \begin{pmatrix} \mathsf{P} & \mathsf{Q}h \\ \mathsf{AXQ}h & \mathsf{P} \end{pmatrix}, \tag{4.74}$$

wherein

$$\mathsf{X} = \frac{\mathsf{H}}{4} - \mathbb{1} \quad \text{with } \mathsf{H} = \mathsf{A}h^2.$$

The commuting entries P, Q are matrix-polynomials in H of degrees p and $p-1$, respectively. For example for $p = 4$ we obtain

$$\begin{aligned} \mathsf{P} &= \frac{\mathsf{H}^4}{2} - 4\mathsf{H}^3 + 10\mathsf{H}^2 - 8\mathsf{H} + 1 \\ \mathsf{Q} &= -\mathsf{H}^3 + 6\mathsf{H}^2 - 10\mathsf{H} + 4. \end{aligned}$$

These matrices satisfy the constraints

$$\mathsf{P}^2 - \mathsf{AXQ}^2 h^2 = \mathbb{1}, \tag{4.75}$$

which express the fact that M is a symplectic matrix or that the map (4.73) in phase space is a *volume preserving* symplectic map—an integrator with this property is called symplectic.

For a detailed study of hybrid-Monte Carlo algorithms for non-interacting models the reader may consult [16]. This paper contains higher-order discretizations of the molecular dynamics equations of motion, results on the autocorrelations functions and on Metropolis acceptance probabilities as a function of the integration step size. For models with dynamical fermions the use of higher-order symplectic integrators in combination with Fourier acceleration [14] often leads to improved algorithms, in particular for intermediate and strong coupling. For example, a fourth-order integrator introduced by FOREST and RUTH [17], and extended in [18] has

been useful in simulations of supersymmetric models with bosonic and fermionic degrees of freedom [19].

For theories with local interactions one may employ a local version of the HMC-algorithm where single site (and link) variables are evolved in a HMC style [20]. In parameter regions where Metropolis and heat bath algorithms have low acceptance rates the local HMC-algorithm may be preferable [21].

4.5 Programs for Chap. 4

This chapter contains the C-programs

- `anharmonic1.c`
- `anharmonic2.c`
- `constants.h`
- `stdanho.h`

to simulate the anharmonic oscillator with the local Metropolis algorithm.

The program `anhamonic1.c` in Listing 4.1 estimates the probability density in position space $|\psi_0(q)|^2$ for the harmonic and anharmonic oscillators. The parameters of the model are stored in the header-files `constants.h` and `stdanho.h`. The program `anharmonic2.c` in Listing 4.2 estimates ground state energies E_0 of the harmonic and anharmonic oscillators with the Metropolis algorithm. Thereby the virial theorem (4.43) is used. The parameters are contained in header-files called by the program.

Header-Files The following files are called by the programs `anharmonic.c`. In the header-file `constants.h` in Listing 4.3 we defined the constants and variables called by the programs. The header-file `stanho.h` in Listing 4.4 contains four functions, which are needed by the main programs.

The first functions `delta_action` calculates the change of the action when the coordinate at a given lattice point is changed from x to y. The function expects the sum of coordinates on the neighboring lattice points, denoted by xs. The variables *muleff, lambdal* and *massl* must be provided.

The next function `mcsweep` performs *MA* successive Monte Carlo-sweeps through the lattice. $*q$ points to the array $q[N]$ and $*zgr$ to the variable *reject*, which counts how often a suggested change has been rejected. The constants N, MA and *DELTA* must be provided.

The third function `binning` bins the values of $q[N]$ between $-INTERV$ and *INTERV* in the array *bin*[*BIN*]. The variables *q[N], bin[BIN], stretch, translate* and *BIN* must be defined and initialized.

The last function *moments* calculates the sums $\frac{1}{N}\sum q_i^n$.

Listing 4.1 Anharmonic oscillator I

```
/*program anharmonic.c*/
/*Metropolis algorithm for the (an)harmonic oscillator*/
/*L=MASS/2 v^2+MU q^2+LAMBDA*q^4*/
/*calcules the square of the ground state wave function*/
#include <stdio.h>
#include <stdlib.h>
#include <math.h>
#include <time.h>
#include "constants.h"
/*defines: N,A,ME,MA,BIN,INTERV,MASS,MU,LAMBDA,DELTA*/
/*init:q[N],qneu,massl,lambdal,muleff,reject,stretch,versch*/
#include "stdanho.h" /*function deltaS(qnew,qold,summenn)*/
                     /*MA MC-iterations: mcsweep(*zgr,*q)*/
int main(void)
{
  unsigned int i,j;
  int *zgr,p,bin[BIN];
  zgr=&reject; srand48(time(NULL));
  /*initialization*/
  for (i=0;i<N;i++)
    q[i]=DELTA*(1-2*drand48());
  for (i=0;i<BIN;i++)
    bin[i]=0;
  /*thermalization*/
  for (i=0;i<ME;i++)
    mcsweep(zgr,q);
  /*calculate binning*/
  reject=0;
  for (i=0;i<M;i++)
    { mcsweep(zgr,q);binning(bin,q);};
  /*output of probability density and rejection rate*/
  printf("bin\t probability\n");
  for (i=0;i<BIN;i++)
    printf("%i\t %7.3f\n",i,20*bin[i]/(double)M);
  printf("\nrejected configurations %.2f percent\n",
        (float)100*reject/(N*M*MA));
  return 0;
}
```

4.6 Problems

4.1 (Detailed balance) A statistical system admits two configurations which in equilibrium are distributed with probabilities $P_\omega > 0, \omega = 1, 2$. Construct the most general stochastic matrix $W(\omega, \omega')$ which obeys the condition of detailed balance,

$$P(\omega)W\left(\omega, \omega'\right) = P\left(\omega'\right)W\left(\omega', \omega\right) \quad \text{for } \omega, \omega' \in \{1, 2\}.$$

What is the optimal choice for W such that W^n converges as quickly as possible to the limit matrix W^{eq}.

Listing 4.2 Anharmonic oscillator II

```
/*program anharmonic2.c*/
/*Metropolis algorithm for anharmonic oscillator*/
/*L=MASS/2 v^2+MU q^2+LAMBDA*q^4 */
/*calculates ground state energy*/
#include <stdio.h>
#include <stdlib.h>
#include <math.h>
#include <time.h>
#include "constants.h"
#include "stdanho.h"
int main(void)
{
  unsigned int i,j;
  int *zgr,p; double moment2=0,moment4=0,wick;
  zgr=&reject;
  srand48(time(NULL));
  /*initialize*/
  for (i=0;i<N;i++)
    q[i]=DELTA*(1-2*drand48());
  /*thermalize*/
  for (i=0;i<ME;i++)
    mcsweep(zgr,q);
  /*simulation and calculation of moments*/
  reject=0;
  for (i=0;i<M;i++)
    {
      mcsweep(zgr,q);
      moment2=moment2+moments(2,q);
      moment4=moment4+moments(4,q);
    };
  /*ground state energy, Wick-test, output*/
  moment2=moment2/M;
  moment4=moment4/M;
  wick=3*moment2*moment2-moment4;
  wick=3*moment2*moment2-moment4;
  printf("2nd moment =\t\t %7.4f\n4th moment =\t\t %7.4f\n"
    "ground state energy =\t %7.4f\nWick-test =\t\t %7.4f\n",
     moment2,moment4,2*MU*moment2+3*LAMBDA*moment4,wick);
    printf("\nrejected configurations %.2f\n",
    (float)reject/(N*M*MA));
  return 0;
}
```

4.2 (Markov process) Consider a system with three energy eigenstates the energies of which are ordered as $E_1 < E_2 < E_3$. The allowed transitions are $\omega \to (\omega + 1) \bmod 1$. This process cannot fulfill the condition of detailed balance. Show that there nevertheless is a stochastic matrix $W(\omega, \omega')$ with the Boltzmann distribution as fixed point.

Listing 4.3 Constants and variables

```
/*program constants.h*/
/*constants: N,A,ME,MA,BIN,INTERV*/
/*MASS,MU,LAMBDA,DELTA*/
/*initial values for q[N],qnew*/
/*massl,lambdal,mueleff,reject,streck,versch*/
#define N 10    /*number of lattice points*/
#define A 1.0   /*lattice constant*/
#define M 1000000 /*number of iterations*/
#define ME 500  /*until equilibrium is reached*/
#define MA 5    /*every MA'th configuration is measured*/
#define BIN 40  /*number of  bins for wave function*/
#define INTERV 2 /*interval for binning [-INTERV,INTERV]*/
#define MASS 1.0
#define MU 1.0  /*coupling of q**2*/
#define LAMBDA 0.0 /*coupling of q**4*/
#define DELTA 0.5 /*change of variable = DELTA(1-2 random)*/
/*rescale to lattice-variables*/
double massl=MASS/A;
double lambdal=A*LAMBDA;
double muleff=MASS/A+A*MU;
double qnew,q[N];
unsigned int reject=0;
double translate=(double)BIN/2.0;
double stretch=0.5*(double)BIN/(double)INTERV;
```

4.3 (Precision of integrators) Show that the numerical integration of an ordinary differential equation of type $df/dt = g(f,t)$ though a leapfrog integrator corresponds to a precision of 2nd order. This means that it should be demonstrated that the global error of the obtained solution is of order $\mathcal{O}(h^2)$, where h is the time-step.

4.4 (Verlet algorithm) If we are not interested in the momenta, but just the trajectory of the particle, we can eliminate the momenta from the leapfrog algorithm and end up with the *Verlet algorithm*. Find this algorithm.

4.5 (Fourth-order symplectic integrator) The simplest higher-order symplectic algorithm is that of Forest, Ruth and Omelyan. If initially $\mathbf{q} = \mathbf{q}(\tau)$, $\mathbf{p} = \mathbf{p}(\tau)$ then, in the Forest–Ruth algorithm, the following steps:

$$
\begin{aligned}
\mathbf{q} &= \mathbf{q} + \frac{\theta h}{2}\mathbf{p},\\
\mathbf{p} &= \mathbf{p} + \theta h \mathbf{F}(\mathbf{q}),\\
\mathbf{q} &= \mathbf{q} + (1-\theta)\frac{h}{2}\mathbf{p},\\
\mathbf{p} &= \mathbf{p} - (1-2\theta)h\mathbf{F}(\mathbf{q}),\\
\mathbf{q} &= \mathbf{q} + (1-\theta)\frac{h}{2}\mathbf{p},\\
\mathbf{p} &= \mathbf{p} + \theta h \mathbf{F}(\mathbf{q}),
\end{aligned}
$$

Listing 4.4 Functions for anharmonic oscillator

```
/*program stdanho.h*/
/*change of action*/
double delta_action(double y,double x,double xs)
{ return (y-x)*((y+x)*(muleff+lambdal*(y*y+x*x))-massl*xs);};
/*MA sweeps*/
/*expects constants N,MA,DELTA*/
/*arguments: array q[N], pointer to reject*/
void mcsweep(int *zgr,double *q)
{ int i,j; double qnew,dS;
  for (i=0;i<MA;i++)
    for (j=0;j<N;j++)
      { qnew=q[j]+DELTA*(1-2*drand48());
        dS=delta_action(qnew,q[j],q[(j+1)%N]+q[(j+N-1)%N]);
        if (dS<0) q[j]=qnew;
        else
          if (exp(-dS)>drand48() ) q[j]=qnew;
          else *zgr=*zgr+1;
      };
}
/*binning of values in q[N]*/
void binning(int *bin,double *q)
{ int i,p;
  for (i=0;i<N;i++)
    {p=(int)(q[i]*stretch+translate);
    if ((0<=p)&&(p<BIN)) bin[p]++;};
}
/*calculation of moments*/
double moments(int n,double *q)
{ int i; double sum=0;
  for (i=0;i<N;i++)
    sum=sum+pow(q[i],n);
  return sum/N;
}
```

$$\mathbf{q} = \mathbf{q} + \frac{\theta h}{2}\mathbf{p},$$

with

$$\theta = \frac{1}{2 - 2^{1/3}} \approx 1.35120719195966$$

yield $\mathbf{q}(\tau + h)$, $\mathbf{p}(\tau + h)$. Prove that this integrator is symplectic.

Remark The algorithm requires three force evaluations per time-step. The middle step is larger in magnitude than h and goes "backwards in time". All higher-order integrators seem to have such steps "backwards in time". If one is willing to accept more than three force evaluations for a fourth-order integrator one can avoid having a step greater in magnitude than h. The algorithm of Omelyan et al. [18] avoids large time-steps and hence is more accurate than the Forest–Ruth algorithm. It reads

$$\mathbf{q} = \mathbf{q} + \xi h\mathbf{p},$$

$$
\begin{aligned}
\mathbf{p} &= \mathbf{p} + (1-2\lambda)\frac{h}{2}\mathbf{F}(\mathbf{q}),\\
\mathbf{q} &= \mathbf{q} + \xi h\mathbf{p},\\
\mathbf{p} &= \mathbf{p} + \lambda h\mathbf{F}(\mathbf{q}),\\
\mathbf{q} &= \mathbf{q} + \big(1-2(\chi+\xi)\big)h\mathbf{p},\\
\mathbf{p} &= \mathbf{p} + \lambda h\mathbf{F}(\mathbf{q}),\\
\mathbf{q} &= \mathbf{q} + \xi h\mathbf{p},\\
\mathbf{p} &= \mathbf{p} + (1-2\lambda)\frac{h}{2}\mathbf{F}(\mathbf{q}),\\
\mathbf{q} &= \mathbf{q} + \xi h\mathbf{p},
\end{aligned}
$$

with parameters

$$
\begin{aligned}
\xi &\approx 0.1786178958448091,\\
\lambda &\approx -0.2123418310626054,\\
\chi &\approx -0.06626458266981849.
\end{aligned}
$$

References

1. K. Jacobs, Markov-Prozesse mit endlich vielen Zuständen (Markov processes with a finite number of states), in *Selecta Mathematica IV* (Springer, Berlin, 1972)
2. M.E.J. Newman, G.G. Barkenna, *Monte Carlo Methods in Statistical Physics* (Clarendon, Oxford, 1999)
3. K. Binder, D.W. Heermann, *Monte Carlo Simulations in Statistical Physics*. Graduate Texts in Physics (Springer, Berlin, 2010)
4. J.S. Liu, *Monte Carlo Strategies in Scientific Computing*. Springer Series in Statistics (Springer, Berlin, 2001)
5. N. Metropolis, A.W. Rosenbluth, M.N. Rosenbluth, A.H. Teller, Equations of state calculations by fast computing machines. J. Chem. Phys. **21**, 1087 (1953)
6. W.K. Hasting, Monte Carlo sampling methods using Markov chains and their applications. Biometrika **170**, 97 (1970)
7. M. Creutz, B.A. Freedman, A statistical approach to quantum mechanics. Ann. Phys. **132**, 427 (1981)
8. S. Duane, A.D. Kennedy, A.D. Pendleton, B.J. Roweth, Hybrid Monte Carlo. Phys. Lett. B **195**, 216 (1987)
9. I. Montvay, G. Münster, *Quantum Fields on a Lattice* (Cambridge University Press, Cambridge, 1994)
10. H.J. Rothe, *Lattice Gauge Theories—An Introduction* (World Scientific, Singapore, 2005)
11. C. Urbach, Untersuchung der Reversibilitätsverletzung beim HMC-Algorithmus. Thesis FU Berlin (2002)
12. M. Griebel, S. Knapek, G. Zumbusch, A. Caglar, *Numerische Simulation in der Moleküldynamik* (Springer, Berlin, 2004)
13. G.G. Batrouni, G.R. Katz, A.S. Kronfeld, G.P. Lepage, B. Svetitsky, K.G. Wilson, Langevin simulation of lattice field theories. Phys. Rev. D **32**, 2736 (1985)
14. D.H. Weingarten, D.N. Petcher, Monte Carlo integration for lattice gauge theories with fermions. Phys. Lett. B **99**, 333 (1981)

15. S. Gupta, A. Irback, F. Karch, B. Petersson, The acceptance probability in the hybrid Monte Carlo method. Phys. Lett. B **242**, 437 (1990)
16. A.D. Kennedy, B. Pendleton, Cost of the generalized hybrid Monte Carlo algorithm for free field theory. Nucl. Phys. B **607**, 456 (2001)
17. E. Forest, R.D. Ruth, Fourth-order symplectic integration. Physica D **43**, 105 (1990)
18. I.P. Omelyan, I.M. Mryglod, R. Folk, Symplectic analytically integrable decomposition algorithms: classification, derivation, and application to molecular dynamics, quantum and celestial mechanics simulations. Comput. Phys. Commun. **151**, 272 (2003)
19. T. Kaestner, G. Bergner, S. Uhlmann, A. Wipf, C. Wozar, Two-dimensional Wess–Zumino models at intermediate couplings. Phys. Rev. D **78**, 095001 (2008)
20. P. Marenzoni, L. Pugnetti, P. Rossi, Measure of autocorrelation times of local hybrid Monte Carlo algorithm for lattice QCD. Phys. Lett. B **315**, 152 (1993)
21. B. Wellegehausen, A. Wipf, C. Wozar, Casimir scaling and string breaking in G2 gluodynamics. Phys. Rev. D **83**, 016001 (2011)

Chapter 5
Scalar Fields at Zero and Finite Temperature

Scalar fields are discussed in many introductory textbooks on quantum field theory [1–4]. They describe spinless particles and from an algebraic point of view they are relatively simple. Gauge bosons and fermions, which are more complicated on account of their polarization and spin degrees of freedom, will be treated in later chapters. More important than the educational value of scalar theories is their role in the electroweak theory, in which a doublet of scalar fields interact with the fields of leptons, quarks and gauge bosons. If we neglect these interactions then we obtain a self-interacting ϕ^4-theory for the scalars.

This subsector of the standard model, the *Higgs sector*, probably defines a non-interacting quantum field theory. It is known that in *more than four dimensions* the removal of the *UV*-cutoff of the regularized ϕ^4-theory leads to a non-interacting theory for scalar fields [5, 6]. There are arguments that this applies to scalar theories in four dimensions as well. In contrast, in less than four dimensions we end up with an interacting field theory. The triviality of the Higgs sector might very well be responsible for the electroweak gauge theory being only an effective theory below a cutoff Λ. This conclusion would not apply if there were a non-Gaussian fixed point. A non-Gaussian fixed point has been intensively searched after in lattice simulations—so far without success. If we accept the idea of a "trivial" standard model, the question about the value of the cutoff Λ arises. The answer to this question depends on the mass of the Higgs particle.

Scalar fields play a pivotal role in many inflationary cosmological scenarios. They could be responsible for the anticipated exponential expansion of the early universe, could trigger various phase transitions and, last not least, their quantum fluctuations could contribute to the structures observed in the cosmic microwave background radiation [7, 8].

5.1 Quantization

This chapter is devoted to scalar field theories in d space-time dimensions. In a given inertial frame we identify an event with its coordinates $x = (x^\mu) = (ct, \mathbf{x})$

A. Wipf, *Statistical Approach to Quantum Field Theory*, Lecture Notes in Physics 864,
DOI 10.1007/978-3-642-33105-3_5,

in $\mathbb{R}^d$. A real scalar field assigns to each space-time point x a real number,

$$\phi : \mathbb{R}^d \to \mathbb{R}, \qquad x \to \phi(x). \tag{5.1}$$

It satisfies a covariant field equation which is the *Euler–Lagrange equation*

$$\frac{\delta S}{\delta \phi(x)} = 0 \quad \Longrightarrow \quad \partial_\mu \frac{\partial \mathscr{L}}{\partial(\partial_\mu \phi(x))} - \frac{\partial \mathscr{L}}{\partial \phi(x)} \tag{5.2}$$

of a Poincaré-invariant classical action

$$S[\phi] = \int \mathrm{d}^d x \, \mathscr{L}(\phi, \partial_\mu \phi) = \int \mathrm{d}^d x \left(\frac{1}{2} \partial_\mu \phi \partial^\mu \phi - V(\phi) \right).$$

For a non-interacting field $V(\phi) = \frac{1}{2} m^2 \phi^2$ and the scalar field fulfills the linear *Klein–Gordon equation* $(\Box + m^2)\, \phi = 0$, with m representing the particle mass.

To quantize the scalar field we apply the well-known quantization rules of quantum mechanics to a system with infinitely many degrees of freedom. The quantum mechanical results can be generalized according to the substitutions

$$q_i(t) \equiv q(t, i) \to \phi(t, \mathbf{x}) = \phi(x) \quad \text{and} \quad \sum_i \to \int \mathrm{d}^{d-1} x. \tag{5.3}$$

For example, the classical field at $\mathbf{x}$ becomes a position-dependent operator $\hat{\phi}(\mathbf{x})$—one operator at every point $\mathbf{x}$—the time dependence of which is determined by the Heisenberg equation.

With these substitution rules we obtain the following (formal) functional integral representation for vacuum expectation values of time-ordered products of field operators:

$$\langle 0 | T \hat{\phi}(x_1) \cdots \hat{\phi}(x_n) | 0 \rangle = \frac{1}{Z} \int \mathscr{D}\phi \, \phi(x_1) \cdots \phi(x_n) \, \mathrm{e}^{\mathrm{i} S[\phi]/\hbar}. \tag{5.4}$$

The symbol $\int \mathscr{D}\phi$ means integration over all scalar fields ϕ. In particular, a one-dimensional field theory for $\phi \equiv q : \mathbb{R} \to \mathbb{R}$ describes a quantum mechanical system. The normalization factor Z in (5.4) represents the vacuum–vacuum amplitude

$$Z = \int \mathscr{D}\phi \mathrm{e}^{\mathrm{i} S[\phi]/\hbar}.$$

Similarly as in quantum mechanics at imaginary time one introduces the Euclidean field operator

$$\hat{\phi}_E(x) \equiv \hat{\phi}_E(\tau, \mathbf{x}) = \mathrm{e}^{\tau \hat{H}} \hat{\phi}(0, \mathbf{x}) \mathrm{e}^{-\tau \hat{H}}, \quad x = (\tau, \mathbf{x}) = \left(-i x^0, \mathbf{x}\right) \tag{5.5}$$

and shows that vacuum expectation values of time-ordered products of such operators have the formal functional integral representations

$$\langle 0 | T \hat{\phi}_E(x_1) \cdots \hat{\phi}_E(x_n) | 0 \rangle = \frac{1}{Z} \int \mathscr{D}\phi \phi(x_1) \cdots \phi(x_n) \mathrm{e}^{-S_\mathrm{E}[\phi]/\hbar}, \tag{5.6}$$

where S_{E} denotes the Euclidean action. These expectation values are the *Schwinger functions* $S_n(x_1, \ldots, x_n)$ and should have the following properties [9–11].

1. *Euclidean covariance:* The S_n are invariant (covariant for fields with spin) under translations and Euclidean "Lorentz-transformations" $x_i \to Rx_i + a$, with R an orthogonal transformation in $\mathbb{R}^d$.
2. *Reflection positivity:* Pick test functions $f_n(x_1, \ldots, x_n)$ with support in the "time-ordered" subsets $0 < \tau_1 < \cdots < \tau_n$. Choose one such f_n for each positive n. Given a point x, let $\bar{x}$ be the reflected point about the $\tau = 0$ hyperplane. Then,

$$\sum_{m,n \le N} \int d^d x_1 \cdots d^d x_m \, d^d y_1 \cdots d^d y_n S_{m+n}(x_1, \ldots, x_m, y_1, \ldots, y_n) \times f_m(\bar{x}_1, \ldots, \bar{x}_m)^* f_n(y_1, \ldots, y_n) \ge 0, \tag{5.7}$$

   where * represents complex conjugation. This property reflects the positivity of the Hilbert space in quantum theory.
3. *Permutation symmetry:* The S_n are symmetric functions of their arguments. This property replaces the locality property in Minkowski space-time.
4. *Cluster property:* If there is a unique vacuum state then the S_n cluster,

$$S_{m+n}(x_1, \ldots, x_m, y_1 + a, \ldots, y_n + a) \xrightarrow{|a| \to \infty} S_m(x_1, \ldots, x_m) S_n(y_1, \ldots, y_n). \tag{5.8}$$

5. *Regularity:* There are different versions of regularity, see [9–11].

Slightly stronger axioms based on measure theory have been formulated in [12].

These Euclidean axioms are due to K. OSTERWALDER and R. SCHRADER and they have significance for the analytically continued Minkowski space quantum fields: one can reconstruct a Minkowski space quantum field theory by assuming these axioms for the Schwinger functions. The vacuum expectation values of products of field operators in Minkowski space are called *Wightman functions* W_n. Thanks to the Euclidean axioms the Euclidean Schwinger functions S_n can be analytically continued to the corresponding Wightman functions, which possess all properties of a relativistic Hilbert-space theory.

5.2 Scalar Field Theory at Finite Temperature

Similarly as in quantum mechanics one argues that thermal expectation values of time-ordered products of Euclidean field operators have the following Euclidean functional integral representations:

$$\begin{aligned} \left\langle T\hat{\phi}_E(x_1) \cdots \hat{\phi}_E(x_n) \right\rangle_\beta &= \frac{1}{Z(\beta)} \operatorname{tr} \mathrm{e}^{-\beta \hat{H}} T\hat{\phi}_E(x_1) \cdots \hat{\phi}_E(x_n) \\ &= \frac{1}{Z(\beta)} \oint \mathscr{D}\phi \, \phi(x_1) \cdots \phi(x_n) \, \mathrm{e}^{-S_{\mathrm{E}}[\phi]/\hbar}, \end{aligned} \tag{5.9}$$

where β denotes the inverse temperature and $S_{\rm E}$ the Euclidean action. We thereby integrate over β-periodic fields, $\phi(\tau+\beta,\mathbf{x})=\phi(\tau,\mathbf{x})$. In the zero-temperature limit $\beta\to\infty$ we integrate over all fields and thus recover the vacuum expectation values given by the *Schwinger functions*. But at finite temperature we integrate only over β-periodic configurations as indicated by the circle on the integration symbol [18–22].

The normalization factor in (5.9) is simply the *partition function*

$$Z(\beta)=\mathrm{e}^{-\beta F}=\oint\mathscr{D}\phi\,\mathrm{e}^{-S_{\rm E}[\phi]/\hbar}, \tag{5.10}$$

the logarithm of which is proportional to the *free energy density* $f=F/V$, an important quantity in quantum statistics. The thermal expectation values (5.9) are generated by the partition function in presence of an external source,

$$Z[\beta,j]=\oint\mathscr{D}\phi\,\mathrm{e}^{-S_{\rm E}[\phi]+\int j(x)\phi(x)}\equiv\mathrm{e}^{W[\beta,j]} \tag{5.11}$$

as follows:

$$\left\langle T\hat{\phi}_E(x_1)\ldots\hat{\phi}_E(x_n)\right\rangle_\beta=\frac{1}{Z[\beta,0]}\frac{\delta^n Z[\beta,j]}{\delta j(x_1)\cdots\delta j(x_n)}\bigg|_{j=0}. \tag{5.12}$$

In contrast, the *connected thermal correlation functions*

$$\left\langle T\hat{\phi}_E(x_1)\ldots\hat{\phi}_E(x_n)\right\rangle_{c,\beta}=\frac{\delta^n W[\beta,j]}{\delta j(x_1)\cdots\delta j(x_n)}\bigg|_{j=0} \tag{5.13}$$

are generated by the functional $W[\beta,j]$ defined in (5.11), which is proportional to the free energy in presence of an external source. At zero temperatures it becomes the *Schwinger functional* $W[j]$, which generates all the connected vacuum expectation values

$$\langle 0|T\hat{\phi}_E(x_1)\ldots\hat{\phi}_E(x_n)|0\rangle_c=\frac{\delta^n W[j]}{\delta j(x_1)\cdots\delta j(x_n)}\bigg|_{j=0}. \tag{5.14}$$

For non-interacting particles the generating functionals at finite temperature can be calculated in closed forms.

5.2.1 Free Scalar Field

The Euclidean action of the free scalar field is quadratic,

$$S_{\rm E,0}[\phi]=\frac{1}{2}\int\mathrm{d}^dx\left(\nabla\phi\cdot\nabla\phi+m^2\phi^2\right)=\frac{1}{2}\int\mathrm{d}^dx\,\phi\left(-\Delta+m^2\right)\phi, \tag{5.15}$$

and the functional integral in (5.11) is Gaussian. Integrating over β-periodic fields yields the generating functional in closed form,

$$Z[\beta, j] = \frac{\text{const}}{\det{}^{1/2}(-\Delta + m^2)} \exp\left(\frac{1}{2}\int \mathrm{d}^d x\, \mathrm{d}^d y\, j(x)\, S_\beta(x-y)\, j(y)\right), \quad (5.16)$$

with the *thermal propagator* in position space

$$S_\beta(x-y) = \left\langle T\hat{\phi}_E(x)\hat{\phi}_E(y)\right\rangle_\beta = \langle x|\frac{1}{-\Delta + m^2}|y\rangle_\beta. \quad (5.17)$$

Its Fourier representation

$$S_\beta(x) = \frac{1}{\beta}\sum_n \int \frac{\mathrm{d}^3 k}{(2\pi)^3} \frac{\mathrm{e}^{-\mathrm{i}\omega_n x^0 - i\mathbf{k}\mathbf{x}}}{\omega_n^2 + \mathbf{k}^2 + m^2}, \quad \omega_n = \frac{2\pi}{\beta} n \quad (5.18)$$

contains a sum over n and an integral over the spatial momenta. The sum originates from the periodicity conditions for the fields at finite temperature. In the limit of very low temperatures the *Matsubara frequencies* ω_n are dense and the Riemann sum turns into a Riemann integral. Thus in the limit $T \to 0$ the function $S_\beta(x)$ approaches the Euclidean propagator

$$S(x) = \lim_{\beta\to\infty} S_\beta(x) = \int \frac{\mathrm{d}^4 k}{(2\pi)^4} \frac{\mathrm{e}^{-\mathrm{i}kx}}{k^2 + m^2}. \quad (5.19)$$

The quadratic action $S_{\mathrm{E},0}[\phi]$ in (5.15) contains the linear operator

$$A = -\Delta + m^2, \quad (5.20)$$

and the corresponding Gaussian functional integral for the partition function (5.10) yields the square root of $1/\det A$, see (5.16), such that the free energy reads

$$F(\beta) = -\frac{\ln Z(\beta)}{\beta} = \frac{1}{2\beta}\log\det A + \text{const}. \quad (5.21)$$

The differential operator A acts on β-periodic functions and the temperature dependence of its eigenvalues and determinant originates from these boundary conditions.

Determinants of differential operators—*functional determinants*—play a prominent role in theoretical and mathematical physics. They appear in a variety of investigations in quantum field theory, for example in tunneling and semiclassical physics, self-consistent Hartree–Fock and Schwinger–Dyson equations or lattice field theories with dynamical fermions to mention a few. Therefore we pause here and have a closer look at functional determinants.

Zeta-Function Regularization As a first simplification we enclose the system in a finite box in order to find *discrete eigenvalues* $\{\lambda_n\}$ of A. We assume that the

eigenvalues are positive—as happens for the particular operator in (5.20). Following [13, 14] we define the ζ-function of A:

$$\zeta_A(s) = \sum_n \lambda_n^{-s}. \tag{5.22}$$

For sufficiently large $\Re(s)$ the spectral sums converge and define an analytic function which can be analytically continued as meromorphic function on the entire complex s-plane [15]. For example, the operator

$$A = -\frac{\mathrm{d}^2}{\mathrm{d}\varphi^2} + 1 \quad \text{on } L_2\big(S^1\big) \tag{5.23}$$

has double degenerate eigenvalues $1^2, 2^2, 3^2, 4^2, \ldots$ and its zeta-function is given by Riemann's celebrated zeta-function,

$$\zeta_R(A) = 2\sum_{n=1}^{\infty} \frac{1}{n^{2s}} = 2\zeta_R(2s). \tag{5.24}$$

The spectral sums converge for $\Re(s) > 1/2$ and their analytic continuation is given by Riemann's zeta-function. The spectral sums for the operator in (5.20) converge for $\Re(s) > d/2$ and define a meromorphic function on the complex s-plane. More generally, with the help of Weyl's formula for the distribution of large eigenvalues [16] one can show that for a second order elliptic operator on a finite domain the sum (5.22) converges for all s with $\Re(s) > d/2$.

For a finite-dimensional matrix A the sum (5.22) exists for all s and with

$$\frac{\mathrm{d}\lambda_n^{-s}}{\mathrm{d}s} = -\lambda_n^{-s}\log(\lambda_n)$$

one finds the useful formula

$$-\frac{\mathrm{d}\zeta_A(s)}{\mathrm{d}s}\bigg|_{s=0} = \sum_n \log\lambda_n = \operatorname{tr}\log A = \log\det A. \tag{5.25}$$

Now we *define* the determinant of an infinite-dimensional matrix, i.e. differential operator, by this formula. For any (elliptic) differential operator the ζ-function is regular at $s = 0$ such that the left hand side in this formula is well-defined. The analytic continuation of the spectral sum to s-values where the sum diverges corresponds to a particular renormalization of functional determinants—the so-called zeta-function regularization. We refer to [17] where the connection to other renormalizations is discussed.

Heat Kernel of a Differential Operator Now we explore the intimate relation between the ζ-function and heat kernel of an elliptic differential operator A. They

are related by a *Mellin transformation*:

$$\zeta_A(s) = \sum_n \frac{1}{\Gamma(s)} \int_0^\infty \mathrm{d}t\, t^{s-1} \mathrm{e}^{-t\lambda_n} = \frac{1}{\Gamma(s)} \int_0^\infty \mathrm{d}t\, t^{s-1}\, \mathrm{tr}\big(\mathrm{e}^{-tA}\big). \tag{5.26}$$

If A were the Hamiltonian of a physical system, the trace of $K(t) = \exp(-tA)$ would be the partition function of that system at inverse temperature $\beta = t$. This explains why the integral kernel $K(t; x, y)$ of $K(t)$ is called a heat kernel. Clearly, the last trace in (5.26) is the integral of $K(t, x, x)$ over space such that

$$\zeta_A(s) = \frac{1}{\Gamma(s)} \int_0^\infty \mathrm{d}t\, t^{s-1} \int \mathrm{d}x\, K(t; x, x). \tag{5.27}$$

In position space the heat kernel fulfills the differential equation

$$\frac{\partial}{\partial t} K(t; x, y) = -A_x K(t; x, y) \quad \text{with } \lim_{t\to 0} K(t; x, y) = \delta(x - y). \tag{5.28}$$

To calculate the determinant of A one proceeds as follows:

1. Construct the unique solution of the initial value problem (5.28) for $x = y$.
2. Insert the solution $K(t, x, x)$ into the representation (5.27) of the ζ-function.
3. Calculate the determinant with the help of formula (5.25).

However, this approach meets several problems: For many operators, for example wave operators in inhomogeneous background fields, one cannot calculate the kernel on the diagonal $K(t, x, x)$ in closed form. Furthermore, the s-integral in (5.27) only exists for sufficiently large $\Re(s)$. Thus we need the analytic continuation of the zeta-function, which even for large $\Re(s)$ is not known analytically. Only for simple systems can one compute the heat kernel explicitly and construct the analytic continuation, for example by a Poisson resummation. However, what is needed is not the zeta-function itself, but its derivative at the origin. Unlike ζ, this quantity is computable for many interesting systems. We refer to the book [15] for further facts about the zeta-function method and the review [23, 24] for an introduction to the theory of heat kernels and their small-t expansions. In [25, 26] the zeta-function is used to calculate Casimir energies, in [27] the regularization is applied to compute the fermionic path integral in the massless Schwinger model in all topological sectors and in [28] it is used to find multi-instanton determinants in 4-dimensional Yang–Mills theories.

Free Energy of Non-interacting Scalars Let us return to the simple operator $A = -\Delta + m^2$, which defines the Euclidean action for free scalars. Since $-\Delta$ is the Schrödinger operator of a free particle we may use the result (2.42) and obtain

$$K\big(t; x, x'\big) = \frac{\mathrm{e}^{-m^2 t}}{(4\pi t)^{d/2}} \sum_{n\in\mathbb{Z}} \mathrm{e}^{-\{(\tau-\tau'+n\beta)^2 + (\mathbf{x}-\mathbf{x}')^2\}/4t}, \quad x = (\tau, \mathbf{x}). \tag{5.29}$$

The contribution with $n = 0$ corresponds to the heat kernel (Euclidean propagator) in $\mathbb{R}^d$. The summation over n enforces periodicity in imaginary time τ with period β and yields the heat kernel on the cylinder $[0, \beta] \times \mathbb{R}^{d-1}$. Inserting $K(t, x, x)$ into (5.27) we end up with the following integral representation of the ζ-function:

$$\zeta_A(s) = \frac{\beta V}{(4\pi)^{d/2}\Gamma(s)} \int \mathrm{d}t\, t^{s-1-d/2} \mathrm{e}^{-m^2 t} \sum_{n=-\infty}^{\infty} \mathrm{e}^{-n^2\beta^2/4t}. \tag{5.30}$$

The spectrum of the operator A on the cylinder is not discrete. This fact expresses itself by a harmless volume-divergence of the ζ-function. We get rid of this divergent factor through the transition to the free *energy density*. One finds the same energy density if ones encloses the particles in a finite box and let the box size tend to infinity.

Now we can do the t-integral via the integral representation

$$\int_0^\infty \mathrm{d}t\, t^a \mathrm{e}^{-bt-c/t} = 2\left(\frac{c}{b}\right)^{(a+1)/2} K_{a+1}(2\sqrt{bc}) \tag{5.31}$$

of the modified Bessel functions of second kind and obtain

$$\zeta_A(s) = \frac{\beta V}{(4\pi)^{d/2}} \frac{m^{d-2s}}{\Gamma(s)} \left(\Gamma\left(s - \frac{d}{2}\right) + 4 \sum_1^\infty \left(\frac{nm\beta}{2}\right)^{s-d/2} K_{d/2-s}(nm\beta) \right). \tag{5.32}$$

Here we introduced the Gamma function $\Gamma(s)$ with simple poles at $s = 0, -1, -2, \ldots$. Now we use the relations

$$\frac{\Gamma(s-2)}{\Gamma(s)} = \frac{1}{(s-1)(s-2)} \quad \text{and} \quad \frac{1}{\Gamma(s)} = s + O\left(s^2\right)$$

to find the explicit expression for the free energy density in four dimensions,

$$f(\beta) = -\frac{1}{2\beta V}\zeta_A'(0) = -\frac{m^4}{128\pi^2}\left(3 - 4\log\frac{m}{\mu} + 64 \sum_{n=1,2\ldots} \frac{K_2(nm\beta)}{(nm\beta)^2}\right). \tag{5.33}$$

Note that the density contains a scale parameter μ with the dimension of a mass. This parameter was introduced to rescale the operator A to a dimensionless operator A/μ^2 with dimensionless eigenvalues, zeta-function and determinant.

In order to obtain the free energy density for massless particles, we use $K_2(x) \sim 2/x^2$, so that

$$\lim_{m\to 0} f(\beta) = -\frac{T^4}{\pi^2}\zeta_R(4), \tag{5.34}$$

where the ubiquitous *Riemann zeta-function* $\zeta_R(s)$ occurs. For $\Re(s) > 1$ it has the simple series representation

$$\zeta_R(s) = \sum_{n=1}^\infty n^{-s}. \tag{5.35}$$

The function is regular in the whole complex plane, except for one simple pole with unit residue at $s = 1$, and it plays a pivotal role in the theory of primes. Some specific values of this function and its derivative are

$$\xi_R(0) = -\frac{1}{2}, \qquad \xi_R(2) = \frac{\pi^2}{6}, \qquad \xi_R(4) = \frac{\pi^4}{90} \quad \text{and} \quad \zeta_R'(0) = -\frac{1}{2}\log(2\pi). \tag{5.36}$$

Thus in the limit $m \to 0$ we obtain the following free energy density and the inner energy density for *scalar particles*:

$$f(\beta) = -\frac{\pi^2 T^4}{90} \quad \text{and} \quad u(\beta) = \partial_\beta(\beta f) = \frac{\pi^2 T^4}{30}. \tag{5.37}$$

The black-body radiation of photons with two polarizations has twice the free energy density of massless scalars.

High-Temperature Expansion To calculate the high-temperature expansion of the free energy density for massive scalars in (5.33) we need the small-x expansions of the series

$$I(\nu, x) = \sum_{n=1}^{\infty} \frac{K_\nu(nx)}{n^\nu}, \qquad \nu \equiv \frac{d}{2}, x \equiv m\beta. \tag{5.38}$$

These expansions have been determined in [29]. In particular in four space-time dimensions we need

$$I(2, x) = \frac{\pi^4}{45x^2} - \frac{\pi^2}{12} + \frac{\pi x}{6} + \frac{x^2}{16}\log\frac{x}{4\pi} - \frac{x^2}{32}\left(\frac{3}{2} - 2\gamma\right) + O\left(x^4\right). \tag{5.39}$$

This leads to the following high-temperature expansion of the energy density:

$$f(\beta) = -\frac{\pi^2 T^4}{90} + \frac{m^2 T^2}{24} - \frac{m^3 T}{12\pi} - \frac{\gamma m^4}{32\pi^2} + \frac{m^4}{32\pi^2}\log\left(\frac{4\pi T}{\mu}\right) + O\left(\frac{m^2}{T^2}\right), \tag{5.40}$$

valid for $T \gg m$, with Euler's constant $\gamma \approx 0.5772$. The high-temperature expansion has been calculated with different regularizations in [18–20]. More details can be found in the textbooks [21, 22].

We may add a potential term to the action of the free field (5.15). This gives rise to the Euclidean action of a self-interacting scalar field

$$S_{\mathrm{E}} = S_{\mathrm{E},0} + \int \mathrm{d}^d x\, V(\phi). \tag{5.41}$$

Expanding the functional integrals (5.9) or (5.10) in powers of the interaction potential V leads to a series expansion for thermal expectation values of time-ordered products of field operators. One can use the *zero-temperature* Feynman rules to calculate the terms in this expansion if one only uses the finite-temperature propagator and replaces each k^0-integral by the sum over Matsubara frequencies [18–22].

5.3 Schwinger Function and Effective Potential

Effective potentials are very often used in the study of phases or phase transitions in physical systems with an order parameter. In field theory, the effective potential is the Legendre transform of the thermal Schwinger function,[1] which is just the Schwinger functional density for a homogeneous source j. In other words, it is the effective action density for a homogeneous field. In statistical physics the thermal Schwinger function corresponds to the free energy density in the presence of an external source, for example a constant magnetic field. One can consider alternatives to this "conventional" effective potential, e.g. the *constraint effective potential* [30], which will be introduced in Chap. 7. The partition function in presence of an external *homogeneous* source j has the functional integral representation [18–20]

$$Z(\beta, j) \equiv \mathrm{e}^{\beta V w(\beta, j)} = C \oint \mathscr{D}\phi \exp\Big(-S_{\mathrm{E}}[\phi] + j \int_0^\beta \mathrm{d}^d x\, \phi(x)\Big), \tag{5.42}$$

where one integrates over β-periodic fields, i.e. fields on the cylinder $[0, \beta] \times V$ over the spatial region V. We denote the spatial region and its volume both by V. Except for the geometric factor βV, the *thermal Schwinger function* $w(\beta, j)$ is equal to the Schwinger functional W in (5.11) with constant source. We can identify the thermal Schwinger function with the negative free energy density of the system with shifted Hamiltonian $\hat{H}_j = \hat{H} - (j, \hat{\phi})$. At low temperatures it converges to the negative ground state energy density $-E_0(j)/V$ of the system with shifted Hamiltonian.

From $w(\beta, j)$ we can calculate the mean of the spatial averaged field in the presence of the source,

$$\frac{\mathrm{d}w}{\mathrm{d}j} = \frac{\oint \mathscr{D}\phi\, M\, \mathrm{e}^{-S_{\mathrm{E}}[\phi] + j \int \phi}}{\oint \mathscr{D}\phi\, \mathrm{e}^{-S_{\mathrm{E}}[\phi] + j \int \phi}} = \langle M \rangle_j, \quad M = \frac{1}{\beta V} \int \phi(x). \tag{5.43}$$

A constant source is compatible with translational invariance of the system such that for periodic boundary conditions $\langle \phi(x) \rangle_j$ is independent of x. Hence we have

$$\big\langle \phi(x) \big\rangle_j = \frac{\mathrm{d}w}{\mathrm{d}j}. \tag{5.44}$$

One should keep in mind that expectation values depend on the external source. Also note that the formula (5.43) cannot be used at points where w is not differentiable.

The thermal Schwinger function is strictly convex, because its second derivative is equal to the expectation value of a positive quantity:

$$\frac{\mathrm{d}^2 w}{\mathrm{d}j^2} = \beta V \big\langle \big(M - \langle M \rangle\big)^2 \big\rangle. \tag{5.45}$$

[1] This should not be confused with the n-point Schwinger functions at zero temperature.

Now we define the finite-temperature *effective potential* u as the *Legendre transform* of the thermal Schwinger function,

$$u(\beta, \varphi) = (\mathscr{L} w)(\varphi) = \sup_j \big(j\varphi - w(\beta, j) \big). \tag{5.46}$$

The maximizing source j is conjugate to φ. The latter is an averaged macroscopic field, in contrast to the microscopic field ϕ entering the functional integral. If the minimum φ_0 of u is not degenerate then it is equal to the expectation value of the field operator:

$$u(\beta, \varphi_0) \leq u(\beta, \varphi), \quad \forall \varphi \Longleftrightarrow \varphi_0 = \big\langle \hat{\phi}(x) \big\rangle_{j=0}. \tag{5.47}$$

For a differentiable u this follows from the second result in (5.55).

Generalizations Both in fundamental and applied physics one is interested in how quantum systems react to a change of external conditions. A prominent example is the Casimir effect [31], which has been measured to great accuracy [32, 33] and which shows how the vacuum energy of a quantum field changes when one moves the walls of the enclosing cavity [34, 35]. In a more general setting one may ask the question how the vacuum structure of an Euclidean scalar field theory with Lagrangian density

$$\mathscr{L}\big(\phi(x)\big) = \int_\Omega \mathrm{d}^d x \left\{ \frac{1}{2} \nabla\phi(x) \nabla\phi(x) + V\big(\phi(x)\big) \right\} \tag{5.48}$$

depends on the geometry of the quantization region Ω, which does not need be a cylinder as in thermal field theory, and on the boundary conditions imposed at the boundary $\partial\Omega$ of Ω [36, 37]. In the *linear sigma models* the field ϕ takes its values in a linear space and transforms non-trivially under a global inner symmetry group. In *non-linear sigma models* the components of ϕ are coordinates of a target-manifold, for example a Lie group or a homogeneous space [38].

The "classical ground state" corresponds to a homogeneous field, which minimizes the potential V. For most systems it is not equal to the quantum mechanical expectation value $\langle \hat{\phi}(x) \rangle$ of the quantum field in Ω. In order to study the quantum corrections to the classical vacuum, one introduces a generalized Schwinger function w on the (Euclidean) space-time region Ω according to

$$Z(\Omega, j) = \int \mathscr{D}\phi \exp\left(-S_{\mathrm{E}}[\phi] + j \int_\Omega \phi(x) \right) = \mathrm{e}^{\Omega w(\Omega, j)}. \tag{5.49}$$

In non-linear sigma models the coupling to the source may look differently. Analogously as in thermal field theory one defines the effective potential $u(\Omega, \varphi)$ as Legendre transform of the Schwinger function.

5.3.1 The Legendre–Frenchel Transformation

The Legendre(–Frenchel) transformation (5.46) shows up in mechanics, thermodynamics, statistical mechanics as well as quantum field theory. In this section we shall collect some relevant properties of this transform. Related and more results are found in [39–41]. Let φ and j be elements of a convex set in $\mathbb{R}^d$.

Corollary 5.1 *The Legendre transform of a* (*for sufficiently large enough arguments*) *convex function is always convex.*

The proof is seen by considering the interpolating field between φ_1 and φ_2,

$$\varphi_\alpha = (1-\alpha)\varphi_1 + \alpha\varphi_2, \quad 0 \le \alpha \le 1. \tag{5.50}$$

Since the supremum of a sum is smaller or equal to the sum of the suprema of each summand we have

$$\begin{aligned} u(\varphi_\alpha) &= \sup_j \big\{(1-\alpha)(j,\varphi_1) + \alpha(j,\varphi_2) - \big((1-\alpha)+\alpha\big)w(j)\big\} \\ &\le (1-\alpha)\sup_j\big\{(j,\varphi_1) - w(j)\big\} + \alpha\sup_j\big\{(j,\varphi_2) - w(j)\big\} \\ &= (1-\alpha)u(\varphi_1) + \alpha u(\varphi_2), \end{aligned} \tag{5.51}$$

such that the graph of u lies below the line connecting the points $(\varphi_i, u(\varphi_i))$. This proves the convexity of u.

Corollary 5.2 *The Legendre transformation is involutive*[2] *for convex functions.*

For every point $(j_0, w(j_0))$ on a convex w we can find a hyperplane below the graph of w. Hence, we find a j_0 that depends on φ_0, so that

$$w(j_0) + (\varphi_0, j - j_0) \le w(j) \quad \text{for all } j,$$

or equivalently

$$(\varphi_0, j) - w(j) \le (\varphi_0, j_0) - w(j_0) \quad \text{for all } j.$$

The supremum of the left hand side with respect to j is the Legendre transform $\mathscr{L}w$ at the point φ_0. The resulting inequality can be written as

$$w(j_0) \le (\varphi_0, j_0) - (\mathscr{L}w)(\varphi_0). \tag{5.52}$$

[2]This means that its square is the identity, i.e. if a the Legendre transform takes f to g, then the Legendre transform of g will be f.

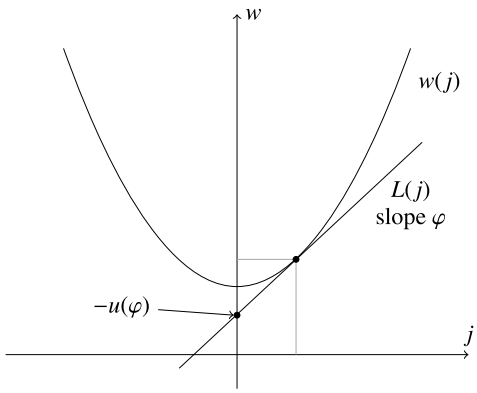

Fig. 5.1 Graphical construction of the Legendre transformation $u(\varphi)$ of a function $w(j)$ $L(j)$ is a linear function of j with slope φ touching the graph of w

The right hand side is the Legendre transform of $(\mathscr{L}w)(\varphi_0)$ and we conclude that $w(j_0)$ is *bounded from above* by $(\mathscr{L}^2 w)(j_0)$. On the other hand, from the very definition of the Legendre transformation it is clear that

$$(\mathscr{L}w)(\varphi) \geq (\varphi, j) - w(j) \quad \text{for all } \varphi \Longrightarrow w(j) \geq (\varphi, j) - (\mathscr{L}w)(\varphi). \tag{5.53}$$

Taking the supremum with respect to φ in the last inequality we see that $w(j)$ is *bounded from below* by $(\mathscr{L}^2 w)(j)$. The two bounds imply that the Legendre transformation is involutive or in other words that $(\mathscr{L}^2 w)(j) = w(j)$.

Corollary 5.3 (Fenchel/Young inequality) *For arbitrary φ and j the inequality*

$$w(j) + u(\varphi) \geq (j, \varphi), \quad u = \mathscr{L}w \tag{5.54}$$

holds true. The inequality becomes an equality if φ and j are conjugate.

This inequality results directly from the inequality (5.53).

Corollary 5.4 *If the continuous Schwinger function shows a cusp then $u = \mathscr{L}w$ has a plateau. In case of a one-component field the width of the plateau is equal to the jump of the slope of w across the cusp. Inversely, a plateau is mapped into a cusp.*

This property follows from the graphical construction of the Legendre transformation as illustrated in Fig. 5.1. The Legendre transform $u(\varphi)$ is $-L(0)$, where $L(j)$ is the linear function with slope φ and tangent to $w(j)$. For a given φ and a convex and *differentiable* w, the conjugate source is defined by the requirement that $L(j)$ defines the hyperplane tangent to the graph of w at the point $(j, w(j))$.

Figure 5.2 illustrates a typical situation for a system which shows spontaneous symmetry breaking. The Schwinger function has a cusp for vanishing source and the effective potential u has a plateau.

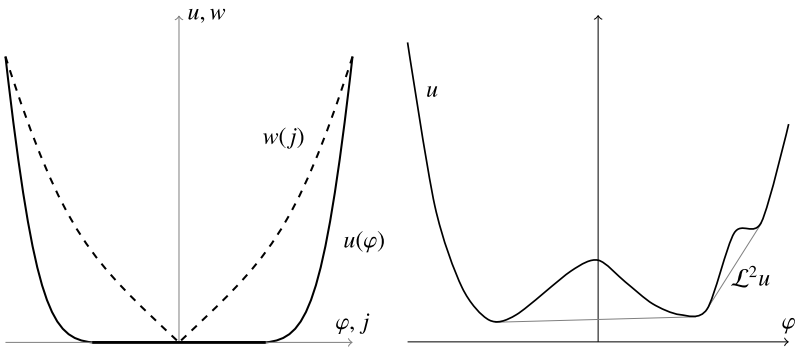

Fig. 5.2 *Left panel*: the Legendre transformation maps cusps to plateaus and plateaus to cusps. *Right panel*: the twofold application of a Legendre transformation produces the convex envelope

Corollary 5.5 *The twofold Legendre transform of a for sufficiently large enough arguments convex function is the convex envelope of this function.*

This corollary results from the previously discussed properties of Legendre transformation and is illustrated in Fig. 5.2.

Corollary 5.6 *Let w and u be differentiable functions. Then the conjugate variables j and ϕ are related according to*

$$\varphi = w'(j) \quad \textit{and} \quad j = u'(\varphi). \tag{5.55}$$

Substituting (j, φ) by $(p, \dot{x})$ and (w, u) by (H, L) this is the well-known Legendre transformation in analytical mechanics. It describes the transition from the Hamiltonian to the Lagrangian formulation.

Defining the rescaled function of a function f according to

$$f_\alpha(x) = \alpha f\left(\frac{x}{\alpha^{1/2}}\right), \quad \alpha > 0, \tag{5.56}$$

it is not difficult to show the

Corollary 5.7 *If u is the Legendre transform of w, then u_α is the Legendre transform of w_α.*

The Legendre transform of the monomial with exponent $\alpha > 1$ is equal to the monomial with the dual exponent β,

$$w(j) = \frac{1}{\alpha}|j|^\alpha \quad \Longleftrightarrow \quad u(\varphi) = \frac{1}{\beta}|\varphi|^\beta, \quad \text{with } \frac{1}{\alpha} + \frac{1}{\beta} = 1. \tag{5.57}$$

With increasing exponent β the function u develops a plateau from -1 to 1. The exponent of the transformed function w approaches one such that it converges to the piecewise linear function $w(j) = |j|$.

Corollary 5.8 *If $w''(j)$ and $u''(j)$ are the matrices of the second derivatives of w and u, then the following identity holds*:

$$w''(j)\,u''(\varphi) = \mathbb{1}, \quad (j, \varphi) \text{ dual}. \tag{5.58}$$

Thus the second derivatives of a function and its Legendre transform are inverse to each other.

This property follows directly from the relations

$$\frac{\partial^2 w}{\partial j_r \partial j_s} = \frac{\partial \varphi_r}{\partial j_s} \quad \text{and} \quad \frac{\partial^2 u}{\partial \varphi_r \partial \varphi_s} = \frac{\partial j_r}{\partial \varphi_s}.$$

In passing we note how the Legendre transformation acts on translated and inverted functions. We obtain

$$\begin{aligned} w(j) = w_1(j) + b \quad &\Rightarrow \quad (\mathscr{L}w)(\varphi) = (\mathscr{L}w_1)(\varphi) - b, \\ w(j) = w_1(j + k) \quad &\Rightarrow \quad (\mathscr{L}w)(\varphi) = (\mathscr{L}w_1)(\varphi) - \varphi \cdot k, \\ w(j) = w_1^{-1}(j) \quad &\Rightarrow \quad (\mathscr{L}w)(\varphi) = -\varphi \cdot (\mathscr{L}w_1)\left(\frac{1}{\varphi}\right). \end{aligned} \tag{5.59}$$

5.4 Scalar Field on a Space-Time Lattice

In a lattice regularization of functional integrals one first discretizes the Euclidean space $\mathbb{R}^d$ by an d-dimensional lattice Λ. Since the lattice constant a defines a minimal length this regulates the quantum field theory at short distances. In a second step one assumes that the lattice Λ is finite. Since the size of the system defines a maximal length this regulates the quantum field theory at long distances. On a finite lattice the formal functional integral (5.9) turns into a well-defined finite-dimensional integral which can be dealt with by the methods of statistical mechanics. To simplify matters we consider a *hyper-cubic lattice*. The lattice points $x \in \Lambda$ have coordinates

$$x^\mu = a\,n^\mu \quad \text{with } n^\mu \in \mathbb{Z}, \tag{5.60}$$

and the extent of the lattice in direction μ is $L_\mu = aN_\mu$, see Fig. 5.3. Typically we impose periodic boundary conditions and thus identify the lattice points $x = (x^1, \ldots, x^\mu, \ldots, x^d)$ and $x' = (x^1, \ldots, x^\mu + L_\mu, \ldots, x^d)$. With this identification the lattice becomes a discretized torus. A scalar field on the lattice defines a map

$$\Lambda \ni x \to \phi_x \in \mathscr{T} \tag{5.61}$$

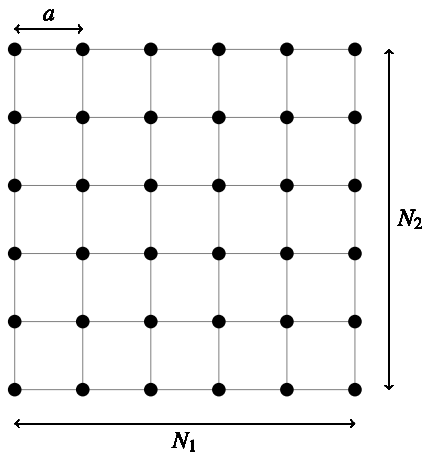

Fig. 5.3 The lattice is characterized by the number of lattice points $N_1 \times N_2 \times \cdots \times N_d$ as well as the lattice constant a. A scalar field is defined on the lattice points

from Λ into the *target space* $\mathscr{T}$. For a real field the target space is $\mathscr{T} = \mathbb{R}$ and in the standard model of the electroweak interaction $\mathscr{T} = \mathbb{C}^2$. Sigma models have a manifold as target space and for Ising-like spin models $\mathscr{T}$ is a finite group.

Boundary Conditions To specify the lattice model we must prescribe the *boundary conditions* for the scalar field. These conditions are classified as follows:

- *Periodic boundary conditions:* With these conditions the lattice is a discrete torus and the lattice field theory is invariant under discrete translations and rotations.
- *Fixed boundary conditions:* Here we prescribe the field on the boundary $\phi|_{\partial\Lambda}$. Such boundary conditions are useful to describe entangled states in quantum field theory.
- *Open boundary conditions:* Here we switch off all interactions between sites on the lattice Λ with sites in the complement of Λ (viewed as subset of $\mathbb{Z}^d$). These boundary conditions are used in solid state physics.
- *Antiperiodic boundary conditions:* They serve as a tool to inhibit unwanted long-range correlations or to study interfaces. This modification of the periodic boundary conditions is frequently used in lattice field theories.

In the remaining part of this chapter we will consider non-interacting scalar fields subject to periodic boundary conditions.

Let us consider the free Klein–Gordon field with target space $\mathscr{T} = \mathbb{R}$. We need to approximate the continuum action (5.15) by an action for the lattice field. We thereby substitute the integral by a Riemann sum according to

$$\int \mathrm{d}^d x \cdots \to a^d \sum \cdots \tag{5.62}$$

and replace differentials by differences. Note that we are free in the choice of the lattice derivative. One often chooses the *forward derivative* or *backward derivative*

$$(\partial_\mu \phi)(x) = \frac{\phi_{x+ae_\mu} - \phi_x}{a} \quad \text{or} \quad (\partial_\mu \phi)(x) = \frac{\phi_x - \phi_{x-ae_\mu}}{a}. \tag{5.63}$$

In both cases the discretized action of the free scalar field is given by

$$\begin{aligned} S &= \frac{a^{d-2}}{2} \sum_{\langle x,y \rangle} (\phi_x - \phi_y)^2 + \frac{m^2 a^d}{2} \sum_x \phi_x^2 \\ &= \frac{a^{d-2}}{2} \big(2d + (am)^2\big) \sum_x \phi_x^2 - a^{d-2} \sum_{\langle x,y \rangle} \phi_x \phi_y, \end{aligned} \tag{5.64}$$

where the factor a^d results from the substitution (5.62) and the last sum includes all nearest-neighbor pairs $\langle x, y \rangle$.

Similar as in quantum mechanics we rescale dimensionful quantities with the appropriate power of the lattice constant in order to obtain dimensionless quantities. The dimensionless mass m_L and the dimensionless lattice field ϕ_L are

$$am = m_L \quad \text{and} \quad a^{(d-2)/2}\phi = \phi_L. \tag{5.65}$$

The rescaled distance between adjacent lattice points is one and the rescaled lattice-length in direction μ is $L_\mu = N_\mu$. The number of lattice points is given by $V = N_1 \cdots N_d$. In the following we suppress the index L.

The lattice action (5.64) defines a quadratic form of the field:

$$S = \frac{1}{2} \sum_{x,y \in \Lambda} \phi_x A_{xy} \phi_y, \quad A_{xy} = \big(m^2 + 2d\big)\delta_{xy} - \sum_{\mu=1}^{d} (\delta_{x,y+e_\mu} + \delta_{x,y-e_\mu}). \tag{5.66}$$

The symmetric matrix (A_{xy}) is thereby positive for a positive m^2. For a linear target space we regard the $\{\phi_x | x \in \Lambda\}$ as components of a vector. For a real field this vector-space is $\mathbb{R}^V$, equipped with the scalar product

$$(\phi, \chi) = \sum_{x \in \Lambda} \phi_x \chi_x. \tag{5.67}$$

The lattice action (5.66) can be rewritten as

$$S = \frac{1}{2}(\phi, A\phi) \quad \text{with } A = (A_{xy}), \tag{5.68}$$

and calculating the 2-point function (or propagator) of the free Euclidean theory reduces to the computation of the simple Gaussian integral

$$\langle \phi_x \phi_y \rangle = \frac{1}{Z} \int \mathscr{D}\phi \, \phi_x \phi_y \, \mathrm{e}^{-\frac{1}{2}(\phi, A\phi)}, \quad \mathscr{D}\phi = \prod_{x \in \Lambda} \mathrm{d}\phi_x \tag{5.69}$$

with the partition function

$$Z = \int \mathscr{D}\phi \, \mathrm{e}^{-\frac{1}{2}(\phi, A\phi)} = (2\pi)^{V/2} \det{}^{-1/2} A. \tag{5.70}$$

Such Gaussian integrals have already appeared in Chap. 2 from which we take the result

$$\langle \phi_x \phi_y \rangle = A^{-1}_{x,y} \equiv G(x, y) \tag{5.71}$$

for the propagator of the free lattice field. In order to calculate this propagator we determine the eigenfunctions and eigenvalues of the symmetric *Toeplitz matrix* A. Thereby we assume that Λ has the same extent N in all directions and hence has $V = N^d$ sites. The eigenvalues and eigenvectors depend on the boundary conditions for the scalar field. For periodic boundary conditions the translational invariant A in (5.66) is circulant and its V orthonormal eigenvectors ψ_p read

$$\psi_p(x) = \frac{1}{\sqrt{V}} \exp(\mathrm{i} px) \quad \text{with } px = \sum_{\mu=1}^{N} p_\mu x^\mu. \tag{5.72}$$

The allowed lattice momenta lie on the *dual lattice* Λ^* with elements

$$p_\mu = \frac{2\pi}{N} n_\mu \in \Lambda^*, \quad n_\mu \in \{1, 2, \ldots, N\}. \tag{5.73}$$

The corresponding V eigenvalues are

$$\lambda(p) = m^2 + 2d - 2\sum_\mu \cos(p_\mu) = m^2 + \hat{p}^2, \quad \hat{p}_\mu = 2 \sin \frac{p_\mu}{2}. \tag{5.74}$$

With these eigenvalues and eigenvectors we find the following spectral resolution of the propagator with V terms:

$$\langle \phi_x \phi_y \rangle = \sum \frac{\psi_p(x) \psi_p^\dagger(y)}{\lambda(p)} = \frac{1}{V} \sum_{\{p_\mu\}} \frac{\mathrm{e}^{\mathrm{i}p(x-y)}}{m^2 + \hat{p}^2}. \tag{5.75}$$

In case of different edge lengths $L_1, \ldots, L_d$ we have to substitute n_μ / L by n_μ / L_μ in the formula above. In the thermodynamic limit $N \to \infty$ the lattice momenta fill in the *Brillouin zone* $(0, 2\pi]^d$ and the Riemann sum

$$\langle \phi_x \phi_0 \rangle = \frac{1}{(2\pi)^d} \sum_{\{p_\mu\}} \Delta p_1 \cdots \Delta p_d \frac{\mathrm{e}^{\mathrm{i}px}}{m^2 + \hat{p}^2}$$

where $\Delta p_\mu = 2\pi / N$ tends to an integral over the Brillouin zone,

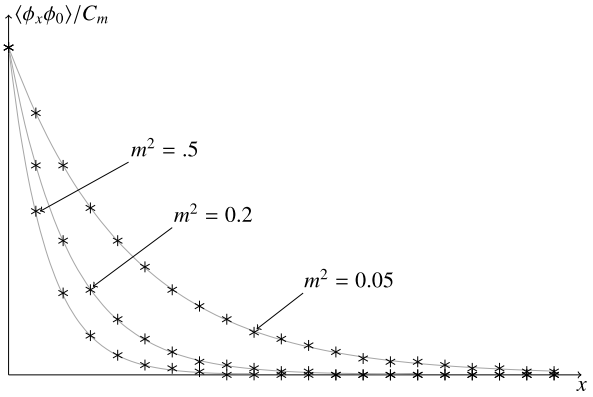

Fig. 5.4 Exponential decay of the two-point function

$$\langle\phi_x\phi_0\rangle \xrightarrow{N\to\infty} \frac{1}{(2\pi)^d}\int_0^{2\pi} \mathrm{d}^d p\,\frac{\mathrm{e}^{\mathrm{i}px}}{m^2+\hat{p}^2}$$
$$= \frac{1}{(2\pi)^d}\int_0^{2\pi} \mathrm{d}^d p\,\frac{\cos(px)}{m^2+\hat{p}^2}, \quad \hat{p}_\mu = 2\sin\frac{p_\mu}{2}. \tag{5.76}$$

The 2-point function on $\Lambda = \mathbb{Z}^d$ is real and invariant under translations and rotations which transform the lattice into itself. The value on the diagonal is given by

$$\langle\phi_0\phi_0\rangle \equiv C_m = \frac{1}{m\sqrt{m^2+4}}. \tag{5.77}$$

Figure 5.4 illustrates the normalized values of the 2-point function for three different masses at the lattice points $x = 0, \ldots, 20$. The exponential fits of the 2-point function are quite excellent. However, for real x the integral (5.76) oscillates around the exponential fit.

5.5 Random Walk Representation of Green's Function

The random walk representation is a reformulation of Euclidean field theory and was introduced by K. Symanzik in his studies of ϕ^4 models [42, 43]. Here we discuss the random walk representation for the 2-point function (5.76) of the free scalar field on $\mathbb{Z}^d$ as "weighted sum over all paths on the lattice" from x to y. This result is useful both for estimates and approximations in lattice field theories.

Let us first consider the quantity

$$G(x) = \mathrm{e}^{-\mu} \sum_{\text{paths } 0\to x} \mathrm{e}^{-\mu\ell} = \mathrm{e}^{-\mu}\sum_{\ell=0}^{\infty} P_\ell(x)\,\mathrm{e}^{-\mu\ell} \tag{5.78}$$

on the infinite lattice. The length of a path (measured in units of the lattice distance) is thereby given by ℓ. In contrast, μ is an arbitrary parameter that will be fixed later

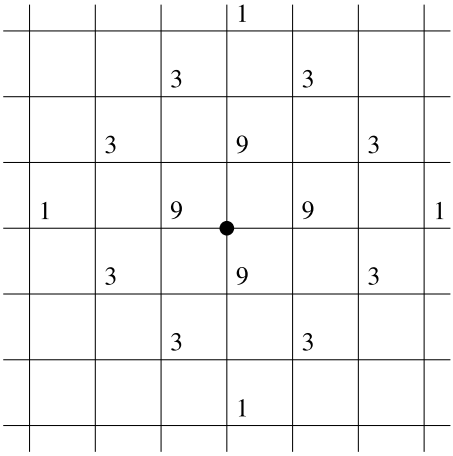

Fig. 5.5 Number of possible paths of length 3 on the lattice. Each path starts at the origin, marked with a *black bullet*

on. The quantity $P_\ell(x)$ represents the number of paths of length ℓ from 0 to $x \in \mathbb{Z}^d$. There exists a simple *generating function* for the P_ℓ:

$$\left(\mathrm{e}^{\mathrm{i}p_1} + \mathrm{e}^{-\mathrm{i}p_1} + \cdots + \mathrm{e}^{\mathrm{i}p_d} + \mathrm{e}^{-\mathrm{i}p_d}\right)^\ell = \sum_{x\in\mathbb{Z}^d} P_\ell(x)\,\mathrm{e}^{\mathrm{i}(p_1x_1+\cdots+p_dx_d)}. \tag{5.79}$$

To prove this formula we compute the left hand side explicitly. We thereby obtain a sum over all possible combinations of ℓ coefficients $\mathrm{e}^{\pm ip_\mu}$. If we interpret $\mathrm{e}^{\pm ip_\mu}$ as a step towards the $\pm\mu$-direction, each of this terms corresponds to one special path of length ℓ on the lattice. Since $P_\ell(x) = 0$ for all points x with a distance greater than ℓ from the origin, the sum over x converges. Figure 5.5 indicates the number of paths of length 3 on a 2-dimensional quadratic lattice. There are nine different paths of length $\ell = 3$ connecting the origin (marked with a bullet) with an arbitrary nearest neighbor. In contrast, there is no path of length $\ell = 3$ that connects the origin with a next-nearest neighbor. Clearly, $P_3(x) = 0$ for points with a distance greater than 3 from the origin. The total number of paths of length 3 is equal to $(2d)^3 = 64$.

Note that we get zero for the integration of the exponential function $\exp(\mathrm{i}px)$ over the Brillouin zone $p_\mu \in [0, 2\pi)$ as long as the exponent does not vanish. Thus we can extract the polynomials P_ℓ according to

$$P_\ell(x) = \frac{1}{(2\pi)^d}\int_0^{2\pi} \mathrm{d}^d p\,\mathrm{e}^{-\mathrm{i}px}\left(\mathrm{e}^{\mathrm{i}p_1} + \mathrm{e}^{-\mathrm{i}p_1} + \cdots + \mathrm{e}^{\mathrm{i}p_d} + \mathrm{e}^{-\mathrm{i}p_d}\right)^\ell. \tag{5.80}$$

Now we insert this result into (5.78). This yields the geometric series

$$\begin{aligned} G(x) &= \frac{\mathrm{e}^{-\mu}}{(2\pi)^d}\int_0^{2\pi} \mathrm{d}^d p\,\mathrm{e}^{-\mathrm{i}px}\sum_\ell \left\{2\mathrm{e}^{-\mu}(\cos p_1 + \cdots + \cos p_d)\right\}^\ell \\ &= \frac{\mathrm{e}^{-\mu}}{(2\pi)^d}\int_0^{2\pi} \mathrm{d}^d p\left(\frac{\mathrm{e}^{-\mathrm{i}px}}{1 - 2\mathrm{e}^{-\mu}\sum_\nu \cos p_\nu}\right) \end{aligned} \tag{5.81}$$

$$= \frac{1}{(2\pi)^d} \int_0^{2\pi} \mathrm{d}^d p \left(\frac{\mathrm{e}^{-\mathrm{i}px}}{\mathrm{e}^{\mu} - 2d + 4\sum_\nu \sin^2 \frac{p_\nu}{2}} \right). \tag{5.82}$$

We recognize the integral representation of the 2-point function of the free Klein–Gordon field (5.76), provided

$$\mathrm{e}^{\mu} - 2d = m^2. \tag{5.83}$$

Inserting this relation into equation (5.78) we end up with the random walk representation for the Green function of the free scalar field on the lattice $\mathbb{Z}^d$ [12]

$$\langle \phi_x \phi_0 \rangle = \frac{1}{(m^2 + 2d)} \sum_{\text{paths } 0 \to x} \frac{1}{(m^2 + 2d)^\ell}. \tag{5.84}$$

This result implies the simple upper bound (see problem 5.90)

$$\langle x | \left(-\Delta + m^2 \right)^{-1} | y \rangle < \frac{1}{m^2} \mathrm{e}^{-\mu |x-y|} \tag{5.85}$$

with $\mu = \log(1 + m^2/2d)$. It is a special case of the energy-entropy bounds as they appear in polymer expansions.

5.6 There Is No Leibniz Rule on the Lattice

When one proves the invariance of a continuum action under infinitesimal space-time symmetries then one employs the ubiquitous Leibniz rule. Unfortunately this rule does not hold on any lattice in accordance with the absence of infinitesimal translational and rotational symmetries and the absence of supersymmetry on a lattice. Now we prove that there exists no lattice derivative which satisfies this rule.

The set of (complex) lattice functions $x \to f_x \in \mathbb{C}$ form a linear space and any lattice derivative D is a linear operator on this space.

Lemma 5.1 *A linear operator* $D\colon \mathrm{map}(\Lambda, \mathbb{C}) \to \mathrm{map}(\Lambda, \mathbb{C})$ *that fulfills Leibniz's rule*

$$D(f \cdot g) = (Df) \cdot g + f \cdot (Dg), \quad \forall\, f, g : \Lambda \to \mathbb{C}, \tag{5.86}$$

vanishes, i.e. $D = 0$. *We denote by* $f \cdot g$ *the pointwise product of functions,* $(f \cdot g)_x = f_x g_x$.

Proof We write the Leibniz rule in component form in order to prove this lemma. For that purpose we identify a lattice function $f : x \to f_x$ with the V-component

vector f_x and the linear operator D with a $V \times V$ matrix D_{xy}, i.e.

$$(Df)_x = \sum_{y \in \Lambda} D_{xy} f_y. \tag{5.87}$$

Then Leibniz's rule may be written as

$$\sum_z D_{xz}(f_z g_z) = g_x \sum_z D_{xz} f_z + f_x \sum_z D_{xz} g_z. \tag{5.88}$$

For both functions in (5.88) we now choose the characteristic function of a *fixed* lattice site, say y. Then f_z and g_z vanish for all $z \neq y$ and in addition $f_y = g_y = 1$. Hence, equation (5.88) simplifies to $D_{xy} = 2\delta_{x,y} D_{xy}$. It immediately follows that $D_{xy} = 0$ for all sites x, y. □

In case of periodic lattice functions we will demand

$$\sum_{x \in \Lambda} (Df)_x = 0, \tag{5.89}$$

following the corresponding formula for fields over $\mathbb{R}^d$. The backward and forward lattice derivatives satisfy this condition. Finally note that the lemma (5.86) does not exclude the possibility that Leibniz's rule is satisfied for a particular subset of lattice functions.

5.7 Programs for Chap. 5

The following `octave`-program:

- `corrscalar`

computes the 2-point function (5.76) of the free scalar field as a function of x, divided by the mass-dependent constant C_m as given in (5.77). The rescaled correlator is equal to 1 for $x = 0$. The correlation function and exponential fit $\exp(-mx)$ with the propagator mass represent the output.

```
1  function corrscalar;
2  # calculates 2-point function for free scalar field
3  # in one dimension with naive lattice derivative.
4  # program asks for square of mass.
5  # stored in corrscalar.dat
6  #
7  m2=input("square of mass");
8  wco=sqrt(m2)*sqrt(4+m2)/(2*pi);# for normalization
9                                    of integrals
10 closeplot;
11 Np=1001; eps=2*pi/(Np-1); # Np sampling points: odd number!
```

```
p=linspace(0,2*pi,Np);ph=0.5*p;
sph=sin(ph);nominator=m2+4*sph.*sph;eps=eps/3;
#z=eps*cos(p).*cos(p);
z=eps./nominator;
# For Simpson integration;
for i=2:2:Np-1;
  z(i)=4*z(i);
endfor;
for i=3:2:Np-2;
  z(i)=2*z(i);
endfor;
x=linspace(0,20,21)';N=length(x);
int0=zeros(N,Np);
s0=zeros(N,1);
for i=1:N
  int0(i,:)=z.*cos(x(i)*p);
  s0(i)=sum(int0(i,:));
endfor;
s0=wco*s0;
data=[x,s0]; # set minimum of u to 0
data1=[x,exp(-sqrt(m2)*x)];
gplot [0:20] data, data1;
corrscalar=fopen("corrscalar.dat","w","native");
for i=1:N
fprintf(corrscalar,"(%4.2f,%4.2f)",x(i),s0(i));
if (rem(i,5)==0) fprintf(corrscalar,"\n");
endif;
endfor;
fclose(corrscalar);
endfunction;
```

5.8 Problems

5.1 (Black-body radiation for massless scalar particles) Compute the free energy density as well as the inner energy density for massless scalar particles in two and three dimensions.

5.2 (High-temperature expansions) Calculate the high-temperature expansions for the free energy densities of massive scalars in two and three dimensions.

5.3 (Legendre transformation) For which φ is the Legendre transform of $w(j) = e^j$ defined? Calculate the transform $u(\varphi)$.

5.4 (Bounds for the free propagator) Prove that for a positive m^2 the propagator (5.84) can be bounded as follows:

$$0 < \langle x|\left(-\Delta + m^2\right)^{-1}|y\rangle < \frac{1}{m^2}\,\mathrm{e}^{-\mu|x-y|} \tag{5.90}$$

with a new mass parameter $\mu = \log(1 + m^2/2d)$.

5.5 (Generalization of Corollary 5.8) Let $W[j]$ be a twice differentiable *functional* and $\Gamma[\varphi]$ its Legendre transform,

$$\Gamma[\varphi] = \inf_{j(x)} \left(\int \mathrm{d}^d x \, j(x)\varphi(x) - W[j] \right). \tag{5.91}$$

The minimizing $j(x)$ is conjugated to the prescribed field $\varphi(x)$. Prove the following generalization of Corollary 5.8 in the section on the Legendre–Fenchel transformation:

$$\int \mathrm{d}^d y \frac{\delta^2 W}{\delta j(x)\delta j(y)} \frac{\delta^2 \Gamma}{\delta\varphi(x)\delta\varphi(z)} = \delta(z, y), \tag{5.92}$$

whereby the second derivatives must be evaluated at conjugated fields $j \leftrightarrow \varphi$. In applications $W[j]$ is the Schwinger functional and $\Gamma[\varphi]$ the effective action. This equation means that the second functional derivative of the effective action is the inverse of the connected two-point function.

References

1. M.E. Peskin, D.V. Schroeder, *An Introduction to Quantum Field Theory* (Addison-Wesley, Reading, 1995)
2. L. Brown, *Quantum Field Theory* (Cambridge University Press, Cambridge, 1992)
3. R. Haag, *Local Quantum Physics: Fields, Particles and Algebras* (Springer, Berlin, 1996)
4. M. Maggiore, *A Modern Introduction to Quantum Field Theory* (Oxford University Press, Oxford, 2005)
5. J. Fröhlich, On the triviality of $\lambda\phi_d^4$ theories and the approach to the critical point in $d \geq 4$ dimensions. Nucl. Phys. B **200**, 281 (1982)
6. R. Fernandez, J. Fröhlich, A.D. Sokal, *Random Walks, Critical Phenomena and Triviality in Quantum Field Theory* (Springer, Berlin, 1992)
7. A. Liddle, D. Lyth, *Cosmological Inflation and Large-Scale Structure* (Cambridge University Press, Cambridge, 2000)
8. V. Mukhanov, *Physical Foundations of Cosmology* (Cambridge University Press, Cambridge, 2005)
9. K. Osterwalder, R. Schrader, Axioms for Euclidean Green's functions. Commun. Math. Phys. **31**, 83 (1973)
10. K. Osterwalder, R. Schrader, Axioms for Euclidean Green's functions II. Commun. Math. Phys. **42**, 281 (1975)
11. J. Fröhlich, Schwinger functions and their generating functionals. Helv. Phys. Acta **47**, 265 (1974)
12. J. Glimm, A. Jaffe, *Quantum Physics—A Functional Integral Point of View* (Springer, New York, 1981)
13. J.S. Dowkder, R. Critchley, Effective Lagrangian and energy–momentum tensor in de Sitter space. Phys. Rev. D **13**, 3224 (1976)
14. S.W. Hawking, Zeta-function regularization of path integrals in curved space. Commun. Math. Phys. **55**, 133 (1977)
15. E. Elizalde, S.D. Odintsov, A. Romeo, A.A. Bytsenko, S. Zerbini, *Zeta Regularization Techniques with Applications* (World Scientific, Singapore, 1994)
16. H. Weyl, Das asymptotische Verteilungsgesetz der Eigenschwingungen eines beliebig gestalteten elastischen Körpers. Rend. Circ. Mat. Palermo **39**, 1 (1915)

17. S. Blau, M. Visser, A. Wipf, Determinants, Dirac operators and one-loops physics. Int. J. Mod. Phys. A **4**, 1467 (1989)
18. S. Weinberg, Gauge and global symmetries at high temperature. Phys. Rev. D **9**, 3357 (1974)
19. L. Dolan, R. Jackiw, Symmetry behavior at finite temperature. Phys. Rev. D **9**, 3320 (1974)
20. C.W. Bernard, Feynman rules for gauge theories at finite temperature. Phys. Rev. D **9**, 3312 (1974)
21. J.I. Kapusta, *Finite-Temperature Field Theory* (Cambridge University Press, Cambridge, 2006)
22. M. Le Bellac, *Thermal Field Theory* (Cambridge University Press, Cambridge, 2000)
23. P.B. Gilkey, *Invariance Theory: The Heat Equation and the Atiyah–Singer Index Theorem* (CRC Press, Boca Raton, 1994)
24. D.V. Vassilevich, Heat kernel expansion: user's manual. Phys. Rep. **388**, 279 (2003)
25. S. Blau, M. Visser, A. Wipf, Zeta functions and the Casimir energy. Nucl. Phys. B **310**, 163 (1988)
26. E. Elizalde, A. Romeo, Expressions for the zeta function regularized Casimir energy. J. Math. Phys. **30**, 1133 (1989)
27. I. Sachs, A. Wipf, Finite temperature Schwinger model. Helv. Phys. Acta **65**, 652 (1992)
28. E. Corrigan, P. Goddard, H. Osborn, S. Templeton, Zeta function regularization and multi—instanton determinants. Nucl. Phys. B **159**, 469 (1979)
29. H.W. Braden, Expansion for field theories on $S^1 \times \Sigma$. Phys. Rev. D **25**, 1028 (1982)
30. L. O'Raifeartaigh, A. Wipf, H. Yoneyama, The constraint effective potential. Nucl. Phys. B **271**, 653 (1986)
31. H. Casimir, On the attraction between two perfectly conducting plates. Proc. K. Ned. Akad. Wet., Ser. B Phys. Sci. **51**, 793 (1948)
32. S.K. Lamoreaux, Demonstration of the Casimir force in the 0.6 to 6 μm range. Phys. Rev. Lett. **78**, 5 (1997)
33. G. Bressi, G. Carugno, R. Onofrio, G. Ruoso, Measurement of the Casimir force between parallel metallic surfaces. Phys. Rev. Lett. **88**, 041804 (2002)
34. M. Bordag, U. Mohideen, V.M. Mostepanenko, New developments in the Casimir effect. Phys. Rep. **353**, 1 (2001)
35. K.A. Milton, *The Casimir Effect* (World Scientific, Singapore, 2001)
36. J.L. Cardy, I. Peschel, Finite size dependence of the free energy in two-dimensional critical systems. Nucl. Phys. B **300**, 377 (1988)
37. C. Wiesendanger, A. Wipf, Running coupling constants from finite size effects. Ann. Phys. **233**, 125 (1994)
38. J. Zinn-Justin, *Quantum Field Theory and Critical Phenomena* (Oxford University Press, London, 2002)
39. R.T. Rockafellar, *Convex Analysis* (Princeton University Press, Princeton, 1970)
40. R. Balian, *From Microphysics to Macrophysics*, vol. 1 (Springer, Berlin, 1991)
41. J.B. Hiriat-Urruty, J.E. Matinez-Legaz, New formulas for the Legendre–Frenchel transform. J. Math. Anal. Appl. **288**, 544 (2003)
42. K. Symanzik, A modified model of Euclidean quantum field theory. Courant Institute of Mathematical Sciences, IMM-NYU 327 (1964)
43. K. Symanzik, Euclidean quantum field theory, in *Local Quantum Field Theory*, ed. by R. Jost (Academic Press, New York, 1968)

Chapter 6
Classical Spin Models: An Introduction

One distinguishes between continuous and discrete spin models (lattice models) depending on whether the spins take their values in a continuous or discrete target space. The previously considered lattice scalar field theory with target space $\mathscr{T} = \mathbb{R}$ defines a *continuous spin model*. A typical representative of the class of *discrete spin models* is the ubiquitous *Ising model* and its generalizations. The target space of the Ising model is the finite group Z_2. It is a simple statistical model for *ferromagnetism* induced by "elementary spins" or "elementary magnets" sitting at the sites of a crystal lattice. The spins can be in one of two states, either spin up or spin down and each spin interacts at most with its nearest neighbors. We will focus on a quantitative understanding of such systems with many or infinitely many degrees of freedom.

In this chapter *phase transitions* as observed in ferromagnets will be of particular interest. The two-dimensional Ising model is one of the simplest statistical models to show a phase transition. Below the *Curie temperature* we observe a spontaneous magnetization, where a majority of spins point in a given direction. Above T_c, the spontaneous magnetization vanishes. Iron, cobalt and nickel with Curie temperatures of 1043, 1403 and 631 K are examples of ferromagnetic materials.

6.1 Simple Spin Models for (Anti)Ferromagnets

When modeling ferromagnets one often assumes that the spins of the atoms on the lattice sites can only attain discrete values. The Hamiltonian of such a spin model has the form

$$H = -\sum_{x,y\in\Lambda} J_{xy} s_x s_y - h \sum_{x\in\Lambda} s_x, \tag{6.1}$$

where s_x denotes the spin associated with the atom at site x, h the magnetic field and J_{xy} the interaction strength (exchange coupling) between the spins at sites x and y. Often it is a good approximation to assume that J_{xy} is non-zero only if the sites x and y are nearest neighbors. In addition, for a translational invariant system

A. Wipf, *Statistical Approach to Quantum Field Theory*, Lecture Notes in Physics 864,
DOI 10.1007/978-3-642-33105-3_6,

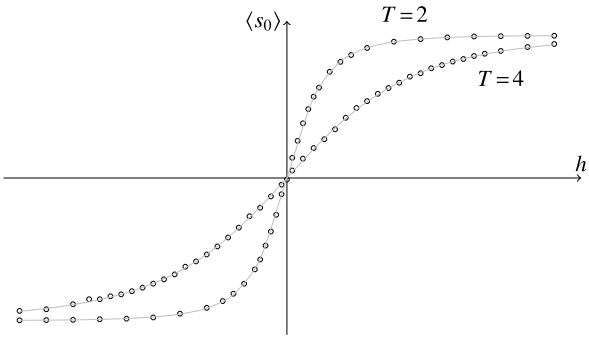

Fig. 6.1 Magnetization as a function of h for the one-dimensional Ising model

we expect that the exchange couplings are independent on the nearest-neighbor pair x, y. In the Ising model a spin s_x parallel to a fixed axis has value 1 and a spin antiparallel to this axis has value -1. The interaction energy has the form

$$H = -J \sum_{\langle x,y \rangle} s_x s_y - h \sum_{x \in \Lambda} s_x, \quad s_x \in \{-1, 1\}, \tag{6.2}$$

where the first sum extends over all pairs of nearest neighbors. A ferromagnetic interaction $J > 0$ tends to align spins, and an antiferromagnetic interaction $J < 0$ tends to anti-align them.

6.1.1 Ising Model

The simple Ising model with energy function (6.2) has been intensively studied and is often referred to as "harmonic oscillator of statistical physics". It was introduced back in 1920 by WILHELM LENZ, the thesis advisor of ERNST ISING [1], to model ferromagnetic systems. Five years later Ising solved the one-dimensional model, the *Ising chain* [2]. The thermodynamic potentials of the Ising chain can be calculated in closed form, for example via its transfer matrix, see Sect. 8.1. Unfortunately this simple model does not show spontaneous magnetization at any finite temperature. With the C-program on p. 114 one can simulate the Ising chain and calculate its magnetization as function of the external magnetic field. In complete agreement with the analytic solutions for the infinitely long chain one obtains a smooth curve for any positive temperature, see Fig. 6.1. This is expected for a system without spontaneous magnetization.

In 1936 RUDOLPH PEIERLS analyzed the *two-dimensional Ising model* and proved the existence of a low-temperature phase exhibiting spontaneous magnetization [3, 4], see Sect. 10.1. For high temperatures there is no magnetization and hence we expect a transition from an ordered low-temperature phase to a disordered high-temperature phase at a critical temperature $T_c > 0$. Without magnetic field this so-called Curie temperature was calculated by KRAMERS and WANNIER in 1941 [5]. We shall discuss their duality transformation in Sect. 10.2. Three years

later LARS ONSAGER found the exact solution by means of the transfer matrix method [6]. He obtained the following analytical formula for the free energy density, measured in units of $k_B T$, as function of $K = \beta J$ (for a lucid discussion see [7–10]):

$$-\beta f(T) = \log\cosh(2K) - 2K + \frac{2}{\pi}\int_0^{\pi/2} \mathrm{d}\theta \log\bigl(1 + \sqrt{1-\kappa^2\sin^2\theta}\bigr), \tag{6.3}$$

with $\kappa = 2\tanh(2K)/\cosh(2K)$. The corresponding internal energy is

$$u(T) = J\frac{\partial}{\partial K}\bigl(\beta f(T)\bigr) = 2J - J\coth 2K\left(1 + \bigl(2\tanh^2 2K - 1\bigr)\frac{2K(\kappa)}{\pi}\right), \tag{6.4}$$

where $K(\kappa)$ is the complete elliptic integral of the first kind, defined as

$$K(\kappa) = \int_0^{\pi/2} \frac{\mathrm{d}\theta}{\sqrt{1-\kappa^2\sin^2\theta}}. \tag{6.5}$$

Differentiating the internal energy with respect to T yields the *specific heat*,

$$c = \frac{4K^2}{\pi\sinh^2 2K}\left\{K(\kappa)\left(\sinh^2 2K + \frac{2}{\cosh^2 2K}\right) - E(\kappa)\cosh^2 2K - \frac{\pi}{2}\right\}, \tag{6.6}$$

which contains the complete elliptic integrals of the second kind,

$$E(\kappa) = \int_0^{\pi/2} \sqrt{1-\kappa^2\sin^2\theta}\,\mathrm{d}\theta.$$

The complete elliptic integral of the first kind has a singularity at $\kappa = 1$ and the phase transition occurs at this point. The temperature at which the phase transition occurs is then given by the condition

$$1 = 2\frac{\tanh(2K_c)}{\cosh(2K_c)} \quad \text{or} \quad 2K_c = \log\bigl(1+\sqrt{2}\bigr). \tag{6.7}$$

This yields the critical temperature $T_c = 2.269J$. In Fig. 6.2 we plotted the internal energy density and the specific heat as functions of $K \propto 1/T$.

The Dutch physicist HENDRIK CASIMIR was not well informed about what had happened in theoretical physics during the Second World War and asked PAULI about new developments. The latter answered:

> Not much interesting ... except Onsager's solution of the two-dimensional Ising model.

This comment should emphasize the importance of Onsager's solution in theoretical physics. After all, two-dimensional Ising-like models are the only non-trivial statistical systems that show a phase transition and can be solved analytically. Today we know several methods for solving these models. We will discuss some of them. The possibility to compare approximation schemes with the exact solution explains the importance of the Ising model in statistical physics.

So far, the *three-dimensional Ising model* could not be solved analytically and one has to rely on approximations, for example the mean field approximation, high-temperature or the low-temperature expansions, or numerical simulations to calculate thermodynamic potentials and (thermal) expectation values. The quality of the mean field approximation increases with the number of nearest neighbors and the approximation yields the correct critical exponents in four or more dimensions.

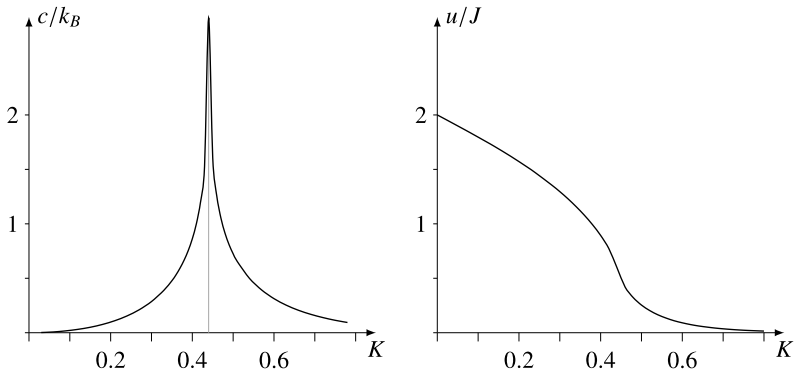

Fig. 6.2 The internal energy per site and the specific heat as a function of $K = \beta J$. The phase transition occurs at the critical value $K_c = 0.4407$

6.2 Ising-Type Spin Systems

Besides Ising models there are many more interesting lattice spin models with discrete or continuous target spaces. Examples with discrete target spaces are the standard and planar Potts models where the spin may assume q different values. Examples with continuous target spaces are non-linear $O(N)$-models for which the spins take their values on the unit sphere in $\mathbb{R}^N$. Also note that lattice regularized Euclidean quantum field theories define particular spin models.

We use the same notation as in Chap. 5 and denote the coordinates of the sites in a hypercubic lattice $\Lambda \subset aZ^d$ by x, where a is the lattice spacing. We impose periodic boundary conditions and thus identify the points x and $x + N_\mu e_\mu$ (no sum), where e_μ denotes the unit vector in direction μ. At the end of the calculation we often take the *thermodynamic limit* where the number of sites $N_1 \cdots N_d$ tends to infinity. After a suitable rescaling we may assume that $a = 1$ such that the unit cell has unit volume and the lattice volume is $V = N_1 \cdots N_d$. To every site we assign a $\mathscr{T}$-valued spin variable s_x. Because of the periodic boundary conditions, we have

$$s_{x'} = s_x \quad \text{for } x' = x + N_\mu e_\mu, \quad \mu = 1, \ldots, d. \tag{6.8}$$

Every point inside a hypercubic lattice has $2d$ nearest neighbors and $2d$ bonds towards these neighbors. A *configuration* $\omega = \{s_x | x \in \Lambda\}$ assigns to all spins on the lattice site certain values,

$$\omega : \Lambda \to \mathscr{T} \times \mathscr{T} \times \cdots \times \mathscr{T} = \mathscr{T}^V, \quad V = |\Lambda|. \tag{6.9}$$

We denote the set of all configurations by Ω. If the target space has a finite number of elements, as happens for the Ising model with $|\mathscr{T}| = 2$, then there exist $|\mathscr{T}|^V$ different configurations $\omega \in \Omega$.

6.2.1 Standard Potts Models

CYRIL DOMB suggested that his student RENFREY POTTS study a class of generalized Ising models with $q > 2$ orientations for the spin. Nowadays these models are named after Potts who described the systems towards the end of his 1952 Ph.D. thesis. His results for the Z_q-models and the standard q-state Potts models were published in [11]. Both lattice systems have q^V different configurations. In two dimensions the q-state Potts model is exactly solvable and shows a phase transition with order parameter. Both the order of the transition and the critical exponents depend on the number q of spin states.

In a lattice gas representation every lattice point is occupied by one of q different atoms. We enumerate the different atoms by $\sigma \in \{1, 2, \ldots, q\}$. Identical nearest-neighbor atoms have an interaction energy of $-J_p$ and different nearest-neighbor atoms have no interaction energy. Thus the energy of a particular distribution of atoms, given by a configuration $\omega = \{\sigma_x | x \in \Lambda\}$, has the form

$$H_{\text{potts}}(\omega) = -J_p \sum_{\langle x,y \rangle} \delta(\sigma_x, \sigma_y) - h \sum_x \delta(\sigma_x, 1), \quad \sigma_x \in \{1, 2, \ldots, q\}, \tag{6.10}$$

where $\delta(\sigma_x, \sigma_y)$ is the Kronecker symbol and the first sum extends only over pairs of nearest neighbors. Note that we added an explicit symmetry-breaking term with magnetic field h. For $h = 0$ the energy is minimal if there is only one type of atoms on the lattice—clearly there are q such classical vacuum configurations.

We may rewrite the energy function (6.10) in the general form (6.2), with s_x being a unit vector pointing to one of q equally spaced points on the unit sphere in $\mathbb{R}^{q-1}$. The particular cases with $q = 2, 3, 4$ are illustrated in Fig. 6.3. So let us pick q unit vectors $\{\mathbf{s}^{(1)}, \ldots, \mathbf{s}^{(q)}\}$ which point from the origin to these q equally spaced points on the unit sphere. Since $\sum_n \mathbf{s}^{(n)} = 0$, the scalar product of any two of these unit vectors is

$$\mathbf{s}^{(n)} \cdot \mathbf{s}^{(m)} = \tilde{q}\delta_{nm} - \frac{1}{q-1} \quad \text{with } \tilde{q} = \frac{q}{q-1}. \tag{6.11}$$

To prove the equivalence of the models (6.10) and (6.2) we map the variable σ_x at site x to the vector $\mathbf{s}_x = \mathbf{s}^{(\sigma_x)}$. This identification yields

$$\mathbf{s}_x \cdot \mathbf{s}_y = \tilde{q}\delta(\sigma_x, \sigma_y) - \frac{1}{q-1}. \tag{6.12}$$

Solving for the Kronecker symbol and inserting into (6.10) yields

$$H_{\text{potts}}(\omega) = -\tilde{J} \sum_{\langle x,y \rangle} \mathbf{s}_x \cdot \mathbf{s}_y - \tilde{h}\mathbf{s}^{(1)} \cdot \sum_x \mathbf{s}_x - C, \tag{6.13}$$

with $J_p = \tilde{q}\tilde{J}$, $h = \tilde{q}\tilde{h}$ and an additive constant C which depends on the volume and the parameters of the model. For positive J_p all vectors are aligned in the classical ground states and the systems show ferromagnetic behavior. For negative J_p it is energetically favorable when two neighboring spins are different and it is not easy to characterize all configurations with minimal energy, at least for $q \geq 3$.

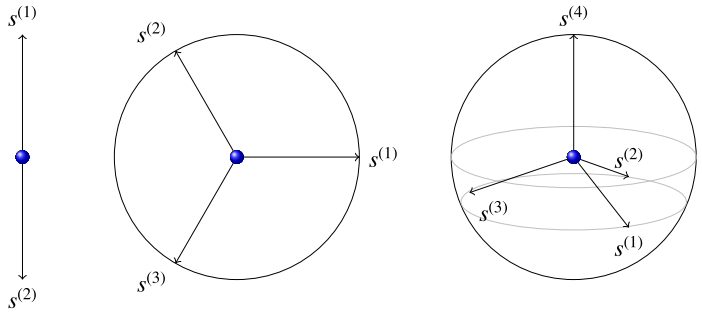

Fig. 6.3 The unit vectors of the vector-Potts model with $q = 2, 3, 4$

The equivalence of the models (6.10) and (6.13) proves that the 2-state Potts model is just the Ising model. In contrast, the 1-state Potts model is very closely related to the bond percolation model. Several exact results are known for the Potts model in two dimensions. On a square lattice a Kramers–Kronig type duality transformation exists and relates the partition functions at high and low temperatures and in particular fixes the critical temperature T_c [11, 12]. Baxter argued that for $q > 4$ the two-dimensional model shows a first-order transition, whereas for $q \leq 4$ the transition is of higher order [13]. The mean field approximation predicts a first-order phase transition for $q \geq 3$. The mean field results agree with all exact results when q is sufficiently large and it is conjectured that the approximation is accurate to leading order in q in a large q expansion.

6.2.2 The Z_q Model (Planar Potts Model, Clock Model)

Now we introduce another generalization of the Ising model where one attaches a unit vector in a fixed plane to each lattice point. The unit vector points towards one of the corners of a *planar* equilateral q-gon, characterized by the angles

$$\theta_n = \frac{2\pi n}{q}, \quad n = 1, 2, \ldots, q. \tag{6.14}$$

Let $\theta_{xy} = \theta_x - \theta_y$ be the angle between the vectors at neighboring sites x, y and $J(\theta)$ a 2π-periodic function, then the energy function for the generalized Z_q-model reads

$$H = -\sum_{\langle x,y \rangle} J(\theta_{xy}). \tag{6.15}$$

Since the interaction only depends on the angle between vectors at neighboring sites it is invariant under the global Z_q-transformations

$$\theta_x \to \theta_x + \frac{2\pi n}{q} \quad \text{with } n \in Z_q. \tag{6.16}$$

The special choice $J(\theta) = J_c \cos\theta$ leads to the *planar Potts model* or *clock model* with energy function

$$H_{\text{clock}} = -J_c \sum_{\langle x,y \rangle} \cos(\theta_x - \theta_y). \tag{6.17}$$

Potts himself solved the two-dimensional model with 2, 3, and 4 states. The system with $q = 3$ states is equivalent to the standard Potts model with $J_p = 3J_c/2$,

$$H_{\text{clock}}(\theta) = H_{\text{Potts}}(\sigma) + \frac{1}{2} J_c, \quad \sigma_x \in \{1, 2, 3\}.$$

The planar Potts model with four states reduces to two standard Potts models with two states each. However, no relation between the standard and planar Potts models is known for $q > 4$.

6.2.3 The $U(1)$ Model

We obtain the $U(1)$ model from the planar Potts model (clock model) in the limit of infinite q. In this limit the angle θ_n in (6.14) assumes any value between 0 and 2π, such that θ_x parametrizes the circle $S^1 \simeq U(1)$. The *two-dimensional* $U(1)$-model shows an unusual phase transition. Unusual because it is of infinite order, which means that the free energy is infinitely many times differentiable though at the critical point it is non-analytic. The transition is due to the existence of topologically stable vortex solutions and not related to any symmetry breaking. We may interpret the phase transition as the condensation of vortices and antivortices: at low temperature there are only bound pairs of vortices with opposite circulations, whereas above the critical temperature we have a plasma of vortices and antivortices. In the disordered high-temperature phase the correlation functions for the spin variables show exponential falloff whereas in the "massless" low-temperature phase they falloff polynomially. This type of transition is called *Kosterlitz–Thouless phase transition* [14–16].

6.2.4 $O(N)$ Models

In the $O(N)$ model the spins take their values on a unit sphere in $\mathbb{R}^N$. For $N = 1, 2, 3$ we may interpret them as possible directions of elementary magnets generated by classical spins—these models come close to our classical conception of a ferromagnet. The energy of a configuration $\omega = \{s_x\}$ is given by

$$H_{O(N)}(\omega) = -J \sum_{\langle x,y \rangle} s_x \cdot s_y, \quad s_x \in \mathbb{R}^N, s_x \cdot s_x = 1. \tag{6.18}$$

A ferromagnetic system is characterized by $J > 0$. The scalar product of two classical spins is invariant under a simultaneous rotation of the spins,

$$Rs_x \cdot Rs_y = s_x \cdot s_y \quad \text{with } R \in O(N).$$

Hence the energy function is invariant under global rotations of the spins:

$$H_{O(N)}(R\omega) = H_{O(N)}(\omega), \quad R\omega = \{Rs_x | x \in \Lambda\}. \tag{6.19}$$

The $O(N)$ invariance justifies the name $O(N)$-*models* for these lattice systems. The model with $N = 1$ is the Ising model, the model with $N = 2$ is known as *XY model* (rotor model) and the model with $N = 3$ is referred to as $O(3)$-*model* or classical *Heisenberg model*. The model with $O(4)$ is a toy model for the Higgs sector of the Standard Model of particle physics. Actually, the model with $N = 0$ describes self-avoiding walks [17].

6.2.5 Interacting Continuous Spins

So far we considered the energy functions of the form (6.1) with couplings J_{xy} and magnetic field h. Now we also admit an interaction of a spin with itself, in which case the energy function can be written as

$$H(\omega) = \frac{1}{2} \sum_{x,y} J_{xy}(s_x - s_y)^2 + \sum_x V(s_x). \tag{6.20}$$

For simplicity we assumed that the self-interaction V is the same at all lattice sites. If $V = 0$ then the energy function belongs to a *Gaussian model*. On the other hand, we may adjust the couplings J_{xy} in order to find the Euclidean action of an interacting scalar field on the lattice. Similarly, we may regard the energy (6.18) of the $O(N)$ spin model as the Euclidean action for the non-linear $O(N)$-sigma model on a lattice:

$$S_{\mathrm{E}}(\omega) = \frac{1}{2g^2} \sum_{\langle x,y \rangle} (\phi_x - \phi_y)^2, \quad \phi_x \in \mathbb{R}^n, \ \phi_x \cdot \phi_x = 1. \tag{6.21}$$

The idea of identifying spin configurations as lattice fields of a discretized Euclidean field theory and energy functions as Euclidean actions according to

$$\begin{array}{c} \omega = \{s_x | x \in \Lambda\} \longleftrightarrow \omega = \{\phi_x | x \in \Lambda\} \\ \beta H(\omega) \longleftrightarrow S_{\mathrm{E}}(\omega)/\hbar \end{array} \tag{6.22}$$

has been very fruitful for the progress of non-perturbative quantum field theory as well as statistical physics.

6.3 Spin Systems in Thermal Equilibrium

In statistical physics we abandon the idea of solving the dynamics for each of the many microscopic degrees of freedom since this is not necessary to determine macroscopic variables such as pressure, temperature or magnetization. Instead we

describe the system by a so-called *density matrix*, which determines the probability of the occurrence of a configuration. In the following we are mainly interested in the *canonical ensemble*, where the energy $H(\omega)$ of a configuration ω determines the probability of its occurrence. In general the energy function depends on several parameters $\lambda = (\lambda_1, \ldots, \lambda_n)$. These parameters may characterize the coupling between two spins or the coupling between the spins and an external field. In the canonical ensemble a configuration ω occurs with probability

$$\exp\bigl(-\beta H_\Lambda(\omega)\bigr), \quad \beta = \frac{1}{k_b T}, \tag{6.23}$$

where T denotes the absolute temperature and k_b the Boltzmann constant. The partition function is defined as

$$Z_\Lambda(\beta) = \sum_{\omega\in\Omega} \exp\bigl(-\beta H_\Lambda(\omega)\bigr), \tag{6.24}$$

where the sum extends over all configurations.

For a continuous target space the sum turns into an integral over the lattice spins. For example, the partition function of the simple Gaussian model reads

$$Z_\Lambda(\beta) = \int \mathscr{D}\omega \mathrm{e}^{-\beta H_\Lambda(\omega)}, \qquad H_\Lambda(\omega) = \frac{1}{2}\sum_{x,y} J_{xy}(s_x - s_y)^2 \tag{6.25}$$

with the Lebesgue measure as single spin distributions,

$$\mathscr{D}\omega = \prod_{x\in\Lambda} \mathrm{d}s_x, \quad s_x \in \mathbb{R}. \tag{6.26}$$

The partition function of the interacting $O(N)$ model with spins on the sphere S^{n-1} looks almost identical,

$$Z_\Lambda(\beta) = \int \mathrm{d}\mu(\omega)\mathrm{e}^{-\beta H_\Lambda(\omega)}, \quad H_\Lambda(\omega) = -J\sum_{\langle x,y\rangle} s_x \cdot s_y, \tag{6.27}$$

but the single spin distribution is the measure on the sphere induced from $\mathbb{R}^n$,

$$\mathrm{d}\mu(\omega) = \prod_{x\in\Lambda} \mathrm{d}\mu(s_x), \qquad \mathrm{d}\mu(s) = \delta\bigl(s^2 - 1\bigr)\mathrm{d}^n s, \quad s_x \in \mathbb{R}^n. \tag{6.28}$$

In general, the partition function and thermodynamic potentials depends on the inverse temperature β, the parameters λ in the Hamilton function and the lattice Λ.

Next we define expectation values of observables $O(\omega)$ in the canonical ensemble. For discrete spin systems they are given by sums,

$$\langle O\rangle_\Lambda(\beta) = \frac{1}{Z_\Lambda(\beta)}\sum_\omega O(\omega)\mathrm{e}^{-\beta H_\Lambda(\omega)} \tag{6.29}$$

and for continuous spin systems by high-dimensional integrals,

$$\langle O\rangle_\Lambda(\beta) = \frac{1}{Z_\Lambda(\beta)}\int \mathrm{d}\mu(\omega) O(\omega)\mathrm{e}^{-\beta H_\Lambda(\omega)}. \tag{6.30}$$

In the following we adopt the notation from the discrete models. The corresponding formulas for continuous models are obtained by the substitution $\sum_\omega \to \int \mathrm{d}\mu(\omega)$.

The basic quantities of thermodynamics are derived from the partition function Z_Λ. For example, the *Helmholtz free energy* is proportional to the logarithm of Z_Λ,

$$F_\Lambda(\beta) = -\frac{1}{\beta} \log Z_\Lambda(\beta). \tag{6.31}$$

Since this extensive quantity diverges in the thermodynamic limit, $V \to \infty$, we mainly use the *free energy density*

$$f_\Lambda(\beta) = \frac{1}{V} F_\Lambda(\beta) \tag{6.32}$$

instead. For systems with short-range interactions the densities f_Λ converge in the thermodynamic limit to the free energy density f of the infinite system,

$$f_\Lambda(\beta) \overset{V\to\infty}{\to} f(\beta). \tag{6.33}$$

Note that the energy of one single configuration is not accessible in an experiment. But we can measure the expectation value of the energy at equilibrium—the *inner energy*. It is given by

$$U_\Lambda(\beta) = \langle H \rangle_\Lambda(\beta) = -\frac{1}{Z_\Lambda(\beta)} \frac{\partial}{\partial\beta} \sum_w \mathrm{e}^{-\beta H_\Lambda(\omega)} = -\frac{\partial}{\partial\beta} \log Z_\Lambda(\beta). \tag{6.34}$$

Substituting the logarithm of the partition function by the free energy leads to the expression

$$U_\Lambda(\beta) = \frac{\partial}{\partial\beta}\big(\beta F_\Lambda(\beta)\big) = F_\Lambda(\beta) - T \frac{\partial}{\partial T} F_\Lambda(\beta). \tag{6.35}$$

To find the macroscopic magnetization $m = \langle s_x \rangle$ we couple the spins to a homogeneous external magnetic field according to Eq. (6.1) and differentiate the corresponding h-dependent free energy density with respect to h. Making use of translational invariance on a lattice with periodic boundary conditions we obtain

$$m := \langle M \rangle = \langle s_x \rangle = -\frac{\partial}{\partial h} f_\Lambda(\beta, h), \quad M = \frac{1}{V} \sum_x s_x. \tag{6.36}$$

We obtain further information about the system via its n-point correlation functions

$$G^{(n)}(x_1, \ldots, x_n) = \langle s_{x_1} \cdots s_{x_n} \rangle, \quad x_1, \ldots, x_n \in \Lambda. \tag{6.37}$$

In particular, the 2-point function

$$G^{(2)}(x, y) \equiv G(x, y) = \langle s_x s_y \rangle \tag{6.38}$$

measures the correlation of the spins at site x and at site y. If $G^{(2)}(x, y)$ is positive these spins have the tendency to align. If this is the case for an arbitrary distance $|x - y|$ between the spins, then the system is *spontaneously magnetized*. If we knew all the correlation functions then we could reconstruct the Gibbs state.

We would like to point to a crucial difference between classical spin models and Euclidean quantum field theories on lattices. In spin models the temperature dependence originates from the temperature-dependent Boltzmann factor of the probability measure

$$\mathrm{d}P_\beta(\omega) = \frac{1}{Z_\Lambda(\beta)} \mathrm{e}^{-\beta H(\omega)} \mathrm{d}\mu(\omega) \tag{6.39}$$

that is used to calculate expectation values. In a lattice field theory with probability measure

$$\mathrm{d}P_\beta(\omega) = \frac{1}{Z_\Lambda(\beta)} \mathrm{e}^{-S(\omega)} \mathrm{d}\mu(\omega), \tag{6.40}$$

the temperature dependence arises from the geometry of the underlying lattice. The lattice has extent $\beta \propto 1/T$ in the imaginary time direction and the (bosonic) lattice fields are periodic with period β.

6.4 Variational Principles

There exists a variational characterization of the partition function and effective action which is useful in approximations, in particular the mean field approximation.[1] The interested reader may also consult [19]. We use the notation for the continuous spin models to underline the connection to lattice field theories.

6.4.1 Principle for Gibbs State and Free Energy

Let P be a probability measure with density $p \geq 0$ over the configuration space Ω. Then we have

$$\mathrm{d}P(\omega) = p(\omega)\mathrm{d}\mu(\omega) \quad \text{with} \int_\Omega \mathrm{d}P(\omega) = 1. \tag{6.41}$$

The *Boltzmann–Gibbs–Shannon entropy* is defined as

$$S_\mathrm{B}(P) = -\int \mathrm{d}\mu(\omega)\, p(\omega) \log p(\omega), \tag{6.42}$$

where the single spin distribution measure μ depends on the geometry of the target space but not on the density p. The free energy has the following variational characterization:

$$\beta F = \inf_P \left(\beta \int \mathrm{d}P(\omega) H(\omega) - S_\mathrm{B}(P) \right), \tag{6.43}$$

[1] There exists an alternative variational approach for the mean field approximation, which is based on Jensen's inequality, see for example [18].

where the infimum is to be taken with respect to all possible probability measures on Ω. We implement the constraint in (6.41) via the addition of the term $\lambda(\int \mathrm{d}P(\omega) - 1)$ with Lagrange multiplier λ. Then the variation of the expression in brackets in (6.43) with respect to $p(\omega)$ leads to

$$0 = \int \mathrm{d}\mu(\omega)\delta p(\omega)\big(\beta H(\omega) + \log p(\omega) + \lambda\big) \quad \Longrightarrow \quad p(\omega) = \mathrm{C}\mathrm{e}^{-\beta H(\omega)}.$$

The constant C is fixed by the requirement that $p\mathrm{d}\mu$ integrates to one. Hence the unique infimum with respect to all *probability measures* is just the Gibbs measure

$$\mathrm{d}P_\beta(\omega) = \frac{1}{Z(\beta)}\mathrm{e}^{-\beta H(\omega)}\mathrm{d}\mu(\omega) \quad \text{with } Z(\beta) = \int \mathrm{d}\mu(\omega)\mathrm{e}^{-\beta H(\omega)}. \tag{6.44}$$

By inserting this result into (6.43) we obtain the well-known expression

$$F(\beta) = -\frac{1}{\beta}\log Z(\beta) \tag{6.45}$$

for the free energy.

6.4.2 Fixed Average Field

The equivalent in statistical physics to the *effective action* in quantum field theory is the free energy functional with prescribed (inhomogeneous) average spin field m_x. Its variational characterization is given by (6.43) with additional constraints,

$$\beta F[m] = \inf_P \left(\beta \int \mathrm{d}P(\omega) H(\omega) - S_\mathrm{B}(P) \,\middle|\, \int \mathrm{d}P(\omega) s_x = m_x \right). \tag{6.46}$$

This means that we minimize with respect to probability densities with *prescribed average spins*. There is one constraint for every lattice site and the constraints are given by the average spins m_x. Since the set of probability measures is convex, the resulting functional $F[m]$ is also convex.

Next we show that the functional F is the Legendre transform of the Schwinger functional W. Thereby we implement the constraints in (6.46) with the help of a Lagrange multiplier field j_x. First we minimize

$$\beta F[m] = \inf_P \left(\int \mathrm{d}P(\omega) \big\{ \beta H(\omega) - (j, s - m) \big\} - S_\mathrm{B}(P) \right)$$

with respect to all probability measures, where $(j, s) = \sum_x j_x s_x$ denotes the ℓ_2 scalar product. The minimizing measure is given by

$$\mathrm{d}P_j(\omega) = \frac{1}{Z[j]}\mathrm{e}^{-\beta H(\omega) + (j,s)}\mathrm{d}\mu(\omega) \quad \text{with } Z[j] = \int \mathrm{d}\mu(\omega)\mathrm{e}^{-\beta H(\omega) + (j,s)}. \tag{6.47}$$

Inserting this result into (6.46) yields the functional,

$$\beta F[m] = (j, m) - W[j] \quad \text{with } W[j] = \log Z[j]. \tag{6.48}$$

The Lagrangian multiplier field j must be chosen such that the constraints

$$m_x = \int \mathrm{d}P_j(\omega) s_x = \frac{\delta W[j]}{\delta j_x} \tag{6.49}$$

are fulfilled on all sites. The formula (6.48) and (6.49) tell us that $F[m]$ is the Legendre transform of the Schwinger function, i.e.

$$\beta F[m] = \sup_j \big((j, m) - W[j] \big) = (\mathscr{L} W)[m]. \tag{6.50}$$

If one is interested only in the average magnetization rather than in general correlation functions, then it suffices to evaluate the free energy functional $F[m]$ for a homogeneous average field $m_x = m$. Since for any translational invariant system the average of s_x is equal to the average of $M = \sum_x s_x / V$ we are lead to the following definition of the free energy density for a homogeneous field:

$$\beta f(m) = \frac{1}{V} \inf_P \left(\beta \int \mathrm{d}P(\omega) H(\omega) - S_{\mathrm{B}}(P) \,\middle|\, \int \mathrm{d}P(\omega) M = m \right). \tag{6.51}$$

This density is given by the Legendre transform of the Schwinger function,

$$\beta f(m) = (\mathscr{L} w)(m) \quad \text{with } w(j) = \frac{1}{V} \log \int \mathrm{d}\mu(\omega) \mathrm{e}^{-\beta H(\omega) + j \sum s_x}. \tag{6.52}$$

The transition from finite temperature spin models to lattice field theories is made by the substitutions

$$\beta H \to S/\hbar, \qquad \beta F[m] \to \Gamma[\varphi]/\hbar, \qquad \beta f(m) \to u(\varphi)/\hbar. \tag{6.53}$$

For example, the effective action of a quantized scalar field is given by

$$\Gamma[\varphi] = \inf_P \left(\int \mathrm{d}P(\omega) S(\omega) - \hbar S_{\mathrm{B}}(P) \,\middle|\, \int \mathrm{d}P(\omega) \phi_x = \varphi_x \right), \tag{6.54}$$

where one minimizes with respect to probabilities on the space of lattice fields with prescribed average field φ_x. The convex functional Γ is the Legendre transform of the Schwinger functional,

$$\Gamma[\varphi] = (\mathscr{L} W)[\varphi] \quad \text{with } W[j] = \log \int \mathrm{d}\mu(\omega) \mathrm{e}^{-S(\omega)/\hbar + (j,\phi)}. \tag{6.55}$$

For a homogeneous φ the effective action density defines the effective potential

$$u(\varphi) = (\mathscr{L} w)(\varphi) \quad \text{with } w(j) = \frac{1}{\beta V} \log \int \mathrm{d}\mu(\omega) \mathrm{e}^{-S(\omega) + j \sum \phi_x}. \tag{6.56}$$

In the classical limit the effective action Γ converges to the classical action and the effective potential to the classical potential. The variational representations introduced above form an adequate starting point for the useful *mean field approximation* discussed in the Chap. 7.

6.5 Programs for the Simulation of the Ising Chain

Here you find the C-programs

- `glgew1d.c`
- `constantsising.h`
- `stdmcising.h`

used in this chapter. The program `glgew1d.c` provides the basis for the simulation of the one-dimensional Ising model with the energy function

$$H(\omega) = -J \sum_{x=1}^{N} s_x s_{x+1} - h \sum_{x=1}^{N} s_x, \quad s_x = \pm 1. \tag{6.57}$$

The first 500 iterations are necessary to thermalize the system. Afterwards, only every 20th configuration is evaluated in order to suppress correlations between the configurations. The program should be self-explanatory. It reads the header files `constantsising.h` containing the global variables and constants N, M, MG, MA and J as well as `stdmcising.h`. The values for the magnetization at temperature $T = 2.0$ are saved in the file `iisingT=2.0`. This file is stored in the subdirectory `is1data` of the directory containing the program `glgew1d.c`.

glgew1d.c (needs `constantsising.h` and `stdmcising.h`):

```
1  /* program ising1d.c */
2  /* simulation of ferromagnetic 1d Ising-model */
3  /* calculates magnetization for different values */
4  /* of magnetic field. Saved in file  ./is1data/isingT */
5  #include <stdio.h>
6  #include <stdlib.h>
7  #include <math.h>
8  #include <string.h>
9  #include <time.h>
10 #include "constantsising.h"
11 #include "stdmcising.h"
12 int main(void)
13 {
14   srand48(time(NULL));
15   /* read temperature  */
16   puts("temperature (3 digits) = ");
17   scanf("%3s",temp);
18   beta=1/atof(temp);
19   strncat(ising1,temp,3);
20   a=4*beta*J;
21   fp=fopen(ising1,"w");
22   fprintf(fp,"# N = %i , T = %.3f\n",N,1/beta);
23   fprintf(fp,"# magnetization 1-d Ising\n");
24   /* initial configuration */
25   for (i=0;i<N;i++)
26     s[i]=-1; */ cold initial configuration */
27   /* if (rand()<1073741823) s[i]=1 else s[i]=-1 */
```

```
  /* coming to equilibrium  */
  h=-5.0;b=2*beta*h;
  /* calculate Boltzmann weights */
  boltzmann();
  for (i=0;i<MG;i++) mcsweep(s);
  /* simulation and calculationfor h
  /* from -5 to 5 in steps of 0.5 */
  for (i=-10;i<11;i++){
    h=0.5*i;b=2*beta*h;
    boltzmann();check();
    ann=0;mean1=0;
    for (j=0;j<M;j++){
      mcsweep(s);
      mean1=mean1+moments(1,s);
    };
    printf(\"accepted %.2f\n",(float)ann/(N*MA*M));
    fprintf(fp,"%4.1f    %6.3f\n",h,2*mean1/M);
    };\draw (100,16)node{$1$};
  fclose(fp);
  return 0;
}
```

constantsising.h defines constants and global variables:

```
/* file constantsising.h */
/* constants N,M,MG,MA,J */
/* variables s[N], ising1[], etc. */
#define N 128  /* number of lattice points */
#define M 10000 /* number of interations */
#define MG 500 /* equilibrium */
#define MA 20 /* every MAth configuration is measured */
#define J 1.0
short nn,si,s[N],test[3][5];
unsigned int j,k;
double mean1;
float a,b,vorz,beta,boltz[3][5],h;
int i,ann=0;
FILE *fp;
char temp[20],ising1[]="./is1data/isingT=";
```

stdmcising.h contains functions called by the main program `glgew1d.c`. The constants, variables and quantities

$$a = 4\beta J \quad \text{and} \quad b = 2\beta h,$$

as declared in `constantsising.h` are used. The arrays *test* and *boltz* are needed for the Mont Carlo iterations. The first argument of these arrays is the value

```
/* header file stdmcising.h */
/* functions check and boltz: */
/* provides  arrays test and boltzmann.*/
```

```
/* mcsweep: MA sweeps over lattice */
/* moments: calculates average of spins */
void check(void)
{
  if (b>0){
    test[2][4]=1;test[2][2]=1;test[0][2]=0;test[0][4]=0;
    if (b>a) {test[0][0]=0;test[2][0]=1;}
    else {test[0][0]=1;test[2][0]=0;};
  }
  else{
    test[2][0]=0;test[0][2]=1;test[2][2]=0;test[0][0]=1;
    if(a+b>0) {test[2][4]=1;test[0][4]=0;}
    else {test[2][4]=0;test[0][4]=1;};};
}
void boltzmann(void)
{
 boltz[2][4]=exp(-a-b);boltz[2][2]=exp(-b);
 boltz[2][0]=exp(a-b);boltz[0][4]=exp(a+b);
 boltz[0][2]=exp(b);boltz[0][0]=exp(-a+b);
}
void mcsweep(short *s)
{
  int p,q;
  for (p=0;p<MA;p++)
         for (q=0;q<N;q++){
           nn=s[(q+1)%N]+s[(q+N-1)%N]+2;
           si=s[q]+1;
           if (test[si,nn]==0) {s[q]=-s[q];ann=ann+1;}
           else
             if (drand48()<boltz[si][nn]){
               s[q]=-s[q];ann=ann+1;};
         };
}
/* calculation of moments */
double moments(short n,short *s)
{
  int p,sum=0;
  for (p=0;p<N;p++)
 sum=sum+s[p];
    /*sum=sum+pow(s[il],n);*/
  return (double)sum/N;
}
```

of the spin s_x plus 1. The next argument is equal to the sum of the spins of the nearest neighbors plus 2. If the energy decreases during the change of s_x, we set $test = 0$. Otherwise we set $test = 1$. The Boltzmann weights are stored in the array *boltz*, in order to spare computing time for the calculation of the exponential function. The basic routine is `mcsweep`, where one finds the $MA \cdot MC$ iterations through the lattice. It is tested how often a change is accepted. We determined the magnetization as a function of h for different temperatures with this code. Figure 6.1 shows the results of the Monte Carlo simulations for $N = 128$. The agreement between the MC-data for $N = 128$ and the exact solution for $N = \infty$ is quite remarkable.

6.6 Problems

6.1 (Two-dimensional Ising model: part I) Determine the inner energy density and the magnetization via the summation over all configurations for a 2×2, 3×3 and 4×4 lattice. Assume thereby periodic boundary conditions and choose $\beta = 0$ to 1 in steps of 0.05. Assume that the external field h vanishes and set J in

$$H = -J \sum_{\langle xy \rangle} s_x s_y$$

equal to 1. Plot your results.

Calculate both $\langle m \rangle$ and $\langle |m| \rangle$. Is it really necessary to calculate $\langle m \rangle$?

6.2 (Two-dimensional Ising model: part II) Adapt the program on p. 114 in order to simulate the *two-dimensional* Ising model via the Metropolis algorithm. Choose $\beta = 0.4406868$ and $h = 0$. Perform the simulations on 4×4, 8×8 and 32×32 lattices with 200000 sweeps over the lattice each time. Determine

$$u = \frac{1}{V} \langle H \rangle, \qquad \big\langle |m| \big\rangle \quad \text{and} \quad \big\langle m^2 \big\rangle.$$

Compare the result for the 4×4 lattice with the outcome of the analytical calculation in Problem 6.1.

6.3 (Minima of energy function) Find the configurations with minimal energy of the following spin models:

1. The Ising chain with first and second neighbor interactions

$$H = -J_1 \sum_x s_x s_{x+1} - J_2 \sum_x s_x s_{x+2}, \quad s_x \in \{-1, 1\}.$$

   Consider both positive and negative values of the couplings J_1, J_2.
2. The one-dimensional clock model

$$H = -J_c \sum_x \cos\big\{2\pi (n_x - n_y + \Delta)/q\big\}$$

   for positive J and all values of Δ.
3. The antiferromagnetic Ising model on a triangular lattice,

$$H = J \sum_{\langle x,y \rangle} s_x s_y, \quad s_x \in \{-1, 1\}$$

   with $J > 0$.

References

1. W. Lenz, Beitrag zun Verständnis der magnetischen Erscheinungen in Festkörper. Z. Phys. **21**, 613 (1920)

2. E. Ising, Beitrag zur Theorie des Ferromagnetismus. Z. Phys. **31**, 253 (1925)
3. R. Peierls, Statistical theory of adsorption with interaction between the adsorbed atoms. Proc. Camb. Philos. Soc. **32**, 471 (1936)
4. R. Peierls, On Ising's model of ferromagnetism. Proc. Camb. Philos. Soc. **32**, 477 (1936)
5. H.A. Kramers, G.H. Wannier, Statistics of the two-dimensional ferromagnet. Part I. Phys. Rev. **60**, 252 (1941)
6. L. Onsager, Crystal statistics. I. A two-dimensional model with an order-disorder transition. Phys. Rev. **65**, 117 (1944)
7. R.P. Feynman, *Statistical Mechanics* (Benjamin, Elmsford, 1972)
8. B.M. McCoy, T.T. Wu, *The Two-Dimensional Ising Model* (Harvard University Press, Harvard, 1973)
9. C. Thompson, *Mathematical Statistical Mechanics* (Princeton University Press, Princeton, 1972)
10. L.E. Reichl, *A Modern Course in Statistical Physics* (Wiley, New York, 1998)
11. R.B. Potts, Some generalized order-disorder transformations. Proc. Camb. Philos. Soc. **48**, 106 (1952)
12. L. Mittag, M. Stephen, Dual transformation in many-component Ising models. J. Math. Phys. **12**, 441 (1971)
13. R. Baxter, Potts model at the critical temperature. J. Phys. C **6**, L445 (1973)
14. J.M. Kosterlitz, D.J. Thouless, Ordering, metastability and phase transitions in two-dimensional systems. J. Phys. C **6**, 1181 (1973)
15. J.M. Kosterlitz, The critical properties of the two-dimensional XY-model. J. Phys. C **7**, 1046 (1974)
16. J.V. Jose, L.P. Kadanoff, S. Kirkpatrick, D.R. Nelson, Renormalization, vortices, and symmetry-breaking perturbations in 2-dimensional planar model. Phys. Rev. B **16**, 1217 (1977)
17. N. Madras, G. Slade, *The Self-Avoiding Walk* (Birkhäuser, Boston, 1993)
18. J.M. Yeomans, *Statistical Mechanics of Phase Transitions* (Clarendon, Oxford, 1992)
19. G. Roepstorff, *Path Integral Approach to Quantum Physics* (Springer, Berlin, 1996)

Chapter 7
Mean Field Approximation

Since only a few lattice models can be solved explicitly one is interested in efficient approximation schemes. A simple and universally applicable approximation is the mean-field approximation (MFA) which yields qualitatively correct results for many lattice systems. When applied to ferromagnets it is often called the *Curie–Weiss approximation* and when applied to lattice gases the *Bragg–Williams approximation*. The approximation appeared in PIERRE WEISS' work back in 1907 [1], where, building on earlier results of PAUL LANGEVIN [2], he obtained a model which explains the Curie point below which ferromagnetism sets in. Often when one deals with systems with very many degrees of freedom one uses the universally applicable MFA to gain information about the qualitative behavior of the system. In some cases the approximation even produces exact results, for example for universal quantities.

In the MFA one replaces the microscopic interaction of a spin with its neighboring spins by an approximate interaction of the spin with the averaged spin generated by all other spins. In the mean-field ensemble the spin variables are independently distributed and under homogeneity assumptions on the interactions they are even equally distributed. Hence the calculation of the free energy density or the order parameter, e.g. the magnetization of the system, reduces to a single spin problem. In this chapter we discuss the approximation for spin models and Euclidean lattice field theories in arbitrary dimensions. The MFA is discussed in many books on statistical mechanics and field theory. It may be useful to consult [3–5].

7.1 Approximation for General Lattice Models

We begin with the variational characterization of the free energy and the free energy with fixed average field as outlined in Sect. 6.4. In the MFA we only admit *product probability measures* on the configuration space Ω in the variational principle (6.46),

$$\mathrm{d}P(\omega) = \prod_x \mathrm{d}\nu_x(s_x), \quad \mathrm{d}\nu_x(s) = \mathrm{d}\mu(s)\, p_x(s), \tag{7.1}$$

A. Wipf, *Statistical Approach to Quantum Field Theory*, Lecture Notes in Physics 864,
DOI 10.1007/978-3-642-33105-3_7, © Springer-Verlag Berlin Heidelberg 2013

where $\nu_x(s)$ is the probability measure for the spin at site x and μ the site-independent single spin distribution. Since we minimize the free energy functional only on a *subset* of all probability measures, the energy functional $F_{\mathrm{mf}}[m]$ in the mean -field approximation bounds the exact functional $F[m]$ from above,

$$F_{\mathrm{mf}}[m] \geq F[m]. \tag{7.2}$$

Note that in contrast to the set of probability measures the set of product measures is not convex such that F_{mf} need not be convex. For a product probability measure we have

$$\mathrm{d}P(\omega)\log p(\omega) = \prod_x \mathrm{d}\nu_x(s_x)\sum_y \log p_y(s_y), \qquad \int \mathrm{d}\nu_x(s) = 1,$$

such that the entropy of the total system is equal to the sum of single-site entropies,

$$S_{\mathrm{B}}(P) = \sum_x s_{\mathrm{B}}(p_x), \quad s_{\mathrm{B}}(p_x) = -\int \mathrm{d}\nu_x(s)\log p_x(s). \tag{7.3}$$

In addition the constraint on the probability measure $P(\omega)$ in (6.46) turns into V independent constraints for the single-site measures ν_x,

$$\int \mathrm{d}\nu_x(s)s = \int \mathrm{d}\mu(s)p_x(s)s = m_x. \tag{7.4}$$

To proceed we must specify the energy functions to be considered. For general spin systems the energy has the form

$$H(\omega) = -\sum_{x\neq y} J_{xy}s_x s_y + \sum_x Q_x(s_x), \tag{7.5}$$

where the last term contains a possible coupling to an external field or a self-interaction of the spin variables. Due to the constraints (7.4) we find the average energy

$$\int \mathrm{d}P(\omega)H(\omega) = -\sum_{x\neq y} J_{xy}m_x m_y + \sum_x \int \mathrm{d}\nu_x(s)Q_x(s). \tag{7.6}$$

It follows that for a product measure the free energy functional takes the form

$$F_{\mathrm{mf}}[m] = -\sum_{x\neq y} J_{xy}m_x m_y + \sum_x \alpha_x(m_x), \tag{7.7}$$

where the function α_x only depends on the prescribed average field on site x and has the variational characterization

$$\alpha_x(m_x) = \inf_{p_x}\left(\int \mathrm{d}\nu_x(s)\big\{Q_x(s) + T\log p_x(s)\big\}\,\Big|\,\int \mathrm{d}\nu_x(s)s = m_x\right). \tag{7.8}$$

Thus for product measures the difficult variational problem on the space of probability measures on Ω simplifies considerably to V variational problems on single sites. The minimizing probability density p_x in (7.8) is given by

$$p_x(s) = \frac{1}{z_x(j_x)}\mathrm{e}^{-\beta Q_x(s)+j_x s}, \quad z_x(j_x) = \int \mathrm{d}\mu(s)\mathrm{e}^{-\beta Q_x(s)+j_x s}, \tag{7.9}$$

whereby the multiplier j_x is determined by the *self-consistency equation*

$$m_x = \int \mathrm{d}\mu(s)\, p_x(s) s = \frac{\mathrm{d}w_x}{\mathrm{d}j_x}, \quad w_x(j_x) = \log z_x(j_x). \tag{7.10}$$

This key equation is often called the *gap equation*. Inserting the result for the density into the expression for α_x finally yields

$$\beta\alpha_x(m_x) = j_x m_x - w_x(j_x) = (\mathscr{L} w_x)(m_x). \tag{7.11}$$

To summarize: In the MFA the free energy functional $F_{\mathrm{mf}}[m]$ for a prescribed average field is given by (7.7), whereby α_x is proportional to the Legendre transform of $w_x = \log z_x$ with one-site partition function z_x given in (7.9).

Let us turn to homogeneous spin systems with $Q_x = Q$ and assume that the average field is constant, in which case

$$\sum_{x \neq y} J_{xy} m_x m_y = \frac{V}{2} \tilde{J} m^2, \quad \text{with } \tilde{J} = \frac{2}{V} \sum_{x \neq y} J_{xy}. \tag{7.12}$$

For lattice models with $J_{xy} = J$ for nearest-neighbor pairs x, y and zero otherwise, the *effective coupling* is

$$\tilde{J} = q J, \tag{7.13}$$

where q denotes the *coordination number*, i.e. the number of nearest neighbors of a given site. For a d-dimensional hyper-cubic lattice $q = 2d$. Homogeneous systems have an extensive free energy and it is advantageous to proceed with the intensive *free energy density*. In the MFA this density is given by

$$f_{\mathrm{mf}}(m) = -\frac{1}{2} \tilde{J} m^2 + T(\mathscr{L} w)(m); \tag{7.14}$$

and hence we remain with evaluating the Legendre transform of

$$w(j) = \log z(j), \quad \text{with } z(j) = \int \mathrm{d}\mu(s) \mathrm{e}^{-\beta Q(s) + js}. \tag{7.15}$$

To calculate $\mathscr{L} w$ we must solve the gap equation. Note that in the MFA the dimension of the lattice enters only via the relations (7.12, 7.13) between the microscopic couplings and the effective coupling $\tilde{J}$.

7.2 The Ising Model

Let us apply the general results to Ising models on hyper-cubic lattices with a single spin (Bernoulli) measure

$$\mathrm{d}\mu(\omega) = \prod_x \mathrm{d}\mu(s_x), \quad \mathrm{d}\mu(s) = \frac{1}{2}\delta(s-1)\,\mathrm{d}s + \frac{1}{2}\delta(s+1)\,\mathrm{d}s. \tag{7.16}$$

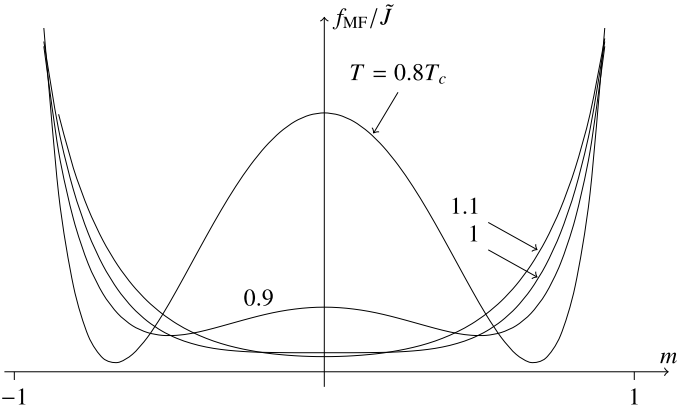

Fig. 7.1 Free energy density as a function of the magnetization m at different temperatures T/T_c

For a vanishing magnetic field in (6.1) the interaction term Q in (7.15) is absent and we obtain the simple one-site partition function $z(j) = 2\cosh(j)$. Note that in contrast to the discrete microscopic spin the average field in the free energy density

$$f_{\mathrm{mf}}(m) = -dJm^2 + T(\mathscr{L}w)(m) \tag{7.17}$$

is a continuous variable with values in the interval $[-1, 1]$. To calculate the Legendre transform of $w(j) = \log(2\cosh j)$ we solve the gap equation $m = \tanh(j)$ for $j(m)$ and insert the result into

$$(\mathscr{L}w)(m) = mj(m) - \log\bigl\{\cosh j(m)\bigr\}. \tag{7.18}$$

Next we insert the Legendre transform into the defining equation (7.17) for the free energy density and obtain the simple expression

$$f_{\mathrm{mf}}(m) = -dJm^2 + \frac{1+m}{2\beta}\log(1+m) + \frac{1-m}{2\beta}\log(1-m). \tag{7.19}$$

Figure 7.1 shows a plot of the density in units of $\tilde{J}$ in the regime near the critical temperature. We observe that the curvature at the origin changes sign at the temperature $T_{c,\mathrm{mf}} = 2dJ$. This defines the critical temperature in the MFA. *Below* this temperature the free energy shows a local maximum at the origin as well as two global minima at $\pm m_0$. Above the critical temperature there is one global minimum at the origin.

The variational characterization of the free energy functional $F[m]$ as discussed in Sect. 6.4 emphasizes that

$$P_{\mathrm{mf}}(m) = \frac{1}{Z_{\mathrm{mf}}}\mathrm{e}^{-\beta V f_{\mathrm{mf}}(m)} \tag{7.20}$$

is to be interpreted as the probability distribution for finding the average field m in the MFA. Clearly, for large volumes this distribution shows distinct maxima at the

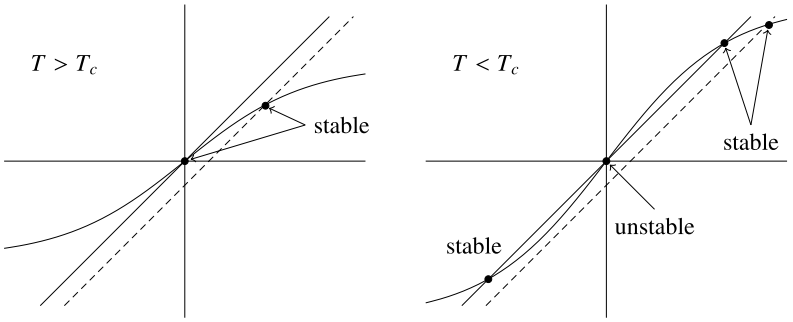

Fig. 7.2 Determination of the critical temperature in the MFA. The *continuous lines* through the origin belong to $h = 0$ and the *dashed lines* to $h \neq 0$

minima of the free energy density. A minimum m_0 of the density (7.19) solves the *gap equation*

$$2dJm_0 = \frac{1}{2\beta}\log\frac{1+m_0}{1-m_0} \quad \Longrightarrow \quad m_0 = \tanh(2dJ\beta m_0). \tag{7.21}$$

To simplify this self-consistency equation for the mean field we define the dimensionless quantity $x := 2dJ\beta m_0$, which obeys

$$\frac{T}{2dJ}x = \tanh x. \tag{7.22}$$

The slope of the linear function on the left-hand side is greater than the slope of the tanh-function on the right-hand side for

$$T > T_{c,\mathrm{mf}} = 2dJ, \tag{7.23}$$

and then there exists only the solution $x = 0$. If the temperature is less than $T_{c,\mathrm{mf}}$, then the transcendental equation (7.22) admits three solutions: $x = 0$ and $x = \pm m_0$. To gain further insight we couple the spins to an external field by adding the term $-h\sum s_x$ to the energy function. This amounts to adding the term $-hm$ to the free energy density f_{mf} such that now the minimizing magnetization obeys

$$m_0 = \tanh(2dJ\beta m_0 + \beta h) = \tanh\left(\frac{T_c}{T}m_0 + \beta h\right). \tag{7.24}$$

Solutions of this *gap equation* are given by the intersection points in Fig. 7.2. For $h \neq 0$ the system is magnetized even for very high temperatures $T \gg T_c$.

7.2.1 An Alternative Derivation

Here we present a derivation of the MFA as it is contained in many textbooks on statistical mechanics, see for example [6]. The main idea is the substitution of the

microscopic interaction of a spin with its neighbors by an *averaged interaction* with all spins:

$$J_{xy} \to \frac{1}{V}\sum_{y} J_{xy} = \frac{\tilde{J}}{V}. \tag{7.25}$$

For translationally invariant systems the effective coupling strength $\tilde{J}$ does not depend on the site. In models with short-range interaction we have $\tilde{J} = qJ$ with coordination number q. With the approximation (7.25) the energy function (6.1) becomes

$$H \to H_{\mathrm{mf}} = -\frac{V\tilde{J}}{2}m^2(s) - Vhm(s), \quad m(s) = \frac{1}{V}\sum s_x. \tag{7.26}$$

For the Ising model with $s_x = \pm 1$ the mean field $m(s)$ takes its values in

$$M = \{-1, -1+\delta, -1+2\delta, \ldots, 1-\delta, 1\}, \quad \delta = \frac{2}{V}.$$

There are $V(1+m)/2$ spins pointing "upward" and $V(1-m)/2$ spins pointing "downward" and the number of possible spin configurations with fixed $m \in M$ is equal to

$$d(m) = \frac{V}{[\frac{1}{2}V(1+m)]![\frac{1}{2}V(1-m)]!}. \tag{7.27}$$

With the help of Stirling's formula

$$\log(n!) = n(\log n - 1) + o(n)$$

we obtain the following approximation for the partition function:

$$Z_{\mathrm{mf}} = \sum_{m\in M} d(m)\mathrm{e}^{-\beta H_{\mathrm{mf}}(m)} = \sum_{m} \mathrm{e}^{-\beta V f_{\mathrm{mf}}(m)}, \tag{7.28}$$

where $f_{\mathrm{mf}}(m)$ is the free energy density (7.19), up to corrections of order $o(V)/V$. In the thermodynamic limit these corrections vanish and at the same time m becomes a continuous field $m \in [-1, 1]$.

7.3 Critical Exponents $\alpha, \beta, \gamma, \delta$

The mean field predicts that the Ising model shows a phase transition from an ordered ferromagnetic phase to a disordered paramagnetic phase. More sophisticated methods presented in the following chapters show that the mean-field prediction is correct in two and more dimensions. A critical temperature separates the low-temperature ferromagnetic phase with non-zero magnetization from the high-temperature paramagnetic phase without magnetization. The free energy is no longer differentiable at the critical temperature $T = T_c$ and the resulting singularities are parametrized by universal *critical exponents*. In this section we calculate the most important critical exponents in the mean-field approximation.

Table 7.1 Most commonly used critical exponents for magnetic systems

zero-field specific heat	α	$c_h \sim \lvert t\rvert^{-\alpha}$
zero-field magnetization	β	$m \sim t^{\beta}$
zero-field isothermal susceptibility	γ	$\chi_T \sim \lvert t\rvert^{-\gamma}$
critical isotherm ($t = 0$)	δ	$h \sim \lvert m\rvert^{\delta}\mathrm{sgn}(m)$
correlation length	ν	$\xi \sim \lvert t\rvert^{-\nu}$
pair correlation function at T_c	η	$G(\mathbf{x}) \sim 1/r^{d-2+\eta}$

Let us introduce the *reduced temperature*, i.e. the relative deviation of the temperature from the critical temperature,

$$t = \frac{T_c - T}{T_c}. \tag{7.29}$$

The critical exponent λ associated with a macroscopic observable $g(t)$ is defined by

$$g(t) \sim |t|^{\lambda}. \tag{7.30}$$

This equation only represents the asymptotic behavior of the function $g(t)$ as $t \to 0$. More generally one might expect

$$g(t) \sim A|t|^{\lambda}\left(1 + bt^{\lambda_1} + \cdots\right) \quad \text{with } \lambda_1 > 0. \tag{7.31}$$

The definitions of the most commonly used critical exponents are listed in Table 7.1. The exponent δ characterizes the singular function $h = h(m)$ and the exponent η the anomalous behavior of the two-point function at the critical temperature. In compiling Table 7.1 we have made the unjustified assumption that the critical exponents associated with a given thermodynamic variable are the same as $T \to T_c$ from above and below. Early series expansions and numerical results suggested that this was the case, but it was only with the advent of the renormalization group that it was indeed proved to be so. A common notation was using a prime to distinguish the value of an exponent as $T \uparrow T_c$ from the value as $T \downarrow T_c$.

In what follows we obtain the mean-field values of the critical exponents α, β, γ and δ in the Ising model. They can be extracted from our previous results for the free energy and magnetization. Later we shall argue that the critical exponents are very universal: two spin models in the same dimension for which the order parameter has the same symmetry should possess identical critical exponents.

7.3.1 Susceptibility

Above the critical temperature the magnetization $m_0(h)$ in Eq. (7.24) approaches zero for $h \to 0$ and the susceptibility

$$\chi = \left(\frac{\partial m_0}{\partial h}\right)\Big|_{h=0} = \sum_y \big(\langle s_x s_y\rangle - \langle s_x\rangle\langle s_y\rangle\big)\Big|_{h=0} \tag{7.32}$$

fulfills the *Curie–Weiss law*

$$\chi \overset{m_0(0)=0}{=} \beta(\chi T_c + 1) \quad \Longrightarrow \quad \chi = \frac{1}{T - T_c}, \tag{7.33}$$

where we made use of (7.21). Hence the susceptibility diverges at the critical point and we obtain for $T \downarrow T_c$ or $T \uparrow T_c$ the scaling law

$$\chi \sim |t|^{-1}. \tag{7.34}$$

The *critical exponent* of the susceptibility is $\gamma = 1$.

7.3.2 Magnetization as a Function of Temperature

Below the critical temperature and for $h > 0$ the magnetization $m_0(h)$ is given by the largest solution to (7.24). In the limit $h \downarrow 0$ we find a spontaneous magnetization $m_0(T)$ which approaches zero for temperatures $T \uparrow T_c$. This justifies a series expansion of the tanh-function in (7.21) in powers of m_0 with the result

$$m_0 = \frac{T_c}{T} m_0 - \frac{1}{3}\left(\frac{T_c}{T} m_0\right)^3 + \cdots,$$

where $T_c = 2dJ$. As expected, this equation has three solutions, given by

$$m_0 = 0 \quad \text{and} \quad m_0 \approx \pm \frac{T}{T_c}(3t)^{1/2}. \tag{7.35}$$

The first solution belongs to an unordered paramagnetic state and the two other solutions describe ordered ferromagnetic low-temperature phases. The ordered states minimize the free energy density at low temperature. Figure 7.3 illustrates the temperature dependence of the spontaneous magnetization $m(T)$. It approaches zero as $T \uparrow T_c$ according to

$$m_0(T) = \frac{T}{T_c}(3t)^{1/2}. \tag{7.36}$$

Since $m_0 \neq 0$ corresponds to an ordered and $m_0 = 0$ to an unordered state, we call the spontaneous magnetization an *order parameter* of the system. We associate the critical exponent β with the order parameter of the transition,

$$m_0(T) \sim t^{\beta}. \tag{7.37}$$

Hence the MFA predicts a critical exponent[1] β of $1/2$.

[1] The exponent β should not be confused with the inverse temperature.

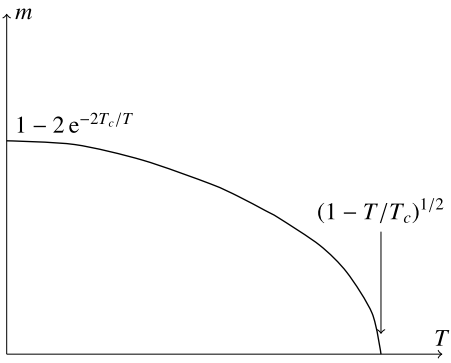

Fig. 7.3 The temperature dependence of the magnetization m in the mean-field approximation

7.3.3 Specific Heat

In the MFA the *inner energy density* of the Ising model is given by

$$u = \frac{\partial}{\partial \beta}(\beta f) = -dJm_0^2 - hm_0, \tag{7.38}$$

such that the specific heat is given in terms of the magnetization by

$$c = \frac{\partial u}{\partial T} = -(T_c m_0 + h)\frac{\partial m_0}{\partial T}, \quad T_c = 2dJ. \tag{7.39}$$

Above T_c the vanishing magnetization leads to a vanishing specific heat and below T_c the gap equation (7.21) implies

$$c = -\frac{(T_c m_0 + h)^2}{TT_c - T^2/(1 - m_0^2)}.$$

We set $h = 0$ and rewrite the denominator by using the formula (7.35) for m_0 at temperature $T \lesssim T_c$. This yields

$$TT_c - \frac{T^2}{1 - m_0^2} \approx T(T_c - T) - T^2 m_0^2 \approx tTT_c\left(1 - \frac{3T^3}{T_c^3}\right).$$

Taking into account that $(T_c m_0)^2 \approx 3tT^2$ we finally arrive at

$$c \approx -\frac{T}{T_c}\frac{3}{1 - 3T^3/T_c^3} \overset{T \nearrow T_c}{\to} \frac{3}{2}. \tag{7.40}$$

This means that the specific heat jumps at $T = T_c$ from the value $3k_B/2$ below T_c to the value 0 above T_c.

7.3.4 Magnetization as a Function of the Magnetic Field

The magnetization as a function of the magnetic field h follows from the self-consistency equation (7.24). We expand the right-hand side of this equation at $T = T_c$ up to third order in h according to

$$m_0 = m_0 + \beta_c h - \frac{1}{3}(m_0 + \beta_c h)^3 + \cdots \quad \Rightarrow \quad \beta_c h = \frac{1}{3}(m_0 + \beta_c h)^3 + \cdots . \tag{7.41}$$

The consistent assumption $\beta_c h \ll m_0$ leads to

$$m_0 \approx (3\beta_c h)^{1/3}, \quad (T = T_c). \tag{7.42}$$

In general, the scaling law

$$m_0 \sim h^{1/\delta} \quad \text{at } T = T_c \tag{7.43}$$

defines the critical exponent δ. Hence, our mean-field studies yield a critical exponent of $\delta = 3$.

7.3.5 Comparison with Exact and Numerical Results

This section is devoted to the comparison of the results of the mean-field approximation with the exact ones near the phase transition. The critical temperature T_c in the MFA only depends on the number of nearest neighbors (the coordination number) q according to the relation

$$T_{c,\mathrm{mf}} = q\,J \tag{7.44}$$

This simple result points to a first deficiency of the MFA: it predicts a phase transition for the Ising chain at a $T_c > 0$ in conflict with the exact result. In Table 7.2 we compare the mean-field predictions for the critical temperatures of Ising models on various two- and three-dimensional lattices with the known values. Note that with increasing coordination number q the MFA becomes more accurate. The MFA correctly predicts scaling laws for the magnetization and susceptibility as functions of the reduced temperature and for the magnetic field as a function of the magnetization in the vicinity of the critical point. But the mean-field critical exponents $\beta = 1/2$, $\gamma = 1$ and $\delta = 3$ are independent of the space dimension and disagree with the exactly known exponents in two dimensions, see Table 7.3. In addition the MFA predicts a jump of the specific heat at T_c in contrast to the exact solution in two dimensions which shows a logarithmic singularity. Similar differences are seen in three dimensions, see Table 7.3. However, the critical exponents of the MFA are the correct ones in $d > 4$ dimensions.

We summarize the main results of the mean-field approximation:

- The dimension d of the lattice enters the MFA only via $T_{c,\mathrm{mf}} = 2d\,J$.
- The order of the phase transition is predicted correctly for $d \geq 2$.

Table 7.2 Critical temperatures depending on dimension d and number q of neighbors

Lattice	d	q	$T_{c,\mathrm{mf}}/T_c$	$T_c/T_{c,\mathrm{mf}}$
square	2	4	1.763	0.567
triangular	2	6	1.648	0.607
simple cubic	3	6	1.330	0.752
body-centered cubic	3	8	1.260	0.794
face-centered cubic	3	12	1.225	0.816

Table 7.3 Critical exponents of the Ising model in two and three dimensions [7, 8]

Quantity		$d=2$ (exact)	$d=3$	Mean-field
zero-field specific heat	α	0 (log.)	0.110(1)	0 (jump)
zero-field magnetization	β	1/8	0.3265(3)	1/2
zero-field isothermal susceptibility	γ	7/4	1.2372(5)	1
critical isotherm ($t=0$)	δ	15	4.789(2)	3
correlation length	ν	1	0.6301(4)	1/2
pair correlation function at T_c	η	1/4	0.0364(5)	0

- The MFA predicts a $T_{c,\mathrm{mf}}$ which is greater than the exact T_c in $d \geq 2$.
- The critical exponents differ from the exact T_c for $d < 4$.
- The MFA does not account for short-range interactions effects.
- The MFA may lead to long-range correlations.

7.4 Mean-Field Approximation for Standard Potts Models

We minimize the free energy of the standard Potts model with the energy (6.10) on the set of product probabilities,

$$P(\omega) = \prod_x p_x(\sigma_x), \quad \sigma_x \in \{1, \ldots, q\}. \tag{7.45}$$

Due to translational invariance p_x does not depend on the site and without magnetic field we obtain the free energy density

$$f_{\mathrm{mf}}(\beta, p_n) = -d J_p \sum_{n=1}^{q} p_n^2 + T \sum_{n=1}^{q} p_n \log p_n, \tag{7.46}$$

where p_n denotes the probability of $\sigma_x = n$. Clearly, in the symmetric phase all probabilities are equal to $1/q$. We now minimize the free energy density with respect to the probability p_1 of σ_1 under the assumption of equal $p_2, \ldots, p_q$. We parametrize the corresponding probabilities as

$$p_1 = \frac{1}{q} + \frac{q-1}{q} x, \qquad p_{n>1} = \frac{1}{q} - \frac{x}{q} \quad \text{with} \quad -\frac{1}{q-1} \leq x \leq 1,$$

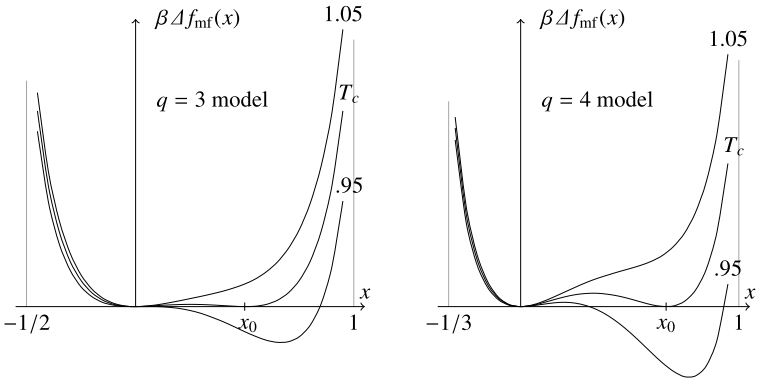

Fig. 7.4 The normalized free energy density for Potts models with $q = 3, 4$ in the MFA

where the value $x = 0$ characterizes the symmetric phase. Setting $q - 1 = q'$ the free energy density reads

$$f_{\rm mf}(x) = -\frac{dJ_p}{q}\left(1 + q'x^2\right) + \frac{1+q'x}{\beta q}\log\frac{1+q'x}{q} + \frac{q'(1-x)}{\beta q}\log\frac{1-x}{q} \tag{7.47}$$

and its curvature at the origin vanishes for $2dJ_p = qT$. This defines the temperature

$$T_c' = \frac{2dJ_p}{q} \tag{7.48}$$

below which the symmetric phase is unstable. But for Potts models with $q \geq 3$ the free energy density has a second minimum at $x_0 > 0$ for temperatures near T_c'. The second minimum turns into an absolute minimum below a critical temperature $T_c > T_c'$. When the temperature drops the order parameter x jumps at the critical temperature

$$T_c = \frac{q-2}{q-1}\frac{dJ_p}{\log(q-1)} > T_c' \tag{7.49}$$

from 0 to $x_0 = (q-2)/(q-1)$. Figure 7.4 illustrates the change of the free energy density $\Delta f_{\rm mf}(x) = f_{\rm mf}(x) - f_{\rm mf}(0)$ in units of $k_B T$ for Potts models with $q = 3, 4$ and temperatures close to T_c. With increasing q we observe an increasing jump of the order parameter and the first-order phase transition gets stronger. For $q = 2$ the jump vanishes and the phase transition is of second order.

For large q the inner energy, free energy and latent heat per site at the critical point have the following expansions:

$$\begin{aligned} e_{\rm mf,c} &\simeq -dJ_p\left(1 - \frac{2}{q}\ldots\right) \\ \beta_c f_{\rm mf,c} &\simeq -\log q\left(1 + \frac{1}{q}\ldots\right) \\ \ell_{\rm mf,c} &\simeq dJ_p\left(1 - \frac{3}{q}\ldots\right). \end{aligned} \tag{7.50}$$

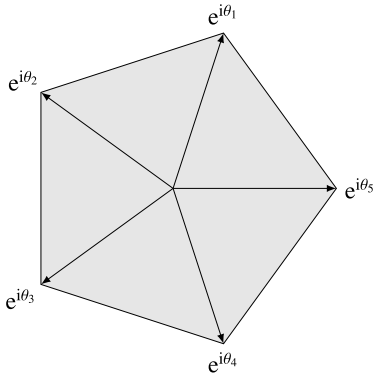

Fig. 7.5 The possible values of the magnetization m in the complex plane for the planar Potts model (clock model) with five states

To leading order in $1/q$ they agree with the exact values for the Potts models on a square lattice. This leads to the conjecture that the mean-field treatment of the Potts model provides an accurate description of the transition in two or higher dimensions if the number of components q is large.

7.5 Mean-Field Approximation for Z_q Models

In the MFA for the planar Potts models with energy functions (6.17) we minimize the free energy with respect to the product probabilities

$$P(\omega) = \prod_x p_x(\theta_x), \quad \theta_x \in \left\{ \theta_n = \frac{2\pi n}{q} \middle| n = 1, 2, \ldots, q \right\}, \tag{7.51}$$

where we fix the average field

$$\sum_{n=1}^{q} p_x(\theta_n) e^{i\theta_n} = m_x. \tag{7.52}$$

The average spin m_x lies in the convex region in the complex plane spanned by the q extremal points $\exp(i\theta_n)$, see the shaded region in Fig. 7.5. If all probabilities are zero except $p_n = 1$, then the magnetization points towards the nth corner of the q-gon and the corresponding states are *pure states* of the planar Potts model. The average energy for fixed m_x is given by

$$\sum_{\omega} p(\omega) H(\omega) = -\frac{J_p}{2} \sum_{\langle x,y \rangle} \left(m_x m_y^* + m_x^* m_y \right). \tag{7.53}$$

For a homogeneous magnetization p_x does not depend on the site and the free energy density takes the form

$$f_{\mathrm{mf}}(m) = \inf_{\{p_n\}} \left(-d J_p m m^* + T \sum_n p_n \log p_n \middle| \sum_n p_n e^{i\theta_n} = m \right), \tag{7.54}$$

where we used the abbreviation $p(\theta_n) = p_n$. The solution of this simple variational problem with constraints leads to

$$f_{\mathrm{mf}}(m) = -dJ_p mm^* + T(\mathscr{L}w)(m), \qquad \mathrm{e}^{w(j)} = \sum_n \exp\bigl(j\mathrm{e}^{\mathrm{i}\theta_n} + j^*\mathrm{e}^{-\mathrm{i}\theta_n}\bigr) \tag{7.55}$$

with the Legendre transform

$$(\mathscr{L}w)(m) = \sup_j \bigl\{jm + j^*m^* - w(j)\bigr\}. \tag{7.56}$$

However, for the models with three and four states we can minimize (7.54) directly. To do this we introduce the *moments* of the probability distribution

$$m_\ell = \sum_n p_n \mathrm{e}^{\mathrm{i}n\theta_\ell} = m^*_{q-\ell}, \quad \text{with } m_q = 1, m_1 \equiv m. \tag{7.57}$$

The individual probabilities can be reconstructed from the moments according to

$$p_n = \frac{1}{q}\bigl(1 + \mathrm{e}^{-\mathrm{i}\theta_n} m + \mathrm{e}^{\mathrm{i}\theta_n} m^*\bigr) + \frac{1}{q}\sum_{\ell=2}^{q-2} m_\ell \mathrm{e}^{-\mathrm{i}\ell\theta_n}. \tag{7.58}$$

The higher moments $m_2, \ldots, m_{q-2}$ as functions of the prescribed order parameter m follow from the requirement that the entropy contribution $\sum p_n \log p_n$ to (7.54) is minimal. For the 3-state model the last sum in (7.58) is absent and m determines all $\{p_n\}$. This leads to the free energy density

$$f_{\mathrm{mf}}^{q=3} = -dJ_p mm^* - T\log 3 + \frac{T}{3}\sum_{n=1}^{3}\bigl(1 + 2\Re\bigl(\mathrm{e}^{\mathrm{i}\theta_n} m\bigr)\bigr)\log\bigl(1 + 2\Re\bigl(\mathrm{e}^{\mathrm{i}\theta_n} m\bigr)\bigr). \tag{7.59}$$

The system shows a (weak) first-order phase transition at the critical temperature $T_c = 3dJ_p/(4\log 2)$. For the 4-state model we rewrite the free energy density as sum of the densities of two Ising models with the coupling $J_p/2$ according to

$$f_{\mathrm{mf}}^{q=4} = f_{\mathrm{mf}}^{\mathrm{Ising}}\left(\frac{J_p}{2}, m_1 + m_2\right) + f_{\mathrm{mf}}^{\mathrm{Ising}}\left(\frac{J_p}{2}, m_1 - m_2\right), \tag{7.60}$$

where $f_{\mathrm{mf}}^{\mathrm{Ising}}$ is the free energy density of the Ising model as given in (7.19). It immediately follows that the 4-state planar Potts model shows a second-order transition at $T_c = dJ_p$. All planar Potts models with $q > 4$ show a second-order transition as well and this fact is illustrated in Fig. 7.6. The critical temperature $T_{c,\mathrm{mf}} = dJ_p$ is independent of q for $q \geq 4$ and with increasing q the free energy density converges quickly to the density at $q \to \infty$.

7.6 Landau Theory and Ornstein–Zernike Extension

Lev Landau developed his celebrated theory of Fermi liquids in 1956 [9, 10]. Some years later experiments indicated that the prediction of his theory were satisfied, at least qualitatively, by liquid ^{3}He. The phenomenological theory based on

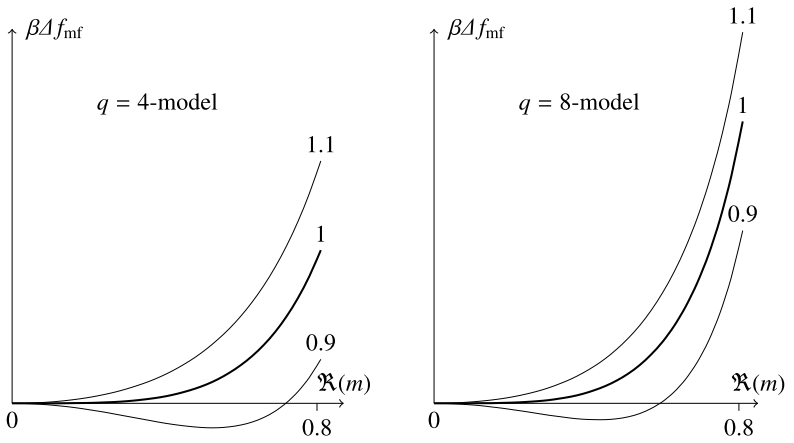

Fig. 7.6 The free energy density for the Z_q models (planar Potts models) with $q = 4$ and $q = 8$ in the vicinity of the critical temperature. The curves are labeled by T/T_c

Landau's original ideas is outlined in [11] and further results based on the methods of quantum field theory are found in [12–14]. The Landau theory is an attempt to formulate a general theory of second-order phase transitions[2] and it is based on very simple assumptions motivated by the MFA. The main assumption is that the free energy can be expanded as a power series in the order parameter m, where only those terms compatible with the symmetries of the system are admitted. Landau theory not only predicts a phase transition but also allows to reproduce the mean-field exponents showing clearly how they depend on the symmetry of the order parameter. Landau theory is an extension of the MFA and thus has similar shortcomings as this approximation. In particular it fails to predict the correct critical exponents below four dimensions. Many details of the Landau theory of phase transitions can be found in the textbook [15].

Consider the free energy of a ferromagnet with real order parameter m. Without a magnetic field the free energy is an even function of m such that in a series expansion only even powers of m occur,

$$f_{\mathrm{L}}(m) = f_0 + a_2 m^2 + a_4 m^4 + \cdots . \tag{7.61}$$

The coefficients in this expansion depend on the parameters of the system and in particular on the temperature. In case $a_4 > 0$ the series can be truncated after the term $O(m^4)$, because, as we shall see, subsequent terms cannot alter the critical behavior of the system. The Landau free energy (7.61) is plotted as a function of m for decreasing values of the coefficient a_2 in Fig. 7.7. For positive a_2 the minimum of the free energy density is at $m_0 = 0$ corresponding to a paramagnetic phase. For negative a_2 the minimum is at finite values $\pm m_0$ corresponding to a ferromagnetic

[2] Extensions of the theory are applicable to first-order phase transitions as well.

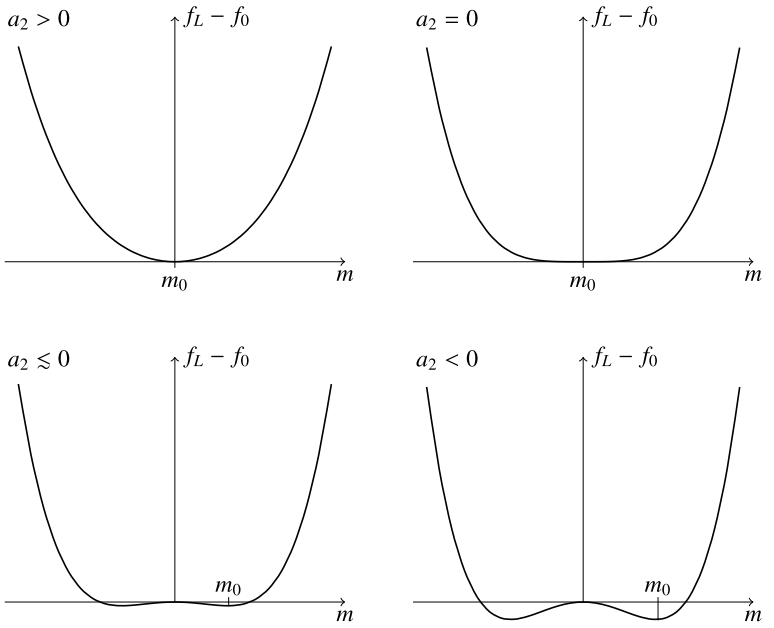

Fig. 7.7 Landau free energy as function of the magnetization for different couplings a_2

phase. The transition happens at $a_2 = 0$ which means that this value corresponds to the critical temperature. This suggests to write

$$a_2 = \tilde{a}_2 t \tag{7.62}$$

with a positive $\tilde{a}_2$ and the reduced temperature $t = (T - T_c)/T_c$. We take a positive coefficient a_4 in the quartic term such that the magnetization is bounded.

7.6.1 Critical Exponents in Landau Theory

The equilibrium *magnetization* corresponds to the minimum of the free energy and thus satisfies the equation

$$\left.\frac{df_{\mathrm{L}}}{dm}\right|_{m_0} = 2\tilde{a}_2 t m_0 + 4a_4 m_0^3 = 0. \tag{7.63}$$

For negative t the minimum is at

$$m_0 = \pm\sqrt{\frac{\tilde{a}_2}{2a_4}}(-t)^{1/2}\theta(-t) \tag{7.64}$$

such that we recover the mean-field critical exponent $\beta_{\rm mf} = 1/2$. The exponent α for the *specific heat* follows from differentiating

$$f_{\rm L}(m_0) = f_0 - \frac{\tilde{a}_2^2}{4a_4} t^2 \theta(-t)$$

twice with respect to the temperature. It is evident that the specific heat jumps at the critical temperature,

$$c_{T\uparrow T_c} - c_{T\downarrow T_c} = \frac{1}{T_c} \frac{\tilde{a}_2^2}{2a_4}\bigg|_{T_c} \tag{7.65}$$

and we recover the mean-field result $\alpha_{\rm mf} = 0$. To find the exponents γ and δ we add a magnetic field term $-hm$ to the Landau free energy,

$$f_{\rm L}(m) = f_0 - hm + \tilde{a}_2 t m^2 + a_4 m^4. \tag{7.66}$$

The minimizing equilibrium magnetization is determined by

$$2\tilde{a}_2 t m_0 + 4a_4 m_0^3 = h. \tag{7.67}$$

At the critical temperature the first term vanishes and the resulting relation $m_0^3 \sim h$ implies that the critical exponent δ attains the mean-field value $\delta_{\rm mf} = 3$. Finally, the variation of the equilibrium magnetization m_0 with the magnetic field at fixed temperature follows from (7.67). Inserting the zero-field value (7.64) yields the susceptibility

$$\chi = \frac{1}{3 - {\rm sgn}(t)} \frac{1}{\tilde{a}_2 |t|}, \tag{7.68}$$

and we recover the mean-field critical exponent $\gamma_{\rm mf} = 1$.

The exponents extracted from the Landau free energy are the same as the mean-field exponents of the Ising model. This is expected since the mean-field free energy of the Ising model (7.19) has the reflection symmetry and hence must have the expansion (7.61). To see this more explicitly we expand (7.19) in powers of m,

$$f_{\rm mf}^{\rm Ising}(J, m) = \frac{T_c}{2} t m^2 + \frac{T}{12} m^4 + \cdots, \quad T_c = qJ, \tag{7.69}$$

from which we can read off the coefficients $\tilde{a}_2$ and a_4. All reflection symmetric models with real order parameter have the Landau expansion (7.61) and thus have the same mean-field critical exponents. However, for some models (7.61) is not the appropriate expansion. For example, the Z_q-symmetry of the Potts models with $q \geq 3$ is compatible with a m^3-term in the Landau free energy. This cubic term gives rise to a first-order phase transition.

7.6.2 Two-Point Correlation Function

To determine the mean-field values of the exponents ν and η in Table 7.1 we need the asymptotic form of the two-point correlation function. For that purpose we invoke

the Ornstein–Zernike extension [16] of Landau's theory. Inspired by the mean-field result for the free energy with fixed inhomogeneous magnetization m_x in (7.7) we set

$$F_{\mathrm{L}}[T,m] - F_{\mathrm{L}}[T,0] = g \int \mathrm{d}^d x (\nabla m)_x^2 + \int \mathrm{d}^d x f_{\mathrm{L}}(m_x) \tag{7.70}$$

with a space dependent magnetization. The first term on the right-hand side is the lowest-order term in a gradient expansion of the spin-spin interaction and takes into account the contribution from non-parallel spins. The second term is just the integral over the Landau free energy density for a constant order parameter. Here we are only interested in the long-distance behavior of the correlation function near a critical point. Near the critical point the lattice spacing is small compared to the correlation length and we may approximate lattice sums by integrals.

To calculate the correlation length and anomalous scaling dimension η we need the connected two-point function of the microscopic spins,

$$G_c(x,y) = \langle s_x s_y \rangle - \langle s_x \rangle \langle s_y \rangle. \tag{7.71}$$

To relate this correlation function to the free energy we recall that $\beta F[m]$ is the Legendre transform of the generating functional for the connected correlation functions,

$$\beta F[m] = (\mathscr{L} W)[m], \quad W[j] = \log \int d\mu(\omega) e^{-\beta H(\omega) + (j,s)}, \tag{7.72}$$

cf. formula (6.48). Note that the second derivative of W is just the connected two-point function G_c. Now we make use of the result (5.92) on p. 98 to relate the second derivatives of W and F,

$$\beta \int \mathrm{d}^d y G_c(x,y) \frac{\delta^2 F}{\delta m_y \delta m_z} = \delta(x,z). \tag{7.73}$$

This result means that the second functional derivative of βF is the inverse of the connected two-point function,

$$G_c(x,y) = kT \left(\frac{\delta^2 F}{\delta m_x \delta m_y} \right)^{-1}. \tag{7.74}$$

The critical exponents ν and η are defined in the vicinity of a second-order transition point where the order parameter vanishes. Thus it suffices to take the Landau free energy to lowest order in the average field,

$$F_L[T,m] = g \int \mathrm{d}^d x \, (\nabla m)_x^2 + \tilde{a}_2 t \int \mathrm{d}^d x \, m_x^2, \tag{7.75}$$

in order to find the two-point function near T_c. The second derivative of F_{L} is

$$\frac{\delta^2 F_L}{\delta m_x \delta m_y} = -2g \Delta_{xy} + 2\tilde{a}_2 t \delta(x-y), \tag{7.76}$$

such that near the critical temperature the connected two-point function of the Landau theory takes the form

$$G_{\mathrm{L},c}(x,y) = \frac{kT}{2g}\langle x|\frac{1}{-\Delta + \tilde{a}_2 t/g}|y\rangle. \tag{7.77}$$

Up to the temperature dependent factor it is just the two-point function of the free scalar field with squared mass $m^2 = \tilde{a}_2 t/g$. It follows at once that for $t > 0$ and large separations $r = |x - y|$ in $d \geq 3$ dimensions

$$G_{\mathrm{L},c}(x,y) \sim \frac{\mathrm{e}^{-mr}}{r^{(d-1)/2}}, \quad T > T_c. \tag{7.78}$$

We conclude that near the critical point the correlation length $\xi = 1/m$ diverges as $\xi \sim t^{-1/2}$ implying that the Landau theory predicts a critical exponent $\nu = 1/2$. On the other hand, at the critical point $t = 0$ such that for $d \geq 3$

$$G_{\mathrm{L},c}(x,y) = \frac{C_d}{r^{d-2}}, \quad T = T_c. \tag{7.79}$$

This means that the Landau theory predicts $\eta = 0$. All critical exponents of the Landau theory are collected in the last column of Table 7.3.

7.7 Antiferromagnetic Systems

We return to general spin systems with energy functions

$$H(\omega) = -\sum_{x \neq y} J_{xy} s_x s_y + \sum_x Q_x(s_x), \quad s_x \in \mathscr{T}. \tag{7.80}$$

For ferromagnetic couplings $J_{xy} > 0$ the contribution $-J_{xy}s_x s_y$ to the energy is minimal for aligned spins and for anti-ferromagnetic couplings $J_{xy} < 0$ it is minimal for anti-parallel spins. Hence, we call a system with negative couplings $\{J_{xy}\}$ an *anti-ferromagnet*. In this section we discuss such systems within the framework of the MFA. We thereby consider translationally invariant systems with $Q_x = Q$ and $J_{xy} = J_{x-y}$. In general, the equilibrium state and average magnetization are not translationally invariant, in contrast to the energy function. Hence, in the MFA we dismiss the assumption of identical site probabilities p_x for the spins. Indeed, for anti-ferromagnets with nearest-neighbor interactions the lattice decomposes into two disjunct sublattices

$$\Lambda = \Lambda_{\mathrm{e}} \cup \Lambda_{\mathrm{o}}, \qquad \Lambda_{\mathrm{e}} \cup \Lambda_{\mathrm{o}} = \emptyset. \tag{7.81}$$

The sites in the even sublattice Λ_{e} have an even $x_1 + \cdots + x_d$ and the sites in the odd sublattice Λ_{o} have an odd $x_1 + \cdots + x_d$. We now suppose that the spins on the even and odd sublattices are identically distributed:

$$p_x = p_{\mathrm{e}} \quad \text{if } x \in \Lambda_{\mathrm{e}} \quad \text{and} \quad p_x = p_{\mathrm{o}} \quad \text{if } x \in \Lambda_{\mathrm{o}}, \tag{7.82}$$

where the probabilities p_e and p_o on the sites of the even and odd sublattices satisfy the constraints

$$\int \mathrm{d}\nu_{\mathrm{e,o}}(s)s = \int \mathrm{d}\mu(s)\, p_{\mathrm{e,o}}(s)s = m_{\mathrm{e,o}}. \tag{7.83}$$

As in (7.12) we introduce the mean coupling strengths

$$J_{\mathrm{ee}} = \frac{2}{V_\mathrm{e}} \sum_{x\neq y\in\Lambda_\mathrm{e}} J_{x-y}, \qquad J_{\mathrm{eo}} = \frac{2}{V_\mathrm{o}} \sum_{x\in\Lambda_\mathrm{e}, y\in\Lambda_\mathrm{o}} J_{x-y} \tag{7.84}$$

and similarly J_{oo} and J_{oe}. For a translationally invariant energy $J_{\mathrm{ee}} = J_{\mathrm{oo}}$ and $J_{\mathrm{eo}} = J_{\mathrm{oe}}$ and the inner energy density in the MFA takes the form

$$\frac{1}{V}\langle H\rangle = -\frac{J_{\mathrm{ee}}}{4}\big(m_\mathrm{e}^2 + m_\mathrm{o}^2\big) - \frac{J_{\mathrm{eo}}}{2} m_\mathrm{e} m_\mathrm{o} + \frac{1}{2}\int \mathrm{d}\nu_e\, Q(s) + \frac{1}{2}\int \mathrm{d}\nu_\mathrm{o}\, Q(s). \tag{7.85}$$

Henceforth one proceeds similarly as for ferromagnetic systems and determines the site probability densities which minimize the free energy subject to the constraints (7.83). With the help of two multipliers j_e and j_o one finds

$$p_{\mathrm{e,o}}(s) = \frac{1}{z(j_{\mathrm{e,o}})} \exp\big(-\beta Q(s) + j_{\mathrm{e,o}} s\big), \tag{7.86}$$

where the multipliers are fixed by the constraints. Inserting p_e and p_o into the expression for the free energy density yields

$$f_{\mathrm{mf}}(m_\mathrm{e}, m_\mathrm{o}) = -\frac{J_{\mathrm{ee}}}{4}\big(m_\mathrm{e}^2 + m_\mathrm{o}^2\big) - \frac{J_{\mathrm{eo}}}{2} m_\mathrm{e} m_\mathrm{o} + \frac{T}{2}(\mathscr{L}w)(m_\mathrm{e}) + \frac{T}{2}(\mathscr{L}w)(m_\mathrm{o}). \tag{7.87}$$

The last two terms contain the Legendre transform of the Schwinger function $w(j)$ on one lattice site as defined in (7.15).

For systems with only nearest-neighbor interactions $J_{\mathrm{ee}} = 0$. If in addition the nearest-neighbor couplings $J_{xy} = J$ are constant, then $J_{\mathrm{eo}} = 2dJ$. In particular, we find the following free energy density of the Ising model:

$$f_{\mathrm{mf}} = -dJ m_\mathrm{e} m_\mathrm{o} + \sum_{\alpha=\mathrm{o,e}} \left(\frac{1+m_\alpha}{4\beta} \log(1+m_\alpha) + \frac{1-m_\alpha}{4\beta} \log(1-m_\alpha) \right). \tag{7.88}$$

For a ferromagnetic coupling $J > 0$ the free energy is minimal for $m_\mathrm{e} = m_\mathrm{o}$ and we recover our previous result (7.19). To find the equilibrium magnetizations for anti-ferromagnetic couplings $J < 0$ we must solve the coupled gap equations

$$m_\mathrm{e} = \tanh(2dJ\beta m_\mathrm{o}) \quad \text{and} \quad m_\mathrm{o} = \tanh(2dJ\beta m_\mathrm{e}). \tag{7.89}$$

Besides the symmetric high-temperature phase with vanishing magnetizations on the two sublattices there exists an anti-ferromagnetic low-temperature phase at temperatures below $T_c = 2d|J|$. In this phase the two magnetizations point in opposite directions, i.e. $m_\mathrm{e} = -m_\mathrm{o}$. The magnetization on the even sublattice is given by the same transcendental equation,

$$m_\mathrm{e} = \tanh\big(2d|J|\beta m_\mathrm{e}\big), \tag{7.90}$$

as we encountered for ferromagnetic systems. For more details on the MFA for anti-ferromagnetic systems you may consult the textbook [17].

7.8 Mean-Field Approximation for Lattice Field Theories

In a lattice field theory the free energy for spin models with prescribed magnetization is replaced by the effective action, see (6.53). Hence we may use the results in Sect. 7.1 to obtain mean-field approximations for lattice scalar field theories. As for the spin models we only admit product measures

$$\mathrm{d}P(\phi) = \prod_x \mathrm{d}\nu_x(\phi_x), \quad \mathrm{d}\nu_x(\phi) = p_x(\phi)\mathrm{d}\mu(\phi), \tag{7.91}$$

in the variational principle for the effective action $\Gamma[\varphi]$ in (6.54). The site probability densities p_x fulfill the constraints

$$\int \mathrm{d}\mu(\phi)\, p_x(\phi)\phi = \varphi_x \tag{7.92}$$

and should minimize the effective action (6.54). The lattice action of a scalar field has the form

$$S[\phi] = -\frac{1}{2}\sum_{x,y} \phi_x \Delta_{xy} \phi_y + \sum_x V(\phi_x), \tag{7.93}$$

where Δ denotes the lattice-Laplacian. Since we assume invariance under lattice-translations, we have $\Delta_{xy} = \Delta_{x-y}$. We now decompose the derivative terms into a part fixed by the constraints $\langle\phi_x\rangle = \varphi_x$ and a remainder,

$$\sum_{x,y} \phi_x \Delta_{xy} \phi_y \to \sum_{x\neq y} \varphi_x \Delta_{xy} \varphi_y + \Delta_0 \sum_x \phi_x^2, \tag{7.94}$$

where $\Delta_0 \equiv \Delta_{xx}$. Except for the missing contribution $\Delta_0 \sum_x \varphi_x^2$ the first sum on the right-hand side is just the kinetic term of the mean field. Thus we add this contribution to the first sum and consequently subtract it from the second sum. Then we obtain for the action averaged with product measures

$$\int \mathrm{d}P(\phi) S[\phi] = -\frac{1}{2}\sum_{x,y} \varphi_x \Delta_{xy} \varphi_y + \sum_x \int \mathrm{d}\nu_x(\phi) V(\varphi_x, \phi), \tag{7.95}$$

wherein the shifted potential

$$V(\varphi, \phi) = \frac{\Delta_0}{2}\varphi^2 - \frac{\Delta_0}{2}\phi^2 + V(\phi) \tag{7.96}$$

with $V(\phi, \phi) = V(\phi)$ occurs. To solve the variational problem we proceed as we did for the spin models and end up with the following MFA for the effective action:

$$\Gamma_{\mathrm{mf}}[\varphi] = \frac{1}{2}\sum_x (\nabla\varphi_x)^2 + \sum_x u_{\mathrm{mf}}(\varphi_x). \tag{7.97}$$

Up to an additive term $\propto \varphi^2$ the effective potential $u_{\mathrm{mf}}(\varphi)$ is the Legendre transform of the convex $w(j) = \log z(j)$, where z is the Laplace transform of $-\Delta_0\phi^2/2 + V(\phi)$:

$$u_{\mathrm{mf}}(\varphi) = \frac{\Delta_0}{2}\varphi^2 + (\mathscr{L}w)(\varphi) \quad \text{with } \mathrm{e}^{w(j)} = \int \mathrm{d}\mu(\phi) \mathrm{e}^{j\phi + \frac{1}{2}\Delta_0\phi^2 - V(\phi)}. \tag{7.98}$$

For a translationally invariant theory with ferromagnetic couplings we may choose a homogeneous average field $\varphi_x = \varphi$. The extensive effective action is then proportional to the lattice volume βV and defines the intensive *effective potential* u_{mf}:

$$\Gamma_{\mathrm{mf}}[\varphi] = \beta V u_{\mathrm{mf}}(\varphi), \quad \varphi_x = \varphi. \tag{7.99}$$

One can show that u_{mf} represents the MFA of the *constraint effective potential*

$$\mathrm{e}^{-\beta V u_c(\varphi)} = \int \mathrm{d}\mu(\phi)\delta\left(\frac{1}{\beta V}\sum_x \phi_x - \varphi\right)\mathrm{e}^{-S[\phi]} \tag{7.100}$$

introduced in [18], see [19]. This result makes it clear that we must interpret

$$\mathrm{d}P_{\mathrm{mf}}(\varphi) = \frac{1}{Z_{\mathrm{mf}}}\mathrm{e}^{-\beta V u_{\mathrm{MF}}(\varphi)}\,\mathrm{d}\mu(\varphi) \tag{7.101}$$

as probability distribution for finding the mean constant field φ in the MFA. Since u_{mf} bounds the convex effective potential u from above, see (7.2), its convex hull

$$\left(\mathscr{L}^2 u_{\mathrm{mf}}\right)(\varphi) \geq u(\varphi) \tag{7.102}$$

is a better approximation for $u(\varphi)$. This improved approximation is the *Maxwell construction*. For a free theory with classical potential $V(\phi) = m^2\phi^2/2$ the effective potential (7.98) is (up to an additive constant) given by

$$w(j) = \frac{1}{2}\frac{j^2}{m_*^2} \quad \Longrightarrow \quad (\mathscr{L}w)(\varphi) = \frac{1}{2}m_*^2\varphi^2, \quad m_*^2 = m^2 - \Delta_0, \tag{7.103}$$

such that the effective potential is simply the classical potential, $u_{\mathrm{mf}}(\varphi) = V(\varphi)$.

7.8.1 ϕ^4 and ϕ^6 Scalar Theories

An interacting ϕ^4-theory with classical potential

$$V(\phi) = \frac{m^2}{2}\phi^2 + \frac{\lambda}{4}\phi^4, \tag{7.104}$$

gives rise to the site Schwinger function

$$w(j) = \log\int \mathrm{d}\phi \exp\left(j\phi - \frac{m_*^2}{2}\phi^2 - \frac{\lambda}{4}\phi^4\right) \tag{7.105}$$

with effective mass m_* defined in (7.103). In order to localize the phase transition in the parameter-space (m, λ) we need the second derivative of w at the origin

$$w''(0) = \frac{4z}{m_*^2}\frac{K_{3/4}(z) - K_{1/4}(z)}{K_{1/4}(z)}, \quad z := \frac{m_*^4}{8\lambda}, \tag{7.106}$$

where the modified Bessel functions of the second kind occur. For any Z_2-symmetric potential the strictly convex and symmetric function w has its (unique)

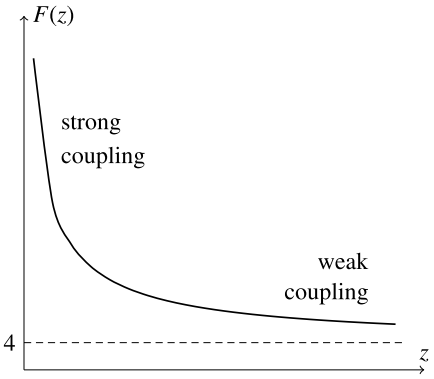

Fig. 7.8 The dependence of the monotonically decreasing function $F(z)$ in (7.109) as a function of the variable $z = m_*^4/8\lambda$

minimum at the origin such that $\varphi(j=0)=0$. According to (5.58) the curvature of $\mathscr{L}w$ at the origin is then equal to

$$(\mathscr{L}w)''(0) = \frac{1}{w''(0)}. \tag{7.107}$$

Thus the curvature of $u_{\rm mf}$ at the origin changes sign if

$$-\Delta_0 = \frac{m_*^2}{4z}\frac{K_{1/4}(z)}{K_{3/4}(z)-K_{1/4}(z)}. \tag{7.108}$$

This gap equation determines a critical curve in the (m^2,λ)-plane, where the symmetric phase with $\varphi=0$ becomes unstable. For the simplest lattice-Laplacian based on the forward or backward derivative we have $\Delta_0=-2d$. Hence the equation for the critical curve reads

$$\frac{4}{1+m^2/2d} = \frac{1}{z}\frac{K_{1/4}(z)}{K_{3/4}(z)-K_{1/4}(z)} \equiv F(z). \tag{7.109}$$

The monotonically decreasing function $F(z)$ approaches the value of 4 from above for large arguments and is plotted in Fig. 7.8. It follows that Eq. (7.109) can only be solved for negative m^2. Conversely, since $F(z)$ reaches infinity for $z\to 0$ there always exists a solution $\lambda_c(m^2)$ for $-2d<m^2<0$.

Next we examine the weak-coupling regime for which z in (7.106) is large. For $z\gg 1$ we insert the asymptotic expansions of the Bessel functions K_ν for large arguments [20] into the gap equation (7.109) and find

$$-\frac{m^2}{2d} = \frac{3}{8z} - \frac{3}{8z^2} + \cdots = \frac{3\lambda}{m_*^4}\left(1-\frac{8\lambda}{m_*^4}+\cdots\right). \tag{7.110}$$

Neglecting terms of the order $O(\lambda^3)$ in this relation we obtain the two solutions

$$\lambda_c(m) = \left(\frac{2d+m^2}{4}\right)^2\left(1\pm\sqrt{1+\frac{16m^2}{3d}}\right). \tag{7.111}$$

Since the "critical mass" vanishes for $\lambda=0$ we only keep the solution with negative sign. We have seen that m^2 must be negative for positive λ_c.

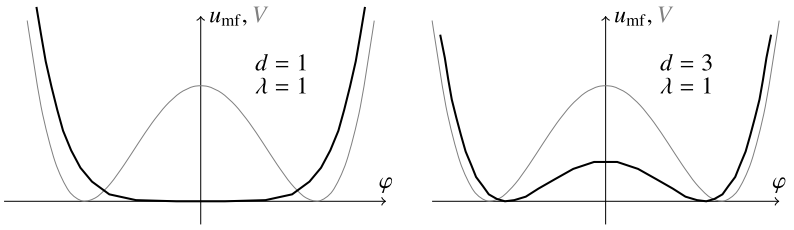

Fig. 7.9 The mean-field effective potential of the interacting ϕ^4-theory with classical double-well potential $\lambda(\phi^2-1)^2$ in one and three dimensions. u_{mf} is the effective potential in the MFA (*black*) and V the classical potential (*gray*)

The classical double-well potential $V(\phi) = \lambda(\phi^2-1)^2$ together with its mean-field effective potential u_{mf} in one and three dimensions are depicted in Fig. 7.9. Observe that with increasing dimension the minima of u_{mf} approach the minima of the classical potential. An `octave` program which computes u_{mf} is contained in the appendix to this chapter.

The Z_2-symmetric classical potential of the sixth order,

$$V(\phi) = \phi^6 - 3\phi^4 + \mu\phi^2, \tag{7.112}$$

and its effective potential in $d = 3$ dimensions are plotted in Fig. 7.10 for four values of the mass parameter μ. In the MFA the system shows a weak first-order transition at $\mu = 2$. For $\mu < 2$ the Z_2-symmetry is spontaneously broken since $\varphi \neq 0$. However, for $\mu \geq 2$ the order parameter vanishes and the Z_2-symmetry is restored.

7.8.2 $O(N)$ Models

The Euclidean action of the nonlinear $O(N)$ sigma model in d dimensions is

$$S = -\frac{1}{2g^2}\int \mathrm{d}^d x(\phi, \Delta\phi) \quad \text{with } \phi(x) \in \mathbb{R}^N,\ \phi(x)\cdot\phi(x) = 1. \tag{7.113}$$

On the lattice we approximate the continuum action by

$$H = -\frac{1}{2g^2}\sum_{x,y}\phi_x \Delta_{xy}\phi_y \quad \text{with } \phi_x \in \mathbb{R}^N,\ \phi_x^2 = 1, \tag{7.114}$$

where $\Delta_{xy} = \Delta_{x-y}$ is some translationally invariant lattice Laplacian. Product measures on the configuration space have the form (7.91) with single spin distribution

$$\mathrm{d}\mu(\phi) = \delta\big(\phi^2 - 1\big)\,\mathrm{d}^N\phi \tag{7.115}$$

and enforce the constraints $\phi_x^2 = 1$ on all lattice sites. The prescribed average field

$$\varphi_x = \int \mathrm{d}\nu_x(\phi)\phi \tag{7.116}$$

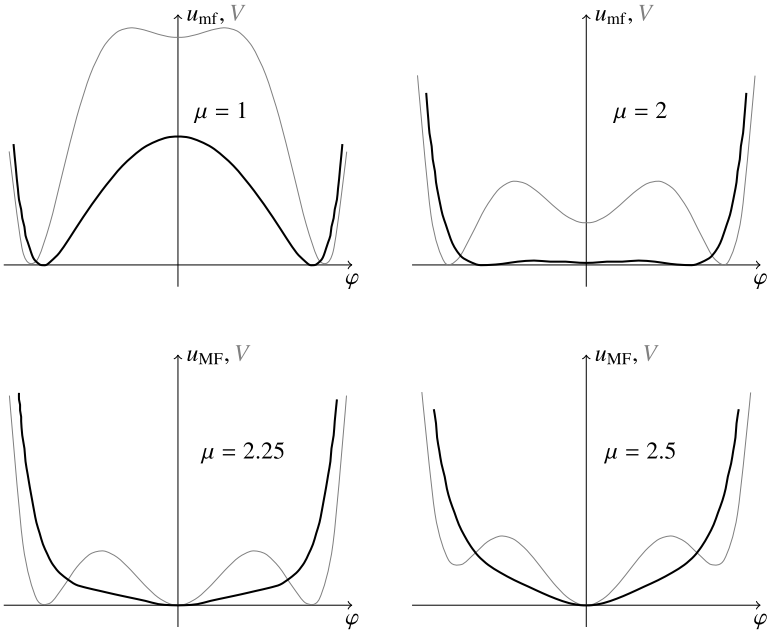

Fig. 7.10 The mean-field effective potential u_{mf} and classical potential V of the ϕ^6-theory with potential (7.112) in $d = 3$ dimensions for different values of the mass parameter μ

takes its values inside or on the boundary of the unit-ball in $\mathbb{R}^N$. For product measures the *averaged action* reads

$$\langle S \rangle = -\frac{1}{2g^2} \sum_{x,y} \varphi_x \Delta_{xy} \varphi_y - \frac{\Delta_0}{2g^2} \sum_x \big(1 - \varphi_x^2\big), \tag{7.117}$$

where $\Delta_0 = \Delta_{xx}$ appeared previously. The constraints (7.116) are implemented by multiplier fields and the solution of the associated variational problem for the site probability densities leads to the mean-field effective action

$$\Gamma_{\mathrm{mf}}[\varphi] = -\frac{1}{2g^2} \sum_{x,y} \varphi_x \Delta_{xy} \varphi_y + \sum_x u_{\mathrm{mf}}(\varphi_x). \tag{7.118}$$

The by now familiar effective potential

$$u_{\mathrm{mf}}(\varphi) = \frac{\Delta_0}{2g^2}\big(\varphi^2 - 1\big) + (\mathscr{L} w)(\varphi) \tag{7.119}$$

contains the Legendre transform of $w = \log z$ with one-site partition function

$$z(j) = \int \mathrm{d}^N \phi \delta\big(\phi^2 - 1\big) \mathrm{e}^{(j,\phi)}, \quad j \in \mathbb{R}^N. \tag{7.120}$$

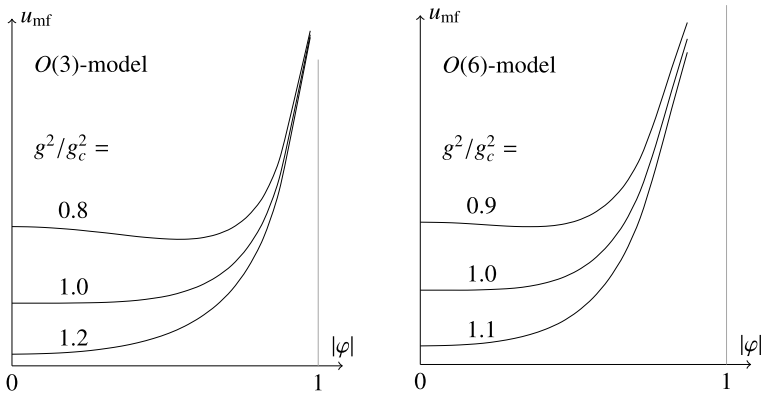

Fig. 7.11 Mean-field effective potentials for the $O(3)$ and $O(6)$ models

To calculate the integral we align the z-axis in ϕ-space with the direction defined by the source j and use polar coordinates in ϕ-space. Then the integral simplifies to

$$z(j) = \mathrm{Vol}\big(S^{N-2}\big) \int \mathrm{d}\theta \mathrm{e}^{|j|\cos\theta} (\sin\theta)^{N-2}. \tag{7.121}$$

With the integral representation for the modified Bessel function

$$I_\nu(z) = \frac{(z/2)^\nu}{\sqrt{\pi}\Gamma(\nu+1/2)} \int_0^\pi \mathrm{d}\theta\, \mathrm{e}^{z\cos\theta} (\sin\theta)^{2\nu}, \tag{7.122}$$

the one-site partition function takes the form

$$z(j) = (2\pi)^{N/2} \frac{I_{N/2-1}(|j|)}{|j|^{N/2-1}} \overset{O(3)}{\to} z(j) = 4\pi \frac{\sinh(|j|)}{|j|}. \tag{7.123}$$

The site partition functions only depend on the modulus of j, in accordance with the underlying $O(N)$ symmetry. It immediately follows that $u_{\rm mf}$ in (7.119) only depends on the modulus of the mean field. To calculate its curvature at the origin,

$$u''_{\rm mf}(0) = \frac{\Delta_0}{g^2} + (\mathscr{L}w)''(0),$$

we use the small-j expansion $w(j) = \text{const.} + j^2/2N + \cdots$ and conclude $(\mathscr{L}w)''(0) = N\mathbb{1}$, such that $u''_{\rm mf}(0)$ changes sign for the critical coupling

$$g^2 = g_c^2 = -\frac{\Delta_0}{N}. \tag{7.124}$$

The lattice Laplacian has diagonal elements $\Delta_0 = -2d$ such that $g_c^2 = 2d/N$. For weak couplings $g < g_c$ the MFA predicts a broken phase. Some typical effective potentials for the $O(3)$ and $O(6)$ models and $g \approx g_c$ are depicted in Fig. 7.11. The MFA predicts a *second-order* transition from an $O(N)$-symmetric strong coupling phase to a spontaneously broken weak-coupling phase. Note that in two dimensions this prediction is in conflict with the Mermin–Wagner theorem [21, 22], according to which a continuous symmetry cannot be spontaneously broken in two dimensions.

7.9 Program for Chap. 7

This section contains the `octave` program

- `mfscalar.m`

which was used in this chapter. This program computes the effective potential u_{mf} in the mean-field approximation with the classical potential $V(\phi) = \lambda(\phi^2 - 1)^2$. The plots on pp. 142 and 143 have been calculated with this program. The dimension of spacetime may be altered by changing d in the source code.

```
function mfscalar;
# calculation of effective potential for scalar field theory
# with potential V(phi)=lambda*(phi**2-1)**2 in the mean-field
# approximation. Dimension and coupling lambda as input.
# Result is stored in file mfscalar.dat.
d=3; # dimension
lam=input("lambda ");
a=(d-2*lam);
closeplot;
Nx=501; eps=2/(Nx-1); # Nx must be odd number
x=linspace(-10,10,Nx);
x2=x.*x; x4=x2.*x2; eps=eps/3;
z=eps*exp(-a*x2-lam*x4-lam);
j=linspace(-20,20,80)'; N=length(j);
# for Simpson integration
for i=2:2:Nx-1;
  z(i)=4*z(i);
endfor;
for i=3:2:Nx-2;
  z(i)=2*z(i);
endfor;
int0=zeros(N,Nx);int1=int2=int0;
L=zeros(N,1);s0=s1=umf=umf1=L;
for i=1:N
  int0(i,:)=z.*exp(j(i)*x);
  s0(i)=sum(int0(i,:));
  int1(i,:)=x.*int0(i,:);
  s1(i)=sum(int1(i,:));
endfor;
# Schwinger function
w0=log(s0);
L=s1./s0;
# calculate, plot and store effective potential
umf=-d*L.*L+j.*L-w0;
# search for minimum of potential
[min1,nmin]=min(umf);
nmin=max(nmin,N+1-nmin);
umf(nmin)=umf(nmin)+.5; # mark minimum
data=[L,umf-min1]; # normalize potential
# classical potential
L2=L.*L;
V=lam*L2.*L2-2*lam*L2+lam;
```

```
[vmin1,vnmin]=min(V);
datav=[L,V-vmin1];
gplot [-1.5:1.5] data,datav;
mfscalar=fopen("mfscalar.dat","w","native");
for i=1:N
fprintf(mfscalar,"(%4.2f,%4.2f)",L(i),umf(i)-min1);
if (rem(i,5)==0) fprintf(mfscalar,"\n");
endif;
endfor;spotts17
fclose(mfscalar);
endfunction;
```

7.10 Problems

7.1 (MFA for the Z_3 model) Determine the partition function of the Z_3-model with energy function

$$H = -\sum_{x,y\in\Lambda} J_{xy}\cos(\theta_x - \theta_y) \quad \text{with } \theta_x \in \left\{ \frac{2\pi n}{3} \middle| n = 0, 1, 2 \right\}$$

in the mean-field approximation. Introduce the order parameter

$$m = \frac{1}{V}\sum_{x\in\Lambda} \exp(i\theta_x)$$

and express the Hamiltonian as a function of m and $\bar{m}$. How many configurations do exist for a given m? Determine the function $f(m, \bar{m})$ occurring in

$$Z = \sum_m \exp\bigl(-\beta V f(m, \bar{m})\bigr)$$

and discuss the result.

Hint Introduce a_0, a_1, a_2 with a_n representing the number of lattice points with $\theta = 2\pi n/3$. Express m as a function of the a_n. Are the a_n uniquely determined for fixed m and V? Use the a_n in order to determine the number of configurations.

7.2 (MFA based on the Bogoliubov inequality) An alternative way of deriving the mean-field theory for a given microscopic system with energy H is to start with the *Bogoliubov inequality*

$$F \le \Phi \equiv F_0 + \langle H - H_0\rangle_0, \tag{7.125}$$

where $F = -kT\log Z$ is the free energy of the system of interest, H_0 is a trial energy function, F_0 the corresponding free energy and $\langle\ldots\rangle_0$ denotes the average taken in the ensemble defines by H_0.

- Prove the inequality (7.125). If you have any difficulties you may consult the book of H.B. Callen [23].
- The mean-field free energy is defined by minimizing Φ with respect to the variational parameters λ in the trial energy $H_0(\lambda)$,

$$F_{\mathrm{mf}} = \min_{\lambda} \Phi(\lambda).$$

The usual choice for H_0 is a free Hamiltonian as this allows for an explicit calculation of Φ. Consider the Ising model without magnetic field on a lattice with V sites and coordination number q. Choose as trial energy

$$H_0 = -\lambda \sum_x s_x \tag{7.126}$$

and compute Φ. Minimize the result with respect to the parameter λ. Calculate the corresponding F_{mf}. What is the meaning of the variational parameter λ?

7.3 (An analytically solvable model) Consider a scalar field theory with

$$V(\phi) = -\log\bigl(1+\phi^2\bigr) + \frac{1}{2}m^2\phi^2, \quad m^2 > 0.$$

For $m^2 < 2$ the origin is a local maximum. Plot the potential for various values of m. Calculate the one-site Schwinger function and discuss the resulting effective potential for small m^2.

7.4 (First-order transition in Landau theory) Consider a Landau expansion of the free energy density of the form

$$f_L(m) = \frac{a}{2}m^2 + \frac{b}{4}m^4 + \frac{c}{6}m^6, \quad c > 0. \tag{7.127}$$

Show that there exists a line of critical transitions $a = 0, b > 0$ which joins a line of first-order transitions $b = -4(ac/3)^{1/2}$ at a tricritical point $a = b = 0$. Sketch $f_L(m)$ in each region of the (a, b) plane, on the transition lines and at the tricritical point.

References

1. P. Weiss, L'Hypothèse du champs moleculairé et la propriete ferromagnéticque. J. Phys. **6**, 661 (1907)
2. P.J. Langevin, Magnétisme et théorie des électrons. J. Chim. Phys. **5**, 70 (1905)
3. L.E. Reichl, *Modern Course in Statistical Mechanics* (Arnold, London, 1980)
4. D. Chandler, *Introduction to Modern Statistical Mechanics* (Oxford University Press, London, 1987)
5. G. Parisi, *Statistical Field Theory* (Addison-Wesley, Reading, 1988)
6. K. Huang, *Introduction to Statistical Physics* (CRC Press, Boca Raton, 2001)
7. A. Pelissetto, E. Vicari, Critical phenomena and renormalization-group theory. Phys. Rep. **368**, 549 (2002)

8. M. Hasenbusch, A finite size scaling study of lattice models in the 3d Ising universality class. Phys. Rev. B **82**, 174433 (2010)
9. L.D. Landau, Theory of Fermi-liquids. Zh. Eksp. Teor. Fiz. **30**, 1058 (1956) [Sov. Phys. JETP **3**, 920 (1957)]
10. L.D. Landau, Oscillations in a Fermi-liquid. Zh. Eksp. Teor. Fiz. **32**, 59 (1957) [Sov. Phys. JETP **5**, 101 (1957)]
11. P. Nozières, *Theory of Interacting Fermi Systems*. Frontiers in Physics: Lecture Note and Reprint Series, vol. 19 (Benjamin-Cummings, Redwood City, 1964)
12. L. Landau, On the theory of Fermi liquid. Sov. Phys. JETP **8**, 70 (1959)
13. V. Galitskii, A. Migdal, Applications of quantum field theory to the many body problem. Sov. Phys. JETP **7**, 96 (1958)
14. A.A. Abrikosov, L.P. Gorkov, I.E. Dzyaloshinksi, *Methods of Quantum Field Theory in Statistical Mechanics* (Dover, New York, 1963)
15. J.C. Toledano, P. Toledano, *The Landau Theory of Phase Transitions* (World Scientific, Singapore, 1987)
16. L.S. Ornstein, F. Zernike, Accidental deviations of density and opalescence at the critical point of a single substance. Proc. Acad. Sci. Amst. **17**, 793 (1914)
17. J.S. Smart, *Effective Field Theories of Magnetism* (Saunders, Philadelphia, 1966)
18. L. O'Raifeartaigh, A. Wipf, H. Yoneyama, The constraint effective potential. Nucl. Phys. B **271**, 653 (1986)
19. Y. Fujimoto, A. Wipf, H. Yoneyama, Symmetry restoration of scalar models at finite temperature. Phys. Rev. D **38**, 2625 (1988)
20. M. Abramowitz, I.A. Stegun, *Handbook of Mathematical Functions with Formulas, Graphs, and Mathematical Tables* (Dover, New York, 1972)
21. N.D. Mermin, H. Wagner, Absence of ferromagnetism or anti-ferromagnetism in one- or two-dimensional isotropic Heisenberg models. Phys. Rev. Lett. **17**, 1133 (1966)
22. S. Coleman, There are no Goldstone bosons in two dimensions. Commun. Math. Phys. **31**, 259 (1973)
23. H.B. Callen, *Thermodynamics and an Introduction to Thermostatistics* (Wiley, New York, 2007)

Chapter 8
Transfer Matrices, Correlation Inequalities and Roots of Partition Functions

In Chaps. 2 and 5 we quantized mechanical systems and classical field theories via the functional integral formalism. Through a Wick rotation of vacuum expectation values we arrived at a (formal) Euclidean functional integral. In a next step the underlying Euclidean space-time is replaced by a lattice and this discretization leads to well-defined lattice field theories—these are particular spin models with continuous target spaces. To calculate thermal expectation values one imposes (anti)periodic boundary conditions in the imaginary time direction for the lattice fields. By these steps one approximates quantum field theories in d space-time dimensions by particular classical statistical systems in d dimensions.

In the first part of this chapter we follow the opposite way. For particular spin models we can reconstruct a state space and a Hamiltonian operator, where the latter converges to the Hamiltonian operator of a relativistic quantum field theory. Thereby we shall make use of the *transfer-matrix method*, which can be applied to general spin models with short-range interactions. To introduce the method we first calculate thermodynamic potentials and correlation functions of simple one-dimensional spin models, so-called "spin chains". Then we present the general formalism and apply it to scalar field theories on the lattice.

In the second part we introduce and prove some useful correlation inequalities for general ferromagnetic systems. These inequalities tell us that certain expectation values or combinations of expectation values are non-negative. In particular the two Griffith–Kelly–Sherman (GKS) inequalities can be used to study the dependence of expectation values on the parameters of a system or to compare correlation functions of spin systems in different volumes or in different dimensions.

In the last part we investigate the Lee–Yang zeros of partition functions, considered as functions of the complex magnetic field (or a complex chemical potential for lattice gases). For the target space $\mathscr{T} = \mathbb{R}$ and an even single-spin density the partition function of a class of ferromagnetic systems can only vanish for imaginary 'magnetic fields'. This theorem of Lee and Yang holds for a system with ferromagnetic couplings provided it holds for zero interaction.

A. Wipf, *Statistical Approach to Quantum Field Theory*, Lecture Notes in Physics 864,
DOI 10.1007/978-3-642-33105-3_8,

8.1 Transfer-Matrix Method for the Ising Chain

The transfer-matrix method is a powerful technique for solving problems in statistical physics. It has been used to find exact solutions, and in particular the famous solution of the two-dimensional Ising model by Lars Onsager [1]. This section contains an introduction to transfer-matrix methods. For more information and applications to spin systems you may consult the textbooks [2, 3]. We explain the method on the basis of the exactly solvable Ising chain on a one-dimensional lattice Λ with N sites [4]. We choose periodic boundary conditions for which s_x and s_{x+N} are identified and the energy function (6.2) takes the form

$$H_\Lambda(\omega) = -J\sum_{x=1}^{N} s_x s_{x+1} - h\sum_{x=1}^{N} s_x, \quad s_x \in \{-1, 1\}. \tag{8.1}$$

Now we will calculate the free energy, inner energy, magnetization and two-point correlation function with the help of the transfer-matrix method.

8.1.1 Transfer Matrix

In a first step we rewrite the partition function of the chain as follows:

$$\begin{aligned} Z_\Lambda(\beta) &= \sum_{\omega} \mathrm{e}^{-\beta H_\Lambda(\omega)} = \sum_{s_1,\dots,s_N} \mathrm{e}^{Ks_1s_2+\beta h(s_1+s_2)/2} \times \mathrm{e}^{Ks_2s_3+\beta h(s_2+s_3)/2} \times \cdots \\ &= \sum_{s_1,\dots,s_N} T_{s_1s_2} T_{s_2s_3} \cdots T_{s_Ns_1} = \operatorname{tr} \hat{T}^N, \quad K = \beta J. \end{aligned} \tag{8.2}$$

Here we defined the two-dimensional *transfer matrix* with matrix elements

$$\langle s|\hat{T}|s'\rangle = \mathrm{e}^{Kss'+\beta h(s+s')/2}, \tag{8.3}$$

where s and s' take the values ± 1. It is real, symmetric and has positive entries,

$$\hat{T} = \begin{pmatrix} \mathrm{e}^{K+\beta h} & \mathrm{e}^{-K} \\ \mathrm{e}^{-K} & \mathrm{e}^{K-\beta h} \end{pmatrix}. \tag{8.4}$$

To calculate the trace in (8.2) we diagonalize the transfer matrix with the help of a rotation matrix R,

$$\hat{T} = RDR^{-1}, \quad R = \begin{pmatrix} \cos\gamma & -\sin\gamma \\ \sin\gamma & \cos\gamma \end{pmatrix}, \; D = \begin{pmatrix} \lambda_+ & 0 \\ 0 & \lambda_- \end{pmatrix}, \tag{8.5}$$

where the diagonal matrix D contains the two positive eigenvalues

$$\lambda_\pm = \mathrm{e}^K(\cosh\beta h \pm B) \quad \text{with } B = \left(\sinh^2\beta h + \mathrm{e}^{-4K}\right)^{1/2}, \tag{8.6}$$

and $\lambda_+ > \lambda_-$. The angle γ in the rotation matrix is determined through

$$\sin 2\gamma = \frac{1}{B}\mathrm{e}^{-2K}, \qquad \cos 2\gamma = \frac{1}{B}\sinh\beta h. \tag{8.7}$$

In terms of the eigenvalues the trace in (8.2) is written as

$$Z_\Lambda(\beta,h) = \operatorname{tr}\hat{T}^N = \lambda_+^N + \lambda_-^N = \lambda_+^N\big(1+p^N\big), \qquad p = \frac{\lambda_-}{\lambda_+}. \tag{8.8}$$

For all values of the magnetic field the last ratio of eigenvalues is bounded, $p < 1$.

Thermodynamic Potentials The result (8.8) means that the thermodynamic potentials are determined by the eigenvalues of the transfer matrix. For example, the *free energy density* is

$$f_\Lambda(\beta,h) = \frac{1}{N}F_\Lambda(\beta,h) = -\frac{1}{\beta}\log\lambda_+ - \frac{1}{\beta N}\log\big(1+p^N\big). \tag{8.9}$$

In the thermodynamic limit $N\to\infty$ the term p^N vanishes and the free energy density is solely determined by the largest eigenvalue of $\hat{T}$,

$$f(\beta,h) = \lim_{N\to\infty} f_\Lambda(\beta,h) = -\frac{1}{\beta}\log\lambda_+. \tag{8.10}$$

Similarly, the inner energy density

$$u_\Lambda(\beta,h) = -\frac{\partial}{\partial\beta}\left(\log\lambda_+ + \frac{1}{N}\log\big(1+p^N\big)\right) \tag{8.11}$$

in the thermodynamic limit is determined by the largest eigenvalue according to

$$u(\beta,h) = \lim_{N\to\infty} u_\Lambda(\beta,h) = -\frac{\partial}{\partial\beta}\log\lambda_+. \tag{8.12}$$

Without external field we simply have $u(\beta,0) = -\tan K$.

Correlation Functions The magnetization of the chain is calculated via the transfer matrix as follows

$$m \equiv \langle s_1\rangle = \frac{1}{Z}\sum_\omega \mathrm{e}^{-\beta H(\omega)} s_1 = \frac{1}{Z}\sum_\omega s_1 T_{s_1 s_2}\cdots T_{s_N s_1} = \frac{1}{Z}\operatorname{tr}\big(\hat{s}\,\hat{T}^N\big), \tag{8.13}$$

where $\hat{s} = \sigma_3$ denotes the third Pauli matrix. Using $\hat{T} = RDR^{-1}$ and that the trace is invariant under cyclic permutations of its arguments we obtain

$$m = \frac{1}{Z}\operatorname{tr}\big(R^{-1}\hat{s}\,R\,D^N\big), \quad \text{where } R^{-1}\hat{s}\,R = \begin{pmatrix} \cos 2\gamma & -\sin 2\gamma \\ -\sin 2\gamma & -\cos 2\gamma \end{pmatrix}. \tag{8.14}$$

Inserting the diagonal matrix D defined in (8.5) leads to

$$m = \frac{1-p^N}{1+p^N}\cos 2\gamma \overset{N\to\infty}{\to} \cosh(2\gamma) = \frac{\sinh\beta h}{(\sinh^2\beta h + \mathrm{e}^{-4K})^{1/2}}. \tag{8.15}$$

Of course, differentiating the free energy density (8.9) with respect to the external field yields the same magnetization.

For any positive temperature the magnetization (8.15) vanishes when the field h is switched off—only at zero temperature a permanent magnetization remains. The Ising chain shares this property with many other one-dimensional lattice models,

since all spin chains with short-range interactions (and further mild assumptions) show no phase transition at any positive temperature [5, 6]. This *van Hove theorem* does not exclude the possibility of phase transitions in one dimension, see for example [7]. For a further reading I refer to the collection of reprints in [8].

For the two-point function we proceed similarly as for the one-point function and obtain for $y \geq x$

$$\begin{aligned}\langle s_x s_y \rangle &= \frac{1}{Z} \sum_{\omega} \mathrm{e}^{-\beta H(\omega)} s_x s_y \\ &= \frac{1}{Z} \sum_{s_1, s_x, s_y} \left(T^{x-1}\right)_{s_1 s_x} s_x \left(T^{y-x}\right)_{s_x s_y} s_y \left(T^{N+1-y}\right)_{s_y s_1} \\ &= \frac{1}{Z} \operatorname{tr}\left(\hat{s}\, \hat{T}^{y-x} \hat{s}\, \hat{T}^{N-(y-x)}\right) \\ &= \frac{1}{Z} \operatorname{tr}\left(\left(R^{-1} \hat{s}\, R\right) D^{y-x} \left(R^{-1} \hat{s}\, R\right) D^{N-(y-x)}\right),\end{aligned}$$

with matrices D and $R^{-1} S R$ given in (8.5) and (8.14). A short calculation leads to

$$\langle s_x s_y \rangle = \cos^2 2\gamma + \frac{p^{y-x} + p^{N-(y-x)}}{1 + p^N} \sin^2 2\gamma, \quad y \geq x. \tag{8.16}$$

Translational invariance and the symmetry relation $\langle s_x s_y \rangle = \langle s_y s_x \rangle$ imply that the two-point function only depends on the distance $|y - x|$ of the spins. In the thermodynamic limit we find

$$\lim_{N \to \infty} \langle s_x s_y \rangle = \cos^2 2\gamma + \mathrm{e}^{-|y-x|/\xi} \sin^2 2\gamma, \tag{8.17}$$

where we introduced the *correlation length*

$$\xi^{-1} = \log \frac{1}{p} \overset{h \to 0}{\to} -\log \tanh K, \quad K = \beta J, \tag{8.18}$$

which is finite for all $T > 0$. The correlation function satisfies the *cluster property*

$$\langle s_x s_y \rangle - \underbrace{\langle s_x \rangle \langle s_y \rangle}_{= m^2} \overset{N \to \infty}{\to} \sin^2 2\gamma \mathrm{e}^{-|y-x|/\xi} \overset{|y-x| \to \infty}{\to} 0. \tag{8.19}$$

At first glance it seems surprising that the Ising chain shows no ordered phase at low temperature since the ordered states with all spins pointing in the same direction have lowest energy. However, they do not minimize the free energy $F = U - TS$. To see this let us consider particular configurations like $\uparrow\uparrow\uparrow\uparrow\uparrow\downarrow\downarrow\downarrow\downarrow\downarrow$, where the spins are partially inverted. Due to the interface between the two sub-chains with aligned spins the inner energy increases by $\Delta U = 4J$. But the N configurations with one interface contribute $k \log N$ to the entropy. We conclude that for large N the free energy is lowered by the interface.

8.1.2 The "Hamiltonian"

We now extract the two-dimensional hermitian matrix $\hat{H}$ via the relation

$$\hat{T} = \mathrm{e}^{-\hat{H}} \tag{8.20}$$

from the positive transfer matrix $\hat{T}$ such that

$$Z_\Lambda(\beta) = \mathrm{tr}\,\hat{T}^N = \mathrm{tr}\,\mathrm{e}^{-N\hat{H}}. \tag{8.21}$$

The operator $\hat{H}$ should not be mistaken with the classical energy H of spin configurations. The result (8.21) suggests that $\hat{H}$ represents the discretized *Hamiltonian* of a quantum theory associated to the spin system. To actually calculate $\hat{H}$ for the Ising chain we use the formula

$$\exp\Big(\alpha \sum_i n_i \sigma_i\Big) = \cosh\alpha + \sinh\alpha \sum_{i=1}^{3} n_i \sigma_i, \tag{8.22}$$

where $\{\sigma_1, \sigma_2, \sigma_3\}$ are the Pauli matrices and $\mathbf{n}$ is a unit vector. To simplify matters we assume $h = 0$ such that the transfer matrix (8.4) takes the simple form

$$\hat{T} = \mathrm{e}^K \mathbb{1} + \mathrm{e}^{-K}\sigma_1 = \frac{\mathrm{e}^K}{\cosh K^*}\,\mathrm{e}^{K^*\sigma_1}, \quad K = \beta J. \tag{8.23}$$

Here we introduced the so-called *dual coupling* K^* in virtue of the relation

$$\tanh K^* = \mathrm{e}^{-2K} \quad \text{or} \quad \tanh K = \mathrm{e}^{-2K^*}. \tag{8.24}$$

From the last representation in (8.23) it is easy to extract the *Hamiltonian*

$$\hat{H} = -\log\hat{T} = -K + \log\cosh K^* - K^*\sigma_1 = E_0 + K^*(1 - \sigma_1) \tag{8.25}$$

with ground state energy $E_0 = \log\cosh K^* - K - K^*$. Using the duality relation between K and K^* we can write this energy as

$$E_0 = -\log(2\cosh K) = \lim_{N\to\infty} \beta f(\beta, 0). \tag{8.26}$$

The only excited energy level lies $2K^*$ above the ground state and yields the inverse correlation length $2K^*$, in agreement with (8.18).

Two Dimensions While it is a relatively simple problem to find the transfer matrix of the Ising chain, the corresponding problem for the two-dimensional model is highly nontrivial. The solution without external field is due to Onsager, who was able to find the analytical expression (6.3) for the free energy in the thermodynamic limit via the transfer-matrix approach. This then gives an exact set of critical exponents, see the discussion on p. 103 in Chap. 6. For a derivation I refer to the textbook [9]. To date, the three-dimensional Ising model remains unsolved.

8.1.3 The Anti-Ferromagnetic Chain

For the anti-ferromagnetic Ising chain with negative $K = \beta J$ the eigenvalue λ_+ of the transfer matrix in (8.6) remains positive whereas the eigenvalue λ_- becomes negative. Actually, without external field the larger eigenvalue does not change under $J \to -J$ whereas the smaller eigenvalue changes its sign,

$$\lambda_+ = 2\cosh(K) > 0 \quad \text{and} \quad \lambda_- = 2\sinh(K) < 0. \tag{8.27}$$

Thus for $h = 0$ the anti-ferromagnetic and ferromagnetic chains share the same free energy density in the thermodynamic limit. However, since $p < 0$ the correlation function (8.16) becomes an oscillating function with different signs at adjacent lattice sites,

$$\lim_{N\to\infty} \langle s_x s_y \rangle_c = (\tanh K)^{|y-x|} = (-1)^{|y-x|} \big(\tanh|K|\big)^{|y-x|}. \tag{8.28}$$

Here we have taken into account that in the absence of the external field $\sin 2\gamma = 1$. The oscillatory behavior originates from the non-positivity of the transfer matrix. Since the exponential of a hermitian matrix is a positive matrix we cannot define a hermitian Hamiltonian for the anti-ferromagnetic chain as we did in (8.20). However, we may define a Hamiltonian by using the positive matrix $\hat{T}^2$ according to

$$\hat{T}^2 = \mathrm{e}^{-2\hat{H}}. \tag{8.29}$$

The hermitian operator $\hat{H}$ agrees with the Hamiltonian of the ferromagnetic Ising chain and determines the long-range behavior of the anti-ferromagnetic system.

8.2 Potts Chain

A configuration $\omega = \{\sigma_1, \ldots, \sigma_N\}$ of the periodic q-state Potts chain has the energy

$$H_\Lambda(\omega) = -J \sum_{x=1}^{N} \delta(\sigma_x, \sigma_{x+1}) - 2h \sum_{x=1}^{N} \delta(\sigma_x, 1), \quad \sigma_x \in \{1, 2, \ldots, q\}. \tag{8.30}$$

For later convenience we rescaled the external field as compared to (6.10). The partition function can be written as

$$\begin{aligned} Z_\Lambda(\beta, J, h) &= \sum_{\sigma_1,\ldots,\sigma_N} \mathrm{e}^{K\delta(\sigma_1,\sigma_2)+2\beta h\,\delta(\sigma_1,1)} \times \mathrm{e}^{K\delta(\sigma_2,\sigma_3)+2\beta h\,\delta(\sigma_2,1)} \times \cdots \\ &= \sum_{\sigma_1,\ldots,\sigma_N} T_{\sigma_1\sigma_2} T_{\sigma_2\sigma_3} \cdots T_{\sigma_N\sigma_1} = \operatorname{tr} \hat{T}^N, \quad K = \beta J, \end{aligned} \tag{8.31}$$

where we introduced the q-dimensional *non-symmetric* transfer matrix

$$(T_{\sigma\sigma'}) = \langle \sigma | \hat{T} | \sigma' \rangle = \begin{pmatrix} \zeta z & z & \ldots & z \\ 1 & \zeta & \ldots & 1 \\ \vdots & \vdots & \ddots & \vdots \\ 1 & 1 & \ldots & \zeta \end{pmatrix}, \quad \zeta = \mathrm{e}^K, z = \mathrm{e}^{2\beta h}. \tag{8.32}$$

Following [10] we calculate the characteristic polynomial $\det(\hat{T} - \lambda\mathbb{1})$ explicitly. Its roots $\lambda_1, \ldots, \lambda_q$ are just the eigenvalues of the transfer matrix and determine the thermodynamic potentials.

Let us subtract the second row of $\hat{T} - \lambda\mathbb{1}$ from the third and each of the subsequent rows, followed by adding the third and all subsequent columns to the second column. The determinant of the resulting matrix

$$\begin{pmatrix} \zeta z - \lambda & z(q-1) & z & \ldots & z \\ 1 & \zeta + q' - \lambda & 1 & \ldots & 1 \\ 0 & 0 & \zeta - 1 - \lambda & \ldots & 0 \\ \vdots & & & \ddots & \\ 0 & & 0 & \ldots & \zeta - 1 - \lambda \end{pmatrix}$$

is equal to the characteristic polynomial of the transfer matrix. It factorizes into a polynomial of degree $q' = q - 2$ and a quadratic polynomial,

$$\det(\hat{T} - \lambda\mathbb{1}) = (\zeta - 1 - \lambda)^{q'}\big(\lambda^2 - \big(\zeta z + \zeta + q'\big)\lambda + z(\zeta - 1)(\zeta + q - 1)\big).$$

The first factor has the root $\zeta - 1$ of order q' and the second factor the simple roots

$$\begin{aligned} \lambda_\pm &= \frac{1}{2}\Big((z+1)\zeta + q' \pm \sqrt{\big(\zeta z - \zeta - q'\big)^2 + 4(q-1)z}\Big) \\ &= \mathrm{e}^{K+\beta h}\cosh\beta h + \frac{q'}{2} \pm \sqrt{\left(\mathrm{e}^{K+\beta h}\sinh\beta h - \frac{1}{2}q'\right)^2 + \mathrm{e}^{2\beta h}(q-1)}. \end{aligned} \tag{8.33}$$

Hence, we obtain the following explicit expression for the partition function:

$$Z_\Lambda(\zeta, z) = \operatorname{tr}\hat{T}^N = \lambda_+^N + \lambda_-^N + q'(\zeta - 1)^N, \tag{8.34}$$

which for $q = 2$ is proportional to that of the Ising chain. In the thermodynamic limit only the contribution of the largest eigenvalue λ_+ remains and determines the free energy and inner energy density according to (8.10) and (8.12), respectively.

8.3 Perron–Frobenius Theorem

We have seen that the largest eigenvalue λ_+ of the transfer matrix determines the thermodynamic potentials of the corresponding spin model in the thermodynamic limit. A theorem of Oskar Perron [11] and Georg Frobenius [12] asserts that a real square matrix with positive entries has a unique largest real eigenvalue and that there is a corresponding eigenvector with strictly positive components:

Theorem 8.1 (Perron–Frobenius) *Let $\hat{T}$ be a hermitian matrix with positive matrix elements T_{ij}. Then the eigenvector with largest eigenvalue $\|\hat{T}\|$ is unique and its components are all unequal to zero and may be chosen as positive numbers.*

Proof We choose the norm given by $\|\psi\|^2 = \sum \psi_i^* \psi_i$ for a vector in $\mathbb{C}^n$. The operator norm of a n-dimensional matrix $\hat{T}$ is defined as

$$\|\hat{T}\| = \sup_{\psi \neq 0} \frac{\|\hat{T}\psi\|}{\|\psi\|}. \tag{8.35}$$

Now let $\tilde{\Omega} = (\tilde{\Omega}_1, \ldots, \tilde{\Omega}_n)^T$ be the eigenvector of $\hat{T}$ with the largest eigenvalue, i.e.

$$(\tilde{\Omega}, \hat{T}\tilde{\Omega}) = \|\hat{T}\|(\tilde{\Omega}, \tilde{\Omega}).$$

Clearly, the vector $\Omega := (|\tilde{\Omega}_1|, \ldots, |\tilde{\Omega}_n|)^T$ has the same norm as $\tilde{\Omega}$. Since the matrix elements of $\hat{T}$ are non-negative we conclude that

$$(\Omega, \hat{T}\Omega) \geq (\tilde{\Omega}, \hat{T}\tilde{\Omega}) = \|\hat{T}\|(\tilde{\Omega}, \tilde{\Omega}) = \|\hat{T}\|(\Omega, \Omega) \tag{8.36}$$

holds. Using the *Cauchy–Schwarz inequality* we have

$$(\Omega, \hat{T}\Omega) \leq \|\Omega\| \, \|\hat{T}\Omega\| \leq \|\hat{T}\| \, \|\Omega\|^2. \tag{8.37}$$

The two inequalities (8.36) and (8.37) imply

$$(\Omega, \hat{T}\Omega) = \|\hat{T}\| \, (\Omega, \Omega)$$

such that also Ω is eigenvector with the same maximal eigenvalue $\|\hat{T}\|$ as $\tilde{\Omega}$. None of the components of this real eigenvector is zero as

$$0 < \sum_j T_{ij}\Omega_j = (\hat{T}\Omega)_i = \|\hat{T}\|\Omega_i \quad \Longrightarrow \quad \Omega_i > 0$$

shows. Now we can prove that the eigenvectors $\tilde{\Omega}$ and Ω are *linearly dependent*. For that purpose we insert

$$\tilde{\Omega}_j = \mathrm{e}^{\mathrm{i}\varphi_j}\Omega_j$$

into $(\tilde{\Omega}, \hat{T}\tilde{\Omega}) = (\Omega, \hat{T}\Omega)$ and find

$$\sum \tilde{\Omega}_j^* T_{jk} \tilde{\Omega}_k = \sum \Omega_j T_{jk} \Omega_k \mathrm{e}^{\mathrm{i}(\varphi_k - \varphi_j)} = \sum \Omega_j T_{jk} \Omega_k.$$

Since $\Omega_j T_{jk} \Omega_k$ is positive we conclude $\varphi_k = \varphi_j \equiv \varphi$, which means that the two eigenvectors Ω and $\tilde{\Omega}$ are linearly dependent, $\tilde{\Omega} = \mathrm{e}^{\mathrm{i}\varphi}\,\Omega$. Now it is not difficult to prove the Perron–Frobenius theorem: Let $\Omega^{(1)}$ and $\Omega^{(2)}$ be two linearly independent eigenvectors corresponding to the largest eigenvalue. According to the previous discussion we may assume that all components of these vectors are positive numbers. Then there exists an $\alpha > 0$, such that the eigenvector corresponding to the same largest eigenvalue

$$\Omega^{(1)} - \alpha\Omega^{(2)}$$

has positive and negative components. But this is impossible as verified above. □

8.4 The General Transfer-Matrix Method

A transfer matrix can be defined for spin systems on lattices of the form $\Lambda = \mathbb{Z} \times \mathscr{R}$. The coordinate $\tau \in \mathbb{Z}$ is sometimes called time coordinate in contrast to the coordinates $\mathbf{x}$ on the spatial lattice $\mathscr{R}$. A lattice site is characterized by its time coordinate and its spatial coordinates, $x = (\tau, \mathbf{x})$. We may view a spin configuration on Λ as the set of spin configurations on $\mathscr{R}$, labeled by τ,

$$\omega = \{s_x | x \in \Lambda\} = \{\boldsymbol{\omega}_\tau | \tau \in \mathbb{Z}\}, \quad \text{with } \boldsymbol{\omega}_\tau = \{s_{\tau,\mathbf{x}} | \mathbf{x} \in \mathscr{R}\}. \tag{8.38}$$

For simplicity we will assume that Λ is a d-dimensional hypercubic lattice in which case $\mathscr{R}$ is a $d-1$-dimensional hypercubic lattice. As earlier on we denote the target space, sometimes called space of *local states*, by $\mathscr{T}$.

To construct the "Hilbert space" of states on the spatial lattice we first introduce the one-site vector space $\mathscr{H}_\mathbf{x}$ of complex-valued functions ψ on the target space,

$$\mathscr{H}_\mathbf{x} = \{\psi | \psi : \mathscr{T} \to \mathbb{C}\}. \tag{8.39}$$

The local states characterize a basis of $\mathscr{H}_\mathbf{x}$ consisting of characteristic functions,

$$|s\rangle = \psi_s \quad \text{with } \psi_s(s') = \delta_{s,s'}. \tag{8.40}$$

We now define the scalar product according to

$$\langle s | s' \rangle = \delta_{s,s'}. \tag{8.41}$$

If $\mathscr{T}$ is infinite discrete, we demand ψ to be square summable, $\psi \in \ell_2$, if $\mathscr{T}$ is continuous, then we demand ψ to be square integrable $\psi \in L_2(\mathscr{T})$, similar as in quantum mechanics. The one-site vector space $\mathscr{H}_\mathbf{x}$ is $\mathbb{C}^2$ for the Ising model and $L_2(\mathbb{R})$ for a real scalar field. We now define a *state space*

$$\mathscr{H} = \bigotimes_{\mathbf{x} \in \mathscr{R}} \mathscr{H}_\mathbf{x}, \tag{8.42}$$

associated with the spatial lattice. This is the space of all (complex-valued) functions over the configurations on $\mathscr{R}$. A basis of $\mathscr{H}$ is given by the product states

$$|\boldsymbol{\omega}\rangle = \bigotimes_{\mathbf{x} \in \mathscr{R}} |s_\mathbf{x}\rangle. \tag{8.43}$$

They are characteristic functions on configurations $\boldsymbol{\omega} = \{s_\mathbf{x} | \mathbf{x} \in \mathscr{R}\}$ at fixed time. We refer to this basis as the *configuration-space basis*. The scalar product of two basis elements is defined as product of the scalar products of their factors in $\mathscr{H}_\mathbf{x}$.

Along with the decomposition of the space-time lattice $\Lambda = \mathbb{Z} \times \mathscr{R}$ goes a decomposition of the energy function. Assuming that the interaction is restricted to nearest-neighbors we obtain

$$H(\omega) = \sum_\tau H_0(\boldsymbol{\omega}_{\tau+1}, \boldsymbol{\omega}_\tau) + \sum_\tau U(\boldsymbol{\omega}_\tau). \tag{8.44}$$

The first term containing the interactions between spins on adjacent time-slices does not change under an interchange of the configurations, i.e. $H_0(\boldsymbol{\omega}', \boldsymbol{\omega}) = H_0(\boldsymbol{\omega}, \boldsymbol{\omega}')$. We may write H_0 and U as

$$H_0 = \sum_{\mathbf{x}} h_0(s_{\tau+1,\mathbf{x}}, s_{\tau,\mathbf{x}}) \quad \text{and} \quad U = \sum_{\langle \mathbf{x},\mathbf{y} \rangle} u(s_{\tau,\mathbf{x}}, s_{\tau,\mathbf{y}}). \tag{8.45}$$

We now introduce the *transfer matrix* as a linear operator on $\mathscr{H}$ through its matrix elements in the configuration-space basis:

$$T_{\omega\omega'} = \langle \boldsymbol{\omega} | \hat{T} | \boldsymbol{\omega}' \rangle = \exp\left(-H_0(\boldsymbol{\omega}, \boldsymbol{\omega}') - \frac{1}{2} U(\boldsymbol{\omega}) - \frac{1}{2} U(\boldsymbol{\omega}') \right). \tag{8.46}$$

This real and symmetric matrix with positive entries has real eigenvalues and the Perron–Frobenius theorem ensures that the largest eigenvalue $\lambda_{\max}$ is positive and non-degenerate. If some eigenvalues of $\hat{T}$ are negative, such as for antiferromagnets, we choose the positive matrix $\hat{T}^2$ to extract a *lattice-Hamiltonian* $\hat{H}$,

$$\hat{T}^2 = \mathrm{e}^{-2\hat{H}}, \quad \hat{H} \text{ self-adjoint.} \tag{8.47}$$

The partition function on a periodic lattice with N time-slices is given by

$$Z_\Lambda = \operatorname{tr} \hat{T}^N = \sum_n \lambda_n^N \overset{N\to\infty}{\to} \lambda_{\max}^N. \tag{8.48}$$

To discuss the continuum limit we define a set of operators in the configuration-space basis: the diagonal operators $\hat{s}_{\mathbf{x}}$ through

$$\hat{s}_{\mathbf{x}} |\boldsymbol{\omega}\rangle = s_{\mathbf{x}} |\boldsymbol{\omega}\rangle \tag{8.49}$$

and the operators $\hat{\pi}_{\mathbf{x}}$ which map basis vectors into different basis vectors,

$$\hat{\pi}_{\mathbf{x}} |\boldsymbol{\omega}\rangle = |\boldsymbol{\omega}_\delta\rangle, \tag{8.50}$$

where $\boldsymbol{\omega}_\delta$ arises from $\boldsymbol{\omega}$ through a shift of $s_{\mathbf{x}}$. The second operator corresponds to the quantum mechanical momentum operator and changes local states at $\mathbf{x}$ by a constant. The exact form of the $\hat{\pi}_{\mathbf{x}}$ depends on the theory of interest. If $s_{\mathbf{x}}$ is real, then $\hat{\pi}_{\mathbf{x}}$ corresponds to the addition of a constant, whereas if $s_{\mathbf{x}}$ is group valued, then (for a cyclic group) it is the multiplication with a generating group element. Every operator on $\mathscr{H}$ may be expressed in terms of the operators $\hat{s}_{\mathbf{x}}$ and $\hat{\pi}_{\mathbf{x}}$. For the simple Ising chain the spatial lattice $\mathscr{R}$ is simply a point. If we choose the basis

$$|1\rangle = \begin{pmatrix} 1 \\ 0 \end{pmatrix} \quad \text{and} \quad |-1\rangle = \begin{pmatrix} 0 \\ 1 \end{pmatrix}, \tag{8.51}$$

then the matrices $\hat{s}$ and $\hat{\pi}$ are given by

$$\hat{s} = \sigma_3 \quad \text{and} \quad \hat{\pi} = \sigma_1. \tag{8.52}$$

8.5 Continuous Target Spaces

Now we consider lattice models with continuous target spaces $\mathscr{T}$ where the transfer 'matrix' is actually an operator. In a suitable basis the transfer matrix becomes a positive integral operator acting on real-valued functions on $\mathscr{T}$.

8.5.1 Euclidean Quantum Mechanics

For a particle on the line we approximate the line by a one-dimensional lattice with N lattice points and lattice spacing ε. In terms of rescaled *dimensionless* variables the Euclidean lattice action reads

$$S = \sum_{j=1}^{N} \left\{ \frac{m}{2}(q_{j+1} - q_j)^2 + V(q_j) \right\}. \tag{8.53}$$

As transfer 'matrix' we choose the integral operator with symmetric kernel

$$\langle q|\hat{T}|q'\rangle = T_{qq'} = \sqrt{\frac{m}{2\pi}}\, \mathrm{e}^{-\frac{1}{2}mq^2 - \frac{1}{2}V(q)}\, \mathrm{e}^{mqq'}\, \mathrm{e}^{-\frac{1}{2}mq'^2 - \frac{1}{2}V(q')}, \tag{8.54}$$

such that the partition function at inverse temperature $\beta = \varepsilon n$ is given by

$$Z_N = \operatorname{tr} \hat{T}^N = \int \mathrm{d}q_1 \cdots \mathrm{d}q_N\, T_{q_1 q_2} T_{q_2 q_3} \times \cdots \times T_{q_N q_1}. \tag{8.55}$$

For the harmonic oscillator with potential $V(q) = m\omega^2 q^2/2$ the kernel is Gaussian and hence $\hat{T}$ has a Gaussian eigenfunction,

$$\int \mathrm{d}q'\, T_{qq'}\, \psi_0(q') = \lambda_0 \psi_0(q), \quad \text{with } \psi_0(q) \propto e^{-m\alpha q^2/2}. \tag{8.56}$$

The parameter α and the eigenvalue λ_0 are

$$\alpha = \omega\sqrt{1 + \omega^2/4} \quad \text{and} \quad \lambda_0 = \sqrt{1 - \alpha + \omega^2/2} < 1. \tag{8.57}$$

Actually one can find all eigenfunctions and eigenvalues of the transfer matrix in closed form. The solution to problem 8.3 tells us that

$$\hat{T}|\psi_n\rangle = \lambda_n |\psi_n\rangle \quad \text{with } \lambda_n = \lambda_0^{2n+1} < \lambda_0,\ n \in \mathbb{N}_0, \tag{8.58}$$

where the $\psi_n(q)$ are calculated from the ground state wave function according to,

$$\psi_n(q) \propto \hat{a}^{\dagger n} \psi_0(q), \quad a^\dagger = \frac{\partial}{\partial q} - m\alpha q. \tag{8.59}$$

This means that the eigenvalues of the lattice Hamiltonian $\hat{H}$ are equidistant,

$$\operatorname{spectrum}(\hat{H}) = \{-(2n+1)\log\lambda_0 | n \in \mathbb{N}_0\}, \tag{8.60}$$

similarly as for the harmonic oscillator on $\mathbb{R}$.

Continuum Limit The dimensionless lattice quantities in the previous formulas (now denoted by an index L, similarly as on p. 59) are related to the dimensionful physical quantities as follows:

$$\omega_L = \varepsilon\omega, \qquad m_L = \varepsilon m, \qquad \hat{H}_L = \varepsilon \hat{H}, \qquad q_L = \varepsilon^{-1} q. \tag{8.61}$$

For a small lattice spacing ε the eigenvalues of the dimensionful Hamiltonian $\hat{H}$ have the expansions

$$-\frac{1}{\varepsilon}\log\lambda_n = \left(\frac{1}{2} + n\right)\omega + O(\varepsilon^2)$$

and in the continuum limit $\varepsilon \to 0$ we recover the energies of the harmonic oscillator on the line together with its ground state wave function $\exp(-m\omega q^2/2)$. In terms of physical parameters the transfer kernel takes the form

$$T_{qq'} = \sqrt{\frac{m}{2\pi\varepsilon}} \exp\left\{-\frac{m}{2\varepsilon}(q-q')^2 - \frac{1}{2}V_\varepsilon(q) - \frac{1}{2}V_\varepsilon(q')\right\},$$

where V_ε is the potential one obtains by substituting q/ε for q_L and the dimensionful couplings for the dimensionless lattice couplings in the lattice potential. Finally, from the proof of the Feynman–Kac formula in Sect. 2.3 it follows that

$$\lim_{\varepsilon\to 0} T_{qq'} = \lim_{\varepsilon\to 0} \langle q|\mathrm{e}^{-\varepsilon\hat{H}}|q'\rangle \quad \text{with } \hat{H} = -\frac{1}{2m}\frac{\mathrm{d}^2}{\mathrm{d}q^2} + V(q). \tag{8.62}$$

Thus in the continuum limit one recovers the well-known Hamiltonian, energies and eigenfunctions of the harmonic oscillator on the line.

8.5.2 Real Scalar Field

Finally we apply the transfer-matrix method to a non-interacting scalar field theory with lattice action

$$S = \frac{1}{2}\sum_{\langle x,y\rangle}(\phi_x - \phi_y)^2 + \frac{m^2}{2}\sum_x \phi_x^2. \tag{8.63}$$

The local degrees of freedom are the real ϕ_x and the one-site Hilbert space is $L_2(\mathbb{R})$. The full Hilbert space is the tensor product of these spaces over all points of the spatial lattice, i.e. $\mathscr{H} = \bigotimes_{\mathbf{x}\in\mathscr{R}} L_2(\mathbb{R})$. In addition, we connect every field configuration $\boldsymbol{\omega}$ on the spatial lattice to a basis vector $|\boldsymbol{\omega}\rangle = |\{\phi_\mathbf{x}|\mathbf{x}\in\mathscr{R}\}\rangle$ in the configuration basis of $\mathscr{H}$. The symmetric transfer matrix can be expressed as

$$\langle\boldsymbol{\omega}|\hat{T}|\boldsymbol{\omega}'\rangle = \mathrm{e}^{-F(\omega)}\exp\left(-\frac{1}{2}\sum_{\mathbf{x}\in\mathscr{R}}\left(\phi_\mathbf{x} - \phi'_\mathbf{x}\right)^2\right)\mathrm{e}^{-F(\omega')}, \tag{8.64}$$

where F only depends on the field values in a given time-slice,

$$F(\boldsymbol{\omega}) = \frac{1}{4}\sum_{\langle\mathbf{x},\mathbf{y}\rangle}(\phi_\mathbf{x} - \phi_\mathbf{y})^2 + \frac{m^2}{4}\sum_\mathbf{x}\phi_\mathbf{x}^2. \tag{8.65}$$

The diagonal operators are represented by the field operators and the displacement operators by the conjugated momentum operators

$$\hat{\phi}_\mathbf{x}|\boldsymbol{\omega}\rangle = \phi_\mathbf{x}|\boldsymbol{\omega}\rangle, \quad \hat{\pi}_\mathbf{x} = \frac{1}{\mathrm{i}}\frac{\delta}{\delta\phi_\mathbf{x}}. \tag{8.66}$$

To rewrite the transfer matrix in terms of these operators we recall the explicit heat kernel of the kinetic operator $K(\hat{\pi}) = \frac{1}{2}\sum_\mathbf{x}\hat{\pi}_\mathbf{x}^2$,

$$\langle\boldsymbol{\omega}|\mathrm{e}^{-K(\hat{\pi})}|\boldsymbol{\omega}'\rangle = \frac{1}{(2\pi)^{|\mathscr{R}|/2}}\exp\left\{-\frac{1}{2}\sum\nolimits_\mathbf{x}\left(\phi_\mathbf{x} - \phi'_\mathbf{x}\right)^2\right\}, \tag{8.67}$$

to obtain the following representation of the matrix elements of the transfer matrix:

$$\langle \boldsymbol{\omega} | \hat{T} \, | \boldsymbol{\omega}' \rangle = (2\pi)^{|\mathscr{R}|/2} \, \mathrm{e}^{-F(\hat{\phi})} \mathrm{e}^{-K(\hat{\pi})} \mathrm{e}^{-F(\hat{\phi})}, \tag{8.68}$$

where the *operator* $F(\hat{\phi})$ is the function (8.65) with the $\phi_{\mathbf{x}}$ replaced by the operators $\hat{\phi}_{\mathbf{x}}$. From the result (8.68) it is evident that $\hat{T}$ is not just the exponential function of a simple differential operator $\hat{H}$. Only in the continuum limit we recover the familiar and simple Hamiltonian of the free scalar field.

8.6 Correlation Inequalities

Correlation inequalities are general inequalities between correlation functions of statistical systems. Many useful inequalities are known for Ising-type models, see the textbooks [6, 13]. With the help of these inequalities one can compare correlations functions of lattice models with different couplings or in different dimensions. For example, knowing that the two-dimensional Ising model shows a spontaneous magnetization at low temperature one can prove that the same holds true for the model in higher dimensions. We shall consider spin models with configuration space $\Omega = \mathbb{R}^V$ and even single-spin measures $\mathrm{d}\mu_x$. Thus we examine *ferromagnetic* lattice systems with real spin variables and energy functions

$$H(\omega) = -\sum_{K \subset \Lambda} J_K s_K, \quad \text{where } J_K \geq 0, \; s_K = \prod_{x \in K} s_x. \tag{8.69}$$

The monomial s_K is the product of spin variables s_x on sites in K (with possible duplications in K). The expectation value of a function $O : \Omega \to \mathbb{R}$ is defined as

$$\langle O \rangle = \frac{1}{Z} \int_{\Omega} O(\omega) \, \mathrm{e}^{-\beta H(\omega)} \, \mathrm{d}\mu(\omega), \quad \mathrm{d}\mu(\omega) = \prod_{x \in \Lambda} \mathrm{d}\mu_x(s_x). \tag{8.70}$$

With a suitable choice of the single-spin measure $\mathrm{d}\mu_x$ we can recover Ising-type systems or scalar field theories on a lattice. We now prove that the correlation of any monomial of the spins is non-negative:

Lemma 8.1 (First GKS inequality) *For a ferromagnetic system with energy function* (8.69) *and even single-spin distribution the inequality*

$$\langle s_A \rangle \geq 0, \quad s_A = \prod_{x \in A} s_x \tag{8.71}$$

holds for all $A \subset \Lambda$ (*we allow duplications in* A).

Proof To prove this inequality we absorb the inverse temperature β in the couplings J_K and expand the Boltzmann factor according to

$$\mathrm{e}^{-H(\omega)} = \sum_{n=0}^{\infty} \frac{1}{n!} \Big(\sum_{K} J_K s_K \Big)^n = \sum_{n_1, \ldots, n_V} a_{n_1 \ldots n_V} s_1^{n_1} \cdots s_V^{n_V}$$

with positive coefficients $a_{n_1 \dots n_V}$ and obtain

$$Z \cdot \langle s_A \rangle = \sum_{n_1,\dots,n_V} a_{n_1 \dots n_V} \int s_1^{m_1} \cdots s_V^{m_V} \, \mathrm{d}\mu_1(s_1) \cdots \mathrm{d}\mu_V(s_V),$$

where m_x is the sum of n_x and the multiplicity of s_x in s_A. For even single-spin measures $\mathrm{d}\mu_x$ the last integral vanishes if only one exponent m_x is odd, and it is non-negative if all exponents are even. This means that $\langle s_A \rangle$ is a sum of non-negative terms and hence is non-negative. □

To proceed further we introduce the important concept of replicas where one considers several independent copies of the original system. Here we consider only two copies characterized by the configurations $(\omega, \omega') \in \Omega \times \Omega$. Since they should be independent we assume that

$$\mathrm{d}\mu\big(\omega, \omega'\big) = \mathrm{d}\mu(\omega)\, \mathrm{d}\mu\big(\omega'\big) \quad \text{and} \quad H\big(\omega, \omega'\big) = H(\omega) + H\big(\omega'\big). \tag{8.72}$$

We also introduce the rotated configurations in $\Omega \times \Omega$,

$$\sigma = \frac{1}{\sqrt{2}}\big(\omega + \omega'\big) \quad \text{and} \quad \sigma' = \frac{1}{\sqrt{2}}\big(\omega - \omega'\big). \tag{8.73}$$

The inverse transformation is

$$\omega = \frac{1}{\sqrt{2}}\big(\sigma + \sigma'\big) \quad \text{and} \quad \omega' = \frac{1}{\sqrt{2}}\big(\sigma - \sigma'\big). \tag{8.74}$$

The spins of the rotated configuration σ are denoted by σ_x and σ_A is defined similarly to s_A. A second interesting inequality is the content of

Lemma 8.2 (Ginibre's inequality) *For a ferromagnetic system with energy function* (8.69) *and even single-spin distributions the rotated spins obey the inequalities*

$$\big\langle \sigma_A \sigma'_B \big\rangle \geq 0 \tag{8.75}$$

for all subsets $A, B \subset \Lambda$.

Proof The negative energy

$$-H\big(\omega, \omega'\big) = \sum_{K \subset \Lambda} J_K \left[\left(\frac{\sigma + \sigma'}{\sqrt{2}} \right)_K + \left(\frac{\sigma - \sigma'}{\sqrt{2}} \right)_K \right] \tag{8.76}$$

is a polynomial in σ and σ' with only *positive coefficients*. All terms with negative coefficients in the expansion of the second contribution on the right hand side in (8.76) chancel against terms with positive coefficients in the expansion of the first contribution. Hence, we obtain an expansion similar to the one discussed in the context of the first GKS inequality. What is left is the proof of

$$I_{mn} = \int_{\mathbb{R}^2} \sigma^m \sigma'^n \, \mathrm{d}\mu(s)\, \mathrm{d}\mu\big(s'\big) \geq 0.$$

Clearly, the inequality holds for even exponents m and n. But for odd m or n the integral vanishes since the measure is even both in σ and σ' as follows from the assumption that $\mathrm{d}\mu(s)$ is even and from

$$(-\omega', -\omega) \to (-\sigma, \sigma'), \qquad (\omega', \omega) \to (\sigma, -\sigma'). \qquad \square$$

With the help of Ginibre's inequality we can prove that the connected two-point correlation function of two monomials of the spins is non-negative:

Lemma 8.3 (Second GKS inequality) *With the same assumption as in the previous lemma we have for all* $A, B \subset \Lambda$

$$\langle s_A s_B \rangle - \langle s_A \rangle \langle s_B \rangle \geq 0. \tag{8.77}$$

Proof We have

$$\begin{aligned} \langle s_A s_B \rangle - \langle s_A \rangle \langle s_B \rangle &= \langle s_A (s_B - s'_B) \rangle \\ &= \left\langle \left(\frac{\sigma + \sigma'}{\sqrt{2}} \right)_A \left[\left(\frac{\sigma + \sigma'}{\sqrt{2}} \right)_B - \left(\frac{\sigma - \sigma'}{\sqrt{2}} \right)_B \right] \right\rangle, \end{aligned}$$

where the product $\langle s_A \rangle \langle s_B \rangle$ turns into one expectation value in the doubled system. The expression between square brackets is a polynomial in σ, σ' with positive coefficients. By using Ginibre's inequality we verify the inequality (8.77). $\square$

Now we specialize to ferromagnetic systems with pair interactions,

$$H(\omega) = -\sum_{x,y \in \Lambda} J_{xy} s_x s_y - \sum_x h_x s_x, \quad J_{xy} > 0 \tag{8.78}$$

for which the following inequality holds:

Lemma 8.4 (Percus' inequality) *In the doubled ferromagnetic system we have*

$$\langle \sigma'_A \rangle \geq 0, \quad \forall A \subset \Lambda. \tag{8.79}$$

Proof The linear transformation (8.74) is a (improper) rotation such that

$$-H(\omega) - H(\omega') = \sum_{x,y \in \Lambda} J_{xy} (\sigma_x \sigma_y + \sigma'_x \sigma'_y) + \sqrt{2} \sum_x h_x \sigma_x.$$

Now we Taylor-expand the exponential of $\sum J_{x,y} \sigma'_x \sigma'_y$ in the expectation value

$$\langle \sigma'_A \rangle = \frac{1}{Z^2} \int_{\Omega \times \Omega} \mathrm{d}\mu(\omega)\, \mathrm{d}\mu(\omega') \sigma'_A \, \mathrm{e}^{-H(\omega) - H(\omega')}$$

and obtain a series with terms

$$\int_{\Omega \times \Omega} \mathrm{d}\mu(\omega)\, \mathrm{d}\mu(\omega') \sigma_1'^{n_1} \cdots \sigma_V'^{n_V} \exp\left(\sum_{x,y} J_{xy} \sigma_x \sigma_y + \sqrt{2} \sum_x h_x \sigma_x \right)$$

and positive coefficients. Since the measure is even in σ' the last integral vanishes if one or more exponents n_x are odd. But for even n_x the integral is non-negative and this proves the inequality of Percus. □

Apart from the inequalities discussed in this section there are numerous other correlation inequalities, for example inequalities for the expectation values of products of three or four spin functions. For a detailed discussion I recommend [14] and the textbooks [6, 13]. In passing we note that almost all inequalities apply to ferromagnetic systems only, the well-known exception being the FKG inequalities. For correlation inequalities for anti-ferromagnetic systems you may consult [15].

Application of Correlation Inequalities The second GKS inequality is of particular importance, since in the form

$$\langle s_A s_B \rangle - \langle s_A \rangle \langle s_B \rangle = \frac{\partial \langle s_A \rangle}{\partial J_B} \geq 0 \tag{8.80}$$

it proves the monotony of correlation functions as functions of the ferromagnetic couplings. The expectation value of any monomial of the spins $\langle s_A \rangle$ increases monotonically with

- an increasing external field,
- an increasing ferromagnetic coupling,
- a decreasing temperature.

Furthermore, the inequality (8.80) allows for a comparison of different models in statistical mechanics. For example, if a ferromagnetic spin model with nearest neighbor interaction has an ordered phase, it remains in the ordered phase if additional *ferromagnetic long-range interactions* are 'switched on' since both the magnetization and the critical temperature increase. Moreover, the inequality shows that the spontaneous magnetization decreases if we heat the system. The same happens if we increase the coordination number of a lattice system since we add additional ferromagnetic terms. For example, for fixed coupling and temperature the magnetization in the three- and four-dimensional hypercubic Ising models are larger than in the two-dimensional model. Also, at fixed Ising coupling J the critical temperature increases monotonically with the dimension of the system. This qualitative but rigorous predictions agree with the mean field results (7.23) and (7.24). The same inequality shows that $\langle s_A \rangle$ increases monotonically with the lattice size. For the Ising model these expectation values are bounded by 1 such that they converge in the thermodynamic limit. The Ginibre inequality was applied to prove the *existence of the thermodynamic limit* for the free energy density and spin correlations of the ferromagnetic classical XY-model [16].

8.7 Roots of the Partition Function

The zeros of the partition function $Z_\Lambda(\beta, h)$ are intimately related to possible phase transitions as was observed by LEE and YANG in their two pioneering papers [17,

18].[1] As a sum of positive terms the partition function is positive in the physical domain with real magnetic field. Thus, in a search of zeros we must admit complex parameters and in particular a complex magnetic field. Following Lee and Yang we study a lattice gas with energy function:

$$H = -\varepsilon \sum_{\langle x,y\rangle} n_x n_y - \mu \sum_x n_x, \quad n_x \in \{0,1\} \tag{8.81}$$

or, what amounts to the same, an Ising model with magnetic field,

$$H(\omega) = -J \sum_{\langle x,y\rangle} s_x s_y - h \sum_x s_x, \quad s_x \in \{-1,1\}. \tag{8.82}$$

The occupation numbers n_x, coupling and chemical potential of the lattice gas are related to the spins s_x, coupling and magnetic field of the Ising model by

$$n_x = (s_x+1)/2, \qquad \varepsilon = 4J \quad \text{and} \quad \mu = 2h - 4dJ.$$

In the expansion of the Ising-model partition function in powers of $\exp(\beta h)$,

$$Z_\Lambda(h) = \sum_{m=-V,-V+2,\dots}^{V} \mathrm{e}^{\beta h m} A_m, \quad A_m = \sum_{\sum s_x = m} \exp\Big(K \sum_{\langle x,y\rangle} s_x s_y\Big), \tag{8.83}$$

we set $m+V = 2n$ such that n takes the values $0,1,\dots,V$ and obtain

$$Z_\Lambda(z) = z^{-V/2} \sum_{n=0}^{V} a_n z^n, \quad \text{where } a_n = A_{2n-V},\ z = \mathrm{e}^{2\beta h}. \tag{8.84}$$

The sum defines a polynomial of degree V in the *fugacity* z. Since all a_n are positive we conclude that on a finite lattice the partition function is non-zero and analytic in a vicinity of the positive real semi-axis in the complex fugacity plane. This means that the free energy has no singularities for any real magnetic field and thus shows no phase transition in a finite volume when h varies.

However, in the thermodynamic limit $V \to \infty$ the partition function zeros may pinch the semi-axis $\mathbb{R}^+$. Phase transitions are localized at the intersection of the set of zeros with the semi-axis. The intersection points determine the critical fields where phase transitions may occur. On the other hand, if there exists a region G in the complex z-plane which contains no zeros and encloses the positive real semi-axis, then the thermodynamic potentials are analytic for $V \to \infty$.

Because the coefficients of the polynomial in (8.84) are real and positive, all roots appear in complex-conjugated pairs in the complex fugacity plane, away from the real, positive semi-axis. There is a further property of the roots which follows from the symmetry $H(\omega,h) = H(-\omega,-h)$, where $-\omega$ is obtained from ω by a flip of all spins. This symmetry implies that the partition function is an even function of h and thus is invariant under $z \to 1/z$:

$$Z_\Lambda(z) = \sum_\omega \mathrm{e}^{-\beta H(\omega,h)} = Z_\Lambda\Big(\frac{1}{z}\Big). \tag{8.85}$$

[1] An elementary discussion of the subject can be found in [9].

It follows that the coefficients of the polynomial in (8.84) are not independent,

$$a_n = a_{V-n} \tag{8.86}$$

and that with z also $1/z$ is a root of the partition function. Thus, the non-real roots which are not on the unit circle in the fugacity plane are members of a quartet $\{z, \bar{z}, 1/z, 1/\bar{z}\}$ of roots. The non-real roots on the unit circle or the real roots which are not on the unit circle are members of a doublet $\{z, 1/z\}$ of roots. Only the root $z = -1$ is not related to another root.

In the high temperature limit $K = 0$ and the partition function

$$\lim_{T\to\infty} Z_\Lambda(z) = z^{-V/2}(1+z)^V \tag{8.87}$$

has the V-fold zero $z = -1$. On the other hand, in the low temperature limit $K = \infty$ and the partition function

$$\lim_{T\to 0} Z_\Lambda(z) = z^{-V/2}\mathrm{e}^{dVK}\left(1+z^V\right) \tag{8.88}$$

has its roots uniformly distributed on the unit circle,

$$z_n = \mathrm{e}^{2\pi \mathrm{i}(n-1/2)/V}, \quad n = 1, \ldots, V.$$

Below we shall argue that for all K between these two extreme values the roots of the partition functions lie on the unit circle. This theorem of Lee and Yang applies to general ferromagnetic systems for which the couplings J_{xy} fall off with the distance rapidly enough in order to ensure the existence of the thermodynamic limit.

8.7.1 Lee–Yang Zeroes of Ising Chain

To find the Lee–Yang zeros for the one-dimensional Ising model we observe that the partition function (8.8) is proportional to a polynomial of degree N in the fugacity $z = \exp(2\beta h)$. It vanishes if and only if

$$\lambda_+ = \mathrm{e}^{\mathrm{i}n\pi/N}\lambda_-, \quad n = 1, 3, \ldots, 2N-1.$$

With the expressions (8.6) for the eigenvalues of the transfer matrix we obtain

$$\mathrm{i}\sin\left(\frac{n\pi}{2N}\right)\cosh(\beta h_n) = \sqrt{\mathrm{e}^{-4K} + \sinh^2(\beta h_n)}\cos\left(\frac{n\pi}{2N}\right),$$

and after setting $\beta h_n = i\theta_n$ we end up with

$$\sin\frac{n\pi}{2N}\cos\theta_n = \sqrt{\sin^2\theta_n - \mathrm{e}^{-4K}}\cos\left(\frac{n\pi}{2N}\right).$$

Squaring this equation yields the following formula for the phases of the Lee–Yang zeros $z_n = \exp(2\mathrm{i}\theta_n)$ in the complex fugacity plane:

$$\cos\theta_n = \sqrt{1-\mathrm{e}^{-4K}}\cos\left(\frac{n\pi}{2N}\right), \quad n = 1, 3, \ldots, 2N-1. \tag{8.89}$$

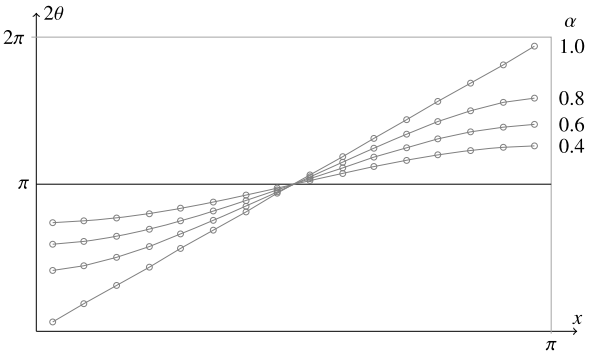

Fig. 8.1 The phases $2\theta_n$ of the Lee–Yang zeros z_n for the Ising chain with 16 sites

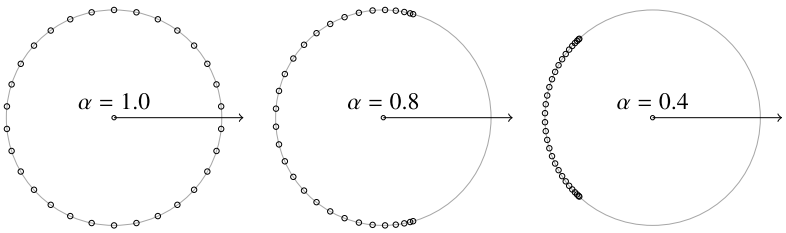

Fig. 8.2 The Lee–Yang zeros in the complex fugacity plane at different temperatures. At $T = 0$ the zeros are uniformly distributed on the unit circle. With increasing temperature the zeros move away from the positive real axis

Since the square root takes its values in the interval $[0, 1]$ we obtain a *real solution* θ_n for every n such that all zeros z_n lie on the unit circle in the complex z-plane. In Fig. 8.1 we plotted the phases

$$2\theta_n = 2\arccos(\alpha \cos x_n) \quad \text{with } \alpha^2 = 1 - \mathrm{e}^{-4K}, x_n = \frac{n\pi}{2N}, \tag{8.90}$$

for different values of α. At zero temperature $\alpha = 1$ and the phases $2\theta_n = 2x_n$ are uniformly distributed within the interval $[0, 2\pi]$. At finite temperatures $\alpha < 1$ and the $2\theta_n$ take their values in the interval $[\Delta, 2\pi - \Delta]$ with $\Delta = 2\arccos\alpha > 0$. This estimate is independent of the lattice size. We conclude that the free energy density shows not singularities at finite temperatures and for any real magnetic field. Only for $T = 0$ and in the thermodynamic limit do the zeros of the partition function pinch the positive real axis. This points to a singularity of the free energy at $z = 1$ and thus to a phase transition at vanishing magnetic field and zero temperature. Figure 8.2 shows the distribution of zeros of $Z_\Lambda(z)$ on the unit circle in the fugacity plane for 30 sites and different values of the temperature dependent parameter α. Figure 8.3 shows the zeros for $\alpha = 0.9$ for three different lattice sizes. In the thermodynamic limit $N \to \infty$ we observe an accumulation of the partition function zeros at the so-called *edge singularity* at

$$\Re z = \cos(2\arccos\alpha) \quad \text{and} \quad \Im z = \sin(2\arccos\alpha).$$

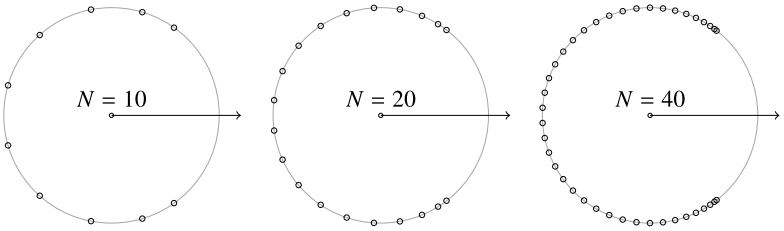

Fig. 8.3 The Lee–Yang zeros, located in the complex fugacity plane for different values of N and at a fixed positive temperature corresponding to $\alpha = 0.9$

8.7.2 General Ferromagnetic Systems

In their two classic papers Lee and Yang showed that the zeros of the Ising-model partition function lie on the unit circle and proposed a program to analyze phase transitions in terms of these zeros. Since their proposal the Lee–Yang theorem has been used to prove the existence of infinite-volume limits for spin models, to prove correlation inequalities and inequalities for critical exponents, see [13].

The Lee–Yang theorem states that the partition function

$$Z_\Lambda(\beta) = \int \mathrm{d}\mu(\omega) \exp\bigl(-\beta H_\Lambda(\omega)\bigr), \quad \mathrm{d}\mu(\omega) = \prod_{x\in\Lambda} \mathrm{d}\mu(s_x), \tag{8.91}$$

of ferromagnetic systems with energies

$$H_\Lambda = -\sum_{x\neq y\in\Lambda} J_{xy} s_x s_y - \sum_{x\in\Lambda} h_x s_x, \quad J_{xy} \geq 0, \tag{8.92}$$

and a certain class of single-spin distributions $\mathrm{d}\mu(s)$ is non-zero whenever $\Re h_x > 0$ on all sites. It was proved by Newman [19–21] for one-component systems with an even single-spin distribution $\mathrm{d}\mu$ with the property that

$$\int \mathrm{e}^{hs}\, \mathrm{d}\mu(s) \neq 0 \quad \text{for } \Re(h) \neq 0. \tag{8.93}$$

For lattice systems with continuous spins, for example lattice field theories, the single-spin distribution should also fall off rapidly,

$$\int e^{\alpha s^2}\, \mathrm{d}\mu(s) < \infty, \quad \alpha < \infty, \tag{8.94}$$

for the partition function to exist. A rapidly decreasing and even measure on $\mathbb{R}$ with property (8.93) is said to have the *Lee–Yang property*. This property means that the Fourier transform of the single-spin distribution has its zeros on the real axis. The Lee–Yang theorem also applies to spin systems with site-dependent single-spin distributions in $\mathrm{d}\mu(\omega) = \prod \mathrm{d}\mu_x(s_x)$, provided all $\mathrm{d}\mu_x$ fulfill the condition (8.93):

Theorem 8.2 (Lee–Yang circle theorem) *If all single-spin distributions* $\mathrm{d}\mu_x$ *of a ferromagnetic spin system with* $\mathscr{T} = \mathbb{R}$ *satisfy the Lee–Yang property and if all* h_x

have a positive real part then the partition function $Z_\Lambda[h]$ is non-zero. If the external field is constant, $h_x = h$, then all zeros of $Z_\Lambda(h)$ are imaginary.

This theorem means that the Lee–Yang property holds for $J_{xy} \geq 0$ in case it holds for $J_{xy} = 0$. For the Ising model with identical single-spin distributions (7.16) the integral (8.93) is $\cosh(h)$ and the theorem applies: all zeros of the Ising-model partition function as function of the fugacity lie on the unit circle, similarly as for the Ising chain. The single-spin distribution of a lattice ϕ^4 theory,

$$\mathrm{d}\mu(\phi) = \exp\bigl(-\lambda\phi^4 - \mu\phi^2\bigr)\,\mathrm{d}\phi, \quad \lambda > 0, \mu \in \mathbb{R}, \tag{8.95}$$

also satisfies the Lee–Yang property such that the circle theorem applies to the Schwinger functional of a lattice ϕ^4 theory.

Recent proofs of the circle theorem use multi-affine Lee–Yang polynomials together with the *Asano contraction*, see [22–24]. For scalar field theories one can easily prove a weaker result [13, 25], which is based on correlation inequalities:

Theorem 8.3 (Dunlop) *Consider a ferromagnetic system with energy function* (8.92) *and single-spin distribution*

$$\mathrm{d}\mu(s) = \mathrm{e}^{-P(s)}, \qquad P(s) = \lambda s^4 + \mu s^2, \quad \lambda > 0,\ \mu \text{ real}. \tag{8.96}$$

If all h_x are in the wedge $|\Im h_x| \leq \Re h_x$ then the partition function is non-zero,

$$\bigl|Z_\Lambda[h]\bigr| \geq Z_\Lambda[h = 0] > 0. \tag{8.97}$$

Proof We introduce two independent copies of the spin system to write

$$\bigl|Z[h]\bigr|^2 = \int \mathrm{d}\mu(\omega)\,\mathrm{d}\mu\bigl(\omega'\bigr)\,\mathrm{e}^{-\beta H(\omega) - \beta H^*(\omega')} \tag{8.98}$$

where H^* is the energy function (8.92) with the h_x replaced by their complex conjugate h_x^*. First we transform to the rotated frame with coordinates σ_x, σ_x' introduced in (8.73), and for these we use polar coordinates

$$\sigma_x = \rho_x \cos\theta_x, \qquad \sigma_x' = \rho_x \sin\theta_x.$$

In terms of polar coordinates the single site measure of the doubled system contains the polynomial

$$P(s) + P\bigl(s'\bigr) = \frac{\lambda\rho^4}{4}(3 - \cos 4\theta) + \mu\rho^2$$

such that the single site measure takes the form

$$\mathrm{e}^{-P(s)-P(s')}\,\mathrm{d}s\,\mathrm{d}s' = \rho \exp\left(-\frac{3}{4}\lambda\rho^4 - \mu\rho^2\right) \exp\left(\frac{1}{4}\lambda\rho^4 \cos 4\theta\right) \rho\,\mathrm{d}\rho\,\mathrm{d}\theta. \tag{8.99}$$

The second step in the proof is to rewrite the integrand in (8.98) in polar coordinates. With

$$\sum_{x\neq y} J_{xy}\big(s_x s_y + s_x s'_y\big) = \sum_{x\neq y} J_{xy}\rho_x\rho_y\cos(\theta_x-\theta_y),$$
$$\sum_{x}\big(h_x s_x + h_x^* s_x\big) = \sum_{x}\rho_x\big(\Delta_+ \mathrm{e}^{\mathrm{i}\theta_x} + \Delta_- \mathrm{e}^{-\mathrm{i}\theta_x}\big),$$

where we abbreviated

$$\sqrt{2}\Delta_\pm = \Re h_x \pm \Im h_x$$

we obtain for the exponent in (8.98)

$$-\beta H(\omega) - \beta H^*\big(\omega'\big) = \sum_{x\neq y} J_{xy}\rho_x\rho_y\cos(\theta_x-\theta_y) + \sum_x \rho_x\big(\Delta_+\mathrm{e}^{\mathrm{i}\theta_x} + \Delta_-\mathrm{e}^{-\mathrm{i}\theta_x}\big).$$

At this point we use the notion of a positive definite function $f(\boldsymbol{\theta}) = f(\theta_1,\ldots,\theta_V)$ of angular variables $\theta_x \in [0, 2\pi]$. Such a function is called *positive definite* if the coefficients $f_{n_1\ldots n_V}$ in its Fourier series

$$f(\theta_1,\ldots,\theta_V) = \frac{1}{(2\pi)^{V/2}}\sum_{n_i\in\mathbb{Z}} f_{n_1\ldots n_V}\exp\Big(\mathrm{i}\sum n_x\theta_x\Big)$$

are all non-negative, $f_{n_1\ldots n_V} \geq 0$. The set of positive definite functions is closed under exponentiation, multiplication and multiplication with a positive real constant.

Clearly, for positive λ the last exponent in (8.99) is a positive definite function such that the density of $\mathrm{d}\mu(\omega)\,\mathrm{d}\mu(\omega')$ is a positive definite function as well. In addition, the condition $|\Im h_x| \leq \Re h_x$ in the theorem implies that $\Delta_\pm$ are both non-negative, such that $-\beta H(\omega) - \beta H^*(\omega)$ and its exponential are both positive definite functions. We conclude that under the assumption in the theorem the integrand of

$$\big|Z_\Lambda[h]\big|^2 = \int\prod_x \rho_s\,\mathrm{d}\rho_x\,\mathrm{d}\theta_x F(\rho_1,\ldots,\rho_V;\theta_1,\ldots,\theta_V)$$

is a positive definite function, the Fourier coefficients of which are monotonic functions of Δ_+ and Δ_-. It follows that the integral, which is proportional to the Fourier coefficient $F_{0\ldots0}$, decreases when we replace the larger of the two numbers Δ_+, Δ_- by the smaller one, which is $\Re h_x - |\Im h_x|$. But then $|Z|^2$ becomes the square of the partition function for the real magnetic field $x \to \Re h_x - |\Im h_x|$ such that

$$\big|Z_\Lambda[h]\big| \geq Z_\Lambda\big[\Re h - |\Im h|\big] \geq Z_\Lambda[h=0] > 0. \tag{8.100}$$

In addition, since $Z_\Lambda[h] = Z_\Lambda[-h]$, it follows that the partition function is also non-zero if all h_x are in the wedge $|\Im h_x| \leq -\Re h_x$. □

In many applications one considers homogeneous fields for which the zeros of the partition function must lie in the forward or backward 'light-cones' in the complex h-plane. Note that the theorem is not as strong as the circle theorem, which nails down the zeros to the imaginary axis in h-space. But the proof given by Dunlop also extends to Z_2 gauge theories [26]. For a general lattice field theory with multidimensional target space (and some invariant single-spin distribution) no variant of the Lee–Yang theorem may exist. Only for simple systems like the $O(2)$ and $O(3)$ models could such theorems be established, see [19–21, 27].

A decade after the work of Lee and Yang, Fisher extended the study of the Ising partition function zeros to the complex temperature plane [28]. After these early results there have been numerous studies of Lee–Yang and Fisher zeros in a variety of models.

8.8 Problems

8.1 (Transfer matrices for modified Ising chains)

(a) Find the transfer matrix for a Ising chain in which the spins may take the three values $\{+1, 0, -1\}$.
(b) Find the transfer matrix for a Ising chain with first and second neighbor interactions,

$$H(\omega) = -J \sum_x s_x s_{x+1} - K \sum_x s_x s_{x+2} - h \sum_x s_x, \quad s_x = \pm 1.$$

Hint: consider the transfer matrix of a pair to the neighboring pair. An analysis of this model which circumvents diagonalizing the resulting 4×4 transfer matrix is given in [29].

8.2 (Potts chain revisited) In Sect. 8.2 we calculated the free energy density for the Potts chain in the thermodynamic limit. Compute the magnetization $m(T, h)$ and the susceptibility $\chi(T, h)$. Compare the results with the corresponding results for the Ising chain.

8.3 (Transfer matrix for harmonic oscillator) Consider the transfer kernel (8.54) for the oscillator on the lattice with harmonic oscillator potential $V(q) = m\omega^2 q^2/2$.

- Prove the useful identity

$$\lambda_0^2 \hat{a}^\dagger T(q, q') = \hat{a}' T(q, q'), \tag{8.101}$$

where $\hat{a}^\dagger$ acts on the argument q and $\hat{a}'$ on the argument q',

$$\hat{a}^\dagger = \frac{\mathrm{d}}{\mathrm{d}q} - m\alpha q, \qquad \hat{a}' = -\frac{\mathrm{d}}{\mathrm{d}q'} - m\alpha q'.$$

The explicit expressions for α and λ_0 are found in Sect. 8.5.1.
- Use the result to show that if ψ is an eigenfunction of the transfer matrix $\hat{T}$ with eigenvalue λ

$$\int \mathrm{d}q' \, T(q, q') \psi(q') = \lambda \psi(q'),$$

and that $\hat{a}^\dagger \psi$ is an eigenfunction as well with eigenvalue $\lambda_0^2 \lambda$.
- In Sect. 8.5.1 we calculated the eigenstate ψ_0 with largest eigenvalue λ_0 of the transfer matrix. Determine the other eigenvalues and eigenfunctions with purely algebraic means.

References

1. L. Onsager, Crystal statistics. I. A two-dimensional model with an order-disorder transition. Phys. Rev. **65**, 117 (1944)
2. E. Lieb, F.Y. Wu, Two-dimensional ferroelectric models, in *Phase Transitions and Critical Phenomena*, vol. 1, ed. by C. Domb, M.S. Green (Academic Press, London, 1972)
3. R.J. Baxter, *Exactly Solved Models in Statistical Mechanics* (Academic Press, New York, 1982)
4. E. Ising, Beitrag zur Theorie des Ferromagnetismus. Z. Phys. **31**, 253 (1925)
5. L. van Hove, Sur l'intégrale de configuration des systèmes des particules à une dimension. Physica **16**, 137 (1950)
6. D. Ruelle, *Statistical Mechanics: Rigorous Results* (Benjamin, New York, 1969)
7. T. Dauxois, M. Peyrand, Entropy-driven transition in a one-dimensional system. Phys. Rev. E **51**, 4027 (1995)
8. E. Lieb, D. Mattis, *Mathematical Physics in One Dimension* (Academic Press, New York, 1966)
9. K. Huang, *Statistical Mechanics* (Wiley, New York, 1963)
10. F.Y. Wu, Self-dual property of the Potts model in one dimension. cond-mat/9805301
11. O. Perron, Zur Theorie der Matrizen. Math. Ann. **64**, 248 (1907)
12. G. Frobenius, Über Matrizen aus nicht negativen Elementen, Sitzungsber. Königl. Preuss. Akad. Wiss. 456 (1912)
13. B. Simon, *The $P(\phi)_2$ Euclidean (Quantum) Field Theory* (Princeton University Press, Princeton, 1974)
14. G.S. Sylvester, Inequalities for continuous-spin Ising ferromagnets. J. Stat. Phys. **15**, 327 (1975)
15. S.B. Shlosman, Correlation inequalities for antiferromagnets. J. Stat. Phys. **22**, 59 (1976)
16. J. Ginibre, General formulation of Griffiths' inequalities. Commun. Math. Phys. **16**, 310 (1970)
17. C.N. Yang, T.D. Lee, Statistical theory of equations of state and phase transitions. I. Theory of condensation. Phys. Rev. **87**, 404 (1952)
18. C.N. Yang, T.D. Lee, Statistical theory of equations of state and phase transitions. II. Lattice gas and Ising model. Phys. Rev. **87**, 410 (1952)
19. C. Newman, Zeros of the partition function of generalized Ising systems. Commun. Pure Appl. Math. **27**, 143 (1974)
20. K.C. Lee, Zeros of the partition function for a continuum system at first-order transitions. Phys. Rev. E **53**, 6558 (1996)
21. W.T. Lu, F.Y. Wu, Partition function zeroes of a self-dual Ising model. Physica A **258**, 157 (1998)
22. T. Asano, Theorems on the partition functions of the Heisenberg ferromagnets. J. Phys. Soc. Jpn. **29**, 350 (1970)
23. D. Ruelle, Extension of the Lee–Yang circle theorem. Phys. Rev. Lett. **26**, 303 (1971)
24. E.H. Lieb, A.D. Sokal, A general Lee–Yang theorem for one-component and multicomponent ferromagnets. Commun. Math. Phys. **80**, 153 (1981)
25. F. Dunlop, Zeros of partition function via correlation inequalities. J. Stat. Phys. **17**, 215 (1977)
26. F. Dunlop, in *Colloquia Mathematica Sociatatis Janos Bolyai 27: Random Fields*, ed. by J. Fritz, J.L. Lebowitz, D. Szasz (North Holland, Amsterdam, 1981)
27. F. Dunlop, C. Newman, Multicomponent field theories and classical rotators. Commun. Math. Phys. **44**, 223 (1975)
28. M.E. Fisher, in *Lectures in Theoretical Physics*, vol. 7c, ed. by W.E. Brittin (University of Colorado Press, Boulder, 1965)
29. J. Stephenson, Two one-dimensional Ising models with disorder points. Can. J. Phys. **48**, 1724 (1979)

Chapter 9
High-Temperature and Low-Temperature Expansions

Series expansions remain, in many cases, one of the most accurate ways of estimating critical exponents. Historically it was the results from series expansions that suggested universality at criticality. Two expansions will be considered in this chapter. In the *high-temperature series* the Boltzmann factor is expanded in powers of the inverse temperature and the sum over all configurations is taken term by term. In the Ising model this leads to an expansion in powers of $\tanh(J/T) \ll 1$. In the *low-temperature expansion* configurations are counted in order of their importance as the temperature is increased from zero. Starting from the ground state the series is constructed by successively adding terms from $1, 2, 3, \ldots$ flipped spins. In the Ising model this leads to an expansion in powers of $\exp(-2J/T) \ll 1$.

Each term in a series is represented by a graph on a lattice and constructing the series amounts to counting the graphs belonging to a fixed order in the expansions. The expansions can be used to approximate the thermodynamic potentials and correlation functions at low and high temperatures. The hope is that the expansions are sufficiently well-behaved in order to extract the singular behavior from a limited number of lowest order terms. Confidence in the method lies in the large body of circumstantial evidence available. Series expansions agree well with high accuracy Monte Carlo simulations, renormalization-group results and results for exactly solvable models.

The high- and low-temperature expansions treated in this chapter are covered in numerous textbooks and papers. For a further reading beyond the introductory material presented in this chapter you may consult the textbooks [1–4].

9.1 Ising Chain

To become acquainted with the high- and low-temperature expansions, we first consider these expansions for the Ising chain.

A. Wipf, *Statistical Approach to Quantum Field Theory*, Lecture Notes in Physics 864,
DOI 10.1007/978-3-642-33105-3_9,

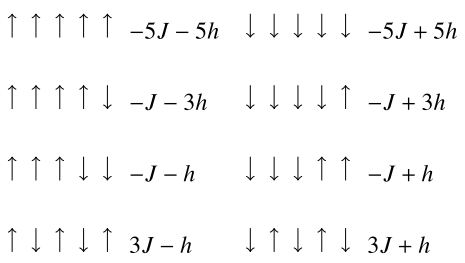

Fig. 9.1 Spin configurations of the Ising chain for different energies

9.1.1 Low Temperature

The configuration with minimal energy is characterized by an alignment of *the spins*—all spins point in the direction of the magnetic field. Configurations with some spins flipped have higher energy and can only be populated for non-zero temperature. But for low temperature the corresponding occupations numbers are exponentially small. For warming up we consider the chain Λ with only five sites. The 2^5 configurations form eight classes and each class is characterized by its energy. Representatives of the classes are depicted in Fig. 9.1. The two classes with aligned spins in the first row contain one element each, whereas all other classes contain five elements. Assuming $h > 0$ the energy of the vacuum configuration is $E_0 = -5J - 5h$ and we obtain the following *low-temperature expansion* of the partition function for $\mathrm{e}^{-\beta J} \ll 1$:

$$Z_\Lambda = \mathrm{e}^{-\beta E_0}\big(1 + \mathrm{e}^{-10\beta h} + 5\mathrm{e}^{-\beta(4J+2h)} + 5\mathrm{e}^{-\beta(4J+8h)} + 5\mathrm{e}^{-\beta(4J+4h)} + 5\mathrm{e}^{-\beta(4J+6h)} + 5\mathrm{e}^{-\beta(8J+4h)} + 5\mathrm{e}^{-\beta(8J+6h)}\big).$$

The systematic low-temperature expansion based on graphs is discussed in Sect. 9.3 for the more interesting Ising models in higher dimensions.

9.1.2 High Temperature

For simplicity we consider the high-temperature expansion for the zero-field Ising model. Thereby we expand the partition function on a hyper-cubic lattice Λ in d dimensions in powers of the small parameter $v = \tanh K = \tanh J/T$,

$$Z_\Lambda = \sum_\omega \prod_{\langle x,y\rangle} \mathrm{e}^{K s_x s_y} = (\cosh K)^P \sum_\omega \prod_{\langle x,y\rangle} (1 + v s_x s_y), \tag{9.1}$$

where $P = dV$ denotes the number of nearest-neighbor pairs and the last equation holds because $s_x s_y \in \{-1, 1\}$.

The periodic *Ising chain* with only three sites has three nearest-neighbor pairs and the product in (9.1) contains three factors,

$$\prod_{\langle x,y\rangle} (1 + v s_x s_y) = (1 + v s_1 s_2)(1 + v s_2 s_3)(1 + v s_3 s_1).$$

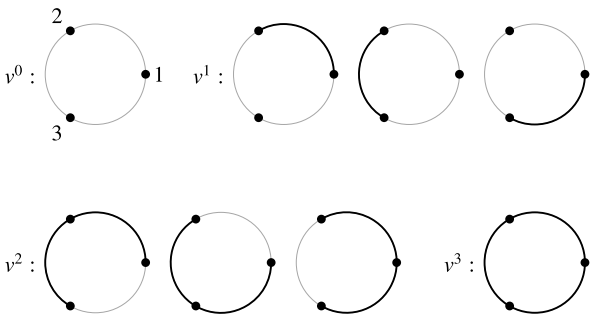

Fig. 9.2 Diagrams associated with the high-temperature expansion of the Ising chain

The expansion of this expression in powers of the parameter v yields $2^P = 8$ terms,

$$Z_\Lambda = (\cosh K)^3 \sum_\omega \big(1 + v(s_1 s_2 + s_2 s_3 + s_3 s_1) + v^2(s_1 s_2 s_2 s_3 + s_1 s_2 s_3 s_1 + s_2 s_3 s_3 s_1) + v^3(s_1 s_2 s_2 s_3 s_3 s_1)\big). \tag{9.2}$$

Next we assign to each term in this expansion a diagram on the periodic chain as follows: we connect two adjacent sites x and y by a line—in the following called bond or link—if the product of their spins occurs in the term under consideration. Those sites where at least one bond ends form the vertices of the associated diagram. We call the number of bonds attached to a vertex the *order of the vertex*.

Figure 9.2 shows the eight diagrams corresponding to the high-temperature expansion (9.2). Since the small parameter v enters via the combination $v s_x s_y$ we see that all diagrams of order n in v have n bonds. Because of the identity

$$\sum_{s_x=-1,1} s_x^n = \begin{cases} 2, & n \text{ even}, \\ 0, & n \text{ odd}, \end{cases} \tag{9.3}$$

only diagrams for which all vertices have an even order contribute to Z_Λ. Such diagrams are called closed. On the chain with three sites only the first and last diagram in Fig. 9.2 are closed such that

$$Z_\Lambda = \cosh^3 K\big(8 + 8v^3\big) = 2^3\big(\cosh^3 K + \sinh^3 K\big).$$

More generally, the chain with N sites has only two closed diagrams: one diagram has no bond and the other has the maximal number of N bonds. It follows that only two diagrams contribute to the partition function,

$$Z_\Lambda = 2^N\big(\cosh^N K + \sinh^N K\big). \tag{9.4}$$

The high-temperature expansion leads to the exact result of the partition function.

9.2 High-Temperature Expansions for Ising Models

The high-temperature expansion is an expansion in the small parameter $v = \tanh K$, where $K = J/T$. It corresponds to the strong-coupling expansion in quantum field theory.

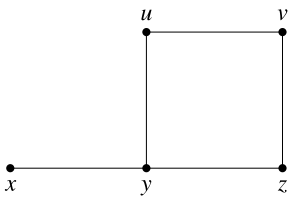

Fig. 9.3 Diagram as it occurs in the high-temperature expansion (9.5). The graph corresponds to the spin product $s_x s_y^3 s_z^2 s_u^2 s_v^2 = s_x s_y$

9.2.1 General Results and Two-Dimensional Model

We consider the zero-field Ising model defined by the Hamiltonian (6.2) with $h = 0$. As starting point we choose the expansion (9.1) in powers of $v \ll 1$,

$$Z_\Lambda = (\cosh K)^P \sum_\omega \left(1 + v \sum_{\langle x,y\rangle} s_x s_y + v^2 \sum_{\langle x,y\rangle \neq \langle x',y'\rangle} s_x s_y s_{x'} s_{y'} + \cdots\right). \tag{9.5}$$

To each spin product we assign the diagram where nearest neighbors are connected by a line if their product occurs in the spin product. Figure 9.3 shows the diagram associated to the spin product $s_x s_y^3 s_z^2 s_u^2 s_v^2$. The diagram does not contribute to the partition function since it has the odd vertices x and y. Only closed diagrams contribute, such that on a *finite* lattice with P nearest neighbor pairs[1]

$$Z_\Lambda = (\cosh K)^P 2^V \sum_{\ell=0}^{P} z'_\ell v^\ell, \quad z'_0 = 1. \tag{9.6}$$

where z'_ℓ counts the number of closed diagrams with ℓ bonds. Table 9.1 contains the closed diagrams for the periodic Ising model on a square lattice with V sites and $P = 2V$ nearest-neighbor pairs with eight or less bonds. The number in the third column counts the number of diagrams of the corresponding class. For example, the number $V(V-5)/2$ in the second to last row of this table is explained as follows: We may place the first plaquette somewhere on the lattice and we have V possibilities to do this. Then the remaining number of locations of the second plaquette subject to the constraint that none of the edges of the two plaquettes coincide is $V - 5$. Hence, there are $V(V-5)$ possibilities to place the two plaquettes on the lattice. However, since we obtain the same diagram under a permutation of the plaquettes we finally end up with $V(V-5)/2$ different diagrams.

The corresponding expansion for the $2d-$Ising model partition function reads

$$Z_\Lambda = (\cosh K)^P 2^V \left(1 + V v^4 + 2V v^6 + \frac{V}{2}(V+9)v^8 + 2V(V+6)v^{10} + \cdots\right). \tag{9.7}$$

[1] Coefficients in an expansion in v are marked with a stroke.

Table 9.1 Closed diagrams contributing to the high-temperature expansion of the partition function of the two-dimensional Ising model to order of v^8

# bonds ℓ	Diagram	Number	z'_ℓ
4		V	V
6		$2V$	$2V$
8		$4V$	
		$2V$	$\frac{1}{2}V^2 + \frac{9}{2}V$
		$\frac{1}{2}V(V-5)$	
		V	

Only intrinsic quantities have a well-defined thermodynamic limit and thus we turn to the free energy density, given by

$$-\beta f = \lim_{V\to\infty} \frac{1}{V} \log Z_\Lambda = \log\bigl(2\cosh^2 K\bigr) + \sum_{\ell\geq 4} f'_\ell v^\ell. \tag{9.8}$$

Inserting the power series for the partition function one obtains the expansion coefficients f'_ℓ of the free energy density. Only connected diagrams contribute to the free energy density such that the coefficients f'_ℓ are volume-independent. For the Ising model on a square lattice

$$-\beta f = \log\bigl(2\cosh^2 K\bigr) + v^4 + 2v^6 + \frac{9}{2}v^8 + 12v^{10} + \cdots. \tag{9.9}$$

Correlation Functions

Above the critical temperature the magnetization vanishes for zero field and the susceptibility χ is given by

$$\chi = \frac{1}{V}\sum_{x,y}\langle s_x s_y\rangle = \sum_y \langle s_x s_y\rangle. \tag{9.10}$$

Again, we associate each term of the high-temperature expansion

$$\langle s_x s_y\rangle = \frac{\cosh^P K}{Z_\Lambda}\sum_\omega s_x s_y \left(1 + v\sum_{\langle uv\rangle} s_u s_v + v^2 \sum_{\langle uv\rangle\neq\langle u'v'\rangle} s_u s_v s_{u'} s_{v'} + \cdots\right) \tag{9.11}$$

with a diagram. For example, consider the diagram in Fig. 9.4 which contributes $2^V v^8$ to the sum over all configurations in (9.11). More generally, a diagram with ℓ bonds contributes $2^V v^\ell$ if the vertices x and y are odd and all other vertices are even. Because of the relation (9.3) the other diagrams do not contribute. The factor $2^V \cosh^P K$ cancels against the same factor in Z_Λ. Thus we have the

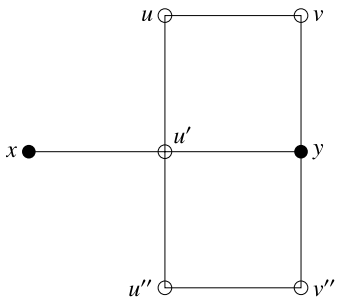

Fig. 9.4 The high-temperature expansion of the 2-point correlation function of the two-dimensional Ising model. The diagram corresponds to the term $s_x^2 s_y^4 s_{u'}^4 s_u^2 s_v^2 s_{u''}^2 s_{v''}^2$

Lemma 9.1 *The high-temperature expansion of the* 2*-point function reads*

$$\langle s_x s_y \rangle = \frac{\sum_\ell g'_\ell v^\ell}{\sum_\ell z'_\ell v^\ell}, \tag{9.12}$$

where g'_ℓ *denotes the number of diagrams with* ℓ *bonds and only even vertices, with the exception of the odd vertices* x *and* y.

This lemma immediately leads to the

Proposition 9.1 *The coefficient* g'_ℓ *vanishes if* ℓ *is less than the shortest distance* $d(x, y)$ *(on the lattice) between* x *and* y.

If the corollary was not true, then there would exist a diagram with less than ℓ bonds and odd vertices x and y, with all other vertices even. It follows that the sites x and y are not connected by a line of bonds or that the diagram consists of at least two disconnected sub-diagrams. At least one connected sub-diagram contains x but not y. According to the relation

$$\sum_{\text{vertices}} \text{vertex order} = 2 \cdot \text{number of bonds} \tag{9.13}$$

the sum of vertex orders for every connected sub-diagram must be even. But for the sub-diagram containing x but not y and contributing to $\langle s_x s_y \rangle$ the sum of vertex orders is odd, since all vertices are even, with the exception of the odd vertex x. But this contradicts the selection rule (9.13) and thus proves Proposition 9.1.

The proposition tells us that for $T \gg J$ the 2-point function falls off exponentially with the shortest distance $d(x, y)$ of x and y on the lattice,

$$\langle s_x s_y \rangle = O\big(v^{d(x,y)}\big) = O\big(\mathrm{e}^{-d(x,y)/\xi}\big), \qquad \frac{1}{\xi} = \log \frac{1}{v} \gg 1. \tag{9.14}$$

As expected, the correlation length ξ decreases with increasing temperature since the thermal fluctuations suppress spin–spin correlations.

ℓ	diagrams	number	g'_ℓ
2		2	2
4		4	4
6	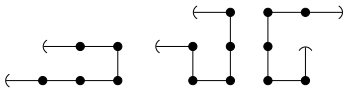	3×4	
	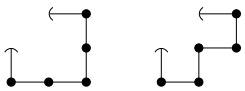	2×2	$2V + 10$
	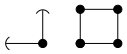	$2(V - 3)$	

Fig. 9.5 The leading high-temperature diagrams contributing to χ

Susceptibility

Only two-point functions with $d(x, y) \leq n$ contribute to the high-temperature expansion of the susceptibility in (9.10) to order n in v. Hence, the susceptibility in every order n is given by a finite number of terms. In the two-point functions (9.12) the volume-factor cancels in the ratio of formal power series. Figure 9.5 shows all diagrams that contribute to the numerator in (9.12) to order v^6. Together with the high-temperature expansion of the denominator given in (9.7) we obtain

$$\begin{aligned} \langle s_x s_y \rangle &= \left(2v^2 + 4v^4 + (2V + 10)v^6 + \cdots\right)/\left(1 + Vv^4 + \cdots\right), \\ &= 2v^2 + 4v^4 + 10v^6 + O\left(v^8\right). \end{aligned} \tag{9.15}$$

The susceptibility χ contains this contribution four times. Similarly, one considers all permitted diagrams for lattice points x, y with $d(x, y) \leq n$ and calculates the corresponding two-point function. Adding these functions as in (9.10) leads to the high-temperature expansion of χ. To order v^{10} one finds

$$\begin{aligned} \chi(v) = \sum \chi'_\ell v^\ell = 1 + 4v + 12v^2 + 36v^3 + 100v^4 + 276v^5 + 740v^6 \\ + 1972v^7 + 5172v^8 + 13492v^9 + 34876v^{10} + \cdots. \end{aligned} \tag{9.16}$$

To convert this series into a series in K,

$$\chi(K) = \sum_{\ell \geq 0} \chi_\ell K^\ell \tag{9.17}$$

we substitute $v = \tanh K$ into (9.16) and expand the resulting expression in powers of K. This yields the following expansion in inverse powers of the temperature:

$$\begin{aligned}\chi(K) = 1 &+ 4K + 12K^2 + 104/3K^3 + 92K^4 + 3608/15K^5 + 3056/5K^6 \\ &+ 484528/315K^7 + 400012/105K^8 + 26548808/2835K^9 \\ &+ 107828128/4725K^{10} + \cdots. \end{aligned} \tag{9.18}$$

This series was calculated to 21st order in [5, 6]. Terms of even higher order are found in [7] and for generalized Ising models with higher spins in [8].[2]

Extrapolation to the Critical Point

The power series (9.18) has a finite radius of convergence $R > 0$, and thus defines an analytical function on the disc $|K| < R$. Since all coefficients χ_ℓ are positive there must be a singularity at the point $K = R$ on the real axis. We identify this singular point with the critical value $K_c = J/T_c$. The *ratio test* yields the critical temperature

$$R = \lim_{\ell\to\infty} \left| \frac{a_\ell}{a_{\ell+1}} \right| = \frac{J}{T_c}. \tag{9.19}$$

More accurate values for the critical temperature and critical exponent γ are obtained by fitting the truncated power series to the expected scaling of the susceptibility near the critical point,

$$\begin{aligned}\chi(K) &= \sum \chi_\ell K^\ell \propto (1 - K/K_c)^{-\gamma} \\ &= 1 + \sum_{\ell=1}^{\infty} \frac{\gamma(\gamma+1)\cdots(\gamma+\ell-1)}{\ell!} \left(\frac{K}{K_c}\right)^\ell. \end{aligned} \tag{9.20}$$

The ratio of coefficients defines a linear function in $1/\ell$,

$$\frac{\chi_\ell}{\chi_{\ell-1}} = \frac{1}{K_c} + \frac{\gamma-1}{K_c}\frac{1}{\ell}, \tag{9.21}$$

and the slope of this function together with its value at $1/\ell \to 0$ yield the critical exponent and the critical temperature. The ratios $\chi_\ell/\chi_{\ell-1}$ of the coefficients to order 25 and the linear fit are depicted in Fig. 9.6. The linear interpolation yields

$$T_c \approx 2.26694J \quad \text{and} \quad \gamma \approx \frac{1.69129}{2.26695} + 1 = 1.74606. \tag{9.22}$$

The estimates agree well with the exact values in (6.7),

$$T_c = \frac{2J}{\log(1+\sqrt{2})} \approx 2.26919J \quad \text{and} \quad \gamma = \frac{7}{4} = 1.75. \tag{9.23}$$

[2] The coefficients of orders 20 and 21 in [6–8] do not agree with those in [5]. According to a private communication by Paolo Butera, the numbers in [5] are probably erroneous.

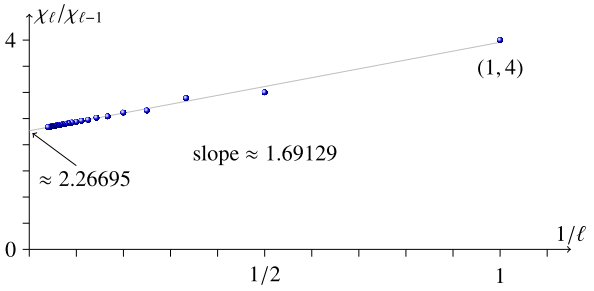

Fig. 9.6 The ratios $\chi_\ell/\chi_{\ell-1}$ for the high-temperature expansion (9.17) to order 25. From the slope and intersection with the vertical axis we read off the critical exponent γ and the critical temperature T_c of the $2d$ Ising model

The on-line library [8] contains further high-temperature expansions of several basic observables in Ising models with spins $1/2, 1, 3/2, 2, 5/2, 3, 7/2, 5$ and ∞—in two dimensions on the square lattice and in three dimensions on the simple-cubic and the body-centered cubic lattices.

9.2.2 Three-Dimensional Model

High-temperature expansions for the three-dimensional Ising model to order 10 in the inverse temperature are found in the early work [9]. With refined techniques more and more higher order terms were calculated in [10–13] and with the steady increase of computer power this was possible for a large class of spin models and lattice field theories. The diagrammatic method has been applied to Ising-type models and the resulting coefficients to order 25 are tabulated in [8].

Free Energy Density and Specific Heat

The finite lattice method developed in [14] avoids the tedious work of counting all the high-temperature diagrams. Nevertheless, the amount of calculation still grows exponentially with the order of the expansion. In [15] a variant of the method was applied to calculate the high-temperature expansion of the free energy density,

$$-\beta f = \log\bigl(2\cosh^3 K\bigr) + \sum_{\ell\geq 4} f'_\ell v^\ell, \quad v = \tanh K, \tag{9.24}$$

to order 46. The expansion coefficients f'_ℓ are listed in Table 9.2. Differentiating $\beta f(K)$ twice with respect to β one obtains the expansion of the specific heat to the same order. The corresponding expansion in K to order 12 reads

$$c = \sum \alpha_\ell K^\ell| = 3K^2 + 33K^4 + 542K^6 + 123547/15K^8 + 14473442/105K^{10} + 11336607022/4725K^{12} + \cdots. \tag{9.25}$$

Table 9.2 High-temperature expansion coefficients f'_ℓ to order 46 [15]

ℓ	f'_ℓ	ℓ	f'_ℓ
2	0	26	4437596650548
4	3	28	525549581866326/7
6	22	30	6448284363491202/5
8	375/2	32	179577198475709847/8
10	1980	34	395251648062268272
12	24044	36	21093662188820520521/3
14	319170	38	126225408651399082182
16	18059031/4	40	45692175331967619977785/2
18	201010408/3	42	291591287110968623857940/7
20	5162283633/5	44	84107222623792350486866604/11
22	16397040750	46	14120314204713719766888210
24	266958797382		

Since this is an expansion in K^2 we fit the high-temperature series to the scaling law

$$c = \sum \alpha_{2\ell} K^{2\ell} \sim \left(1 - \frac{K^2}{K_c^2}\right)^{-\alpha}. \tag{9.26}$$

For large ℓ the ratio of coefficients define a linear function of $1/\ell$, similarly as for the susceptibility,

$$\frac{\alpha_{2\ell}}{\alpha_{2\ell-2}} \to \frac{1}{K_c^2} + \frac{\alpha - 1}{K_c^2}\frac{1}{\ell}. \tag{9.27}$$

Figure 9.7 shows the ratios for all coefficients to order 46. The three ratios involving the coefficients of lowest orders 2, 4, 6 and 8 do not fall onto a straight line and are left out in the data analysis. The linear fit included in Fig. 9.7 yields

$$T_c = 4.5102J \quad \text{and} \quad \alpha = 0.1226. \tag{9.28}$$

We can do even better when we estimate the critical temperature and exponent from the ratios $r_\ell = \alpha_{2\ell}/\alpha_{2\ell-2}$ of two neighboring ℓ according to

$$T_c^{(\ell)} = J\sqrt{(\ell+1)r_{\ell+1} - \ell r_\ell} \quad \text{and} \quad \alpha^{(\ell)} = -\frac{(\ell^2-1)r_{\ell+1} - \ell^2 r_\ell}{(\ell+1)r_{\ell+1} - \ell r_\ell} \tag{9.29}$$

and let ℓ become large. Figure 9.8 contains the estimates for T_c/J for all available orders. Leaving out the lowest five estimates which do not fall onto a straight line the linear extrapolation leads to

$$T_c = 4.512176J. \tag{9.30}$$

Computer simulations in combination with finite size scaling analysis predict a critical temperature $T_c \approx 4.511516J$ [16].

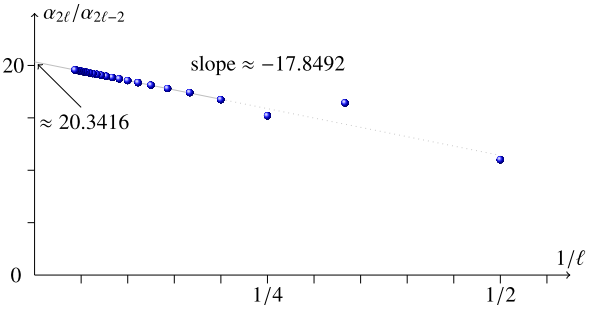

Fig. 9.7 The ratios $\alpha_{2\ell}/\alpha_{2\ell-2}$ for the high-temperature expansion (9.25) to order 46. From the slope and intersection with the vertical axis we read off the critical exponent α and the critical temperature T_c of the $3d$ Ising model

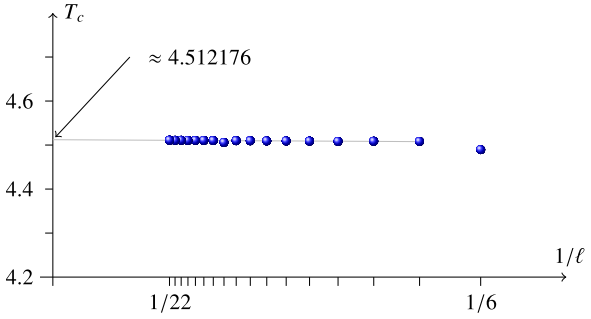

Fig. 9.8 The local estimates $T_c^{(\ell)}$ for the critical temperature given in (9.29) for the high-temperature expansion to order 46

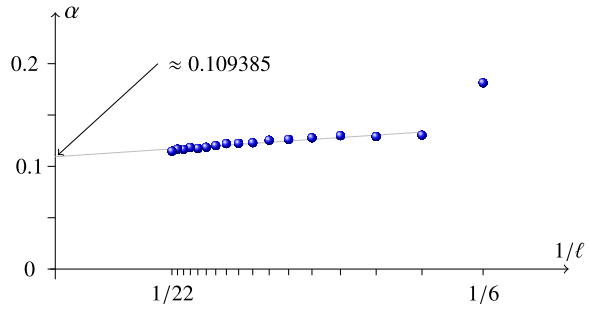

Fig. 9.9 The local estimates $\alpha^{(\ell)}$ for the critical exponent α according to (9.29) for the high-temperature expansion to order 46

Figure 9.9 shows the local estimates $\alpha^{(\ell)}$ defined in (9.29) for ℓ up to 22. Discarding the five lowest orders in the high-temperature expansion a linear fit yields the critical exponent

$$\alpha = 0.109385. \tag{9.31}$$

This compares well with the precise estimate $\alpha = 0.110(1)$ taken from [17]. Further improvement is possible if one uses the modified-ratio method and also includes corrections to scaling.

Table 9.3 Expansion coefficients of $\chi(v)$ for the Ising model on a cubic lattice (taken from [8])

ℓ	χ'_ℓ	ℓ	χ'_ℓ
1	6	14	3973784886
2	30	15	18527532310
3	150	16	86228667894
4	726	17	401225368086
5	3510	18	1864308847838
6	16710	19	8660961643254
7	79494	20	40190947325670
8	375174	21	186475398518726
9	1769686	22	864404776466406
10	8306862	23	4006394107568934
11	38975286	24	18554916271112254
12	182265822	25	85923704942057238
13	852063558		

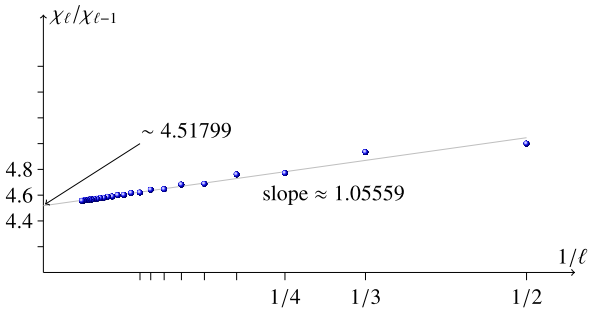

Fig. 9.10 Ratios $\chi_\ell/\chi_{\ell-1}$ for the high-temperature expansion $\sum \chi_\ell K^\ell$ for the three-dimensional Ising model

Susceptibility

The high-temperature expansion of the susceptibility for the three-dimensional Ising model on a hyper-cubic lattice,

$$\chi(v) = 1 + \sum_{\ell \geq 1} \chi'_\ell v^\ell, \tag{9.32}$$

to order 20 was computed earlier on in [10] and then continued to order 25 in [8]. The known coefficients χ'_ℓ are listed in Table 9.3. The coefficient ratios of the derived series $\chi(K) = \sum \chi_\ell K^\ell$ to order 25 are depicted in Fig. 9.10. Similarly as in two dimensions we fit this series expansion with the expected scaling law for the susceptibility and find the critical values

$$T_c \approx 4.51799J \quad \text{and} \quad \gamma \approx 1 + \frac{1.05559}{4.51799} = 1.23364. \tag{9.33}$$

These values differ by less than 1 percent from the best known values.

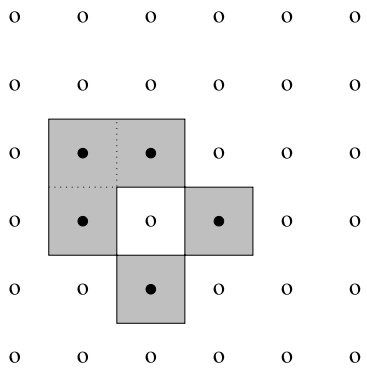

Fig. 9.11 A spin configuration is uniquely determined by the set of sites with flipped spins marked as •

9.3 Low-Temperature Expansion of Ising Models

In spin systems at zero temperature only the configuration(s) with minimal energy is occupied. At low temperature, configurations with higher energies may occur, but they are exponentially suppressed. Thus in a low-temperature expansion we study the deviation of the system from the state with minimal energy. The expansion corresponds to the weak-coupling expansion in field theory. Indeed, for a continuous target space we recover the perturbation theory in quantum field theory.

The energy of the Ising-model is minimal if all spins point in the direction of the magnetic field. Hence, for a positive magnetic field the configuration

$$\omega_0 = \{s_x = 1 \mid x \in \Lambda\} \tag{9.34}$$

has the lowest energy:

$$E_0 = -PJ - Vh. \tag{9.35}$$

The number of nearest neighbor pairs is $P = dV$. There is only one configuration with minimal energy, $g_0 = 1$. We reach configurations with higher energies by flipping the spins at certain lattice points. A configuration ω is uniquely characterized by the set $X(\omega) \subset \Lambda$ of lattice points with flipped spins. All spins in the complement of X are parallel to the magnetic field and all spins in X are anti-parallel. This means that the number of flipped spins is equal to the volume $|X|$ of X and the number of nearest-neighbor pairs with anti-parallel spins is equal to the area $|\partial X|$ of its boundary. Figure 9.11 shows a configuration of the Ising model on a square lattice with $|X| = 5$ and $|\partial X| = 16$. A configuration ω is almost uniquely characterized by its polygon ∂X (in higher dimensions: polyhedron). The only ambiguity is that ω and $-\omega$ possess the same polygons—the graphical representation does not distinguish between the inner and outer part of ∂X.

9.3.1 Free Energy and Magnetization of Two-Dimensional Model

Every lattice point • with spin anti-parallel to the magnetic field contributes $2h$ to the energy. Similarly, a nearest-neighbor pair •◦ with opposite spins contributes $2J$. Hence, we have

$$E(X) = E_0 + 2J|X| + 2h|\partial X|, \tag{9.36}$$

and the partition function may be written as

$$Z = \mathrm{e}^{-\beta E_0} \sum_X \mathrm{e}^{-2\beta J|X| - 2\beta J|\partial X|} \equiv \mathrm{e}^{-\beta E_0}\, \Xi, \tag{9.37}$$

where we introduced the function Ξ, which has the low-temperature expansion

$$\Xi(z, \zeta) \sum_{n,p=0}^{\infty} z^n u^p G_V(n, p). \tag{9.38}$$

We assume a positive h such that the fugacity[3] satisfies

$$z = \mathrm{e}^{-2\beta h} < 1. \tag{9.39}$$

For a ferromagnetic system on a hyper-cubic lattice $|\partial X|$ is an even integer and thus we choose

$$u = \mathrm{e}^{-4\beta J} \ll 1 \tag{9.40}$$

as small expansion parameter at low temperatures, such that the order of the series expansion is the power $p = |\partial X|/2$ of u. The combinatorial factor $G_V(n, p)$ is just the number of subsets $X \subset \Lambda$ with volume $|X| = n$ and surface area $|\partial X| = 2p$.

The sets X and X' corresponding to the configurations ω and $-\omega$ have different statistical weights, namely

$$X : z^{|X|} u^{|\partial X|/2} \quad \text{and} \quad X' : z^{V-|X|} u^{|\partial X|/2},$$

such that in the thermodynamic limit the statistical weight of X' vanishes relative to that of X. This is why the low-temperature system shows a spontaneous magnetization for $h \neq 0$ and infinite volume. However, without magnetic field $E(X) = E(X')$ and the configurations ω and $-\omega$ have identical weights. Thus, in a finite volume there is no magnetization for $h = 0$.

Next we must enumerate the low-temperature diagrams to obtain the combinatorial factors G_V in Eq. (9.38). Table 9.4 shows all diagrams on the square to order $p = 5$ in the expansion parameter u. Observe the close relationship with the high-temperature expansion in Table 9.1. This relation is a two-dimensional peculiarity and originates from the self-duality of the two-dimensional Ising model. From

$$\begin{aligned} \Xi = 1 &+ Vu^2 z + 2Vu^3 z^2 + Vu^4\big(z^4 + 6z^3 + (V-5)z^2/2\big) \\ &+ Vu^5\big(2z^6 + 8z^5 + 18z^4 + 2(V-8)z^3\big) + \cdots \end{aligned} \tag{9.41}$$

[3] It is the inverse of the fugacity used in Sect. 8.7.

Table 9.4 Leading diagrams contributing to the low-temperature expansion of Ξ

p	n	Diagram	Number	p	n	Diagram	Number
2	1		V	5	3		$2V(V-8)$
3	2		$2V$	5	4		$2V$
4	2		$\frac{1}{2}V(V-5)$	5	4		$8V$
4	3		$2V$	5	4		$4V$
4	3		$4V$	5	4		$4V$
4	4		V	5	5		$8V$
				5	6		$2V$

follows the low-temperature expansion of the temperature dependent contribution to the free energy density,

$$-\beta\Delta f = \frac{\log \Xi}{V} = zu^2 + 2z^2u^3 + \big(z^4 + 6z^3 - 5z^2/2\big)u^4 + \big(2z^6 + 8z^5 + 18z^4 - 16z^3\big)u^5 + \cdots. \tag{9.42}$$

The field dependence of the magnetization m for $h > 0$ is given by

$$\begin{aligned} m &= -\frac{\partial f}{\partial h} = 1 + 2z\frac{\partial}{\partial z}(\beta\Delta f) \\ &= 1 - 2zu^2 - 8z^2u^3 - \big(8z^4 + 36z^3 - 10z^2\big)u^4 \\ &\quad - \big(24z^6 + 80z^5 + 144z^4 - 96z^3\big)u^5 + \cdots. \end{aligned} \tag{9.43}$$

Now we switch off the h-field and remain with the spontaneous magnetization

$$m = \sum m_\ell u^\ell = 1 - 2u^2 - 8u^3 - 34u^4 - 152u^5 - \cdots. \tag{9.44}$$

In the zero-temperature limit all spins are aligned in direction defined by the magnetic field before it was switched off. The systems shows a spontaneous magnetization. In [18] the finite lattice method has been applied to obtain the low-temperature series for the partition function, order parameter and susceptibility of the Ising model on the square lattice. In particular the expansion for the magnetization was calculated to order 38. Half of the known coefficients are listed in Table 9.5.

Figure 9.12 shows a plot of the spontaneous magnetization $m = \sum m_\ell u^\ell$ with the coefficients in Table 9.5. The magnetization vanishes for values u larger than the critical value of u_c.

Table 9.5 Coefficients m_ℓ and ratios of coefficients for the $2d$ Ising model [18]

ℓ	m_ℓ	$m_\ell/m_{\ell-1}$	ℓ	m_ℓ	$m_\ell/m_{\ell-1}$
0	1		10	−454378	5.16056
1	0		11	−2373048	5.22263
2	−2		12	−12515634	5.27408
3	−8	4.00000	13	−66551016	5.31743
4	−34	4.25000	14	−356345666	5.35447
5	−152	4.47059	15	−1919453984	5.38649
6	−714	4.69737	16	−10392792766	5.41445
7	−3472	4.86275	17	−56527200992	5.46093
8	−17318	4.98790	18	−308691183938	5.48046
9	−88048	5.08419	19	−1691769619240	

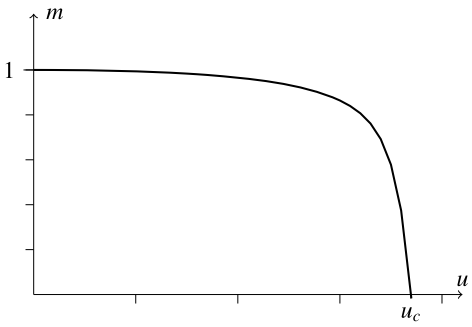

Fig. 9.12 The magnetization as a function of $u = \mathrm{e}^{-4\beta J}$ in the low-temperature expansion

Extrapolation to the Critical Point

The low-temperature series for m has only negative coefficients m_ℓ except for m_0. Hence, if the series has a finite radius of convergence, then a singularity of $m(u)$ lies on the positive real axis at some value u_c. As earlier on we fit the low-temperature expansion to the expected scaling,

$$m = \sum m_\ell u^\ell \sim \left(1 - \frac{u}{u_c}\right)^\beta, \tag{9.45}$$

and analyze the series with the help of the ratio test,

$$\frac{m_\ell}{m_{\ell-1}} = \frac{1}{u_c} - \frac{1+\beta}{u_c}\frac{1}{\ell}. \tag{9.46}$$

Figure 9.13 shows the ratios of successive coefficients for the orders given in [18] and the corresponding linear fit for $\ell \geq 4$. The slope of the fitting function is approximately -6.80717 and the intersection with the ordinate is given by $1/u_c \approx 5.837266$. This yields the estimates

$$T_c = 2.26985J \quad \text{and} \quad \beta = 0.13056 \tag{9.47}$$

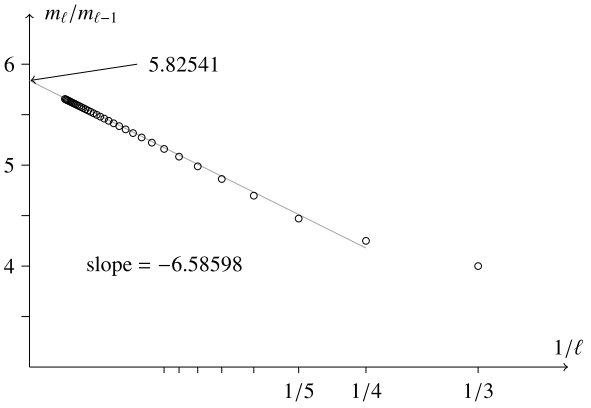

Fig. 9.13 Extrapolation for the determination of the critical temperature and the critical exponent β in the low-temperature approximation

for the critical temperature and critical exponent. This critical temperature is very close to the exact value in (9.23) and the exponent is near the exact value $\beta = 1/8$.

9.3.2 Three-Dimensional Model

While the high-temperature series are well-behaved the situation at low temperatures is less satisfactory, in particular above two dimensions. With finite lattice methods it was possible to calculate low-temperature expansions on the simple-cubic lattice in powers of the small parameter $u = \mathrm{e}^{-4J/T}$. For example, the magnetization was calculated to order 20 in [19, 20] and later on to order 26 in [21]. Using a modification of the shadow-lattice techniques Vohwinkel obtained low-temperature series for the free energy, magnetization and susceptibility [22]. The magnetization was calculated to order 32 and the corresponding coefficients m_ℓ are listed in Table 9.6. Note that in three dimensions the coefficients have alternating signs and we expect the first singularity of $m(u)$ on the negative real axis. The ratio test shows that the first singularity for the series occurs near $u \approx -0.3$. This unphysical singularity makes it difficult to apply the ratio method and thus we use Padé approximants to analyze the low-temperature series. The $[p, q]_f$ Padé approximant of a function $f(u)$ is the ratio of a polynomial $p(u)$ of degree p and a polynomial $q(u)$ of degree q such that the series expansion of $p(u)/q(u)$ agrees with the series expansion of $f(u)$ through order $p + q$ [23]. Figure 9.14 shows the high-temperature expansion of the magnetization which becomes singular at $u \approx \pm 0.3$ together with its $[5, 5]$ Padé approximant.

To extract the critical point u_c and the critical exponent β we analyze the Padé approximants to the low-temperature series of $f(u) = m(u)/m'(u)$, which near the critical point should behave like $(u - u_c)/\beta$, such that the critical coupling u_c is identified with the first zero of the Padé approximant on the positive real axis, and the inverse critical exponent is equal to the slope at the critical value u_c. The critical

Table 9.6 Coefficients m_ℓ and ratios of coefficients for the $3d$ Ising model [22]

ℓ	m_ℓ	ℓ	m_ℓ
0	1	18	30371124
3	−2	19	−101585544
4	0	20	338095596
5	−12	21	−1133491188
6	14	22	3794908752
7	−90	23	−12758932158
8	192	24	42903505030
9	−792	25	−144655483440
10	2148	26	488092130664
11	−7716	27	−1650000819068
12	2326	28	5583090702798
13	−79512	29	−18918470423736
14	252054	30	64167341172984
15	−846628	31	−217893807812346
16	2753520	32	740578734923544
17	−9205800		

Table 9.7 Critical coupling u_c and critical exponent β from various Padé approximants

$[r, s] =$	[3, 3]	[4, 4]	[5, 5]	[6, 6]	[7, 7]	Averages
$u_c =$	0.4177	0.4033	0.4124	0.4031	0.4098	0.4093
$\beta =$	0.3204	0.2595	0.3063	0.2586	0.2848	0.2859

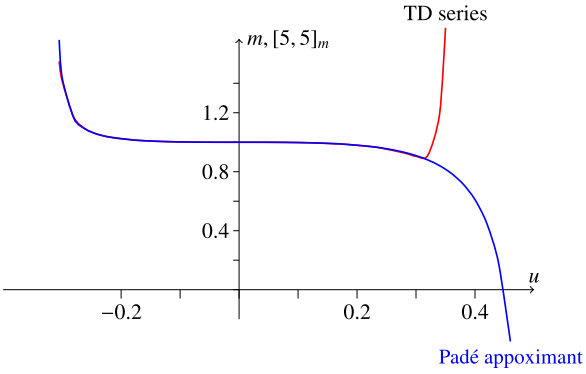

Fig. 9.14 Plot of the high-temperature series of order 32 and its [5, 5] Padé approximant

values for several Padé approximants are listed in Table 9.7. The prediction for u_c of the approximant [5, 5] comes closest to the precise number $u_c = 0.41205$ from simulations and for this best fit we read off a critical exponent $\beta = 0.3063$.

Table 9.8 Critical parameters of Ising model on the square from Padé approximants

$[r,s]=$	[2, 2]	[3, 3]	[4, 4]	[5, 5]	[6, 6]	Exact
$u_c=$	0.166666	0.171573	0.171573	0.171573	0.171573	0.171573...
$T_c/J=$	2.232443	2.269186	2.269185	2.269185	2.269185	2.269185...
$\beta=$	0.111111	0.125000	0.125000	0.125000	0.125000	0.125

9.3.3 *Improved Series Studies for Ising-Type Models*

Typically the Padé approximant method yields more accurate results for the critical parameters as the ratio method. For example, for the $2d$-Ising model on the square lattice the lowest Padé approximant to $m(u)/m'(u)$, where $m(u)=\sum m_\ell u^\ell$ is the low-temperature expansion up order 38, yields the critical parameters listed in Table 9.8. Already the fourth-order approximant agrees with the exact result in all digits given in the table. To achieve a further improvement in the precision of the estimates of the critical parameters from the analysis of extended high- or low-temperature series one should properly allow for the expected non-analytic correction to the leading power law behavior or thermodynamic quantities near a critical point. A singular quantity is expected to behave, in the vicinity of the critical point β_c as

$$g(\beta)\sim A_\gamma|t|^\lambda\left(1+a_\chi|t|^{\lambda_1}+a'_\chi|t|^{2\lambda_1}+\cdots+e_\chi t+e'_\chi t^2+\cdots\right) \tag{9.48}$$

when $t=1-\beta/\beta_c\to 0$, see [24]. The critical exponent λ and the leading confluent correction exponents λ_1 are universal. The established ratio extrapolation and Padé approximant methods are generally inadequate to solve the numerical problem of extracting β_c, the critical exponent and the leading confluent exponent. Instead one may use the differential approximants method put forward in [25]. With such improvements it is possible to find rather precise values for critical exponents for a large class of spin models in various dimensions, for a detailed discussion see the textbook [3]. In Table 9.9 we compiled results from high-temperature expansions for the *Ising model on a simple-cubic lattice*. From scaling relations between critical exponents one finds $\beta\approx 0.3265$. In [29] the low-temperature series for the partition function, order parameter and susceptibility of the q-state *Potts model on the square lattice* to high order in u for $q=2,3,4,\ldots,10$ are given. The on-line library [8] contains high-temperature expansions of basic observables in two- and three-dimensional Ising models with spins $1/2,1,\ldots,5,\infty$. Beside the critical exponents there are further universal quantities, namely the universal amplitude ratios. Critical exponents and universal amplitude ratios for many interesting spin models are compiled in the review [17].

9.4 High-Temperature Expansions of $O(N)$ Sigma Models

For $N>1$ the high-temperature series for the widely studied $O(N)$ sigma model with energy function (6.18) are significantly less well known than those for the

Table 9.9 Critical parameters for $3d$ Ising model from high-temperature expansions

β_c	γ	ν	η	α	From
0.22165459(10)	1.2373(2)	0.63012(16)	0.03639(15)		[26]
0.2216545(1)	1.2369(2)	0.6298(3)		0.1035(5)	[27]
0.221655(2)	1.2371(1)	0.6299(2)	0.0360(8)		[28]

Ising model. For $N = 0$ (the self-avoiding walk model) the susceptibility has been calculated to order β^{23} on the simple-cubic lattice in [30]. With the linked cluster expansion technique the high-temperature series has been extended to order β^{23} for the non-linear models with $N \leq 12$ in [31, 32].

Actually, the linked cluster expansion technique can be adapted to produce expansions for the general class of models with partition functions

$$Z = \int \mathrm{d}\mu(\omega) \mathrm{e}^{-\beta H + \sum h_x s_x}, \quad \text{where } H = -\sum_{\langle x,y \rangle} s_x s_y, \tag{9.49}$$

contains nearest-neighbor interactions between the spins $s_x \in \mathbb{R}^N$. The $h_x \in \mathbb{R}^N$ represent an external field and $\mathrm{d}\mu$ is the product of $O(N)$-invariant single-spin measures,

$$\mathrm{d}\mu(\omega) = \prod_x \mathrm{d}\mu(s_x), \qquad \mathrm{d}\mu(Rs) = \mathrm{d}\mu(s). \tag{9.50}$$

We absorbed the nearest-neighbor coupling J in the inverse temperature β. For small β and without external field we obtain the expansion

$$Z = 1 + \sum_{\ell=1}^{\infty} \frac{\beta^{2\ell}}{(2\ell)!} \int \mathrm{d}\mu(\omega) H^{2\ell}, \tag{9.51}$$

with only even powers of H, since $\mathrm{d}\mu$ is invariant under rotations of the individual spins. For the product measure $\mathrm{d}\mu$ the averages on the right hand side are expressed in terms of moments of the single-spin distribution $\mathrm{d}\mu(s)$ and these moments are generated by $z(h) = \int \mathrm{d}\mu(s) \exp(hs)$. For $O(N)$-invariant systems the generating function depends only on the modulus of h such that for a vanishing field the moments are totally symmetric $O(N)$ invariant tensors, e.g.

$$\begin{aligned} \int \mathrm{d}\mu(s) s_a s_b &= \mathscr{C}_2 \delta_{ab} \equiv \mathscr{C}_2 C_{ab}, \\ \int \mathrm{d}\mu(s) s_a s_b s_c s_d &= \mathscr{C}_4 (\delta_{ab}\delta_{cd} + \delta_{ac}\delta_{bd} + \delta_{ad}\delta_{bc}) \equiv \mathscr{C}_4 C_{abcd}. \end{aligned} \tag{9.52}$$

The totally symmetric tensor

$$C_{a_1 \dots a_{2\ell}} = \delta_{a_1 a_2} \delta_{a_3 a_4} \cdots \delta_{a_{2k-1} a_{2\ell}} + \cdots \tag{9.53}$$

contains $(2\ell - 1)!!$ terms corresponding to the possible Wick-contractions. For the *Gaussian model* with normalized single-spin distribution

$$\mathrm{d}\mu(s) = \left(\frac{\alpha}{2\pi}\right)^{N/2} \mathrm{e}^{-\alpha s^2/2}, \quad s \in \mathbb{R}^N \tag{9.54}$$

the coefficients of the invariant tensors are

$$\mathscr{C}_{2\ell} = \frac{1}{\alpha^\ell}. \tag{9.55}$$

For the *non-linear $O(N)$ sigma model* with single spins randomly distributed on the unit-sphere the normalized single-spin measure is proportional to $\delta(s^2-1)\mathrm{d}^N s$. The generating function in (7.123), normalized to $z(0)=1$, has the Taylor expansion

$$z(h) = \sum_{\ell=0}^{\infty} \frac{\Gamma(N/2)}{\Gamma(\ell+N/2)} \frac{1}{\ell!} \left(\frac{h^2}{4}\right)^\ell, \tag{9.56}$$

from which one extracts the coefficients

$$\mathscr{C}_{2\ell} = \frac{\Gamma(N/2)}{2^\ell \Gamma(N/2+\ell)} = \frac{1}{N(N+2)\cdots(N+2\ell-2)}. \tag{9.57}$$

9.4.1 Expansions of Partition Function and Free Energy

The term of order $\beta^{2\ell}$ in (9.51) contains sums of products of 2ℓ spins. Thus the high-temperature expansion involves products of links $s_x s_y$ and because for each site each s_x must appear an even number of times, one generates closed polygons. Since the spins also carry an internal index we must attach an internal index to each link. A link may now be chosen several times. More precisely, a link connecting two nearest neighbors ℓ-times represents the average of $(s_x s_y)^\ell$, where x, y are the endpoints of the link. If 2ℓ links with indices $a_1, \ldots, a_{2\ell}$ end at a given site (a vertex of the graph), we assign the factor $\mathscr{C}_{2\ell} C_{a_1 \ldots a_{2\ell}}$ to the vertex. In addition $s_x s_y = s_x^a s_y^a$ involves a contraction over internal indices and hence we must finally contract all internal indices occurring in the graph. For example, to $(s_x s_y)^2 (s_y s_u)^2$ we assign a graph with two lines from x to its neighbor y and two lines from y to its neighbor u. Since indices of nearest-neighbor pairs are contracted the average yields

$$C_{ab} C_{abcd} C_{cd} = \big(N^2+2N\big)\mathscr{C}_2^2 \mathscr{C}_4.$$

Below we need the following contractions of invariant tensors:

$$\begin{aligned}
C_{ab}C_{ab} &= N,\\
C_{abcd}C_{abcd} &= 3\big(N^2+2N\big),\\
C_{abcdef}C_{abcdef} &= 15\big(N^3+6N^2+8N\big),\\
C_{abcd}C_{bcde} &= 3(N+2)C_{ae},\\
C_{abcd}C_{cd} &= (N+2)C_{ab},\\
C_{abcdef}C_{ef} &= (N+4)C_{abcd},\\
C_{abcdef}C_{cdef} &= 3(N+2)(N+4)C_{ab},\\
C_{ab}C_{abcdef}C_{cdef} &= 3N(N+2)(N+4).
\end{aligned} \tag{9.58}$$

Now we are ready to calculate the partition functions of $O(N)$ models to order β^6. The emerging diagrammatic expansion is also very useful to obtain the high-temperature expansions for other objects of interest, for example the susceptibility.

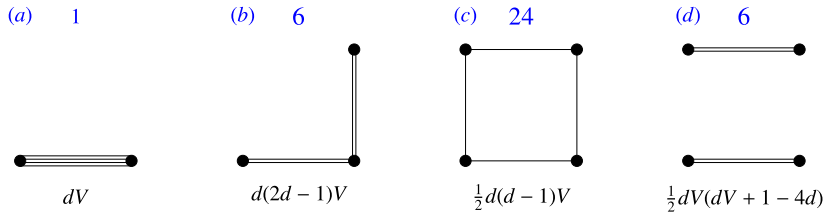

Fig. 9.15 Diagram contributing in order β^4

Order β^2

The second order contribution to Z is proportional to $\langle H^2\rangle$. Setting $\sigma_b = s_x s_y$ for a bond b with endpoints x, y we obtain

$$\langle H^2\rangle = \sum_b \langle \sigma_b^2\rangle = \sum_c C_{ac}C_{ac}\mathscr{C}_2^2 = dVN\mathscr{C}_2^2, \tag{9.59}$$

where dV comes from the sum over all links and is the number of associated graphs

on the lattice.

Order β^4

The function H^4 is a sum of all terms $\sigma_{b_1}\sigma_{b_2}\sigma_{b_3}\sigma_{b_4}$ associated to four bonds. Only graphs with even vertices contribute and these graphs are depicted in Fig. 9.15. The number of graphs of a given type is listed below the graph. In the contribution

$$\langle H^4\rangle = \sum \langle \sigma_b^4\rangle + 6\sum \langle \sigma_{b_1}^2\sigma_{b_2}^2\rangle + 24\sum \langle \sigma_{b_1}\sigma_{b_2}\sigma_{b_3}\sigma_{b_4}\rangle, \tag{9.60}$$

one only sums over distinct links. All terms in the second sum belonging to disconnected links are represented by the disconnected graph (d) Fig. 9.15. The four links in the last sum in (9.60) define the loop graph (c). Thus every term of $\langle H^4\rangle$ is represented by a graph. The number related to a graph is the product of its multiplicity and the combinatorial factor in (9.60), and both are given in Fig. 9.15. Therefore we find

$$\begin{aligned}\langle H^4\rangle = {} & dVC_{abcd}C_{abcd}\mathscr{C}_4^2 \\ & + 6dV(2d-1)C_{abcd}C_{ab}C_{cd}\mathscr{C}_4\mathscr{C}_2^2 \\ & + 12dV(d-1)C_{ab}C_{bc}C_{cd}C_{da}\mathscr{C}_2^4 \\ & + 3dV(dV-4d+1)C_{ab}C_{ab}C_{cd}C_{cd}\mathscr{C}_2^4.\end{aligned} \tag{9.61}$$

Contracting the invariant tensors according to (9.58) leads to

$$\begin{aligned}\langle H^4\rangle = {} & 3dVN\big((N+2)C_4^2 + 2(2d-1)(N+2)\mathscr{C}_4\mathscr{C}_2^2 \\ & + 4(d-1)\mathscr{C}_2^4 + (dV-4d+1)N\mathscr{C}_2^4\big).\end{aligned} \tag{9.62}$$

Order β^6

The function H^6 is a sum of all terms $\sigma_{b_1}\sigma_{b_2}\sigma_{b_3}\sigma_{b_4}\sigma_{b_5}\sigma_{b_6}$ associated to six links. The following terms contribute to the partition function:

$$\begin{aligned}\langle H^6\rangle = &\sum\langle\sigma_b^6\rangle + 15\sum\langle\sigma_{b_1}^4\sigma_{b_2}^2\rangle + 90\sum\langle\sigma_{b_1}^2\sigma_{b_2}^2\sigma_{b_3}^2\rangle\\ &+ 360\sum\langle\sigma_{b_1}^2\sigma_{b_2}\sigma_{b_3}\sigma_{b_4}\sigma_{b_5}\rangle + 120\sum\langle\sigma_{b_1}^3\sigma_{b_2}\sigma_{b_3}\sigma_{b_4}\rangle\\ &+ 720\sum\langle\sigma_{b_1}\sigma_{b_2}\sigma_{b_3}\sigma_{b_4}\sigma_{b_5}\sigma_{b_6}\rangle. \end{aligned} \tag{9.63}$$

The first and last sums are represented by the connected diagrams a, f and f' in Fig. 9.16. The remaining sums are represented by connected and disconnected diagrams. The disconnected ones are depicted in Fig. 9.17. The analytical expression for $\langle H^6\rangle$ in terms of the invariant tensors, coefficients $\mathscr{C}_\ell$ and dimension of space d is now easily found

$$\begin{aligned}\langle H^6\rangle = &\, dV C_{abcdef}C_{abcdef}\mathscr{C}_6^2\\ &+ 30dV(2d-1)C_{abcdef}C_{abcd}C_{ef}\mathscr{C}_6\mathscr{C}_4\mathscr{C}_2\\ &+ 90dV(2d-1)^2C_{ab}C_{abcd}C_{cdef}C_{ef}\mathscr{C}_4^2\mathscr{C}_2^2\\ &+ 60dV(2d-1)(d-1)C_{ab}C_{abcdef}C_{cd}C_{ef}\mathscr{C}_6\mathscr{C}_2^3\\ &+ 1440dV(d-1)^2C_{ab}C_{abcd}C_{ce}C_{ef}C_{fd}\mathscr{C}_4\mathscr{C}_2^4\\ &+ 240dV(d-1)C_{abcd}C_{bcde}C_{ef}C_{fa}\mathscr{C}_4^2\mathscr{C}_2^2\\ &+ 720dV(d-1)(2d-3)C_{ab}C_{bc}C_{cd}C_{de}C_{ef}C_{fa}\mathscr{C}_2^6\\ &+ 480dV(d-1)(d-2)C_{ab}C_{bc}C_{cd}C_{de}C_{ef}C_{fa}\mathscr{C}_2^6\\ &+ 15dV(dV+1-4d)C_{abcd}C_{abcd}C_{ef}C_{ef}\mathscr{C}_4^2\mathscr{C}_2^2\\ &+ 90dV(2d-1)(dV+2-6d)C_{ab}C_{abcd}C_{cd}C_{ef}C_{ef}\mathscr{C}_4\mathscr{C}_2^4\\ &+ 180dV(d-1)(dV+4-8d)C_{ab}C_{bc}C_{cd}C_{da}C_{ef}C_{ef}\mathscr{C}_2^6\\ &+ 15dV\big(d^2\big(V^2-12V+40\big)+3dV-24d+4\big)(C_{ab}C_{ab})^3\mathscr{C}_2^6. \end{aligned}$$

After contracting the invariant tensors this becomes

$$\begin{aligned}\langle H^6\rangle = &\, 15dVn(N+2)(N+4)\mathscr{C}_6^2\\ &+ 90dV(2d-1)N(N+2)(N+4)\mathscr{C}_6\mathscr{C}_4\mathscr{C}_2\\ &+ 90dV(2d-1)^2N(N+2)^2\mathscr{C}_4^2\mathscr{C}_2^2\\ &+ 60dV(2d-1)(d-1)N(N+2)(N+4)\mathscr{C}_6\mathscr{C}_2^3\\ &+ 1440dV(d-1)^2N(N+2)\mathscr{C}_4\mathscr{C}_2^4\\ &+ 720dV(d-1)N(N+2)\mathscr{C}_4^2\mathscr{C}_2^2\\ &+ 720dV(d-1)(2d-3)N\mathscr{C}_2^6\\ &+ 480dV(d-1)(d-2)N\mathscr{C}_2^6\\ &+ 45dV(dV+1-4d)N^2(N+2)\mathscr{C}_4^2\mathscr{C}_2^2 \end{aligned}$$

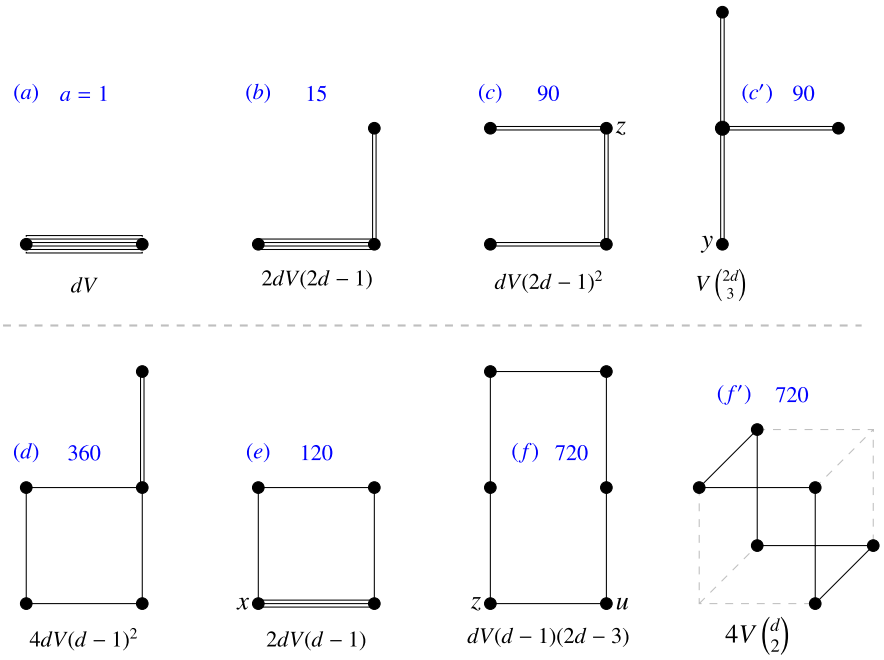

Fig. 9.16 All connected diagrams contributing to $\langle H^6 \rangle$. The numbers below the graphs count the number of diagrams. The combinatorial factors in (9.63) are also listed

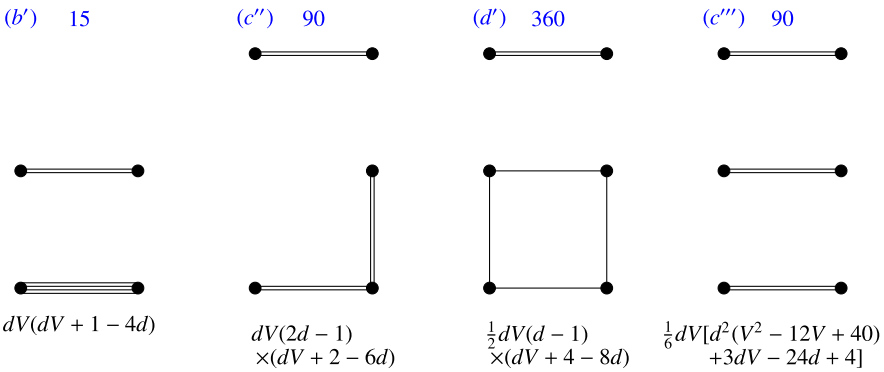

Fig. 9.17 Disconnected diagrams contributing to $\langle H^6 \rangle$. The numbers below the graphs count the number of diagrams

$$
\begin{aligned}
&+ 90dV(2d-1)(dV+2-6d)N^2(N+2)\mathscr{C}_4\mathscr{C}_2^4 \\
&+ 180dV(d-1)(dV+4-8d)N^2\mathscr{C}_2^6 \\
&+ 15dV\left(d^2\left(V^2-12V+40\right)+3dV-24d+4\right)N^3\mathscr{C}_2^6 .
\end{aligned}
$$

The disconnected graphs cancel in the free energy density

$$-\beta V f_\beta = \frac{\beta^2}{2}\langle H^2\rangle + \frac{\beta^4}{4!}\big(\langle H^4\rangle - 3\langle H^2\rangle^2\big) + \frac{\beta^6}{6!}\big(\langle H^6\rangle - 15\langle H^4\rangle\langle H^2\rangle + 30\langle H^2\rangle^3\big) + \cdots.$$

In particular for the non-linear $O(N)$ sigma model in d dimensions we find

$$-\beta f(\beta) = \frac{d\beta^2}{2N} + \frac{d\beta^4}{4N^3}\frac{2dN+4d-3N-4}{N+2} + \frac{d\beta^6}{3N^5}\left(8d^2 - \frac{3d(9N^2+50N+56)-2(10N^2+51N+52)}{(N+2)(N+4)}\right), \tag{9.64}$$

and for $N = 1$ we recover the leading order contributions to the Ising model free energy density in dimension d. The internal energy density for the models in two and three dimensions have the expansions

$$\begin{aligned} u_{d=2} &= \frac{2\beta}{N} + \frac{2\beta^3}{N^3}\frac{N+4}{N+2} - \frac{8\beta^5}{N^5}\frac{N^2+3N-12}{(N+2)(N+4)} + \cdots, \\ u_{d=3} &= \frac{3\beta}{N} + \frac{3\beta^3}{N^3}\frac{3N+8}{N+2}\beta^4 + \frac{6\beta^5}{N^5}\frac{11N^2+84N+176}{(N+2)(N+4)} + \cdots. \end{aligned} \tag{9.65}$$

When one tries to calculate higher order contributions the way we did then the process becomes very laborious after the first few terms in the high-temperature expansion. One runs into the problem of polygon counting on the lattice. Such polygons can be generated by an n-step random walk on the lattice. The major difficulty is to ensure that no diagrams have been overlooked at each stage.

It is advantageous to consider intrinsic quantities, for example the free energy density or the susceptibility, to which only connected diagrams contribute. The linked cluster expansion is a systematic method to construct all connected diagrams [31]. Each term in the expansion is represented by a graph consisting of vertices $v \in \mathscr{V}$ and lines joining them. There are internal lines $\ell \in \mathscr{L}$ and external lines (the graphs belonging to the free energy have no external lines). Lines with only one terminal point are external. We denote the number of external lines attached to a vertex v by $E(v)$. All lines ℓ have an initial point $i(\ell)$ and a final point $f(\ell)$ and the two endpoints are different. For the $O(N)$-models the order of all vertices, i.e. the total number of lines (internal and external) ending at v, must be even.

We associate four numbers to each graph $G \in \mathscr{G}$. These are the (topological) symmetry number $S(G)$, the lattice embedding number $I(G)$, the $O(N)$ symmetry factor $C(G)$ and the weight $\mathring{W}(G)$. First one tabulates all graphs of a particular topological class which contribute to a given order. Figure 9.16 contains the six classes:

$$\{a\}, \qquad \{b\}, \qquad \{c, c'\}, \qquad \{d\}, \qquad \{e\}, \quad \text{and} \quad \{f, f'\}.$$

Table 9.10 Ratios $r_\ell = \alpha_{2\ell}/\alpha_{2\ell-2}$ for various $O(N)$ models in three dimensions

ℓ	2	3	4	5	6
$N=2$	2.62500	3.84921	3.45242	3.86091	4.03943
$N=3$	1.13333	1.64021	1.43292	1.61356	1.69459
$N=4$	0.62500	0.89583	0.76566	0.86438	0.90978
$N=5$	0.394286	0.561031	0.470829	0.53166	0.56018

Table 9.11 Critical temperature for $O(N)$ models in three dimensions

N	2	3	4	5	6
β_c	0.45460	0.69507	0.94265	1.19509	1.45209

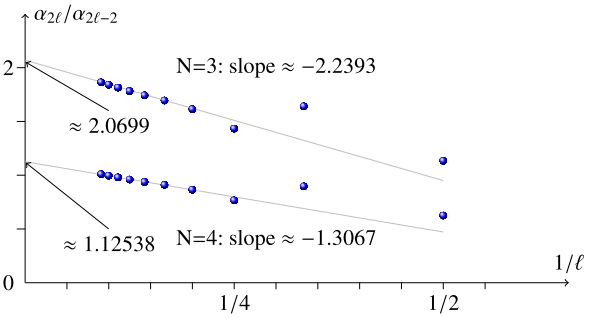

Fig. 9.18 The ratios of coefficients $r_\ell = \alpha_{2\ell}/\alpha_{2\ell-2}$ in the high-temperature expansion of the specific heat for the $O(3)$ and $O(4)$ models in three dimensions

In [31] the following linked cluster expansion for the coefficient in the high-T expansion of the susceptibility is given:

$$\chi_{2k} = \sum_{G \in \mathcal{G}_{2k}} (2\kappa)^L I(G) C(G) \mathring{W}(G) \frac{E!}{S_E(G)}, \tag{9.66}$$

where the sum extends over all topologically inequivalent graphs with k internal lines. The symmetry number $S(G)$ is given by the incidence matrix associated to the graph. Although we shall not go further into algorithmic considerations we shall use the results obtained by the linked cluster expansion in combination with efficient computer programs. We shall only consider simple hyper-cubic lattices.

For example, Butera and Comi computed through order β^{21} the high temperature expansions for the inner energies of non-linear $O(N)$ models on hyper-cubic lattices for arbitrary N [33]. For the simple ratio test we calculated the ratios of coefficients in the expansion of the specific heat. The ratios for $N = 2, 3, 4$ and 5 are listed in Table 9.10. For large ℓ these ratios depend linearly on $1/\ell$ and this linear dependence is seen in Fig. 9.18. With the linear extrapolation (9.27) one obtains reasonable accurate values for the critical temperatures, given in Table 9.11. Unfortunately the series for the inner energy are too short to extract reliable values for the critical

Table 9.12 Critical temperatures, susceptibility exponent and heat capacity exponent of $O(N)$ models on simple-cubic lattices from high-temperature expansions (hte). Also listed are the exponents obtained from strong-coupling expansions (sc), from six-loop approximations combined with the Padé–Borel resummation technique (6-loop), from renormalization-group equation with full-momentum dependence of correlation function (rge) and from lattice simulations (mc)

N	1	2	3	4	6	8	10	12	From
$\beta_{\text{hte,c}}$	0.2217	0.4542	0.6930	0.9359	1.4286	1.9263	2.4267	2.929	[32]
$\beta_{\text{mf,c}}$	0.1667	0.3333	0.5000	0.6667	1.0000	1.3333	1.6667	2.000	MF
γ_{hte}	1.244	1.327	1.404	1.474	1.582	1.656	1.712	1.759	[32]
γ_{sc}	1.241	1.318	1.387	1.451	1.558	1.638	1.275	1.763	[34]
$\gamma_{\text{6-loop}}$	1.239	1.315	1.3386	1.449	1.556	1.637	1.697	1.743	[35]
ν_{hte}	0.634	0.677	0.715	0.750	0.804	0.840	0.867	0.889	[32]
ν_{sc}	0.630	0.670	0.705	0.737	0.790	0.829	0.866	0.890	[34]
$\nu_{\text{6-loop}}$	0.631	0.670	0.706	0.738	0.790	0.830	0.859	0.881	[35]
ν_{rge}	0.632	0.674	0.715	0.754			0.889		[36]
ν_{mc}	0.630	0.672	0.711	0.749	0.818				[37–39]
α_{hte}	0.098	−0.031	−0.145	−0.250	−0.412	−0.520	−0.601	−0.667	
α_{sc}	0.107	−0.010	−0.117	−0.213	−0.370	−0.489	−0.576	−0.643	[34]
α_{mc}	0.1101		−0.1336						[37–39]

exponent α. In [32] the high-temperature expansions for the susceptibility and the second correlation length

$$\mu_2(\beta) = \sum_x x^2 \langle s_0 s_x \rangle = \sum s_\ell(N) \beta^\ell \tag{9.67}$$

have been extended to order β^{21} with the help of the (vertex renormalized) linked cluster expansion [31]. The corresponding estimates for the critical point and critical exponents γ and ν are listed in Table 9.12. The critical exponent α_{hte} is calculated with the hyperscaling relation. Also listed in the table are the critical exponents from strong-coupling expansions and six-loop approximations, improved by the Padé–Borel resummation technique. A comparison of the numbers may indicate how uncertain they are. For small N there are precise data from lattice simulations or other methods, see the references on p. 202.

9.5 Polymers and Self-Avoiding Walks

Polymers are long molecules composed of many, say n, monomers. When the interaction between the monomers is negligible, the geometric configuration is similar to a Brownian chain of n successive independent steps, made at random. This is the analogue of a random walk on a lattice. If the monomers are interacting, the problem

is more difficult. If they repel then the chain is more extended than the Brownian chain. The simplest realization for a repulsion is to imagine a random walk on a lattice in which it is forbidden to visit again a previously visited site: this is called a self-avoiding walk. The resulting model is non-Markovian since the nth step depends on the whole past of the chain. It is expected that the typical size of the chain will be larger as a function of n than that of the Brownian chain, because of this geometric repulsion.

It was shown by P. de Gennes that the problem of self-avoiding walks on the lattice may be mapped onto a singular $N = 0$ limit of the $O(N)$ model. To perform this limit we choose a different normalization for the spins, namely

$$s_x s_x = N, \quad \text{for all } x \in \Lambda. \tag{9.68}$$

As a consequence the coefficients in (9.57) are rescaled,

$$\mathscr{C}_{2\ell} = \frac{N^\ell}{N(N+2)\cdots(N+\ell k-2)}, \tag{9.69}$$

and have the scaling limit

$$\lim_{N\to 0} \mathscr{C}_{2\ell} = \begin{cases} 1, & \text{for } \ell = 1, \\ 0, & \text{for } \ell > 1. \end{cases} \tag{9.70}$$

In the previously considered expectation values $\langle H^{2\ell}\rangle$ all totally symmetric $O(N)$-invariant tensors are contracted. But a contraction of all indices yield at least one power of N. Actually the contraction of all indices in the terms belonging to disconnected graphs yield at least two powers of N. This means that all expectation values $\langle H^{2\ell}\rangle$ vanish and this gives the trivial result $Z = 1$. However, let us go a bit further and consider the high-temperature expansion of the spin–spin correlation function

$$G^{1,1}(x) = \langle s_0^1 s_x^1\rangle_{N\to 0} = \lim_{N\to 0} \frac{1}{Z} \sum_{\ell=0}^{\infty} \frac{\beta^\ell}{\ell!} \int \mathrm{d}\mu(\omega) s_0^1 s_x^1 H^\ell, \tag{9.71}$$

where x is any site on the lattice. In the limit $N \to 0$ all terms containing coefficients $\mathscr{C}_4, \mathscr{C}_6, \mathscr{C}_8, \ldots$ vanish. This means that graphs with vertices that have more than two lines attached, or equivalently with several lines between nearest neighbors, do not contribute. All graphs must be connected since disconnected graphs contain at least one full contraction of indices and hence are suppressed by at least one power of N. We conclude that only non-intersecting connected graphs contribute which connect the lattice points 0 and x. Two examples are shown in Fig. 9.19. Since $\langle s^a s^b\rangle \propto \delta_{ab}$ the internal index is preserved along the line connecting 0 and x and hence all spins on the line have the same index as the spins at the endpoints. The contribution of a graph is equal to $\ell!\mathscr{C}_2^\ell$, where 0 and x are connected by a line with length ℓ. Thus we find

$$G^{1,1}(x) = \sum_\ell c_\ell(x)\beta^\ell, \tag{9.72}$$

where $c_\ell(x)$ is the number of self-avoiding random walks from $0 \to x$ with length ℓ. Averaging over x yields the susceptibility

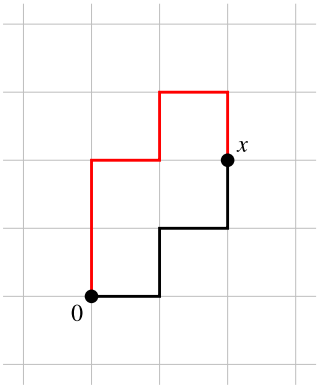

Fig. 9.19 Only graphs contribute in which the two points 0 and x are connected by a non-intersecting line on the lattice

$$\chi = \sum_{\ell} c_\ell \beta^\ell, \tag{9.73}$$

with coefficient c_ℓ counting the number of random walk of length ℓ beginning at the origin. The singularity of χ at the critical temperature is related to the behavior of the coefficients c_ℓ for large ℓ. With the help of Stirlings approximation for large factorials one estimates the coefficients in the expansion (9.20) and finds

$$\chi \sim \sqrt{\frac{\gamma}{2\pi}} \left(\frac{\mathrm{e}}{\gamma}\right)^\gamma \sum_{\ell} \ell^{\gamma-1} \left(\frac{\beta}{\beta_c}\right)^\ell. \tag{9.74}$$

Another quantity of interest is the mean square displacement over all ℓ-step self-avoiding walks

$$R_\ell^2 = \frac{1}{c_\ell} \sum_{x} x^2 c_\ell(x). \tag{9.75}$$

Its root is the average size of a walk consisting of ℓ steps. If the 2-point correlation function of the $N \to 0$ vector model falls off exponentially with a correlation length ξ which diverges near β_c as $(\beta_c - \beta)^{-\nu}$, this is compatible with (9.75) if, for large ℓ, $R_\ell \sim \ell^\nu$. This provides a surprising connection between the problem of self-avoiding walks and properties of N-vector models.

In two dimensions the exact critical temperature on a honeycomb lattice is known, $\beta_c^{-2} = 2 + \sqrt{2}$, and the critical exponents are [40],

$$\gamma = \frac{43}{32} \quad \text{and} \quad \nu = \frac{3}{4}. \tag{9.76}$$

The computation of c_ℓ for not too small ℓ is a formidable computational problem since, according to (9.74), the number of self-avoiding random walks grows as

$$c_\ell \sim \frac{\ell^{\gamma-1}}{\beta_c^\ell}. \tag{9.77}$$

Table 9.13 Critical temperatures for the self-avoiding random walks for $4 \leq d \leq 8$ [41]

d	4	5	6	7	8
β_c	0.147622	0.1131	0.09193	0.07750	0.06703

In three dimensions the critical exponents were calculated with a self-avoiding walk enumeration technique in [41]. From walks with up to 30 steps (for example, $c_{30} = 270569905525454674614$) one extracts

$$\beta_c \approx 0.2134907, \qquad \gamma \approx 1.1567, \quad \text{and} \quad \nu \approx 0.5875, \tag{9.78}$$

and from self-avoiding walks with 24 or less steps in $d \geq 4$ dimensions one can estimate the non-universal critical temperatures, see Table 9.13. An earlier conjecture for the exponent ν is due to the chemist Flory. The Flory exponents are

$$\nu_{\text{Flory}} = \begin{cases} 3/(2+d), & \text{for } d \leq 4, \\ 1/2, & \text{for } d > 4. \end{cases} \tag{9.79}$$

This value is correct in $d = 2$ and $d \geq 4$ (apart from logarithmic corrections in four dimensions) and comes very close for $d = 3$, where $\nu = 0.5888$. We expect that in $d \geq 4$ dimensions the second critical exponent is $\gamma = 1$.

9.6 Problems

9.1 (High-temperature expansion for the $3d$-Ising model) Examine the diagrams for the high-temperature expansion of the partition function of the three-dimensional Ising model with Hamiltonian

$$H = -J \sum_{\langle xy \rangle} s_x s_y, \quad s_x, s_y \in \{-1, 1\}.$$

The number of nearest-neighbor pairs is equal to $P = 3V$. You will find the following series expansion:

$$Z = (\cosh K)^{3V} 2^V \left(1 + 3V v^4 + 22V v^6 + \frac{1}{2}\{9V(V-1) + 375V\} v^8 + \cdots \right)$$

with $v = \tanh(\beta J)$. Furthermore, determine the series expansion of $\mathrm{e}^{-\beta f}$ (with f denoting the free energy density) to order v^8.

9.2 (Correlation functions of $O(N)$ models) Compute, up to order β^4, the correlation function $\langle s(x)s(0) \rangle$ of the three-dimensional $O(N)$ models at high temperature.

References

1. C. Domb, in *Phase Transitions and Critical Phenomena*, vol. 3, ed. by C. Domb, M.S. Green (Academic Press, London, 1974)

2. G.A. Baker, *Quantitative Theory of Critical Phenomena* (Academic Press, London, 1990)
3. J. Oitmaa, C. Hamer, W. Zheng, *Series Expansion Methods for Strongly Interacting Lattice Models* (Cambridge University Press, Cambridge, 2006)
4. C. Itzykson, J.M. Drouffe, *Statistical Field Theory*, vol. 2 (Cambridge University Press, Cambridge, 1989)
5. M.F. Sykes, D.S. Gaunt, P.D. Roberts, J.A. Wyles, High temperature series for the susceptibility of the Ising model. I. Two dimensional lattices. J. Phys. A **5**, 624 (1972)
6. B.G. Nickel, J.J. Rehr, High-temperature series for scalar-field lattice models: generation and analysis. J. Stat. Phys. **61**, 1 (1990)
7. W.P. Orrick, B.G. Nickel, A.J. Guttmann, J.H.H. Perk, The susceptibility of the square lattice Ising model: new developments. J. Stat. Phys. **102**, 795 (2001)
8. P. Butera, M. Comi, A library of extended high-temperature expansions of basic observables for the spin S Ising models on two- and three-dimensional lattices. J. Stat. Phys. **109**, 311 (2002)
9. W.J. Camp, J.P. Van Dyke, High-temperature series for the susceptibility of the spin-s Ising model: analysis of confluent singularities. Phys. Rev. B **11**, 2579 (1975)
10. D.S. Gaunt, M.F. Sykes, The critical exponent γ for the three-dimensional Ising model. J. Phys. A **12**, L25 (1979)
11. G. Bhanot, M. Creutz, U. Glässner, K. Schilling, Specific heat exponent for the 3-d Ising model from a 24-th order high temperature series. Phys. Rev. B **49**, 12909 (1994)
12. A.J. Guttmann, I.G. Enting, The high-temperature specific heat exponent of the 3-dimensional Ising model. J. Phys. A **27**, 8007 (1994)
13. P. Butera, M. Comi, Extension to order β^{23} of the high-temperature expansions for the spin $1/2$ Ising model on the simple-cubic and body-centered-cubic lattices. Phys. Rev. B **62**, 14837 (2000)
14. T. de Neef, I.G. Enting, Series expansions from the finite lattice method. J. Phys. A **10**, 801 (1977)
15. H. Arisue, T. Fujiwara, New algorithm of the finite lattice method for the high-temperature expansion of the Ising model in three dimensions. Phys. Rev. E **67**, 066109 (2003)
16. K. Binder, E. Luijten, Monte Carlo tests of renormalization-group predictions for critical phenomena in Ising models. Phys. Rep. **344**, 179 (2001)
17. A. Pelissetto, E. Vicari, Critical phenomena and renormalization-group theory. Phys. Rep. **368**, 549 (2002)
18. I.G. Enting, A.J. Guttmann, I. Jensen, Low-temperature series expansions for the spin-1 Ising model. J. Phys. A **27**, 6987 (1994)
19. M.F. Sykes, D.S. Gaunt, J.W. Essam, C.J. Elliot, Derivation of low-temperature expansions for Ising model. VI three-dimensional lattices-temperature grouping. J. Phys. A **6**, 1507 (1973)
20. G. Bhanot, M. Creutz, J. Lacki, Low temperature expansion for the Ising model. Phys. Rev. Lett. **69**, 1841 (1992)
21. A.J. Guttmann, I.G. Enting, Series studies of the Potts model: I. The simple cubic Ising model. J. Phys. A **26**, 807 (1993)
22. C. Vohwinkel, Yet another way to obtain low temperature expansions for discrete spin systems. Phys. Lett. B **301**, 208 (1993)
23. G.A. Baker, P. Graves-Morris, *Padé Approximants* (Cambridge University Press, Cambridge, 2010)
24. F. Wegner, Corrections to scaling laws. Phys. Rev. B **5**, 4529 (1972)
25. H.D. Hunter, G.A. Baker, Methods of series analysis. III. Integral approximant methods. Phys. Rev. B **19**, 3808 (1979)
26. M. Campostrini, A. Pelissetto, P. Rossi, E. Vicari, 25th order high temperature expansion results for three-dimensional Ising like systems on the simple cubic lattice. Phys. Rev. E **65**, 066127 (2002)
27. H. Arisue, T. Fujiwara, K. Tabata, Higher orders of the high-temperature expansion for the Ising model in three dimensions. Nucl. Phys. B, Proc. Suppl. **129**, 774 (2004)

28. P. Butera, M. Comi, Critical universality and hyperscaling revisited for Ising models of general spin using extended high temperature series. Phys. Rev. B **65**, 144431 (2002)
29. P. Butera, M. Comi, Series studies of the Potts model. 2. Bulk series for the square lattice. J. Phys. A **27**, 1503 (1994)
30. D. MacDonald, D.L. Hunter, K. Kelly, N. Jan, Self avoiding walks in two to five dimensions: exact enumerations and series studies. J. Phys. A **25**, 1429 (1992)
31. M. Lüscher, P. Weisz, Application of the linked cluster expansion to the n-component ϕ^4 theory. Nucl. Phys. B **300**, 325 (1988)
32. P. Butera, M. Comi, N-vector spin models on the sc and the bcc lattices: a study of the critical behavior of the susceptibility and of the correlation length by high temperature series extended to order β^{21}. Phys. Rev. B **56**, 8212 (1997)
33. P. Butera, M. Comi, Critical specific heats of the N-vector spin models on the sc and the bc lattices. Phys. Rev. B **60**, 6749 (1999)
34. H. Kleinert, Strong-coupling behavior of ϕ^4-theories and critical exponents. Phys. Rev. D **57**, 2264 (1998)
35. S.A. Antonenko, A.I. Sokolov, Critical exponents for $3d$ $O(n)$-symmetric models with $n > 3$. Phys. Rev. E **51**, 1894 (1995)
36. F. Benitez, J.P. Blaizot, H. Chaté, B. Delamotte, R. Méndes-Galain, N. Wschebor, Non-perturbative renormalization group preserving full-momentum dependence: implementation and quantitative evaluation. Phys. Rev. E **85**, 026707 (2012)
37. M. Hasenbusch, A finite scaling study of lattice models in the three-dimensional Ising universality class. Phys. Rev. B **82**, 174433 (2010)
38. M. Campostrini, M. Hasenbusch, A. Pelissetto, P. Rossi, E. Vicari, Critical exponents and equation of state of the three dimensional Heisenberg universality class. Phys. Rev. B **82**, 174433 (2010)
39. S. Holtmann, T. Schulze, Critical behavior and scaling functions of the three-dimensional $O(6)$ model. Phys. Rev. E **68**, 036111 (2003)
40. B. Nienhuis, Exact critical exponents of the $O(n)$ models in 2 dimensions. Phys. Rev. Lett. **49**, 1062 (1982)
41. N. Clisby, R. Liang, G. Slade, Self-avoiding walk enumeration via lattice expansion. J. Phys. A **40**, 10973 (2007)

Chapter 10
Peierls Argument and Duality Transformations

In this chapter we shall present exact results which apply to many lattice models of interest. Even before the exact solution of the two-dimensional Ising model by ONSAGER, PEIERLS [1] proved the existence of two ordered phases at low temperatures. His argument can be extended to many other models with discrete target spaces. Here we present Peierls' argument for the two- and three-dimensional Ising models.

We continue with the duality transformations which relate two lattice models. A duality transformation maps a system at weak coupling or low temperature into a system at strong coupling or high temperature and thus leads to new insights into the strong-coupling regime of lattice models. *Duality transformations* exist for many Abelian theories even in higher dimensions. In case the two lattice models are identical up to a rescaling of the couplings we call the transformation *self-dual*. The two-dimensional Ising model without magnetic field is self-dual [2, 3]. For non-self-dual models the dual theory maybe considerably more complex than the original one. For example the dual of the three-dimensional Ising model is a Z_2-gauge theory on the dual lattice [4]. In this chapter we shall study lattice systems for which the target spaces form Abelian groups. Unfortunately, it is difficult or impossible to find duality transformations for non-Abelian models. A detailed account of duality transformations in field theories and statistical mechanics is given in [5–7].

10.1 Peierls' Argument

First we present the beautiful reasoning due to Peierls to prove that at sufficient low temperatures the two-dimensional Ising model is in an ordered phase. The proof can be extended to other discrete spin models in two or more dimensions and this will be discussed later in this section.

To begin with, we choose fixed boundary conditions and set all Ising spins at the boundary to one. The choice of non-periodic boundary conditions will be important

A. Wipf, *Statistical Approach to Quantum Field Theory*, Lecture Notes in Physics 864,
DOI 10.1007/978-3-642-33105-3_10,

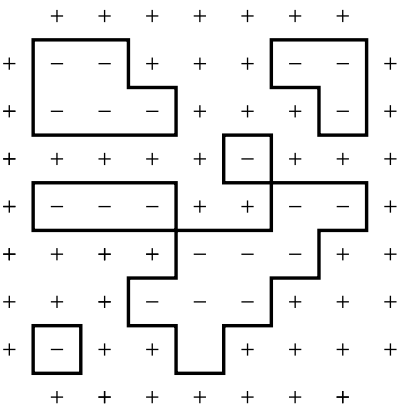

Fig. 10.1 The Peierls contours (loops) enclose regions on the lattice where the spins are -1. With the $+$ boundary conditions the $+$ spins are outside the contours and the $-$ spins are inside

at a later stage. Every spin configuration ω is uniquely characterized by a set of non-intersecting loops on the dual lattice,

$$\Gamma_\omega = \{\gamma_1, \gamma_2, \ldots, \gamma_n\},$$

where every loop, called Peierls contour, encloses an island with spins down, see Fig. 10.1. If $|\gamma_i|$ denotes the length of γ_i then a configuration ω has exactly $\sum_i |\gamma_i|$ nearest-neighbor pairs with anti-parallel spins. Hence its energy is given by

$$\begin{aligned} H_\Lambda(\omega) &= -J\#(\text{pairs with equal spins}) \\ &\quad + J\#(\text{pairs with unequal spins}) \\ &= -JP + 2J \sum_{\gamma_i \in \Gamma_\omega} |\gamma_i|, \end{aligned}$$

where P is the total number of nearest-neighbor pairs. The constant contribution cancels in expectation values such that we obtain the following probability for the occurrence of a configuration ω (recall that $K = \beta J$):

$$P[\omega] = \frac{1}{Z} \exp\Big(-2K \sum_{\gamma_i \in \Gamma_\omega} |\gamma_i|\Big), \quad Z = \sum_{\Gamma} \exp\Big(-2K \sum_{\gamma_i \in \Gamma} |\gamma_i|\Big). \tag{10.1}$$

Lemma 10.1 (Peierls' inequality) *The probability for the occurrence of a contour γ may be bounded from above as follows*:

$$P[\gamma] \equiv P\big[\{\omega : \gamma \in \Gamma_\omega\}\big] \le \mathrm{e}^{-2K|\gamma|}. \tag{10.2}$$

Proof The left hand side may be written as

$$\begin{aligned} \frac{1}{Z} \sum_{\omega:\gamma\in\Gamma_\omega} \exp\Big(-2K \sum_{\gamma'\in\Gamma_\omega} |\gamma'|\Big) &= \frac{1}{Z} \mathrm{e}^{-2K|\gamma|} \sum_{w:\gamma\in\Gamma_\omega} \exp\Big(-2K \sum_{\gamma'\in\Gamma_\omega\setminus\gamma} |\gamma'|\Big) \\ &= \frac{1}{Z} \mathrm{e}^{-2K|\gamma|} \sum_{\omega:\gamma\in\Gamma_{P_\gamma\omega}} \exp\Big(-2K \sum_{\gamma'\in\Gamma_\omega} |\gamma'|\Big), \end{aligned}$$

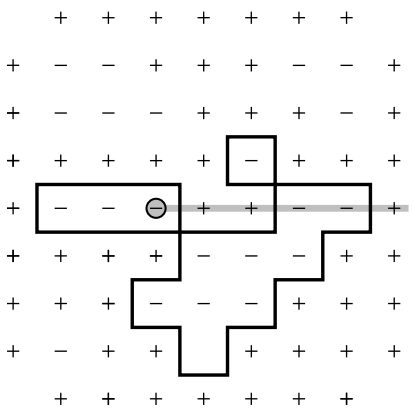

Fig. 10.2 Estimation of the number of loops which enclose a fixed lattice point

where we have used the fact that if we remove γ from a contour gas Γ_ω with $\gamma \in \Gamma_\omega$, we obtain the contour gas of the configuration $P_\gamma \omega$, where $P_\gamma \omega$ originates from ω by a flip of all spins enclosed by γ. Since the last term represents a summation over a *subset* of all configurations, we have proved the inequality (10.2). □

The inequality shows that the probability for the occurrence of a long contour decreases exponentially with its length, independent of the lattice size. We now use this inequality to estimate the probability of spin configurations with $s_x = -1$. Here it will be important to recall that we imposed fixed boundary conditions with all spins $+1$ at the boundary. Note that any x with $s_x = -1$ is enclosed by *at least* one contour and the number of horizontal and vertical edges of a contour is always even. Thus we have $|\gamma| \in \{4, 6, 8, \ldots\}$.

Lemma 10.2 *The number $A(n)$ of contours of length n which enclose a certain point $x \in \Lambda$ is bounded from above according to*

$$A(n) \leq \frac{n-2}{2} 3^{n-1}.$$

Proof First of all, we notice that the ray $y(\lambda) = x + \lambda e_1$, $\lambda > 0$, emanating from x, intersects a contour at least once. This is sketched in Fig. 10.2. Now let us consider the vertical link of a given contour γ_x enclosing x which intersects the ray at a maximal distance λ_{may} from x. The possible values of $\lambda_{\max}$ are $1/2, 3/2, \ldots, (n-3)/2$, i.e. we have $(n-2)/2$ possible values of $\lambda_{\max}$. The largest value is attained for the rectangle of height 1 and length $(n-2)/2$. If we now move along the contour then each of the remaining $n-1$ links may "choose" between three possible directions with respect to its predecessor: left, right or straight on. This gives a multiplicative factor of 3^{n-1} and this yields the upper bound for $A(n)$. □

Theorem 10.1 *If $K > 0.7$, then there exist two different Gibbs measures P_β^+, P_β^- for the Ising model on the infinite square lattice, where*

$$\langle s_x \rangle_{P_\beta^+} > 0 \quad \textit{and} \quad \langle s_x \rangle_{P_\beta^-} < 0 \tag{10.3}$$

holds for all sites x.

Thus we observe spontaneous magnetization at low temperatures. We know already from the exact solution or the duality arguments that spontaneous magnetization occurs for $K > K_c$ with $K_c = \frac{1}{2}\log(1+\sqrt{2}) \approx 0.44$.

Proof Firstly, we estimate the probability of the occurrence of $s_x = -1$ when the spins on the boundary are $+1$. If $\{\gamma_x\}$ is the set of contours enclosing x then

$$\begin{aligned} P^+[s_x = -1] &\le \sum_{\gamma_x} P[\gamma] \le \sum_{n\in\mathbb{N}} A(n)\mathrm{e}^{-2Kn} = \sum_{m\in\mathbb{N}} A(2m)\mathrm{e}^{-4Km} \\ &\le \sum_{m\in\mathbb{N}} (m-1)3^{2m-1}\mathrm{e}^{-4Km} = \frac{1}{3}\sum_{m\in\mathbb{N}} (m-1)\mathrm{e}^{-\alpha m} \\ &= \frac{1}{3}\mathrm{e}^{-\alpha}\sum_{n\in\mathbb{N}_0} n\mathrm{e}^{-n\alpha} = \frac{1}{3}\mathrm{e}^{-\alpha}\left(-\frac{\partial}{\partial\alpha}\sum_{n\in\mathbb{N}_0}\mathrm{e}^{-n\alpha}\right) = \frac{1}{3}\frac{y^2}{(1-y)^2}, \end{aligned}$$

wherein we assumed that the constant $\alpha \equiv 4K - 2\log 3$ is positive and in the last step we defined $y = \mathrm{e}^{-\alpha} \in (0,1)$. Next we determine the y-values for which the probability is less than $1/2$. The upper bound $1/2$ is attained for

$$2y^2 = 3(1-y)^2 \quad \text{or} \quad y = y_p \equiv 3 \pm \sqrt{6}.$$

We conclude that the probability for any given spin being -1 is less than $1/2$ for $y < y_p$ or equivalently for $\alpha > -\log(3-\sqrt{6})$. With $+1$-boundary conditions we thus observe spontaneous magnetization, if

$$\beta J > K_p, \quad K_p = \frac{1}{2}\log 3 - \frac{1}{4}\log\bigl(3-\sqrt{6}\bigr) \approx 0.69853. \tag{10.4}$$

The estimate holds for all sites x and lattice sizes. At low temperature the system is therefore characterized by a positive magnetization $\langle s_x \rangle^+ > 0$ in the thermodynamic limit. On the other hand, setting all Ising spins at the boundary to -1 we would find a probability $P^-[s_x = 1] < 1/2$ for $K > K_p$ for all lattice sizes. This implies a negative magnetization in the thermodynamic limit. Different boundary conditions force the statistical system into different phases in the thermodynamic limit. Hence there exist at least two different equilibrium states at low temperature. □

10.1.1 Extension to Higher Dimensions

To which other spin systems can one extend Peierls' argument? The argument begins with a minimal energy configuration ω_0 compatible with the imposed bound-

ary conditions. For the Ising model with +1-boundary conditions this is the ordered configuration

$$\omega_0 = \{s_x = 1 | x \in \Lambda\}. \tag{10.5}$$

Then one studies configurations with higher energies which are exponentially suppressed. Although the excited configurations carry lots of entropy—there are many of them—the energy suppression wins at sufficiently low temperatures. To generalize this type of energy-entropy arguments one needs a generalization of the *Peierls' contours* for other lattices and more general target spaces. Actually the Peierls argument can be extended to spin models with a discrete Abelian group G as target space. Here we focus on the Ising model in higher dimensions with target space Z_2 for which the closed contours are borderless hypersurfaces on the dual lattice. A contour thereby separates the interior from its complement, the exterior.

There exists a one-to-one relation between configurations ω with +1-boundary conditions and sets of non-intersection contours. We find the following estimate for the number of counters of a given size:

Lemma 10.3 *In d dimensions the number $A(n)$ of different Peierls' contours of size n fulfills the inequality*

$$\exp\left(\frac{n-2d}{2d-2}\log d\right) < A(n) < \frac{n-2}{2d-2}(6d-9)^{n-1}. \tag{10.6}$$

Proof To prove the lower bound we construct elongated contours of size n which enclose the site x. To that aim we consider a chain of k adjacent lattice points starting at x. Moving along the chain from one site to the next site we jump one step towards one of the d *positive coordinate directions*. This guarantees that two chains are different if only one of their jumps is in a different direction. Clearly there exist d^{k-1} different chains of this type. We now consider the corresponding dual d-chain, the border of which is a Peierls contour which encloses x. More explicitly, the d-chain is just the union of the k elementary cubes dual to the sites along the chain. The size of such a contour is the surface area of the d-chain which is $n = (2d-2)k + 2$, since the inner areas of the chain-segments cancel. Thus the length of the chain is

$$k(n) = \frac{n-2}{2d-2}, \tag{10.7}$$

and we obtain the lower bound

$$A(n) > d^{k(n)-1} = d^{(n-2d)/(2d-2)} = \exp\left(\frac{n-2d}{2d-2}\log d\right). \tag{10.8}$$

To derive the upper bound we proceed similarly as in two dimensions. Thereby we call a k-dimensional cube on the lattice k-cube. In particular 2-cubes and 1-cubes are plaquettes and links, respectively. The corresponding objects from the dual lattice are called dual cubes, dual plaquettes and dual links. Here we are mostly dealing with dual $(d-1)$-cubes which we call *cells*.

The ray $x + \lambda e_1$ emanating from x intersects every contour γ_x around x at least once. We focus on that cell in the contour γ_x with maximal distance $\lambda_{\max}$ from x.

The possible values of $\lambda_{\max}$ are $-\frac{1}{2}+k$ with $k \in \{1, \ldots, k(n)\}$ and $k(n)$ from (10.7). Thereby the largest value is realized for a column with base area of 1 and length $k(n)$ towards the e_1-direction. Beginning with the cell with maximal distance from x we construct a Peierls contour around x by successively gluing more and more cells together. We can glue a cell to one of the $2d-3$ free faces of an already attached cell. Actually there are three ways to glue a cell to the face of a given cell: A face is a dual $(d-2)$-cube and defines a unique plaquette on the original lattice. The newly glued cell must be dual to one of the links forming the boundary of this plaquette. But one of the four links on the boundary of the plaquette is dual to the already attached cell and hence must be excluded. Thus we are left with three possible ways of gluing. Multiplying the combinatorial factors yields the upper bound in (10.6). □

To prove spontaneous symmetry breaking at low temperatures we assume that the constant $\alpha = 4K - 2\log(6d-9)$ is positive. The probability for the spin at x to be -1 is bounded from above as

$$P^+[s_x = -1] \le \sum_{m \in \mathbb{N}} A(2m) \mathrm{e}^{-4Km} \le \frac{1}{\zeta^2} \frac{y^2}{(1-y)^2}, \tag{10.9}$$

where we used the abbreviations

$$y = \mathrm{e}^{-\alpha} \quad \text{and} \quad \zeta^2 = 3(2d-3)(d-1). \tag{10.10}$$

This probability is less than $1/2$ for

$$y < \frac{\zeta}{\zeta + \sqrt{2}} \quad \text{or} \quad K > \frac{1}{4}\log\left(1 + \frac{\sqrt{2}}{\zeta}\right) + \frac{1}{2}\log(6d-9). \tag{10.11}$$

In two dimensions $\zeta^2 = 3$ and we recover our previous result. For $d = 3$ we have $\zeta^2 = 9/2$ and we observe two phases, if

$$K > \frac{1}{4}\log 135 \quad \text{or} \quad T < 0.1359 T_{c,\mathrm{mf}}. \tag{10.12}$$

From the mean field result we expect that K_c decreases as $1/d$. Hence the lower bounds (10.11) are by no means optimal. The inequality derived in [8] is much better in high dimensions,

$$A(n) \le \exp\bigl(64n(\log d)/d\bigr). \tag{10.13}$$

However, an easier way to prove the existence of an ordered low temperature phase in higher-dimensional ferromagnetic systems makes use of the correlation inequalities in Sect. 8.6 in conjunction with the known results for the two-dimensional system.

10.2 Duality Transformation of Two-Dimensional Ising Model

In their pioneering work KRAMERS and WANNIER discovered a transformation which maps the 2d-Ising model with couplings $(\beta, h = 0)$ into itself, but with couplings $(^*\beta, h = 0)$ [2, 3]. The temperature after the transformation is a monotonously

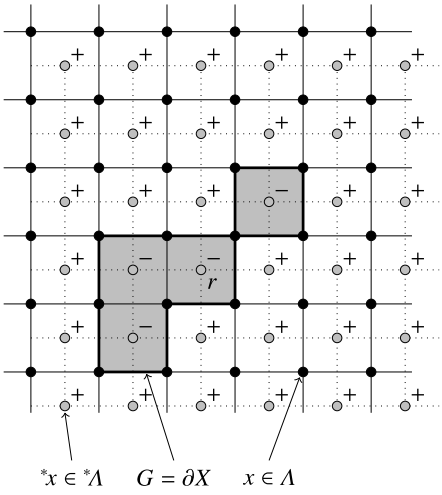

Fig. 10.3 A high-temperature graph G of the two-dimensional Ising model of length $L(G) = 12$. The dual lattice ${}^*\Lambda$ with its lattice points ${}^*x$ is illustrated as well

decreasing function of the temperature of the original model such that the high-temperature phase maps into the low-temperature phase and vice versa. We begin with rewriting the high-temperature series expansion of the partition function in Sect. 9.2 as follows ($K = \beta J$):

$$Z = (\cosh K)^P \sum_{\omega} \prod_{\langle x,y \rangle} (1 + \nu s_x s_y) = (\cosh K)^P 2^V \sum_{G \in \mathcal{G}} \nu^{L(G)}$$
$$= (\cosh K)^P 2^V \sum_{G} \prod_{x} \nu^{n_x(G)/2}, \quad \nu = \tanh(K) \ll 1. \tag{10.14}$$

Here P is the number of nearest-neighbor pairs and $\mathcal{G}$ the set of high-temperature graphs. These are diagrams with closed curves (loops) and even vertices only. $L(G)$ denotes the length of the graph G or the number of its links. Figure 10.3 shows a high-temperature graph with $L(G) = 12$. Finally, the even number $n_x(G)$ in the last representation of the partition function is equal to the number of links ending at vertex x. In two dimensions $n_x(G)$ takes the values 0, 2, or 4.

Now we shall argue that the sum (10.14) may be viewed as partition function on the *dual lattice*. The dual lattice ${}^*\Lambda$ of a square lattice is again a square lattice with sites at the centers of the plaquettes of the original lattice. Now we assign a spin configuration ${}^*\omega = \{s_{{}^*x}\}$ on the dual lattice to every spin configuration $\omega = \{s_x\}$ on the lattice as follows: For two nearest neighbors ${}^*x, {}^*y$ on the dual lattice we set $s_{{}^*x} s_{{}^*y} = -1$ if a loop of the high-temperature graph belonging to ω crosses the link between ${}^*x$ and ${}^*y$. Else we set $s_{{}^*x} s_{{}^*y} = 1$. Actually the mapping from the high-temperature graphs to ${}^*\omega$ is not bijective since ${}^*\omega$ and $-{}^*\omega$ belong to the same graph. On the other hand, ω and $-\omega$ also belong to the same high-temperature graph and this implies that there is a bijective mapping $\omega \to {}^*\omega$. The loops of a graph G encircle a set X of sites on the dual lattice and all spins $s_{{}^*x}$ in X have the same sign. The spins in the complement of X have the other sign.

Let us consider the plaquette $p(x)$ on the dual lattice with vertices ${}^*x, {}^*y, {}^*u, {}^*v$ and center point $x \in \Lambda$. Now it easy to see that the order of the vertex x is

$$n_x = 2 - \frac{1}{2}(s_{{}^*x}s_{{}^*y} + s_{{}^*y}s_{{}^*u} + s_{{}^*u}s_{{}^*v} + s_{{}^*v}s_{{}^*x}) \equiv 2 - \frac{1}{2}p(x). \tag{10.15}$$

Inserting this result into the partition function (10.14) yields

$$\begin{aligned} Z &= (\cosh K)^P 2^V \sum_{{}^*\omega} \prod_x \left(v \cdot v^{-p(x)/4}\right) \\ &= (\cosh K)^{2V} (2v)^V \sum_{{}^*\omega} v^{-\frac{1}{2}\sum_{\langle {}^*x, {}^*y\rangle} s_{{}^*x}s_{{}^*y}} \\ &= (2\sinh K \cosh K)^V \sum_{{}^*\omega} \mathrm{e}^{-{}^*\beta {}^*H(s)}, \end{aligned} \tag{10.16}$$

where we took into account that every dual link belongs to two plaquettes. In the last step we defined $v = \exp(-2{}^*K)$. We may rewrite this relation as follows,

$$2\sinh\left(2{}^*K\right) = \mathrm{e}^{2{}^*K} - \mathrm{e}^{-2{}^*K} = \frac{1}{v} - v = \coth K - \tanh K = \frac{2}{\sinh 2K}.$$

Hence, the duality relation takes the symmetric form

$$\sinh 2K \cdot \sinh 2{}^*K = 1. \tag{10.17}$$

This duality relation links the temperature T of the Ising model with the temperature ${}^*T$ of the Ising model on the dual lattice. It is a *symmetric* and reciprocal relation: If K increases monotonically from 0 to ∞ then ${}^*K$ decreases monotonically from ∞ to 0. Figure 10.4 shows the function ${}^*K(K)$ as well as the fixed point of the map $K \to {}^*K$. By using (10.17) we obtain the relation

$$(2\sinh K \cosh K)^2 = \sinh 2K \sinh 2K \overset{(10.17)}{=} \frac{\sinh 2K}{\sinh 2{}^*K}.$$

Together with (10.16) this leads to the duality relation

$$\frac{Z(K)}{(\sinh 2K)^{V/2}} = \frac{Z({}^*K)}{(\sinh 2{}^*K)^{V/2}}. \tag{10.18}$$

Let us now assume that there is a critical coupling K_c where the free energy density (in the thermodynamic limit) is singular. Then the duality relation (10.18) implies that there must exist another singularity at ${}^*K_c$. Hence, in the case of there being a unique critical point, it would be located at $K_c = {}^*K_c$. Then K_c is a solution of

$$\sinh 2K_c = \pm 1 \quad \Longrightarrow \quad K_c = \pm\frac{1}{2}\log\left(1 + \sqrt{2}\right) \approx \pm 0.4407.$$

The negative solution thereby corresponds to the anti-ferromagnetic case $J < 0$. For the ferromagnetic Ising model we obtain the critical temperature

$$T_c = \frac{2J}{\log(1 + \sqrt{2})} \approx 2.2692J. \tag{10.19}$$

For systems with several critical points the duality relation leads to relations between pairs of critical couplings only.

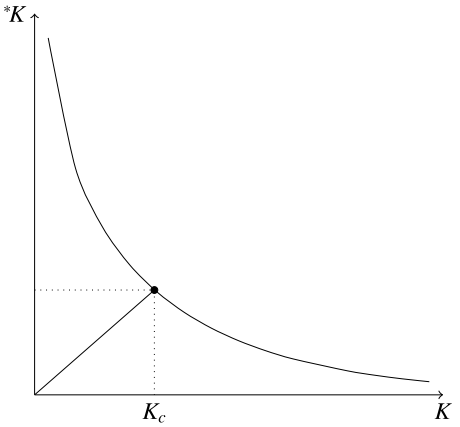

Fig. 10.4 Relation between the reduced temperature K on the lattice Λ and the reduced temperature ${}^*K$ on the dual lattice ${}^*\Lambda$

10.2.1 An Algebraic Derivation

We now present a second, more algebraic, derivation of the duality relation which generalizes more easily to higher dimensions and to other spin systems. We rewrite the Ising model partition function in d dimensions as follows,

$$Z = \sum_{\omega} \prod_{\langle x,y\rangle} (\cosh K + \sinh K s_x s_y) = \sum_{\omega} \prod_{\langle x,y\rangle} \sum_{k=0,1} c_k(K)(s_x s_y)^k, \qquad (10.20)$$

where we defined $c_0(K) := \cosh K$ and $c_1(K) := \sinh K$. At this point we are lead to introduce a field which assigns to every link either 0 or 1,

$$k : \langle x, y\rangle \to k_{xy} \in \{0, 1\}.$$

For a fixed configuration of link variables $\{k_{xy}\}$ we obtain the following contribution to the partition function:

$$\begin{aligned} \sum_{\omega} \prod_{\langle x,y\rangle} c_{k_{xy}}(K)(s_x s_y)^{k_{xy}} &= \prod_{\langle x,y\rangle} c_{k_{xy}}(K) \sum_{\omega} \prod_{\langle x,y\rangle} (s_x s_y)^{k_{xy}} \\ &= \prod_{\langle x,y\rangle} c_{k_{xy}}(K) \sum_{\omega} \prod_{x} s_x^{\partial k(x)}, \end{aligned} \qquad (10.21)$$

where $\partial k(x)$ is the sum of all variables defined on links ending at x,

$$\partial k(x) = \sum_{y:\langle y,x\rangle} k_{xy} = \sum_{\ell: x\in\partial\ell} k_\ell.$$

The operator ∂ represents the discrete version of the divergence and in d dimensions and takes the values $\{0, 1, \ldots, 2d\}$. For any integer n we have

$$\sum_{s=-1,1} s^n = 2\delta_2(n), \quad \delta_2(n) = \begin{cases} 1, & n \text{ even}, \\ 0, & n \text{ odd}, \end{cases} \qquad (10.22)$$

such that the sum over all spin configurations in (10.21) is performed easily and leads to the following representation of the partition function in arbitrary dimensions:

$$Z = 2^V \sum_{\{k\}} \prod_{\ell} c_{k_\ell}(K) \prod_{x} \delta_2\big(\partial k(x)\big). \tag{10.23}$$

We now assign a spin configuration ${}^*\omega$ on the dual lattice to each configuration $k = \{k_\ell\}$ on the links as follows: If the link $\langle {}^*x, {}^*y\rangle$ between two nearest neighbors ${}^*x$ and ${}^*y$ on the dual lattice crosses the link ℓ we set

$$k_\ell = \frac{1}{2}(1 - s_{{}^*x} s_{{}^*y}). \tag{10.24}$$

We recover the relation (10.15) wherein n_x is equal to the divergence of k at x,

$$\partial k(x) = 2 - \frac{1}{2} p(x).$$

Since $p(x) \in \{-4, 0, 4\}$ the right hand side is always even and all δ_2-constraints in (10.23) are fulfilled. This means that the transformation (10.24) yields all link configurations $\{k\}$ that satisfy the δ_2-constraints. The sum over link configurations turns into the sum over spin configurations on the dual lattice. Since every link corresponds to exactly one link on the dual lattice, the product over all ℓ becomes the product over all nearest-neighbor pairs $\langle {}^*x, {}^*y\rangle$. Thus (10.23) can be written as

$$Z = 2^V \sum_{{}^*\omega} \prod_{\langle {}^*x, {}^*y\rangle} c_{(1 - s_{{}^*x} s_{{}^*y})/2}(K). \tag{10.25}$$

Rewriting $c_k(K)$ according to

$$c_{k_\ell}(K) \overset{(10.24)}{=} (\cosh K \sinh K)^{1/2} \exp\left(-\frac{1}{2} s_{{}^*x} s_{{}^*y} \log\tanh K\right)$$

and inserting this into (10.25) gives

$$\begin{aligned} Z &= (2\cosh K \sinh K)^V \sum_{{}^*\omega} \exp\left(-\frac{1}{2} \log\tanh K \sum_{\langle {}^*x, {}^*y\rangle} s_{{}^*x} s_{{}^*y}\right) \\ &= \big(\sinh 2{}^*K\big)^{-V} \sum_{{}^*\omega} \exp\left({}^*K \sum_{\langle {}^*x, {}^*y\rangle} s_{{}^*x} s_{{}^*y}\right), \end{aligned} \tag{10.26}$$

where ${}^*K$ is related to K as in (10.17). Thus we recovered our previous result.

10.2.2 Two-Point Function

In order to interpret the dual spins $s_{{}^*x}$ we slightly modify the previous derivation to determine the 2-*point function* of the dual model:

$$\langle s_{{}^*x} s_{{}^*y}\rangle = \frac{1}{{}^*Z} \sum_{{}^*\omega} s_{{}^*x} s_{{}^*y} \exp\left({}^*K \sum_{\langle {}^*u, {}^*v\rangle} s_{{}^*u} s_{{}^*v}\right).$$

The partition function ${}^*Z$ in the denominator has already been dualized and we focus on the numerator,

$$\begin{aligned} Z_{{}^*x{}^*y} &= \sum_{{}^*\omega} s_{{}^*x} s_{{}^*y} \exp\Bigg({}^*K \sum_{\langle {}^*u, {}^*v\rangle} s_{{}^*u} s_{{}^*v} \Bigg) \\ &= \sum_{{}^*\omega} s_{{}^*x} s_{{}^*y} \prod_{\langle {}^*u, {}^*v\rangle} \sum_{k=0,1} c_k\big({}^*K\big) (s_{{}^*u} s_{{}^*v})^k, \end{aligned}$$

where the product extends over all nearest-neighbor pairs on ${}^*\Lambda$. Thus we have

$$Z_{{}^*x{}^*y} = 2^V \sum_{\{k\}} \prod_{{}^*\ell} c_{k_{{}^*\ell}}\big({}^*K\big) \prod_{{}^*u} \delta_2\big(\delta_{{}^*u{}^*x} + \delta_{{}^*u{}^*y} + \partial k\big({}^*u\big)\big). \tag{10.27}$$

We now wish to find a representation for the configurations $\{k\}$ on the dual links such that all δ_2-constraints in (10.27) are fulfilled. We proceed as follows: We connect the points ${}^*x$ and ${}^*y$ by an arbitrary path $\mathcal{C}_{{}^*x{}^*y}$ on the dual lattice as illustrated in Fig. 10.5. We then choose the following representation for the dual-link variables:

$$k_{{}^*\ell} = \begin{cases} \frac{1}{2}(1 - s_x s_y), & {}^*\ell \notin \mathcal{C}_{{}^*x{}^*y}, \\ \frac{1}{2}(1 + s_x s_y), & {}^*\ell \in \mathcal{C}_{{}^*x{}^*y}. \end{cases}$$

In other words if the link $\langle x, y\rangle$ on the lattice intersects the path ${}^*\mathcal{C}_{{}^*x{}^*y}$ on the dual lattice, then we modify the transformation rule. According to this representation, ∂k is an even number for all lattice points ${}^*\Lambda$, except for ${}^*x, {}^*y$, where it is odd. Hence, we may cast the representation (10.27) in the form

$$Z_{{}^*x{}^*y} = 2^V \sum_{\omega} \prod_{\langle x,y\rangle \in \mathcal{S}_{{}^*x{}^*y}} c_{(1+s_x s_y)/2}\big({}^*K\big) \prod_{\langle x,y\rangle \notin \mathcal{S}_{{}^*x{}^*y}} c_{(1-s_x s_y)/2}\big({}^*K\big),$$

where $\mathcal{S}_{{}^*x{}^*y}$ denotes the set of links on the lattice Λ which intersect the path $\mathcal{C}_{{}^*x{}^*y}$. With a calculation similar to the one above (10.26) we arrive at

$$Z_{{}^*x{}^*y} = (\sinh 2K)^{-V} \sum_{\omega} \exp\Bigg(\sum_{\langle x,y\rangle} K_{xy} s_x s_y \Bigg). \tag{10.28}$$

Note that the couplings in the exponent depend on the nearest neighbor pair: if the link between a pair does not intersect the path $\mathcal{C}_{{}^*x{}^*y}$, then the corresponding coupling is given by βJ. If the link between the pair does intersect the path $\mathcal{C}_{{}^*x{}^*y}$, then the corresponding coupling $-\beta J$ is negative and anti-ferromagnetic. In summary, the numerator $Z_{{}^*x{}^*y}$ itself is a partition function with ferromagnetic as well as anti-ferromagnetic couplings between nearest neighbors. Thus the correlation function $\langle s_{{}^*x} s_{{}^*y}\rangle$ of the dual Ising model is the ratio of two partition functions on Λ. One contains ferromagnetic and anti-ferromagnetic couplings, whereas the other one includes only ferromagnetic couplings.

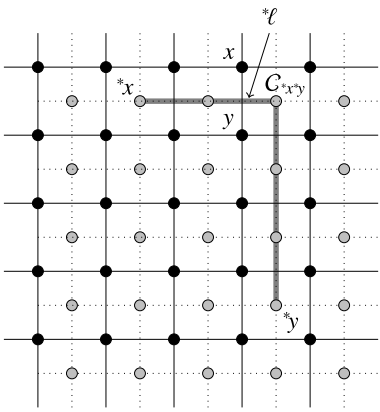

Fig. 10.5 A path on the dual lattice connecting the arguments ${}^*x$ and ${}^*y$ of the two-point correlation function

10.2.3 Potts Models

The two-dimensional standard q-state Potts model with energy function (6.10) is self-dual and the duality relation between the couplings reads

$$\mathrm{e}^{-{}^*K_p} = \frac{1-\mathrm{e}^{-K_p}}{1+(q-1)\mathrm{e}^{-K_p}}, \quad K_p = \beta J_p, \tag{10.29}$$

see the problem on p. 227. A particular simple proof based on the random-bond model was given in [9]. On a finite lattice the duality transformation can be extended to Potts models subject to cyclic boundary conditions,

$$s_{\mathbf{x}+N\mathbf{e}_i} = s_{\mathbf{x}} + c_i, \quad c_i \bmod q, \tag{10.30}$$

and this generalization may be utilized to study universal aspects of phase transitions in three-dimensional gauge theories [10].

10.2.4 Curl and Divergence on a Lattice

Consider a hypercubic lattice Λ in d dimensions and its dual lattice ${}^*\Lambda$. Suppose that there are some statistical variables k_ℓ defined on the oriented links of Λ. If we change the orientation of ℓ, then k_ℓ changes its sign, $k_{\langle x,y\rangle} = -k_{\langle y,x\rangle}$. The k_ℓ should belong to an Abelian group with the addition as group operation. The circulation along the perimeter of a elementary plaquette p is

$$\mathrm{d}k\big({}^*x\big) = \sum_{\ell\in\partial p} k_\ell, \tag{10.31}$$

where the site ${}^*x$ on the dual lattice sits in the center of the plaquette p. If k is curl-free, $\mathrm{d}k = 0$, then it is (locally) the gradient of a function φ

$$k_{\langle y,x\rangle} = \varphi(y) - \varphi(x). \tag{10.32}$$

In this case the 'integral' along any contactable loop $\mathcal{C}$ on the lattice vanishes,

$$\oint_{\mathcal{C}} k = \sum_{\ell \in \mathcal{C}} k_\ell = 0. \tag{10.33}$$

The links must have the same orientation as the loop. Besides the curl we can define a discrete version of the divergence on the lattice. The divergence of k is

$$(\partial x)(x) = \sum_{\ell : x \in \partial \ell} k_\ell, \tag{10.34}$$

where all links are emanating from x. For a divergence-free field the flux through elementary cubes of the dual lattice vanish.

We do not want to go any further at this point. However, if one goes beyond hypercubic lattices in higher dimensions it is useful to know some basic facts about the difference calculus on lattices. A comprehensive and exhaustive representation based on simplices, chains, border and co-border operators and Stokes theorem is contained in [11].

10.3 Duality Transformation of Three-Dimensional Ising Model

The three-dimensional Ising model is not self-dual—the application of the duality transformation yields the Z_2 lattice gauge theory. Thus we cannot predict its critical point form duality alone. But a duality relating two different models can be useful for studying the excitations in the high- and low-temperature regimes since it is still true that the transformation relates the high-temperature phase of one model to the low-temperature phase of the other model and vice versa.

Our point of departure is the representation (10.23) of the partition function,

$$Z = 2^V \sum_{\{k\}} \prod_{\ell} c_{k_\ell}(K) \prod_{x} \delta_2\big(\partial k(x)\big), \tag{10.35}$$

which holds in all dimensions. In three dimensions the divergence at a given site

$$(\partial k)(x) = \sum_{\ell : x \in \partial \ell} k_\ell \tag{10.36}$$

is the sum of six terms—one term for every link ending at x—and attains the values $\{0, 1, \ldots, 6\}$. Again we can fulfill the δ_2-constraints on $\partial k(x)$ in (10.35) by introducing suitable variables on the dual lattice ${}^*\Lambda$. The dual of a hypercubic lattice is again a hypercubic lattice with sites in the centers of the elementary cells of the original lattice. Nearest neighbors of ${}^*\Lambda$ sit in adjacent cells. Every link ℓ crosses exactly one plaquette ${}^*p_\ell$ of the *dual lattice* as depicted in Fig. 10.6. We now assign to every link ${}^*\ell$ of the dual lattice a variable $U_{*\ell}$ with values in the Abelian group $Z_2 = \{-1, 1\}$. Next we map a link configuration $\{U_{*\ell}\}$ on the dual lattice to a link

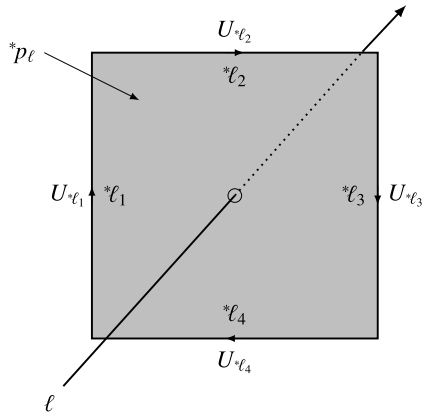

Fig. 10.6 Every link ℓ of the lattice crosses exactly one plaquette ${}^*p_\ell$ of the dual lattice and a dual plaquette has four dual links as edges

configuration $\{k_\ell\}$ on the original lattice as follows: If ${}^*p_\ell$ is the plaquette dual to ℓ, then we set

$$k_\ell = \frac{1}{2}(1 - U_{*p_\ell}), \quad \text{where } U_{*p} = \prod_{{}^*\ell \in \partial {}^*p} U_{*\ell} \tag{10.37}$$

is the product of the link variables of the four edges bounding the dual plaquette. Now we shall prove that the divergence of k only takes the values 0, 2, 4 and 6 and thus satisfies all δ_2-constraints in (10.35).

To calculate the divergence of k at x we consider the elementary cube c_x of the dual lattice with center x. The six links ending at x intersect the six plaquettes on the boundary of c_x, such that the divergence in (10.36) takes the form

$$\partial k(x) = 3 - \frac{1}{2} \sum_{{}^*p \in \partial c_x} U_{*p}. \tag{10.38}$$

The plaquette variables U_{*p} have the values 1 or -1 and if all dual-link variables $U_{*\ell}$ on the edges of the cube c_x are 1, then the divergence at x is zero. In contrast, if we change the sign of one link variable then exactly two plaquette variables change sign such that the sum changes by a multiple of 4 or the divergence by a multiple of 2. This then proves that ∂k takes the values in $\{0, 2, 4, 6\}$ and thus fulfills the δ_2-constraints.

We now rewrite the product over all links in (10.35) as a product over all dual plaquettes. Since k in (10.37) satisfies all δ_2-constraints in (10.35) we find

$$Z = 2^V \sum_{\{k(U)\}} \prod_{\{{}^*p\}} c_{\frac{1}{2}(1-U_{*p})}(K). \tag{10.39}$$

Below we shall see that there are many different configurations $\{U_{*\ell}\}$ belonging to the same configuration $\{k_\ell\}$. Configurations which are mapped into the same k are called equivalent. By construction equivalent configurations have the same weight c in (10.39) and the sum over $\{k\}$ in the partition function (10.35) becomes a sum over equivalence classes. This is indicated by the sum over $\{k(U)\}$ in (10.39). Using the relation

$$c_{k_\ell} = \cosh K \, \mathrm{e}^{k_\ell \log\tanh K} \overset{(10.37)}{=} (\cosh K \sinh K)^{1/2} \exp\left(-\frac{1}{2}\log\tan K U_{{}^*p_\ell}\right)$$

we end up with the following representation of the partition function:

$$Z = 2^V (\cosh K \sinh K)^{3V/2} \sum_{\{k(U)\}} \exp\left({}^*K \sum_{\{{}^*p\}} \prod_{{}^*\ell \in \partial {}^*p} U_{{}^*\ell}\right). \tag{10.40}$$

Note that the sum in the exponent extends over all plaquettes of the dual lattice. Besides, the relation ${}^*K(K)$ is of the same form as in two dimensions,

$${}^*K = -\frac{1}{2}\log\tanh K. \tag{10.41}$$

10.3.1 Local Gauge Transformations

Let us now determine the set of configurations $\{U_{{}^*\ell}\}$ which are mapped into the same configuration $\{k_\ell\}$ by the mapping (10.37). Multiplying the group elements $U_{{}^*\ell}$ on all links ${}^*\ell$ ending at a fixed ${}^*x$ with -1 does not change $\{k_\ell\}$ and $\{U_{{}^*p_\ell}\}$ since every dual plaquette contains either two or none of these links. This operation may be performed at each site of the dual lattice independently such that there are 2^{V^*} equivalent configurations in each class. Thus we conclude that the variables $\{k_\ell\}$ and $\{U_{{}^*p}\}$ do not change under so-called *gauge transformations* of the dual-link variables,

$$U_{\langle {}^*x, {}^*y\rangle} \to U'_{\langle {}^*x, {}^*y\rangle} = g_{{}^*x} U_{\langle {}^*x, {}^*y\rangle} g^{-1}_{{}^*y}, \qquad g : {}^*\Lambda \to Z_2 = \{-1, 1\}. \tag{10.42}$$

They are examples of gauge invariant variables. Other gauge invariant objects are the so-called *Wilson loop variables*: for any closed path (loop) ${}^*\mathcal{C}$ on the dual lattice the gauge invariant loop variable is

$$W({}^*\mathcal{C}) = \prod_{\ell \in {}^*\mathcal{C}} U_{{}^*\ell} \in Z_2. \tag{10.43}$$

Now the question arises how to perform the sum in (10.40) over gauge-nonequivalent configurations $\{U_{{}^*\ell}\}$, i.e. configurations with different $k(U)$. There are two possible approaches: e.g. one *fixes the gauge* and picks from each gauge class

$$\{U_{\langle {}^*x, {}^*y\rangle}\} \sim \left\{g_{{}^*x} U_{\langle {}^*x, {}^*y\rangle} g^{-1}_{{}^*y}\right\} \equiv {}^g U_{\langle {}^*x, {}^*y\rangle} \tag{10.44}$$

one representative and sums over these representatives. Since equivalent configurations give the same contribution it does not matter which representatives are picked. Alternatively, one simply sums over *all* configurations $\{U_{{}^*\ell}\}$ in (10.40). Of course, we over-count, but since every class contains the same number of configurations this over-counting results in the same factor 2^{V^*}, independently of k. In doing so, we find for cubic lattices with $V = V^*$ the result

$$Z = (\cosh K \sinh K)^{3V/2} \cdot \sum_{\{U\}} \exp\left({}^*K \sum_{\{{}^*p\}} \prod_{{}^*\ell \in \partial {}^*p} U_{{}^*\ell}\right). \tag{10.45}$$

Since $\{g_{*x}\}$ entering a gauge transformation ${}^{g}U$ is a site-dependent lattice field we call the gauge transformation *local* and theories which admit a local (space-dependent) symmetry are called gauge theories. What we have proven then is that the three-dimensional Ising model is dual to a Z_2 *gauge theory*. This duality holds in both directions and the transformation is idempotent [6].

Finally, we may cast the gauge transformation (10.42) into a form that emphasizes the connection with electrodynamics in three Euclidean spacetime dimensions. We therefore write

$$U_{\langle *x,*y\rangle} = \exp(\mathrm{i}\pi A_{\langle *x,*y\rangle}), \quad g_{*x} = \exp(\mathrm{i}\pi\lambda_{*x}),$$

where the variables $A_{\langle *x,*y\rangle}$ and λ_{*x} belong to the additive group $\mathbb{Z}_2 = \{0, 1\}$. The gauge transformation (10.42) for the gauge potential A assumes the well-known form

$$A_{\langle *x,*y\rangle} \to A'_{\langle *x,*y\rangle} = A_{\langle *x,*y\rangle} + (\lambda_{*x} - \lambda_{*y}). \tag{10.46}$$

Since the last term between brackets represents the discretized gradient of the lattice field λ this formula is just the lattice version of the well-known gauge transformation $A'_\mu = A_\mu + \partial_\mu\lambda$ in electrodynamics.

10.4 Duality Transformation of Three-Dimensional Z_n Gauge Model

Here we extend the results of the previous section to Z_n models. This time the point of departure are the Z_n gauge theories which are mapped into Z_n spin models by the duality transformation. We shall use a slightly different method which emphasizes the close relationship between finite Fourier transformations and duality transformations [12]. The link variables of the Z_n gauge theory are elements of the multiplicative cyclic group, the elements of which can be written as

$$U_\ell = \mathrm{e}^{2\pi\mathrm{i}\theta_\ell/n}, \quad \theta_\ell \in \{0, 1, \ldots, n-1\}. \tag{10.47}$$

The θ_ℓ are in the additive group of integers with addition performed modulo n. As in the previous section we introduce the plaquette variables,

$$U_p = \prod_{\ell\in\partial p} U_\ell = \mathrm{e}^{2\pi\mathrm{i}\theta_p/n}, \quad \theta_p = \sum_{\ell\in\partial p} \theta_\ell, \tag{10.48}$$

where the orientation of a link on the boundary of a plaquette is inherited from the orientation of the plaquette. The real and gauge invariant energy function contains the sum over all plaquettes,

$$S = \sum_p (1 - \Re U_p) = \sum_p \left(1 - \cos\frac{2\pi\theta_p}{n}\right). \tag{10.49}$$

Here we interpret the energy function as Euclidean action of a lattice gauge theory with coupling constant g related to β according to $\beta = 1/g^2$. In the partition function one sums over the $3V$ link variables,

$$Z(\beta) = \sum_{\{\theta_\ell\}} \mathrm{e}^{-\beta S} = \mathrm{e}^{-3\beta V} \sum_{\{\theta_\ell\}} \prod_p \exp\left(\beta \cos \frac{2\pi\theta_p}{n}\right). \tag{10.50}$$

To extend the duality transformation from the Ising model to Z_n models we perform for each plaquette a finite Fourier transform on $\mathbb{Z}_n$,

$$\exp\left(\beta \cos \frac{2\pi\theta}{n}\right) = \sum_{k=0}^{n-1} c_k(\beta) \cos\left(\frac{2\pi\theta k}{n}\right). \tag{10.51}$$

At a fixed plaquette the Fourier coefficients are given by the inverse transformation

$$c_k(\beta) = \frac{1}{n} \sum_{\theta=0}^{n-1} \exp\left(\beta \cos \frac{2\pi\theta}{n}\right) \cos\left(\frac{2\pi\theta k}{n}\right). \tag{10.52}$$

Inserting the Fourier representation into (10.50) yields

$$\begin{aligned} Z(\beta) &= \mathrm{e}^{-3\beta V} \sum_{\{\theta_\ell\}} \prod_p \sum_{k_p=0}^{n-1} c_{k_p}(\beta) \exp\left(\frac{2\pi \mathrm{i} \theta_p k_p}{n}\right) \\ &= \mathrm{e}^{-3\beta V} \sum_{\{\theta_\ell\}} \sum_{\{k\}} \left(\prod_p c_{k_p}(\beta)\right) \exp\left(\sum_p \frac{2\pi \mathrm{i} \theta_p k_p}{n}\right). \end{aligned} \tag{10.53}$$

Writing every plaquette variable θ_p as a sum of link variables as in (10.48) the exponent takes the form

$$\frac{2\pi \mathrm{i}}{n} \sum_\ell \theta_\ell \sum_{p:\ell\in\partial p} k_p, \tag{10.54}$$

and the sum over θ_ℓ leads to the constraint

$$\sum_{p:\ell\in\partial p} k_p = 0 \bmod n, \tag{10.55}$$

where the summation symbol is defined to include the sign corresponding to the relative orientation of p and ℓ. The sum extends over the plaquettes of the staple belonging to ℓ, i.e. the plaquettes with a boundary containing the link ℓ. The staple of ℓ in Fig. 10.7 consists of the four plaquettes $p, \ldots, p''''$. To summarize, the sum over the configurations $\{\theta_\ell\}$ can calculated and yields

$$Z(\beta) = \mathrm{e}^{-3\beta V} \sum_{\text{constrained}\{k\}} \prod_p c_{k_p}. \tag{10.56}$$

To solve for the constraints it is convenient to switch to the dual lattice. With each link ℓ and plaquette p of the original lattice we associate the dual plaquette ${}^*p$ and

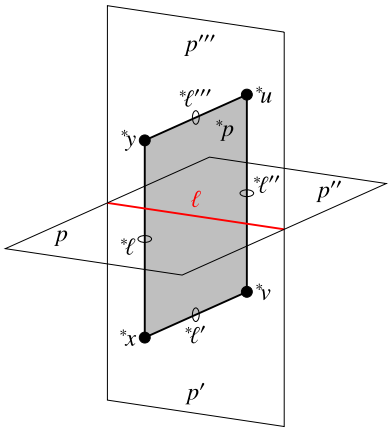

Fig. 10.7 The link ℓ is at the boundary of the four plaquettes p, p', p'' and p''' defining the staple belonging to the link. The links ${}^*\ell$, ${}^*\ell'$, ${}^*\ell''$ and ${}^*\ell'''$ dual to these plaquettes form a loop which encircles ℓ and form the boundary of the plaquette ${}^*p$ dual to ℓ

dual link ${}^*\ell$ of the dual lattice. One may write $k_p = k_{{}^*\ell}$ such that the constraint (10.55) can be written as

$$\sum_{{}^*\ell \in \partial {}^*p} k_{{}^*\ell} = 0 \bmod n. \tag{10.57}$$

We conclude that the configurations $\{k_{{}^*\ell}\}$ on the dual lattice have no circulation and thus can be written as gradients of Z_n-spin configurations on the dual lattice,

$$k_{{}^*\ell} = s_{{}^*x} - s_{{}^*y}, \tag{10.58}$$

where ${}^*x$ and ${}^*y$ are the two end points of ${}^*\ell$ and the difference is modulo n. In terms of the unconstrained spin variables $\{s_{{}^*x} | {}^*x \in {}^*\Lambda\}$ the partition function takes the form

$$Z(\beta) = \text{const} \times \sum_{\{s\}} \mathrm{e}^{-{}^*\beta {}^*S[s]}. \tag{10.59}$$

The action (energy) of the dual spin model is the sum of nearest neighbor terms,

$${}^*S[s] = \sum_{{}^*\ell} {}^*s(k_{{}^*\ell}), \quad k_{{}^*\ell} = s_{{}^*x} - s_{{}^*y}, \ {}^*\ell = \langle {}^*x, {}^*y \rangle, \tag{10.60}$$

and the nearest neighbor interaction is given by the Boltzmann weights

$$\mathrm{e}^{-{}^*\beta {}^*s(k)} = c_k(\beta) = \frac{1}{n} \sum_{\ell=0}^{n-1} \mathrm{e}^{\beta \cos(2\pi \ell/n)} \cos\left(2\pi \ell \frac{k}{n}\right), \quad k \in \mathbb{Z}_n. \tag{10.61}$$

Note that the contributions with ℓ and $n - \ell$ are identical. The Boltzmann weights of the Z_2, Z_3 and Z_4 spin models are listed in Table 10.1. For $n \leq 4$ we find the energy functions of the clock (planar Potts) models, see Sect. 6.2.2. In particular, for $n = 2$ we recover the nearest neighbor interaction of the 2-state clock model,

$${}^*\beta {}^*s(k) = \tilde{c}_0(\beta) - {}^*\beta \cos\left(\frac{2\pi k}{2}\right), \quad {}^*\beta = \frac{1}{2} \log \coth \beta, \tag{10.62}$$

Table 10.1 The Boltzmann weights $\exp[-{}^*\beta {}^*s(k)]$ for the Z_2, Z_3 and Z_4 spin models dual to gauge theories in three dimensions

n	$k=0$	$k=1$	$k=2$	$k=3$
2	$e^{\beta}+e^{-\beta}$	$e^{\beta}-e^{-\beta}$		
3	$e^{\beta}+2e^{-\beta/2}$	$e^{\beta}-e^{-\beta/2}$	$e^{\beta}-e^{-\beta/2}$	
4	$e^{\beta}+2+e^{-\beta}$	$e^{\beta}-e^{-\beta}$	$e^{\beta}-2+e^{-\beta}$	$e^{\beta}-e^{-\beta}$

Table 10.2 The critical couplings ${}^*\beta_c$ of the planar Potts models [13] and the corresponding critical couplings β_c of the dual Z_n spin systems in three dimensions

	$n=2$	$n=3$	$n=4$
${}^*\beta_c$(Potts models)	0.2217	0.367	0.4434
$\beta_c(Z_n$ gauge models)	0.7613	1.084	1.5226

which is equivalent to the ubiquitous Ising model, together with the already known dual coupling. Recall that k is the difference of neighboring spin variables. Similarly, the Z_3-gauge theory is dual to the 3-state clock model with nearest neighbor interaction

$$ {}^*\beta {}^*s(k) = \tilde{c}_0(\beta) - {}^*\beta \cos\left(\frac{2\pi k}{3}\right), \quad \beta^* = \frac{2}{3}\log\left(\frac{e^{\beta}+2e^{-\beta/2}}{e^{\beta}-e^{-\beta/2}}\right), \tag{10.63} $$

where $k \in \{0, 1, 2\}$. Finally, the Z_4 gauge theory is dual to the 4-state clock model with nearest neighbor interaction given by

$$ {}^*\beta {}^*s(k) = c_0(\beta) - {}^*\beta \cos\left(\frac{2\pi k}{4}\right), \quad {}^*\beta = \log\coth\frac{\beta}{2}, \tag{10.64} $$

which is equivalent to two copies of the Ising model. For $n > 4$ the dual models are not clock models but belong to the class of generalized Z_n spin models with energy functions (6.15).

The three-dimensional Ising model and more generally the n-state Potts model shows a phase transition from an ordered low-temperature phase into a disordered high-temperature phase at a critical point β_c. From the duality map we conclude that the dual gauge theory also shows a transition at ${}^*\beta_c = {}^*\beta(\beta_c)$. For small n the critical temperatures of the clock models are known [13] and the resulting critical couplings of the dual gauge theories are listed in Table 10.2.

10.4.1 Wilson Loops

Let us discuss the gauge invariant Wilson loops as correlation function. Recall that the Wilson loop $W_{\mathcal{C}}$ is the product of the link variables U_ℓ around a closed curve $\mathcal{C}$, where the orientation of ℓ is inherited from the orientation of the loop $\mathcal{C}$. Thus

$$ W_{\mathcal{C}} = \prod_{\ell\in\mathcal{C}} U_\ell = \exp\left(\frac{2\pi i}{n}\sum_{\ell\in\mathcal{C}}\theta_\ell\right). \tag{10.65} $$

The expectation value of Wilson loops

$$\langle W_{\mathcal{C}} \rangle = \frac{1}{Z(\beta)} \sum_{\theta_\ell} W_{\mathcal{C}}[\theta] e^{-\beta S[\theta]} \tag{10.66}$$

can be dualized similarly as the partition function. The constraint (10.55) is thereby changed to

$$\sum_{p:\ell \in \partial p} k_p + \delta_{\ell,\mathcal{C}} = 0 \bmod n, \tag{10.67}$$

where the additional term is 1 if $\ell \in \mathcal{C}$ and else is 0. On the dual lattice this additional term leads to the modified constraint

$$\sum_{^*\ell \in \partial^* p} k_{^*\ell} + \text{linking}\big(\partial^* p, \mathcal{C}\big) = 0 \bmod n, \tag{10.68}$$

where $\text{linking}(\partial^* p, \mathcal{C}) = 1$ if the boundary of the plaquette $^*p$ and the loop $\mathcal{C}$ are linked and otherwise is 0. Consider now an arbitrary surface $\mathcal{S}$ bounded by $\mathcal{C}$ and made up or plaquettes $p_1, \ldots, p_r$. Let $^*\ell_1, \ldots, ^*\ell_r$ be the variables on links dual to these plaquettes. They intersect the surface $\mathcal{S}$ such that the constraints are solved by

$$k_{^*\ell} = s_{^*x} - s_{^*x} + \text{intersect}\big(^*\ell, \mathcal{S}\big). \tag{10.69}$$

This then leads to the following result:

$$\langle W_{\mathcal{C}} \rangle = \left\langle \prod_{^*\ell \cap \mathcal{S} \neq 0} \frac{c_{^*\ell+1}}{c_{^*\ell}} \right\rangle, \tag{10.70}$$

where the expectation value is evaluated in the dual spin model with Boltzmann weights (10.61). In particular, when $\mathcal{C}$ is the boundary of a single plaquette with dual link $^*\ell$, we obtain

$$\langle W_p \rangle = \left\langle \frac{c_{^*\ell+1}}{c_{^*\ell}} \right\rangle. \tag{10.71}$$

Since the gauge action (energy) is proportional to the sum of the W_p we interpret $\langle W_p \rangle$ as average action density given by the derivative of the free energy density with respect to the coupling β. This means that an nth-order phase transition is a discontinuity in the $(n-1)$th derivative of $\langle W_p \rangle(\beta)$.

10.4.2 Duality Transformation of U(1) Gauge Model

Numerical and theoretical arguments indicate the absence of phase transitions in the three-dimensional $U(1)$ lattice gauge theory [12, 14, 15]. The model shows confinement for all values of the coupling β, analogous to the expected behavior of non-Abelian gauge theory in four dimensions. The theory is defined as the $n \to \infty$ limit of the Z_n gauge theories. In this limit a link variables

$$\frac{2\pi\theta_\ell}{n} \quad \text{with } \theta_\ell \in \mathbb{Z}_n \tag{10.72}$$

turn into real variables θ_ℓ with values in $[0, 2\pi)$ and the link variables $\exp(\mathrm{i}\theta_\ell)$ into elements of the Abelian group $U(1)$. The lattice action becomes

$$S = \sum_p (1 - \cos\theta_p), \quad \theta_p = \sum_{\ell \in \partial p} \theta_\ell, \tag{10.73}$$

and it is invariant under local gauge transformations

$$\theta_{\langle x,y\rangle} \to \theta_{\langle x,y\rangle} + \lambda_x - \lambda_y, \quad \lambda_{x,y} \in [0, 2\pi). \tag{10.74}$$

The sum over θ_ℓ in the Z_n-partition function (10.50) becomes an integral such that the partition function of the $U(1)$ model takes the form

$$Z(\beta) = \int \prod_\ell \mathrm{d}\theta_\ell \, \mathrm{e}^{-\beta S}. \tag{10.75}$$

with the action (10.73). The dual of the $U(1)$ gauge theory is the $n \to \infty$ limit of the spin systems dual to the Z_n gauge models. In particular the sum in (10.52) turns into an integral which can be expressed in terms of modified Bessel functions,

$$c_k(\beta) = \frac{1}{2\pi} \int_0^{2\pi} \mathrm{d}\theta \, \mathrm{e}^{\beta\cos\theta} \cos(k\theta) = I_k(\beta), \quad k \in \mathbb{Z}. \tag{10.76}$$

Now the sum defining the constraint (10.55) must vanish in $\mathbb{Z}$ and not only in $\mathbb{Z}_n$ such that the partition function has the dual representation

$$Z(\beta) = \text{const} \times \sum_{\{s\}} \prod_{\langle {}^*x, {}^*y\rangle} I_{s_{{}^*x} - s_{{}^*y}}(\beta), \tag{10.77}$$

where one averages over all spin configuration $\{s_{{}^*x} \in \mathbb{Z}\}$ defined on the sites of the dual lattice. For weak couplings one can use the approximation

$$I_k(\beta) \to \frac{\mathrm{e}^\beta}{\sqrt{2\pi\beta}} \mathrm{e}^{-k^2/4\beta} \quad \text{for } \beta \to \infty \tag{10.78}$$

to further simplify the partition function. Various expressions for the partition function in the weak-coupling regime and physical pictures of the phases have been obtained in [16].

10.5 Duality Transformation of Four-Dimensional Z_n Gauge Model

The dual of an Abelian lattice gauge theory in four dimensions is again an Abelian lattice gauge theory [4]. In particular, the Z_2, Z_3 and Z_4 systems are self-dual and show one phase transition at their self-dual points. Z_n gauge theories based on the Wilson action (10.49) are no longer self-dual for $n \geq 5$ and show two phase transitions with a massless phase appearing between the strong- and weak-coupling phases [17–19]. However, systems with gauge invariant Villain action [20] instead of the Wilson action are self-dual for all n.

To find the dual of the Z_n-gauge theory with Wilson action we proceed as in Sect. 10.4 up to the result (10.56). To solve the constraint (10.55) we again switch to the dual lattice. In four dimensions the dual of a plaquette p is a plaquette ${}^*p$ on the dual lattice and the dual of a link ℓ is a cube ${}^*c$ on the dual lattice. We set $k_p = \theta_{{}^*p}$. The constraint (10.55) on the original lattice translates into

$$\sum_{{}^*p \in \partial {}^*c} \theta_{{}^*p} = 0 \bmod n \tag{10.79}$$

on the dual lattice. Since the configuration $\{\theta_{{}^*p}\}$ has no circulation it can be written as (generalized) gradient of a configuration defined on the dual links,

$$\theta_{{}^*p} = \sum_{{}^*\ell \in \partial {}^*p} \theta_{{}^*\ell}, \tag{10.80}$$

where the summation symbol is defined to include the sign corresponding to the relative orientation of ${}^*p$ and ${}^*\ell \in \partial {}^*p$. In terms of the unconstrained link variables $\{\theta_{{}^*\ell}\}$ the partition function takes the form

$$Z(\beta) = \text{const} \times \sum_{\{\theta_{{}^*\ell}\}} \mathrm{e}^{-{}^*\beta {}^*S}, \tag{10.81}$$

where the action contains a sum over the plaquettes of the dual lattice,

$${}^*S = \sum_{{}^*p} {}^*s(\theta_{{}^*p}). \tag{10.82}$$

The contribution of a single plaquette to the Boltzmann weight is

$$\mathrm{e}^{-{}^*\beta {}^*s(\theta)} = \sum_{\ell=0}^{n-1} \mathrm{e}^{\beta \cos(2\pi \ell/n)} \cos\left(2\pi \ell \frac{\theta}{n}\right). \tag{10.83}$$

From Table 10.1 we can read off the single plaquette action of the dual Z_2, Z_3 and Z_4 gauge models. They define the Wilson actions

$${}^*S(\theta_p) = \text{const}(\beta) - \sum_{{}^*p} \cos\left(\frac{2\pi \theta_{{}^*p}}{n}\right), \quad n = 2, 3, 4, \tag{10.84}$$

on the dual lattice with dual couplings ${}^*\beta = {}^*\beta(\beta)$ given below Table 10.1. We conclude that the Z_2, Z_3 and Z_4 gauge models with Wilson action are self-dual in four dimensions. If any of these models possess one critical coupling, then it must be the self-dual coupling defined by ${}^*\beta = \beta$. The self-dual couplings for the Z_2, Z_3, and Z_4 gauge theories are listed in Table 10.3.

Probably the most attractive feature of duality transformations is the relation between strong-coupling and weak-coupling regimes, or between high temperature and low temperature phases of dual theories. For small couplings we can trust weak-coupling perturbation theory and with duality we may use the perturbative results to study the non-perturbative sector of the dual theory. Further results on dualities, in particular on the representation of various correlation functions in the dual model can be found in the reviews cited at the end of this chapter.

Table 10.3 Self-dual couplings $\beta(^*\beta = \beta)$ of the Z_n gauge theories in four dimensions

	$n=2$	$n=3$	$n=4$
$\beta_{\text{self-dual}}$	$\frac{1}{2}\log(1+\sqrt{2})$ ≈ 0.44069	$\frac{2}{3}\log(1+\sqrt{3})$ ≈ 0.67004	$\log(1+\sqrt{2})$ ≈ 0.88137

10.6 Problems

10.1 (Self-duality of Potts chain in magnetic field) We wish to show that the q-state Potts chain with partition function (8.34) admits a duality transformation. To this aim we consider the auxiliary function

$$\begin{aligned}\tilde{Z}_\Lambda(\zeta,z) &= \big((\zeta-1)(z-1)\big)^{-N/2} Z_\Lambda(\zeta,z)\\ &= q'\left(\frac{\zeta-1}{z-1}\right)^{N/2} + \left(\frac{\lambda_+^2}{(\zeta-1)(z-1)}\right)^{N/2} + \left(\frac{\lambda_-^2}{(\zeta-1)(z-1)}\right)^{N/2}\end{aligned}$$

depending on the couplings $z = \mathrm{e}^{2\beta h}$ and $\zeta = \mathrm{e}^{\beta J}$.

1. Show that $\tilde{Z}$ is invariant under duality transformation

$$\big({}^*\zeta - 1\big)(z-1) = q, \qquad \big({}^*z - 1\big)(\zeta - 1) = q$$

according to

$$\tilde{Z}_\Lambda(\zeta,z) = \tilde{Z}_\Lambda\big({}^*\zeta, {}^*z\big).$$

Actually all three terms between brackets in the right hand side of the formula for $\tilde{Z}_\Lambda$ are invariant.

2. Show that the duality relations relating the old to the new couplings define two broken linear Möbius transformations

$${}^*\zeta = \frac{z+q-1}{z-1} \quad \text{and} \quad {}^*z = \frac{\zeta+q-1}{\zeta-1},$$

and these transformations map circles to circles.

3. The partition function of the *Ising chain* is given by

$$Z_\Lambda(\zeta,z) = \left(\frac{(\zeta-1)(z-1)}{({}^*\zeta-1)({}^*z-1)}\right)^{N/2} Z_\Lambda\big({}^*\zeta, {}^*z\big),$$

and in Sect. 8.7.1 we determined the Lee–Yang zeros of the partition function in the complex fugacity plane. Use the duality transformation to show that the zeros of the partition function in the complex ζ-plane (for fixed $\beta h \in \mathbb{R}$) are on the imaginary axis. Compare your results with [21].

10.2 (Self-duality of two-dimensional Potts models) Prove that the standard q-state Potts model without external field is self-dual in two dimensions. Its energy function is given in (6.10) wherein $h = 0$. Show that the relation between the couplings of the Potts model and dual Potts model is given by (10.29). Use this result to find the critical temperature of the two-dimensional Potts models.

10.3 (Dual of Z_6-gauge theory in three dimensions) Calculate the dual model of the Z_6 gauge theory with Wilson action in three dimensions. Show that the dual model belongs to the class of *generalized* Potts models.

References

1. R. Peierls, Statistical theory of adsorption with interaction between the adsorbed atoms. Proc. Camb. Philos. Soc. **32**, 471 (1936)
2. H.A. Kramers, G.H. Wannier, Statistics of the two-dimensional ferromagnet. Part I. Phys. Rev. **60**, 252 (1941)
3. H.A. Kramers, G.H. Wannier, Statistics of the two-dimensional ferromagnet. Part II. Phys. Rev. **60**, 263 (1941)
4. F. Wegner, Duality in generalized Ising models and phase transitions without local order parameter. J. Math. Phys. **12**, 2259 (1971)
5. L. Kadanoff, Lattice Coulomb representations of two-dimensional problems. J. Phys. A **11**, 1399 (1978)
6. R. Savit, Duality in field theory and statistical systems. Rev. Mod. Phys. **52**, 453 (1980)
7. C. Gruber, A. Hintermann, D. Merlini, *Group Analysis of Classical Lattice Systems*. Lecture Notes in Physics, vol. 60 (Springer, Berlin, 1977)
8. J.L. Lebowitz, A.E. Mazel, Improved Peierls argument for high-dimensions Ising models. J. Stat. Phys. **90**, 1051 (1998)
9. F.Y. Wu, The Potts model. Rev. Mod. Phys. **54**, 235 (1982) [Erratum-ibid **55**, 315 (1983)]
10. L. von Smekal, Universal aspects of QCD-like theories. Nucl. Phys. Proc. Suppl. **228**, 179 (2012)
11. W. Schwalm, B. Moritz, M. Giona, M. Schwalm, Vector difference calculus for physical lattice models. Phys. Rev. E **59**, 1217 (1999)
12. G. Bhanot, M. Creutz, Phase diagram of $Z(N)$ and $U(1)$ gauge theories in three dimensions. Phys. Rev. D **21**, 2892 (1980)
13. W.J. Blöte, R.H. Swendsen, First order phase transitions and the three state Potts model. J. Appl. Phys. **50**, 7382 (1979)
14. A.M. Polyakov, Compact gauge fields and the infrared catastrophe. Phys. Lett. B **59**, 82 (1975)
15. A.M. Polyakov, Quark confinement and topology of gauge groups. Nucl. Phys. B **120**, 429 (1977)
16. T. Banks, R. Myerson, J. Kogut, Phase transitions in Abelian lattice gauge theories. Nucl. Phys. B **129**, 493 (1977)
17. J.M. Drouffe, Series analysis in four-dimensional Z_n lattice gauge systems. Phys. Rev. D **18**, 1174 (1978)
18. M. Creutz, L. Jacobs, C. Rebbi, Experiments with a gauge invariant Ising system. Phys. Rev. Lett. **42**, 1390 (1979)
19. A. Ukawa, P. Windey, A.H. Guth, Dual variables for lattice gauge theories and the phase structure of $Z(N)$ systems. Phys. Rev. D **21**, 1023 (1980)
20. J. Villain, Theory of one- and two-dimensional magnets with an easy magnetization plane. II. The planar, classical, two-dimensional magnet. J. Phys. **36**, 581 (1975)
21. F.Y. Wu, Self-dual property of the Potts model in one dimension. cond-mat/9805301

Chapter 11
Renormalization Group on the Lattice

Previously we considered a variety of equilibrium systems which undergo second order phase transitions. In this chapter we will show how the idea of scaling leads to a universal theory of critical phenomena, and we will derive some exact results for order–disorder transitions.

Simulations of systems with second order transition characterized by an order parameter show typical configurations in the high- and low-temperature phases and in the vicinity of a critical point. Characteristic configurations of the two-dimensional Ising model near the critical temperature are depicted in Fig. 11.1. At high temperature the spins are randomly oriented and there is only a short-range correlation between the fluctuating spins. With increasing temperature the system becomes more and more disordered, the already small regions of aligned spins become even smaller and the correlation length tends to zero. At low temperature, on the other hand, we typically see aligned spins within macroscopic *domains* and some few, finite regions with an opposite alignment. With decreasing temperature the fluctuations over the mean field become more and more decorrelated and as a result the correlation length decreases when we cool the system. When we approach the critical point by heating the system in the low-temperature phase or cooling it in the high temperature phase then long wave length excitations are most easily excited and dominate the properties in the critical region. At the critical point there are domains of arbitrary size and we may not distinguish between images taken at different length scales. The observed scale invariance is rather unusual since specific physical systems usually have specific scales. Therefore, in the vicinity of a critical point these specific scales must in some sense become irrelevant.

What happens to typical configurations in the high- and low-temperature phases when we gradually change the scale (and not the temperature) by some coarse-graining procedure, for example by decreasing the resolution of our microscope? In the disordered high-temperature phase the small domains become even smaller and this has the same effect as an increase in temperature. In contrast, in the ordered low-temperature phase the typical size of the macroscopic domains shrink and this effect is similar to the one obtained by lowering the temperature of the system. In either case a change in scale with decimation factor $b > 1$ decreases the correla-

A. Wipf, *Statistical Approach to Quantum Field Theory*, Lecture Notes in Physics 864,
DOI 10.1007/978-3-642-33105-3_11,

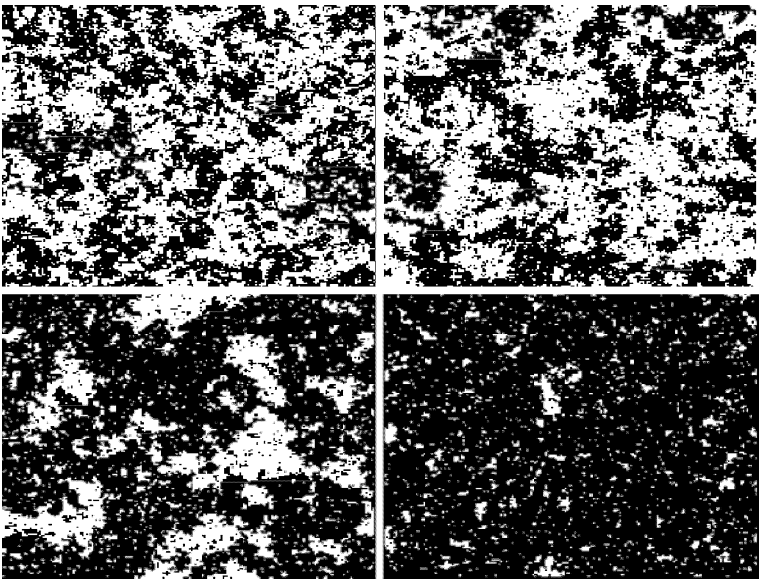

Fig. 11.1 Typical configurations from Monte Carlo simulations above and below the critical temperature $T_c = 2.2692$. The configurations belong to ensembles with $T = 2.5$ (*upper left*), $T = 2.4$ (*upper right*), $T = 2.3$ (*lower left*) and $T = 2.2$ (*lower right*)

tion length and drives the system away from its critical point. Only at criticality, where the correlation length diverges, does a typical configuration not change under coarse graining. These considerations lead to the natural question whether a scale transformation is indeed equivalent to a change in temperature and of further coupling constants. Thereby the word equivalent means that the partition function and correlation functions do not alter.

K. WILSON was awarded the Nobel prize for his major contributions to the physics of scale transformations or more generally of renormalization group (RG) transformations. This non-perturbative approach to the description of critical phenomena has become a very powerful tool in statistical physics as well as in quantum field theory. Early contributions to quantum field theory and particle physics have been obtained by STUECKELBERG, PETERMAN, GELL-MAN, LOW and by BREZIN. Some ten years later KADANOV [1], FISHER [2, 3] and WILSON [4–6] developed the renormalization group method in statistical systems. The textbooks [7–11] present the renormalization group approach within quantum field theory and statistical physics with applications to critical phenomena. The following sections are devoted to the following problem: What general properties of the system may be extracted from RG transformations?

There are many ways to construct scale transformations or more general RG transformations. Examples of real space RG transformations are the cumulant method, finite-cluster method, Migdal–Kadanov transformation and Monte Carlo renormalization. In particular, the latter method yields precise values for the critical

exponents and will be discussed. Alternatively one may set up the RG transformation in momentum space with continuous momenta in the Brilloin zone. The momentum space RG transformation may be performed by integrating out the high momentum modes. Since high momenta correspond to *short* length scales, this amounts to a coarse-gaining in real space. In momentum space the rescaling factor may be continuous and arbitrarily close to 1. Hence we may consider infinitesimal transformations. Examples of momentum space RG transformations include the ε expansion, Callan–Symanzik equation and functional renormalization group equations. The latter can be formulated in the continuum and will be discussed in Chap. 12.

11.1 Decimation of Spins

The decimation of spins can be done exactly for the Ising chain with external field. The "thinned out" system is identical to the original system at different temperature and with different external field. However, for spin systems in two and more dimensions each decimation of spins generates new terms in the energy function and the iterated decimation cannot be performed analytically as for the Ising chain.

11.1.1 Ising Chain

We consider the partition function of the periodic Ising chain with N spins and energy proportional to

$$-\beta H = K \sum_{x=1}^{N} s_x s_{x+1} + h \sum_{x=1}^{N} s_x \quad \text{with } K = \beta J. \tag{11.1}$$

We assume N to be an even number. Summing only over every second spin ($b = 2$), i.e. over spins at even lattice points, the partition function takes the form

$$\begin{aligned} Z(N, K, h) &= \sum_{s_1, s_2, \ldots} \mathrm{e}^{K s_1 s_2 + \frac{1}{2} h (s_1 + s_2)} \mathrm{e}^{K s_2 s_3 + \frac{1}{2} h (s_2 + s_3)} \times \cdots \\ &= \sum_{s_1, s_2, \ldots} \mathrm{e}^{K (s_1 s_2 + s_2 s_3) + \frac{1}{2} h (s_1 + 2 s_2 + s_3)} \times \cdots \\ &= \sum_{s_1, s_3, \ldots} \left(\mathrm{e}^{(K + \frac{1}{2} h)(s_1 + s_3) + h} + \mathrm{e}^{-(K - \frac{1}{2} h)(s_1 + s_3) - h} \right) \cdots . \end{aligned} \tag{11.2}$$

Thus, after decimation we obtain an Ising-type system with spins located at the odd lattice points. We now may introduce new coupling constants K', h' as well as a function $g(K, h)$ such that

$$\mathrm{e}^{(K + \frac{1}{2} h)(s_1 + s_3) + h} + \mathrm{e}^{-(K - \frac{1}{2} h)(s_1 + s_3) - h} = \mathrm{e}^{2 g(K, h)} \mathrm{e}^{K' s_1 s_3 + \frac{1}{2} h' (s_1 + s_3)}. \tag{11.3}$$

We shall calculate the new couplings and g at a later stage. Inserting the expression (11.3) for every factor in (11.2) yields the partition function on the thinned out lattice with couplings K', h':

$$\begin{aligned} Z(N,K,h) &= \mathrm{e}^{Ng} \sum_{s_1,s_3,\ldots} \mathrm{e}^{K's_1s_3+\frac{1}{2}h'(s_1+s_3)} \mathrm{e}^{K's_3s_5+\frac{1}{2}h'(s_3+s_5)} \times \cdots \\ &= \mathrm{e}^{Ng} Z\left(\frac{N}{2}, K', h'\right). \end{aligned} \tag{11.4}$$

We summarize this remarkable result: the decimation of spins reproduces the Ising model on the thinned out chain with twice the lattice spacing. The energy on the coarser lattice has the same functional form as on the microscopic lattice,

$$\beta H \to \beta' H' - g(K,h)N, \qquad -\beta' H' = K' \sum_{x' \text{odd}} s_{x'} s_{x'+2} + h' \sum_{x' \text{odd}} s_{x'}. \tag{11.5}$$

We have used a very particular *decimation procedure* to get to this transformation of the energy function. Other decimation procedures, where the set of degrees of freedom after decimation is not necessarily a subset of the original degrees of freedom shall be discussed below.

In order to extract the new coupling constants we evaluate Eq. (11.3) for three different configurations of the two spins (s_1, s_3). We have

$$\begin{aligned} (s_1,s_3) = (1,1): &\qquad 2\mathrm{e}^{h}\cosh(2K+h) = \mathrm{e}^{2g}\mathrm{e}^{K'+h'}, \\ (s_1,s_3) = (-1,-1): &\qquad 2\mathrm{e}^{-h}\cosh(2K-h) = \mathrm{e}^{2g}\mathrm{e}^{K'-h'}, \\ (s_1,s_3) = (1,-1): &\qquad 2\cosh(h) = \mathrm{e}^{2g}\mathrm{e}^{-K'}. \end{aligned}$$

Solving these equations for K', h' and g, we obtain the map

$$\begin{aligned} K \xrightarrow{R_2} K' &= \frac{1}{4}\log\frac{\cosh(2K+h)\cosh(2K-h)}{\cosh^2 h}, \\ h \xrightarrow{R_2} h' &= h + \frac{1}{2}\log\frac{\cosh(2K+h)}{\cosh(2K-h)}, \\ g(K,h) &= \frac{1}{8}\log\bigl(16\cosh(2K+h)\cosh(2K-h)\cosh^2 h\bigr). \end{aligned} \tag{11.6}$$

Figure 11.2 shows the trajectories of the couplings in the (K,h)-plane after the repeated application of the decimation transformation R_2. The decimation doubles the distance between neighboring lattice sites as sketched in Fig. 11.3 and this scale factor appears as index or R. The initial couplings in the plot are $K = 2$ and $h \in \{\pm 0.2, \pm 0.05, 0\}$. The series of points

$$(K,h) \xrightarrow{R_2} \bigl(K',h'\bigr) \xrightarrow{R_2} \bigl(K'',h''\bigr) \xrightarrow{R_2} \bigl(K''',h'''\bigr) \xrightarrow{R_2} \cdots$$

in the plane of couplings is *attracted* to the axis $K = 0$. This means that the nearest neighbor coupling K decreases for every decimation of spins. If the magnetic field of the microscopic system is zero then it stays zero since the Z_2 symmetry without field is preserved by the decimation map. Thus the line $h = 0$ is a trajectory of

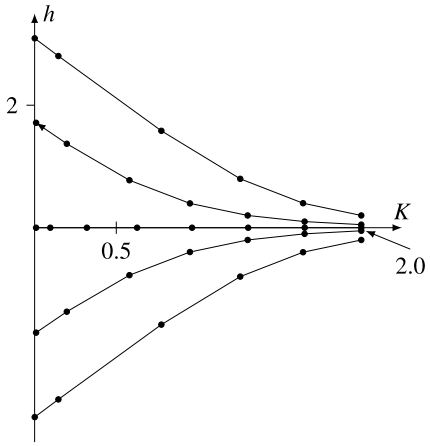

Fig. 11.2 The flow of the couplings (K, h) under repeated application of the decimation transformation R_2 for the Ising chain. For the chain the exact transformation is known and reproduces the energy function with nearest neighbor coupling. The same flow expressed in terms of the variables e^{-2h} and e^{-2K} has been obtained in [12]

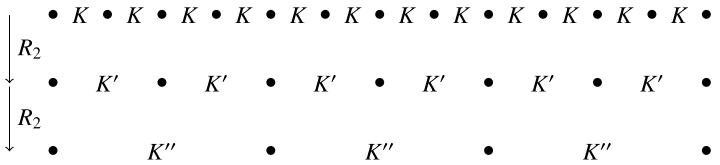

Fig. 11.3 Decimation of degrees of freedom by successive blocking transformations. Each decimation R_2 reproduces the energy function with different couplings and doubles the distance between nearest neighbors

the renormalization group (RG). More generally, if R_b is a renormalization group transformation with scaling factor b, then we have

$$R_b \circ R_b = R_{b^2}. \tag{11.7}$$

Note that there is no inverse of R_b, since we cannot reverse the procedure of integrating out degrees of freedom. Hence the transformations R_b form only a semigroup and not a group.

Let us see how the partition functions on the microscopic lattice and on the coarse-grained lattices are related when R_2 is repeated several times. For two decimations the relation (11.4) leads to

$$Z(N, K, h) = e^{Ng(K,h)} e^{\frac{1}{2}Ng(K',h')} Z\left(\frac{N}{4}, K'', h''\right). \tag{11.8}$$

Further iterations yield the following relation between the free energy densities of the microscopic and coarse-grained systems,

$$f(K,h) = -\frac{1}{\beta}\left(g(K,h) + \frac{1}{2}g\big(K',h'\big) + \frac{1}{2^2}g\big(K'',h''\big) + \frac{1}{2^3}g\big(K''',h'''\big) + \cdots\right). \tag{11.9}$$

Note that the function g has the same form for every iteration step. For simplicity we consider the decimation without magnetic field,

$$K' = R_2(K) = \frac{1}{2}\log\cosh(2K), \qquad g = \frac{1}{4}\log\bigl(4\cosh(2K)\bigr). \tag{11.10}$$

Only the couplings $K = 0$ and $K = \infty$ are inert under decimation—they are *fixed points* of the RG transformation R_2. These two couplings represent the high-temperature and low-temperature fixed points of the Ising chain.

The previous derivation shows that the correlation between two spins defined on both the microscopic and diluted lattice is the same before and after decimation,

$$\begin{aligned}&\frac{1}{Z(N,K)}\sum_{\Omega} s_{x'}s_{y'}\exp\biggl(K\sum_{\langle u,v\rangle} s_u s_v\biggr)\\ &\quad=\frac{1}{Z(\frac{1}{2}N,K')}\sum_{\Omega'} s_{x'}s_{y'}\exp\biggl(K'\sum_{\langle u',v'\rangle} s_{u'}s_{v'}\biggr).\end{aligned}$$

In the decimation (11.4) the sites x' and y' must be odd lattice points. Now we rescale the coarse-grain lattice such that the distance between neighboring sites shrinks from 2 to 1. Thus, if two points are separated by a distance $2n$ on the microscopic lattice, then they are separated by a distance n on the rescaled coarse-grained lattice. It follows that the two-point correlation

$$\langle s_x s_y\rangle \sim \mathrm{e}^{-|x-y|/\xi}, \quad |x-y| \gg \xi \tag{11.11}$$

falls off faster after decimation and rescaling. We conclude that every transformation R_2 halves the correlation length ξ, i.e.

$$\xi' = \frac{\xi}{2}. \tag{11.12}$$

According to (8.18) the correlation length diverges at the low-temperature fixed point and vanishes at the high-temperature fixed point. The low-temperature fixed point is a critical point, whereas at the high-temperature fixed point the interaction vanishes. The RG trajectories flow into the trivial fixed point with $\xi = 0$ since the coupling constant K and correlation length ξ both decrease with every decimation of spins.

11.1.2 The Two-Dimensional Ising Model

Let us consider the two-dimensional Ising model without external field, given by

$$\beta H = -K\sum_{\langle x,y\rangle} s_x s_y. \tag{11.13}$$

We shall see that the decimation generates, besides nearest-neighbor interactions, interactions between next-nearest neighbors. Iterating the decimation generates interactions between widely separated spins.

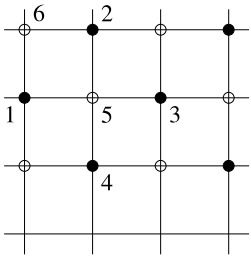

Fig. 11.4 In one decimation step one sums over the spins on the lattice sites marked with *open circles*

Again we consider the sum over all configuration in the partition function. In the decimation we sum over the spins marked by open circles in Fig. 11.4 and thus construct an effective spin model with spins located at the filled circles. These sites define the coarse-grained lattice. For example, the contribution of the spin located at lattice site denoted by 5 is given by

$$\sum_{s_5=\pm 1} \mathrm{e}^{K s_5(s_1+s_2+s_3+s_4)} = \mathrm{e}^{K(s_1+s_2+s_3+s_4)} + \mathrm{e}^{-K(s_1+s_2+s_3+s_4)}. \tag{11.14}$$

The most general Boltzmann weight involving s_1, s_2, s_3 and s_4 compatible with the symmetries of the system has the form

$$\mathrm{e}^{2g} \exp\left(\frac{1}{2} K_1' \underbrace{(s_1 s_2 + s_2 s_3 + s_3 s_4 + s_4 s_1)}_{\mathrm{NN}} + K_2' \underbrace{(s_1 s_3 + s_2 s_4)}_{\mathrm{nNN}} + K_3' \underbrace{(s_1 s_2 s_3 s_4)}_{\mathrm{Q}} \right),$$

where (NN) and (nNN) denote nearest neighbors and next-nearest neighbors and (Q) represents squares. The last two expressions are equal for all configurations of spins s_1, s_2, s_3 and s_3 if the following independent equations are satisfied:

$$\begin{aligned}
&(s_1, s_2, s_3, s_4) = (1, 1, 1, 1): && 2\cosh(4K) = \mathrm{e}^{2g} \mathrm{e}^{2K_1' + 2K_2' + K_3'}, \\
&(s_1, s_2, s_3, s_4) = (1, -1, -1, -1): && 2\cosh(2K) = \mathrm{e}^{2g} \mathrm{e}^{-K_3'}, \\
&(s_1, s_2, s_3, s_4) = (1, 1, -1, -1): && 2 = \mathrm{e}^{2g} \mathrm{e}^{-2K_2' + K_3'}, \\
&(s_1, s_2, s_3, s_4) = (1, -1, 1, -1): && 2 = \mathrm{e}^{2g} \mathrm{e}^{-2K_1' + 2K_2' + K_3'}.
\end{aligned}$$

Solving these equations for the new couplings, we obtain the relations

$$\begin{aligned}
K_1' &= 2K_2' = \frac{1}{4} \log\cosh(4K), \\
K_3' &= \frac{1}{8} \log\cosh(4K) - \frac{1}{2} \log\cosh(2K), \\
g &= \frac{1}{16} \big(\log\cosh(4K) + \log\cosh(2K) + 8 \log 2 \big).
\end{aligned} \tag{11.15}$$

We get such contributions from all spins on the open circles. Thereby a term like $\exp(K_1' s_1 s_2/2)$ occurs in the sum over s_6 as well. Denoting the spin configuration on the coarse-grained lattice by ω' we can write

$$Z(V,K) = Z'\left(\frac{V}{2}, K'\right) = \sum_{\omega'} \mathrm{e}^{-(\beta H)'(\omega')}. \tag{11.16}$$

The so-called *Landau–Ginzburg–Wilson* energy function

$$-(\beta H)' = Vg + K_1' \sum_{\mathrm{NN}} s_{x'} s_{y'} + K_2' \sum_{\mathrm{nNN}} s_{x'} s_{y'} + K_3' \sum_{\mathrm{Q}} s_{x'} s_{y'} s_{u'} s_{v'}, \tag{11.17}$$

where x', y', u', v' are sites on the dilute lattice, is not of the same form as the energy function of the microscopic system.

If we iterated the decimation without approximation, we would generate more and more terms involving interactions between widely separated spins. To proceed analytically one needs some sort of truncation. In a first attempt we could set the coupling constants $K_2' = K_3'$ equal to zero, but this approximation would be quite insufficient. This becomes apparent by inspecting the fixed points which are simply $K_1 = 0$ and $K_1 = \infty$ as in the one-dimensional model. Thus we would *not* observe any phase transition. A better approximation is to set $K_3 = 0$ and to count next-nearest neighbors as nearest neighbors. With this truncation the partition function becomes

$$Z(V,K) = \mathrm{e}^{Vg} \sum_{\omega'} \exp\left(K' \sum_{\langle x', y' \rangle} s_{x'} s_{y'}\right), \quad K' = K_1' + K_2'. \tag{11.18}$$

Inserting the results in (11.15) we find the renormalization group map

$$K \to K'(K) = \frac{3}{8} \log\cosh 4K, \tag{11.19}$$

which is depicted in Fig. 11.5. The map has fixed points at $K = 0$, $K = \infty$ and at

$$K^* = 0.50698. \tag{11.20}$$

This is reasonably close to the known critical point $K_c = 0.4407$. Actually the fixed point is instable: starting at $K \neq K^*$, the flow drives the system either to the high-temperature fixed point at $K = 0$ or the low-temperature fixed point at $K = \infty$.

11.2 Fixed Points

We now turn towards a more general discussion of the RG method. For this purpose we consider a d-dimensional lattice model, characterized by its coupling constants

$$K = \{K_A | A \subset \Lambda\} = (K_1, K_2, \ldots), \tag{11.21}$$

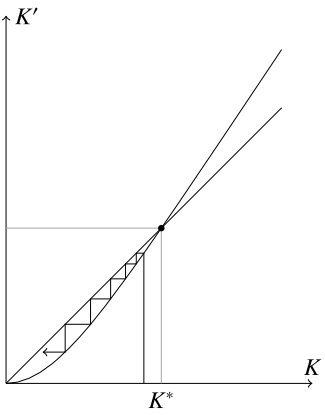

Fig. 11.5 The fixed point of the truncated block-spin transformation (11.19). The non-trivial fixed point at $K^* = 0.50698$ is unstable

where we enumerated the subsets of the lattice.[1] The set of couplings should be complete in the following sense: A RG transformation that substitutes b^d microscopic degrees of freedom on the lattice Λ by one degree of freedom on the coarser lattice Λ' leads to an *energy function* with the same kind of interactions as the energy function of the original system. Thus, starting with the energy function of the form

$$H(\omega) = -\sum_{A\subset\Lambda} K_A s_A, \quad s_A = \prod_{x\in A} s_x, \tag{11.22}$$

the renormalized energy function on Λ' has the same form, up to an additive extensive constant,

$$H(\omega) \to H'(\omega') - Vg(K), \quad H'(\omega') = -\sum_{A\subset\Lambda'} K'_A S_A, \tag{11.23}$$

where A denotes the same set as in (11.21). We thereby assume a set $\{A\}$ to exist on the original lattice as well as on the diluted lattice. Furthermore we assume the reduced degrees of freedom $S_{x'}$ to exhibit the same algebraic properties as the s_x.

Note that the constant term $Vg(K)$ in (11.23) occurs in all RG transformations. Unfortunately, only simple models as the Ising chain may be described by a *finite* number of couplings. However, we may assume the couplings K_A corresponding to long-range interactions are suppressed and thus may be neglected. Hence, in practice, we work with a finite number of coupling constants $\{K_1, \ldots, K_n\}$. A dilution of the system changes the couplings according to the *renormalization group map*

$$K'_i = R_i(K_1, K_2, \ldots), \tag{11.24}$$

where the partition function remains unchanged, i.e.

$$\mathrm{e}^{-F(V,K)} = \sum_{\omega\in\Omega} \mathrm{e}^{-H(\omega)} = \mathrm{e}^{Vg(K)} \sum_{\omega'\in\Omega'} \mathrm{e}^{-H'(\omega')} = \mathrm{e}^{Vg(K)-F(V',K')}. \tag{11.25}$$

[1] $x \in A$ may appear several times, similarly as in Sect. 8.6.

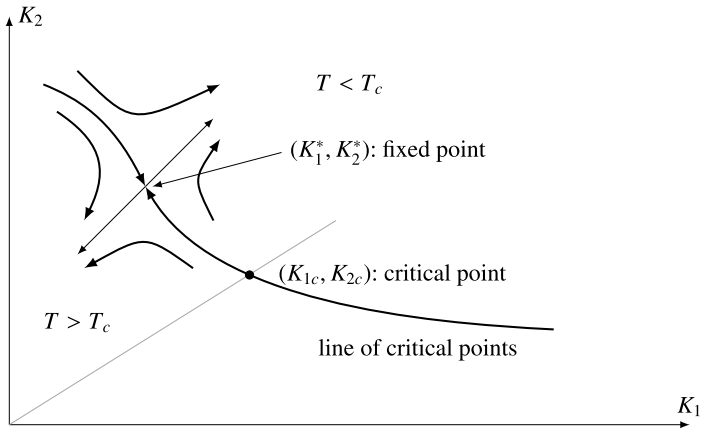

Fig. 11.6 The fixed point K^* has one relevant and one irrelevant direction

Now we assume that the thermodynamic limit $V \to \infty$ exists. Hence, the free energy densities of the two systems are related by the recursion relation

$$f(K) = b^{-d} f\left(K'\right) - g(K), \qquad V = b^d V' \tag{11.26}$$

in the thermodynamic limit. This relation is quite familiar since it occurred in (11.5) in connection with the Ising chain. We have already argued that a *fixed point* K^* of the RG transformation either defines a critical point of the system characterized by a divergent correlation length $\xi_c = \infty$ or belongs to a non-interacting system with vanishing correlation length $\xi = 0$. The converse needs not be true, i.e. there may exist critical points which are *no* fixed points.

Now let us consider a two-dimensional space of couplings (K_1, K_2), where we denote the critical couplings by $K_c = (K_{1c}, K_{2c})$. The generic case as illustrated in Fig. 11.6 shows a *line of critical points*, where K^* lies on this curve. This may be explained as follows: since we absorbed the temperature in the couplings, a change of temperature in

$$(K_{1c}, K_{2c}) = (\beta J_1, \beta J_2)$$

is equivalent to a dilation in the space of coupling $\{K_i\}$. Thus, when we lower the temperature then we move away from $K = 0$ on a ray with constant ratio K_2/K_1 and expect to find a critical point at some critical temperature T_c. This temperature will depend on this ratio K_2/K_1 and when the ratio changes, then the point

$$(K_{1c}, K_{2c}) = \left(\frac{J_1}{T_c}, \frac{J_2}{T_c}\right)$$

describes a curve in the (K_1, K_2)-plane. If we admit more couplings we expect to find critical hyper-surfaces on which $\xi = \infty$ instead of critical lines.

Let us now see how the properties of a statistical system are related to its critical points, critical surfaces or fixed points. Some simple properties of the RG flow are:

- Near the critical surface a RG trajectory moves away from the surface, since $\xi = \infty$ on the surface and every RG transformation reduces ξ.
- A RG transformation cannot change the phase of the system, since a dilution of the system cannot generate order from disorder and vice versa.
- If we start above the critical temperature then the system should evolve to the free fixed point, characterized by $T = \infty$. In contrast, if we start below the critical temperature then we should end up at the "ground state" fixed point $T = 0$.
- If the flow begins exactly on the critical surface then it stays on this surface, since $\xi = \infty$ implies $\xi' = \xi/b = \infty$.
- It is the exception and not the rule that a critical point is a fixed point. In general we expect a finite set of isolated fixed points. Only in lower-dimensional systems there may be an infinite set of fixed points.

11.2.1 The Vicinity of a Fixed Point

Let $K^* = (K_1^*, K_2^*, \ldots)$ be a fixed point of the RG transformation,

$$K^* = R\big(K^*\big). \tag{11.27}$$

To examine the RG flow in the vicinity of K^* we write $K = K^* + \delta K$ and linearize the flow around the fixed point,

$$K_i' = K_i^* + \delta K_i' = R_i\big(K_j^* + \delta K_j\big) = K_i^* + \left.\frac{\partial R_i}{\delta K_j}\right|_{K^*} \delta K_j + O\big(\delta K^2\big).$$

We read off the linearized RG transformation,

$$\delta K_i' = \sum_j M_i^j \delta K_j, \quad M_i^j = \left.\frac{\partial R_i}{\partial K_j}\right|_{K^*}. \tag{11.28}$$

This linear map determines the flow in the vicinity of the critical point. It is characterized by the eigenvalues and left-eigenvectors of the associated matrix M,

$$\sum_j \Phi_\alpha^j M_j^i = \lambda_\alpha \Phi_\alpha^i = b^{y_\alpha} \Phi_\alpha^i. \tag{11.29}$$

If K^* lies on a critical surface, then a subset of eigenvectors span the space tangential to the critical surface at K^*. Note that the eigenvalue λ_α has been substituted by b^{y_α}. This is justified, since we have

$$\lambda_\alpha(b)\lambda_\alpha(b) = \lambda_\alpha\big(b^2\big)$$

by virtue of the semigroup-property of the RG transformation. Thus every eigenvalue λ_α defines a critical exponent y_α which will enter our discussion of scaling relations below. We now consider the new variables

$$g_\alpha = \sum_i \Phi_\alpha^i \delta K_i. \tag{11.30}$$

These are projections of δK onto the eigenvectors Φ_α. We have

$$g'_\alpha = \sum_i \Phi^i_\alpha \delta K'_i = \sum_{ij} \Phi^i_\alpha M^j_i \delta K_j = \sum_j b^{y_\alpha} \Phi_{\alpha j} \delta K_j = b^{y_\alpha} g_\alpha . \tag{11.31}$$

We now return to the recursion relation (11.26) for the free energy density. The contribution $g(K)$ thereby originates from integrating out the short-range fluctuations and thus represents a *smooth function*. Thus the singular part of the free energy density fulfills the homogeneous relation

$$f_s(K) = b^{-d} f_s\big(K'\big). \tag{11.32}$$

We linearize the flow around the fixed point and obtain the following scaling behavior for the singular part of the free energy density

$$f_s\big(K^* + \delta K\big) = b^{-d} f_s\big(K^* + \delta K'\big). \tag{11.33}$$

We now omit the argument K^* and write

$$f_s\big(K^* + \delta K\big) \equiv f_s(g_1, g_2, \ldots), \quad \delta K \overset{(11.30)}{=} \delta K(g).$$

Performing ℓ iteration steps, we find

$$f_s(g_1, g_2, \ldots) = b^{-d\ell} f_s\big(b^{\ell y_1} g_1, b^{\ell y_2} g_2, \ldots\big). \tag{11.34}$$

Depending on the sign of the exponent y_α, we observe a qualitatively different scaling behavior:

- For $y_\alpha > 0$ the deviation g_α increases continuously and the flow moves the point $K^* + g_\alpha$ away from the fixed point K^*. This is called a *relevant perturbation*.
- For $y_\alpha < 0$ the deviation g_α decreases and the flow carries the point $K^* + g_\alpha$ towards the fixed point K^*. This corresponds to an *irrelevant perturbation*.
- Deviations with $y_\alpha = 0$ are called *marginal*.

Physical quantities corresponding to relevant perturbations are e.g. the temperature or the (dimensionless) external field,

$$t = \frac{T - T_c}{T_c} \equiv g_1 \quad \text{and} \quad h = g_2. \tag{11.35}$$

Let us slightly reinterpret these findings: The RG transformation acts on the space of coupling constants or equivalently on the space of interactions parametrized by the energy function. In general, this is an ∞-dimensional space. Let us now consider again the general class of energy functions (11.22), i.e.

$$H = -\sum_{A \subset \Lambda} K_A s_A \equiv -\sum K_i O_i . \tag{11.36}$$

An expansion of the Hamiltonian around the fixed point, $H = H^* + \delta H$, yields

$$H^* = -\sum K^*_i O_i , \quad \delta H = -\sum \delta K_i O_i = -\sum_\alpha g_\alpha Q_\alpha . \tag{11.37}$$

Applying the linearized RG transformation ℓ times changes H according to

$$H^* + \delta H \to H^* - \sum g'_\alpha Q_\alpha \to H^* - \sum g''_\alpha Q_\alpha \to \cdots$$
$$\to H^* - \sum_\alpha b^{\ell y_\alpha} g_\alpha Q_\alpha,$$

where the Q_α are called *scaling operators* and the g_α *scaling fields*. Operators with positive y_α are relevant, operators with $y_\alpha < 0$ are irrelevant and operators with $y_\alpha = 0$ are marginal. The relevant operators of the Ising model are its energy H and its average field $\sum s_x$.

11.2.2 Derivation of Scaling Laws

Let us assume that $g_1 = t$ and $g_2 = h$ in (11.35) are relevant couplings and $g_3, g_4, \ldots$ are irrelevant ones. Moreover, we choose ℓ such that

$$b^{y_1 \ell} = \frac{1}{t} \quad \text{or} \quad b^\ell = t^{-1/y_1}. \tag{11.38}$$

Then the scaling relation (11.34) yields

$$f_s\big(K^* + \delta K\big) \equiv f_s(t, h, g_3, \ldots) = t^{d/y_1} f_s\left(1, \frac{h}{t^{y_2/y_1}}, \frac{g_3}{t^{y_3/y_1}}, \ldots\right). \tag{11.39}$$

Similarly, setting $b^\ell = h^{-1/y_2}$ we arrive at

$$f_s(t, h, g_3, \ldots) = h^{d/y_2} f_s\left(\frac{t}{h^{y_1/y_2}}, 1, \frac{g_3}{h^{y_3/y_2}}, \ldots\right). \tag{11.40}$$

Note that the arguments

$$\frac{g_i}{t^{y_i/y_1}} \overset{t\to 0}{\to} 0 \quad \text{and} \quad \frac{g_i}{h^{y_i/y_2}} \overset{h\to 0}{\to} 0, \quad i = 3, 4, \ldots \tag{11.41}$$

of the singular part f_s of the free energy density vanish at the fixed point, since the exponents of t and h are negative.

Now we can relate the thermodynamic critical exponents to the exponents of the linearized RG transformation by differentiating the singular part of the free energy density with respect to the relevant couplings t and h. At this point it is useful to collect the relevant thermodynamic quantities as introduced in Sect. 7.3:

$$\text{magnetization:} \quad m(t, h) = \langle s_x \rangle = -\frac{\partial f}{\partial h}, \tag{11.42}$$

$$\text{susceptibility:} \quad \chi(t, h) = \beta \sum_x \langle s_0 s_x \rangle_c = -\frac{\partial^2 f}{\partial h^2}, \tag{11.43}$$

$$\text{inner energy density:} \quad u(t, h) = \lim_{\Lambda \to \mathbb{Z}^d} \frac{1}{V} \langle H \rangle = \frac{\partial(\beta f)}{\partial \beta}, \tag{11.44}$$

$$\text{specific heat:} \quad c(t, h) = \frac{\partial u}{\partial T} = -\beta^2 \frac{\partial u}{\partial \beta} = -T \frac{\partial^2 f}{\partial T^2}. \tag{11.45}$$

Their singular behavior is characterized by the critical exponents α, β, γ and δ:

$$c(t,0) \sim E_{\pm}|t|^{-\alpha}, \qquad m(t,0) \sim Bt^{\beta}, \tag{11.46}$$

$$\chi(t,0) \sim A_{\pm}|t|^{-\gamma}, \qquad m(0,h) \sim |h|^{-1/\delta}\mathrm{sign}(h). \tag{11.47}$$

The correlation length and two-point function define the critical exponents η and ν,

$$\text{correlation length:} \quad \xi^{-1} = -\lim_{|x|\to\infty} \frac{1}{|x|} \log\langle s_0 s_x\rangle_c \sim |t|^{\nu}, \tag{11.48}$$

$$\text{Green's function:} \quad \langle s_0 s_x\rangle \sim \frac{1}{|x|^{d-2+\eta}}. \tag{11.49}$$

Since the specific heat is proportional to the second t-derivative of f we conclude

$$f_s \sim |t|^{2-\alpha}. \tag{11.50}$$

A comparison with (11.39) immediately results in $2-\alpha = d/y_1$. A similar reasoning for the other derivatives of f yields further relations between the critical exponents β, γ and δ and the relevant exponents y_1 and y_2. To relate ν and η to the relevant exponents we must allow for an inhomogeneous external field $h(\mathbf{x})$, similarly as in the Ornstein–Zernike extension of Landau's theory. Finally one ends up with the following important relations between $\alpha, \beta, \gamma, \delta, \nu, \eta$ and y_1, y_2:

$$\begin{aligned} 2-\alpha &= \frac{d}{y_1}, \qquad \beta = \frac{d-y_2}{y_1}, \\ \gamma &= \frac{2y_2-d}{y_1}, \qquad \frac{1}{\delta} = \frac{d-y_2}{y_2}, \\ \nu &= \frac{1}{y_1}, \qquad d-2+\eta = 2(d-y_2). \end{aligned} \tag{11.51}$$

Since the six critical exponents only depend on the two relevant exponents y_1 and y_2 and the dimension of the system we find the following scaling relations between the critical exponents,

$$\begin{aligned} \gamma &= \nu(2-\eta) && \text{(Fisher)}, \\ \alpha+2\beta+\gamma &= 2 && \text{(Rushbrooke)}, \\ \gamma &= \beta(\delta-1) && \text{(Widom)}, \\ \nu d &= 2-\alpha && \text{(Josephson, "hyperscaling relation")}. \end{aligned} \tag{11.52}$$

The critical exponents of the two- and three dimensional Ising models and the three-dimensional Heisenberg model are found in Table 11.1 As expected the scaling relations are fulfilled. In $d \neq 4$ they are not fulfilled for the mean field exponents in the last row of Table 11.1.

The critical exponents do not depend on the microscopic details of the interactions, since the correlation length diverges at the critical point. This *universality* of the critical behaviour arises from the singular part of the free energy which is independent of the (infinitely many) *irrelevant* couplings $g_i, i \geq 3$. The critical exponents of a system are fixed by the space-dimension, the number of components of the order parameter and the symmetry of the interaction. Two models which share these properties belong to the same universality class.

Table 11.1 Critical exponents for the Ising model and the Heisenberg model

	α	β	γ	δ	η	ν
$d=2$ Ising	0	1/8	7/4	15	1/4	1
$d=3$ Ising	0.11	0.32	1.24	4.8	0.05	0.63
class. Heisenberg $d=3$	−0.12	0.36	1.37	4.6	0.04	0.7
MFA, arbitrary d	0	1/2	1	3	0	1/2

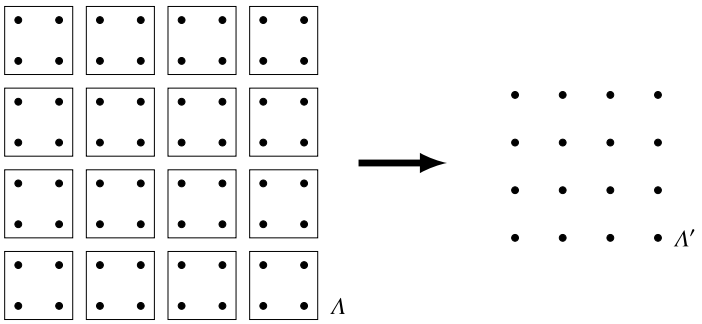

Fig. 11.7 A blocking transformation which combines four microscopic spins to one block spin

11.3 Block-Spin Transformation

The Monte Carlo renormalization group (MCRG) method has been developed by MA, SWENDSEN and others [13–15]. This powerful method is based on the block-spin transformation which maps a microscopic system to a coarse-grained system. It is a generalization of the previously considered decimation procedure. We present the transformation for two-dimensional Ising-type models on a square lattice with general energy function

$$\beta H = -\sum_{A\subset\Lambda} K_A s_A, \quad s_A = \prod_{x\in A} s_x,\ s_x \in \{-1.1\}, \tag{11.53}$$

and subject to periodic boundary conditions. We absorb the inverse temperature β in the couplings K_A and we write H instead of βH.

We partition the lattice into blocks of size b^2 and assign a *block spin* to the spins in every block. Figure 11.7 shows a possible blocking with rescaling factor of $b=2$. Let us denote by $x=(x_1,x_2)$ with $x_i \in \{1,\dots,N\}$ the sites on a square lattice Λ. Then a block consisting of b^2 lattice points is mapped onto one lattice point x' of the coarse-grained lattice,

$$x'(x) = \big(x_1'(x_1), x_2'(x_2)\big) = \left(\mathrm{ceil}\frac{x_1}{b}, \mathrm{ceil}\frac{x_2}{b}\right), \tag{11.54}$$

where $\mathrm{ceil}(x)$ is the smallest integer not less than x. If $b=2$ then all sites $(1,1)$, $(1,2)$, $(2,1)$ and $(2,2)$ are mapped onto the site $(1,1)$ on the diluted lattice Λ'. Thereby the lattice shrinks by the factor $1/b$.

A *block-spin transformation* maps a microscopic configuration $\omega = \{s_x\}$ with a certain probability onto a configuration $\omega' = \{S_{x'}\}$ on the coarser lattice and is characterized by its *kernel* $T(\omega', \omega)$ according to

$$\omega' = \sum_{\omega \in \Omega} T\big(\omega', \omega\big), \tag{11.55}$$

where $T(\omega', \omega)$ is the probability that ω is mapped to ω'. This blocking kernel should satisfy the conditions

$$0 \leq T\big(\omega', \omega\big) \leq 1 \quad \text{and} \quad \sum_{\omega'} T\big(\omega', \omega\big) = 1. \tag{11.56}$$

The Boltzmann factors of the microscopic configurations determine the Boltzmann factors of the block-spin configurations via

$$\mathrm{e}^{-H'(\omega')} = \sum_{\omega \in \Omega} T\big(\omega', \omega\big)\mathrm{e}^{-H(\omega)}. \tag{11.57}$$

The previously considered decimation of the Ising chain is a particular blocking transformation with kernel

$$T\big(\omega', \omega\big) = \prod_{x' \in \Lambda'} \delta(s_{2x'}, S_{x'}),$$

i.e. two neighboring spins are mapped to one block spin. Thus, decimation is a particular blocking, where all but one spin from each block are discarded. The block spin is then equal to the one spin left.

Assuming that the energy of the block spins may be written again in the form

$$H'\big(\omega'\big) = -\sum_{A' \subset \Lambda'} K_{A'} S_{A'} \tag{11.58}$$

we can derive a recursion relation for the coupling constants. Because of the second relation in (11.56) the partition function of the blocked system is equal to that of the microscopic system,

$$Z'_{H'} = \sum_{\omega' \in \Omega'} \mathrm{e}^{-H'(\omega')} = \sum_{\omega' \in \Omega'} \sum_{\omega \in \Omega} T\big(\omega', \omega\big)\mathrm{e}^{-H(\omega)} = \sum_{\omega \in \Omega} \mathrm{e}^{-H(\omega)} = Z_H. \tag{11.59}$$

The connected correlation functions of the s_A are obtained by differentiating $\log Z$ with respect to the corresponding couplings. for example

$$\begin{aligned} \langle s_A \rangle &= \frac{\partial \log Z}{\partial K_A}, \\ \langle s_A; s_B \rangle &\equiv \langle s_A s_B \rangle - \langle s_A \rangle \langle s_B \rangle = \frac{\partial \langle s_A \rangle}{\partial K_B}. \end{aligned} \tag{11.60}$$

The correlation functions of the blocked system are given by

$$\langle S_{A'} \rangle' \equiv \frac{\sum_{\omega'} S_{A'} \mathrm{e}^{-H'(\omega')}}{\sum_{\omega'} \mathrm{e}^{-H'(\omega')}} = \frac{\sum_{\omega'} S_{A'} \sum_{\omega} T(\omega', \omega)\mathrm{e}^{-H(\omega)}}{\sum_{\omega} \mathrm{e}^{-H(\omega)}}. \tag{11.61}$$

The last relation shows how one can calculate correlations of the block spins from the microscopic ensemble. To proceed we introduce the derivative of $\langle S_{A'}\rangle'$ in the blocked system with respect to the coupling constant K_B of the microscopic system,

$$T_{A'B} = \frac{\partial \langle S_{A'}\rangle'}{\partial K_B} = \frac{\partial}{\partial K_B} \frac{\sum_{\omega'} S_{A'} \sum_{\omega} T(\omega', \omega) \mathrm{e}^{-H(\omega)}}{\sum_{\omega} \mathrm{e}^{-H(\omega)}}$$
$$= \frac{\sum_{\omega} \{\sum_{\omega'} S_{A'} T(\omega', \omega)\} s_B \mathrm{e}^{-H(\omega)}}{\sum_{\omega} \mathrm{e}^{-H(\omega)}} - \langle S_{A'}\rangle' \langle s_B\rangle.$$

This yields

$$T_{A'B} = \left\langle s_B \sum_{\omega'} S_{A'} T\left(\omega', \omega\right)\right\rangle - \langle S_{A'}\rangle' \langle s_B\rangle, \tag{11.62}$$

and with the help of (11.61) all expectation values on the right hand side can be calculated from the microscopic ensemble and the blocking kernel. We use the chain rule to find the alternative expression

$$T_{A'B} = \frac{\partial \langle S_{A'}\rangle'}{\partial K_B} = \sum_{C'} \frac{\partial \langle S_{A'}\rangle'}{\partial K_{C'}} \frac{\partial K_{C'}}{\partial K_B} = \sum_{C'} \langle S_{A'}; S_{C'}\rangle' \frac{\partial K_{C'}}{\partial K_B}. \tag{11.63}$$

Again the connected correlation functions on the right hand side can be extracted from the microscopic ensemble. Thus, from the two expressions (11.62) and (11.63) for $T_{A'B}$ we can read off how the couplings of the blocked system vary when we vary the microscopic couplings.

In order to illustrate the MCRG transformation we return to the two-dimensional Ising model and combine four spins to one block spin as indicated in Fig. 11.7. For the blocking kernel we choose the *majority rule*: Four spins $\{s_x\}$ are mapped onto one block spin $S_{x'}$ according to

$$T\left(\omega', \omega\right) = \prod_{x' \in \Lambda'} t\left(S_{x'}, \sum_{x \in x'} s_x\right) \tag{11.64}$$

with

$$\begin{aligned} \sum s_x > 0 \quad &\Longrightarrow \quad S_{x'} = 1 \quad \text{with probability 1,} \\ \sum s_x < 0 \quad &\Longrightarrow \quad S_{x'} = -1 \quad \text{with probability 1,} \\ \sum s_x = 0 \quad &\Longrightarrow \quad \begin{cases} S_{x'} = +1 & \text{with probability } 1/2, \\ S_{x'} = -1 & \text{with probability } 1/2. \end{cases} \end{aligned} \tag{11.65}$$

Let us determine the RG transformation for the Ising model without external field on a small 4×4 lattice. The $2^{16} = 65536$ microscopic configurations are easily generated such that (11.57) allows for a direct calculation of the energy of the coarse-grained system. In two dimensions H' has not the same functional form as H, but on the blocked 2×2 lattice there are only three different types of interactions: between nearest neighbors, next-nearest neighbors and all four spins (for simplicity we drop the prime at the couplings)

Table 11.2 Grouping of the blocked configurations on the 2×2 lattice into classes. Configurations in the same class have equal weight

Class	Configurations	$-H'$
$\mathscr{C}_1$	++ −− ++ −−	$8K_1 + 8K_2 + 4K_3 + 4K_4$
$\mathscr{C}_2$	−+ +− ++ ++ +− −+ −− −− ++ ++ −+ +− −− −− +− −+	$-4K_3 + 4K_4$
$\mathscr{C}_3$	++ +− −− −+ −− +− ++ −+	$-8K_2 + 4K_3 + 4K_4$
$\mathscr{C}_4$	+− −+ −+ +−	$-8K_1 + 8K_2 + 4K_3 + 4K_4$

$$
\begin{aligned}
H' = &-K_1 \sum_{x'} S_{x'}(S_{x'+(1,0)} + S_{x'+(0,1)}) \\
&- K_2 \sum_{x'} S_{x'}(S_{x'+(1,1)} + S_{x'+(1,-1)}) \\
&- K_3 \sum_{x'} S_{x'} S_{x'+(1,0)} S_{x'+(0,1)} S_{x'+(1,1)} \\
&- K_4 \sum_{x'} 1.
\end{aligned} \tag{11.66}
$$

Note that we deliberately over-counted, since, for instance, the two terms in the second row, which are identical on a 2×2 lattice, are different on larger lattices. The $2^4 = 16$ configurations on the coarse-grained lattice fall into one of the four classes listed in Table 11.2, and members of the same class share the same Boltzmann factor. Hence we end up with four equations for the couplings K_1, K_2, K_3, K_4 in Eq. (11.66). In each class we pick the first representative and obtain the equations

$$
\mathrm{e}^{-H'(\omega_i')} = \sum_{\omega} T\left(\omega_i', \omega\right) \mathrm{e}^{-H(\omega)} \equiv \mathrm{e}^{c_i}, \quad i = 1, 2, 3, 4. \tag{11.67}
$$

From Table 11.2 we can find the couplings of block spins in terms of these constants as follows:

$$
\begin{aligned}
K_1 &= \frac{1}{16}(c_1 - c_4), \\
K_2 &= \frac{1}{32}(c_1 - 2c_3 + c_4), \\
K_3 &= \frac{1}{32}(c_1 - 4c_2 + 2c_3 + c_4), \\
K_4 &= \frac{1}{32}(c_1 + 4c_2 + 2c_3 + c_4).
\end{aligned}
$$

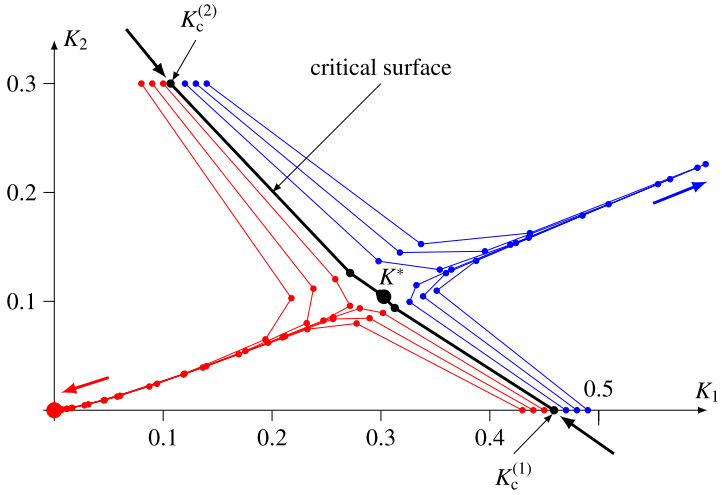

Fig. 11.8 Renormalization group flow in the (K_1, K_2)-plane. Besides the trivial high-temperature fixed point at $K = 0$ we find a non-trivial fixed point. The intersection of the critical surface with the K_1-axis yields the critical temperature of the Ising model with nearest neighbor interaction

The iteration of the RG transformation is then performed by using the couplings K_i again on a 4×4 lattice. Figure 11.8 shows the projection of some renormalization group trajectories onto the K_1, K_2-plane. These trajectories are obtained with the program `rengroupis2d.c` on p. 252 and is based on the discussion found at http://www-zeuthen.desy.de/~hasenbus/lecture.html. Points in the space of couplings that flow into the fixed point define the *critical surface*, and the intersection of this surface with the line $(K_1, 0, 0)$ yields the critical coupling of the Ising model with nearest-neighbor interaction. Besides the trivial high-temperature fixed point at $K^* = 0$ we find a non-trivial fixed point at

$$K^* = \left(K_1^*, K_2^*, K_3^*\right) = (0.302796, 0.104246, 0.023298). \tag{11.68}$$

The numerical value of the critical coupling of the $2d$ Ising model with nearest-neighbor interactions lies at

$$K_{1,c}^{(1)} \approx 0.458961,$$

and this value can be compared with the exact result $\frac{1}{2}\log(1+\sqrt{2}) \approx 0.4407$. In order to obtain the critical exponents we examine the linearized RG transformation close to the fixed point K^*, i.e. the matrix

$$T_{ab} = \left.\frac{\partial K_a'}{\partial K_b}\right|_{K^*}. \tag{11.69}$$

The corresponding difference quotients as calculated with `rengroupis2d.c` read

$$T = \begin{pmatrix} 1.37342 & 0.50762 & 0.06027 \\ 1.66800 & 0.79017 & 0.00564 \\ 0.55608 & 0.22621 & 0.20882 \end{pmatrix}. \tag{11.70}$$

Next we have to diagonalize this non-symmetric matrix in order to determine the critical exponents:

$$\sum_a \Phi_a^i T_{ab} = \lambda^i \Phi_b^i.$$

The eigenvalues and left-eigenvectors are

$$\begin{aligned} \lambda_1 &= 2.0658, \qquad \Phi_1 = (0.9268, 0.3743, 0.0312), \\ \lambda_2 &= 0.1890, \qquad \Phi_2 = (0.3027, 0.1010, -0.9477), \\ \lambda_3 &= 0.1176, \qquad \Phi_3 = (-0.7695, 0.4185, 0.4825), \end{aligned} \tag{11.71}$$

and yield the following exponents y_i in $\lambda_i = b^{y_i}$:

$$\frac{1}{\nu} = y_1 \approx 1.0467, \qquad y_2 \approx -2.4037, \qquad y_3 \approx -3.0880. \tag{11.72}$$

Without external field the Ising model has only one relevant coupling t and infinitely many irrelevant couplings with negative exponents. The truncated model has just two irrelevant couplings. With $h = 0$ we may confirm only the relation $\nu = 1/y_1$ in (11.51). We see that the result (11.72) for ν approximates the exact value $\nu = 1$ rather well in contrast to the mean field approximation, which predicts $\nu_{\mathrm{mf}} = 0.5$.

11.4 Continuum Limit of Non-interacting Scalar Fields

We begin our discussion of the continuum limit by reconsidering the simple free scalar field theory. For that purpose we introduce explicitly a *lattice spacing* a (earlier denoted by ε) and study the *continuum limit* $a \to 0$ of the two-point function. Thereby we should distinguish between sites, parameters and fields of the system on the unit lattice and on the lattice with lattice spacing a. We use the following conventions: n, k and m_{L} refer to the dimensionless sites, momenta and mass on the unit lattice and x, p and m to the corresponding dimensionful quantities on the lattice with spacing a. We begin with the Fourier representation of the two-point function on the unit lattice,

$$G_{\mathrm{L}}(n) = \frac{1}{(2\pi)^d} \int_{-\pi}^{\pi} \mathrm{d}^d k \frac{\mathrm{e}^{\mathrm{i}kn}}{m_{\mathrm{L}}^2 + \hat{k}^2}, \quad \hat{k}_\mu = 2 \sin \frac{k_\mu}{2}. \tag{11.73}$$

Setting $n = x/a, k = pa$ and $m_{\mathrm{L}} = am$ we obtain

$$G_{\mathrm{L}}(x) = \left(\frac{a}{2\pi}\right)^d \frac{1}{a^2} \int_B \mathrm{d}^d p \frac{\mathrm{e}^{\mathrm{i}px}}{m^2 + \hat{p}^2}, \quad \hat{p}_\mu = \frac{2}{a} \sin \frac{a p_\mu}{2}, \tag{11.74}$$

where the momentum is inside the Brillouin zone $B = [-\pi/a, \pi/a]^d$ which becomes $\mathbb{R}^d$ in the continuum limit. The Green function satisfies the difference equation

$$-\sum_\mu \big(G_{\mathrm{L}}(x + ae_\mu) - 2G_{\mathrm{L}}(x) + G_{\mathrm{L}}(x - ae_\mu)\big) + (am)^2 G_{\mathrm{L}}(x) = \delta_{x,0}.$$

The rescaled dimensionful two-point function

$$G_a(x) = \frac{1}{a^{d-2}} G_{\mathrm{L}}(x) = \frac{1}{(2\pi)^d} \int_B \mathrm{d}^d p \, \frac{\mathrm{e}^{\mathrm{i}px}}{m^2 + \hat{p}^2} \tag{11.75}$$

satisfies the rescaled difference equation

$$-\sum_\mu \frac{1}{a^2} \big(G_a(x + a e_\mu) - 2 G_a(x) + G_a(x - a e_\mu) \big) + m^2 G_a(x) = \frac{1}{a^d} \delta_{x,0}.$$

In the continuum limit the right hand side approaches the Dirac delta function,

$$\frac{1}{a^d} \delta_{x,0} \overset{a \to 0}{\to} \delta(x), \tag{11.76}$$

such that the difference equation turns into the linear *differential* equation

$$\big(-\Delta + m^2 \big) G(x) = \delta^d(x), \quad \text{where } \lim_{a \to 0} G_a = G. \tag{11.77}$$

It is just the defining equation for the Green function of the operator $-\Delta + m^2$ on the Euclidean space $\mathbb{R}^d$. In the same limit the Fourier representation (11.75) becomes

$$\frac{1}{(2\pi)^d} \int_{\mathbb{R}^d} \mathrm{d}^d p \, \frac{\mathrm{e}^{\mathrm{i}px}}{m^2 + p^2}. \tag{11.78}$$

Several remarks are in order at this point:

- The rescaling of the two-point function in (11.75) corresponds to a *field renormalization*. The mass parameter m_{L} and the lattice field ϕ_{L} in the lattice action

$$\begin{aligned} S &= \frac{1}{2} \sum_{\langle n,m \rangle} \big(\phi_{\mathrm{L}}(m) - \phi_{\mathrm{L}}(n) \big)^2 + \frac{m_{\mathrm{L}}^2}{2} \sum_n \phi_{\mathrm{L}}^2(n) \\ &= \frac{1}{2} \sum_{x \in (a\mathbb{Z})^d} \frac{a^d}{a^{d-2}} \left(\sum_{\mu=1}^d \frac{(\phi_{\mathrm{L}}(x + a e_\mu) - \phi_{\mathrm{L}}(x))^2}{a^2} + \frac{m_{\mathrm{L}}^2}{a^2} \phi_{\mathrm{L}}^2(x) \right) \end{aligned} \tag{11.79}$$

  are *dimensionless*. In the continuum limit the difference quotients become partial derivatives and, if we rescale the field according to

$$\phi_{\mathrm{L}}(n) \to \phi(x) = \frac{1}{a^{(d-2)/2}} \phi_{\mathrm{L}}(an), \tag{11.80}$$

  then the Riemann sum turns into an integral over $\mathbb{R}^d$, such that the lattice action approaches the continuum action of the Klein–Gordon field

$$S = \frac{1}{2} \int \mathrm{d}^d x \big(\big(\nabla\phi(x), \nabla\phi(x) \big) + m^2 \phi^2(x) \big), \quad \text{where } m = \frac{m_{\mathrm{L}}}{a}.$$

  In d space-time dimensions a scalar field has mass-dimension $[\text{mass}]^{(d-2)/2}$ such that the naive rescaling (11.80) just restores the correct mass-dimension of ϕ. The rescaling implies a rescaling of the k-point function

$$G_{\mathrm{L}}(n_1, \ldots, n_k) \to G_{\mathrm{L}}(x_1, \ldots, x_k) = a^{-k(d-2)/2} G(an_1, \ldots, an_k). \tag{11.81}$$

- For large arguments the two-point function on the lattice and in the continuum fall off exponentially,

$$G_{\mathrm{L}}(n) \overset{m_{\mathrm{L}}|n|\gg 1}{\to} \mathrm{e}^{-m_{\mathrm{L}}|n|}, \qquad G(x) \overset{m|x|\gg 1}{\to} \mathrm{e}^{-m|x|}. \tag{11.82}$$

- The lattice Green function becomes approximately rotationally invariant for large arguments $|n| \gg 1/m_{\mathrm{L}}$ and this is needed to obtain an $SO(\mathrm{d})$-invariant correlation function in the continuum limit. Hence, although the lattice regularization breaks the rotation invariance, the rotational symmetry is restored in the continuum limit.

11.4.1 Correlation Length for Interacting Systems

For interacting theories the correlation length on a lattice or in the continuum is intimately related to a mass parameter, similarly as for a non-interacting theory. To explain this connection we recall the definition of a mass and a correlation length:

1. The dimensionless *bare mass* m_{L} directly appears in the lattice action.
2. The dimensionless *correlation length* ξ_{L} is defined via the two-point function

$$\frac{1}{\xi_{\mathrm{L}}} = -\lim_{|n|\to\infty} \frac{\log G_{\mathrm{L}}(n)}{|n|}. \tag{11.83}$$

   For the free field we simply have $\xi_{\mathrm{L}} = 1/m_{\mathrm{L}}$, but in general ξ_{L} depends on all bare couplings of the lattice theory.
3. A particle described by the field ϕ is characterized by a dimensional *physical mass* m as measured in experiments.
4. The choice of bare parameters determines the correlation length ξ_{L} in lattice units from which we extract the physical mass according to

$$m = \frac{1}{\xi} = \frac{1}{a\xi_{\mathrm{L}}(m_{\mathrm{L}}, \ldots)}. \tag{11.84}$$

   Thus, the *lattice spacing* a depends on the fixed physical mass m, the dimensionless mass parameter m_{L} and possible further bare couplings.

We may interpret the connection between the bare and the physical mass as follows: Firstly, we may set the lattice spacing a equal to some arbitrarily chosen physical distance. If ϕ describes a particle of mass m then the product $\xi_{\mathrm{L}} = 1/am$ is identified with its Compton wavelength in units of a. When we specify a and m then we fix the bare parameter $m_{\mathrm{L}}(\xi_{\mathrm{L}})$ provided the remaining bare parameters are specified as well. A change of the (unobservable) lattice spacing a is compensated by a change of the (unobservable) bare parameter m_{L} whereby physical quantities remain unchanged. Thus the trajectory $m_{\mathrm{L}}(a)$ represents a *curve of constant physics*.

To reach the continuum limit $a \to 0$ we should adjust the free lattice parameters such that the correlation length ξ_{L} is very large compared to the lattice spacing or equivalently that $\xi \gg a$. This means that we perform the limits $\xi_{\mathrm{L}} \to \infty$ or $m_{\mathrm{L}} \to 0$ so that the dimensional correlation functions have a well-defined continuum limit characterized by a correlation length $\xi > 0$. More generally, for each free lattice bare

parameter we identify a physical quantity (mass, vacuum expectation value, decay constant, ...) which should be reached in the continuum limit. The a-dependence of the bare parameters can be fixed by the requirement that the physical quantities do not change. This step also relates the lattice spacing to a physical scale.

In *MC simulations* one typically chooses a set of bare parameters and extracts the corresponding lattice spacing for a prescribed physical mass m according to (11.84). Thereby the correlation length should be much larger than the lattice spacing in order to avoid lattice effects and much smaller than the volume in order to avoid finite volume effects. This means that the inequality

$$1 \ll \xi_{\mathrm{L}} \ll N \tag{11.85}$$

should always be satisfied. Currently, high performance computer clusters admit simulations of scalar field theories on lattices with up to 128^4 sites.

11.5 Continuum Limit of Spin Models

In the vicinity of a critical point (curve, surface) of a general spin model the correlation length ξ_{L} becomes large. Thus, near criticality the correlations extend over very many lattice spacings such that the discreteness of the lattice becomes irrelevant. This is the reason why certain lattice models at criticality can be interpreted as Euclidean quantum field theories or a quantum field theories at finite temperature. At finite temperature we perform the limit $a \to 0$ such that

$$T = \frac{1}{aN_d} \tag{11.86}$$

is fixed. Away from criticality the lattice model is viewed as lattice regularized theory. Performing a continuum limit means then that we approach a critical point along a particular curve in the space of couplings. Close to a critical point the correlation length in units of a diverges as

$$\frac{\xi}{a} = \xi_{\mathrm{L}} = \kappa(\beta_c - \beta)^{-\nu} \tag{11.87}$$

with critical exponent ν. For a *fixed correlation length* this equation determines the lattice spacing $a = a(\beta)$ and the continuum limit is reached for $\beta \to \beta_c$ with ξ being fixed. For a given lattice spacing the dimensionless parameter β can be expressed in terms of the dimensional length ξ. The physical mechanism that transforms a dimensionless parameter into a dimensional parameter is called *dimensional transmutation*. It is observed in many relevant field theories with dimensionless couplings.

We consider a correlation function with long-range behavior

$$\big\langle O(n)O(m)\big\rangle \sim \mathrm{e}^{-m_{\mathrm{L}O}|n-m|}, \tag{11.88}$$

wherein $m_{\mathrm{L}O}$ acts as screening parameter. Since the distance $|n-m|$ is measured in units of the lattice spacing, the correlation function yields the screening mass in units of $a(\beta)$. Universality implies that near a critical point

$$m_O a(\beta) = m_{\mathrm{L}O} = \kappa_O(\beta_c - \beta)^{\nu}, \quad \beta \uparrow \beta_c, \tag{11.89}$$

such that the product $m_O\xi$ attains a constant value in the vicinity of the critical point,

$$m_O\xi = \kappa_m\kappa. \tag{11.90}$$

The dimensionless numbers κ and κ_m are accessible to numerical simulations. Thus we can "measure" the screening mass m_O in units of the free parameter $1/\xi$.

11.6 Programs for Chap. 11

The program `rengroupis2d.c` computes the trajectories of the block-spin transformation of the $2d$ Ising model on a 4×4 lattice. The blocking kernel is based on the *majority rule* with block-spin Hamiltonian (11.66). The trajectories in Fig. 11.8 were computed with this program. When one runs the program it first wants to know an initial K_1-value and then computes `ig` points on the renormalization group trajectory beginning at $(K_1, 0, 0, 0)$. One also may change the initial couplings in line 10 of the code. With a fine tuning we localized the non-trivial fixed point K^* listed in lines 11 and 12. The two critical points in Fig. 11.8 are localized at

$$K_c^{(1)} = (0.4589605276967553, 0, 0, 0),$$
$$K_c^{(2)} = (0.106770494, 0.3, 0, 0).$$

To compute the critical exponents one needs to set `ig=1` in line 21 and uncomment the lines beginning with X.

```
1  /* Program rengroupis2d.c */
2  /* computes trajectories of MC_RG  transformation*/
3  /* numerically. Blocking according to majority rule.*/
4  #include <stdio.h>
5  #include <stdlib.h>
6  #include <math.h>
7  #include <string.h>
8  #include "constrenising2.h"
9  #include "stdrenising.h"
10 double k1,k2=0.3,k3=0,k4=0;
11 /*X double k1=0.30279597088,k2=0.10424577852;*/
12 /*X double k3=0.02329831163,k4=2.66479130426;*/
13 int main(void){
14   /*X k1o=k1;k2o=k2;k3o=k3;*/
15   /*X puts("delta = ");scanf("%lf",&delta);*/
16   /*X k1=k1+delta;*/
17   conf=1<<V; /* number of configurations */
18   neighbors();
19   puts("K1 = ");scanf("%lf",&k1);
20   printf("(%1.4f, %1.4f)",k1,k2);
21   for (ig=0;ig<20;ig++){
22     c1=0;c2=0;c3=0;c4=0;
23     for (i=0;i<conf;i++){
24       /* binary code of i =  configurations */
```

```
      for (p=0;p<V;p++){
        s[p]=(i>>p)%2;s[p]=2*s[p]-1;
      };
      h1=0;h2=0;h3=0;
      for (p=0;p<V;p++){
        h1=h1+s[p]*(s[nr[p]]+s[no[p]]);
        h2=h2+s[p]*(s[nro[p]]+s[nru[p]]);
        h3=h3+s[p]*s[nr[p]]*s[no[p]]*s[nro[p]];
      };
      boltz=exp(k1*h1+k2*h2+k3*h3);
      block spin(s);
      for (p=0;p<VB;p++){
        kc1[p]=bs[p]*kl1[p];
        kc2[p]=bs[p]*kl2[p];
        kc3[p]=bs[p]*kl3[p];
        kc4[p]=bs[p]*kl4[p];
      };
      if ((kc1[0]>=0)&&(kc1[1]>=0)&&(kc1[2]>=0)&&(kc1[3]>=0)){
        if (kc1[0]*kc1[1]*kc1[2]*kc1[3]==0) c1=c1+0.5*boltz;
        else c1=c1+boltz;}
      if ((kc2[0]>=0)&&(kc2[1]>=0)&&(kc2[2]>=0)&&(kc2[3]>=0)){
        if (kc2[0]*kc2[1]*kc2[2]*kc2[3]==0) c2=c2+0.5*boltz;
        else c2=c2+boltz;}
      if ((kc3[0]>=0)&&(kc3[1]>=0)&&(kc3[2]>=0)&&(kc3[3]>=0)){
        if (kc3[0]*kc3[1]*kc3[2]*kc3[3]==0) c3=c3+0.5*boltz;
        else c3=c3+boltz;}
      if ((kc4[0]>=0)&&(kc4[1]>=0)&&(kc4[2]>=0)&&(kc4[3]>=0)){
        if (kc4[0]*kc4[1]*kc4[2]*kc4[3]==0) c4=c4+0.5*boltz;
        else c4=c4+boltz;}
    };
    l1=log(c1);l2=log(c2);l3=log(c3);l4=log(c4);
    k1=(l1-l4)/16;
    k2=(l1-2*l3+l4)/32;
    k3=(l1-4*l2+2*l3+l4)/32;
    k4=(l1+4*l2+2*l3+l4)/32;
    printf("(%1.4f,%1.4f)",k1,k2);
  };
   /*X printf("[%1.8f,%1.8f,%1.8f]\n",*/
   /*X (k1-k1o)/delta,(k2-k2o)/delta,(k3-k3o)/delta);*/
  printf("\n");
  return 0;
}
```

The following header-file defines the constants and variables. The arrays $kl1[VB]$, ... represent the four distinct classes of configurations on the blocked lattice.

```
/* header-file constrenising2.h*/
#define N 4 /* lattice length*/
#define V (N*N) /* number of lattice points*/
#define VB (V/4) /* volume of blocked lattice*/
short x,y,xm,xp,ym,yp;
short s[V],nr[V],no[V],nro[V],nru[V];
short bs[VB],kc1[VB],kc2[VB],kc3[VB],kc4[VB];
```

```
short kl1[VB]={1,1,1,1},kl2[VB]={1,1,-1,1};
short kl3[VB]={-1,-1,1,1},kl4[VB]={-1,1,1,-1};
unsigned int ig,i,il,j,jl,conf;
unsigned short p,q;
double k1o,k2o,k3o,delta,c1,c2,c3,c4,l1,l2,l3,l4,boltz;
int h1,h2,h3;
```

The header-file `stdrenising.h` determines the nearest neighbors and next-nearest neighbors of a given lattice point and provides the block-spin configuration $bs[VB]$ of a given spin configuration $s[V]$.

```
/* header-file stdrenising.h */
/* provides (next-)nearest neighbours and block spins */
void neighbors(void){
  for (il=0;il<V;il++){
    y=il/N;x=il-y*N;
    xp=x+1,yp=y+1,ym=y-1;
    nr[il]=y*N+xp%N;
    no[il]=(yp%N)*N+x;
    nro[il]=(yp%N)*N+xp%N;
    nru[il]=((ym+N)%N)*N+xp%N;
  };
}
void blockspin(short *s)
{
  for (il=0;il<VB;il++){
    p=(2*il)/N;jl=p*N+2*il;
    bs[il]=s[jl]+s[jl+1]+s[jl+N]+s[jl+N+1];
  };
}
```

11.7 Problems

11.1 (Scaling relations) Starting from the scaling relation for the singular part of the free energy,

$$f_s(t,h) \sim b^{-d} f_s\left(b^{y_1} t, b^{y_2} h\right),$$

derive the four relations in (11.51) which contain α, β, γ and δ.

11.2 (Decimation for spin-1 Ising chain) Generalize the decimation procedure to the spin-1 Ising chain with energy function

$$H = -J \sum_x s_x s_{x+s} - \sum_x C, \quad s_x = \pm 1, 0.$$

New interactions are generated by the decimation. Show that if all possible even interactions between nearest neighbors are included in the energy function,

$$H = -J \sum_x s_x s_{x+1} - K \sum_x s_x^2 s_{x+1}^2 - D \sum_x s_x^2 - \sum_x D$$

a set of consistent recursion equations for the couplings is obtained. The recursion equations take a simple form in terms of the parameters

$$x = \mathrm{e}^{-\beta(J+K+D/2)}, \qquad y = \mathrm{e}^{-2\beta J} \quad \text{and} \quad z = \mathrm{e}^{-\beta(J+K+D)}.$$

Study the trajectories of the renormalization group transformation.

11.3 (Decimation of $2d$ Ising model) Rewrite the program `rengroupis2d.c` on p. 252 by using the decimation procedure inplace of the majority rule to define the blocking kernel. Calculate the couplings $K_1^*, K_2^*, K_3^*, K_4^*$ at the non-trivial fixed point and the corresponding critical exponents. Compare with the flow obtained with the majority rule and depicted in Fig. 11.8.

References

1. L.P. Kadanoff, Scaling laws for Ising models near T_c. Physica **2**, 263 (1966)
2. M.E. Fisher, The renormalization group in the theory of critical behavior. Rev. Mod. Phys. **46**, 597 (1974)
3. M.E. Fisher, Renormalization group theory: its basis and formulation in statistical physics. Rev. Mod. Phys. **70**, 653 (1998)
4. K.G. Wilson, Renormalization group and critical phenomena. I. Renormalization group and the Kadanoff scaling picture. Phys. Rev. B **4**, 3174 (1971)
5. K.G. Wilson, Renormalization group and critical phenomena. II. Phase-space cell analysis of critical behavior. Phys. Rev. B **4**, 3184 (1971)
6. K.G. Wilson, The renormalization group and critical phenomena. Rev. Mod. Phys. **55**, 583 (1983)
7. N.N. Bogoliubov, D.V. Shirkov, *Introduction to the Theory of Quantized Fields* (Interscience, New York, 1959)
8. E. Brezin, J.C. Le Guillou, J. Zinn-Justin, Field theoretical approach to critical phenomena, in *Phase Transitions and Critical Phenomena*, vol. 6, ed. by C. Domb, M.S. Green (Academic Press, London, 1976), p. 125
9. P. Pfeuty, G. Toulouse, *Introduction to the Renormalization Group and to Critical Phenomena* (Wiley, New York, 1977)
10. D.J. Amit, *Field Theory, the Renormalization Group and Critical Phenomena* (World Scientific, Singapore, 1993)
11. J.I. Binney, N.J. Dowrick, A.J. Fisher, M.E.J. Newmann, *The Theory of Critical Phenomena. An Introduction to the Renormalization Group* (Clarendon, Oxford, 1992)
12. D.R. Nelson, M.E. Fisher, Soluble renormalization groups and scaling fields for low-dimensional Ising systems. Ann. Phys. **91**, 226 (1975)
13. R.H. Swendsen, Monte Carlo renormalization group. Phys. Rev. Lett. **42**, 859 (1979)
14. R.H. Swendsen, Monte Carlo calculation of renormalized coupling parameters. Phys. Rev. Lett. **52**, 1165 (1984)
15. S.K. Ma, Renormalization group by Monte Carlo methods. Phys. Rev. Lett. **37**, 461 (1976)

Chapter 12
Functional Renormalization Group

The functional renormalization group (FRG) is a particular implementation of the renormalization group concept which combines the functional methods of quantum field theory with the renormalization group idea of KENNETH WILSON. It interpolates smoothly between the known microscopic laws and the complex macroscopic phenomena in physical systems. It is a momentum-space implementation of the renormalization group idea and can be formulated directly for a continuum field theory—no lattice regularization is required. In most approaches one uses a scale-dependent Schwinger functional or scale-dependent effective action. The scale parameter acts similarly as an adjustable screw of a microscope. For large values of a momentum scale k or equivalently for a high resolution of the microscope one starts with the known microscopic laws. With decreasing scale k or equivalently with decreasing resolution of the microscope one moves to a coarse-grained picture adequate for macroscopic phenomena. The flow from microscopic to macroscopic scales is given by a conceptionally simple but technically demanding flow equation for scale dependent functionals. A priori the method is non-perturbative and does not rely on an expansion in a small coupling constant.

The flow of the scale-dependent Schwinger functional $W_k[j]$ is determined by the Wilson–Polchinski functional renormalization group equation. Actually the flow equations used by K. WILSON [1] with a specific cutoff procedure (the incomplete integration) is equivalent to the equation of J. POLCHINSKI [2] containing an arbitrary cutoff function, as was observed in [3].

In this chapter we will use the flow equation for the scale-dependent effective action $\Gamma_k[\varphi]$. Apart from a cutoff term it is just the Legendre transform of the scale-dependent Schwinger functional. The flow of Γ_k from microscopic to macroscopic scales is determined by the flow equation [4] due to C. WETTERICH. The flow interpolates between the classical action $S[\varphi]$ and the full effective action $\Gamma[\varphi]$ is depicted in Fig. 12.1. To actually calculate Γ_k one incorporates quantum fluctuations between a momentum scale k and a large cutoff scale Λ. For large k near the cutoff one should recover the classical action $S[\varphi]$. With decreasing scale long-range effects are included and for $k \to 0$ one recovers the complete effective action containing quantum fluctuations on all momentum scales. In recent years the functional

A. Wipf, *Statistical Approach to Quantum Field Theory*, Lecture Notes in Physics 864,
DOI 10.1007/978-3-642-33105-3_12,

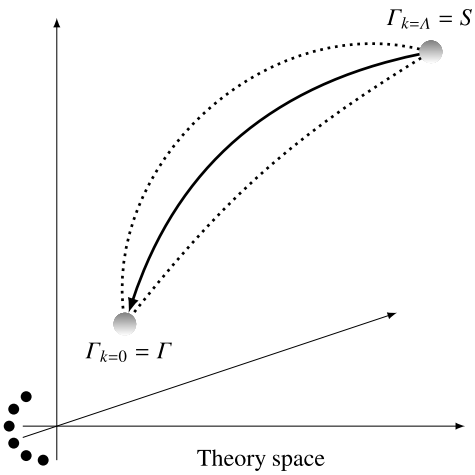

Fig. 12.1 Sketch of the renormalization group flow in theory space. Each axis labels a different operator which may enter the effective action, e.g. φ^2, φ^4, $(\partial\varphi)^2$, etc. For a given initial condition at the cutoff scale Λ the functional renormalization group equation determines the flow of Γ_k. Different regulator functions R_k lead to different trajectories in theory space, but in principle all trajectories end at the full quantum effective action Γ

renormalization group has been applied to many physical systems of interest: in particle physics to the theory of strong interaction, the electroweak phase transition and the gauge hierarchy problem, in gravity to the asymptotic safety scenario and in condensed matter theory to a unified description of classical bosons, the Hubbard model, disordered systems, liquid He^4, frustrated magnets, nucleation processes, superconductivity, and non equilibrium systems. In nuclear physics it has been applied to effective models and the equation of state of nuclear matter, and, finally, in atomic physics to investigate ultra-cold atoms. Useful reviews on various aspects and applications of the functional renormalization group method are contained in [5–11].

12.1 Scale-Dependent Functionals

To find an effective average action we begin with the generating functional of the Euclidean n-point correlation functions

$$Z[j] = \int \mathscr{D}\phi \mathrm{e}^{-S[\phi]+(j,\phi)}, \quad (j,\phi) = \int \mathrm{d}^d x j(x)\phi(x). \tag{12.1}$$

Its logarithm defines the Schwinger functional $W[j] = \log Z[j]$ which generates all connected correlation functions. The Legendre transform of $W[j]$ is the effective action

$$\Gamma[\varphi] = (j,\varphi) - W[j] \quad \text{with } \varphi(x) = \frac{\delta W[j]}{\delta j(x)} \tag{12.2}$$

which generates the one-particle irreducible correlation functions. The last equation in (12.2) determines $j[\varphi]$ which must be inserted into the right hand side of the first equation. The functional Γ encodes all properties of the underlying quantum field theory in a most economic way.

In order to introduce scale-dependent functionals we add a scale-dependent *IR-cutoff* term ΔS_k to the classical action in the functional integral (12.1) and obtain the scale-dependent generating functional

$$Z_k[j] = \int \mathscr{D}\phi \mathrm{e}^{-S[\phi]+(j,\phi)-\Delta S_k[\phi]}. \tag{12.3}$$

The corresponding scale-dependent Schwinger functional $W_k[j]$ is given by

$$W_k[j] = \log Z_k[j]. \tag{12.4}$$

As regulator we choose a quadratic functional with a momentum-dependent mass,

$$\Delta S_k[\phi] = \frac{1}{2}\int \frac{\mathrm{d}^d p}{(2\pi)^d}\phi^*(p)R_k(p)\phi(p) \equiv \frac{1}{2}\int_p \phi^*(p)R_k(p)\phi(p), \tag{12.5}$$

such that the flow equation will have a one-loop structure. We impose the following natural conditions on the cutoff function $R_k(p)$:

- For $k \to 0$ and fixed momentum p the function should vanish such that we recover the conventional effective action for $k \to 0$. Hence we demand

$$R_k(p) \xrightarrow{k\to 0} 0 \quad \text{for fixed } p. \tag{12.6}$$

- When k approaches the large cutoff scale Λ then we should recover the classical theory. With the help of the saddle point approximation one shows that the scale-dependent effective action $\Gamma_{k\to\Lambda}$ defined below tends to the classical action if

$$R_k \xrightarrow{k\to\Lambda} \infty. \tag{12.7}$$

- The cutoff function must regularize the theory in the IR, and this is the case if

$$R_k(p) > 0 \quad \text{for } p \to 0. \tag{12.8}$$

In many cases one demands $R_k(p) \longrightarrow k^2$ for small momenta p and in addition sends the cutoff to infinity. Possible cut-offs are

$$\text{the exponential regulator:} \quad R_k(p) = \frac{p^2}{\mathrm{e}^{p^2/k^2}-1}, \tag{12.9}$$

$$\text{the optimized regulator:} \quad R_k(p) = \left(k^2 - p^2\right)\theta\left(k^2 - p^2\right), \tag{12.10}$$

$$\text{the quartic regulator:} \quad R_k(p) = k^4/p^2, \tag{12.11}$$

$$\text{the sharp regulator:} \quad R_k(p) = \frac{p^2}{\theta(k^2-p^2)} - p^2, \tag{12.12}$$

$$\text{the Callan–Symanzik regulator:} \quad R_k(p) = k^2. \tag{12.13}$$

The exponential cutoff function and its derivative are plotted in Fig. 12.2.

Similarly as for the conventional effective action one introduces the average field of the cutoff theory with external source,

$$\varphi(x) = \frac{\delta W_k[j]}{\delta j(x)}. \tag{12.14}$$

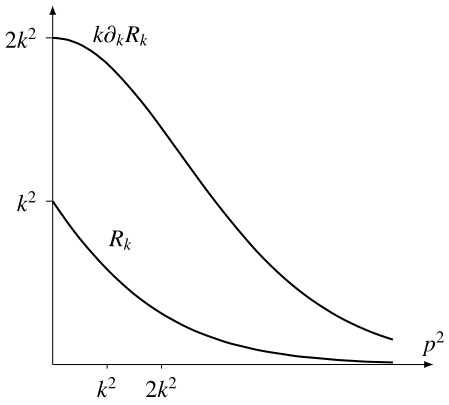

Fig. 12.2 Plots of the exponential cutoff function $R_k(p^2)$ and its derivative $k\partial_k R_k(p^2)$. The cutoff function vanishes for $k \to 0$ and fixed p^2, it becomes large for $k \to \infty$ and it is positive for small arguments p^2

Note that for a fixed source the average field depends on the cutoff function and vice versa for a fixed average field the source depends on the cutoff function. Next we perform a modified Legendre transformation and define the *scale-dependent effective action*

$$\Gamma_k[\varphi] = (j, \varphi) - W_k[j] - \Delta S_k[\varphi]. \tag{12.15}$$

Here it is understood that (12.14) has been solved for $j = j[\varphi]$ and the solution is used on the right hand side. Note that (12.15) is not the Legendre transform of $W_k[j]$ because of the additional term ΔS_k and hence does not need to be convex. But for $k \to 0$ the additional term vanishes and $\Gamma_{k\to 0}$ must become convex. Now we vary the effective average action with respect to φ to derive its equation of motion for the average field,

$$\frac{\delta \Gamma_k}{\delta \varphi(x)} = \int \frac{\delta j(y)}{\delta \varphi(x)} \varphi(y) + j(x) - \int \frac{\delta W_k[j]}{\delta j(y)} \frac{\delta j(y)}{\delta \varphi(x)} - \frac{\delta \Delta S_k[\varphi]}{\delta \varphi(x)}.$$

With (12.14) the first term on the right hand side cancels against the third term and

$$\frac{\delta \Gamma_k}{\delta \varphi(x)} = j(x) - \frac{\delta}{\delta \varphi(x)} \Delta S_k[\varphi] = j(x) - (R_k \varphi)(x). \tag{12.16}$$

12.2 Derivation of the Flow Equation

Now we derive the flow equation for the scale-dependent effective action. Its argument φ is kept fixed such that its conjugated current defined in (12.16) depends on the scale. Differentiating Γ_k in (12.15) results in

$$\partial_k \Gamma_k = \int \mathrm{d}^d x \, \partial_k j(x) \varphi(x) - \partial_k W_k[j] - \int \frac{\partial W_k[j]}{\partial j(x)} \partial_k j(x) - \partial_k \Delta S_k[\varphi],$$

where the variation of W_k yields two contributions: the second term on the right hand side comes from the scale dependence of the parameters in W_k and the third

term from the scale dependence of its argument j. Hence, in the partial derivative $\partial_k W_k[j]$ one varies the parameters and not the argument. With (12.14) the first and third term cancel and

$$\begin{aligned}\partial_k \Gamma_k &= -\partial_k W_k[j] - \partial_k \Delta S_k[\varphi] \\ &= -\partial_k W_k[j] - \frac{1}{2}\int \mathrm{d}^d x\, \mathrm{d}^d y\, \varphi(x)\partial_k R_k(x,y)\varphi(y). \end{aligned} \tag{12.17}$$

Clearly, the partial derivative of W_k in (12.4) is given by

$$\partial_k W_k[j] = -\frac{1}{2}\int \mathrm{d}^d x\, \mathrm{d}^d y \big\langle \phi(x)\partial_k R_k(x,y)\phi(y)\big\rangle_k,$$

and it relates to the connected two-point function

$$G_k^{(2)}(x,y) \equiv \frac{\delta^2 W_k[j]}{\delta j(x)\delta j(y)} = \big\langle \phi(x)\phi(y)\big\rangle_k - \varphi(x)\varphi(y) \tag{12.18}$$

as follows:

$$\begin{aligned}\partial_k W_k[j] &= -\frac{1}{2}\int \mathrm{d}^d x\, \mathrm{d}^d y\, \partial_k R_k(x,y) G_k^{(2)}(y,x) - \partial_k \Delta S_k[\varphi] \\ &= -\frac{1}{2}\,\mathrm{tr}\big(\partial_k R_k G_k^{(2)}\big) - \partial_k \Delta S_k[\varphi]. \end{aligned} \tag{12.19}$$

Now we insert this simple result into the flow equation (12.17) and find

$$\partial_k \Gamma_k = \frac{1}{2}\int \mathrm{d}^d x\, \mathrm{d}^d y\, \partial_k R_k(x,y) G_k^{(2)}(y,x). \tag{12.20}$$

It is known that the second functional derivatives of a convex functional and its Legendre transform define two operators which are inverses of each other, see Eq. (5.58) on p. 89. But since Γ_k is only the modified Legendre transform of W_k we must first calculate the corrections to the quoted result. With

$$\varphi(x) = \frac{\delta W_k[j]}{\delta j(x)} \quad \text{and} \quad j(x) = \frac{\delta \Gamma_k}{\delta \varphi(x)} + \int \mathrm{d}^d y\, R_k(x,y)\varphi(y)$$

we find the following relation between the second derivatives:

$$\delta(x-y) = \int \mathrm{d}^d z \frac{\delta\varphi(x)}{\delta j(z)}\frac{\delta j(z)}{\delta\varphi(y)} = \int \mathrm{d}^d z\, G_k^{(2)}(x,z)\big\{\Gamma_k^{(2)} + R_k\big\}(z,y). \tag{12.21}$$

Between the curly brackets there appears the second functional derivative of Γ_k,

$$\Gamma_k^{(2)}(x,y) = \frac{\delta^2 \Gamma_k}{\delta\varphi(x)\delta\varphi(y)}. \tag{12.22}$$

We conclude that the expression between the curly brackets in (12.21) is the inverse of the connected two-point function G_k. In operator notation this identity reads

$$G_k^{(2)} = \frac{1}{\Gamma_k^{(2)} + R_k}. \tag{12.23}$$

Inserting this result into (12.20) provides us with the flow equation for the scale-dependent effective action [4]

$$\partial_k \Gamma_k[\varphi] = \frac{1}{2}\,\mathrm{tr}\left(\frac{\partial_k R_k}{\Gamma_k^{(2)}[\varphi] + R_k}\right). \tag{12.24}$$

The closed *Wetterich equation* (12.24) is a non-linear functional integro-differential equation which contains the full propagator. It is the starting point for many applications in various branches of theoretical physics.

In passing we note that the intermediate result (12.19) is just the *Polchinski equation* for the scale-dependent Schwinger functional,

$$\partial_k W_k = -\frac{1}{2}\,\mathrm{tr}\big(\partial_k R_k G_k^{(2)}\big) - \frac{1}{2}\big(G_k^{(1)}, \partial_k R_k G_k^{(1)}\big). \tag{12.25}$$

On the right hand side the scale-dependent connected one- and two-point functions appear. These are just the first and second functional derivatives of $W_k[j]$ with respect to its argument.

Both the Polchinski equation (12.25) and Wetterich equation (12.24) are exact functional renormalization group equations. They are related by a (modified) Legendre transformation and as such they are equivalent. The Polchinski equation has a more simple structure since the Schwinger functional and its derivatives appear at most quadratically in this equation. This is not the case for the Wetterich equation in which the second functional derivative of the effective action occurs in the denominator. But it is exactly this property which stabilizes the flow when one tries to actually solve the flow equation in some approximation. This explains why Polchinski's equation is favored in structural investigations whereas Wetterich's equation is mainly used in explicit calculations.

In applications the flow equation must be truncated which means that it is projected onto some finite-dimensional sub-space. Unfortunately it is a highly nontrivial task to find some controlled error estimate for the flow. Typically one improves the truncation in successive steps by including more and more running couplings to see how quickly the flow stabilizes. This gives a first impression about the stability and quality of the flow. In addition one may compare the flows for different regulator functions in a given truncation scheme. For a 'good truncation' the resulting couplings in the infrared should vary little with the regulator function. The most difficult part in any truncation is to include all relevant degrees of freedom in the infrared. If the effective action at the cutoff is quadratic,

$$\Gamma_\Lambda[\varphi] = \frac{1}{2}\int \mathrm{d}^d x\, \varphi\big(-\Delta + m_\Lambda^2\big)\varphi,$$

then the unique solution of the FRG-equation reads

$$\Gamma_k[\varphi] = \Gamma_\Lambda[\varphi] + \frac{1}{2}\log\det\left(\frac{-\Delta + m_\Lambda^2 + R_k}{-\Delta + m_\Lambda^2 + R_\Lambda}\right). \tag{12.26}$$

For the optimized cutoff in (12.10) the last term is

in two dimensions: $\frac{1}{8\pi}\left(m_\Lambda^2 \log\frac{m_\Lambda^2+\Lambda^2}{m_\Lambda^2+k^2}+k^2-\Lambda^2\right)$,

in three dimensions: $\frac{1}{6\pi^2}\left(m_\Lambda^3 \arctan\frac{m_\Lambda(k-\Lambda)}{m_\Lambda^2+k\Lambda}+m_\Lambda^2(\Lambda-k)+\frac{k^3}{3}-\frac{\Lambda^3}{3}\right)$,

in four dimensions: $\frac{1}{64\pi^2}\left(m_\Lambda^4 \log\frac{m_\Lambda^2+k^2}{m_\Lambda^2+\Lambda^2}+m_\Lambda^2\left(\Lambda^2-k^2\right)+\frac{k^4}{2}-\frac{\Lambda^4}{2}\right)$.

12.3 Functional Renormalization Applied to Quantum Mechanics

Before applying the flow equation to quantum field theory we study approximate solutions for the ubiquitous anharmonic oscillator with classical Euclidean action

$$S[\omega]=\int \mathrm{d}\tau\left(\frac{1}{2}\dot{q}^2+V(q)\right), \tag{12.27}$$

depending on a classical potential V. Many techniques and approximations used in field theories can nicely be illustrated and checked against semi-analytic results for this simple quantum-mechanical model. Here we are mainly interested in the *effective potential* and consider the following low energy approximation to the effective average action

$$\Gamma_k[\omega]=\int \mathrm{d}\tau\left(\frac{1}{2}\dot{q}^2+u_k(q)\right) \tag{12.28}$$

with scale-dependent effective potential u_k. We have neglected higher derivative terms or mixed terms of the form $q^n\dot{q}^m$. The truncation (12.28) is the local potential approximation (LPA). It is the leading order in a systematic gradient expansion of the effective action.

On the right hand side of the flow equation the second functional derivative of Γ_k enters, which in the LPA has the simple form $\Gamma_k^{(2)}=-\partial_\tau^2+u_k''(q)$. In order to find the flow projected onto the effective potential it suffices to consider a constant q, for which

$$\begin{aligned}\int \mathrm{d}\tau\,\partial_k u_k(q)&=\frac{1}{2}\int \mathrm{d}\tau\,\mathrm{d}\tau'\,\partial_k R_k\left(\tau-\tau'\right)\left(-\partial_\tau^2+u_k''(q)+R_k\right)^{-1}\left(\tau'-\tau\right)\\&=\frac{1}{2}\int \mathrm{d}\tau\int_{-\infty}^{\infty}\frac{\mathrm{d}p}{2\pi}\frac{\partial_k R_k(p)}{p^2+u_k''(q)+R_k(p)}.\end{aligned} \tag{12.29}$$

To proceed we must choose a regulator function which conforms to the above mentioned conditions. It has been argued in [12, 13] that the regulator function in (12.10) is optimal since it improves the stability properties of the flow equation. Its derivative is $\partial_k R_k(p)=2k\theta(k^2-p^2)$ such that for a constant q we obtain the following non-linear partial differential equation for the effective potential,

$$\partial_k u_k(q)=\frac{1}{\pi}\frac{k^2}{k^2+u_k''(q)}. \tag{12.30}$$

Note that the minimum of $u_k(q)$ cannot be the ground state energy but differs by a q-independent contribution. This already becomes clear by studying the free particle case for which $u_\Lambda = 0$ and (12.30) yields $u_k = (k - \Lambda)/\pi$. In order to extract the true ground state energy from u_k we perform a subtraction to avoid the build up of unphysical zero-point energy contributions [10]. The free particle limit fixes this subtraction in the flow equation and we end up with

$$\partial_k u_k = \frac{1}{\pi}\left(\frac{k^2}{k^2 + u_k''(q)} - 1\right) = -\frac{1}{\pi}\frac{u_k''(q)}{k^2 + u_k''(q)}. \tag{12.31}$$

Let us consider an even potential at the cutoff scale. Then the right hand side of (12.31) is an even function at the cutoff and the solution of the flow equation will be even at all scales. To proceed we make a polynomial ansatz for the even potential,

$$u_k(q) = \sum_{n=0,1,2,\ldots} \frac{1}{(2n)!} a_{2n}(k) q^{2n}, \tag{12.32}$$

where the effects of the fluctuation with short wavelengths are encoded in scale-dependent couplings a_{2n}. Inserting the second derivative of u_k with respect to q into (12.31) and comparing coefficients in a series expansion in powers of q^2 yields an infinite set of coupled ordinary differential equations,

$$\begin{aligned}
\frac{\mathrm{d}a_0}{\mathrm{d}k} &= -\frac{1}{\pi} a_2 \Delta_0, \quad \Delta_0 = \frac{1}{k^2 + a_2}, \\
\frac{\mathrm{d}a_2}{\mathrm{d}k} &= -\frac{k^2}{\pi} a_4 \Delta_0^2, \\
\frac{\mathrm{d}a_4}{\mathrm{d}k} &= -\frac{k^2 \Delta_0^2}{\pi}\left(a_6 - 6a_4^2 \Delta_0\right), \\
\frac{\mathrm{d}a_6}{\mathrm{d}k} &= -\frac{k^2 \Delta_0^2}{\pi}\left(a_8 - 30 a_4 a_6 \Delta_0 + 90 a_4^3 \Delta_0^2\right), \\
&\vdots \quad \vdots
\end{aligned} \tag{12.33}$$

where the dots indicate the equations for the higher coefficients. As initial conditions we use the parameters a_{2n} at the cutoff—the parameters in the classical potential.

We first project the flow onto the space of fourth-order polynomials and hence impose $a_6 = 0$ in Eqs. (12.33). Using the standard notation

$$a_0 = E, \qquad a_2 = \omega^2 \quad \text{and} \quad a_4 = \lambda, \tag{12.34}$$

we find the following truncated system of flow equations

$$\frac{\mathrm{d}E_k}{\mathrm{d}k} = -\frac{\omega_k^2}{\pi}\Delta_0, \qquad \frac{\mathrm{d}\omega_k^2}{\mathrm{d}k} = -\frac{k^2 \lambda_k}{\pi}\Delta_0^2, \qquad \frac{\mathrm{d}\lambda_k}{\mathrm{d}k} = \frac{6k^2\lambda_k^2}{\pi}\Delta_0^3. \tag{12.35}$$

With the `octave`-program on p. 286 we solved these differential equations subject to the initial conditions $E_\Lambda = 0, \omega_\Lambda = 1$ and a varying quartic coupling λ at the cutoff scale. The scale-dependent couplings E_k and ω_k^2 are depicted in Fig. 12.3. They hardly change for $k \gg \omega$ and only when the scale parameter is comparable

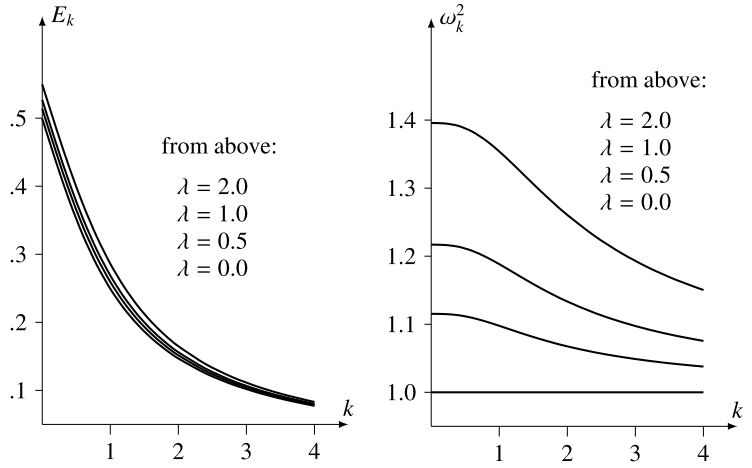

Fig. 12.3 The flow of the couplings E_k and ω_k^2 of the anharmonic oscillator for the cutoff values $E_\Lambda = 0$ and $\omega_\Lambda^2 = 1$. The values at $k = 0$ contain quantum corrections from all length scales

to the characteristic scale ω of the oscillator do the couplings begin to flow. For a positive $\omega = \omega_{k=0}$ the effective potential is minimal at the origin such that the *ground state* energy is just $E_0 = \min(u_{k=0})$. The energy of the *first excited state* is given by the curvature of the effective potential at its minimum,

$$E_1 = E_0 + \sqrt{u''_{k=0}(0)} = E_0 + \omega_{k=0}. \tag{12.36}$$

The second and sixth columns in Table 12.1 contain the energies of the ground state and first excited state for varying values of the quartic coupling λ of the anharmonic oscillator. The fifth and last columns contain the 'exact values' for E_0 and E_1 obtained by a numerical diagonalization of the matrix-Schrödinger operator of the anharmonic oscillator with SLAC lattice derivative [14, 15]. A comparison reveals that the simple projection of the LPA-flow onto polynomials of order four already leads to rather accurate values for the energies.

12.3.1 Projection onto Polynomials of Order 12

To judge the quality of the polynomial truncation we also calculated the flow projected onto even polynomials of order 12 with the `octave`-program on p. 286. The corresponding energies are listed in the columns 3 and 7 in Table 12.1 and they are almost identical to the values obtained for the projection onto fourth-order polynomials. For positive ω^2 we do not gain much by including higher-order terms in the polynomial truncation.

Table 12.1 Energies of the ground state and first excited state of the anharmonic oscillator with varying λ extracted from the flow in the LPA projected onto polynomials of order 4 and order 12. We used the optimized regulator and the Callan–Symanzik regulator $R_k(p) = k^2$. The fifth and last column contain the 'exact values'. The energies and couplings are given in units of $\hbar\omega$

Cutoff	Ground state energy				Energy of first excited state			
	optimal order 4	optimal order 12	Callan order 4	exact result	optimal order 4	optimal order 12	Callan order 4	exact result
$\lambda = 0$	0.5000	0.5000	0.5000	0.5000	1.5000	1.5000	1.5000	1.5000
$\lambda = 1$	0.5277	0.5277	0.5276	0.5277	1.6311	1.6315	1.6307	1.6313
$\lambda = 2$	0.5506	0.5507	0.5504	0.5508	1.7324	1.7341	1.7314	1.7335
$\lambda = 3$	0.5706	0.5708	0.5703	0.5710	1.8177	1.8207	1.8159	1.8197
$\lambda = 4$	0.5885	0.5889	0.5882	0.5891	1.8923	1.8968	1.8898	1.8955
$\lambda = 5$	0.6049	0.6054	0.6045	0.6056	1.9593	1.9652	1.9562	1.9637
$\lambda = 6$	0.6201	0.6207	0.6196	0.6209	2.0205	2.0278	2.0168	2.0260
$\lambda = 7$	0.6343	0.6350	0.6336	0.6352	2.0771	2.0857	2.0728	2.0836
$\lambda = 8$	0.6476	0.6484	0.6469	0.6487	2.1299	2.1397	2.1250	2.1374
$\lambda = 9$	0.6602	0.6611	0.6594	0.6614	2.1794	2.1905	2.1741	2.1879
$\lambda = 10$	0.6721	0.6732	0.6713	0.6735	2.2263	2.2385	2.2205	2.2357
$\lambda = 20$	0.7694	0.7714	0.7679	0.7719	2.5994	2.6209	2.5898	2.6166

12.3.2 Changing the Regulator Function

In order to study the dependence of the flow on the regulator function we now use the momentum-independent Callan–Symanzik regulator $R_k(p) = k^2$. After subtracting the unphysical zero-point energy contributions the flow equation for the effective potential (12.29) takes the form

$$\partial_k u_k = \frac{1}{2}\left(\frac{k^2}{k^2 + u_k''(q)}\right)^{1/2} - \frac{1}{2}. \tag{12.37}$$

As before we choose an even potential at the cutoff such that u_k stays even at all scales. Expanding u_k in even powers of q and comparing coefficients we find the following equations for the flow projected onto fourth-order polynomials,

$$\begin{aligned} \frac{\mathrm{d}a_0}{\mathrm{d}k} &= \frac{1}{2}\left(k\Delta_0^{1/2} - 1\right), \\ \frac{\mathrm{d}a_2}{\mathrm{d}k} &= -\frac{k}{4}a_4\Delta_0^{3/2}, \\ \frac{\mathrm{d}a_4}{\mathrm{d}k} &= \frac{9k}{8}a_4^2\Delta_0^{5/2}. \end{aligned} \tag{12.38}$$

Similarly as for the optimized regulator we calculated the energies of the ground state and first excited state with the `octave`-program on p. 286 and the results are collected in the 5th and second to last columns in Table 12.1. The values are almost as accurate as those obtained with the optimized cutoff function.

12.3.3 Solving the Flow Equation for Non-convex Potentials

The classical potential with negative ω^2 shows a local maximum at the origin and two minima at $\pm v$, where $v^2 = -6\omega^2/\lambda$. The flow equation (12.30) reveals that u_k changes most rapidly near positions where its curvature is minimal which happens at maxima of u_k. The denominator $k^2 + u_k''$ in the equation is positive for large scales and the structure of the flow equation ensures that it remains positive during the flow. It follows from the flow equation (12.31) that $u_k(q)$ increases with decreasing k if $u_k''(q)$ is positive and it decreases if $u_k''(q)$ is negative. This implies that a double-well potential flattens when it flows to the infrared and finally becomes convex for $k \to 0$. This is expected on general grounds and has been discussed in the context of the Wetterich equation in [16]. Figure 12.4 shows the solution of the partial differential equation (12.31) for a classical double-well potential with couplings $\omega^2 = -1$ and $\lambda = 1$. Here we see explicitly how the potential becomes convex at small scales. The parabolic differential equation (12.31) has been solved numerically with the `octave` function `flowpde` on p. 288. For the numerical treatment we discretized *coordinate space* and replaced the continuous position variable q by equidistant points $q_1, \ldots, q_N$ in a suitable chosen interval $[-L, L]$. Then the function $u_k(q)$ of the two variables k and q becomes a vector-valued function $u_k(q_i)$ of the continuous flow parameter k. At the same time the partial differential equation (12.31) turns into a system of N ordinary differential equations

$$\partial_k u_k(q_i) = -\frac{1}{\pi} \frac{(\Delta u_k)(q_i)}{k^2 + (\Delta u_k)(q_i)}, \tag{12.39}$$

where Δ is a discretized second derivative. In the function `flowpde` we use

$$(\Delta u_k)(q_i) = \frac{u_k(q_{i+1}) + u_k(q_{i-1}) - 2u_k(q_i)}{(\Delta q)^2}$$

for which an *even* classical potential flows into an even effective potential.

The energies of the ground state and first excited state of the anharmonic oscillators with double-well potential are given in Table 12.2. We see that the projection of the flow onto fourth-order polynomials yields inaccurate results for weak couplings. The reason is that for small λ/ω^3 the potential near the minimum of the classical potential changes rapidly and this happens away from the origin where the polynomial approximation applies. The numerical solution of the flow equation (12.31) does better. But for decreasing λ or equivalently increasing barrier of the classical potential it becomes more and more difficult to extract reliable results from the LPA. For large barriers the low-lying energies come in almost degenerate pairs and the splitting of the doublet is induced by instanton effects. To detect these exponentially suppressed non-perturbative effects one needs to go beyond the leading order LPA [17].

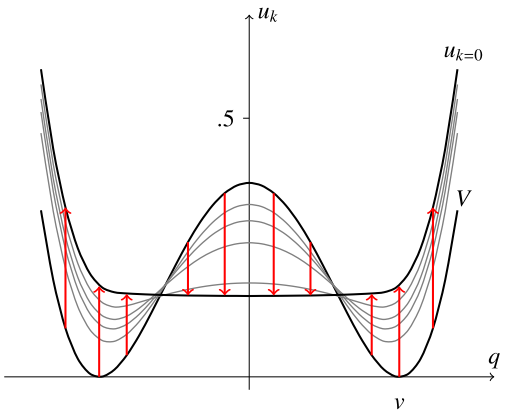

Fig. 12.4 Flow of the scale-dependent effective potential in the local potential approximation. At the cutoff the flow begins with a non-convex double-well potential and for small scales ends up with a convex potential $u_{k=0}$. Depicted is the solution of (12.31) with initial couplings $\omega^2 = -1$ and $\lambda = 1$

Table 12.2 Energies of the ground state and first excited state for the anharmonic oscillator with $\omega^2 = -1$ and varying λ. All energies are calculated with the optimized regulator. For small λ the polynomial approximation of order 4 fails. Also shown are the energies calculated from the numerical solution of the partial differential equation (12.31). In the fifth and last column we listed the 'exact values'. Energies and couplings are given in units of $\hbar\omega$

	Ground state energy				Energy of first excited state			
	optimal order 4	optimal order 12	pde	exact	optimal order 4	optimal order 12	pde	exact
$\lambda = 1$			−0.8732	−0.8556			−0.7887	−0.8299
$\lambda = 2$		−0.2474	−0.2479	−0.2422		0.0049	0.0063	−0.0216
$\lambda = 3$	0.2473	−0.0681	−0.0679	−0.0652	−0.2241	0.3514	0.3500	0.3307
$\lambda = 4$	−0.0186	0.0286	0.0290	0.0308	0.3511	0.5753	0.5755	0.5598
$\lambda = 5$	0.0654	0.0949	0.0953	0.0967	0.5835	0.7455	0.7462	0.7324
$\lambda = 6$	0.1234	0.1457	0.1461	0.1472	0.7509	0.8842	0.8851	0.8723
$\lambda = 7$	0.1688	0.1871	0.1876	0.1885	0.8851	1.0021	1.0030	0.9909
$\lambda = 8$	0.2063	0.2223	0.2228	0.2236	0.9987	1.1052	1.1061	1.0944
$\lambda = 9$	0.2671	0.2530	0.2535	0.2543	1.1863	1.1972	1.1981	1.1866
$\lambda = 10$	0.2386	0.2803	0.2808	0.2816	1.0978	1.2805	1.2814	1.2701
$\lambda = 20$	0.4536	0.4632	0.4639	0.4643	1.7866	1.8638	1.8648	1.8538

Comparison with Weak-Coupling Perturbation Expansion

From ordinary weak-coupling stationary perturbation theory for the anharmonic oscillator one obtains a series expansion for the ground state energy in powers of λ/ω^3. The leading terms are [18]

$$E_0 = \frac{\omega}{2} + \frac{3\omega}{4}\varepsilon - \frac{21\omega}{8}\varepsilon^2 + \cdots, \quad \varepsilon = \frac{\lambda}{24\omega^3}. \tag{12.40}$$

We wish to extract a similar weak-coupling expansion from the truncated flow equations (12.35). For the harmonic oscillator with a vanishing λ the coupling ω_k is scale independent and $\lambda_k = 0$ for all k. This points to the following series expansion for the (dimensionless) scale-dependent couplings in powers of the dimensionless small parameter $\varepsilon \ll 1$,

$$\begin{aligned} E_k/\omega &= \alpha_0 + \alpha_1\varepsilon + \alpha_2\varepsilon^2 + \cdots, \\ \omega_k^2/\omega^2 &= 1 + \beta_1\varepsilon + \beta_2\varepsilon^2 + \cdots, \\ \lambda_k/24\omega^3 &= \varepsilon + \gamma_2\varepsilon^2 + \cdots. \end{aligned} \tag{12.41}$$

Inserting these expansions into the truncated flow equations (12.35) and comparing coefficients of $\varepsilon^0, \varepsilon^1$ and ε^2 leads to simple flow equations for the coefficient functions $\alpha_0, \alpha_1, \alpha_2, \beta_1, \beta_2$ and γ_2. For large scales the coefficients must vanish and this initial condition determines the solution. Details of the calculation are found in problem 12.1.

It is easier to find an explicit solution of these equations if we first neglect the running of the anharmonic coupling and set $\lambda_k = \lambda$ or equivalently $\gamma_2 = 0$. For this crude truncation the coefficient functions α_0, α_1 are given in (12.114) and α_2 in (12.115). The ground state energy is obtained if we set $x = k/\omega = 0$ in these results, such that

$$E_0 = \frac{\omega}{2} + \frac{3\omega}{4}\varepsilon - \frac{21\omega}{8}\kappa\varepsilon^2 + \cdots, \quad \kappa = \frac{8\pi^2 + 29}{14\pi^2} = 0.7813. \tag{12.42}$$

Already from our crude approximation we have obtained the correct coefficient 3/4 for the first-order contribution. The coefficient of the second-order contribution is off by the factor $\kappa \approx 0.78$. Even for a running λ_k we can integrate the differential equations for the coefficients analytically. The small-x expansions of the coefficients are given in (12.114) in the Appendix and lead to

$$E_0 = \frac{\omega}{2} + \frac{3\omega}{4}\varepsilon - \frac{21\omega}{8}\kappa'\varepsilon^2 + \cdots, \quad \kappa' = \frac{10\pi^2 - 29}{7\pi^2} = 1.0088. \tag{12.43}$$

We see that the simple local potential approximation projected onto polynomials of degree four reproduces the second-order coefficient in the weak-coupling expansion very well. It exceeds the correct value by less than 1 %.

12.4 Scalar Field Theory

A quantum-mechanical system can be interpreted as one-dimensional field theory, and this explains why the previous methods and results are easily extended to field theories—at least to field theories without local symmetries. In this section we study the flow equation for a scalar field theory in d dimensions with Euclidean action

$$\mathscr{L} = \frac{1}{2}(\partial_\mu\phi)^2 + V(\phi). \tag{12.44}$$

First we consider the local potential approximation of the effective average action

$$\Gamma_k[\varphi] = \int \mathrm{d}^d x \left(\frac{1}{2} (\partial_\mu \varphi)^2 + u_k(\varphi) \right). \tag{12.45}$$

Its second functional derivative $\Gamma_k^{(2)} = -\Delta + u_k''(\varphi)$ enters the flow equation. Projecting the flow onto constant average fields we arrive at the following flow equation for the scale-dependent effective potential,

$$\partial_k u_k(q) = \frac{1}{2} \int \frac{\mathrm{d}^d p}{(2\pi)^d} \frac{\partial_k R_k(p)}{p^2 + u_k''(q) + R_k(p)}. \tag{12.46}$$

For the optimized regulator the integral can be calculated in closed form and the result contains the volume of the d-dimensional ball divided by $(2\pi)^d$,

$$\mu_d = \frac{\pi^{d/2}}{(2\pi)^d \Gamma(d/2+1)} = \frac{1}{(4\pi)^{d/2} \Gamma(d/2+1)}. \tag{12.47}$$

The flow equation has the simple form

$$\partial_k u_k(\varphi) = \mu_d \frac{k^{d+1}}{k^2 + u_k''(\varphi)}, \tag{12.48}$$

where prime denotes the derivative with respect to the field. For $d = 1$ we recover the flow equation for the anharmonic oscillator (12.30). Inserting the polynomial ansatz (12.32) for an even potential into the flow equation and comparing coefficients we end up with similar flow equations as in quantum mechanics,

$$\begin{aligned}
\frac{\mathrm{d}a_0}{\mathrm{d}k} &= -\mu_d k^{d+2} \Delta_0, \quad \Delta_0 = \frac{1}{k^2 + a_2}, \\
\frac{\mathrm{d}a_2}{\mathrm{d}k} &= -\mu_d k^{d+2} \Delta_0^2 a_4, \\
\frac{\mathrm{d}a_4}{\mathrm{d}k} &= -\mu_d k^{d+2} \Delta_0^2 \big(a_6 - 6a_4^2 \Delta_0\big), \\
\frac{\mathrm{d}a_6}{\mathrm{d}k} &= -\mu_d k^{d+2} \Delta_0^2 \big(a_8 - 30 a_4 a_6 \Delta_0 + 90 a_4^3 \Delta_0^2\big), \\
&\vdots \quad \vdots
\end{aligned} \tag{12.49}$$

where the geometric factor μ_d was introduced earlier in (12.47).

12.4.1 Fixed Points

To localize the fixed points of RG flow in the local potential approximation we introduce the dimensionless field and potential

$$\varphi = k^{(d-2)/2} \sqrt{\mu_d}\, \chi \quad \text{and} \quad u_k(\varphi) = k^d \mu_d v_k(\chi) \tag{12.50}$$

and rewrite the flow equation for $u_k(\varphi)$ in terms of these rescaled quantities,

$$k\partial_k v_k + d v_k - \frac{d-2}{2}\chi v_k' = \frac{1}{1+v_k''}, \tag{12.51}$$

where a prime is now the derivative with respect to the dimensionless field χ. At a fixed point of the flow the first term on the left hand side vanishes, such that a fixed-point potential v_* satisfies the following second-order differential equation:

$$d v_* - \frac{d-2}{2}\chi v_*' = \frac{1}{1+v_*''}. \tag{12.52}$$

In any dimension this equation has the constant solution $d v_* = 1$ corresponding to a trivial Gaussian fixed point. Does it also possess other regular solutions corresponding to non-Gaussian fixed points? The answer to this question depends on the dimension d of spacetime.

For an even classical potential v_k is even as well and we can set

$$v_k(\chi) = w_k(\rho), \quad \text{with } \rho = \frac{\chi^2}{2}. \tag{12.53}$$

The flow equation for $w_k(\rho)$ takes the form

$$k\partial_k w_k(\rho) + d w_k(\rho) - (d-2)\rho w_k'(\rho) = \frac{1}{1+w_k'(\rho)+2\rho w_k''(\rho)}, \tag{12.54}$$

where the prime denotes the derivative with respect to ρ. Note that in two dimensions a classical scalar field is dimensionless such that the last term on the left hand side of the associated fixed-point equation

$$d w_*(\rho) - (d-2)\rho w_*'(\rho) = \frac{1}{1+w_*'(\rho)+2\rho w_*''(\rho)} \tag{12.55}$$

is absent. This property is the main reason why two-dimensional scalar field theories admit infinitely many fixed-point solutions [19]. Actually the same happens for two-dimensional Yukawa theories with scalars and fermions in interaction [20].

In a polynomial truncation to order m we expand the dimensionless potential in powers of ρ,

$$w^{(m)} = \sum_{n=0}^{m} c_n \rho^n. \tag{12.56}$$

The corresponding flow equations for the couplings c_n read

$$\begin{aligned}
k\partial_k c_0 &= -d c_0 + \Delta_0, \quad \Delta_0 = (1+c_1)^{-1},\\
k\partial_k c_1 &= -2c_1 - 6c_2\Delta_0^2,\\
k\partial_k c_2 &= (d-4)c_2 - 15c_3\Delta_0^2 + 36c_2^2\Delta_0^3,\\
k\partial_k c_3 &= (2d-6)c_3 - 28c_4\Delta_0^2 + 180c_2c_3\Delta_0^3 - 216c_2^3\Delta_0^4,\\
k\partial_k c_4 &= (3d-8)c_4 - 45c_5\Delta_0^2 + \left(336c_2c_4 + 225c_3^2\right)\Delta_0^3\\
&\quad - 1620c_2^2c_3\Delta_0^4 + 1296c_2^4\Delta_0^5.\\
&\vdots \quad \vdots
\end{aligned} \tag{12.57}$$

Scalar Fields in Three Dimensions

Many three-dimensional field theories admit non-trivial fixed points and the scalar theory is no exception. As we cannot solve the fixed-point equation (12.55) exactly, we have to find ways to get at least approximate solutions. We use the polynomial truncation which leads to (12.57) with vanishing left hand sides. Thus we find m algebraic equations for the $m+1$ fixed-point couplings,

$$0 = f_0\big(c_0^*, c_1^*\big) = f_1\big(c_1^*, c_2^*\big) = \cdots = f_{m-1}\big(c_1^*, \ldots, c_m^*\big).$$

The functions are just the right hand sides of the system of equations (12.57) for $d = 3$. They are polynomials in $c_0^*, c_2^*, \ldots, c_m^*$ and $\Delta_0 = 1/(1 + c_1^*)$. Since the slope at the origin c_1^* is the only non-polynomial variable we solve the system for $c_0^*, c_2^*, c_3^*, \ldots, c_m^*$ in terms of c_1^*. Algebraic computer programs[1] find the solution for polynomials of order 42. In the intermediate manipulation it is useful to introduce $c_1^* - 1$ as new variable. The explicit expressions for the lowest couplings read

$$\begin{aligned}
c_0^* &= \frac{1}{3}\frac{1}{1+c_1^*}, \\
c_2^* &= -\frac{c_1^*(1+c_1^*)^2}{3}, \\
c_3^* &= \frac{c_1^*(1+c_1^*)^3(1+13c_1^*)}{45}, \\
c_4^* &= -\frac{c_1^{*2}(1+c_1^*)^4(1+7c_1^*)}{21}, \\
&\vdots \quad \vdots \\
c_m^* &= c_1^{*2}\big(1+c_1^*\big)^m P_{m-3}\big(c_1^*\big),
\end{aligned} \tag{12.58}$$

where P_k is a polynomial of order k. We recover the trivial solution

$$c_0^* = \frac{1}{3}, \qquad 0 = c_2^* = c_3^* = c_4^* = \cdots \tag{12.59}$$

corresponding to the Gaussian fixed point $w_*' = 1$. To find an approximate non-trivial fixed-point solution we truncate the tower of algebraic equations and set $c_m^* = 0$ which leads to $P_{m-3}(c_1^*) = 0$. Generically, the polynomials P_k has several real roots and we must pick a particular one. We choose roots c_1^* such that for large m they converge to a fixed value. For this choice of slopes at the origin the approximating polynomials converge to a power series with maximal radius of convergence. For example, for polynomials of order 20 and 42 we find the two roots $c_1^* = -.186066$ and $c_1^* - .186041$ in agreement with [21]. Inserting the solution for $m = 20$ and for $m = 42$ into (12.58) yields the coefficients of the polynomials given in Table 12.3.

In Fig. 12.5 we plotted the polynomials of order 10, 20, 30 and 40 which approximate the fixed-point solution in the local potential approximation. The potentials are compared with the numerical solution of the fixed-point equation.

[1] The calculation in this section were performed with REDUCE 3.8.

Table 12.3 With $n!$ multiplied coefficients c_n^* of two polynomial approximations to the fixed-point solution. The lowest coefficients do not change much when one increases the polynomial degree from $m = 20$ to $m = 42$

	c_0^*	c_1^*	c_2^*	c_3^*	c_4^*	c_5^*	c_6^*
$m = 20$	0.409534	−0.186066	0.082178	0.018981	0.005253	0.001104	−0.000255
$m = 42$	0.409533	−0.186064	0.082177	0.018980	0.005252	0.001104	−0.000256

	c_7^*	c_8^*	c_9^*	c_{10}^*	c_{11}^*	c_{12}^*	c_{13}^*
$m = 20$	−0.000526	−0.000263	0.000237	0.000632	0.000438	−0.000779	−0.002583
$m = 42$	−0.000526	−0.000263	0.000236	0.000629	0.000431	−0.000799	−0.002643

	c_{14}^*	c_{15}^*	c_{16}^*	c_{17}^*	c_{18}^*	c_{19}^*	c_{20}^*
$m = 20$	−0.002029	0.007305	0.028778	0.034696	−0.077525	−0.381385	0.000000
$m = 42$	−0.002216	0.006677	0.026544	0.026320	−0.110498	−0.517445	−0.587152

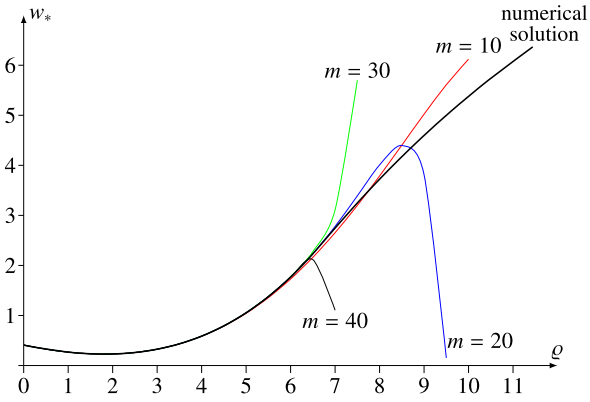

Fig. 12.5 Fixed-point solution w_* of a scalar field theory with even potentials in three dimensions. Depicted are the numerical solution to the differential equation (12.60) and results of polynomial approximations with polynomials of degree 10, 20, 30 and 40

Numerical Solution

When we try to solve the fixed-point equation by numerical means we generically run into a singularity at a finite value of ρ. At the singular point the potential and its derivative are both finite but its higher derivatives are divergent. A solution of the fixed-point equation

$$w_*'' = \frac{1}{2\rho}\,\frac{1}{d\,w_* - (d-2)\rho\,w_*'} - \frac{1 + w_*'}{2\rho}, \quad (d = 3), \tag{12.60}$$

may become singular when the denominator $3w_*(\rho) - \rho\,w_*'(\rho)$ vanishes. Regularity at the origin demands that the 'initial values' $w_*(0)$, $w_*'(0)$ are related as

$$w_*'(0) = c^* \quad \text{and} \quad w_*(0) = \frac{1}{3}\,\frac{1}{1 + c^*}. \tag{12.61}$$

This is just the first relation in (12.58). From the polynomial truncation we already know that the slope at the origin is $w'_*(0) \approx -0.18606$. We applied the shooting method with a seventh-order Runge–Kutta integrator and determined the slope for which the numerical solution is regular for $\rho \leq 120$. The resulting slope $w'_*(0) \approx -0.186064249376$ is almost identical with the slope -0.186064279993 of the approximating polynomial of degree 42.

12.4.2 Critical Exponents

Let us study the solution to the flow equation in the vicinity of a prescribed fixed-point solution w_*. Thus we write $w_k = w_* + \delta_k$ and linearize the flow equation (12.54) in the small perturbation δ_k. Using the fixed-point equation of w_* we end up with the following linear differential equation for the small fluctuation δ_k:

$$k\partial_k \delta_k = -d\delta_k + (d-2)\rho\delta'_k - \big(dw_* - (d-2)\rho w'_*\big)^2\big(\delta'_k + 2\rho\delta''_k\big). \tag{12.62}$$

To make progress we insert the polynomial approximation for the fixed-point solution and make a polynomial ansatz for the perturbation,

$$\delta_k(\rho) = \sum_{n=0}^{m-1} d_n \rho^n, \quad \rho = \frac{\chi^2}{2}. \tag{12.63}$$

The resulting linear system for the coefficients d_m has the form

$$k\partial_k \begin{pmatrix} d_0 \\ d_1 \\ \vdots \\ d_{m-1} \end{pmatrix} = M\big(c_0^*\big) \begin{pmatrix} d_0 \\ d_1 \\ \vdots \\ d_{m-1} \end{pmatrix} \tag{12.64}$$

and the critical exponents are identified with the eigenvalues of the m-dimensional matrix M. With an algebraic computer program we calculated the eigenvalues for polynomial truncations up to order 46. The results are listed in Table 12.4. The Z_2-symmetric model has two negative exponents $\omega_0 = -3$ and $\omega_1 = -1/\nu$. The former corresponds to the trivial scaling of the ground state energy and is unrelated to the critical behavior. The remaining exponents $\omega_2, \omega_3, \ldots$ are all positive. We see that the smallest exponents extracted from the polynomial truncations converge with increasing m and can be extrapolated to $m = \infty$. The LPA-prediction obtained in this way $\nu = 0.649562$ should be compared with the accurate prediction $\nu = 0.630$ of the high-temperature expansion, see Table 9.9. To obtain more accurate results one needs to go beyond the local potential approximation.

12.5 Linear $O(N)$ Models

The previous results are readily extended to the linear $O(N)$ models in d dimensions. So let us assume that the scalar field ϕ has N real components and that the interaction term in the Lagrangian density

$$\mathscr{L} = \frac{1}{2}(\partial_\mu \phi)^2 + V(\phi), \tag{12.65}$$

Table 12.4 The five smallest non-trivial eigenvalues of the stability matrix corresponding to the Wilson–Fisher fixed point. The exponents are calculated for different polynomial truncations up to degree $m = 46$ of the LPA. The eigenvalue $\omega_0 = -3$ of the scaling operator 1 is not listed

m	$\nu = -1/\omega_1$	ω_2	ω_3	ω_4	ω_5
10	0.648617	0.658053	2.985880	7.502130	17.913494
14	0.649655	0.652391	3.232549	5.733445	9.324858
18	0.649572	0.656475	3.186784	5.853987	9.141093
22	0.649554	0.655804	3.170538	5.977066	8.522811
26	0.649564	0.655629	3.182910	5.897290	8.844632
30	0.649562	0.655791	3.180847	5.903039	8.907607
34	0.649561	0.655749	3.178636	5.922910	8.702583
38	0.649562	0.655731	3.180577	5.908885	8.814225
42	0.649562	0.655755	3.180216	5.909910	8.847386
46	0.649562	0.655746	3.179541	5.915754	8.738608

is $O(N)$ invariant. This means that the potential depends only on the modulus of $\phi \in \mathbb{R}^N$. In the fixed-point analysis we use the dimensionless field χ and the dimensionless potential v_k in (12.50). For the $O(N)$ models it is convenient to introduce the invariant composite field

$$\rho = \frac{1}{2}\sum_{i=1}^{N} \chi_i^2, \tag{12.66}$$

since the invariant scaling potential is a function of ρ only, $v_k(\chi) = w_k(\rho)$. For several components the flow equation (12.51) generalizes to

$$\partial_k v_k(\chi) = d v_k - \frac{d-2}{2}\chi v_k' = \mathrm{tr}\left(\frac{1}{1+\partial_i\partial_j v_k(\chi)}\right). \tag{12.67}$$

For $v_k = w_k(\rho)$ the matrix in the denominator becomes $\partial_i\partial_j v_k = \delta_{ij} w_k' + \chi_i\chi_j w_k''$ and has just two eigenvalues: the single eigenvalue $w_k' + 2\rho w_k''$ and the highly degenerate eigenvalue w_k'. Hence for multi component fields with $O(N)$ invariant interaction the flow equation (12.51) translates into

$$k\partial_k w_k + d w_k - (d-2)\rho w_k' = \frac{N-1}{1+w_k'} + \frac{1}{1+w_k'+2\rho w_k''}, \tag{12.68}$$

where a prime denotes the derivative with respect to the invariant field ρ. The first term on the right hand side is easily recognized as the contribution of the $N-1$ Goldstone modes. The last term is related to the massive radial mode. For large N the Goldstone modes give the main contribution to the flow equation.

To study the critical behavior we linearize the flow equation about a fixed-point solution w_* and hence set $w_k = w_* + \delta_k$. The fluctuation δ_k obeys the linear differential equation

$$k\partial_k\delta_k = -d\delta_k + (d-2)\rho\delta_k' - \frac{(N-1)\delta_k'}{(1+w_*')^2} - \frac{\delta_k' + 2\rho\delta_k''}{(1+w_*'+2\rho w_*'')^2}. \tag{12.69}$$

Table 12.5 The slope of the fixed-point solution at the origin and the three smallest non-trivial eigenvalues of the stability matrix corresponding to the Wilson–Fisher fixed point of the $O(N)$ models. The eigenvalue $\omega_0 = -3$ of the scaling operator 1 is not listed. The numbers are calculated with a polynomial truncation of degree 40

N	1	2	3	100	1000
$-w_*'(0)$	0.186064	0.230186	0.263517	0.384172	0.387935
$\nu = -1/\omega_1$	0.64956	0.70821	0.76113	0.99187	0.99923
ω_2	0.6556	0.6713	0.6990	0.97218	0.99844
ω_3	3.1798	3.0710	3.0039	2.98292	2.99554

Now we proceed exactly in the same way as for the one-component model without Goldstone modes considered in the previous section. The fixed-point solution and the critical exponents in the polynomial truncation are computed with an algebraic computer program. We used polynomials of degree 40 to determine the eigenvalues of the stability matrix listed in Table 12.5. For a given N we must find polynomial approximations which for small values of ρ converge to a fixed-point solution. For this purpose one picks that root of the polynomial $P_{m-3}(c_1^*)$ for which the roots converge with increasing degree of the polynomials. This amounts to a fine tuning of the slope at the origin. The correct slopes are calculated beforehand and are used in the algebraic computer program.

Actually we can do better and extend the polynomial truncation to much higher order. For example, for the Z_2-model we obtain the value $\nu = 0.649561776$ from a truncation to polynomials of degree $m = 60$. With the help of a conformal mapping one can further extend the polynomial truncation to order 75 which yields the more accurate value[2] $\nu = 0.649561773880\ldots$. Plots of the scaling potentials w_* of various $O(N)$ models and more critical exponents are found in [21].

Looking at the exponents in the table one may conjecture that for large N the critical exponents converge to $\omega_n^\infty = 2n - 3$. Since it was shown in [22] that the LPA is exact in the large N limit for the effective potential we expect that the ω_n^∞ are the exact critical exponents in this limit. In the following section we shall see that this indeed the case. Actually the exponents ω_n converge to their limiting values ω_n^∞ as

$$\omega_n = \omega_n^\infty + \frac{\delta_n}{N} + \cdots. \tag{12.70}$$

Linear fits in the small parameter $1/N$ to the slope as well as the critical exponent ν for $N = 100, 500$ and 1000, as depicted in Fig. 12.6, yield the asymptotic formulas

$$w_*'(0) \approx -0.3881 + 0.4096/N, \qquad \nu \approx 0.9998 - 0.9616/N. \tag{12.71}$$

The number -0.3881 is close to that of the large N expansion, which is $-0.3883\ldots$. Our prediction for ν is also close to the exact result $\nu \approx 1 - 1.081/N$ derived in

[2] Private communication by Daniel Litim.

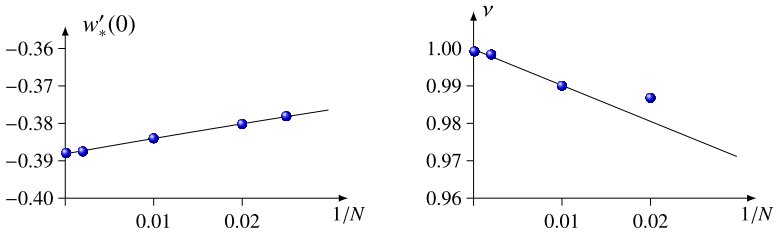

Fig. 12.6 The slope $w'_*(0)$ and the critical exponent ν for large values of N. Fitting the data points for $N \geq 100$ with a linear function in $1/N$ yields (12.71). The interpolating linear functions are plotted in the figure

Table 12.6 Critical exponents from the derivative expansion (de) [25], the BMW approximation [26] and lattice simulation combined with the high-temperature expansion [27–29], see Table 9.12

N	1	2	3	4	10	100
ν_{de}	0.631	0.666	0.704	0.739	0.881	0.990
ν_{bmw}	0.632	0.674	0.715	0.754	0.889	0.990
$\nu_{\mathrm{mc,hte}}$	0.630	0.672	0.711	0.749	0.867	
ω_{bmw}	0.78	0.75	0.73	0.72	0.80	1.00
ω_{mc}	0.832	0.785	0.773	0.765		

[23]. Notice that the subleading terms are very small for the N used in the fit. To make further progress one must go beyond the LPA. In a next step in the derivative expansion one would include a momentum- and field-dependent wave function renormalization and terms containing derivatives of the fields. Also, to determine critical exponents like the anomalous dimension one should allow for a momentum dependence of the correlation functions. An approximation which keeps the momentum dependence in the two-point function has been proposed in [24]. This approximation was used to obtain better values for critical exponents of the $O(N)$ models. Table 12.6 contains the results obtained with such approximations. They are compared with the exponents extracted from simulations and high-temperature expansions. Including the momentum dependence has become more important over the last years. This leads to a higher numerical effort and the recently published numerical toolbox `FlowPy` [30] can be used to find solutions of a broad class of partial differential equations that are encountered in next to leading-order approximations.

12.5.1 Large N Limit

For a large number of field components N we only keep the terms of order N on the right hand side of the flow equation (12.68). In the resulting differential equation

$$k\partial_k w_k = (d-2)\rho w'_k - d w_k + \frac{N}{1+w'_k} \tag{12.72}$$

the contribution of the radial mode is missing. Thus in the large-N limit only the fluctuating Goldstone modes are responsible for a non-trivial flow to the infrared. To obtain a differential equation which is linear in the first derivatives and hence can be solved with the methods of characteristics, we differentiate (12.72) with respect to the field ρ. Introducing the dimensionless scale parameter $t = \log(k/\Lambda)$ we obtain the flow equation for $w'(t,\rho) = w_k'(\rho)$:

$$\partial_t w' = (d-2)\rho w'' - 2w' - \frac{N}{(1+w')^2} w''. \tag{12.73}$$

Before we present and discuss the analytical solutions of this differential equation we study the fixed-point solutions and calculate the critical exponents.

Fixed-Point Analysis

It is not difficult to solve the ordinary differential equation for a fixed-point solution $w_*'(\rho)$. The general solution depends on a free parameter c and reads

$$\frac{1}{\sqrt{\pm w'}} \frac{\rho}{N} = H_\pm\big(w_*'\big) + c, \quad \pm w_*' \geq 0, \tag{12.74}$$

where we introduced the functions

$$H_+\big(w'\big) = \frac{1}{\sqrt{w'}} \frac{3w'+2}{2w'+2} + \frac{3}{2} \arctan\big(\sqrt{w'}\big), \tag{12.75}$$

$$H_-\big(w'\big) = \frac{1}{\sqrt{-w'}} \frac{3w'+2}{2w'+2} - \frac{3}{2} \operatorname{arctanh}\big(\sqrt{-w'}\big). \tag{12.76}$$

Setting $\rho = 0$ in (12.74) yields the slope at the origin, $w_*'(0) = -0.3883467189\ldots$, and this result can be compared with the values in Table 12.5. All solutions vanish at $\rho_0 = N$. An expansion around this node reveals that only the solution with $c = 0$ is analytic. For the non-analytic solutions w_*' vanishes at ρ_0. Solutions with positive c are globally defined and solutions with negative c are multi-valued. We plotted solutions for different values of c as functions of ρ/N in Fig. 12.7. To find all critical exponents it is more convenient to use the fixed-point equation for w_* in place of w_*',

$$(d-2)\rho w_*' - d w_* + \frac{N}{(1+w_*')} = 0. \tag{12.77}$$

To linearize the flow equation (12.72) near a fixed point we set $w \approx w_*(\rho) + \mathrm{e}^{\omega t}\delta(\rho)$. The small fluctuations obey the eigenvalue problem

$$(\omega + d)\delta = (d-2)\rho\delta' - \frac{N}{(1+w_*')^2}\delta'. \tag{12.78}$$

Following [33] we now express the fluctuation in terms of the fixed-point solution. To that aim we use the ρ-derivative of the fixed-point equation,

$$(d-2)\rho w_*'' - 2w_*' - \frac{N}{(1+w_*')^2} w_*'' \tag{12.79}$$

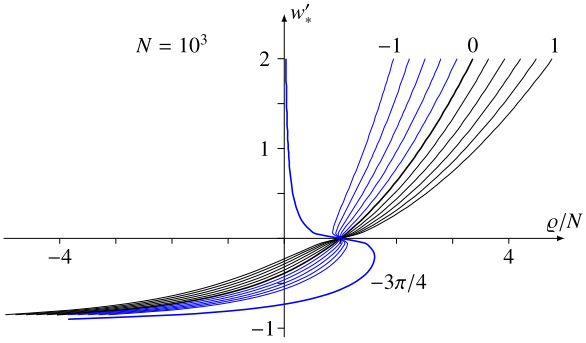

Fig. 12.7 One parametric family of derived fixed-point potentials in the large N limit. Depicted are solutions with c-values between -1 and 1 and the particular solution with $c = -3\pi/4$ which touches the w'_* axis. All solutions have a node at $\rho = N$. The solutions with $c \neq 0$ are non-analytic and have zero slope w''_* at the node

to simplify the right hand side of (12.78) as follows:

$$(\omega + d)\delta = \frac{2\omega'_*}{\omega''_*}\delta'. \tag{12.80}$$

This equation is easily solved and leads to

$$w(t, \rho) \approx w_*(\rho) + \text{const} \times \mathrm{e}^{\omega t} w'_*(\rho)^{(\omega+d)/2}. \tag{12.81}$$

If the solutions $w(t, \rho)$ and w_* have Taylor expansions in powers of ρ with a finite radius of convergence, the result (12.81) implies that the eigenvalues of the stability matrix must be quantized,

$$\omega \in \{2n - d \mid n = 0, 1, 2, \ldots\}. \tag{12.82}$$

In three dimensions there exist two relevant perturbations. The eigenvalue -3 belongs to the scaling operator 1 and the eigenvalue -1 yields the critical exponent $\nu = 1$. Note that already in the polynomial truncation we have anticipated this simple result for the exponents in the large-N limit.

12.5.2 Exact Solution of the Flow Equation

The most general solution of the first-order evolution equation (12.73) was derived in [31, 32] with the method of characteristics. It is the solution (12.74) with the constant c replaced by an arbitrary function of $F(\mathrm{e}^{2t} w')$ and thus has the form

$$H_{\pm}(w') - \frac{1}{\sqrt{\pm w'}}\frac{\rho}{N} = F\big(\mathrm{e}^{t} w'\big), \quad \pm w' > 0, \tag{12.83}$$

where the functions $H_{\pm}$ have been defined in (12.75) and (12.76). To prove that this is indeed a solution of the flow equation (12.73) one differentiates with respect to ρ and t, solves the resulting equations for $\partial_t w'$ and w'' and inserts the solutions back into the flow equation. The free function F is fixed by initial conditions. Here it is the requirement that at the cutoff scale Λ the effective potential u_k is equal to

the classical potential $V(\phi)$. Recalling the relation between the dimensionful and dimensionless fields and potentials this means

$$w'_\Lambda(\rho) = \frac{1}{\Lambda^2} V'(\tilde{\rho}), \quad \tilde{\rho} = \frac{1}{2}\phi^2 = \mu_d \Lambda \rho. \tag{12.84}$$

Now we evaluate equations (12.83) at the cutoff scale where ρ is a known function of w'_Λ, determined by solving

$$w'_\Lambda(\rho) = \frac{1}{\Lambda^2} V'(\mu_3 \Lambda \rho), \quad \mu_3 = \frac{1}{6\pi^2}, \tag{12.85}$$

for ρ in terms of w'_Λ. Collecting our results we end up with the following rather simple solution of the flow equation,

$$H_\pm\big(w'\big) - \frac{1}{\sqrt{\pm w'}} \frac{\rho}{N} = H_\pm\big(\mathrm{e}^{2t} w'\big) - \frac{\mathrm{e}^{-t}}{\sqrt{\pm w'}} \frac{\rho(\mathrm{e}^{2t} w')}{N}, \quad \pm w' > 0. \tag{12.86}$$

Note that ρ on the left hand side is an independent parameter whereas the function $\rho(\mathrm{e}^{2t} w')$ on the right hand side is obtained by inverting (12.85). Also note that the dependence on the number of fields only enters via ρ/N. Thus we may set $N = 1$ if we use ρ/N in place of ρ as field variable.

Let us consider a theory with a quartic classical potential,

$$V(\tilde{\rho}) = \frac{\tilde{\lambda}_\Lambda}{2} (\tilde{\rho} - \tilde{\kappa}_\Lambda)^2. \tag{12.87}$$

At the cutoff scale it is defined in the regime with spontaneous symmetry breaking, with the minimum of the potential at $\tilde{\kappa}_\Lambda$. The corresponding w'_Λ in (12.84) reads

$$w'_\Lambda(\rho) = \lambda_\Lambda(\rho - \kappa_\Lambda) \quad \text{with } \lambda_\Lambda = \mu_3 \frac{\tilde{\lambda}_\Lambda}{\Lambda}, \ \kappa_\Lambda = \frac{1}{\mu_3} \frac{\tilde{\kappa}_\Lambda}{\Lambda}. \tag{12.88}$$

This means that for a quartic potential

$$\rho\big(\mathrm{e}^{2t} w'\big) = \frac{\mathrm{e}^{2t} w'}{\lambda_\Lambda} + \kappa_\Lambda, \tag{12.89}$$

and this result is inserted into the right hand side of (12.86). To actually calculate the scale-dependent potential we prescribe at every scale the values of w' and determine the corresponding values of the composite field ρ from the mappings

$$\frac{\rho}{N} = \frac{\mathrm{e}^{-t}}{N} \left(\frac{\mathrm{e}^{2t} w'}{\lambda_\Lambda} + \kappa_\Lambda \right) + \sqrt{\pm w'} \big(H_\pm\big(w'\big) - H_\pm\big(\mathrm{e}^{2t} w'\big) \big), \quad \pm w' > 0. \tag{12.90}$$

For small w' the right hand side converges to $(1 - \mathrm{e}^{-t})$ such that a node ρ_0 of w' flows according to

$$\rho_0(t) = N + \mathrm{e}^{-t}(\kappa_\Lambda - \kappa_{\mathrm{crit}}), \quad \kappa_{\mathrm{crit}} = N. \tag{12.91}$$

If we tune the cutoff parameter κ_Λ to κ_{crit} then the node of the dimensionless w' becomes scale invariant. Any other choice of this parameter leads to an instability since the $\rho_0(t) - \rho_0(0)$ grows exponentially fast. For small scales equation (12.91) reads

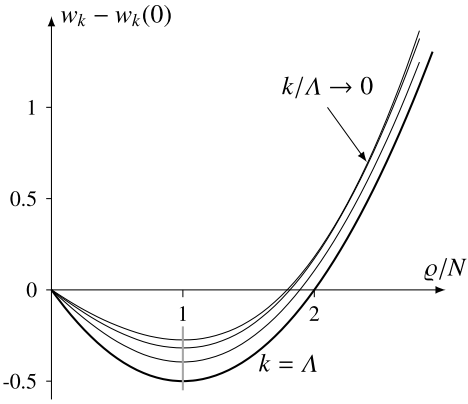

Fig. 12.8 Flow of the *dimensionless* effective potential with cutoff parameters $\lambda_\Lambda = 1$ and $\kappa_\Lambda = 1$. For this fine tuned value of κ_Λ the potential flows into the regular fixed-point solution with $c = 0$. Shown are potentials with scale parameter $k/\Lambda = 1, 0.95, 0.8$ and 0.6. All dimensionless potentials have their minimum at $\rho/N = 1$

$$\frac{\rho}{N} = \mathrm{e}^{-t}\left(\frac{\kappa_\Lambda}{N} - 1\right) + \sqrt{\pm w'}\, H_\pm\big(w'\big), \quad t \ll -1. \tag{12.92}$$

As expected, this is only a solution of the fixed-point equation if $\kappa_\Lambda = \kappa_{\mathrm{crit}}$. For this fine tuned value the potential flows into the fixed-point solution with $c = 0$. Figure 12.8 shows the flow of the dimensionless potential with critical coupling κ_{crit}.

Symmetry Breaking

To study the phases of the $O(N)$ models for large N we return to the dimensionful effective potential

$$\frac{u_k(\tilde{\rho})}{\Lambda^3} = \mu_3 \mathrm{e}^{3t} w_k\left(\frac{\mathrm{e}^{-t}\tilde{\rho}}{\mu_3 \Lambda}\right). \tag{12.93}$$

In the far infrared u_k is minimal at

$$\frac{\tilde{\rho}_0(t)}{\mu_3 \Lambda} = \mathrm{e}^t \rho_0(t) \to \kappa_\Lambda - \kappa_{\mathrm{crit}} \equiv \delta\kappa_\Lambda \quad \text{for } t \to -\infty. \tag{12.94}$$

Thus for any *positive* control parameter $\delta\kappa_\Lambda$ the system flows into the ordered phase with broken $O(N)$ symmetry. When we lower the scale the minimum moves inwards and the normalized field settles at $\delta\kappa_\Lambda$. The flow of the potential with cutoff parameter $\kappa_\Lambda/\kappa_{\mathrm{crit}} = 1.5$ is depicted in Fig. 12.9. For any *negative* control parameter $\delta\kappa_\Lambda$ the minimum of the full effective potential is always at the origin. Even if the classical potential has a minimum at $\kappa_\Lambda < \kappa_{\mathrm{crit}}$ the system flows into the disordered $O(N)$ symmetric phase and this is shown in Fig. 12.10. In other words if the symmetry breaking of the classical theory is not strong enough, the quantum fluctuations drive the system into the symmetric phase. No secondary minimum develops, and hence there is a second-order phase transition at $\kappa_\Lambda = \kappa_{\mathrm{crit}}$. Clearly there is just one relevant coupling, namely κ_Λ. Only the control parameter $\delta\kappa_\Lambda$ must be tuned to fix the qualitative behavior of the quantum system in the infrared. Since in the large-N limit the LPA for the effective potential becomes exact our conclusions will not be modified if one considers other truncations.

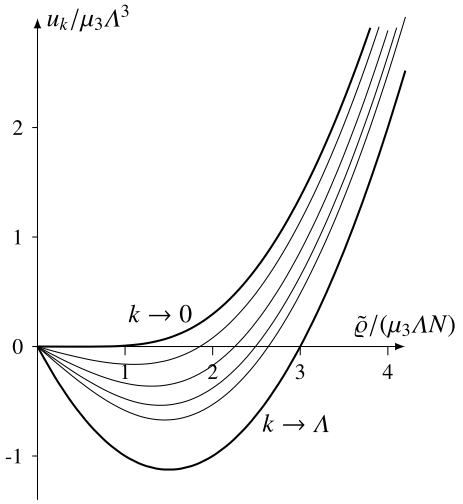

Fig. 12.9 Flow of the *dimensionful* effective potential for $\kappa_\Lambda/\kappa_{\rm crit} = 1.5$ and $\lambda_\Lambda = 1$. With decreasing k the minimum moves inwards until it settles as $\delta\kappa_\Lambda$. For $k = 0$ the potential is flat between 0 and $\delta\kappa_\Lambda$. Shown are potentials with k/Λ values 1, 0.95, 0.9, 0.8, 0.6 and 0. Since $\kappa_\Lambda > \kappa_{\rm crit}$ the system ends up in the phase with broken $O(N)$

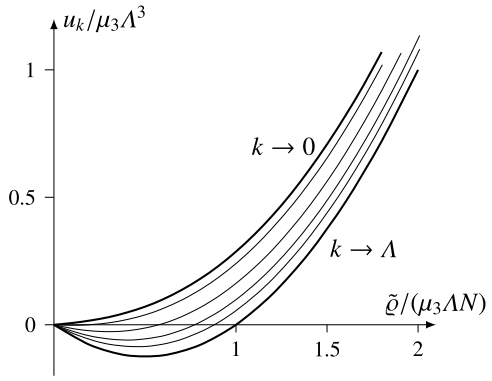

Fig. 12.10 Flow of the *dimensionful* effective potential for $\kappa_\Lambda/\kappa_{\rm crit} = 0.5$ and $\lambda_\Lambda = 1$. Due to quantum fluctuations the minimum of the classical potential moves to the origin. From below to above the scale parameter k/Λ has the values 1, 0.95, 0.9, 0.8, 0.6 and 0. Since $\kappa_\Lambda < \kappa_{\rm crit}$ the system ends up in the symmetric phase

12.6 Wave Function Renormalization

In a full next-to-leading order approximation in the derivative expansion one would include a wave function renormalization $Z_k(p, \varphi)$ depending on the scale, fields, and momenta. Typically this leads to non-linear parabolic partial differential RG-equations which are not always easy to solve. Here we neglect the field and momentum dependence and consider a scale-dependent wave function renormalization Z_k in the effective action

$$\Gamma_k[\varphi] = \int \mathrm{d}^d x \left(\frac{1}{2} Z_k (\partial_\mu \varphi)^2 + u_k(\varphi) \right). \tag{12.95}$$

Thereby the scale-dependent constant Z_k is the field-dependent wave function renormalization at zero field, $Z_k = Z_k(\phi = 0)$. The variation of Γ_k contains the

derivatives of the couplings in the effective potential as well as the derivative of the wave function renormalization,

$$\partial_k \Gamma_k = \int \mathrm{d}^d x \left(\frac{1}{2} (\partial_k Z_k)(\partial_\mu \varphi)^2 + \partial_k u_k(\varphi) \right), \tag{12.96}$$

and its second functional derivative with respect to the field is

$$\Gamma_k^{(2)} = -Z_k \Delta + u_k''(\varphi). \tag{12.97}$$

The flow equation simplifies if we use $Z_k R_k$ in place of R_k in the regulator term ΔS_k. This is also suggested by preserving the invariance under field rescalings. With this parametrization the flow equation in the truncation (12.95) reads

$$\partial_k \Gamma_k = \frac{1}{2} \operatorname{tr} \left(\frac{\partial_k (Z_k R_k)}{Z_k (p^2 + R_k) + u_k''} \right). \tag{12.98}$$

As earlier on we employ the optimized regulator in (12.10) for which the flow equation for the effective potential takes the form

$$\partial_k u_k = \frac{\mathscr{Z}_k}{Z_k k^2 + u_k''}, \quad \text{where } \mathscr{Z}_k = \frac{\mu_d}{d+2} \partial_k \left(k^{d+2} Z_k \right). \tag{12.99}$$

The geometric constant μ_d was introduced earlier in (12.47). Without wave function renormalization the differential equation simplifies to the flow equation (12.48). Inserting the series expansion

$$u_k(\varphi) = a_0 + \sum_{n=1}^{\infty} \frac{a_n(k)}{n!} \varphi^n \tag{12.100}$$

and comparing coefficients we obtain the flow equations for the couplings a_n. The lowest couplings obey

$$\begin{aligned}
\frac{\mathrm{d}a_0}{\mathrm{d}k} &= \mathscr{Z}_k \Delta_0, \quad \Delta_0 = \frac{1}{Z_k k^2 + a_2}, \\
\frac{\mathrm{d}a_1}{\mathrm{d}k} &= -\mathscr{Z}_k \Delta_0^2 a_3, \\
\frac{\mathrm{d}a_2}{\mathrm{d}k} &= -\mathscr{Z}_k \Delta_0^2 \left(a_4 - 2\Delta_0 a_3^2 \right), \\
\frac{\mathrm{d}a_3}{\mathrm{d}k} &= -\mathscr{Z}_k \Delta_0^2 \left(a_5 - 6\Delta_0 a_3 a_4 + 6\Delta_0^2 a_3^3 \right), \\
\frac{\mathrm{d}a_4}{\mathrm{d}k} &= -\mathscr{Z}_k \Delta_0^2 \left(a_6 - 8\Delta_0 a_3 a_5 - 6\Delta_0 a_4^2 + 36\Delta_0^2 a_3^2 a_4 - 24\Delta_0^3 a_3^4 \right), \\
\frac{\mathrm{d}a_5}{\mathrm{d}k} &= -\mathscr{Z}_k \Delta_0^2 \left(a_7 - 10\Delta_0 a_3 a_6 - 20\Delta_0 a_4 a_5 + 60\Delta_0^2 a_3^2 a_5 \right. \\
&\quad \left. + 90\Delta_0^2 a_3 a_4^2 - 240\Delta_0^3 a_3^3 a_4 + 120\Delta_0^4 a_3^5 \right), \\
\frac{\mathrm{d}a_6}{\mathrm{d}k} &= -\mathscr{Z}_k \Delta_0^2 \left(a_8 - 12\Delta_0 a_3 a_7 - 30\Delta_0 a_4 a_6 - 20\Delta_0 a_5^2 + 90\Delta_0^2 a_3^2 a_6 \right. \\
&\quad + 90 G_2^2 a_4^3 + 360\Delta_0^2 a_3 a_4 a_5 - 480\Delta_0^3 a_3^3 a_5 - 1080\Delta_0^3 a_3^2 a_4^2 \\
&\quad \left. + 1800\Delta_0^4 a_3^4 a_4 - 720\Delta_0^5 a_3^6 \right).
\end{aligned} \tag{12.101}$$

In leading order $Z_k = 1$ and we recover the flow equations without wave function renormalization in (12.49).

12.6.1 RG Equation for Wave Function Renormalization

To extract the scale dependence of Z_k in the flow equation

$$\int \mathrm{d}^d x \left(\frac{1}{2} (\partial_k Z_k)(\partial_\mu \varphi)^2 + \partial_k u_k(\varphi) \right) = \frac{1}{2} \mathrm{tr} \left(\frac{\partial_k (Z_k R_k)}{Z_k (p^2 + R_k) + u_k''(\varphi)} \right) \tag{12.102}$$

we project the right hand side onto the operator $(\partial\varphi)^2$. Clearly, this is only possible if we admit an inhomogeneous average field for which p^2 and $u_k''(\varphi)$ do not commute. But it is sufficient to expand the full propagator on the right hand side in powers of the field up to second order. For this expansion we set $u_k''(\varphi) = a_2 + \Delta u_k'' + \cdots$ and expand in powers of the field-dependent $\Delta u_k''$,

$$\frac{1}{Z_k (p^2 + R_k) + u_k''(\varphi)} = \sum_{n=0}^{\infty} (-)^n G_0 \big(\Delta u_k''(\varphi) G_0 \big)^n . \tag{12.103}$$

For the optimized regulator the free propagator

$$G_0 = \frac{1}{Z_k (p^2 + R_k) + a_2} \tag{12.104}$$

becomes p-independent below the scale k,

$$G_0 \big(|p| < k \big) = \Delta_0 = \frac{1}{Z_k k^2 + a_2} . \tag{12.105}$$

In order to project the right hand side of (12.102) onto the operator $(\partial\varphi)^2$ we only need to consider terms quadratic in φ. With $\Delta u_k'' = a_3 \varphi + a_4 \varphi^2/2 + \cdots$ we obtain

$$\int \mathrm{d}^d x \, \partial_k Z_k (\partial_\mu \varphi)^2 = \mathrm{tr} \left\{ \partial_k (Z_k R_k) \left(a_3^2 G_0 \varphi G_0 \varphi G_0 - \frac{a_4}{2} G_0 \varphi^2 G_0 \right) \right\}_{(\partial\varphi)^2} . \tag{12.106}$$

In momentum space the left hand side takes the form

$$\partial_k Z_k \int_p \varphi(-p) p^2 \varphi(p), \quad \text{where} \quad \int_p \equiv \int \frac{\mathrm{d}^d p}{(2\pi)^d} . \tag{12.107}$$

We distinguish between a function in x space and its Fourier transform in p space via their arguments. Inserting the Fourier transform of the free propagator

$$G_0(x) = \int_p \mathrm{e}^{\mathrm{i} p x} G_0(p) \tag{12.108}$$

and that of the average field into the last term in (12.106) yields

$$-\frac{a_4}{2} \varphi^2(p = 0) \int_p \partial_k \big(Z_k R_k(p) \big) G_0^2(p) .$$

Only the field at zero momentum enters here, and hence no term like the one in (12.107) is generated. We conclude that for systems with even potentials for a series

expansion at the origin (12.100) the wave function renormalization Z_k does not flow in the truncation considered here. For more general potentials or expansions of even potentials around a non-vanishing vacuum expectation value $a_3 \neq 0$ and the second to last term in (12.106) reads in momentum space

$$a_3^2 \int_p \int_q \partial_k \big(Z_k R_k(q)\big) G_0^2(q) \varphi(-p) G_0(p+q) \varphi(p). \tag{12.109}$$

Its projection onto $(\partial\varphi)^2$ is

$$\frac{1}{2} a_3^2 \int_q \partial_k \big(Z_k R_k(q)\big) G_0^2(q) \Delta_q G_0(q) \int_p \varphi(-p) p^2 \varphi(p). \tag{12.110}$$

Using these results in the projected flow equation (12.106) finally yields

$$\partial_k Z_k = \frac{a_3^2}{2} \int_q \partial_k \big(Z_k R_k(q)\big) G_0^2(q) \Delta_q G_0(q). \tag{12.111}$$

For the optimized regulator the integrand contains products of distributions, and for this reason we expand the q-integral in (12.109) directly in powers of p. The detailed calculation can be found in the Appendix to this section. The final answer is

$$k\partial_k Z_k = -\mu_d k^{d+2} \big(Z_k a_3 \Delta_0^2\big)^2 \quad \text{with } \frac{1}{\mu_d} = (4\pi)^{d/2} \Gamma\left(\frac{d}{2}+1\right). \tag{12.112}$$

The differential equations (12.99) and (12.112) yield the flow of the effective potential and scale-dependent wave function renormalization in the next to leading-order approximation. Actually the anomalous dimension

$$\eta = -k\partial_k \log Z_t \tag{12.113}$$

of the $O(N)$ model vanishes in the large N limit. But there exist perturbatively non-renormalizable but asymptotically safe field theories with a large anomalous dimension at the non-Gaussian fixed point. For example, the Gross–Neveu model in three dimensions is asymptotically safe and has a large anomalous dimension [34].

12.7 Outlook

It has already been stressed that functional renormalization group equations have been applied to a variety of quantum and statistical systems. In this chapter we could only give an introduction into this powerful method with applications to simple quantum-mechanical systems and scalar field theories. For a further reading I refer to the textbooks and reviews [5–11]. Here it suffices to mention some interesting recent developments. Of course the flow equations can be formulated for and applied to fermionic systems as well. Thereby one can dynamically bosonize the emerging four-fermion operators with the Hubbard–Stratonovich trick [34–36]. For gauge theories with local gauge symmetries the background field method has

Listing 12.1 Flow of couplings in polynomial LPA

```
function x=truncflowanho_lambda)
# calculates the flow for even potentials projected onto
# quartic polynomials. At the cutoff E=0. The program asks
# for lambda at the cutoff in units of omega. The running
# of the effective couplings  in the infrared is plotted.
# couplLambda=[0;-1;0];         # for 4th order polynomial
couplLambda=[0;-1;0;0;0;0;0];  # for 12th order polynomial
Nk=100000;disp=20;
couplLambda(3)=lambda;
k=linspace(10000,0,Nk);
#[coupl]=lsode("flowOpt4",couplLambda,k);
#[coupl]=lsode("flowCallan4",couplLambda,k);
[coupl]=lsode("flowOpt12",couplLambda,k);
xh=coupl(Nk-disp:Nk,:,:);
kh=k(Nk-disp:Nk);
plot(kh,xh(:,1),kh,xh(:,2),kh,xh(:,3));
legend('E','omega**2','lambda');
printf("E0 = \t %4.4f\n",coupl(Nk,1));
printf("E1 = \t %4.4f\n",coupl(Nk,1)+sqrt(coupl(Nk,2)));
endfunction
```

been adjusted to calculate the flow for the coupled systems of gauge, matter, and ghost fields [9, 37–40]. A similar technique has been used to study gravity theories with local diffeomorphism invariance and to argue that gravity very probably is an asymptotically safe theory with a non-trivial UV fixed point [41–43]. Also for many supersymmetric quantum field theories a manifest supersymmetric flow can be constructed in superspace [20, 33, 44, 45]. Supersymmetry relates the regulator functions of the bosons and fermions and thus gives a new perspective on regulator functions in theories with interacting bosons and fermions. One can investigate for which parameter region the quantum systems are supersymmetric and for which region supersymmetry is broken. Implementing space time symmetries is not so much an issue for functional renormalization group flow equations as it is for a lattice regularization.

The flexible functional method offers great potential for theoretical advances in both hot and dense QCD, gravity, supersymmetry as well as many-body physics. The method is somehow complementary to the ab initio lattice approach. In cases where a lattice regularization based on a positive Boltzmann factor fails, for example for gauge theories at finite density, the functional method may work. Thus it is probably a good strategy to consider both methods when it comes to properties of strongly coupled systems under extreme conditions.

12.8 Programs for Chap. 12

The `octave`-program in Listing 12.1 calculates the flow of the couplings E_k, ω_k^2 and λ_k in the LPA-approximation and the truncation with $a_6 = 0$. The flow begins at $k = 10^5$, but only the values of the couplings for $k = 2$ down to $k = 0$ are plotted.

Listing 12.2 Called by program 12.1: optimized regulator and fourth-order polynomial

```
%\ref{truncflowanho.m}
%, optimal regulator, 4th order polynomial}
%,\label=flowOpt4.m]
function coupldot=flowOpt4(coupl,k)
ksquare=k*k;
P=1/(ksquare+coupl(2));xh=ksquare*P/pi;
coupldot(1)=xh-1/pi;
coupldot(2)=-xh*P*coupl(3);
coupldot(3)=-6*coupldot(2)*P*coupl(3);
endfunction
```

Listing 12.3 Called by program 12.1: Callan–Symanzik regulator and fourth-order polynomial

```
function coupldot=flowCallan4(coupl,k)
P=1/(k*k+coupl(2));
rootP=k*sqrt(P);
coupldot(1)=0.5*(rootP-1);
coupldot(2)=-0.25*rootP*P*coupl(3);
coupldot(3)=-4.5*coupldot(2)*P*coupl(3);
endfunction
```

Listing 12.4 Called by program 12.1: optimized regulator and 12th-order polynomial

```
function coupldot=flowOpt12(coupl,k)
a0=coupl(1);a2=coupl(2);a4=coupl(3);a6=coupl(4);
a8=coupl(5);a10=coupl(6);a12=coupl(7);
ks=k*k;numflow1
P=1/(ks+a2);P2=P*P;P2pi=ks*P2/pi;P3=P*P2;P4=P*P3;
a4s=a4*a4;a4q=a4s*a4s;a6s=a6*a6;
coupldot(1)=-a2*P/pi;
coupldot(2)=-a4;
coupldot(3)=-a6+6*a4s*P;
coupldot(4)=-a8+30*a4*a6*P-90*a4s*a4*P2;
coupldot(5)=-a10+(56*a4*a8+70*a6s)*P\
-1260*a6*a4s*P2+2520*a4q*P3;
coupldot(6)=-a12+(90*a4*a10+420*a6*a8)*P\
 -(3780*a8*a4s+9450*a6s*a4)*P2\
+75600*a4s*a4*a6*P3-113400*a4q*a4*P4;
coupldot(7)=(132*a4*a12+924*a8*a8+990*a10*a6)*P\
-(8910*a10*a4s+83160*a4*a6*a8+34650*a6s*a6)*P2\
+(332640*a8*a4s*a4+1247400*a4s*a6s)*P3\
-6237000*a4q*a6*P4+7484400*a4q*a4s*(P4*P);
coupldot(2:7)=P2pi*coupldot(2:7);
endfunction
```

The functions defined in Listings 12.2, 12.3 and 12.4 are called by program 12.1 to calculate the flow for different regulators and truncation orders.

Listing 12.5 Flow of effective potential in LPA

```
function flowpde(a4)
# Solves the partial differential equation for the
# flow of the effective potential by rewriting it
# as a system of coupled ode's. Calls fa.m
global Nq;
global dqsquareinv;
global W;
Nq=151;L=5;Nk=800;
q=linspace(-L,L,Nq);
a2=-1;
qsquare=q.*q;
dq=2*L/(Nq-1);
dqsquareinv=1/(dq*dq);
k=linspace(800,0,Nk);
V=0.5*a2*qsquare+a4*qsquare.*qsquare/24;
Veff=lsode("fa",V,k);
u=Veff(Nk,:);
plot(q,V,'r',q,u,'b')
legend('Vclass','Veff');
[umin,index]=min(u);
upp=(u(index+1)+u(index-1)-2*u(index))*dqsquareinv;
printf("\nE0 = %4.f\nE1 = %4.f \n",umin,umin+sqrt(upp));
endfunction
```

Listing 12.6 Called by program 12.5: right hand side of ode

```
function xdot=fa(V,x)
global dqsquareinv;
global Nq;
global W;
xs=x*x;
W=dqsquareinv*(shift(V,1)+shift(V,-1)-2*V);
xdot=(xs./(xs+W)-1)/pi;
xdot(1)=0;
xdot(Nq)=0;
endfunction
```

The `octave` function 12.5 solves the partial differential equation for the scale-dependent effective potential in (12.31). It calls the function defined in Listing 12.6.

12.9 Problems

12.1 (Weak-coupling expansion for anharmonic oscillator) In this exercise we solve the truncated flow equations (12.35) for weak couplings $\lambda/\omega^3 \ll 1$. First we introduce dimensionless variables,

$$x = \frac{k}{\omega}, \qquad e_k = \frac{E_k}{\omega}, \qquad o_k = \frac{\omega_k}{\omega} \quad \text{and} \quad \ell_k = \frac{\lambda_k}{24\omega^3}.$$

(a) Show that the truncated flow equations for the dimensionless variables read

$$\frac{de_k}{dx} = -\frac{o_k^2}{\pi}\frac{1}{x^2+o_k^2}, \qquad \frac{do_k^2}{dx} = -\frac{\ell_k}{\pi}\frac{24x^2}{(x^2+o_k^2)^2},$$
$$\frac{d\ell_k}{dx} = \frac{144\ell_k^2}{\pi}\frac{x^2}{(x^2+o_k^2)^3}.$$

(b) For the harmonic oscillator with vanishing λ we have $e_k = 1/2, o_k = 1$ and $\ell_k = 0$. The initial conditions are $e_{x\to\infty} = 0, o_{x\to\infty} = 1$ and $\ell_{x\to\infty} = \lambda/24\omega^3$. Thus for weak coupling the expansion has the form

$$e_k = \alpha_0 + \alpha_1\varepsilon + \alpha_2\varepsilon^2 + \cdots,$$
$$o_k^2 = 1 + \beta_1\varepsilon + \beta_2\varepsilon^2 + \cdots,$$
$$\ell_k = \varepsilon + \gamma_2\varepsilon^2 + \cdots$$

with $\varepsilon = \lambda/24\omega^3 \ll 1$ and scale-dependent coefficient functions. Show that these functions satisfy the differential equations

$$\dot\alpha_0 = -\frac{P}{\pi}, \qquad \dot\alpha_1 = -\frac{x^2P^2}{\pi}\beta_1, \qquad \dot\alpha_2 = \frac{x^2P^2}{\pi}\big(\beta_1^2 P - \beta_2\big),$$
$$\dot\beta_1 = -\frac{24x^2P^2}{\pi}, \qquad \dot\beta_2 = \frac{24x^2P^2}{\pi}(2\beta_1 P - \gamma_2), \qquad \dot\gamma_2 = 144\frac{x^2P^3}{\pi},$$

where we defined $P \equiv 1/(1+x^2)$. The coefficient functions vanish for $x \to \infty$ and the first differential equation has the solution $\alpha(x) = 1/2 - \arctan(x)/\pi$.

(c) Calculate β_1, γ_2 and β_2 with an algebraic computer program. Insert the solutions to find the functions α_2 and α_3.

(d) Prove that the coefficient functions have the following small-x expansions:

$$\begin{aligned}
\alpha_0(x) &\sim \frac{1}{2} - \frac{1}{\pi}x + \frac{1}{3\pi}x^3 + \cdots,\\
\alpha_1(x) &\sim \frac{3}{4} - 2\pi x^3 + \cdots,\\
\alpha_2(x) &\sim -\frac{3}{8}\left(10 - \frac{29}{\pi^2}\right) + 8\left(3 - \frac{4}{\pi^2}\right)x^3 + \cdots,\\
\beta_1(x) &\sim 6 - \frac{8}{\pi}x^3 + \cdots,\\
\beta_2(x) &\sim -12\left(3 - \frac{8}{\pi^2}\right) + \frac{168}{\pi}x^3 + \cdots,\\
\gamma_2(x) &\sim -9 + \frac{48}{\pi}x^3 + \cdots.
\end{aligned} \tag{12.114}$$

(e) If we make a cruder truncation with $\lambda_k = \lambda$ of equivalently with $\gamma_2 = 0$, how does the results change? Prove that in this case

$$\begin{aligned} \alpha_2(x) &\sim -\frac{3}{16}\left(8 + \frac{29}{\pi^2}\right) + \frac{1}{\pi^3}\left(15\pi^2 + 16\right)x^3 + \cdots, \\ \beta_2(x) &\sim -2\left(3 + \frac{16}{\pi^2}\right) + \frac{96}{\pi}x^3 + \cdots. \end{aligned} \tag{12.115}$$

12.2 (Fixed-point solution and critical exponents) Write a program with your favorite algebraic computer system to find the fixed-point solution and the critical exponents of the Z_2 scalar field theory. You should be able to reproduce the plots in Fig. 12.5 and the critical exponents in Table 12.4.

Appendix: A Momentum Integral

In this appendix we calculate the $O(p^2)$ contribution to the integral

$$F(p) = \int \mathrm{d}^d q \, \partial_k \big\{ Z_k R_k(q) \big\} G_0^2(q) G_0(p+q) \tag{12.116}$$

for the optimized regulator function (12.10). The integrand is only non-zero for $q^2 \le k^2$ and in this region

$$\partial_k \big\{ Z_k R_k(q) \big\} G_0^2(q) = \big((k^2 - q^2) \partial_k Z_k + 2k Z_k \big) \Delta_0^2. \tag{12.117}$$

To proceed we need to consider two cases: $|p+q| \le k$ and $|p+q| > k$ separately.

The Case $|p+q| < k$ This is the region located inside of both spheres in Fig. 12.11 where the Green function $G_0(q) = G_0(p+q) = \Delta_0$ is independent of the integration variable q. Let us decompose this variable as $q = q_\parallel + q_\perp$, where $q_\parallel$ is parallel and $q_\perp$ perpendicular to the fixed momentum p. Then the integral has the form

$$I_1 = \mathrm{Vol}(S_{d-2}) \Delta_0^3 \int \mathrm{d}q_\parallel \int \mathrm{d}|q_\perp| |q_\perp|^{d-2} \big((k^2 - q^2) \partial_k Z_k + 2k Z_k \big), \tag{12.118}$$

where $q^2 = q_\parallel^2 + q_\perp^2$. The volume of the unit sphere $S_{d-2} \subset \mathbb{R}^{d-1}$ originates from the integration over the directions of $q_\perp$. Now we split the integration domain inside of both spheres, the region marked gray in Fig. 12.11, into two spherical caps,

$$\begin{aligned} -k \le q_\parallel < -\frac{p}{2} \quad &\text{and} \quad 0 \le q_\perp^2 \le k^2 - q_\parallel^2, \\ -\frac{p}{2} \le q_\parallel < k - p \quad &\text{and} \quad 0 \le q_\perp^2 \le k^2 - (p + q_\parallel)^2. \end{aligned}$$

The domain of integration in (12.118) is just the union of these two caps. After a shift $q_\parallel \to q_\parallel - p$ in the integral over the second cap we are left with the one-dimensional integral

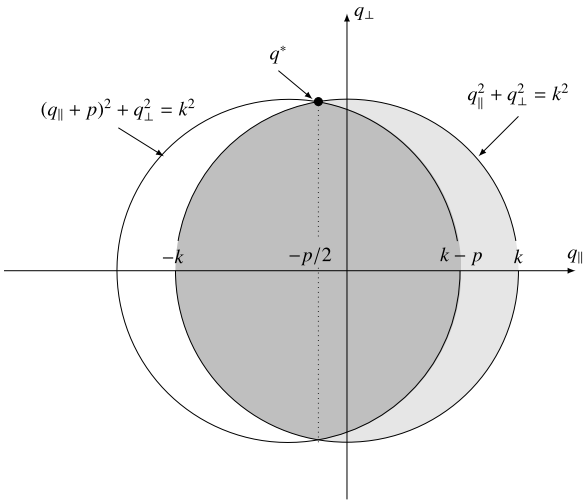

Fig. 12.11 Sketch of the integration regions in momentum space. Only momenta inside of the ball centered at the origin contribute to the integral. The Green functions are constant in the *gray region* inside of both spheres. Inside the sickle-shaped *light-gray region* $G_0(p,q)$ is momentum dependent. The two spheres intersect at the lower-dimensional sphere defined by $\{q_\parallel^*, q_\perp^*\} = \{-p/2, k^2 - p^2/4\}$

$$\frac{\mathrm{Vol}(S_{d-2})\Delta_0^3}{d-1}\int_{p/2}^{k}\mathrm{d}q_\parallel\left\{\left(\frac{4k^2-4q_\parallel^2}{d+1}+2q_\parallel p-p^2\right)\partial_k Z_k+4kZ_k\right\}$$
$$\times\left(k^2-q_\parallel^2\right)^{(d-1)/2}.$$

Its second derivative with respect to p at $p=0$ is

$$\left.\frac{\mathrm{d}^2 I_1}{\mathrm{d}p^2}\right|_{p=0} = -k^d V(B_d)\Delta_0^3\partial_k Z_k. \tag{12.119}$$

The Case $|p+q|<k$ This is the sickle-shaped region inside of the sphere centered at the origin but outside the displaced sphere, marked light-gray in Fig. 12.11. The integral over this region can be written as a difference of two integrals as follows:

$$I_2 = \Delta_0^2\left(\int_{-p/2}^{k}\mathrm{d}q_\parallel\int_0^{\sqrt{k^2-q_\parallel^2}}\mathrm{d}q_\perp h(q_\parallel,q_\perp)\right.$$
$$\left.-\int_{-p/2}^{k-p}\mathrm{d}q_\parallel\int_0^{\sqrt{k^2-(q_\parallel+p)^2}}\mathrm{d}q_\perp h(q_\parallel,q_\perp)\right).$$

The integrand of both integrals is

$$h(q_\parallel,q_\perp) = \frac{(k^2-q_\parallel^2-q_\perp^2)\partial_k Z_k + 2kZ_k}{Z_k(q_\parallel+p)^2 + Z_k q_\perp^2 + a_2}.$$

It is convenient to shift the variable $q_\parallel$ in the second integral by $-p$ such that

$$I_2 = \Delta_0^2 \Bigg(\int_{-p/2}^{k} \mathrm{d}q_\parallel \int_0^{\sqrt{k^2-q_\parallel^2}} \mathrm{d}q_\perp h(q_\parallel, q_\perp) - \int_{p/2}^{k} \mathrm{d}q_\parallel \int_0^{\sqrt{k^2-q_\parallel^2}} \mathrm{d}q_\perp h(q_\parallel - p, q_\perp) \Bigg).$$

The second derivative of this integral with respect to p at $p = 0$ is given by

$$\left. \frac{\mathrm{d}^2 I_2}{\mathrm{d}p^2} \right|_{p=0} = k^d V(B_d) \Delta_0^4 \big(a \partial_k Z_k + k^2 Z_k \partial_k Z_k - 2k Z_k^2 \big). \tag{12.120}$$

Adding the two results (12.119) and (12.120) leads to the simple expression

$$\left. \frac{\mathrm{d}^2 F}{\mathrm{d}p^2} \right|_{p=0} = -2k^{d+1} V(B_d) \Delta_0^4 Z_k^2 \tag{12.121}$$

for the curvature of $F(p)$ in (12.116) at the origin in momentum space.

References

1. K.G. Wilson, The renormalization group: critical phenomena and the Kondo problem. Rev. Mod. Phys. **47**, 773 (1975)
2. J. Polchinski, Renormalization and effective lagrangians. Nucl. Phys. B **231**, 269 (1984)
3. T.R. Morris, On truncations of the exact renormalization group. Phys. Lett. B **334**, 355 (1994)
4. C. Wetterich, Exact evolution equation for the effective potential. Phys. Lett. B **301**, 90 (1993)
5. K. Aoki, Introduction to the nonperturbative renormalization group and its recent applications. Int. J. Mod. Phys. B **14**, 1249 (2000)
6. C. Bagnus, C. Bervillier, Exact renormalization group equations: an introductiory review. Phys. Rep. **348**, 91 (2001)
7. J. Berges, N. Tetradis, C. Wetterich, Nonperturbative renormalization flow in quantum field theory and statistical physics. Phys. Rep. **363**, 223 (2002)
8. J. Polonyi, Lectures on the functional renormalization group methods. Cent. Eur. J. Phys. **1**, 1 (2003)
9. J. Pawlowski, Aspects of the functional renormalisation group. Ann. Phys. **322**, 2831 (2007)
10. H. Gies, Introduction to the functional RG and applications to gauge theories, in *Renormalization Group and Effective Field Theory Approaches to Many-Body Systems*, ed. by A. Schwenk, J. Polonyi. Lect. Notes Phys., vol. 62 (2012)
11. P. Kopietz, L. Bartosch, F. Schütz, *Introduction to the Functional Renormalization Group*. Lecture Notes in Physics, vol. 798 (Springer, Berlin, 2010)
12. D. Litim, Optimization of the exact renormalization group. Phys. Lett. B **486**, 92 (2000)
13. D. Litim, Optimized renormalization group flows. Phys. Rev. D **64**, 105007 (2001)
14. S.D. Drell, M. Weinstein, S. Yankielowicz, Variational approach to strong coupling theory. 1. ϕ^4 theory. Phys. Rev. D **14**, 487 (1976)
15. D. Lange, A. Kirchberg, A. Wipf, From the Dirac operator to Wess–Zumino models on spatial lattices. Ann. Phys. **316**, 357 (2005)
16. D.F. Litim, J.P. Pawlowski, L. Vergara, Convexity of the effective action from functional flows. arXiv:hep-th/0602140
17. D. Zappala, Improving the renormalization group approach to the quantum-mechanical double well potential. Phys. Lett. A **290**, 35 (2001)
18. C.M. Bender, T.T. Wu, Anharmonic oscillator. Phys. Rev. D **184**, 1231 (1969)

19. T. Morris, The renormalization group and two-dimensional multicritical effective scalar field theory. Phys. Lett. B **345**, 139 (1995)
20. F. Synatschke, H. Gies, A. Wipf, Phase diagram and fixed-point structure of two dimensional $N = 1$ Wess–Zumino model. Phys. Rev. D **80**, 085007 (2009)
21. D.F. Litim, Critical exponents from optimized renormalization group flows. Nucl. Phys. B **631**, 128 (2002)
22. M. D'Attanasio, T.R. Morris, Large N and the renormalization group. Phys. Lett. B **409**, 363 (1997)
23. M. Moshe, J. Zinn-Justin, Quantum field theory in the large N limit: a review. Phys. Rep. **385**, 69 (2003)
24. J.P. Blaizot, R. Mendéz-Galain, N. Wschebor, A new method to solve the non perturbative renormalization group equations. Phys. Lett. B **632**, 571 (2006)
25. V. Von Gersdorff, C. Wetterich, Nonperturbative renormalization flow and essential scaling for the Kosterlitz–Thouless transition. Phys. Rev. B **64**, 054513 (2001)
26. F. Benitez, J.P. Blaizot, H. Chaté, B. Delamotte, R. Méndez-Galain, N. Wschebor, Nonperturbative renormalization group preserving full-momentum dependence: implementation and quantitative evaluation. Phys. Rev. E **85**, 026707 (2012)
27. M. Hasenbusch, Finite scaling study of lattice models in the three-dimensional Ising universality class. Phys. Rev. B **82**, 174433 (2010)
28. M. Campostrini, M. Hasenbusch, A. Pelissetto, P. Rossi, E. Vicari, Critical exponents and equation of state of the three dimensional Heisenberg universality class. Phys. Rev. B **65**, 144520 (2002)
29. S. Holtmann, T. Schulze, Critical behavior and scaling functions of the three-dimensional $O(6)$ model. Phys. Rev. E **68**, 036111 (2003)
30. T. Fischbacher, F. Synatschke-Czerwonka, FlowPy—a numerical solver for functional renormalization group equations. arXiv:1202.5984
31. N. Tetradis, C. Wetterich, Critical exponents from effective average action. Nucl. Phys. B **422**, 541 (1994)
32. N. Tetradis, D. Litim, Analytical solutions of exact renormalization group equations. Nucl. Phys. B **464**, 492 (1996)
33. D. Litim, M. Mastaler, F. Synatschke-Czerwonka, A. Wipf, Critical behavior of supersymmetric $O(N)$ models in the large-N limit. Phys. Rev. D **84**, 125009 (2011)
34. J. Braun, H. Gies, D. Scherer, Asymptotic safety: a simple example. Phys. Rev. D **83**, 085012 (2011)
35. H. Gies, C. Wetterich, Renormalization flow of bound states. Phys. Rev. D **65**, 065001 (2002)
36. J. Braun, Fermion interaction and universal behavior in strongly interacting theories. J. Phys. G **39**, 033001 (2012)
37. M. Reuter, C. Wetterich, Effective average action for gauge theories and exact evolution equations. Nucl. Phys. B **417**, 181 (1994)
38. U. Ellwanger, Flow equations and BRS invariance for Yang–Mills theories. Phys. Lett. B **335**, 364 (1994)
39. H. Gies, Running coupling in Yang–Mills theory: a flow equation study. Phys. Rev. D **66**, 025006 (2002)
40. D. Litim, J. Pawlowski, Wilsonian flows and background fields. Phys. Lett. B **546**, 279 (2002)
41. M. Reuter, Nonperturbative evolution equation for quantum gravity. Phys. Rev. **57**, 971 (1998)
42. M. Reuter, M. Niedermeier, The asymptotic safety scenario in quantum gravity. Living Rev. Relativ. **9** (2006)
43. M. Reuter, F. Saueressing, Functional renormalization group equations, asymptotic safety and quantum Einstein gravity. arXiv:0708.1317
44. M. Bonini, F. Vian, Wilson renormalization group for supersymmetric gauge theories and gauge anomalies. Nucl. Phys. B **532**, 473 (1998)
45. F. Synatschke, J. Braun, A. Wipf, $N = 1$ Wess Zumino model in $d = 3$ at zero and finite temperature. Phys. Rev. D **81**, 125001 (2010)

Chapter 13
Lattice Gauge Theories

According to present day knowledge *all fundamental interactions* in nature are described by *gauge theories*. The best known example is electrodynamics with Abelian symmetry group $U(1)$. In contrast, the electroweak and the strong interactions are modeled by gauge theories with the non-Abelian symmetry groups $SU(2) \times U(1)$ and $SU(3)$, respectively. In a sense, general relativity also represents a non-Abelian gauge theory, albeit with a non-compact symmetry group [1, 2]. Continuum gauge theories are dealt with in many excellent textbooks [3–6] and it is useful, but not a necessity that the reader has some basic knowledge of these theories. For those who are not acquainted with continuum gauge theories we summarized those properties and concepts which are needed in the remaining chapters of this book.

The first systematic investigation of a lattice gauge theory goes back to F. WEGNER [7]. He examined Ising-like systems with *local* Z_2-invariance. In Chap. 10 we already encountered the three-dimensional Z_2 gauge theory as dual of the Ising model and introduced the object that is known today in a more general setting as *Wilson loop*. Three years after Wegner's contribution K. WILSON formulated non-Abelian gauge theories on a space-time lattice as possible discretization and regularization of continuum gauge theories [8]. Thereby he replaced the Lie-algebra valued continuum gauge field by link variables with values in a compact Lie group in a way that the discretized theory possesses a gauge symmetry for any size of the lattice spacing. In a naive continuum limit where the lattice spacing tends to zero the lattice action turns into the Yang–Mills action for the continuum field. He formulated a useful and often used criterion for confinement based on the Wilson loop: if the logarithm of the Wilson loop shows an *area-law* behavior then charged particles are confined.

By working on a discrete space-time the path integral becomes finite-dimensional and can be evaluated by stochastic simulation techniques such as the Monte Carlo method. Shortly after the seminal work of Wilson the first numerical simulations of pure lattice gauge theories in three and four dimensions were performed. At first, this was done for the finite gauge group Z_2 in [9] and later on for non-Abelian lattice gauge theories with gauge groups $SU(2)$ as well as $SU(3)$ in [10, 11]. Observable quantities such as particle masses and decay widths are calculated with the Monte

A. Wipf, *Statistical Approach to Quantum Field Theory*, Lecture Notes in Physics 864,
DOI 10.1007/978-3-642-33105-3_13,

Carlo method. Thereby gauge field configurations are generated with probabilities proportional to e^{-S}, where S is the lattice action. When one includes fermions then the calculations are often expensive and can require the use of the largest computers available. The simulations typically utilize algorithms based upon molecular dynamics. For more introductory material on lattice gauge theories as presented in this and the following chapters I recommend the textbooks [12–15] and the classic review papers [16] and [17, 18].

13.1 Continuum Gauge Theories

In this section we summarize the relevant properties of gauge theories in the continuum. Thereby the emphasis is put on the underlying structures and principles. We begin with the extremely successful *gauge principle*. For that purpose we consider a scalar field ϕ with values in a vector space V with scalar product denoted by $(.,.)$. The scalar product is left invariant when its arguments are transformed with an element Ω of some symmetry group G. The most important example is $V = \mathbb{C}^n$ with hermitian scalar product. Choosing an orthonormal basis ϕ is identified with its components

$$\phi = \begin{pmatrix} \phi_1 \\ \phi_2 \\ \vdots \\ \phi_n \end{pmatrix}, \qquad \phi^\dagger = \left(\phi_1^*, \phi_2^*, \ldots, \phi_n^*\right) \tag{13.1}$$

and the scalar product of two fields is

$$(\phi, \chi) = \sum_{a=1}^{n} \phi_a^* \chi_a. \tag{13.2}$$

It is invariant under a simultaneous $U(n)$ transformation of its arguments,

$$(\phi, \chi) = (\Omega\phi, \Omega\chi), \quad \Omega \in U(n). \tag{13.3}$$

Let us now assume that the components of ϕ are free fields with equal masses, such that they all obey the Klein–Gordon equation,

$$\left(\Box + \frac{m^2c^2}{\hbar^2}\right)\phi_a = 0. \tag{13.4}$$

We follow the habit in high energy physics and use natural units $\hbar = c = 1$. The field equations (13.4) are the Euler–Lagrange equations of the Lorentz-invariant action

$$S = \int \mathrm{d}^d x \, \mathscr{L}(\phi, \partial_\mu \phi) \quad \text{with } \mathscr{L} = \left(\partial_\mu \phi, \partial^\mu \phi\right) - m^2(\phi, \phi). \tag{13.5}$$

Clearly, the Lagrangian density $\mathscr{L}$ is invariant under *global* $U(n)$ transformations

$$\phi(x) \to \phi'(x) = \Omega\phi(x), \quad \Omega \in U(n), \tag{13.6}$$

since the scalar product is invariant. The transformation $\phi \to \Omega\phi$ is called *global transformation* since it does not depend on the space-time point. Invariant Lagrangians can be constructed for symmetry groups G which leave a scalar product invariant.

However, the Lagrangian density is not invariant under *local* gauge transformations, given by

$$\phi(x) \to \phi'(x) = \Omega(x)\phi(x), \quad \Omega(x) \in G, \tag{13.7}$$

since the derivatives in (13.5) act on a space-time independent $\Omega(x)$. But it is possible to extend a global symmetry to a local symmetry by coupling the charged scalar field ϕ to a *gauge potential* A_μ. In the minimal coupling one replaces the partial derivative ∂_μ by the *covariant derivative*,

$$D_\mu(A) = \partial_\mu - \mathrm{i}gA_\mu. \tag{13.8}$$

Here g is the constant which couples the gauge field and the matter field. The two objects on the right hand side should transform identically under Lorentz transformation. This means that the A_μ are components of a vector field A. Now we impose the important condition that $D_\mu(A)\phi$ transforms exactly like the field ϕ under gauge transformation:

$$D_\mu\big(A'\big)\phi'(x) = \Omega(x)\, D_\mu(A)\phi(x). \tag{13.9}$$

Inserting the transformation of ϕ this condition is equivalent to

$$D_\mu\big(A'\big) = \Omega D_\mu(A)\Omega^{-1} \tag{13.10}$$

and this transformation rule for the covariant derivative is fulfilled if

$$A_\mu \to A'_\mu = \Omega A_\mu \Omega^{-1} - \frac{\mathrm{i}}{g}\partial_\mu \Omega \Omega^{-1}. \tag{13.11}$$

For notational simplicity we did not write the space-time dependence of the fields and gauge transformation. If $\Omega(x)$ takes its values from a Lie group G then $\partial_\mu \Omega \Omega^{-1}$ is in the Lie algebra $\mathbf{g}$ of the group. The transformation formula suggests that $\mathrm{i}A_\mu$ should be in the Lie algebra as well such that all three terms in (13.11) are (up to a factor i) Lie-algebra valued. For the gauge group $U(n)$ the Lie algebra contains all anti-hermitian matrices.

The antisymmetric *field strength tensor* is defined as the commutator of two covariant derivatives,

$$F_{\mu\nu}(A) = \frac{\mathrm{i}}{g}\big[D_\mu(A), D_\nu(A)\big] = \partial_\mu A_\nu - \partial_\nu A_\mu - ig[A_\mu, A_\nu]. \tag{13.12}$$

The transformation rule (13.10) for the covariant derivatives implies that it transforms according to an adjoint representation of the gauge group,

$$F_{\mu\nu}(x) \to \Omega(x) F_{\mu\nu}(x) \Omega_x^{-1}. \tag{13.13}$$

Similarly as in electrodynamics we square the field strength tensor to obtain a Lorentz-invariant contribution to the Lagrangian density. Since $F^{\mu\nu}F_{\mu\nu}$ is not gauge

invariant—it transforms according to the adjoint representation—we take its trace and end up with the following Lorentz and gauge-invariant Lagrangian density:

$$\mathscr{L}(\phi, A_\mu) = -\frac{1}{4}\,\mathrm{tr}\big(F_{\mu\nu}F^{\mu\nu}\big) + \big(D_\mu\phi, D^\mu\phi\big) - m^2(\phi,\phi) = \mathscr{L}\big(\phi', A'_\mu\big) \quad (13.14)$$

for the coupled system of scalar fields and gauge fields. The first Yang–Mills term generalizes the Maxwell term in electrodynamics. The remaining terms are obtained from (13.5) by the substitution $\partial_\mu \to D_\mu$.

Let us specialize to the Abelian gauge group $U(1)$ for which the components A_μ of the vector potential are real fields. For an Abelian gauge theory the field strength is gauge invariant, since Ω in (13.13) commutes with $F_{\mu\nu}$, and no trace is needed in (13.14). Thus we obtain the Lagrangian density of the vector potential in electrodynamics coupled to a charged scalar field. Upon quantization the theory based on (13.14) describes photons and charged scalar particles in interaction. In Chap. 15 we shall see how one couples fermions to the gauge field. If ϕ is replaced by the electron field, then the resulting quantized gauge theory is *quantum electrodynamics*, one of the most successful theories in theoretical physics.

The electroweak interaction, described by the *Salam–Weinberg model*, is based on the non-Abelian gauge group $SU(2) \times U(1)$. In this theory the scalar field ϕ is a complex doublet and transforms under both factors of the gauge group. The field ϕ is very important since after condensation it is responsible for the masses of elementary particles. Finally, the theory of strong interaction, quantum chromodynamics, is a gauge theory with gauge group $SU(3)$. The matter sector of this theory contains quarks—fermions which are confined within baryons and mesons and which cannot be liberated. Many quantitative results about this strongly interacting theory stem from numerical simulations of the corresponding lattice gauge theory.

Let us discuss in more detail the minimal coupling of matter fields to the gauge field. In general the vector space V carries a representation R of the gauge group, in which case the matter field transforms according to this representation, $\phi' = R(\Omega)\phi$. For example, for the gauge group $SU(2)$ a real field ϕ with three components could transform according to the three-dimensional triplet-representation. The important covariance condition (13.6) is automatically fulfilled, if we choose

$$D_\mu\phi = \partial_\mu\phi - \mathrm{i}g\,R_*(A_\mu)\phi \quad (13.15)$$

as covariant derivative. Here R_* is the representation of the Lie algebra, induced by the group representation R. Thus the commutator of covariant derivatives in the representation R is given by

$$\mathrm{i}[D_\mu, D_\nu] = g\,R_*(F_{\mu\nu}). \quad (13.16)$$

Certain properties of quantized gauge theories may depend on the representation of the gauge group. For example, locally the gauge groups $SU(2)$ and $SO(3)$ are identical, but this does not imply that the corresponding quantized gauge theories show the same phases and phase structure [19].

Finally let us summarize the main ingredients of a gauge theory. A gauge theory is determined by

- the gauge group G,
- the matter fields including the representations under which they transform,
- the *universal* coupling constant g.

Unfortunately that is not all. We also must specify the masses and self-couplings of the matter fields. The Salam–Weinberg theory contains additional parameters, for example the elements of the KMS matrix.

13.1.1 Parallel Transport

A lattice gauge theory has parallel transporters between neighboring sites as fundamental fields. These transporters are defined in the continuum theory, and their definition is carried over to the corresponding lattice theory. Here we consider a scalar field in the defining representation, i.e. $\phi \to \Omega\phi$. The field is called *covariantly constant* if

$$D_\mu \phi = 0, \quad \text{i.e. } \partial_\mu \phi = \mathrm{i} g A_\mu \phi. \tag{13.17}$$

With (13.12) this implies the integrability condition

$$0 = [D_\mu, D_\nu]\phi = -\mathrm{i} g F_{\mu\nu}\, \phi.$$

In a non-Abelian gauge theory $F_{\mu\nu}(x)$ is Lie-algebra valued and $\phi(x)$ is a vector with n components. For a generic field strength these n algebraic equations have no non-trivial solution.

Let us instead study the equation of covariant constancy *along a path* $\mathscr{C}_{yx}$ from x to y. The parametrized path $x(s)$ with $s \in [0, 1]$ fulfills

$$x(0) = x \quad \text{and} \quad x(1) = y.$$

The field ϕ is covariantly constant along the path if

$$0 = \dot{x}^\mu D_\mu \phi = \frac{\mathrm{d}\phi(s)}{\mathrm{d}s} - \mathrm{i} g A_\mu\big(x(s)\big)\dot{x}^\mu(s)\, \phi(s), \tag{13.18}$$

where we used the shorthand notation $\phi(s)$ for $\phi(x(s))$. If we interpret the curve parameter s as time, then the equation above is a time-dependent Schrödinger equation with time-dependent "Hamiltonian" $\sim A_\mu(x(s))\dot{x}^\mu(s)$. Hence, the solution of the system of ordinary differential equations may be written as

$$\phi(s) = \mathscr{P} \exp\left(\mathrm{i} g \int_0^s \mathrm{d}u\, A_\mu\big(x(u)\big)\dot{x}^\mu(u) \right) \phi(x), \tag{13.19}$$

where $\mathscr{P}$ indicates the ordering with respect to the curve parameter s. For non-Abelian fields this *path ordering* is necessary since the Lie-algebra valued Hamiltonians at different points on the curve do not commute. Evidently, path ordering is obsolete for Abelian gauge groups.

Setting $s = 1$ we obtain the *parallel transporter* along the curve $\mathscr{C}_{yx}$,

$$\phi(y) = U(\mathscr{C}_{yx}; A)\phi(x), \quad U(\mathscr{C}_{yx}; A) = \mathscr{P} \exp\left(\mathrm{i} g \int_0^1 \mathrm{d}s\, A_\mu \dot{x}^\mu \right). \tag{13.20}$$

The components of the gauge potential define a one-form, $A = A_\mu dx^\mu$, and the line integral in the exponent is just the integral of this one-form along the path $\mathscr{C}_{yx}$. Thus for an arbitrary path $\mathscr{C}$ we may write

$$U(\mathscr{C}; A) = \mathscr{P} \exp\left(\mathrm{i}g \int_{\mathscr{C}} A \right). \tag{13.21}$$

For a Lie-algebra valued potential this parallel transporter along $\mathscr{C}$ is an element of the gauge group.

Composition of Paths

If the path $\mathscr{C}$ connects x and y and $\mathscr{C}'$ connects y and z then the composite path $\mathscr{C}' \circ \mathscr{C}$ (first $\mathscr{C}$ and afterwards $\mathscr{C}'$) connects x and z. The parallel transporter along the composite path is just the product of the individual transporters,

$$U\big(\mathscr{C}' \circ \mathscr{C}; A\big) = U\big(\mathscr{C}'; A\big) U(\mathscr{C}; A). \tag{13.22}$$

This property follows from the uniqueness of the solution of the system of ordinary differential equation (13.18) for fixed end points.

Stokes' Theorem

The parallel transport between two points depends on the path. If $\mathscr{C}'$ and $\mathscr{C}''$ are two different paths from x to y, then $\mathscr{C} = \mathscr{C}'^{-1} \circ \mathscr{C}''$ is a loop beginning and ending at x. For an Abelian theory Stokes' theorem implies

$$U(\mathscr{C}; A) = \exp\left(\mathrm{i}g \oint_{\mathscr{C} = \partial \mathscr{S}} A \right) = \exp\left(\mathrm{i}g \int_{\mathscr{S}} F \right), \tag{13.23}$$

where $\mathscr{S}$ is a surface enclosed by $\mathscr{C}$ and F denotes the field strength two-form

$$F = \frac{1}{2} F_{\mu\nu}\, dx^\mu \wedge dx^\nu = dA. \tag{13.24}$$

Unfortunately, no comparable simple generalization for non-Abelian gauge theories is known, although a non-Abelian Stokes theorem exists in the mathematical literature [20, 21]. There are not many interesting applications of this theorem in physics. Note, however, that, mathematically, the theorem implies that for $F = 0$ the parallel transport is path-independent as long as the considered paths may be deformed into each other.

Gauge Transformation

Parallel transporters are not gauge invariant, they are only gauge covariant. We shall prove that under a gauge transformation a transporter along $\mathscr{C}_{yx}$ transforms as

$$U\big(\mathscr{C}_{yx}; A'\big) = \Omega(y)\, U(\mathscr{C}_{yx}; A)\, \Omega_x^{-1}. \tag{13.25}$$

It immediately follows that for an arbitrary loop the trace of the associated transporter

$$\operatorname{tr} U\big(\mathscr{C}, A'\big) = \operatorname{tr} U(\mathscr{C}, A) \tag{13.26}$$

represents a gauge-invariant quantity—the *Wilson loop*. The set of all Wilson loops form an overcomplete system of gauge-invariant functions on configuration space [22].

Let us now prove the important result (13.25). The parallel transport belonging to the right hand side of (13.25) is given by

$$\phi'\big(x(s)\big) = \Omega\big(x(s)\big) \exp\left(\mathrm{i}g \int_0^s A_\mu \dot{x}^\mu \,\mathrm{d}s\right) \Omega_x^{-1} \phi(x). \tag{13.27}$$

Differentiating with respect to the parameter s we obtain the Schrödinger equation

$$\frac{\mathrm{d}\phi'(s)}{\mathrm{d}s} = \big(\partial_\mu \Omega \Omega^{-1} + \mathrm{i}g \Omega A_\mu \Omega^{-1}\big)|_{x(s)} \dot{x}^\mu \, \phi'(s) = \mathrm{i}g A'_\mu(s) \dot{x}^\mu(s) \, \phi'(s),$$

which has the unique solution

$$\phi'\big(x(s)\big) = \mathscr{P} \exp\left(\mathrm{i}g \int_0^s \mathrm{d}s \, A'_\mu \dot{x}^\mu\right) \phi(x). \tag{13.28}$$

A comparison of (13.27) with (13.28) for $s = 1$ yields the transformation rule (13.25).

Matter Fields

The matter field $\phi(x)$ transforms under a gauge transformation into $\Omega(x)\phi(x)$. It follows immediately that the bilinear expression

$$\big(\phi(y), U(\mathscr{C}_{yx}; A)\phi(x)\big) \tag{13.29}$$

is gauge invariant. However, for a non-vanishing $F_{\mu\nu}$ this expression depends on the path from x to y. A complete list of gauge-invariant composite fields in a theory with scalar and gauge fields is presented in [23].

From this point on we switch to the *Euclidean formulation* of gauge theories. After a Wick rotation from the Lorentzian to the Euclidean signature the Lagrangian density of the Higgs model (13.14) transforms into

$$\mathscr{L}_E = \frac{1}{4} \operatorname{tr} F^{\mu\nu} F_{\mu\nu} + \big(D_\mu \phi, D^\mu \phi\big) + m^2(\phi, \phi). \tag{13.30}$$

The connection between gauge potential and field strength as well as the definitions of the covariant derivatives remain unchanged. In Euclidean theory the metric is $\delta_{\mu\nu}$ and this implies, for example, $F_{\mu\nu} = F^{\mu\nu}$ or $F^{\mu\nu} F_{\mu\nu} = \sum F_{\mu\nu}^2$.

13.2 Gauge-Invariant Formulation of Lattice Higgs Models

In this section we will formulate a theory with *local* gauge invariance on a lattice Λ with lattice sites $\{x\}$ and lattice spacing a. First we discretize a scalar field theory such that the resulting theory on the lattice remains invariant under *global* gauge transformations $\phi_x \to \Omega\phi_x$. The kinetic part of the lattice Lagrangian will contain nearest neighbor terms

$$(\phi_x, \phi_y). \tag{13.31}$$

These terms are invariant under global, but not under *local* transformations,

$$\phi_x \to \phi'_x = \Omega_x \phi_x, \quad x \in \Lambda, \Omega_x \in G, \tag{13.32}$$

since the field at different sites enters the scalar product (13.31). Before comparing the field at different points we should parallel transport it from one point to the other. This suggests that the correct nearest neighbor coupling reads

$$(\phi_x, U_{\langle x,y\rangle}\phi_y), \tag{13.33}$$

were $U_{\langle x,y\rangle}$ is the parallel transporter from y to its neighbor x. This expression is invariant under local gauge transformations if the transporter transforms as expected,

$$U_{\langle x,y\rangle} \to U'_{\langle x,y\rangle} = \Omega_x U_{\langle x,y\rangle} \Omega_y^{-1}. \tag{13.34}$$

In general the parallel transport depends on the chosen path. On the lattice we may think of $U_{\langle x,y\rangle}$ as the parallel transporter along the link,

$$U_{\langle x,y\rangle} = P \exp\left(\mathrm{i}g \int_y^x A_\mu(z)\, \mathrm{d}z^\mu \right) = \mathbb{1} + \mathrm{i}g(x-y)^\mu A_\mu(x) + O\big(a^2\big), \tag{13.35}$$

although this interpretation is not of much relevance on the lattice. Inserting this expansion into the difference between the field at a given lattice site and on a neighboring site, parallel transported to the given site, we obtain the expansion

$$\phi_x - U_{\langle x,y\rangle}\phi_y = (x-y)^\mu D_\mu \phi(x) + O\big(a^2\big). \tag{13.36}$$

Taking the square of this relation and bearing in mind that nearest neighbors are separated by the lattice spacing a yields (no sum over μ)

$$\begin{aligned} a^2\big(D_\mu\phi(x), D_\mu\phi(x)\big) = (\phi_x, \phi_x) + (\phi_y, \phi_y) \\ - 2\Re(\phi_s, U_{\langle x,y\rangle}\phi_y) + O\big(a^3\big). \end{aligned} \tag{13.37}$$

These considerations suggest that we choose the parallel transporters $U_{\langle x,y\rangle}$ between neighboring sites rather than the vector potential $A_\mu(x)$ as the basic object for constructing an invariant action and path integral. Since all relevant symmetry groups are compact[1] this means that the dynamical variables on the lattice $\{U_{x,\mu}\}$ take their values in a *compact* group. This will be relevant for the functional integrals of lattice gauge theories.

[1] Gravity is an exception.

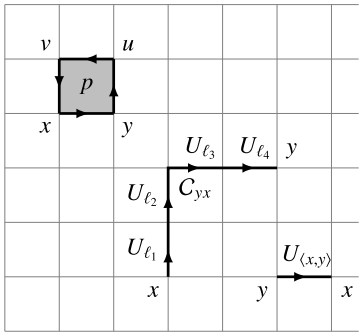

Fig. 13.1 The elementary variables are the parallel transporters $U_{\langle x,y\rangle}$ between nearest neighbors. The parallel transporter along a path $\mathscr{C}_{yx}$ from x to y is the product of elementary variables on the oriented links along the path. A plaquette is characterized by four sites x, y, u and v

13.2.1 Wilson Action of Pure Gauge Theories

Our first task is to construct an action that describes the dynamics of the gauge variables $U_{\langle x,y\rangle} \in G$ defined on the oriented links of the lattice. A gauge field configuration on the lattice is a map from the set of directed links E into G,

$$U : E = \{\ell\} \to G. \tag{13.38}$$

The parallel transporter $U(\mathscr{C})$ along an arbitrary path $\mathscr{C}$ on the lattice is the product of the elementary transporters assigned to the directed links along the path:

$$U(\mathscr{C}_{yx}) = U_{\ell_n} \cdots U_{\ell_3} U_{\ell_2} U_{\ell_1},$$

cf. Fig. 13.1. Similarly as in the continuum we have

$$U^{-1}(\mathscr{C}) = U\big(\mathscr{C}^{-1}\big) \quad \text{e.g. } U^{-1}_{\langle x,y\rangle} = U_{\langle y,x\rangle}. \tag{13.39}$$

The Lagrangian density of a continuum Yang–Mills theory contains the square of the field strength. The field strength is interpreted as curvature and determines how much the matter field changes (per area) when it is parallel transported along an infinitesimally small loop. Naturally, there is no infinitesimal transport on a lattice. The most elementary transport along a closed path results from the product of the transporters along the edges of an elementary plaquette, which is defined by its corners x, y, u and v:

$$U_p = U_{\langle x,v\rangle} U_{\langle v,u\rangle} U_{\langle u,y\rangle} U_{\langle y,x\rangle}, \tag{13.40}$$

see Fig. 13.1. Similarly as in Sect. 10.4 we use the notation

$$U_p = \prod_{\ell \in \partial p} U_\ell. \tag{13.41}$$

This notation does not reveal the dependence of U_p on x. Sometimes it is convenient to use an alternative notation: if x and $x + e_\mu$ are neighboring sites then we denote the parallel transporter from x to $x + e_\mu$ by $U_{x,\mu}$. Similarly, a plaquette is characterized by a point and two (positive) directions, $p = (x, \mu, \nu)$, and we can write

$U_p = U_{x,\mu\nu}$. The plaquette variable $U_{x,\mu\nu}$ transforms under gauge transformations according to

$$U_{x,\mu\nu} \to \Omega_x U_{x,\mu\nu} \Omega_x^{-1}. \tag{13.42}$$

To motivate Wilson's choice of a gauge-invariant and real lattice action we introduce a small lattice spacing a and write

$$U_{x,\mu} = \mathrm{e}^{\mathrm{i}gaA_\mu(x)}, \tag{13.43}$$

where the interpolating field $A_\mu(x) = A_\mu^a(x)T_a$ takes its values in the Lie algebra. With the help of the Baker–Hausdorff formula [24]

$$\mathrm{e}^A \mathrm{e}^B = \mathrm{e}^{A+B+\frac{1}{2}[A,B]+\cdots} \tag{13.44}$$

we rewrite the product of parallel transporters around a plaquette p as follows:

$$\begin{aligned} U_{x,\mu\nu} &= \mathrm{e}^{-\mathrm{i}gaA_\nu(x)} \mathrm{e}^{-\mathrm{i}gaA_\mu(x+ae_\nu)} \mathrm{e}^{\mathrm{i}gaA_\nu(x+ae_\mu)} \mathrm{e}^{\mathrm{i}gaA_\mu(x)} \\ &= \mathrm{e}^{-\mathrm{i}gaA_\nu(x)} \mathrm{e}^{-\mathrm{i}gaA_\mu(x) - \mathrm{i}ga^2\partial_\nu A_\mu(x) + O(a^3)} \\ &\quad \times \mathrm{e}^{\mathrm{i}gaA_\nu(x) + \mathrm{i}ga^2\partial_\mu A_\nu(x) + O(a^3)} \mathrm{e}^{\mathrm{i}gaA_\mu(x)} \\ &= \mathrm{e}^{\mathrm{i}ga^2(\partial_\mu A_\nu(x) - \partial_\nu A_\mu(x) - \mathrm{i}g[A_\mu(x), A_\nu(x)]) + O(a^3)} = \mathrm{e}^{\mathrm{i}ga^2 F_{\mu\nu}(x) + O(a^3)}. \end{aligned} \tag{13.45}$$

Only terms up to order a^2 are considered in the exponent. This yields

$$U_{x,\mu\nu} + U_{x,\mu\nu}^{-1} \approx 2 \cdot \mathbb{1} - ga^4 F_{\mu\nu}^2(x) + O\big(a^6\big). \tag{13.46}$$

Since the relevant term is $O(a^4)$ you would think that all terms up to this order in the exponent will contribute. However, for $U = \exp(\mathrm{i}T)$ we obtain

$$U + U^{-1} = 2 - T^2 + O\big(T^4\big).$$

It follows that only the *leading* term of order a^2 in T contributes to the fourth order term in $U + U^{-1}$. This naive continuum limit motivates the following choice for the action of a Euclidean gauge theory with unitary gauge group:

$$S_{\text{gauge}} = \beta \sum_p \mathrm{tr}\left\{\mathbb{1} - \frac{1}{2}\big(U_p + U_p^\dagger\big)\right\}, \quad \beta = \frac{2}{Ng^2}. \tag{13.47}$$

The sum extends over all $Vd(d-1)/2$ elementary plaquettes of the lattice and the factor $1/N$ in the gauge coupling β takes into account that the link variables are N-dimensional matrices. The non-negative action is minimal for configurations with $U_p = \mathbb{1}$ for all p. These "vacuum configurations" have zero action. For real or pseudo-real groups like $SU(2)$ the trace of U is real and the plaquette action simplifies to $\beta\ \mathrm{tr}(\mathbb{1} - U_p)$. For the finite gauge group Z_n we recover the action (10.55).

The *Wilson action* (13.47) approximates the continuum Yang–Mills action up to an error of order $O(a^2)$, similarly to the trapezoidal rule which approximates an integral up to order $O(a^2)$. A natural question is whether there is something like Simpson's rule with an error of order $O(a^4)$ in lattice gauge theory. Such improvements of the Wilson action have been suggested. One improvement based on the

renormalization group method was given by K. Wilson himself [25]. Another improvement program based on perturbation theory was initiated by K. Symanzik [26] and further developed in [27]. A lattice action which gives two-loop scaling was constructed in [28].

Now we can write down a gauge-invariant action for the Higgs model on a lattice. For the gauge fields we choose the Wilson action (13.47). For the scalar field we take the right hand side of (13.37), summed over all lattice sites, since this sum approximates the kinetic term in (13.30). Thereby the terms (ϕ_x, ϕ_x) and (ϕ_y, ϕ_y) can be absorbed in the potential term. Hence as gauge-invariant interaction between the gauge field and scalar field we take

$$S_{\mathrm{m}} = -\kappa \sum_{\langle x,y \rangle} \Re(\phi_x, U_{\langle x,y \rangle} \phi_y) \tag{13.48}$$

with hopping parameter κ. Thus we end up with the Yang–Mills–Higgs action

$$S_{\mathrm{YMH}}(U, \phi) = S_{\mathrm{gauge}}(U) + S_{\mathrm{m}}(U, \phi) + \sum_x V(\phi_x) \tag{13.49}$$

with an invariant potential for the scalar field, $V(\Omega\phi) = V(\phi)$.

We have argued that on a lattice the $\{U_\ell\}$ should be taken as dynamical variables. Thus, the formal integration over all gauge potentials in the continuum theory turns into an integration over the group valued fields on the links and we end up with the following functional representation of the partition function:

$$Z(\beta, \kappa) \int \prod_x \mathrm{d}\phi_x \prod_\ell \mathrm{d}U_\ell \, \mathrm{e}^{-S_{\mathrm{YMH}}(U,\phi)}. \tag{13.50}$$

Since the resulting lattice theory should be gauge invariant we better choose an invariant integration,

$$\mathrm{d}(\Omega\phi) = \mathrm{d}\phi, \qquad \mathrm{d}\big(\Omega' U \Omega^{-1}\big) = \mathrm{d}U. \tag{13.51}$$

Invariant measures on compact groups exist and are studied in Chap. 14.

13.2.2 Weak and Strong Coupling Limits of Higgs Models

Here we will consider the four simplifying limits of the Higgs model in which $\beta \to 0$ or ∞ and $\kappa \to 0$ or ∞. Along the way we will learn about selecting gauges.

Vanishing β and Unitary Gauge

In this limit the Wilson term is absent and it is a trivial limit of the theory. This is most easily seen in the unitary gauge which can be achieved for all models for which the scalar field can be gauge transformed into a fixed direction defined by a constant unit vector ϕ_0,

$$\phi_x = \rho_x \Omega_x \phi_0 \quad \text{with } \Omega_x \in G. \tag{13.52}$$

This condition fixes the gauge transformations $\{\Omega_x\}$ completely in case the little group of ϕ_0

$$H = \{\Omega \in G \,|\, \Omega\phi_0 = \phi_0\} \tag{13.53}$$

is a trivial subgroup $H = \{\mathbb{1}\}$ of the gauge group. Now we use the gauge invariance of the action and measure to rewrite the partition function as

$$Z = \int \prod_x \mathrm{d}\phi_x \prod_\ell \mathrm{d}U_\ell \, \mathrm{e}^{-S_{\text{gauge}}(U') - S_{\text{m}}(U', \rho\phi_0) - V(\rho)} \tag{13.54}$$

with gauge transformed link variables $U'_{\langle x,y\rangle} = \Omega_x^{-1} U_{\langle x,y\rangle} \Omega_y$. But since $\mathrm{d}U_\ell$ is gauge invariant we may skip the prime at U' in the integrand. Since the integrand only depends on ρ and U we may change variables and find

$$Z = (\mathrm{Vol}_{G/H})^V \int \prod_x \mathrm{d}\rho_x \, \rho_x^{n-1} \prod_\ell \mathrm{d}U_\ell \, \mathrm{e}^{-S_{\text{gauge}}(U) - S_{\text{m}}(U, \rho\phi_0) - V(\rho)}, \tag{13.55}$$

where the first factor contains the volume of the coset space G/H and n denotes the number of ϕ-components. If we freeze the length ρ of the scalar field by setting $\exp(-V(\rho)) = \delta(\rho - 1)$, we are dealing with gauged nonlinear sigma models. For these models the integration over the radial modes $\{\rho_x\}$ yields 1 and for $\beta = 0$ the partition function Z factors into a product of independent terms and thus is trivial,

$$Z \xrightarrow{\beta \to 0} (\mathrm{Vol}_{G/H})^V \left(\int \mathrm{d}U \mathrm{e}^{\kappa(\phi_0, U\phi_0)} \right)^{|E|}, \tag{13.56}$$

where $|E|$ is the number of links on the lattice. The free energy density is an analytic function of κ given by a simple group integral.

Infinite β and Axial Gauge on Periodic Lattices

Again we impose periodic boundary conditions in all directions and thus may view the hyper-cubic lattice as torus. In the limit $\beta = \infty$ the system is most comprehensible in an axial-like gauge where one uses the gauge freedom to choose as many U's as possible to be the unit matrix. In a first step of the gauge fixing all time-like link variables $U_{x,0}$ for $t > 1$ are gauged to the unit element. These are the thick vertical links in Fig. 13.2. The remaining time-like link variables at $t = 1$ cannot be gauged to the unit element and in the axial gauge they are equal to the *Polyakov loops*

$$\mathscr{P}_{\mathbf{x}} \equiv \prod_{t=1}^{N} U_{(t,\mathbf{x}),0} \overset{\text{gf}}{=} U_{(1,\mathbf{x}),0}. \tag{13.57}$$

These particular Wilson loops wind around the periodic time direction and will be relevant at finite temperatures. The gauge transformations Ω_x in the time slice $t = 1$ are not used for this first gauge fixing step. In a second step we use these gauge transformations to fix all variables on links in the x_1-direction and with $x_1 > 1$ in the time slice $t = 1$ to the unit element. These are the thick links at the bottom of the

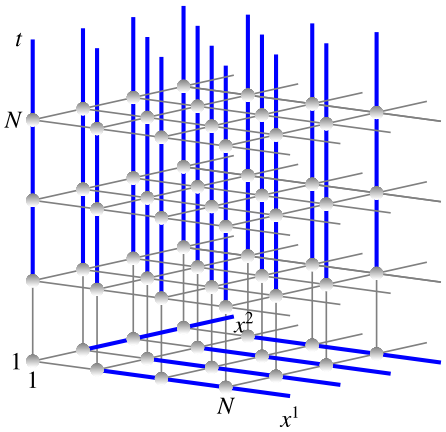

Fig. 13.2 In the axial-like gauge the variables on the thick marked links are fixed to the unit element

cube in Fig. 13.2 pointing towards the x_1-direction. The gauge transformations Ω_x in the slice $t = x_1 = 1$ are not used for this second gauge fixing step but in the third step were one fixes the variables in this slice with $x_2 > 1$ to the unit element. After these three steps all variables on the thick links in Fig. 13.2 are gauge fixed to the unit element. This is almost a complete gauge fixing—only the gauge transformation at the point $(1, 1, 1)$ remains unfixed and acts as a residual *global* gauge symmetry. After gauge fixing the number of links with $U_{x,\mu} = \mathbb{1}$ is

$$N^2(N-1) + N(N-1) + (N-1) = N^3 - 1 \tag{13.58}$$

in three dimensions and more generally $V - 1$ in arbitrary dimensions. This is exactly the number of gauge transformations $\{\Omega_x\}$ minus the residual gauge transformation.

In the limit $\beta \to \infty$ we require that each term of S_{gauge} be minimized which means that all plaquette variables occurring in the Wilson action are the unit matrix. Let us see what this implies for a gauge fixed configuration in three dimensions:

Considering the time-space plaquettes of a gauge fixed configuration we see that the link variables in x_1 and x_2-directions are t-independent. Considering the space plaquettes in the slice $t = 1$ we conclude that the link variable in x_2-direction are also x_1-independent. Thus we are left with the non-trivial variables $U_{x,0}$ in the slice $t = 1$, the variables $U_{x,1}$ in the slice $x_1 = 1$ and the variables $U_{x,2}$ in the slice $x_2 = 1$. Recalling that all other variables are the identity one concludes that the variables in each slice are constant. The same reasoning applies in d dimensions and one is left with just d constant group elements. In four dimensions:

$$\begin{aligned} U_{x,0} &\equiv \mathscr{P} \quad \text{if } x = (1, x_1, x_2, x_3), \\ U_{x,1} &\equiv U_1 \quad \text{if } x = (t, 1, x_2, x_3), \\ U_{x,2} &\equiv U_2 \quad \text{if } x = (t, x_1, 1, x_3), \\ U_{x,3} &\equiv U_3 \quad \text{if } x = (t, x_1, x_2, 1). \end{aligned} \tag{13.59}$$

Actually for a gauge theory with open boundary conditions we can gauge fix *all* link variables to the unit element such that the Higgs model reduces to a spin model for the scalar field,

$$Z \overset{\beta\to\infty}{\longrightarrow} C \int \prod_x \mathrm{d}\phi_x \exp\Big(-\kappa \sum_{\langle x,y\rangle} (\phi_x, \phi_y)\Big). \tag{13.60}$$

Vanishing κ

In this limit the matter field decouples and we are left with a pure gauge theory. This is a non-trivial limit and much of the rest of the present chapter concerns this limit.

The Limit $\kappa \to \infty$

This limit is most easily studied in the unitary gauge. In this gauge we require that $(\phi_0, U\phi_0)$ takes its maximum value on each link which implies $U\phi_0 = \phi_0$. If the little group H of ϕ_0 is trivial then all link variables must be the identity. If we freeze the length of the scalar field then no degrees of freedom are left. If the little group is non-trivial then the limiting theory is a pure gauge theory with gauge group H.

13.3 Mean Field Approximation

First we discuss the mean field approximation for pure gauge theories. Our starting point is the variational characterization of the free energy

$$F = \inf_P \Big(\int \mathrm{d}P(U)\, S_{\text{gauge}}(U) - S_{\text{B}}(P) \Big). \tag{13.61}$$

In the mean field approximation, as described in Chap. 7, $\mathrm{d}P(U)$ is assumed to be a product measure with associated Boltzmann entropy S_{B}. We use the Wilson action S_{gauge} in the variational principle. In spite of a priori difficulties, such as Elitzur's theorem discussed in Sect. 13.5, this simple approximation allows for a first exploration of the phase diagram. We choose the non-invariant product measure

$$\mathrm{d}P(U) = \prod_\ell \mathrm{d}\nu_\ell(U_\ell), \quad \mathrm{d}\nu(U) = p(U)\,\mathrm{d}U, \tag{13.62}$$

where $\mathrm{d}U$ denotes the invariant Haar measure on the gauge group (as discussed in Chap. 14) and p is the probability density

$$p(U) = \frac{1}{z(h)} \exp\Big(\frac{h}{N} \Re \operatorname{tr} U\Big), \tag{13.63}$$

normalized with the single-link partition function

$$z(h) = \mathrm{e}^{v(h)} = \int \mathrm{d}U \exp\Big(\frac{h}{N} \Re \operatorname{tr} U\Big) = 1 + O\big(h^2\big). \tag{13.64}$$

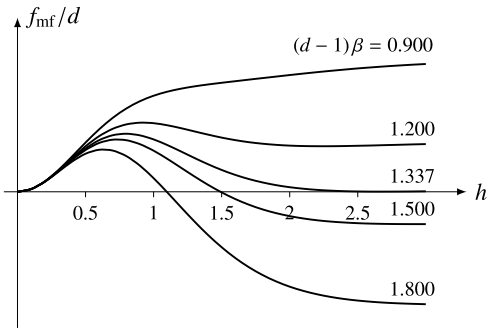

Fig. 13.3 The free energy per link $f_{\rm mf}/d$ of the Z_2 gauge theory in the mean field approximation. The minimum jumps at $(d-1)\beta_* \approx 1.3776$

In matrix notation, the mean value is proportional to the unit matrix [29]

$$\langle U\rangle_h = \int \mathrm{d}\nu(U)\, U = v'(h)\mathbb{1}. \tag{13.65}$$

The Boltzmann entropy is the number of links dV times the single-link entropy

$$s_{\rm B} = -\int \mathrm{d}\nu \log p = \nu(h) - h\nu'(h). \tag{13.66}$$

The expectation value of $S_{\rm gauge}$ for the product measure is proportional to the number of plaquettes $Vd(d-1)/2$ times the average single plaquette action,

$$\langle U_p\rangle_h = \int \mathrm{d}\nu_1(U_1)\cdots \mathrm{d}\nu_4(U_4)\Re\,\mathrm{tr}(U_p) = N v'^4(h). \tag{13.67}$$

Inserting the average action and entropy into (13.61) one obtains the mean field free energy per link,

$$\frac{f_{\rm mf}}{d} = \inf_h\left(h\nu'(h) - \nu(h) - \frac{1}{2}\beta N(d-1)\, v'^4(h)\right), \tag{13.68}$$

where the function $\nu(h)$ is the single-link free energy defined in (13.64) and hence a convex function with a minimum at the origin where it behaves as h^2. Since the term $v'^4(h)$ behaves as h^4 the minimization always leads to the solution $h = 0$, and this minimum is unique for small β. As β increases this minimum does not remain the lowest one.

13.3.1 Z_2 Gauge Model

For the gauge group Z_2 the single site free energy is $v(h) = \log\cosh(h)$ and

$$\frac{f_{\rm mf}}{d} = \inf_h\left(h\tanh(h) - \log\cosh(h) - \frac{1}{2}\beta(d-1)\tanh^4(h)\right). \tag{13.69}$$

The behavior of the free energy density for different values of β is displayed in Fig. 13.3. At the critical value $(d-1)\,\beta_* \approx 1.3776$ the absolute minimum suddenly changes its location as depicted in Fig. 13.3 and this jump signals a first order tran-

sition at β_*. In four dimensions we find $\beta_* = 0.4592$ to be compared with the exact value 0.44069 known from self-duality, see Table 10.3. The transition is known to be of first order as predicted by the mean field approximation. In three dimensions the mean field yields $\beta_* = 0.6888$ to be compared with the value 0.7613, known from duality, see Table 10.2. But since the three-dimensional Z_2 gauge theory is dual to the Ising model the transition is in fact a second order transition.

13.3.2 $U(1)$ Gauge Theory

For this gauge theory $z(h) = I_0(h)$ and the corresponding mean field free energy density looks similar as in Fig. 13.3 and signals a first order transition at $(d-1)\beta_* = 3.6460$. This yields the mean field critical gauge coupling $\beta_* = 1.215$ in four dimensions. High precision MC simulations, supplemented by a finite size analysis, indeed spotted a weakly first order transition at $\beta_* = 1.011133$ [30, 31].

13.3.3 $SU(N)$ Gauge Theories

The upper critical dimension for non-Abelian gauge theories should be four, where the theory becomes asymptotically free. Above the critical dimension we can trust the mean field approximation. To determine $f_{\rm mf}$ of $SU(N)$ gauge theories we need the single-link partition function, which is a sum of products of modified Bessel functions [32, 33],

$$z_{SU(N)}(h) = \sum_{n\in\mathbb{Z}} \det \begin{pmatrix} I_n & I_{n+1} & \cdots & I_{n+N-1} \\ I_{n-1} & I_n & \cdots & I_{n+N-2} \\ \vdots & \vdots & & \vdots \\ I_{n-N+1} & I_{n-N+2} & \cdots & I_n \end{pmatrix} \left(\frac{h}{N}\right). \tag{13.70}$$

The infinite sums entering $v = \log z$ and its derivative (here one uses Bessel function identities) can be evaluated with `octave`. The resulting $f_{\rm mf}(h)$ of the gauge group $SU(2)$ in the vicinity of the critical gauge coupling, $(d-1)\,\beta_* = 4.2394$ is depicted in Fig. 13.4. As expected, the mean field approximation predicts a first order transition at some critical gauge coupling β_*. In five dimensions $\beta_* \approx 1.0598$, which agrees well with numerical simulations which find a first order transition at $\beta_* = 0.82$. In four dimensions the mean field approximation fails. There is no evidence for any transition in numerical simulations.

13.3.4 Higgs Model

For a lattice Higgs model with normalized scalar field the mean field free energy per link is

$$\frac{f_{\rm mf}}{d} = \inf_h \left((h-\kappa)v'(h) - v(h) - \frac{1}{2}\beta N(d-1)\, v'^4(h) \right). \tag{13.71}$$

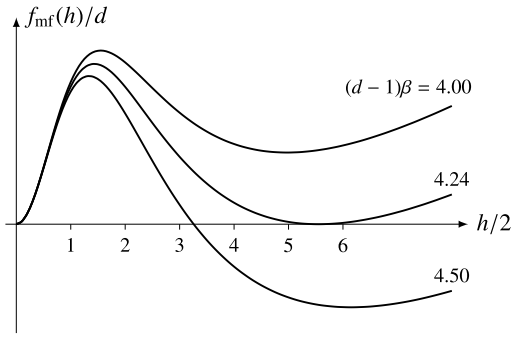

Fig. 13.4 The free energy per link f_{mf}/d of the $SU(2)$ gauge theory in the mean field approximation. The minimum jumps at $(d-1)\beta_* \approx 4.2394$

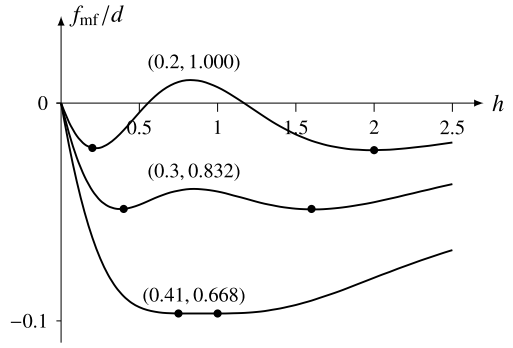

Fig. 13.5 The free energy f_{mf}/d per link of the gauged Ising model in the mean field approximation. Shown are the energies for three pairs of critical parameters (κ_*, β_*) for which the two minima are degenerate. The first order transitions becomes weaker and finally becomes a second order transition when κ_* increases

For small h it behaves as $-2c\kappa h + ch^2 + O(h^4)$ with some positive constant c such that the origin ceases to be a minimum for a non-vanishing hopping parameter κ. With increasing κ the two minima of the free energy approach each other and the first order transition becomes weaker as depicted in Fig. 13.5. At the critical point $(\kappa_*, \beta_*) \approx (0.41, 0.668)$ the two minima merge to one minimum.

13.4 Expected Phase Diagrams at Zero Temperature

Consider a lattice Higgs model with scalar field in a fundamental representation of the gauge group. For $\kappa = 0$ the model reduces to a pure gauge theory and for a discrete gauge group we expect a phase transition at some critical hopping parameter. In three dimensions it is a second order transition and in four dimensions a first order transition. For a non-Abelian gauge theory there is no such transition in either three or four dimensions. For $\beta = \infty$ the Higgs model collapses to a spin model with global symmetry. Generically there will be a second order phase transition from a symmetric phase at large κ to a spontaneously broken phase at small κ. For $\beta = 0$ the theory is analytic in κ and there is no phase transition.

For non-zero but small β OSTERWALDER and SEILER proved that the expansion in powers of β exists with a finite radius of convergence, and that in this strong

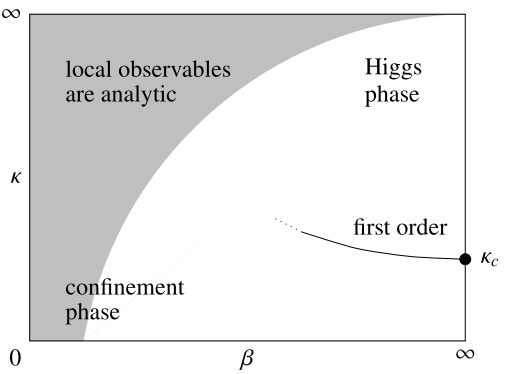

Fig. 13.6 Sketch of phase diagram for $SU(2)$ gauge plus fundamental scalars. The Osterwalder–Seiler–Fradkin–Shenker theorem says that local observables are analytic in the *gray region*

coupling phase the theory is confining [34]. Their proof is combinatoric in nature. It is reassuring though not very surprising that this is the case since most theories are analytic in the high temperature phase. Later on we will show that the Wilson loop obeys an area law in the strong coupling region. Finally, for $\kappa = \infty$ the Higgs model has no dynamics if the unitary gauge is a complete gauge fixing. If it is not a complete gauge fixing then one is left with a pure gauge theory with gauge group $H = \{\Omega \in G | \, \Omega\phi_0 = \phi_0\}$. Hence we do not expect a phase transition at $\kappa = \infty$ for a trivial or non-Abelian H. On the other hand, if the little group H is discrete then there will be a second order transition in three dimensions and a first order transition in four dimensions. There exists a generalization of the Osterwalder–Seiler theorem due to FRADKIN and SHENKER, which states that for a scalar field in a fundamental representation the Higgs model is analytic for sufficiently large κ [35]. The two theorems together imply that in the coupling constant plane there is always a path from a point $\beta, \kappa \ll 1$ deep in the confinement region, where the Wilson loop obeys an area law, to a point $\beta, \kappa \gg 1$ in the Higgs phase where the Wilson loop obeys a perimeter law, such that the expectation values of all *local*, gauge-invariant observables vary analytically along the path. This means that the Higgs phase and the confining phase are smoothly connected and that they are as different as a liquid is from a gas. When the Higgs fields transform according to a non-fundamental representation then a phase boundary may exist. This is the case for $SU(N)$ with all Higgs fields in the adjoint representation and for $U(1)$ with all Higgs fields in the charge-N ($N > 1$) representation.

The $SU(2)$ *Higgs model* with fundamental scalars has been studied by Monte Carlo techniques, and the situation is depicted schematically in Fig. 13.6. One finds that for intermediate values of β certain observables vary rapidly with the coupling, but still analytically in the thermodynamic limit. This is interpreted as a crossover [36]. For larger values of β a line of probably first order transitions are seen. At $\kappa = \infty$, marked by a dot in the figure, the transition must be second order. For a further discussion and an interpretation of these results you may consult the textbook [37].

The Z_2 theory has a similar phase diagram. A crucial difference is that at $\kappa = 0$ the resulting pure gauge model shows a first order transition at some critical β.

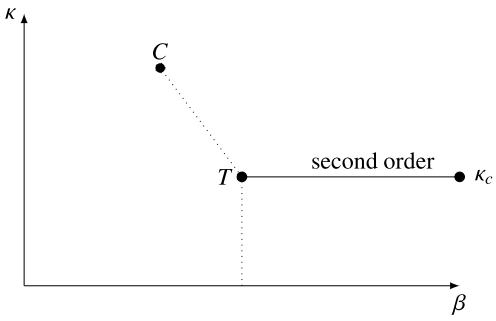

Fig. 13.7 Schematic plot of the phase diagram of the Z_2 gauged Ising model. The *dashed lines* represent a first order phase transition, and the *continuous line* represents a second order transition. The critical point is marked with C and the triple point by T

The diagram is shown schematically in Fig. 13.7. The three transition lines meet at the triple point and split the phase space into three regions. Again the phase diagram includes familiar limits. In the limit $\beta \to \infty$ the gauge degrees of freedom disappear and the system reduces to that of a four-dimensional Ising model with a second order transition which is seen in the expectation value $\langle s_x U_{\langle x,y\rangle} s_y \rangle$. This second order line is of Ising type all the way to the triple point T. On the $\kappa = 0$ axis the system reduces to a pure gauge theory and the expectation value of the plaquette variable $\langle U_p \rangle$ shows a first order transition. This behavior continues all the way up to the triple point. A first order line seen in both expectation values is then formed and ends with the critical point C [39].

13.5 Elitzur's Theorem

The phenomenon of spontaneously broken symmetries happens in large macroscopic systems where the breaking of a global symmetry involves a macroscopic number of degrees of freedom. This is not the case for a local gauge symmetry. The quantum fluctuations tend to smear the ground-state wave function of the system homogeneously over the whole orbit under the group. This results in

Theorem 13.1 (Elitzur) *A local gauge symmetry cannot break spontaneously. The expectation value of any gauge non-invariant local observable must vanish.*

Elitzur's original proof in [38] applies to Abelian gauge theories but was later extended to non-Abelian models [40]. The proofs of Elitzur's theorem are all based on the fact that inequalities which hold for any field configuration continue to hold after integrating with respect to a positive measure. In fact, positivity of the measure and gauge invariance are sufficient to prove the theorem. The theorem means that there is no analog of a magnetization: expectation values of a spin or link variables are zero, even if we introduce an external field (which explicitly breaks gauge invariance) and then carefully take first the infinite volume limit, and then the $h \to 0$ limit. We must look, instead, to gauge-invariant observables which are unaffected by gauge transformations. These can be constructed by taking parallel transporters around closed loops, known as Wilson loops.

Elitzur's theorem raises the question of whether the Higgs mechanism, which gives masses to the fermions and gauge bosons of the standard model, may perhaps not work. As demonstrated in [23] such fears are ungrounded, since the physical phenomena which are associated with the Higgs mechanism can be recovered in an approach that uses gauge-invariant fields only. The masses are extracted from expectation values of gauge-invariant combinations of the Higgs and gauge fields, without any need of introducing a non-zero expectation value of the Higgs field. In particular the electroweak phase transition can be described in purely gauge-invariant terms. For example, the expectation value of (ϕ, ϕ) exhibits a "jump" along the phase transition line in parameter space where the electroweak phase transition occurs.

13.5.1 Proof for Pure Z_2 Gauge Theory

First we consider the simplest possible gauge theory, the pure lattice gauge theory with gauge group Z_2 and link variables $U_\ell \in \{-1, 1\}$ on a finite lattice Λ. We couple the system to an external field h and hence add a source term to the Wilson action,

$$S_{\text{gauge},\Lambda}(U) = -\beta \sum_p U_p - h \sum_\ell U_\ell. \tag{13.72}$$

In expectation values one sums over all elements of the configuration space $\Omega = \{U_\ell | \ell \in E\}$. Now we prove

Theorem 13.2 *The magnetization $\langle U_\ell \rangle$ converges to zero,*

$$\lim_{h \downarrow 0} \langle U_\ell \rangle_\Lambda(h) = 0, \tag{13.73}$$

uniformly in Λ and β. This also holds in the thermodynamic limit.

Proof We bound the numerator and denominator in the expectation value

$$\langle U_{\ell_0} \rangle_\Lambda(h) = \frac{\sum_\Omega U_{\ell_0} \exp(-S_{\text{gauge},\Lambda})}{\sum_\Omega \exp(-S_{\text{gauge},\Lambda})}. \tag{13.74}$$

Let x denote an end point of the link under consideration and perform a local gauge transformation at x with $\Omega_x = \pm 1$. Only variables defined on the $2d$ links ending at this point are affected, $U_\ell \to U'_\ell = \Omega_x U_\ell$ if $x \in \partial\ell$, and this is depicted in Fig. 13.8. Both the original configuration $\{U_\ell\}$ and the transformed configuration $\{U'_\ell\}$ are already contained in Ω such that the partition function in the denominator can be written as

$$Z = \frac{1}{2} \sum_{\Omega_x = \pm 1} \sum_\Omega \exp\Big(\beta U_p + h \sum_{\ell : x \notin \partial\ell} U_\ell\Big) \exp\Big(h \sum_{\ell : x \in \partial\ell} \Omega_x U_\ell\Big),$$

where we took into account that the plaquette variables are gauge invariant. Thus we obtain

$$Z = \sum_\Omega \exp\Big(\beta U_p + h \sum_{\ell : x \notin \partial\ell} U_\ell\Big) \cosh\Big(h \sum_{\ell : x \in \partial\ell} U_\ell\Big). \tag{13.75}$$

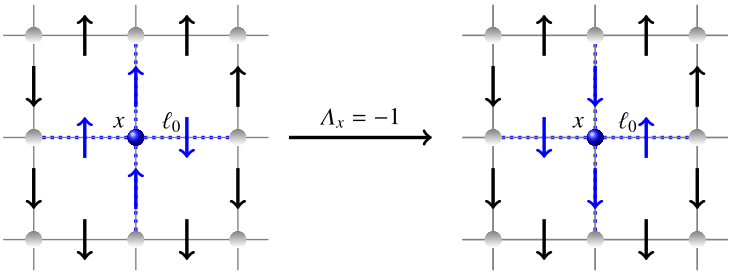

Fig. 13.8 Gauge transformation on the central site. All spins U_ℓ on the links touching the central site (*dotted lines* in the figure) are flipped

Repeating the argument for the numerator N in (13.74) yields

$$N = \sum_{\Omega} \exp\Big(\beta U_p + h \sum_{\ell: x \notin \partial\ell} U_\ell\Big) U_{\ell_0} \sinh\Big(h \sum_{\ell: x \in \partial\ell} U_\ell\Big). \tag{13.76}$$

The argument of the hyperbolic functions varies between $-2dh$ and $2dh$ such that for all configurations

$$\cosh(\ldots) \geq \mathrm{e}^{-2dh}, \quad \big|U_{\ell_0} \sinh(\ldots)\big| \leq \sinh(2dh). \tag{13.77}$$

This yields the bound

$$\big|\langle U_{\ell_0}\rangle_\Lambda(h)\big| \leq \mathrm{e}^{2dh} \sinh(2dh) \xrightarrow{h \downarrow 0} 0, \tag{13.78}$$

uniformly in Λ and β. If one couples the Z_2-gauge field minimally to a scalar field and adds a symmetry breaking term $h \sum_x \phi_x$ then one can prove

$$\langle \phi_x \rangle(h) \xrightarrow{h \downarrow 0} 0, \tag{13.79}$$

uniformly in Λ and the couplings β and κ, see problem 13.1. □

13.5.2 General Argument

Let $\Phi = \{U_\ell, \phi_x, \ldots\}$ denote the collection of fields of a gauge theory and $\int \mathscr{D}\phi \cdots$ the invariant integration. We study the expectation value of a local and non-invariant function $O(\Phi)$ of the fields. Local means that it only depends on a finite number of variables $\{\Phi'\}$ defined on the sites and links in some finite area A. Non-invariant means that $\mathscr{O}$ has no invariant component, i.e.

$$\int \prod_{x \in \mathscr{R}} \mathrm{d}\Omega_x \mathscr{O}\big({}^{\Omega}\Phi\big) = 0, \tag{13.80}$$

where ${}^{\Omega}\Phi$ denotes the gauge transformed configuration. Following [40] we decompose the set of fields $\{\Phi\}$ into $\{\Phi'\} \cup \{\Phi''\}$. Now we average over the subgroup of

gauge transformations which leave the $\{\Phi''\}$ invariant. The invariance of the action without source term and of the integration implies

$$\big\langle \mathscr{O}(\Phi)\big\rangle_{\lambda,J} = \frac{1}{Z_{\Lambda,J}} \int \mathscr{D}\Phi \prod_{x\in\mathscr{R}} \mathrm{d}\Omega_x \, \mathrm{e}^{-S[\Phi]+(J,{}^{\Omega}\Phi')+(J,\Phi'')} \, \mathscr{O}\big({}^{\Omega}\Phi\big). \tag{13.81}$$

Since $\{\Phi'\}$ contains a finite and Λ-independent number of degrees of freedom

$$|\,\mathrm{e}^{(J,\Phi')} - 1| \le \varepsilon(J) \xrightarrow{J\downarrow 0} 0,$$

and this bound is uniform in Λ and in Φ, at least if the latter is a compact variable. Inserting

$$\mathrm{e}^{(J,\,{}^{\Omega}\Phi')} = 1 + \big(\mathrm{e}^{(J,\,{}^{\Omega}\Phi')} - 1\big)$$

into (13.81) the contribution of the first term vanishes because of (13.80). The contribution of the second term vanishes in the limit $\lim_{J\downarrow 0} \lim_{\Lambda\to\mathbb{Z}^d}$. This proves (together with a similar bound on the partition function) that

$$\big\langle \mathscr{O}(\Phi)\big\rangle = \lim_{J\downarrow 0} \lim_{\Lambda\to\mathbb{Z}^d} \big\langle \mathscr{O}(\Phi)\big\rangle_{\Lambda,J} = 0. \tag{13.82}$$

The reasoning in the proofs hinges very much on the *local* gauge invariance and on the positivity of the measure.

13.6 Observables in Pure Gauge Theories

For a gauge-invariant lattice action the normalized probability measure

$$\mathrm{d}\mu[U] = \frac{1}{Z}\,\mathrm{e}^{-S_{\mathrm{gauge}}(U)} \prod_{\ell\in E} \mathrm{d}U_\ell, \quad Z = \int \mathrm{e}^{-S_{\mathrm{gauge}}(U)} \prod_{\ell\in E} \mathrm{d}U_\ell, \tag{13.83}$$

which defines the functional integral, is gauge invariant. The dimensionality of the integral on a finite d-dimensional lattice is $dV\dim(G)$. For example for the pure $SU(2)$ gauge theory on a hyper-cubic 16^4-lattice one is confronted with a 786 432-dimensional integral. According to Elitzur's theorem it is only reasonable to consider expectation values of *gauge-invariant* quantities. For a pure gauge theory the gauge-invariant functions of the link variables are given by *traces* of parallel transporters along closed paths (loops). Thus, we define

$$W[\mathscr{C}] = \mathrm{tr}(U_{\ell_n}\cdots U_{\ell_1}), \quad \mathscr{C} = \ell_n \circ \cdots \circ \ell_1. \tag{13.84}$$

In most work $W[\mathscr{C}]$ is called Wilson loop. Sometimes the product of the $U's$ along the loop, i.e. the argument of the trace in (13.84), is called a Wilson loop. It also occurs that a Wilson loop is defined as the expectation value of $W[\mathscr{C}]$. With a *Wilson loop* we will associate the gauge-invariant quantity W defined in (13.84).

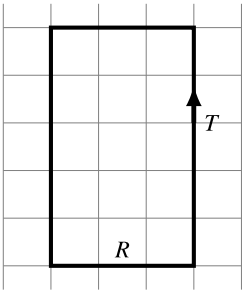

Fig. 13.9 Wilson loop belonging to a rectangular loop with edge lengths R and T. From its expectation value one may extract the string tension between two static charges

Fig. 13.10 Between a static quark–antiquark pair a flux tube develops and leads to a linearly rising potential

13.6.1 String Tension

Let $W[R,T]$ denote the Wilson loop associated with a plane rectangular loop of edge lengths R and T, respectively, as illustrated in Fig. 13.9. The function

$$V_{q\bar{q}}(R) = -\lim_{T\to\infty}\frac{1}{T}\log\langle W[R,T]\rangle \tag{13.85}$$

is interpreted as potential energy of a static $q\bar{q}$-pair separated by a distance R. From the static potential we can extract the *string tension*

$$\sigma = \lim_{R\to\infty}\frac{V_{q\bar{q}}(R)}{R}. \tag{13.86}$$

The justification of this interpretation will be given at a later stage.

A positive string tension means that the potential energy of the static charges increases linearly with increasing distance R. The potential becomes infinitely large for asymptotically separated charges and hence this state does not exist in a dynamical theory. The formation of a flux tube of constant energy density between the charges, as depicted in Fig. 13.10, could explain the linear rising potential: the energy of the tube is proportional to its length R and would give rise to a constant force between the charges. On the other hand, a vanishing string tension would imply that the force between the charges decreases with increasing separation. If it decreases sufficiently fast then a finite amount of energy suffices to separate the two charges. Color-electric flux tubes have indeed been observed in lattice simulations [42].

We assumed that the test particles are infinitely heavy charged objects without their own dynamics. In the real world with dynamical matter the energy between the departing charges increases only as long as the potential energy is smaller than the energy necessary for pair production from vacuum. In the string picture the pair production gives rise to *string breaking*. If pair production sets in then the created pairs screen the test charges and finally we observe two neutral states departing

from each other. Even without dynamical matter string breaking happens if the test particles are in particular representations of the gauge group or if the gauge group has a trivial center [41].

K. Wilson proposed the *area* or *perimeter law* for the expectation value of the Wilson loop as a criterion for confinement in lattice gauge theories:

$$\begin{aligned} \langle W[R,T]\rangle &\sim \mathrm{e}^{-TV_{q\bar{q}}(R)} \sim \mathrm{e}^{-\sigma \times \text{ area}} \quad \text{confinement,} \\ \langle W[R,T]\rangle &\sim \mathrm{e}^{-TV_{q\bar{q}}(R)} \sim \mathrm{e}^{-\gamma \times \text{ perimeter}} \quad \text{deconfinement.} \end{aligned} \tag{13.87}$$

For a plane rectangular loop the area and perimeter are TR and $2(T+R)$, respectively. E. Seiler and C. Borgs proved that the static potential increases monotonously, i.e. $V'_{q\bar{q}} \geq 0$. They also showed that this increase is at most linear, $V''_{q\bar{q}} \leq 0$ [43, 44]. Hence, for large separation of the charges the static potential should have the form

$$V_{q\bar{q}}(R) \sim \sigma R + \text{ const.} - \frac{c}{R} + o\big(R^{-1}\big), \tag{13.88}$$

where c is a universal and positive constant. The term $-c/R$ is the so-called *Lüscher term* and originates from the quantum fluctuations of the flux tube connecting the two static charges [45].

Let us finally *motivate* why $V_{q\bar{q}}$ represents a static $q\bar{q}$-potential. In quantum electrodynamics the phase factor entering the functional integral in the presence of an external four-current density is modified to

$$\exp(\mathrm{i}S) \to \exp\left(\mathrm{i}S + \mathrm{i}\int \mathrm{d}^4x\, j^\mu A_\mu\right). \tag{13.89}$$

We parametrize the world line $\mathscr{C}$ of an electrically charged point particle by $z^\mu(\tau)$ with time-like four-velocity $\dot{z}^\mu$. The four-current density is

$$j^\mu(x) = g\int_{\mathscr{C}} \mathrm{d}\tau\, \dot{z}^\mu(\tau)\delta^4\big(x - z(\tau)\big)$$

and gives rise to the additional phase factor

$$\exp\left(\mathrm{i}\int \mathrm{d}^4x j^\mu A_\mu\right) = \exp\left(\mathrm{i}g\int_{\mathscr{C}} \mathrm{d}z^\mu A_\mu(z)\right) = \exp\left(\mathrm{i}g\int_{\mathscr{C}} A\right), \tag{13.90}$$

where the integral is taken along the particle path $\mathscr{C}$. We obtain the Euclidean version by the substitutions $\mathrm{d}z^0 \to -\mathrm{i}\,\mathrm{d}z^0$ and $A_0 \to \mathrm{i}A_0$. The Wick rotation transforms the phase (13.90) again into a phase. If we choose for $\mathscr{C}$ a loop representing the world-lines of a heavy test particle and its antiparticle put into the system at a given time and removed at a later time, then the partition function in presence of the particles reads

$$\frac{1}{Z}\int \mathscr{D}A_\mu \exp\big(-S_\mathrm{E}[A] + \mathrm{i}g\oint_{\mathscr{C}} A\big) = \left\langle \exp\left(\mathrm{i}g\oint_{\mathscr{C}} A\right)\right\rangle = \langle W[\mathscr{C}]\rangle. \tag{13.91}$$

This is just the continuum result for the expectation value of the Wilson loop.

13.6.2 Strong Coupling Expansion for Pure Gauge Theories

The Wilson action of a pure lattice gauge theory

$$S_{\text{gauge}} = \beta \sum_p \operatorname{tr}(\mathbb{1} - \Re U_p), \quad \beta = \frac{2}{Ng^2}, \tag{13.92}$$

contains only the bare coupling constant g as free parameter. The theory may be considered as classical spin system with inverse temperature $1/kT \propto 1/g^2$. Thus the perturbation theory in g^2 corresponds to the low-temperature expansion in the spin model and the strong coupling limit $g \gg 1$ corresponds to the high-temperature limit of the spin model. We now argue that expectation values of Wilson loops,

$$\langle W[\mathscr{C}] \rangle = \frac{\int \prod_\ell \mathrm{d}U_\ell \, W[\mathscr{C}] \, \mathrm{e}^{-S_{\text{gauge}}(U)}}{\int \prod_\ell \mathrm{d}U_\ell \, \mathrm{e}^{-S_{\text{gauge}}(U)}}, \tag{13.93}$$

obey an area law in the strong-coupling regime. To perform the strong-coupling expansion, we expand the exponential of the lattice action in powers of β. Then the problem is to calculate integrals over the group,

$$I^{a_1 \cdots a_m, c_1 \cdots c_n}_{b_1 \cdots b_m, d_1 \cdots d_n} = \int_G \mathrm{d}U \, U^{a_1}_{b_1} \cdots U^{a_m}_{b_m} U^{\dagger c_1}_{d_1} \cdots U^{\dagger c_n}_{d_n}, \tag{13.94}$$

where the Haar measure is normalized to 1, $\int \mathrm{d}U = 1$. For the cases $(m, n) = (1, 0)$ and $(1, 1)$ the answers derive from the Peter–Weyl theorem (cf. Sect. 14.3.1)

$$\int_G \mathrm{d}U \, U^a_b = 0, \qquad \int_G \mathrm{d}U \, U^a_b U^{\dagger c}_d = \frac{1}{\dim(U)} \, \delta^a_d \delta^c_b. \tag{13.95}$$

The integral

$$\int_G \mathrm{d}U \, U^a_b U^c_d \tag{13.96}$$

is zero if the tensor product $U \otimes \bar{U}$ does not contain the trivial singlet representation. It vanishes for the group $SU(N)$ with $N > 3$. More generally, the center of these groups is Z_N and as a result the integral (13.94) is non-vanishing only if $n = m + kN$ with integer k. The integral (13.96) does not vanish for $SU(2)$ and G_2.

In the expectation value (13.93) the constant contribution $\beta \sum_p \operatorname{tr} \mathbb{1}$ to the Wilson action cancels and hence will be dropped such that

$$\mathrm{e}^{-S_{\text{gauge}}(U)} = \prod_p \big(1 + \beta \, \Re U_p + O\big(\beta^2\big)\big).$$

Because of (13.95) the terms of order β do not contribute to the partition function,

$$Z = 1 + O\big(\beta^2\big) = 1 + O\big(1/g^4\big). \tag{13.97}$$

The numerator in (13.93) has the strong coupling expansion

$$\int \prod_\ell \mathrm{d}U_\ell \, W[\mathscr{C}] \prod_p \big(1 + \beta \, \Re U_p + O\big(\beta^2\big)\big). \tag{13.98}$$

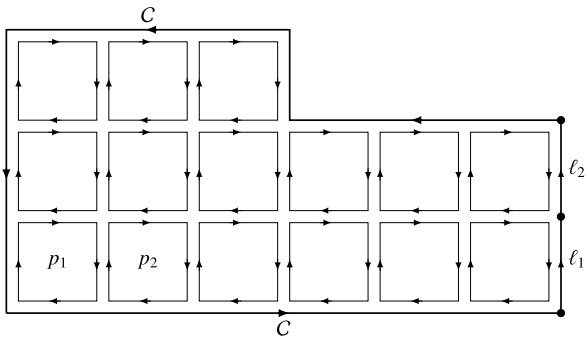

Fig. 13.11 Filling of a loop $\mathscr{C}$ with plaquettes $p_1, p_2, \ldots$

Consider a loop $\mathscr{C} = \ell_n \circ \cdots \circ \ell_2 \circ \ell_1$ as depicted in Fig. 13.11. Because of (13.95) every link variable must appear at least twice in the integrand. Hence only those products of plaquettes contribute that define a surface with boundary $\partial\mathscr{C}$. Besides a connected surface with boundary $\partial\mathscr{C}$ the plaquettes may define further surfaces without boundaries. If the integral (13.96) vanishes then the plaquettes of the surface with boundary $\partial\mathscr{C}$ must have opposite orientation to $\partial\mathscr{C}$. Since every plaquette contributes a factor β the surface with *minimal* area A gives the leading order contribution. Hence, in leading order the expectation value (13.93) is given by

$$\langle W[\mathscr{C}]\rangle \sim \left(c^2\beta\right)^A = \exp\left(-A\log\frac{Ng^2}{c^2}\right). \tag{13.99}$$

For a rectangular Wilson loop the minimal area is $A = RT$. The constant c originates from the group integrations and depends on the gauge group.

Let us briefly comment on the sub-leading terms in the strong-coupling expansion. Only products of plaquettes which define a surface with boundary $\mathscr{C}$ contribute to the numerator in (13.93). The contributions of the additional closed surfaces that are not connected to the surface enclosed by $\mathscr{C}$ cancel with the corresponding contributions in the denominator. An area A may self-intersect or may be tangent to a closed surface. In any case, we expect a series expansion of the form

$$\langle W[C]\rangle = \sum_{A:\,\partial A=\mathscr{C}} \mathrm{e}^{-\sigma A} \tag{13.100}$$

with string tension σ. Actually this area law should hold for all couplings and in particular for weak couplings corresponding to small lattice sizes. Unfortunately, up to now there exists no proof of this expectation.

13.6.3 Glueballs

Gluons, the "photons" of quantum chromodynamics, carry color charge and hence interact strongly with each other. Thus we may expect bound states of several gluons even in the absence of matter. These states, called *glueball*, are characterized

by three quantum numbers J^{PC}: the total angular momentum J and the discrete quantum numbers P and C. The latter characterize the behavior under parity transformation and charge conjugation. Gluons have spin 1 such that glueballs carry an integer spin. We neglect the quark exchange between gluons and consider pure gauge theories.

The energy of excited states are extracted from the exponential tails of suitable two-point functions. Let $G(\tau)$ be the Euclidean two-point function of a gauge-invariant operator $\hat{\mathcal{O}}$ (an observable) given by the vacuum expectation value

$$G_{\mathrm{E}}(\tau) = \langle 0|T\,\hat{\mathcal{O}}(\tau)\hat{\mathcal{O}}(0)|0\rangle = \langle 0|\hat{\mathcal{O}}\mathrm{e}^{-\tau\hat{H}}\hat{\mathcal{O}}|0\rangle = \sum_n \left|\langle n|\hat{\mathcal{O}}|0\rangle\right|^2 \mathrm{e}^{-\tau E_n}, \quad (13.101)$$

where the $|n\rangle$ form a complete set of eigenstates of the Hamiltonian $\hat{H}$ with energies E_n. For large Euclidean times the two-point function behaves as

$$G_{\mathrm{E}}(\tau) \to \left|\langle 0|\hat{\mathcal{O}}|0\rangle\right|^2 + \left|\langle 1|\hat{\mathcal{O}}|0\rangle\right|^2 \mathrm{e}^{-E_1\tau}\left(1 + \mathcal{O}\left(\mathrm{e}^{-\tau(E_2-E_1)}\right)\right). \quad (13.102)$$

We see that the excited state with lowest energy and non-vanishing matrix element $\langle 1|\hat{\mathcal{O}}|0\rangle$ determines the large time behavior. This matrix elements can only be non-zero if the states $\hat{\mathcal{O}}|0\rangle$ and $|1\rangle$ have identical quantum numbers with respect to all conserved charges. Thus, to calculate the mass of a glueball with specified quantum numbers we must pick a suitable $\hat{\mathcal{O}}$ which projects onto a subsector specified by the quantum numbers J^{PC}.

In a pure gauge theory every gauge-invariant operator is given in terms of Wilson loops in the framework of the functional integral quantization. Hence we consider a sum of Wilson loops

$$\mathcal{O} = \sum \alpha_i W[\mathscr{C}_i] \quad \text{with } \left\langle \mathcal{O}(\tau)\mathcal{O}(0)\right\rangle = \sum_{i,j} \bar{\alpha}_i \alpha_j \left\langle W\left[\mathscr{C}_i^\tau\right] W[\mathscr{C}_j]\right\rangle. \quad (13.103)$$

Thereby $\mathscr{C}^\tau$ denotes the loop $\mathscr{C}$ shifted by τ lattice points in the Euclidean time direction. To project onto states with zero momentum one often averages over the spatial directions of the lattice. The eigenvalues of parity P and charge conjugation C are ± 1 and it is not difficult to implement the corresponding projections. It is not so easy to project onto a subspace with fixed angular momentum since a lattice theory is invariant only under a finite subgroup of the rotation group.

Cubic Group

The symmetry transformations of a lattice with fixed point form a finite subgroup of the rotation group. In case of a hyper-cubic lattice it is the cubic group, i.e. one of the platonic groups. There are three types of symmetry axis: the axes going through the centers of opposite faces of the cube, the axes going through the centers of opposite edges and the body diagonals as depicted in Fig. 13.12. Hence the order of the group is $1 + F/2 \times 3 + E/2 \times 1 + V/2 \times 2 = 24$, where F, E and V denote the numbers of faces, edges and vertices of the cube. The group is isomorphic to the octahedral group $\mathscr{O}_{24}$ or the permutation group $\mathscr{S}_4$ and contains five conjugacy classes:

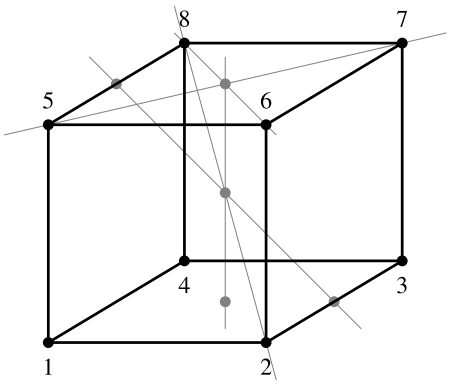

Fig. 13.12 The symmetry operations of a hyper-cubic lattice has three types of symmetry axis: the six axes going through the centers of opposite faces, the six axes going through the centers of opposite edges and the four body diagonals

Table 13.1 Character table of the five irreducible representations of the cubic group

class	# elements	A_1	A_2	E	T_1	T_2
e	1	1	1	2	3	3
$\mathscr{C}_2$	3	1	1	2	-1	-1
$\mathscr{C}_3$	8	1	1	-1	0	0
$\mathscr{C}_2'$	6	1	-1	0	1	-1
$\mathscr{C}_4$	6	1	-1	0	-1	1

1. the trivial class with neutral element e,
2. the class $\mathscr{C}_2$ with the π-rotations about the axes connecting opposite faces,
3. the class $\mathscr{C}_3$ with the $2\pi/3$-rotations about the body diagonals,
4. the class $\mathscr{C}_2'$ with the π-rotations about the axes connecting opposite edges,
5. the class $\mathscr{C}_4$ of the $\pm\pi/2$-rotations about the axes connecting opposite faces.

There are as many irreducible representations as there are conjugacy classes and according to *Burnside's theorem* the sum of squares of the dimensions of these representations is equal to the order of the group. Hence, the cubic group has five irreducible representations and the sum of the squares of their dimensions is 24. There is the ubiquitous one-dimensional trivial representation A_1, a second one-dimensional representation A_2, a two-dimensional representation E and two three-dimensional representations T_1 and T_2. The latter consists of the symmetry transformations of the cube. Table 13.1 contains the characters of the five irreducible representations on the conjugacy classes $e, \mathscr{C}_2, \mathscr{C}_3, \mathscr{C}_2'$ and $\mathscr{C}_4$.

Projecting on Fixed Quantum Numbers

Now we are ready to construct an irreducible representation of parity, charge conjugation and the cubic group from a given Wilson loop $W[\mathscr{C}]$. Let $\mathscr{C}_{a,P,g}$ denote the

loop resulting from $\mathscr{C}$ by a translation on the lattice with $a \in \mathbb{Z}_3$, a parity transformation $P \in \{\mathbb{1}, -\mathbb{1}\}$ and a group transformation $g \in \mathscr{O}_{24}$. Then we introduce

$$\mathscr{W}_{\theta^{PC}}[\mathscr{C}] = \sum_a \sum_{P,g} (-1)^P \chi_\theta(g) \big(W[\mathscr{C}_{a,P,g}] + (-)^C W^*[\mathscr{C}_{a,P,g}] \big), \tag{13.104}$$

where θ denotes one of the five irreducible representations of the cubic group. This combination of Wilson loops has quantum numbers θ^{PC} and a vanishing spatial momentum. Simple loops may lead to a vanishing $\mathscr{W}_{\theta^{PC}}[\mathscr{C}]$ for some representations.

The infinitely many irreducible representations θ_ℓ of the rotation group are labeled by the angular momentum $\ell = 0, 1, 2, \ldots$ and have dimension $2\ell + 1$. In general, the irreducible representation θ_ℓ branches into several irreducible representations of the subgroup $\mathscr{O}_{24}$. The branching rules are obtained by comparing the characters of the rotation group with those of $\mathscr{O}_{24}$. In the rotation group the character $\chi_\ell(\phi)$ of a rotation with fixed axis and angle ϕ in the representation θ_ℓ is

$$\chi_\ell(\phi) = 1 + 2 \sum_{k=1}^{\ell} \cos(k\phi). \tag{13.105}$$

The symmetries of the cube are rotations through $\pi, 2\pi/3$ and $\pi/2$ such that

$$\begin{aligned} \chi_\ell(e) &= 2\ell + 1, \\ \chi_\ell(\mathscr{C}_2) &= (-1)^\ell, \\ \chi_\ell(\mathscr{C}_3) &= 1 - (\ell \bmod 3), \\ \chi_\ell(\mathscr{C}_2') &= (-1)^\ell, \\ \chi_\ell(\mathscr{C}_4) &= 1 + (\ell \bmod 2) - (\ell \bmod 4). \end{aligned} \tag{13.106}$$

Now we are ready to determine the coefficients α_ℓ in the branching rules

$$\theta_\ell = \sum_\theta \alpha_\ell(\theta)\, \theta \quad \text{and} \quad \chi_\ell = \sum_\theta \alpha_\ell(\theta)\, \chi_\theta \tag{13.107}$$

by using the orthonormality of the $\mathscr{O}_{24}$-characters:

$$\alpha_\ell(\theta) = \frac{1}{24} \sum_{g \in \mathscr{O}_{24}} \chi_\theta(g) \chi_\ell(g).$$

The characters are constant on a conjugacy class such that (13.106) yields

$$\begin{aligned} 24\alpha_\ell(A_1) &= 2\ell + 15 + 9(-1)^\ell + 6(\ell \bmod 2) - 8(\ell \bmod 3) - 6(\ell \bmod 4), \\ 24\alpha_\ell(A_2) &= 2\ell + 3 - 3(-1)^\ell - 6(\ell \bmod 2) - 8(\ell \bmod 3) + 6(\ell \bmod 4), \\ 24\alpha_\ell(E) &= 4\ell - 6 + 6(-1)^\ell + 8(\ell \bmod 3), \\ 24\alpha_\ell(T_1) &= 6\ell - 3 + 3(-1)^\ell - 6(\ell \bmod 2) + 6(\ell \bmod 4), \\ 24\alpha_\ell(T_2) &= 6\ell + 9 - 9(-1)^\ell + 6(\ell \bmod 2) - 6(\ell \bmod 4). \end{aligned} \tag{13.108}$$

Inserting these results back into (13.107) yields the branching rules given in Table 13.2, see also [46, 47]. As expected θ_0 branches into A_1 and θ_1 branches into T_2.

Table 13.2 Angular momenta for the irreducible representations of the cubic group

	θ_0	θ_1	θ_2	θ_3	θ_4	θ_5	θ_6	θ_7	θ_8	θ_9	θ_{10}	θ_{11}	θ_{12}	θ_{13}	θ_{14}	θ_{15}
A_1	1	0	0	0	1	0	1	0	1	1	1	0	2	1	1	1
A_2	0	0	0	1	0	0	1	1	0	1	1	1	1	1	1	2
E	0	0	1	0	1	1	1	1	2	1	2	2	2	2	3	2
T_1	0	0	1	1	1	1	2	2	2	2	3	3	3	3	4	4
T_2	0	1	0	1	1	2	1	2	2	3	2	3	3	4	3	4

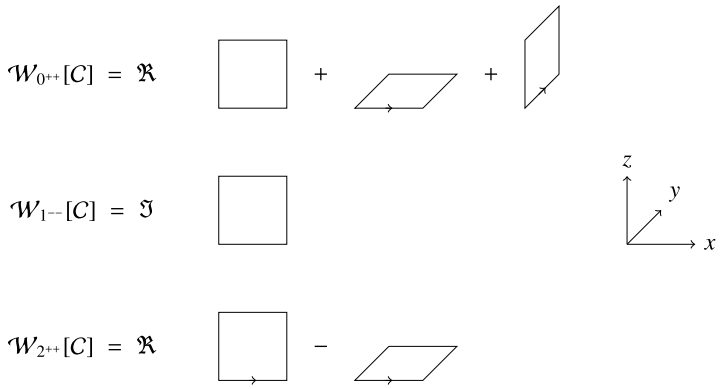

Fig. 13.13 Examples of operators with fixed quantum numbers J^{PC}

But already the five-dimensional representation θ_2 branches into two representations of the cubic group: $\theta_2 = E \oplus T_1$. In a lattice theory we can project onto one of the five irreducible representations of the cubic group. In general the corresponding subspace contains states with different angular momenta. For example, according to Table 13.2 the angular momenta $\ell = 0, 4, 6, 8, 9, \ldots$ all contribute to the trivial representation A_1. This already illustrates the problem with filtering out representations with $\ell > 3$ on a cubic lattice. Figure 13.13 shows some simple combinations of Wilson loops with fixed quantum numbers J^{PC}.

To extract glueball masses with sufficient accuracy from simulations the overlap $\langle 1|\hat{O}|0\rangle$ should be as large as possible. We may increase the overlap by selecting a suitable linear combination of the operators with fixed quantum numbers in (13.104),

$$\mathscr{W}_{\theta^{PC}} = \sum_{\mathscr{C}} \alpha(\mathscr{C})\, \mathscr{W}_{\theta^{PC}}[\mathscr{C}] \quad \text{with} \quad \sum_{\mathscr{C}} \left|\alpha(\mathscr{C})\right|^2 = 1. \tag{13.109}$$

The optimal weights $\alpha(\mathscr{C})$ used in this smearing procedure are extracted from Monte Carlo simulations. The masses of the lowest lying glueballs, converted to physical units and corresponding to a Sommer parameter $r_0^{-1} = 410(20)$, are listed in Table 13.3 and are taken from [48]. The reader interested in details concerning the use of non-local smeared operators to improve the signal to noise ratio for small lattice spacings may consult [49] and the textbooks cited at the end of this chapter.

Table 13.3 Glueball masses for different quantum numbers J^{PC} (taken from [48])

J^{PC}	0^{++}	2^{++}	0^{-+}	1^{+-}	2^{-+}	3^{+-}	3^{++}	1^{--}	2^{--}	3^{--}	2^{+-}	0^{+-}
m_G [MeV]	1710	2390	2560	2980	3940	3600	3670	3830	4010	4200	4230	4780

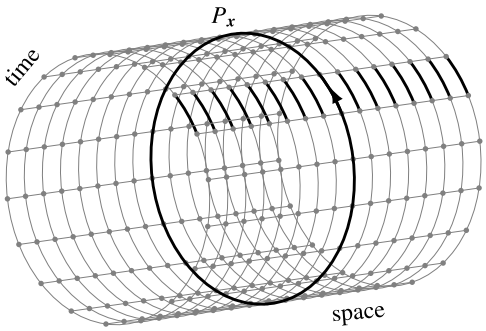

Fig. 13.14 A gauge theory at finite temperature is discretized on a cylinder with circumferences $\beta_T = aN_0$. Even in the thermodynamics limit there exist parallel transporters which wind around the periodic time direction—these are the Polyakov loops

13.7 Gauge Theories at Finite Temperature

The partition function of a canonical ensemble at temperature T is given by

$$Z(\beta_T) = \operatorname{tr} \mathrm{e}^{-\beta_T H}, \quad \beta_T = \frac{1}{k_{\mathrm{B}} T}. \tag{13.110}$$

We set the Boltzmann constant $k_{\mathrm{B}} = 1$ and use the symbol β_T for the inverse temperature since β is reserved for the gauge coupling. In the path integral representation of the partition function and the thermal correlation functions one integrates over fields which are periodic in the Euclidean time with period β_T. An exhaustive introduction to finite-temperature continuum gauge theories is contained in [50].

In the regularized lattice theory $\beta_T = aN_0$. In order not to mess up finite-temperature and finite-volume effects we always assume $N_0 \ll N_i$, $i = 1, 2, 3$, or equivalently that β_T is much smaller than the spatial extent of the system. In the continuum limit $a \to 0$ the inverse temperature β_T is kept fixed and this implies $N_0, N_i \to \infty$. But when we perform the thermodynamic limit $N_i \to \infty$ at fixed lattice spacing a then the number of lattice points in the time direction remains finite and the lattice forms a cylinder as depicted in Fig. 13.14. From the partition function

$$Z(V, \beta_T) = \oint \prod_x \mathrm{d}\phi_x \prod_\ell \mathrm{d}U_\ell \, \mathrm{e}^{-S_{\mathrm{YMH}}(U,\phi)}, \tag{13.111}$$

where one integrates over time-periodic fields,

$$\Phi_{x+N_0 e_0} = \phi_x, \quad U_{\langle x,y\rangle} = U_{\langle x+N_0 e_0, y+N_0 e_0\rangle}, \tag{13.112}$$

one extracts the free energy density $f = -\beta_T (\log Z)/V$. The first derivatives of this density yield the inner energy density and pressure of the thermodynamic system,

$$\varepsilon = \left.\frac{\partial f(V,\beta_T)}{\partial \beta_T}\right|_V \quad \text{and} \quad p = -\left.\frac{\partial (V f(V,\beta_T))}{\partial V}\right|_{\beta_T}. \tag{13.113}$$

In the absence of a chemical potential, a change of the volume of a relativistic gas alters its pressure by changing the particle numbers. The specific heat c_V is given by the derivative of ε with respect to temperature at constant volume. Using thermodynamic identities, one can extract the speed of sound from ε and p. It is an important problem to calculate the pressure and energy density with lattice simulations and to extrapolate them to the continuum limit, see the nice review [51] for more details. For sufficiently high temperatures a pure gauge theory should behave as a gas of free gluons. This is actually not the case. For $SU(3)$ one finds a deviation from the ideal gas behavior of (15–20) % even at temperatures as high as $T \approx 3T_c$, where T_c is the critical temperature above which gluons, confined to glueballs at low temperatures, become free and form a plasma [52].

We are not going further in this direction but instead discuss an interesting order parameter. At finite temperature there are additional (nonlocal) observables, namely the Polyakov loops winding around the periodic time direction [55, 56],

$$P_{\mathbf{x}} = \operatorname{tr} \mathscr{P}(\mathbf{x}), \qquad \mathscr{P}(\mathbf{x}) = \prod_{t=1}^{N_0} U_{(t,\mathbf{x}),0}. \tag{13.114}$$

We already encountered these loop variables when we discussed the axial gauge on a periodic lattice, see (13.57). Polyakov loops are particular Wilson loops such that

$$\mathrm{e}^{-\beta_T \Delta f(\mathbf{x}-\mathbf{y})} = \left\langle P_{\mathbf{y}}^* P_{\mathbf{x}} \right\rangle \tag{13.115}$$

defines the free energy Δf which is needed to insert a static quark at $\mathbf{x}$ and a static antiquark at $\mathbf{y}$ into the thermodynamic system. In the confining phase Δf grows without limits when we try to separate the pair whereas in the deconfined phase we can separate the pair with a finite amount of energy Δf. The cluster property

$$\left\langle P_{\mathbf{y}}^* P_{\mathbf{x}} \right\rangle \to \left\langle P_{\mathbf{y}}^* \right\rangle \langle P_{\mathbf{x}} \rangle = \left| \langle P \rangle \right|^2 \quad \text{for } |\mathbf{x}-\mathbf{y}| \to \infty$$

implies that

$$\langle P \rangle = \begin{cases} 0, & \text{confining phase,} \\ P_0 \neq 0, & \text{deconfining phase.} \end{cases} \tag{13.116}$$

The expectation value of the Polyakov loop distinguishes between the phase with confined quarks and the phase with liberated quarks, similarly as the magnetization distinguishes between the ordered and disordered phases of spin systems.

13.7.1 Center Symmetry

In pure gauge theories with non-trivial centers the Polyakov loop is an order parameter, similarly as the magnetization is an order parameter in the Ising model. The

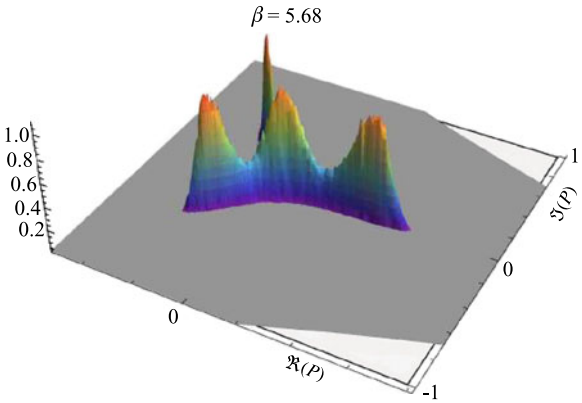

Fig. 13.15 Histograms of the Polyakov loop for the $SU(3)$ gauge theory at the critical temperature [53]. Below the critical temperature the order parameter is zero and above the critical temperature it takes one of the three center values. The expectation values jumps at the critical temperature

center of a group is the maximal subgroup consisting of elements which commute with all elements of the group. The center of $SU(N)$ is the finite group

$$Z_N = \left\{ z_n = z^n \mathbb{1} | z = \mathrm{e}^{2\pi \mathrm{i}/N}, n = 1, 2, \ldots, N \right\} \subset SU(N). \tag{13.117}$$

If a gauge group contains a non-trivial center, then the corresponding gauge theory is invariant under global center transformation. A center transformation multiplies all time-oriented link variables in a fixed time slice with the same center element,

$$U_{(t,\mathbf{x}),0} \to z_n U_{(t,\mathbf{x}),0}, \quad z_n \in Z_N, t \text{ fixed}. \tag{13.118}$$

For example, we could multiply all fat links in Fig. 13.14 with the same center element. A center transformation is just a non-periodic gauge transformation which maps periodic fields into periodic fields. It follows that the lattice action is invariant since the traces of all parallel transporters around contactable loops (i.e. the plaquette variables) are invariant under center transformations, see problem 13.3. But the Polyakov loops are not invariant since just one link variable in (13.114) picks up a center element such that

$$P_{\mathbf{x}} \to z^n P_{\mathbf{x}}. \tag{13.119}$$

Hence, if the expectation value of $P_{\mathbf{x}}$ is non-zero, then the global center symmetry is broken. This means that in the confining phase the center symmetry is realized whereas in the deconfining phase it is spontaneously broken.

Figure 13.15 shows the histogram of the Polyakov loop in $SU(3)$ gauge theory just at the critical temperature. The order parameter jumps and this points to a first order transition. The simulations reveal that the deconfinement transition in $SU(N)$ gauge theories without matter is first order for $N \geq 3$. The transitions becomes stronger with increasing N. The N-dependence of the critical temperature for $2 \leq N \leq 8$ in units of the string tension is well fitted by $T_c/\sqrt{\sigma} \approx 0.596 + 0.453/N^2$, see [54].

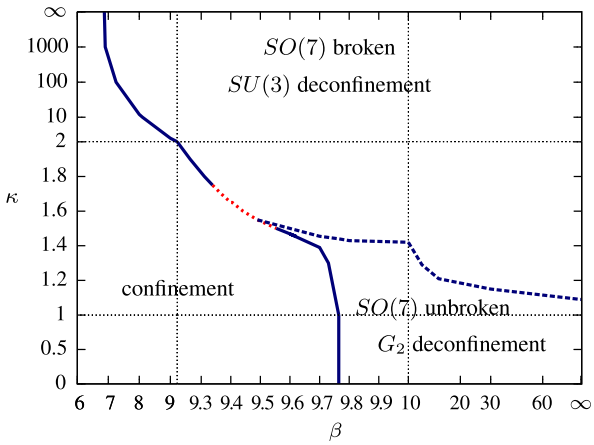

Fig. 13.16 Complete phase diagram of the G_2-Higgs model with scalar field in the fundamental representation in the (β, κ)-plane on a $16^3 \times 6$ lattice [58]. The *solid line* indicates a first order transition, the *dashed line* a second order transition and the *dotted line* a second order transition or a crossover. Note that the scales are non-linear

13.7.2 G_2 Gauge Theory

One may wonder whether a non-trivial center is essential for confinement since the Polyakov loop ceases to be an order parameter if the center is trivial. An interesting theory with trivial center is the Higgs model with exceptional gauge group G_2. This theory interpolates between pure G_2 gauge theory for $\kappa = 0$ and pure $SU(3)$ gauge theory for $\kappa \to \infty$ [57]. The pure G_2 gauge theory shows a first order confinement-deconfinement transition. The Polyakov loop jumps at the critical temperature and is very small but non-zero in the confining phase. Well below the critical temperature it is difficult to measure its non-zero value in simulations. Hence, although P is not an order parameter in the strict sense it is still a very useful quantity to spot the phase transition. Figure 13.16 taken from [58] shows the full phase diagram of the G_2 Higgs model in the (β, κ) plane on a $16^3 \times 6$ lattice. The Higgs field is in the seven-dimensional fundamental representation of G_2 and for $\beta = \infty$ the model collapses to a $O(7)$ non-linear sigma model. This model shows a second order transition from a $O(7)$-symmetric to a $O(7)$-broken phase and this transition persists for finite β. At the same time the first order confinement-deconfinement transition at $\kappa = 0$ extends into the coupling constant plane until it meets the second order line. The first order line beginning at $\kappa = \infty$ almost meets the two other lines. There remains a small window with a cross-over (or a weak transition) connecting the confining and deconfining phases.

13.8 Problems

13.1 (Elitzur theorem for Z_2 gauge theory with matter) Consider a Z_2-gauge theory coupled to a scalar field. The action with source term is

$$S = -\beta \sum_p U_p - \kappa \sum_{\langle x,y \rangle} \phi_x U_{\langle x,y \rangle} \phi_y + h \sum_x \phi_x + \sum_x V(\phi_x),$$

where V is a Z_2 symmetric potential. Prove that

$$\lim_{h\downarrow 0}\langle\phi_x\rangle = 0$$

uniformly in Λ and the couplings.

13.2 (Metropolis simulation of the Z_2 gauge model in three dimensions) Consider a three-dimensional Z_2 gauge theory with matter on a cubic lattice with N^3 lattice sites (a related analysis of the four-dimensional theory gives e.g. [39]). The action is of the form

$$S = -\beta\sum_p U_p - \kappa\sum_{\langle x,y\rangle} s_x U_{xy} s_y,$$

where U_{xy} is Z_2-valued. The free energy density $f(\beta,\kappa) = -1/N^3 \log Z$ is proportional to the logarithm of the partition function.

(a) Derive the relations

$$\langle U_p\rangle = -\frac{1}{3}\frac{\partial}{\beta} f(\beta,\kappa), \quad \text{and} \quad \left\langle s_x U_{\langle x,y\rangle} s_y\right\rangle = -\frac{1}{3}\frac{\partial}{\partial\kappa} f(\beta,\kappa). \tag{13.120}$$

(b) Investigate the phase diagram in the (β,κ)-plane with the help of the Metropolis algorithm by considering the expectation values (13.120). Before doing the simulation you should study the limiting case $\beta = 0$.

13.3 (Center transformations) Show that the center transformations introduced in Sect. 13.7 can be regarded as gauge transformations. Why do we admit these gauge transformations although they are not periodic in time. Show that parallel transporters around contractible loops are invariant under center transformations.

References

1. D. Ivanenko, G. Sardanashvily, The gauge treatment of gravity. Phys. Rep. **94**, 1 (1983)
2. F.W. Hehl, J.D. McCrea, E.W. Mielke, Y. Ne'eman, Metric affine gauge theory of gravity: field equations, Noether identities, world spinors, and breaking of dilation invariance. Phys. Rep. **258**, 1 (1995)
3. S. Pokorski, *Gauge Field Theories* (Cambridge University Press, Cambridge, 2000)
4. K. Huang, *Quarks, Leptons and Gauge Fields* (World Scientific, Singapore, 1992)
5. L. O'Raifeartaigh, *Group Structure of Gauge Theories* (Cambridge University Press, Cambridge, 1986)
6. A. Das, *Lectures on Quantum Field Theory* (World Scientific, Singapore, 2008)
7. F.J. Wegner, Duality in generalized Ising models and phase transitions without local order parameters. J. Math. Phys. **10**, 2259 (1971)
8. K.G. Wilson, Confinement of quarks. Phys. Rev. D **10**, 2445 (1974)
9. M. Creutz, L. Jacobs, C. Rebbi, Experiments with a gauge invariant Ising system. Phys. Rev. Lett. **42**, 1390 (1979)
10. M. Creutz, Confinement and the critical dimensionality of spacetime. Phys. Rev. Lett. **43**, 553 (1979)

11. M. Creutz, Monte Carlo simulations in lattice gauge theories. Phys. Rep. **95**, 201 (1983)
12. I. Montvay, G. Münster, *Quantum Fields on a Lattice* (Cambridge University Press, Cambridge, 1994)
13. H.J. Rothe, *Lattice Gauge Theories: An Introduction* (World Scientific, Singapore, 2012)
14. T. DeGrand, C. DeTar, *Lattice Methods for Quantum Chromodynamics* (World Scientific, Singapore, 2006)
15. C. Gattringer, C. Lang, in *Quantum Chromodynamics on the Lattice*. Lect. Notes Phys., vol. 788, (2010)
16. L.P. Kadanoff, The application of renormalization group techniques to quarks and strings. Rev. Mod. Phys. **49**, 267 (1977)
17. J.B. Kogut, An introduction to lattice gauge theory and spin systems. Rev. Mod. Phys. **51**, 659 (1979)
18. J.B. Kogut, The lattice gauge theory approach to quantum chromodynamics. Rev. Mod. Phys. **55**, 775 (1983)
19. P. de Forcrand, O. Jahn, Comparison of $SO(3)$ and $SU(2)$ lattice gauge theory. Nucl. Phys. B **651**, 125 (2003)
20. R.L. Karp, F. Mansouri, J.S. Rho, Product integral formalism and non-Abelian Stokes theorem. J. Math. Phys. **40**, 6033 (1999)
21. R.L. Karp, F. Mansouri, J.S. Rho, Product integral representations of Wilson lines and Wilson loops, and non-Abelian Stokes theorem. Turk. J. Phys. **24**, 365 (2000)
22. R. Giles, Reconstruction of gauge potentials from Wilson loops. Phys. Rev. D **24**, 2160 (1981)
23. J. Fröhlich, G. Morchio, F. Strocchi, Higgs phenomenon without symmetry breaking order parameter. Nucl. Phys. B **190**, 553 (1981)
24. F. Hausdorff, Die symbolische Exponentialformel in der Gruppentheorie. Ber. Verh. Saechs. Akad. Wiss. Leipz. **58**, 19 (1906)
25. K. Wilson, in *Recent Developments of Gauge Theories*, ed. by G. 't Hofft, et al. (Plenum, New York, 1980)
26. K. Symanzik, Continuum limit and improved action in lattice theories. 1. Principles and ϕ^4 theory. Nucl. Phys. B **226**, 187 (1983)
27. M. Luscher, P. Weisz, Computation of the action for on-shell improved lattice gauge theories at weak coupling. Phys. Lett. B **158**, 250 (1985)
28. K. Langfeld, Improved actions and asymptotic scaling in lattice Yang–Mills theory. Phys. Rev. D **76**, 094502 (2007)
29. J.M. Drouffe, J.B. Zuber, Strong coupling and mean field methods in lattice gauge theories. Phys. Rep. **102**, 1 (1983)
30. G. Arnold, B. Bunk, T. Lippert, K. Schilling, Compact QED under scrutiny: its first order. Nucl. Phys. B, Proc. Suppl. **119**, 864 (2003)
31. K. Langfeld, B. Lucini, A. Rago, The density of states in gauge theories. Phys. Rev. Lett. **109**, 111601 (2012)
32. J. Carlsson, B. McKellar, $SU(N)$ glueblall masses in $2+1$ dimensions. Phys. Rev. D **68**, 074502 (2003)
33. S. Uhlmann, R. Meinel, A. Wipf, Ward identities for invariant group integrals. J. Phys. A **40**, 4367 (2007)
34. K. Osterwalder, E. Seiler, Gauge field theories on a lattice. Ann. Phys. **10**, 440 (1978)
35. E. Fradkin, S. Shenker, Phase diagrams of lattice gauge theories with Higgs fields. Phys. Rev. D **19**, 3682 (1979)
36. C. Bonati, G. Cossu, M. D'Elia, A. Di Giacomo, Phase diagram of the lattice $SU(2)$ Higgs model. Nucl. Phys. B **828**, 390 (2010)
37. J. Greensite, *An Introduction to the Confinement Problem*. Lecture Notes in Physics (Springer, Berlin, 2011)
38. S. Elitzur, Impossibility of spontaneously breaking local symmetries. Phys. Rev. D **12**, 3978 (1975)
39. Y. Blum, P.K. Coyle, S. Elitzur, E. Rabinovici, S. Solomon, H. Rubinstein, Investigation of the critical behavior of the critical point of the Z2 gauge lattice. Nucl. Phys. B **535**, 731 (1998)

40. C. Itzikson, J.M. Drouffe, *Statistical Field Theory*, vol. I. Cambridge Monographs on Mathematical Physics (Cambridge University Press, Cambridge, 1989)
41. B. Wellegehausen, A. Wipf, C. Wozar, Casimir scaling and string breaking in G2 gluodynamics. Phys. Rev. D **83**, 016001 (2011)
42. G.S. Bali, K. Schilling, C. Schlichter, Observing long color flux tubes in $SU(2)$ lattice gauge theory. Phys. Rev. D **51**, 5165 (1995)
43. E. Seiler, Upper bound on the color-confining potential. Phys. Rev. D **18**, 482 (1978)
44. C. Bachas, Convexity of the quarkonium potential. Phys. Rev. D **33**, 2723 (1986)
45. M. Lüscher, K. Symanzik, P. Weisz, Anomalies of the free loop wave equation in WKB approximation. Nucl. Phys. B **173**, 365 (1980)
46. M. Lax, *Symmetry Principles in Solid State and Molecular Physics* (Wiley, New York, 1974)
47. J.S. Lomount, *Applications of Finite Groups* (Academic Press, New York, 1959)
48. Y. Chen et al., Glueball spectrum and matrix elements on anisotropic lattices. Phys. Rev. D **73**, 014516 (2006)
49. M. Teper, An improved method for lattice glueball calculations. Phys. Lett. B **183**, 345 (1986)
50. J.I. Kapusta, C. Gale, *Finite-Temperature Field Theory: Principles and Applications* (Cambridge University Press, Cambridge, 2006)
51. F. Karsch, Lattice QCD at high temperature and density. Lect. Notes Phys. **583**, 209 (2002)
52. G. Boyd, J. Engels, F. Karsch, E. Laermann, C. Legeland, M. Lütgemeier, B. Petersson, Equation of state for the SU(3) gauge theory. Phys. Rev. Lett. **75**, 4169 (1995)
53. B. Wellegehausen, Effektive Polyakov-Loop Modelle für SU(N)- und G2-Eichtheorien (Effective Polyakov loop models for SU(N) and G2 gauge theories). Diploma Thesis, Jena (2008)
54. B. Lucini, M. Teper, U. Wenger, The high temperature phase transition in SU(N) gauge theories. J. High Energy Phys. **0401**, 061 (2004)
55. A.M. Polyakov, Quark confinement and topology of gauge groups. Nucl. Phys. B **120**, 429 (1977)
56. B. Svetitsky, L.G. Yaffe, Critical behavior at finite temperature confinement transitions. Nucl. Phys. B **210**, 423 (1982)
57. K. Holland, P. Minkowski, M. Pepe, U.J. Wiese, Exceptional confinement in G(2) gauge theory. Nucl. Phys. B **668**, 207 (2003)
58. B. Wellegehausen, A. Wipf, C. Wozar, Phase diagram of the lattice G2 Higgs Model. Phys. Rev. D **83**, 114502 (2011)

Chapter 14
Two-Dimensional Lattice Gauge Theories and Group Integrals

In two dimensions a pure lattice gauge theory with the simple Wilson action can be solved analytically. With open boundary conditions and in the axial gauge the partition function becomes a product of one-dimensional chains, each of which is the same as a spin theory, and the area law behavior is exact for all values of the gauge coupling β. In this chapter we impose periodic boundary conditions in all directions, adequate for finite temperature and finite volume studies. On a torus the solution is a bit less trivial, and the exact solution can be used as a test bed for new Monte Carlo algorithms. First we study simple Abelian gauge models for which the calculation parallels our treatment of one-dimensional spin models. The second part deals with non-Abelian theories on the torus for which we use the character expansion and a recursion formula due to Migdal [1, 2] (for a review see [3]). We calculate the free energy and the potential energy between a static quark–antiquark pair. Two dimensional gauge theories confine a static $q\bar{q}$-pair, since in one space dimension the field energy cannot spread out in space. For weak couplings the string tension shows an exact Casimir scaling, similarly as gauge theories in three and four dimensions. Towards the end of this chapter we collect some facts on invariant group integration which are useful in strong-coupling expansions, mean field approximations and exact solutions. Further material can be found in the textbook [4].

14.1 Abelian Gauge Theories on the Torus

For an Abelian theory the calculation simplifies considerably if we choose an axial-type gauge for the link variables in the partition function

$$Z_V(\beta) = \mathrm{e}^{-\beta V} \int \prod_\ell \mathrm{d}U_\ell \prod_p \mathrm{e}^{\beta \Re(U_p)}, \quad U_p = \prod_{\ell \in \partial p} U_\ell. \tag{14.1}$$

A. Wipf, *Statistical Approach to Quantum Field Theory*, Lecture Notes in Physics 864,
DOI 10.1007/978-3-642-33105-3_14,

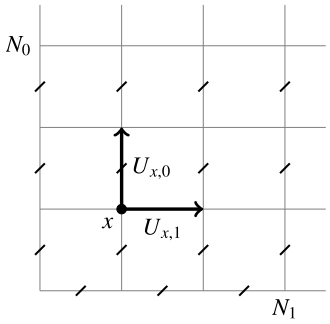

Fig. 14.1 If periodic boundary conditions are imposed then only the variables on the marked links can be gauged to the identity

On p. 307 we have argued that on a periodic lattice the variables on the marked links in Fig. 14.1 can be transformed to the identity. As gauge-invariant variables we may choose the plaquette variables and the *Polyakov loops* in both directions,

$$P_0(t) = \prod_{n=1}^{N_0} U_{x+ne_0,0}, \qquad P_1(x) = \prod_{n=1}^{N_1} U_{x+ne_1,1}. \tag{14.2}$$

For periodic boundary conditions not all plaquette variables are independent since $U_1 U_2 \dots U_V = 1$. Only $V-1$ plaquette variables are independent and we choose these as new variables, together with a subset of Polyakov loops. To find this subset we observe that the Polyakov loop at $x_1 + m$ is equal to the Polyakov loop at x_1 multiplied by the plaquette variables enclosed by the two loops. Thus only one Polyakov loop in the time direction is independent. The same applies to Polyakov loops in the x_1 direction. Thus there are $V+1$ independent gauge-invariant variables. Together with the variables on the $V-1$ marked links in Fig. 14.1, denoted by E', we obtain a complete set of $2V$ variables

$$\{U_p | p = 1, \dots, V-1\}, \qquad P_0, P_1 \quad \text{and} \quad \{U_\ell | \ell \in E'\}. \tag{14.3}$$

Exploiting the invariance of the Haar measure we can write

$$Z_V(\beta) = \mathrm{e}^{-\beta V} \int \prod_{p=1}^{V-1} \mathrm{d}U_p \prod_{p=1}^{V} \mathrm{e}^{\beta \Re U_p} \int \mathrm{d}P_0 \, \mathrm{d}P_1 \int \prod_{\ell \in E'} \mathrm{d}U_\ell, \tag{14.4}$$

wherein the plaquette variable U_V is given in terms of the other plaquette variables. The integrand does not depend on the link variables on E' and on the Polyakov loops and with $1 = \int \mathrm{d}U_V \delta(\mathbb{1}, U_1 U_2 \cdots U_V)$ we obtain

$$Z_V(\beta) = \mathrm{e}^{-\beta V} \prod_{p=1}^{V} \int \mathrm{d}U_p \mathrm{e}^{\beta \Re U_p} \delta\Big(\mathbb{1}, \prod U_p\Big). \tag{14.5}$$

For an Abelian group every irreducible representation R_n is one-dimensional and the formula (14.65) reads $\delta(1, U) = \sum_n R_n(U)$. In addition $R_n(UV) = R_n(U) R_n(V)$ such that the partition function for an Abelian gauge group factorizes

$$Z_V(\beta) = \mathrm{e}^{-\beta V} \sum_n (Z_n)^V, \quad Z_n = \int \mathrm{d}U \mathrm{e}^{\beta \Re U} R_n(U), \tag{14.6}$$

where the sum extends over all irreducible representation of the group. Expectation values of Wilson loops in a given representation R_{n_0} are calculated similarly. For an Abelian theory Stokes theorem applies and the Wilson loop is the product of plaquette variables

$$W[\mathscr{C}] = \prod_{\ell \in \mathscr{C}} R_{n_0}(U_\ell) = \prod_{p \in A} R_{n_0}(U_p), \tag{14.7}$$

where A is an area with boundary $\mathscr{C}$. One obtains

$$\langle W[\mathscr{C}] \rangle = \frac{\sum_n Z_n^{V-A} Z_{n,n_0}^A}{\sum_n Z_n^V}, \quad Z_{n,n_0} = \int \mathrm{d}U \mathrm{e}^{\beta \Re U} R_n(U) R_{n_0}(U), \tag{14.8}$$

such that the expectation value of the Wilson loop only depends on the charges of the static $q\bar{q}$ pair, the area of the loop and the lattice size. Later we shall see that this formula implies confinement.

14.1.1 Z_2 Gauge Theory

There are two irreducible representations of $Z_2 = \{1, -1\}$. The trivial representation assigns 1 to every group element such that $Z_{\text{trivial}} = \cosh(\beta)$ and for the defining representation $Z_{\text{defining}} = \sinh(\beta)$. Thus (14.6) yields

$$Z_V(\beta) = \left(\frac{1 + \mathrm{e}^{-2\beta}}{2}\right)^V + \left(\frac{1 - \mathrm{e}^{-2\beta}}{2}\right)^V. \tag{14.9}$$

In the thermodynamic limit $V \to \infty$ we may neglect the last term and find the ground state energy density

$$e(\beta) = -\lim_{V \to \infty} \frac{Z_V(\beta)}{V} = -\log \frac{1 + \mathrm{e}^{-2\beta}}{2}. \tag{14.10}$$

In the weak-coupling limit $\beta \to \infty$ it converges to the constant value $\log(2)$. By contrast, in the strong-coupling limit the energy density converges to $\beta = 1/g^2$. In between it is a monotonically decreasing function of g as depicted in Fig. 14.2.

14.1.2 $U(1)$ Gauge Theory

The continuous group $U(1)$ has infinitely many one-dimensional irreducible representation characterized by the integer charge,

$$R_n\left(\mathrm{e}^{\mathrm{i}\alpha}\right) = \mathrm{e}^{\mathrm{i}n\alpha}, \quad n \in \mathbb{Z}, \tag{14.11}$$

such that Z_n in (14.6) is given by a modified Bessel function of order n,

$$Z_n(\beta) = \frac{1}{2\pi} \int_{-\pi}^{\pi} \mathrm{e}^{\beta \cos\alpha + \mathrm{i}n\alpha} = I_n(\beta). \tag{14.12}$$

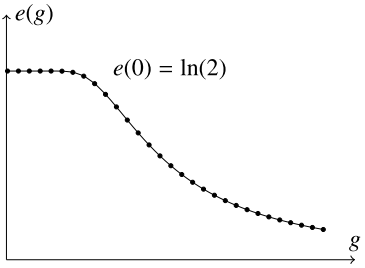

Fig. 14.2 Ground state energy density for the two-dimensional Z_2-gauge theory in the thermodynamic limit $V \to \infty$ as function of the coupling constant g. For $g > 0$ it is an analytic function of g

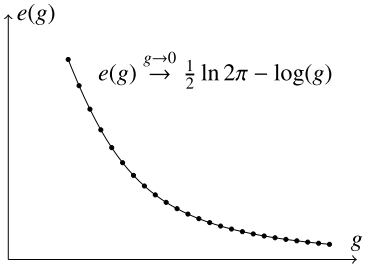

Fig. 14.3 Ground state energy density of the two-dimensional $U(1)$ gauge theory in the infinite volume limit

Since $I_0(\beta) > I_1(\beta) > \cdots$ we obtain the following ground state energy density in the thermodynamic limit:

$$e(\beta) = \beta - \log I_0(\beta). \tag{14.13}$$

In the weak-coupling regime it diverges as $-\log(g)$ and for strong coupling it falls off as $1/g^2 - 1/4g^4 + \cdots$. Figure 14.3 shows the energy density as a function of the coupling g. In passing we note that if one is only interested in the thermodynamic limit then one may neglect the constraint $U_1 \cdots U_V = 1$ imposed by the periodic boundary conditions. This already indicates that the thermodynamic limit $V \to \infty$ is insensitive to the boundary conditions. Actually this is true for two-dimensional gauge theories with general boundary conditions, see [5].

Equation (14.11) shows that $R_n R_{n_0} = R_{n+n_0}$ such that the formula for the Wilson loop (14.8) yields the following simple result in the thermodynamic limit:

$$\lim_{V\to\infty} \langle W[\mathscr{C}] \rangle = \left(\frac{I_{n_0}(\beta)}{I_0(\beta)} \right)^A. \tag{14.14}$$

We see that in all representations the Wilson loops obey an area law. The string tension in the charge n_0 representation has the strong- and weak-coupling limits

$$\sigma_{n_0} = \log \frac{I_0(\beta)}{I_{n_0}(\beta)} \to \begin{cases} n_0 \log(2/\beta), & \text{for } \beta \ll 1, \\ \log(1 + n^2/2\beta), & \text{for } \beta \gg 1. \end{cases} \tag{14.15}$$

14.2 Non-Abelian Lattice Gauge Theories on the 2d Torus

For free boundary conditions it is easy to calculate the partition function and ground state energy density. For example, for the gauge group $SU(2)$ one finds

$$e(\beta) = 2\beta - \log\left(\frac{I_1(2\beta)}{\beta}\right). \tag{14.16}$$

The energy density shows a similar dependency on the gauge coupling as the energy density of the $U(1)$ theory. In the strong-coupling regime $e \sim 1/g^2 - 1/8g^4 + \cdots$ and in the weak-coupling regime $e \sim 3\log(g) + \frac{1}{2}\log(\pi/2)$.

For periodic boundary conditions in all directions the models can still be solved but the solution involves several steps. Since there is no simple Stoke theorem for non-Abelian theories the constraint on the plaquette variables is not as simple as for Abelian theories. In place of Stokes' theorem we shall apply the gluing rule (14.63).

Gluing Loops and Migdal's Recursion Relation Let us consider two loops $\mathscr{C}_x, \mathscr{C}'_x$ starting at x and sharing one edge as illustrated in Fig. 14.4. We denote the variable on the common edge by V. The parallel transporter along $\mathscr{C}_x$ is given by $U_{\mathscr{C}_x} = WV$ and the transporter along $\mathscr{C}'_x$ is $V^{-1}W'$. A class function obeys $f(\Omega U \Omega^{-1}) = f(U)$ and is a linear combination of the orthonormal characters,

$$f(U) = \sum_R c_R \chi_R(U), \tag{14.17}$$

where the expansion coefficients are given by

$$c_R = (\chi_R, f) \equiv \int \mathrm{d}U\, \bar{\chi}_R(U) f(U). \tag{14.18}$$

This expansion allows for the integration over the common link variable V in the product function $f(U_{\mathscr{C}_x}) f(U_{\mathscr{C}'_x})$. By using the gluing rule (14.63), we find

$$\int \mathrm{d}V f(U_{\mathscr{C}}) f(U_{\mathscr{C}'}) = \sum_R \frac{c_R^2}{d_R} \chi_R\big(WW'\big) = \sum_R \frac{c_R^2}{d_R} \chi_R(U_{\mathscr{C}\circ\mathscr{C}'}). \tag{14.19}$$

If the two loops share several edges and if these edges are *connected*, then only one of the edges is glued. For example, if we glue together the loops $\mathscr{C}_x$ and $\mathscr{C}'_x$ along x, y in Fig. 14.5, the parallel transporter $U_{\langle x,z\rangle}$ in $\mathscr{C}_x$ and its inverse $U_{\langle z,x\rangle}$ in $\mathscr{C}'_x$ cancel in the class function $\chi_R(U_{\mathscr{C}\circ\mathscr{C}'})$. More generally, after gluing along one common edge the link variables on the other common edges connected to the glued edge cancel on the right hand side of (14.19). Hence $U_{\mathscr{C}\circ\mathscr{C}'}$ in this formula describes the parallel transporter along the exterior boundary of the area enclosed by $\mathscr{C}$ and $\mathscr{C}'$. However, if the two loops $\mathscr{C}$ and $\mathscr{C}'$ share several unconnected edges, then only those variables cancel that are defined on common links connected to the glued edge. Now we can iterate the gluing process, for example by gluing $\mathscr{C}\circ\mathscr{C}$ and $\mathscr{C}''$ at a common edge V',

$$\int \mathrm{d}V' \mathrm{d}V f(U_{\mathscr{C}}) f(U_{\mathscr{C}'}) f(U_{\mathscr{C}''}) = \sum_R \frac{c_R^3}{d_R^2} \chi_R(U_{\mathscr{C}\circ\mathscr{C}'\circ\mathscr{C}''}). \tag{14.20}$$

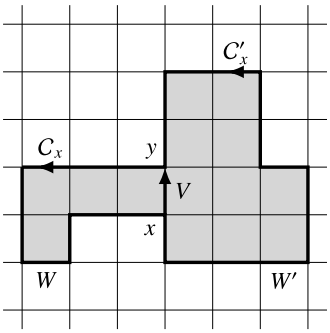

Fig. 14.4 Gluing a class function on two loops which share a common link V

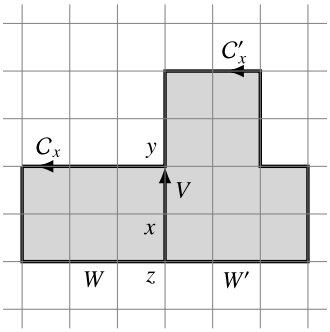

Fig. 14.5 Gluing together two loops at several connected links

Every surface A without holes is built from single plaquettes by gluing one plaquette after another along a connected set of edges, $A = p_1 \cup \cdots \cup p_n$. This way we obtain for a surface without holes the *Migdal* recursion formula [1, 2]

$$\int \prod_{\ell=1}^{n-1} \mathrm{d}V_\ell \prod f(U_{p_1}) \cdots f(U_{p_n}) = \sum_R d_R \left(\frac{c_R}{d_R}\right)^n \chi_R(U_{\partial A}). \qquad (14.21)$$

14.2.1 Partition Function

Now we are ready to calculate the partition function with the help of the recursion formula applied to $f(U) = \exp(-\beta \operatorname{tr}(\mathbb{1} - \Re U_p))$. We assume A to be the union of all plaquettes such that the boundary ∂A contains the link variables V, V' and W depicted in Fig. 14.6. If we fix the link variables on the spatial boundary, then we obtain the partition function

$$Z(V, V') = \sum d_R \left(\frac{c_R}{d_R}\right)^V \int \mathrm{d}W \chi_R\left(V^{-1} W^{-1} V' W\right).$$

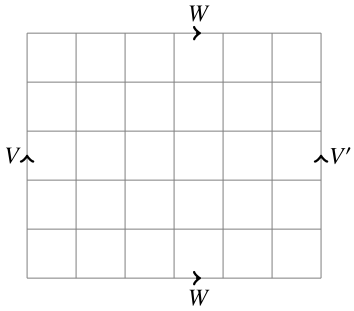

Fig. 14.6 Calculating the partition function with the help of the gluing and separation rules

With the separation rule (14.64) the integral can be calculated,

$$Z(V, V') = \sum \left(\frac{c_R}{d_R}\right)^V \chi_R(V^{-1})\chi_R(V'). \tag{14.22}$$

If in addition we choose periodic boundary conditions in the spatial direction then we must set $V' = V$ and integrate over V,

$$Z_{\text{per}} = \mathrm{e}^{-2\beta V} \sum_R \left(\frac{c_R(\beta)}{d_R}\right)^V, \quad c_R(\beta) = \int \mathrm{d}U\, \bar{\chi}_R(U) \mathrm{e}^{\beta \mathrm{tr} \Re U}. \tag{14.23}$$

The irreducible representations of $SU(2)$ are characterized by their half-integer spin j. The spin-j representation has dimension $d_j = 2j + 1$ and its character is

$$\chi_j(U) = \frac{\sin(d_j\theta)}{\sin\theta}. \tag{14.24}$$

With $\mathrm{tr}\,\Re U = 2\cos\theta$ the integral (14.23) yields a modified Bessel function:

$$\begin{aligned} c_j(\beta) &= \frac{2}{\pi}\int_0^\pi \mathrm{d}\theta (\sin\theta)^2 \frac{\sin(d_j\theta)}{\sin\theta} \mathrm{e}^{2\beta\cos\theta} = -\frac{1}{\pi\beta}\int \sin(d_j\theta)\frac{\mathrm{d}}{\mathrm{d}\theta}\mathrm{e}^{2\beta\cos\theta} \\ &= \frac{d_j}{\pi\beta}\int \cos(d_j\theta)\mathrm{e}^{2\beta\cos\theta} = \frac{d_j}{\beta} I_{2j+1}(2\beta). \end{aligned}$$

Hence we end up with the following exact formula for the partition function of the $SU(2)$ gauge theory on the torus:

$$Z(\beta) = \mathrm{e}^{-2\beta V}\left(\frac{1}{\beta}\right)^V \sum_{n=1,2,\ldots}^{\infty} \big(I_n(2\beta)\big)^V. \tag{14.25}$$

In the thermodynamic limit we recover the result (14.16) for the vacuum energy density.

14.2.2 Casimir Scaling of Polyakov Loops

At finite temperature we must impose periodic boundary conditions in the Euclidean time direction. In this section we compute the expectation value of correlators of the

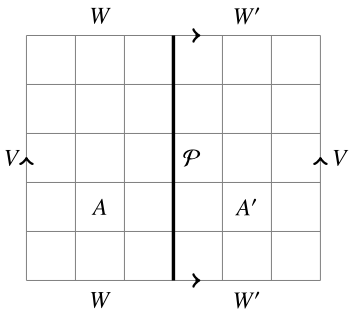

Fig. 14.7 Calculating the expectation value of the Polyakov loop with the cutting rule

Polyakov loop $\mathscr{P}_x$ for static charges in a fixed representation R_0. The expectation value of one Polyakov loop is given by

$$\langle P\rangle = \frac{1}{Z}\int \prod \mathrm{d}U_\ell \mathrm{e}^{-S_{\text{gauge}}(U)}\chi_{R_0}(\mathscr{P}_{\mathbf{x}}). \tag{14.26}$$

The straight Polyakov loop winding around the Euclidean time direction divides the lattice into two regions, denoted by A and A' in Fig. 14.7. We choose periodic boundary conditions in the spatial direction. First we glue together the plaquettes in each of the two regions. Decomposing the parallel transporters along ∂A and $\partial A'$ as depicted in the figure and using Migdal's recursion relation we obtain for the integral in (14.26) the double sum

$$\sum_{R,R'} d_R\left(\frac{c_R}{d_R}\right)^A \chi_R\big(WV^{-1}W^{-1}\mathscr{P}\big)d_{R'}\left(\frac{c'_R}{d'_R}\right)^{A'}\chi_{R'}\big(\mathscr{P}^{-1}W'^{-1}VW'\big)\chi_{R_0}(\mathscr{P}).$$

With the separation rule (14.64) the integration over W and W' can easily be done and one obtains a double sum containing the factor $\chi_R(V^{-1})\chi_{R'}(V)$. Owing to the orthogonality of the characters the integration over V reduces the double sum to a single sum and we end up with

$$\langle P\rangle = \frac{1}{Z}\mathrm{e}^{-2\beta V}\sum_R\left(\frac{c_R}{d_R}\right)^V \int d\mathscr{P}\chi_{R_0}(\mathscr{P})\chi_R(\mathscr{P})\chi_R\big(\mathscr{P}^{-1}\big).$$

We now focus again on the gauge group $SU(2)$ with characters χ_j. The Clebsch–Gordon decomposition $\chi_{j_0}\chi_j = \chi_{j_0+j} + \cdots + \chi_{|j_0-j|}$ immediately yields

$$\int d\mathscr{P}\chi_{j_0}(\mathscr{P})\chi_j(\mathscr{P})\chi_j\big(\mathscr{P}^{-1}\big) = \begin{cases} 0, & \text{for half-integer } j_0,\\ 1, & \text{for integer } j_0 \text{ and } j \geq j_0/2.\end{cases}$$

Thus we obtain the interesting result that for static quarks transforming according to a half-integer spin representation the Polyakov loop expectation value vanishes. This means that these particles are confined. Actually, a non-vanishing expectation value would violate the center symmetry. On the other hand, for static quarks transforming according to an integer spin representation of the gauge group we obtain

$$\big\langle \chi_{j_0}(\mathscr{P})\big\rangle = \frac{\sum_{n\geq 1} I^V_{j_0+n}(2\beta)}{\sum_{n\geq 1} I^V_n(2\beta)}, \quad j_0 \in \{0,1,2,\ldots\}. \tag{14.27}$$

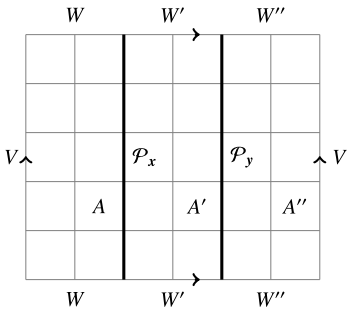

Fig. 14.8 Calculation of the two-point function of Polyakov loops via the gluing technique

The terms with $n = 1$ dominate for large volumes V such that we find the asymptotic formula

$$\left\langle \chi_{j_0}(\mathscr{P}) \right\rangle \approx \left(\frac{I_{j_0+1}(2\beta)}{I_1(2\beta)} \right)^V, \quad j_0 \in \{0, 1, 2, \ldots\}. \tag{14.28}$$

Since the ratio is less than one the expectation value vanishes in the thermodynamic limit.

In order to compute the two-point function of the Polyakov loop corresponding to a static quark–antiquark pair in the representation R_0,

$$\left\langle \bar{\chi}_{R_0}(\mathscr{P}_\mathbf{x}) \chi_{R_0}(\mathscr{P}_\mathbf{y}) \right\rangle = \frac{1}{Z} \int \prod \mathrm{d}U_\ell \mathrm{e}^{-S_{\text{gauge}}(U)} \bar{\chi}_{R_0}(\mathscr{P}_\mathbf{x}) \chi_{R_0}(\mathscr{P}_\mathbf{y}), \tag{14.29}$$

we divide the lattice into three domains A, A', A'' as depicted in Fig. 14.8. Again we impose periodic boundary conditions in all directions. First we glue the plaquettes in each of the three domains and this yields a triple sum for the integral in (14.29). Then we glue together the variables W, W' and W'' in every domain in Fig. 14.8. After a further integration over V the triple sum collapses to the double sum

$$\begin{aligned} &\mathrm{e}^{-2\beta V} \sum_{R,R'} \left(\frac{c_R}{d_R} \right)^{A+A'} \left(\frac{c_{R'}}{d_{R'}} \right)^{A'} \chi_R(\mathscr{P}_\mathbf{x}) \bar{\chi}_{R_0}(\mathscr{P}_\mathbf{x}) \bar{\chi}_{R'}(\mathscr{P}_\mathbf{x}) \chi_{R'}(\mathscr{P}_\mathbf{y}) \\ &\quad \times \chi_{R_0}(\mathscr{P}_\mathbf{y}) \bar{\chi}_R(\mathscr{P}_\mathbf{y}). \end{aligned}$$

The final integration over $\mathscr{P}_y$ (or equivalently over $\mathscr{P}_x$) counts how often R appears in the tensor product $R_0 \otimes R'$. After the integration over the Polyakov loops the absolute squares of these generalized Clebsch–Gordon coefficients appear on the right hand side. In particular, for the gauge group $SU(2)$ and static quarks in fundamental representation we find

$$\langle \operatorname{tr} \mathscr{P}_\mathbf{x} \operatorname{tr} \mathscr{P}_\mathbf{y} \rangle = \frac{\mathrm{e}^{2\beta V}}{Z} \left(\frac{1}{\beta} \right)^V \sum_{n \geq 1} \left(I_n^{A+A''}(2\beta) I_{n+1}^{A'}(2\beta) + I_n^{A'}(2\beta) I_{n+1}^{A+A''}(2\beta) \right), \tag{14.30}$$

with partition function given in (14.25). In the thermodynamic limit both A and A'' tend to infinity and only the term proportional to $I_1^{A+A''}$ contributes. By using the relation $V = A + A' + A''$ we end up with

$$\langle \operatorname{tr} \mathscr{P}_{\mathbf{x}} \operatorname{tr} \mathscr{P}_{\mathbf{y}} \rangle = \left(\frac{I_2(2\beta)}{I_1(2\beta)} \right)^{A'}. \tag{14.31}$$

We see that the two-point function obeys a Wilson's area law. The free energy of the two static charges grows linearly with their separation,

$$f\big(|\mathbf{x}-\mathbf{y}|\big) = \sigma_{\frac{1}{2}} |\mathbf{x}-\mathbf{y}| \quad \text{with } \sigma_{\frac{1}{2}} = -\log\left(\frac{I_2(2\beta)}{I_1(2\beta)} \right). \tag{14.32}$$

Actually, one finds a similar behavior of static charges in higher representations of $SU(2)$. The free energy rises linearly with the separation and defines a string tension

$$\sigma_j = -\log\left(\frac{I_{2j+1}(2\beta)}{I_1(2\beta)} \right) \to \begin{cases} j(j+1)/\beta, & \beta \to \infty, \\ 2j \log(1/\beta), & \beta \to 0. \end{cases} \tag{14.33}$$

Interestingly in the weak-coupling limit $\beta \to \infty$ the string tension σ_j for static $q\bar{q}$-pair in the representation j is proportional to the eigenvalue $j(j+1)$ of the Casimir operator. In two dimensions this *Casimir scaling* holds for higher groups as well. In general the string tension is proportional to the quadratic Casimir.

In higher dimensions there is no proof of Casimir scaling, although there are good reasons to believe that it holds. For example, for pure $SU(2)$ and $SU(3)$ gauge theories in three and four dimensions there is conclusive numerical evidence for Casimir scaling from Monte Carlo simulations. In particular the simulations for $SU(3)$ in four dimensions confirm Casimir scaling within 5 % for separations up to 1 fm for static quarks with Casimir values (normalized by the Casimir of {3}) up to 7 [6]. Dynamical quarks can screen the static charges in which case we expect Casimir scaling only on intermediate scales. If the separation of the static $q\bar{q}$ pair becomes too large then string breaking sets in and the static potential flattens. String breaking has been seen in $SU(2)$ gauge theory with fundamental fermions [7]. There are gauge theories where the gauge bosons can screen the static quarks as well. In such theories we expect string breaking even without matter. Indeed, for the exceptional G_2 gauge theory Casimir scaling holds only at intermediate distances. At large separations one observes string breaking [8].

Pure gauge theories in two dimensions are analytic for $\beta > 0$. They behave similarly as one-dimensional spin chains and in particular there is no phase transition. However, it was shown by Gross and Witten that, in two dimensions, the $U(N)$ lattice gauge theory with Wilson action exhibits a third order phase transition when N approaches infinity [9]. The phase transition is due to the presence of an infinite number of degrees of freedom in group space.

14.3 Invariant Measure and Irreducible Representations

Here we present some facts and formulas about invariant integration on group manifolds which are useful when dealing with lattice gauge theories. On every compact

group there exists a distinguished *Haar measure* which is positive, left-invariant and right-invariant:

$$\mathrm{d}U = \mathrm{d}(\Omega U) = \mathrm{d}(U\Omega), \quad \Omega \in G. \tag{14.34}$$

It was introduced by the Hungarian mathematician ALFRED HAAR back in 1933 and represents a generalization of the Lebesgue measure. When we normalize the invariant measure, i.e. $\int \mathrm{d}U = 1$, then it is unique. The conditions (14.34) are equivalent to the left- and right-invariance of averages

$$\mathscr{M}(f) \equiv \int_G \mathrm{d}U f(U) = \int_G \mathrm{d}U f(\Omega U) = \int_G \mathrm{d}U f(U\Omega) \tag{14.35}$$

for functions $f : G \to \mathbb{C}$. The map $\mathscr{M}$ is linear, positive, normalized and invariant.

For a *finite group* the average of a function is just its mean value,

$$\mathscr{M}(f) = \frac{1}{|G|} \sum_{U \in G} f(U), \tag{14.36}$$

and the properties (14.35) are evident. Another simple example is the Abelian Lie group $U(1)$ consisting of unimodular complex numbers parametrized by their phase according to $U = \mathrm{e}^{\mathrm{i}\alpha}$, $\alpha \in [-\pi, \pi)$. A function $f : U(1) \to \mathbb{C}$ is a 2π-periodic function of the real phase α and its average is given by the integral

$$\mathscr{M}(f) = \frac{1}{2\pi} \int_{-\pi}^{\pi} \mathrm{d}\alpha f\left(\mathrm{e}^{\mathrm{i}\alpha}\right). \tag{14.37}$$

For an Abelian group left- and right-multiplication are identical. The invariance of the measure is easily proved,

$$\frac{1}{2\pi} \int_{-\pi}^{\pi} \mathrm{d}\alpha\, f\left(\Omega \mathrm{e}^{\mathrm{i}\alpha}\right) \overset{\Omega = \mathrm{e}^{\mathrm{i}\beta}}{=} \frac{1}{2\pi} \int_{-\pi}^{\pi} \mathrm{d}\alpha\, f\left(\mathrm{e}^{\mathrm{i}\beta + i\alpha}\right) = \frac{1}{2\pi} \int_{-\pi}^{\pi} \mathrm{d}\alpha\, f\left(\mathrm{e}^{\mathrm{i}\alpha}\right).$$

Haar Measure of $SU(2)$ First we study the geometric meaning of left- and right-translations on the group. To that aim we use the following bijective parametrization of the group elements:

$$\alpha \to U(\alpha) = \begin{pmatrix} \alpha_1 + i\alpha_2 & \alpha_3 + i\alpha_4 \\ -\alpha_3 + i\alpha_4 & \alpha_1 - i\alpha_2 \end{pmatrix} \quad \text{with } \alpha = \begin{pmatrix} \alpha_1 \\ \alpha_2 \\ \alpha_3 \\ \alpha_4 \end{pmatrix} \in S^3. \tag{14.38}$$

By definition a Lie group is a differentiable manifold and we see here explicitly that the group $SU(2)$ is identified with the sphere S^3. A short calculation reveals that the left-translation $U \to \Omega U$ with $\Omega = U(\beta)$ is given by

$$U(\beta)U(\alpha) = U\big(O(\beta)\alpha\big), \quad O(\beta)\alpha = \begin{pmatrix} \beta_1 & -\beta_2 & -\beta_3 & -\beta_4 \\ \beta_2 & \beta_1 & -\beta_4 & \beta_3 \\ \beta_3 & \beta_4 & \beta_1 & -\beta_2 \\ \beta_4 & -\beta_3 & \beta_2 & \beta_1 \end{pmatrix} \begin{pmatrix} \alpha_1 \\ \alpha_2 \\ \alpha_3 \\ \alpha_4 \end{pmatrix}. \tag{14.39}$$

Since β has unit norm the four-dimensional matrix $O(\beta)$ represents a rotation, i.e. $O^T O = \mathbb{1}$. Clearly the volume form on S^3, inherited from the embedding space $\mathbb{R}^4$, is rotationally invariant. A similar argument shows that the induced volume form is also invariant under right-translations and this proves that

$$\mathrm{d}U = \delta\big(\alpha^2 - 1\big)\,\mathrm{d}\alpha_1\,\mathrm{d}\alpha_2\,\mathrm{d}\alpha_3\,\mathrm{d}\alpha_4 \tag{14.40}$$

is the unique Haar measure on the group $SU(2)$. Alternatively one may introduce "spherical coordinates" on the group manifold S^3, given by

$$\begin{pmatrix}\alpha_1\\ \alpha_2\\ \alpha_3\\ \alpha_4\end{pmatrix} = \begin{pmatrix}\cos\theta\\ \sin\theta\cos\psi\\ \sin\theta\sin\psi\cos\varphi\\ \sin\theta\sin\psi\sin\varphi\end{pmatrix}, \tag{14.41}$$

and this leads to the following parametrization of the group elements:

$$U(\theta,\psi,\varphi) = \begin{pmatrix}\cos\theta + i\sin\theta\cos\psi & \sin\theta\sin\psi\,\mathrm{e}^{\mathrm{i}\varphi}\\ -\sin\theta\sin\psi\,\mathrm{e}^{-i\varphi} & \cos\theta - i\sin\theta\cos\psi\end{pmatrix}. \tag{14.42}$$

The angles are restricted to the intervals

$$0<\theta<\pi, \qquad 0<\psi<\pi \quad \text{and} \quad 0<\varphi<2\pi. \tag{14.43}$$

For the spherical coordinates the Haar measure reads

$$\mathrm{d}U = \frac{1}{2\pi^2}(\sin\theta)^2\sin\psi\,\mathrm{d}\theta\,\mathrm{d}\psi\,\mathrm{d}\varphi. \tag{14.44}$$

Haar Measure for a General Lie Group For other Lie groups the Haar measure is constructed as follows: first one (locally) parametrizes the n-dimensional group with n parameters $\{\alpha^1,\ldots,\alpha^n\} = \alpha$. Then $\mathrm{d}UU^{-1}$ is a linear combination of the differentials $\mathrm{d}\alpha^a$, where the coefficients belong to the Lie algebra $\mathbf{g}$, and the line element

$$\mathrm{d}s^2 = -\,\mathrm{tr}\big(\mathrm{d}U\,U^{-1}\mathrm{d}U\,U^{-1}\big) = \mathrm{tr}\left(\frac{\partial U^{-1}}{\partial\alpha^a}\frac{\partial U}{\partial\alpha^b}\right)\mathrm{d}\alpha^a\,\mathrm{d}\alpha^b = g_{ab}\,\mathrm{d}\alpha^a\,\mathrm{d}\alpha^b \tag{14.45}$$

defines a left- and right-invariant metric on the group. Note that unitary groups have anti-hermitian $U^{-1}\mathrm{d}U$ such that the minus sign in (14.45) yields a metric with positive signature. Now the Haar measure is proportional to the volume form associated with the invariant metric,

$$\mathrm{d}U = \mathrm{const}\sqrt{g}\,\mathrm{d}\alpha^1\cdots\mathrm{d}\alpha^n, \quad g = \det(g_{ab}). \tag{14.46}$$

The constant is fixed by the normalization of the measure. As an example consider the parametrization (14.42) of $SU(2)$. The invariant line element is

$$\mathrm{d}s^2 = \mathrm{d}\theta^2 + \sin^2\theta\,\mathrm{d}\psi^2 + \sin^2\theta\sin^2\psi\,\mathrm{d}\phi^2 \tag{14.47}$$

and the corresponding normalized volume form is the Haar measure (14.44). One may use the *exponential map* to parametrize the group: an element near the identity may be written as the exponential of an element T of the *Lie algebra*,

$$U = \mathrm{e}^{\mathrm{i}T} = \mathrm{e}^{\mathrm{i}(\alpha^1 T_1+\cdots+\alpha^n T_n)} = U(\alpha). \tag{14.48}$$

It is convenient to choose a trace-orthogonal basis of the Lie algebra,

$$\operatorname{tr} T_a T_b = \kappa \delta_{ab}. \tag{14.49}$$

The parameters $\{\alpha^1, \ldots, \alpha^n\}$ are continuous local coordinates of the Lie group. Now we introduce the one-parametric group

$$U(t) = \mathrm{e}^{\mathrm{i}tT} \quad \text{with } U(0) = \mathbb{1},\ U(1) = U. \tag{14.50}$$

The n elements of the Lie algebra may be written as

$$L_a(t) = -i \frac{\partial U(t)}{\partial \alpha^a} U^{-1}(t).$$

They satisfy the simple differential equations

$$\frac{\mathrm{d}L_a(t)}{\mathrm{d}t} = T_a + \mathrm{i}\big[T, L_a(t)\big]. \tag{14.51}$$

If we rewrite the L_a as linear combinations of the base elements T_a, i.e. $L_a = L_a^b T_b$, then the coefficient matrix $L = (L_a^b)$ fulfills the simple differential equation

$$\dot{L}(t) = \mathbb{1} + L(t)X, \qquad X = \big(X_a^b\big), \qquad X_a^b = f_{ac}^b \alpha^c. \tag{14.52}$$

The structure constants f_{ab}^c of the Lie algebra satisfy the relation

$$[T_a, T_b] = \mathrm{i} f_{ab}^c T_c \tag{14.53}$$

which means that they are real and antisymmetric in a and b (for compact groups). Hence, the matrix X is antisymmetric as well. The solution to the differential equation (14.52) for the matrix function $L(t)$ reads

$$L(t) = \int_0^t \mathrm{e}^{(t-t')X} = \frac{\mathrm{e}^{tX} - 1}{X}. \tag{14.54}$$

We now may calculate the invariant metric tensor as introduced in (14.45) by virtue of

$$g_{ab} = \operatorname{tr} L_a L_b|_{t=1} = \kappa \big(LL^T\big)_{ab}|_{t=1}, \tag{14.55}$$

where κ emerges from the normalization of the base elements. This leads to the invariant volume form (up to a multiplicative factor)

$$\mathrm{d}V = \sqrt{g} \prod_a \mathrm{d}\alpha^a \propto \big(\det LL^T\big)_{t=1}^{1/2} \prod_a \mathrm{d}\alpha^a \tag{14.56}$$

which is proportional to the Haar measure. The matrix LL^T appearing in (14.56) has the form

$$\begin{aligned} LL^T|_{t=0} &= -\frac{1}{X^2}\big(\mathrm{e}^X - \mathbb{1}\big)\big(\mathrm{e}^{-X} - \mathbb{1}\big) = -4X^{-2}\sinh^2(X/2) \\ &= -\prod_{n\neq 0}\big(1 + X^2/(2\pi n)^2\big), \end{aligned} \tag{14.57}$$

where we have used the Weierstrass product representation of the sinh function. For example, the gauge group $SU(2)$ with $T = \alpha^a \sigma_a$ implies

$$X = \begin{pmatrix} 0 & -\alpha_3 & \alpha_2 \\ \alpha_3 & 0 & -\alpha_1 \\ -\alpha_2 & \alpha_1 & 0 \end{pmatrix} \quad \text{and} \quad \mathrm{d}V \propto \frac{8}{|\boldsymbol{\alpha}|^3} \sin^3\left(\frac{|\boldsymbol{\alpha}|}{2}\right) \mathrm{d}^3\alpha. \tag{14.58}$$

14.3.1 The Peter–Weyl Theorem

The Haar measure is used to define an *invariant* scalar product for functions $G \to \mathbb{C}$,

$$(f, g) \equiv \int_G \bar{f}(U) g(U)\, \mathrm{d}U. \tag{14.59}$$

One obtains an orthonormal basis of the Hilbert space $L_2(G, \mathrm{d}U)$ of square integrable functions by considering all irreducible representations of the group G. We recall that a *representation* R of G is a homomorphism from the group to the group of invertible linear maps $V \to V$. This means that a representation preserves the *structure* of the group:

$$R : G \to L(V), \qquad R(U_1 U_2) = R(U_1) R(U_2), \qquad R(\mathbb{1}) = \mathbb{1}. \tag{14.60}$$

For a fixed basis in V we can identify a linear map with a matrix. Thus a representation assigns to each group element U an invertible matrix such that the conditions (14.60) are satisfied. The dimension d_R of a representation R is given by the dimension of the vector space V. For example, the infinitely many representations of $SU(2)$ are classified by the angular momentum j and the dimension of the representation is $2j + 1$.

For a group with invariant measure every representation is equivalent to a unitary representation, hence we may assume that the matrices R are unitary. A representation is called *irreducible* if the linear maps $\{R(U) | U \in G\}$ have no common *invariant* subspace in V, apart from the empty set and V itself. Let $\{R(U)\}$ denote the set of all irreducible representations. Then we have the following important theorem [10–13].

Theorem 14.1 (Peter–Weyl theorem) *The functions* $\{R(U)^a_b\}$ *define a complete orthogonal system of* $L_2(\mathrm{d}U)$ *with*

$$\left(R^a_b, R'^c_d\right) \equiv \int \bar{R}^a_b(U) R'^c_d(U)\, \mathrm{d}U = \frac{\delta_{RR'}}{d_R} \delta^{ac} \delta_{bd}, \tag{14.61}$$

where $d_R = \operatorname{tr} R(\mathbb{1})$ *denotes the dimension of the representation* R.

This theorem provides a generalization of the Fourier analysis of functions on the unit circle to functions on groups. A useful consequence of this theorem is

Lemma 14.1 *The characters* $\chi_R(U) = \operatorname{tr} R(U)$ *of the irreducible representations form a orthogonal basis of the space of invariant functions* $f(U) = f(\Omega U \Omega^{-1})$ *in* $L_2(\mathrm{d}U)$. *In particular, we have* $(\chi_R, \chi_{R'}) = \delta_{RR'}$.

This lemma can be used to decompose a reducible representation into its irreducible parts. In the strong-coupling expansions and the exact solutions of two-dimensional gauge theories we shall need further useful identities which are the content of

Lemma 14.2 *The following identities hold*:

$$\text{orthogonality:} \quad \left(R_b^a, \chi_{R'}\right) = \frac{\delta_{RR'}}{d_R}\delta_b^a, \tag{14.62}$$

$$\text{gluing:} \quad \int \mathrm{d}\Omega\, \chi_R\left(U\Omega^{-1}\right)\chi_{R'}(\Omega V) = \frac{\delta_{RR'}}{d_R}\chi_R(UV), \tag{14.63}$$

$$\text{separation:} \quad \int \mathrm{d}\Omega\, \chi_R\left(\Omega U \Omega^{-1} V\right) = \frac{1}{d_R}\chi_R(U)\chi_R(V), \tag{14.64}$$

$$\text{decomposition of } \mathbb{1}: \quad \sum_R d_R \chi_R(U) = \delta(\mathbb{1}, U). \tag{14.65}$$

For example, the gluing property is proven quite easily:

$$\begin{aligned}\int \mathrm{d}\Omega\, \chi_R\left(U\Omega^{-1}\right)\chi_{R'}(\Omega V) &= \sum_{a,b,c,d} R_b^a(U) \int \mathrm{d}\Omega\, \bar{R}_a^b(\Omega) R'^c_d(\Omega) R'^d_c(V) \\ &= \sum_{a,b,c,d} R_b^a(U) R'^d_c(V) \frac{\delta_{RR'}}{d_R}\delta_a^c \delta_d^b = \frac{\delta_{R,R'}}{d_R}\chi_R(UV).\end{aligned}$$

The decomposition of the identity follows from the orthogonality relation (14.61). Proofs and further relations are found in the rich literature on groups and representations, for example in [10–13].

14.4 Problems

14.1 (Solution of Z_2 gauge theories in two dimensions) Calculate the partition function of the Z_2 gauge theory

$$Z_V(\beta) = \frac{1}{2^{|E|}} \sum_{\{U\}} \mathrm{e}^{-\sum_p \beta(1-U_p)} = \frac{1}{2^{|E|}} \left(\frac{\cosh\beta}{\mathrm{e}^{\beta}}\right)^V \sum_{\{U\}} \prod_p (1 + \tanh\beta U_p)$$

without gauge fixing. Thereby U_p denote a plaquette variable and the link variables take the values $U_\ell \in \{-1, 1\}$. Expand the product and use

$$\sum_U U^k = \begin{cases} 2, & k \text{ odd}, \\ 0, & k \text{ even}. \end{cases}$$

The solution is very similar to that of the Ising spin chain.

14.2 (Peter–Weyl theorem and Fourier analysis) Apply the Peter–Weyl theorem to the group $U(1)$ and show that it reduces to a well-known property of the Fourier series for periodic functions on an interval.

References

1. A.A. Migdal, Phase transitions in gauge and spin-lattice systems. J. Exp. Theor. Phys. **69**, 1457 (1975)
2. K.R. Ito, Analytic study of the Migdal–Kadanoff recursion formula. Commun. Math. Phys. **93**, 379 (1984)
3. J.M. Drouffe, J.B. Zuber, Strong coupling and mean field methods in lattice gauge theories. Phys. Rep. **102**, 1 (1983)
4. H.J. Rothe, *Lattice Gauge Theories: An Introduction* (World Scientific, Singapore, 2012)
5. H.G. Dosch, V.V. Müller, Lattice gauge theory in two spacetime dimensions. Fortschr. Phys. **27**, 547 (1979)
6. G. Bali, Casimir scaling of $SU(3)$ static potentials. Phys. Rev. D **62**, 114503 (2000)
7. O. Philipsen, H. Wittig, String breaking in non-Abelian gauge theories with fundamental matter fields. Phys. Rev. Lett. **81**, 4059 (1998)
8. B. Wellegehausen, A. Wipf, C. Wozar, Casimir scaling and string breaking in G2 gluodynamics. Phys. Rev. D **83**, 016001 (2011)
9. D.J. Gross, E. Witten, Possible third order phase transition in the large N lattice gauge theory. Phys. Rev. D **21**, 446 (1980)
10. T. Bröcker, T. tom Dieck, *Representations of Compact Lie Groups* (Springer, Berlin, 2003)
11. G. Segal, Lie Groups, in *Lectures on Lie Groups and Lie Algebras* (Cambridge University Press, Cambridge, 1995)
12. C. Chevalley, *Theory of Lie Groups* (Princeton University Press, Princeton, 1946)
13. M. Hammermesh, *Group Theory and Its Application to Physical Problems* (Dover, New York, 1989)

Chapter 15
Fermions on a Lattice

In the previous chapters we considered quantum field theories for bosons with spin 0 and spin 1 and discussed the regularization of these theories on a spacetime lattice. But all fundamental microscopic theories of nature contain both bosonic and fermionic fields. Hence it remains to put fermions with spin $1/2$ onto a lattice. Electrons, muons or quarks are all described by a four-component spinor field $\psi(x) \in \mathbb{C}^4$. The corresponding quantum field $\hat{\psi}(x)$ creates and annihilates the particles together with their anti-particles which have identical mass but opposite charge. In this chapter we briefly recall the basic properties of a Dirac field in Euclidean space. By using anticommuting Grassmann variables we formulate the path integral for Fermi fields. With the most naive approach we encounter the species-doubling phenomenon—the fact that a naively discretized Dirac field leads to more excitations than expected. We discuss various proposals to discretize fermion fields, these include Wilson fermions, staggered fermions and Ginsparg–Wilson fermions. Towards the end we shall comment on problems with formulating supersymmetric systems on a lattice. A discussion of fermions on a lattice is contained in several textbooks, see [1–8].

15.1 Dirac Equation

We assume that the reader has basic knowledge of the Dirac theory, and hence we will not present many details regarding particular properties of the Dirac equation and its solutions. In particular we only discuss the internal and spacetime symmetries in Euclidean space. We begin with the relativistic wave equation of a spinor field ψ, the *Dirac equation*, in Minkowski spacetime,

$$(\mathrm{i}\partial\!\!\!/ - m)\psi(x) = 0, \qquad \partial\!\!\!/ = \gamma^\mu \partial_\mu, \qquad \{\gamma^\mu, \gamma^\nu\} = 2\eta^{\mu\nu}\mathbb{1}, \tag{15.1}$$

where $(\eta_{\mu\nu})$ denotes the metric tensor $\mathrm{diag}(1, -1, -1, -1)$ and $\gamma^0, \ldots, \gamma^3$ are the four-dimensional gamma matrices that satisfy the relation in (15.1). In the following we shall consider Euclidean Fermi fields. The gamma matrices in Euclidean space

A. Wipf, *Statistical Approach to Quantum Field Theory*, Lecture Notes in Physics 864,
DOI 10.1007/978-3-642-33105-3_15, © Springer-Verlag Berlin Heidelberg 2013

$\gamma_{\mathrm{E}}^{\mu}$ are related to those in Minkowski spacetime according to $\gamma_{\mathrm{E}}^{0} = \gamma^{0}$ and $\gamma_{\mathrm{E}}^{i} = \mathrm{i}\gamma^{i}$. They satisfy anticommutation rules with the Euclidean metric,

$$\left\{\gamma_{\mathrm{E}}^{\mu}, \gamma_{\mathrm{E}}^{\nu}\right\} = 2\delta^{\mu\nu}\mathbb{1}. \tag{15.2}$$

Since we are dealing with the Euclidean theory we omit the index E in what follows. The Euclidean gamma matrices are hermitian

$$\gamma_{\mu}^{\dagger} = \gamma_{\mu} = \gamma^{\mu} \tag{15.3}$$

and the Euclidean Dirac equation reads

$$D\psi(x) \equiv (\not{\partial} + m)\psi(x) = 0, \tag{15.4}$$

with an anti-hermitian operator $\not{\partial}$. Lorentz transformations in Minkowski space turn into rotations in four-dimensional Euclidean space and a spinor field transforms under these rotations according to $\psi(x') = S\psi(x)$ with $S^{\dagger}S = \mathbb{1}$.[1] Here S is a spin transformation from the covering group of the rotation group $SO(4)$. The bilinear $\bar{\psi}\psi$ is *not* invariant under "Lorentz transformations" in Euclidean space if we stick to the definition $\bar{\psi} = \psi^{\dagger}\gamma^{0}$, valid in Minkowski spacetime. In Euclidean space $\bar{\psi}$ should be considered as $\psi^{\dagger}$ when it comes to spin transformations. The hermitian matrix

$$\gamma_5 = \gamma^0\gamma^1\gamma^2\gamma^3 = \gamma_5^{\dagger} \tag{15.5}$$

anticommutes with all gamma matrices:

$$\left\{\gamma_5, \gamma^{\mu}\right\} = 0 \quad \text{and} \quad \gamma_5^2 = \mathbb{1}, \tag{15.6}$$

and has the degenerate eigenvalues ± 1. The Dirac operator D fulfills the relation

$$\gamma_5 D \gamma_5 = D^{\dagger} \tag{15.7}$$

which implies that all non-real eigenvalues appear in complex-conjugate pairs and that the determinant of D is real. This non-Hermitian Dirac operator is also obtained by a careful derivation of the path-integral representation of the partition function. The Dirac equation (15.4) is the Euler–Lagrange equation derived from the action

$$S_{\mathrm{F}} = \int \mathrm{d}^4x \left(\frac{1}{2}\left(\bar{\psi}(x)\gamma^{\mu}\partial_{\mu}\psi(x) - \partial_{\mu}\bar{\psi}(x)\gamma^{\mu}\psi(x)\right) + m\bar{\psi}(x)\psi(x)\right). \tag{15.8}$$

Up to a surface term the action can be written as

$$S_{\mathrm{F}} = \int \mathrm{d}^4x\, \bar{\psi}(x) D \psi(x), \tag{15.9}$$

and the latter form is most commonly used in the literature.

[1] Recall that in Minkowski space $S^{\dagger} = \gamma^0 S^{-1} \gamma^0$.

15.1.1 Coupling to Gauge Fields

Realistic theories contain several Dirac fields and these fields combine to a field ψ with values in $V \otimes \mathbb{C}^4$. Here V is a vector space equipped with a G-invariant scalar product, i.e. $(\chi, \psi) = (\Omega\chi, \Omega\psi)$ for all $\Omega \in G$. Expanding χ and ψ in an orthonormal basis of V the scalar product reads $(\chi, \psi) = \sum_a \bar{\chi}_a \psi_a$, where each term is the Lorentz-invariant bilinear of the corresponding Dirac spinors. The linear transformation Ω only acts on the internal index a (and not on the spinor index) such that the Lagrangian density is invariant under global transformations,

$$\mathscr{L} = (\psi, D\psi) = \big(\psi', D\psi'\big), \quad \psi' = \Omega\psi, \ \Omega \in G. \tag{15.10}$$

Similarly as for a scalar field we can promote the global symmetry to a local one by introducing a Lie-algebra valued gauge potential to define a covariant derivative. The resulting covariant Dirac operator reads

$$D = \not{D} + m, \qquad \not{D} = \gamma^\mu D_\mu, \qquad D_\mu = \partial_\mu - \mathrm{i}g A_\mu, \tag{15.11}$$

and the Lagrangian (15.9) with this operator is invariant under local gauge transformations $(\psi, A_\mu) \to (\psi', A'_\mu)$. If there is only one Dirac field the gauge transformations are local $U(1)$ transformations,

$$\psi'(x) = \mathrm{e}^{\mathrm{i}g\lambda(x)}\psi(x), \qquad \bar{\psi}'(x) = \bar{\psi}(x)\mathrm{e}^{-\mathrm{i}g\lambda(x)}, \qquad A'_\mu(x) = A_\mu(x) + \partial_\mu\lambda(x). \tag{15.12}$$

In the chiral limit $m = 0$ the Lagrangian (15.9) for one Dirac field in addition is invariant under global chiral transformations,

$$\psi(x) \to \mathrm{e}^{\gamma_5\alpha}\psi(x), \qquad \bar{\psi}(x) \to \bar{\psi}(x)\mathrm{e}^{\alpha\gamma_5}, \quad \alpha \in \mathbb{R}. \tag{15.13}$$

In Euclidean space the chiral transformations form the *non-compact* group $\mathbb{R}_+$, whereas in Minkowski spacetime they form the compact group $U(1)$. The chiral symmetry group is enlarged for a multiplet of Dirac fields.

15.2 Grassmann Variables

To motivate why we need anticommuting variables in the path-integral quantization of theories with fermions we briefly return to bosonic fields. A scalar field entering the path integral is a real and commuting function,

$$\big[\phi(x), \phi(y)\big] = 0. \tag{15.14}$$

This property may be regarded as the limiting case $\hbar \to 0$ of the commutation rules for the quantum field $\hat{\phi}$. A fermionic quantum field, on the other hand, must satisfy the equal-time anticommutation relations

$$\big\{\hat{\psi}(t, \mathbf{x}), \hat{\psi}(t, \mathbf{y})\big\} = 0, \quad \mathbf{x} \neq \mathbf{y},$$

so that the Pauli exclusion principle and Fermi–Dirac statistics are fulfilled. This serves as motivation for using an anticommuting field:

$$\{\psi(x), \psi(y)\} = 0, \quad \forall x, y, \tag{15.15}$$

in the fermionic path integral. We may view an anticommuting field as classical limit of a fermionic quantum field. Classical bosonic fields are built with commuting c-numbers whereas 'classical fermionic fields' are built with anticommuting Grassmann variables. We refer the reader interested in details to the literature [5, 9]. The objects $\{\eta_i, \bar{\eta}_i\}$ form a complex *Grassmann algebra* if

$$\{\eta_i, \eta_j\} = \{\bar{\eta}_i, \bar{\eta}_j\} = \{\eta_i, \bar{\eta}_j\} = 0, \quad i, j = 1, 2, \ldots, n, \tag{15.16}$$

holds. Note that the square of a Grassmann variable is zero. For the path integral we need to integrate over functions of Grassmann variables. The integration is a linear map and defined by the rules

$$\int \mathrm{d}\eta_i (a + b\eta_i) = b, \qquad \int \mathrm{d}\bar{\eta}_i (a + b\bar{\eta}_i) = b \tag{15.17}$$

with arbitrary complex numbers a, b. The integration is invariant under a translation of the Grassmann variables.

15.2.1 Gaussian Integrals

Most path integrals for fermionic systems lead to Gaussian integrals of the form

$$Z = \int \mathscr{D}\bar{\eta}\mathscr{D}\eta \mathrm{e}^{-\bar{\eta}A\eta}, \quad \bar{\eta}A\eta = \sum_{ij} \bar{\eta}_i A_{ij} \eta_j, \tag{15.18}$$

where the integration extends over all Grassmann variables

$$\mathscr{D}\bar{\eta}\mathscr{D}\eta = \prod \mathrm{d}\bar{\eta}_i \, \mathrm{d}\eta_i. \tag{15.19}$$

The Gaussian integral can be evaluated by an expansion of the exponential function. Due to the integration rules (15.17) the only non-vanishing contribution is given by

$$\begin{aligned}
\frac{(-1)^n}{n!} \int \mathscr{D}\bar{\eta}\mathscr{D}\eta (\bar{\eta}A\eta)^n &= (-1)^n \int \mathscr{D}\bar{\eta}\mathscr{D}\eta \sum_{i_1,\ldots,i_n} (\bar{\eta}_1 A_{1i_1}\eta_{i_1}) \cdots (\bar{\eta}_n A_{ni_n}\eta_{i_n}) \\
&= (-1)^n \int \mathscr{D}\bar{\eta}\mathscr{D}\eta \prod_i (\bar{\eta}_i \eta_i) \sum_{i_1,\ldots,i_n} \varepsilon_{i_1\ldots i_n} A_{1i_1} \cdots A_{ni_n} \\
&= \int \prod_i (\mathrm{d}\bar{\eta}_i \, \bar{\eta}_i \, \mathrm{d}\eta_i \, \eta_i) \det A = \det A.
\end{aligned}$$

Thus we end up with the simple formula

$$Z = \int \mathscr{D}\bar{\eta}\mathscr{D}\eta \mathrm{e}^{-\bar{\eta}A\eta} = \det A. \tag{15.20}$$

Next we consider the slightly more general Gaussian integral

$$Z(\bar{\alpha},\alpha)=\int \mathscr{D}\bar{\eta}\mathscr{D}\eta \mathrm{e}^{-\bar{\eta}A\eta+\bar{\alpha}\eta+\bar{\eta}\alpha} \tag{15.21}$$

with Grassmann-valued sources $\alpha=(\alpha_1,\ldots,\alpha_n)$ and $\bar{\alpha}=(\bar{\alpha}_1,\ldots,\bar{\alpha}_n)$. We used the abbreviation $\bar{\eta}\alpha=\sum\bar{\eta}_i\alpha_i$. Shifting the integration variables $\bar{\eta}_i$, η_i according to

$$\eta\to\eta+A^{-1}\alpha \quad \text{and} \quad \bar{\eta}\to\bar{\eta}+\bar{\alpha}A^{-1}$$

and using the translational invariance of the integration, we obtain the following generalization of (15.20):

$$Z(\bar{\alpha},\alpha)=\int \mathscr{D}\bar{\eta}\mathscr{D}\eta \mathrm{e}^{-\bar{\eta}A\eta+\bar{\alpha}\eta+\bar{\eta}\alpha}=\mathrm{e}^{-\bar{\alpha}A^{-1}\alpha}\det A. \tag{15.22}$$

Expanding both sides in powers of $\bar{\alpha}$, α, we find the useful formula

$$\langle\bar{\eta}_i\eta_j\rangle\equiv\frac{1}{Z}\int \mathscr{D}\bar{\eta}\mathscr{D}\eta \mathrm{e}^{-\bar{\eta}A\eta}\bar{\eta}_i\eta_j=\left(A^{-1}\right)_{ij}. \tag{15.23}$$

The integral is zero when the number of variables $\bar{\eta}$ and η do not match,

$$\langle\bar{\eta}_{i_1}\cdots\bar{\eta}_{i_n}\eta_{j_1}\cdots\eta_{j_m}\rangle=0 \quad \text{if } m\neq n. \tag{15.24}$$

In passing we note that path integrals for Majorana fermions lead to Gaussian integrals of the from

$$\int \mathscr{D}\eta \mathrm{e}^{\frac{1}{2}\eta^t M\eta}=\mathrm{Pf}(M), \quad \mathscr{D}\eta=\prod \mathrm{d}\eta_a, \tag{15.25}$$

where $\eta=(\eta_1,\ldots,\eta_{2N})$ denotes an even number of real Grassmann variables with anticommutation rules

$$\{\eta_a,\eta_b\}=0, \tag{15.26}$$

and M is a real and antisymmetric matrix. Up to a sign the Pfaffian $\mathrm{Pf}(M)$ is the square root of $\det(M)$. Further properties of Grassmann integrals for real anticommuting parameters are found on p. 379.

15.2.2 Path Integral for Dirac Theory

After these algebraic preliminaries we return to quantum field theory. An anticommuting field assigns several Grassmann variables to each spacetime point. For a Dirac field in four dimensions these are the anticommuting variables $\{\psi_\alpha(x),\bar{\psi}_\alpha(x)\}$, where the spinor index α takes the values $1,2,3,4$. The 'classical' Dirac field satisfies

$$\left\{\psi_\alpha(x),\psi_\beta(y)\right\}=\left\{\bar{\psi}_\alpha(x),\bar{\psi}_\beta(y)\right\}=\left\{\psi_\alpha(x),\bar{\psi}_\beta(y)\right\}=0. \tag{15.27}$$

The functional integration over the fermion field is the (formal) Grassmann integral

$$\int \mathscr{D}\psi\mathscr{D}\bar{\psi}\ldots\equiv\int\prod_x\prod_\alpha \mathrm{d}\psi_\alpha(x)\,\mathrm{d}\bar{\psi}_\alpha(x)\ldots, \tag{15.28}$$

and the expectation value of an observable $\hat{A}$ is given by the functional integral

$$\langle 0|\hat{A}|0\rangle = \frac{1}{Z_{\mathrm{F}}} \int \mathscr{D}\psi \mathscr{D}\bar{\psi} A(\bar{\psi}, \psi) \mathrm{e}^{-S_{\mathrm{F}}(\psi,\bar{\psi})} \tag{15.29}$$

normalized by the partition function

$$Z_{\mathrm{F}} = \int \mathscr{D}\psi \mathscr{D}\bar{\psi} \mathrm{e}^{-S_{\mathrm{F}}}. \tag{15.30}$$

The integrands contain the classical action S_{F} for the fermion field. Most physically relevant theories have a bilinear action

$$S_{\mathrm{F}} = \int \mathrm{d}^d x \, \mathscr{L}(\psi, \bar{\psi}), \quad \mathscr{L} = \bar{\psi}(x) D \psi(x), \tag{15.31}$$

which contains the Dirac operator D. Exceptions are the Thirring, Gross–Neveu and supergravity models which contain terms that are quartic in the Fermi fields.

Applying (15.20) we can calculate the partition function of a theory with bilinear action (15.31). Formally it is just the determinant of the Dirac operator,

$$Z_{\mathrm{F}} = \int \mathscr{D}\psi \mathscr{D}\bar{\psi} \exp\left(- \int \mathrm{d}^d x \, \bar{\psi}(x) D \psi(x) \right) = \det D. \tag{15.32}$$

The corresponding formula for a *complex* scalar fields reads

$$Z_{\mathrm{B}} = \int \mathscr{D}\phi \mathscr{D}\bar{\phi} \exp\left(- \int \mathrm{d}^d x \, \bar{\phi}(x) A \phi(x) \right) = \frac{1}{\det A}. \tag{15.33}$$

There are interesting field theories with an additional supersymmetry for which the contributions of the bosons and fermions to the partition function chancel. For these theories the bosonic operator A and the fermionic operator D are related. In a lattice regularization the Dirac operator becomes a huge matrix, and one of the main difficulties in MC simulations is to calculate the determinant and the inverse of this matrix.

15.3 Fermion Fields on a Lattice

To obtain a lattice regularization for fermionic systems we proceed similarly as for scalar field theories by substituting differentials by differences. In contrast to the bosonic fields the most naive discretization is afflicted with the doubling problem and we shall discuss how to deal with this problem. In many cases the lengths and dimensionful parameters are measured in units defined by the lattice spacing a.

15.3.1 Lattice Derivative

The discretization of differential operators within fermionic systems is a subtle point since the field equations contain the first-order Dirac operator D. According to (15.23) the two-point function (before averaging over the other fields) reads

$$G_{\mathrm{F}}(x,y) = \big\langle \psi(x)\bar{\psi}(y)\big\rangle \equiv G_{\mathrm{F}}(x-y) = \langle x|\frac{1}{D}|y\rangle \tag{15.34}$$

and the inverse of the Dirac operator depends on the discretization. We assume that the lattice Dirac operator is γ_5-symmetric

$$\gamma_5 D\gamma_5 = D^\dagger, \tag{15.35}$$

such that its eigenvalues come in complex conjugated pairs $\{\lambda, \lambda^*\}$ and its determinant is real. To prove this proposition we consider the characteristic polynomial of the operator on a finite lattice,

$$P(\lambda) \equiv \det(\lambda - D) = \det\gamma_5(\lambda - D)\gamma_5 = \det\big(\lambda - D^\dagger\big) = P^*\big(\lambda^*\big). \tag{15.36}$$

This means that if λ is a root of the characteristic polynomial then λ^* is also a root and this proves the proposition. A Dirac operator $D = \not{\partial} + m + \mathscr{O}$ is γ_5-hermitian if the lattice derivatives are anti-hermitian and the operator $\mathscr{O}$ is hermitian with respect to the ℓ_2-scalar product on the space of lattice functions and also commutes with γ_5,

$$\gamma_5 D\gamma_5 = \gamma_5(\not{\partial} + m + \mathscr{O})\gamma_5 = -\not{\partial} + m + \mathscr{O} = \not{\partial}^\dagger_\mu + m + \mathscr{O}^\dagger = D^\dagger, \tag{15.37}$$

where we used that the γ^μ anticommute with γ_5.

Forward and Backward Derivative

The frequently used nearest-neighbor forward and backward derivatives

$$(\hat{\partial}_\mu f)(x) = f(x+e_\mu) - f(x), \qquad \big(\hat{\partial}'_\mu f\big)(x) = f(x) - f(x-e_\mu) \tag{15.38}$$

are not anti-hermitian with respect to the scalar product $(f,g) = \sum_x \bar{f}(x)g(x)$. In fact for periodic boundary conditions we have $\hat{\partial}^\dagger_\mu = -\hat{\partial}'_\mu$. Both derivatives define circulant matrices and thus commute with each other,

$$[\hat{\partial}_\mu, \hat{\partial}_\nu] = \big[\hat{\partial}'_\mu, \hat{\partial}'_\nu\big] = \big[\hat{\partial}_\mu, \hat{\partial}'_\nu\big] = 0. \tag{15.39}$$

Plane waves on the periodic lattice

$$\varphi_p = \frac{1}{\sqrt{V}}\mathrm{e}^{\mathrm{i}px}, \qquad p_\mu = \frac{2\pi}{N}n_\mu, \quad n_\mu \in \mathbb{Z}_N \tag{15.40}$$

are simultaneous eigenfunctions of the derivative operators,

$$\hat{\partial}_\mu\varphi_p = \mathrm{i}\hat{p}_\mu \mathrm{e}^{\mathrm{i}p_\mu/2}\varphi_p, \qquad \hat{\partial}'_\mu\varphi_p = \mathrm{i}\hat{p}_\mu \mathrm{e}^{-\mathrm{i}p_\mu/2}\varphi_p, \quad \hat{p}_\mu = 2\sin\frac{p_\mu}{2}. \tag{15.41}$$

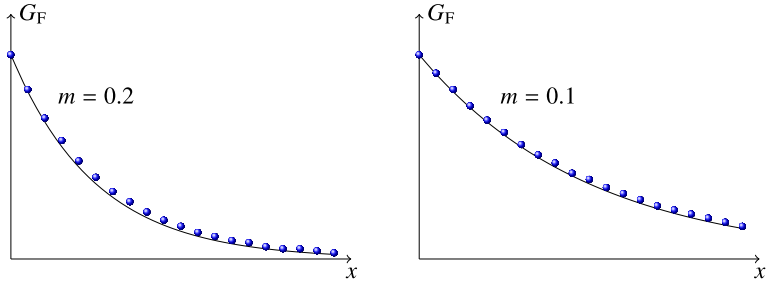

Fig. 15.1 The fermionic Green function for the forward derivative on the one-dimensional lattice with $N = 20$ lattice sites as well as its interpolating exponential function

In particular the inverse of $\hat{\partial} + m$ on a one-dimensional lattice reads

$$\langle x|\frac{1}{\hat{\partial}+m}|y\rangle = \frac{1}{N}\sum_p \frac{\mathrm{e}^{\mathrm{i}p(x-y)}}{m+\mathrm{i}\mathrm{e}^{\mathrm{i}p/2}\hat{p}} \overset{N\to\infty}{\to} \frac{1}{2\pi}\int_{-\pi}^{\pi}\mathrm{d}p\,\frac{\mathrm{e}^{\mathrm{i}p(x-y)}}{m+\mathrm{i}\mathrm{e}^{\mathrm{i}p/2}\hat{p}}. \tag{15.42}$$

This Green function is very well approximated by an exponential fit for small bare masses $m < 0.2$ or equivalently for large correlation lengths $\xi > 5$. Figure 15.1 shows both the propagator and its exponential fit for the masses $m = 0.1$ and $m = 0.2$.

Antisymmetric Derivative

In place of the forward and backward derivatives one may employ the *antisymmetric* discretization of ∂_μ, defined by

$$\mathring{\partial}_\mu = \frac{1}{2}\big(\hat{\partial}_\mu + \hat{\partial}'_\mu\big) \quad\Longrightarrow\quad (\mathring{\partial}_\mu f)(x) = \frac{1}{2}\big(f(x+e_\mu) - f(x-e_\mu)\big). \tag{15.43}$$

These commuting derivatives can be diagonalized simultaneously. The plane waves (15.40) are the eigenfunctions with eigenvalues

$$\mathring{\partial}_\mu \varphi_p(x) = \mathrm{i}\mathring{p}_\mu \varphi_p(x), \quad \mathring{p}_\mu = \sin p_\mu, \tag{15.44}$$

and we find the following Green function on the one-dimensional lattice:

$$\langle x|\frac{1}{\mathring{\partial}+m}|0\rangle = \frac{1}{N}\sum_p \frac{\mathrm{e}^{\mathrm{i}px}}{m+\mathrm{i}\mathring{p}} \overset{N\to\infty}{\to} \frac{1}{2\pi}\int_{-\pi}^{\pi}\mathrm{d}p\,\frac{\mathrm{e}^{\mathrm{i}px}}{m+\mathrm{i}\mathring{p}}. \tag{15.45}$$

Figure 15.2 shows the Green function on the lattice with 40 sites. Note that the restriction of the propagator to even (odd) lattice sites defines an even (odd) lattice function. The functions on the two sub-lattices approach each other for small x, whereas they have opposite signs near $x = N$. This means that the lattice Green function with antisymmetric derivative oscillates with a large amplitude around the mean value 0 for $x \to N$. The figure also shows that the exponential function $\exp(-mx)$ fits the Green function rather well for $x \ll N$ and $5 \ll \xi \ll N/2$.

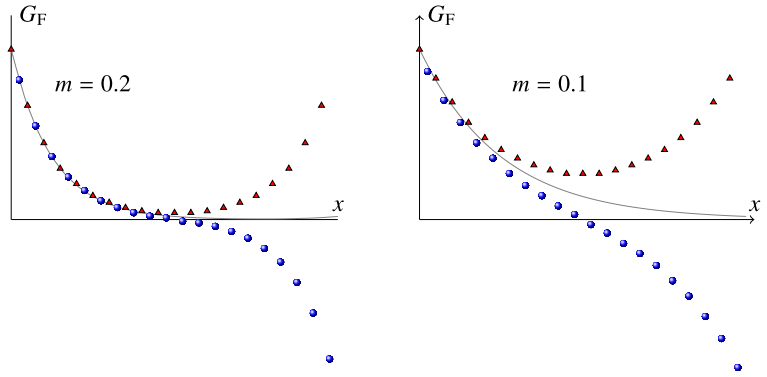

Fig. 15.2 The fermion Green function for the antisymmetric derivative on a one-dimensional lattice with $N = 40$

SLAC Derivative

Here we introduce yet another lattice derivative—the SLAC derivative [13, 14]—which can be used in fermionic systems without local gauge invariance.[2] This derivative yields the best values for the bound state energies of quantum mechanical Hamiltonians discretized on lattices of moderate sizes [15, 16]. In addition, simulations of supersymmetric Yukawa models show that in these models observables approach their continuum values most rapidly when one employs the SLAC derivative [17, 18]. This lattice derivative has the interesting property of having exactly the same spectrum as the continuum derivative below the UV-cutoff. A particular simple choice of the SLAC derivative has the following matrix elements in position space:

$$(\partial_{\text{slac}})_{kk} = 0, \qquad (\partial_{\text{slac}})_{k\neq k'} = \frac{\pi}{N}(-)^{k-k'}\frac{1}{\sin(\pi t_{kk'})}, \qquad t_{kk'} = \frac{k-k'}{N}. \quad (15.46)$$

Clearly, the SLAC derivative is antisymmetric. Further properties of this derivative are discussed in the Appendix to this chapter. Figure 15.3 shows the Green functions of the Dirac and Klein–Gordon operators

$$G_F(x) = \langle x|\frac{1}{m+\partial_{\text{slac}}}|0\rangle \quad \text{and} \quad G_B(x) = \langle x|\frac{1}{m^2-\partial^2_{\text{slac}}}|0\rangle \qquad (15.47)$$

on a one-dimensional lattice. Near the origin the amplitude of the fermionic Green function overshoots since in momentum space the SLAC derivative jumps at the edge of the Brillouin zone. The overshooting is the well-known Gibbs phenomenon of Fourier transforms of discontinuous functions. The fits in Fig. 15.3 are normal-

[2] The problems with the SLAC derivative in gauge theories as discussed in [19] are absent in theories without local gauge invariance [17].

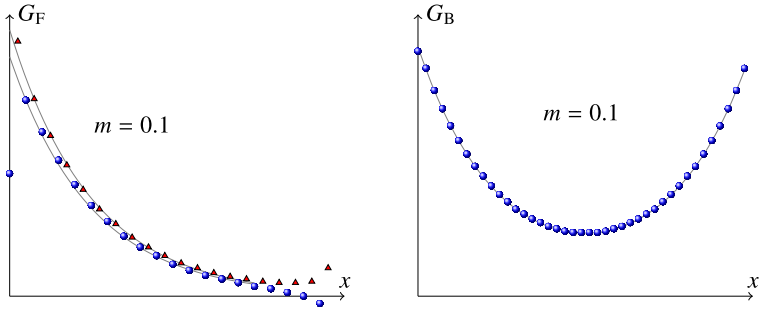

Fig. 15.3 The fermion and boson Green function on a chain with $N = 41$ sites, evaluated with the non-local SLAC derivative

ized such that they match the propagator at $x = 2$ and $x = 3$, respectively. The interpolating function

$$G_B(x) \sim \text{const}\left(e^{-mx} + e^{-m(N-x)}\right)$$

approximates the bosonic Green function very well.

15.3.2 Naive Fermions on the Lattice

In this section we shall discuss various types of lattice fermions distinguished by the different discretization of the Dirac operator. Since the main focus is on the discretizations of $\partial\!\!\!/$ it is sufficient to consider free fermions. We do not specify the dimension of the Euclidean lattice. In d dimensions a Dirac spinor has $\Delta_f = 2^{[d/2]}$ complex components, where $[d/2]$ is the largest integer which is smaller or equal to $d/2$. For even d there exists a generalization of γ_5 which anticommutes with all γ^μ. If we use the forward (or backward) derivative $\hat{\partial}_\mu$ in the discretization of the continuum action (15.9) in the absence of gauge fields we obtain

$$S_{\text{naive}} = \sum_x \bar{\psi}_x \hat{D} \psi_x, \quad \hat{D} = \gamma^\mu \hat{\partial}_\mu + m. \tag{15.48}$$

But in even dimensions the operator $\hat{D}$ does not possess the γ_5-symmetry (15.7),

$$\gamma_5 \hat{D} \gamma_5 = -\hat{\partial}\!\!\!/ + m \neq D^\dagger,$$

since the hermite conjugate of a forward derivative is the backward derivative. In addition, this implementation violates the cubic symmetry on a hypercubic lattice which is useful to recover the rotational $O(4)$ symmetry on large scales or in the continuum limit. Besides, the reflection hermiticity (the Euclidean counterpart of the hermiticity in Minkowski spacetime) is violated and the theory in Minkowski spacetime lacks unitarity.

One may believe that the antisymmetric lattice derivative $\mathring{\partial}_\mu$ in (15.43) leads to an acceptable lattice Dirac operator since it is γ_5-Hermitian. But this operator

suffers from the *species-doubling problem*. To see this more clearly we calculate the eigenvalues, eigenfunctions and Green function

$$G_{\mathrm{F}}(x,y) = \langle \psi_x \bar{\psi}_y \rangle = \langle x | \frac{1}{\mathring{D}} | y \rangle, \quad \mathring{D} = \gamma^\mu \mathring{\partial}_\mu + m \tag{15.49}$$

with antisymmetric derivatives. First we observe that the lattice Laplacian $\mathring{\Delta}$ in

$$\mathring{D}\mathring{D}^\dagger = \big(\gamma^\mu \mathring{\partial}_\mu + m\big)\big(-\gamma^\mu \mathring{\partial}_\mu + m\big) = \big(-\mathring{\Delta} + m^2\big)\mathbb{1} \tag{15.50}$$

only connects next-to-nearest neighbors on the lattice,

$$(\mathring{\Delta} f)(x) = \frac{1}{4}\sum_\mu \big(f(x+2e_\mu) - 2f(x) + f(x-2e_\mu)\big). \tag{15.51}$$

The plane waves (15.40) are eigenvectors of $\mathring{\Delta}$ with eigenvalues

$$\mathring{p}^2, \quad \mathring{p}_\mu = \sin(p_\mu) \tag{15.52}$$

and this spectrum causes the doubling problem. This becomes clear when we compare (15.51) with the standard lattice Laplacian

$$(\hat{\Delta} f)(x) = \big(\hat{\partial}'_\mu \hat{\partial}^\mu f\big)(x) = \sum_\mu \big(f(x+e_\mu) - 2f(x) + f(x-e_\mu)\big), \tag{15.53}$$

which connects nearest neighbors on the lattice and has the eigenvalues

$$\hat{p}^2, \qquad \hat{p}_\mu = 2\sin\left(\frac{p_\mu}{2}\right). \tag{15.54}$$

Figure 15.4 shows the dispersion relations (15.52) and (15.54) together with the dispersion relation $p \to p^2$ of the continuum operator on the interval of "length" N. We see that for small p_μ the three dispersion relations are identical and in particular that the constant function with zero momentum is an eigenfunction with eigenvalue zero (a zero-mode) of all three operators. But for even N the operator $\mathring{\Delta}$ has not only one but 2^d zero-modes[3] with momenta in the first Brillouin zone,

$$p = (p_0, \ldots, p_{d-1}) \quad \text{and} \quad p_\mu \in \{0, \pi\}. \tag{15.55}$$

The Green function G_{F} of the naive lattice Dirac operator is

$$G_{\mathrm{F}}(x,y) = \frac{1}{V}\sum_p G_{\mathrm{F}}(p) \mathrm{e}^{\mathrm{i}p(x-y)}, \quad G_{\mathrm{F}}(p) = \frac{1}{\mathrm{i}\gamma^\mu \mathring{p}_\mu + m}. \tag{15.56}$$

In the thermodynamic limit the sum over the discrete momenta in (15.56) turns into a Riemann integral over the Brillouin zone,

$$G_{\mathrm{F}}(x,y) \overset{N\to\infty}{\to} \frac{1}{(2\pi)^d}\int_B \mathrm{d}^4 p\, G_{\mathrm{F}}(p). \tag{15.57}$$

[3] Strictly speaking there is only one zero-mode for odd N. But in the thermodynamic limit the momenta on the edge of the Brillouin zone again give rise to zero-modes.

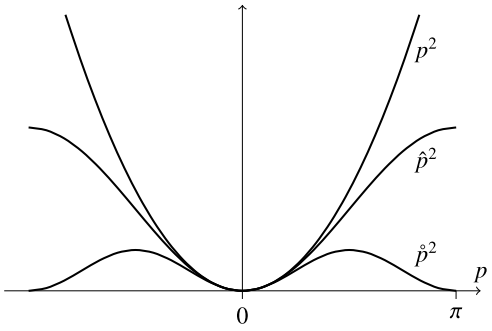

Fig. 15.4 The spectra of two discretizations $\mathring{\Delta}$ and $\hat{\Delta}$ of the Laplace operator on a one-dimensional lattice. For a comparison we also plotted the dispersion relation of the continuum operator on the finite interval

For small momenta the propagator $G_{\mathrm{F}}(p)$ reproduces the correct continuum propagator $G_{\mathrm{F}}(p) \propto (\mathrm{i}\gamma^\mu p_\mu + m)^{-1}$ and for massless fermions has a pole at $p = 0$. The problem is, however, that $G_{\mathrm{F}}(p)$ has not just one but 2^d poles in the Brillouin zone. Thus, the most naive discretization of the continuum theory leads to a lattice discretization with 2^d fermionic species.

15.3.3 Wilson Fermions

K. Wilson has been aware of the doubling problem since the starting years of lattice field theories and suggested a modification of the action in order to get rid of the doublers in the continuum limit [11]. He added a particular momentum-dependent mass term—the Wilson term—to the naive action. This contribution gives a mass to the doublers. In the continuum limit the doublers become infinitely heavy and thus unobservable. Unfortunately at the same time the Wilson term breaks the chiral symmetry of massless theories explicitly. In more detail, on a lattice with lattice spacing a the modified new action reads

$$S_{\mathrm{w}} = S_{\mathrm{naive}} - \frac{r}{2}\sum_x \bar{\psi}_x a\hat{\Delta}\psi_x = \sum_x \bar{\psi}_x D_{\mathrm{w}}\psi_x, \tag{15.58}$$

where the Wilson parameter r in the modified Dirac operator

$$D_{\mathrm{w}} = \mathring{D} - \frac{ar}{2}\hat{\Delta} \tag{15.59}$$

has values in the interval $(0, 1]$. For positive r the Wilson term proportional to r acts like a momentum-dependent mass such that in the massless limit D_{w} does not anticommute with γ_5. This means that the chiral symmetry is explicitly *broken* by the Wilson term. In even dimensions D_{w} is γ_5-hermitian. Without gauge fields it has the eigenvalues

$$\lambda_p = \left(m + \frac{ar}{2}\hat{p}^2\right) \pm \mathrm{i}|\mathring{p}|, \tag{15.60}$$

where we recall the definitions of $\hat{p}_\mu$ and $\mathring{p}_\mu$,

$$\hat{p}_\mu = \frac{2}{a}\sin\left(\frac{ap_\mu}{2}\right), \qquad \mathring{p}_\mu = \frac{1}{a}\sin(ap_\mu), \qquad p_\mu \in \frac{2\pi}{a}\frac{n_\mu}{N}. \tag{15.61}$$

In the following we often use the lattice spacing a as length scale. To localize the eigenvalues of the Wilson operator in the complex plane we set $t_\mu = -\cos(p_\mu)$. In the thermodynamic limit the lattice momentum has its values in the Brillouin zone such that the t_μ vary smoothly between -1 and 1 and define a d-dimensional cube. The map $\{t_\mu\} \to \lambda(t)$ defined by (15.60) maps the edges of this cube into d ellipses with semi-major axes r and 1 and equidistant centers on the real axis,

$$(m + r, 0), (m + 3r, 0), \ldots, (m + 2d - 1, 0). \tag{15.62}$$

The ellipses are symmetrical to the real axis, touch each other on the real axis and form the inner boundary of the spectrum of the Wilson operator, i.e. the set of eigenvalues of D_w. Next we observe that the momenta with equal coordinates $t_\mu = t$ are mapped to an ellipse with semi-major axes rd and $d^{1/2}$ and center at $(0, m + rd)$. This ellipse encloses the smaller ellipses and forms the outer boundary of the spectrum.

Thus the shaded area in Fig. 15.5 represents the spectrum of the 4-dimensional Wilson operator in the thermodynamic limit. For $r \to 0$ we recover the spectrum of the naive Dirac operator $\mathring{D}$, i.e. the interval connecting $m - \mathrm{i}d^{1/2}$ and $m + \mathrm{i}d^{1/2}$. In the massless limit the eigenvalues on the real axis at $0, 2r, 4r, \ldots$ become the annoying doublers of the naive Dirac operator when $r \to 0$. In one dimension there is only one inner ellipse and this ellipse coincides with the outer one. Hence all eigenvalues are located on the ellipse centered at $m + r$ with semi-major axes r and 1. The value $r = 1$ corresponds to the backward derivative, the value $r = -1$ to the forward derivative and the value $r = 0$ to the antisymmetric derivative. In the latter case all eigenvalues are located on the interval $m + \mathrm{i}[-1, 1]$. In the limit $r \to 0$ the eigenvalues $m + 2r$ and m are degenerate and we recover the species-doubling problem.

To investigate the naive continuum limit of the Wilson operator we momentarily re-install the lattice spacing a in the mass, eigenvalues and momenta. With decreasing a the center of the outer ellipse at $(m + rd/a, 0)$ moves away from the origin and at the same time the semi-major axes rd/a and $d^{1/2}/a$ become large. The same applies to the inner ellipses at

$$(m + r/a, 0), (m + 3r/a, 0), \ldots, \big(m + (2d - 1)/a, 0\big)$$

with semi-major axes r/a and $1/a$. In the continuum limit only the inner ellipse next to the imaginary axis and the outer ellipse remain, and they converge to the line $m \pm \mathrm{i}|p|$ defining the spectrum of the continuum operator. More accurately, the dimensionful eigenvalues of D_w have the following expansion for small a:

$$\lambda_p = m + \frac{ar}{2}\hat{p}^2 \pm \mathrm{i}|\mathring{p}| = m \pm \mathrm{i}|p| + \frac{1}{2}(ar)p^2 + O\big(a^2\big). \tag{15.63}$$

Thus for $a \to 0$ we recover the spectrum of the free Dirac operator in the continuum. For Wilson's choice $r = 1$ the eigenvalues contain errors of order a, to be compared with $O(a^2)$ for naive, staggered or SLAC fermions.

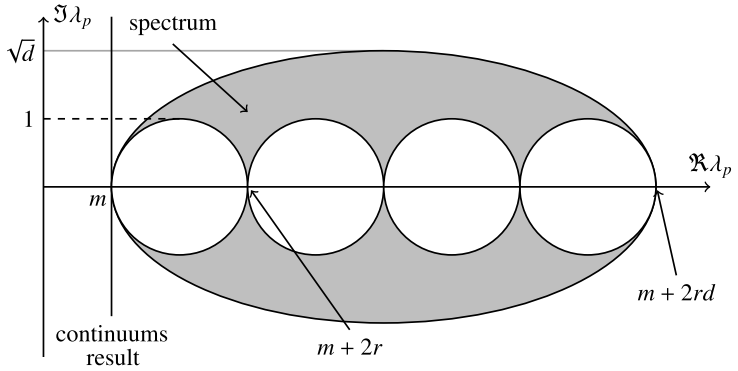

Fig. 15.5 The complex eigenvalues of the free massive Wilson operator D_w in the thermodynamic limit define the shaded region. Depicted is the spectrum for Wilson parameter $r = 1$ for which the inner ellipses become circles

15.3.4 Staggered Fermions

Staggered fermions are obtained from naive fermions by redistributing the spinor degrees of freedom across different lattice sites [12]. As a result, staggered fermions describe a theory with much less doublers as naive fermions. In addition they are relatively easy and fast to implement in simulations. To begin with, consider the naive fermion action for spinor field with $\Delta_f = 2^{[d/2]}$ components,

$$S_\mathrm{naive} = \sum_{x,\mu} \bar{\psi}_x \gamma^\mu (\mathring{\partial}_\mu \psi)_x + m \sum_x \bar{\psi}_x \psi_x . \tag{15.64}$$

Now we perform the site-dependent similarity transformation

$$\psi_x = T(x)\chi_x, \qquad \bar{\psi}_x = \bar{\chi}_x T^\dagger(x), \qquad T(x) = \gamma_0^{x_0} \cdots \gamma_{d-1}^{x_{d-1}}, \tag{15.65}$$

which diagonalizes the Dirac operator in spin space. With the help of

$$T^\dagger(x)\gamma^\mu T(x \pm e_\mu) = \Gamma_\mu(x)\mathbb{1}_{\Delta_f}, \quad \Gamma_\mu(x) = (-1)^{x_0 + x_1 \ldots + x_{\mu-1}} \tag{15.66}$$

the action transforms into a sum of identical actions for the components χ_α of ψ,

$$S_\mathrm{naive}[\bar{\psi}, \psi] = \sum_{\alpha=1}^{\Delta_f} S_\mathrm{s}[\bar{\chi}_\alpha, \chi_\alpha], \qquad S_\mathrm{s}[\bar{\chi}, \chi] = \sum_x \chi_x^* (Q_\mathrm{s}\chi)_x , \tag{15.67}$$

where the (normal) matrix Q_s acts on the one-component χ as follows,

$$(Q_\mathrm{s}\chi)(x) = \sum_\mu \Gamma_\mu(x)(\mathring{\partial}_\mu \chi)_x + m\chi_x . \tag{15.68}$$

To decrease the number of doublers we keep only *one* of the Δ_f identical terms and this single term is just the action for staggered fermions. As a result we are dealing with only one fermionic degree of freedom per lattice site. The site-dependent phases $\Gamma_\mu(x)$ in Q_s are remnants of the Dirac structure. With this clever trick, one

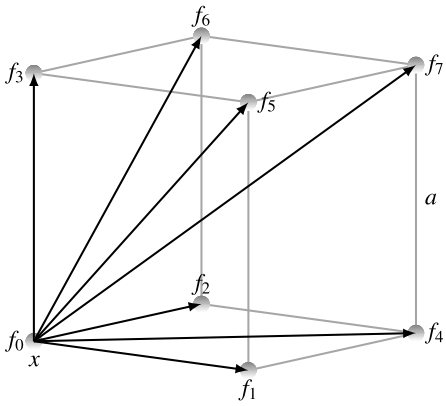

Fig. 15.6 Dirac spinor fields at x are constructed from the one-component field χ on the 2^d corners of the hypercubes of the lattice specified by the base point x and the vectors f_ρ. The vector f_0 is the null vector

can reduce the 2^d-fold degeneracy by a factor Δ_f without losing the original chiral symmetry completely. The action for staggered fermions still admits an Abelian $U(1) \times \mathbb{R}_+$ symmetry. We show this by introducing the lattice function

$$\varepsilon(x) = (-1)^{x_0+x_1+\cdots+x_{d-1}}, \tag{15.69}$$

which is 1 on the even sub-lattice and -1 on the odd sub-lattice. In the massless limit the action is a sum of nearest-neighbor interaction terms and each term contains the product of the field on an even site and the field on an odd site. Thus the reduced action retains the $U(1) \times \mathbb{R}_+$ part of the original symmetry:

$$\chi_x \to \mathrm{e}^{\mathrm{i}g\lambda+\alpha\varepsilon(x)}\chi_x, \qquad \chi_x^* \to \chi_x^* \mathrm{e}^{-\mathrm{i}g\lambda+\alpha\varepsilon(x)}. \tag{15.70}$$

Clearly the mass term $\chi_x^*\chi_x$ acquires a factor $\mathrm{e}^{2\alpha\varepsilon(x)}$ and is not invariant under transformations with non-zero α. The symmetry (15.70) is enough to prevent the occurrence of mass counterterms in the renormalization process: $m_{\text{bare}} = 0$ implies $m_{\text{ren}} = 0$. The $\mathbb{R}_+$ symmetry becomes a flavor non-singlet axial symmetry in the continuum limit. Its possible spontaneous breaking produces a Goldstone boson for any value of the lattice spacing.

By keeping just one of the Δ_f identical contributions to the action in (15.67) we did not remove all of the 2^d doublers from the theory. In even dimensions we are still left with $2^{d/2}$ fermion species and in odd dimensions with $2^{(d+1)/2}$ species. For simplicity we assume now that d is even. From the one-component field χ we can reconstruct $2^{d/2}$ flavors of Dirac spinors on 2^d disjoint sub-lattices $\{\Lambda_\rho\}$ with lattice spacing $2a$. The sub-lattices are defined by the 2^d corners of a given elementary hyper-cube on the lattice, see Fig. 15.6, as follows: Let $\{f_\rho\}$ be the lattice vectors pointing from a fixed corner x of the cube to all corners of the cube. In particular $f_0 = 0$. Then the field χ_ρ on the sub-lattice Λ_ρ is given by (we set $a = 1$)

$$\chi_{\rho,x} = \chi_{2x+f_\rho}, \quad \rho = 0, \ldots, 2^d - 1. \tag{15.71}$$

Finally from the one-component fields $\{\chi_\rho\}$ on the coarse lattices we may reconstruct $2^{d/2}$ flavors of Dirac fields ψ^f, usually called 'tastes' to distinguish them from real flavors, with components ψ^f_α as follows:

$$\hat{\psi}^f_{\alpha,x} = \mathcal{N}_0 \sum_\rho (T_\rho)_{\alpha f}\, \chi_{\rho,x}, \quad \alpha, f = 1, \ldots 2^{d/2}, \tag{15.72}$$

where the matrices T_ρ are given by

$$T_\rho = \gamma_0^{\rho_0} \gamma_1^{\rho_1} \cdots \gamma_{d-1}^{\rho_{d-1}}. \tag{15.73}$$

The staggered fermion description has, however, some unpleasant features as well. Flavor (or taste) symmetry is explicitly broken and hoped to be recovered only in the continuum limit. In addition it is non-trivial to construct baryon operators with definite quantum numbers. Finally, in order to obtain a theory with a single physical flavor, one usually takes the fourth root of the fermionic determinant for staggered fermions. This is correct in the free theory, but we do not know for sure whether this non-local prescription makes sense non-perturbatively [20, 21].

15.4 Nielsen–Ninomiya Theorem

The lattice fermions discussed so far are all afflicted with certain problems. Naive fermions and staggered fermions show fermion doubling, Wilson fermions break chiral symmetry explicitly and staggered fermions break chiral symmetry partially. In this section we shall shed light on the doubling problem in a more general fashion with the help of the *Nielsen–Ninomiya no-go theorem* [22–24]. First, consider an arbitrary bilinear action

$$S = \sum_{x,y} \bar{\psi}_x M(x, y) \psi_y \tag{15.74}$$

for spin-1/2 lattice fermions. Because of translational invariance, the Dirac operator depends only on the difference $x - y$, i.e.

$$M(x, y) = D(x - y). \tag{15.75}$$

We may now ask the question, why the discretization of fermions without doublers and under conservation of chiral symmetry is as hard as it is? This question is answered by the no-go theorem which says that the phenomenon of fermion doubling occurs, provided that we only assume some general properties of the action as locality, hermiticity and translational invariance. Thereby, one finds an equal number of left- and right-handed fermions. More precisely, the theorem states:

Theorem 15.1 (Nielsen–Nynomyia theorem) *There exists no translational invariant Dirac operator that fulfills the four following properties*:

1. *locality*: $D(x - y) \lesssim \mathrm{e}^{-\gamma|x-y|}$,
2. *continuum limit*: $\lim_{a\to 0} \tilde{D}(p) = \sum_\mu \gamma^\mu p_\mu$,

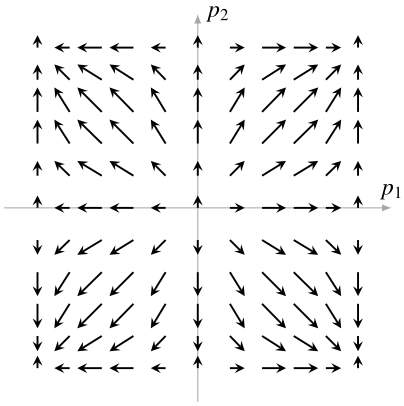

Fig. 15.7 The vector field $\tilde{D}_\mu(p)$ of the naive Dirac operator in two dimensions. The vector field has four zeroes in the Brillouin zone. Two zeros have winding number 1 and two zeros have winding number -1

3. *no doublers*: $\tilde{D}(p)$ *is invertible if* $p \neq 0$,
4. *chirality*: $\{\gamma_5, D\} = 0$.

Locality implies the Fourier transform $\tilde{D}$ of D to be an analytic and periodic function of the momenta p_μ with period $2\pi/a$. The second and third assumption guarantee the correct continuum limit of D. References [22–24] give a proof of the theorem by homotopy theory. Readers interested in a proof based on elegant arguments from differential geometry should consult [25].

Proof We shall give a proof under the additional assumption [10]

$$\tilde{D}(p) = \sum \gamma^\mu \tilde{D}_\mu(p) \quad \text{with } \tilde{D}_\mu(p) \in \mathbb{R} \tag{15.76}$$

in momentum space, where the *analytic* functions $\tilde{D}_\mu$ tend to p_μ for small momenta. Since the Brillouin zone shows the topology of a torus in d dimensions, $\tilde{D}_\mu$ defines a vector field $\tilde{D}$ on T^d. We now assign an index to every zero p_i of this vector field, whereby we assume the number of zeros to be finite. According to a theorem by HOPF and POINCARÉ, the sum of the indices of all zeros on a compact and oriented manifold is equal to the Euler characteristic of the manifold,

$$\sum_{\text{zeroes}\, p_i} \text{index}\big(\tilde{D}(p_i)\big) = \chi\big(\mathrm{T}^d\big). \tag{15.77}$$

Thereby the index of $\tilde{D}$ at a zero p_i is equal to the degree of the induced map (the winding number) from the boundary of a small ball centered at p_i into $\mathbb{R}^d - 0$. Figure 15.7 shows the vector field $\tilde{D}(p)$ of the naive Dirac operator in two dimensions in the first Brillouin zone. The vector field has index 1 at the zeros $p = (0, 0)$ and (π, π) and index -1 at the zeros $p = (0, \pi)$ and $(\pi, 0)$. The sum of the indices vanishes in accordance with the fact that the Euler-characteristics of the torus vanishes, $\chi(\mathrm{T}^d) = 0$. The figure shows clearly the doublers at momenta $(\pi, 0), (0, \pi)$ and (π, π).

Similarly, on the d-dimensional torus the zeros of $\tilde{D}$ occur in pairs with opposite indices. To see this we expand $\tilde{D}$ around a zero p_0 according to

$$\tilde{D}_\mu(p) = A_{\mu\nu}(p-p_0)^\nu + \cdots, \quad A_{\mu\nu} = \frac{\partial \tilde{D}_\mu}{\partial p_\nu}\bigg|_{p_0}.$$

The index of the vector field $\tilde{D}$ at its zero is equal to the sign of $\det A$. For example, if A is diagonal at the zero $p_0 = 0$ then we have $\tilde{D}_\mu(p) = A_\mu p_\mu + O(p^2)$. If in four dimensions $A = \mathrm{diag}(1,1,1,1)$, the index is equal to 1 and we find

$$\bar{\psi}\gamma^\mu \tilde{D}_\mu(p)\psi \approx \bar{\psi}\gamma^\mu p_\mu \psi \tag{15.78}$$

in the vicinity of the zero. Recall that the field ψ transforms under a chiral transformation into $\exp(\alpha\gamma_5)\psi$. In contrast, if $A = \mathrm{diag}(-1,1,1,1)$, the vector field has index -1 and the Lagrangian density in the vicinity of the zero $p_0 = 0$ has the form

$$\bar{\psi}\gamma^\mu \tilde{D}_\mu(p)\psi \approx \bar{\psi}\gamma_5\gamma^0\big(\gamma^\mu p_\mu\big)\gamma^0\gamma_5\psi \equiv \bar{\chi}\not{p}\chi. \tag{15.79}$$

Clearly $\chi = \gamma^0\gamma_5\psi$ is to be interpreted as Dirac field of the doubler. Under chiral transformations it transforms according to $\exp(-\alpha\gamma_5)\chi$ such that the two fermion species have opposite chirality. Every pole of the massless propagator corresponds to a fermionic one-particle state. Thus, we conclude that a fermion of chirality $+1$ is always accompanied by a fermion of chirality -1. □

15.5 Ginsparg–Wilson Relation and Overlap Fermions

The Nielsen–Ninomiya no-go theorem makes clear that under certain conditions it is impossible to find a chirally invariant Dirac operator without the appearance of doublers. Similarly as with many other no-go theorems there is a way to bypass it. The solutions of the doubler problem are based on a paper published in 1982 by GINSPARG and WILSON [26]. They asked thereby the question "... how can a lattice theory serve to represent a continuum situation where the symmetry does not suffer explicit breaking?".

To begin with they considered a chirally invariant continuum theory which is mapped to a lattice theory via a block spin transformation. In detail, the continuum field ϕ on $\mathbb{R}^d$ is related via a block spin transformation to the lattice field ψ:

$$\psi_x = \int \mathrm{d}^d y\, \alpha(x-y)\phi(y), \quad x \in \Lambda. \tag{15.80}$$

Thereby the exact form of the weight function α is irrelevant. Then Ginsparg and Wilson analyzed the lattice action induced by the blocking transformation and how much it deviates from a chirally invariant action. They discovered that operators which solve the *Ginsparg–Wilson relation*

$$\gamma_5 D + D\gamma_5 = aD\gamma_5 D \tag{15.81}$$

yield optimal lattice operators. The lattice spacing a on the right hand side ensures the proper continuum relation $\gamma_5 D + D\gamma_5 = 0$ on macroscopic scales (or for sufficiently small a). By multiplying the relation (15.81) with $S = D^{-1}$, we find

$$S\gamma_5 + \gamma_5 S = a\gamma_5 \quad \text{or} \quad S(x,y)\gamma_5 + \gamma_5 S(x,y) = a\gamma_5 \delta_{x,y}. \tag{15.82}$$

This means that chiral symmetry breaking as encoded in the propagator is *ultralocal*, i.e. we obtain a chirally invariant propagator for all finite distances $|x - y| > 0$. The property (15.82) is sufficient to preserve many relevant consequences of chiral symmetry as e.g. the absence of an additive mass renormalization on the lattice.

The new developments have been triggered by the rediscovery of the Ginsparg–Wilson relation by P. HASENFRATZ [34–36] and an explicit solution of the Ginsparg–Wilson relation by H. NEUBERGER [40, 41]. M. LÜSCHER noticed that the fermionic action

$$S_{\mathrm{F}} = a^d \sum_{x,y} \bar{\psi}_x D(x-y)\psi_y \tag{15.83}$$

admits a continuous symmetry if the Dirac operator satisfies the Ginsparg–Wilson relation [27]. The symmetry is interpreted as lattice version of the chiral symmetry and reads

$$\psi \to \psi_{(\alpha)} = \mathrm{e}^{\alpha\gamma_5(1-aD/2)}\psi \quad \text{and} \quad \bar{\psi} \to \bar{\psi}_{(\alpha)} = \bar{\psi}\mathrm{e}^{\alpha(1-aD/2)\gamma_5}. \tag{15.84}$$

It is not difficult to show that the bilinear $\bar{\psi} D\psi$ is invariant:

$$\frac{\mathrm{d}}{\mathrm{d}\alpha}\left(\bar{\psi}_{(\alpha)} D \psi_{(\alpha)}\right) = \bar{\psi}_{(\alpha)} \left\{ \left(1 - \frac{1}{2}aD\right)\gamma_5 D + D\gamma_5 \left(1 - \frac{1}{2}aD\right) \right\} \psi_{(\alpha)} \overset{(15.81)}{=} 0.$$

However, in general the fermionic integration measure $\mathscr{D}\psi\mathscr{D}\bar{\psi}$ is not invariant under the deformed chiral transformations (15.84). This fact ensures the occurrence of the *axial anomaly* in presence of an external gauge field. Examples of lattice Dirac operators that satisfy the Ginsparg–Wilson relations are:

1. domain wall fermions [28–30],
2. overlap operators [31–33, 40, 41],
3. fixed-point operators [34–36],
4. chirally improved operators [37–39].

In the following section we shall discuss the overlap operators introduced by Neuberger and Narayanan.

15.5.1 Overlap Fermions

An elegant solution of the Ginsparg–Wilson relation—the overlap operator—has been constructed in the pioneering contributions [31–33, 40, 41]. The operator has the form

$$D_o = \frac{1}{a}(\mathbb{1} + V), \qquad V = \left(D_{\mathrm{w}} D_{\mathrm{w}}^{\dagger}\right)^{-1/2} D_{\mathrm{w}}, \quad m < 0, \tag{15.85}$$

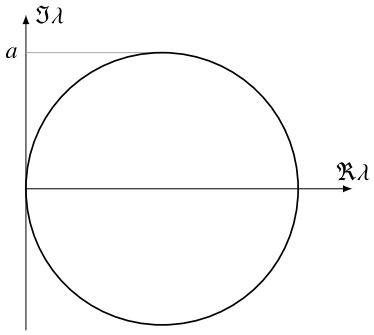

Fig. 15.8 The eigenvalues of the overlap operator are located on a Ginsparg–Wilson circle that touches the imaginary axis at the origin

where D_{w} denotes the Wilson operator. Dividing D_{w} by its modulus yields a unitary operator V with its spectrum on the unit circle. Correspondingly, the overlap operator has its eigenvalues on a circle that touches the imaginary axis at the origin, as shown in Fig 15.8. Let us show that the overlap operator solves the Ginsparg relation (15.81). In terms of the unitary operator V the left hand side reads

$$D_o\gamma_5 + \gamma_5 D_o = \frac{2}{a}\gamma_5 + \frac{1}{a}\{\gamma_5, V\}. \tag{15.86}$$

To rewrite the right hand side we use the following properties of the Wilson operator:

$$\left[D_{\mathrm{w}}, D_{\mathrm{w}}^\dagger\right] = 0, \qquad \gamma_5 D_{\mathrm{w}} = D_{\mathrm{w}}^\dagger \gamma_5, \qquad \left[D_{\mathrm{w}} D_{\mathrm{w}}^\dagger, \gamma_5\right] = 0, \tag{15.87}$$

which imply $V\gamma_5 V = \gamma_5$. Now the right hand side of the relation reads

$$a D_o \gamma_5 D_o = \frac{1}{a}\big(\gamma_5 + \{\gamma_5, V\} + V\gamma_5 V\big) = \frac{2}{a}\gamma_5 + \frac{1}{a}\{\gamma_5, V\} \tag{15.88}$$

and it is equal to the left hand side in (15.86).

15.5.2 Locality

One disadvantage of the overlap operator is the appearance of the inverse of the modulus $(D_{\mathrm{w}} D_{\mathrm{w}}^\dagger)^{1/2}$ of the Wilson operator. It is not evident that D_o is a local operator. In general, we distinguish between *ultralocal* operators, where $D(x-y)$ vanishes exactly if $|x-y| > \ell$ and *local* operators, where $D(x-y)$ decreases exponentially as a function of the distance $|x-y|$ on the lattice. In the continuum limit local operators become *exact* local operators. By considering the spectral representation of the operator D_o, we can analyze its locality behavior. Since

$$D_{\mathrm{w}} D_{\mathrm{w}}^\dagger = -\mathring{\Delta} + \left(m - \frac{ar}{2}\Delta\right)^2, \tag{15.89}$$

the overlap operator in Fourier space may be written as

$$a\tilde{D}_o(p) = 1 + \left\{\mathrm{i}\gamma^\mu \mathring{p}_\mu + m + \frac{ar}{2}\hat{p}^2\right\}\left\{\mathring{p}^2 + \left(m + \frac{ar}{2}\hat{p}^2\right)^2\right\}^{-1/2}. \tag{15.90}$$

The operator satisfies the first three conditions stated in the Nielsen–Ninomiya theorem. In particular, $\tilde{D}_o(p)$ is analytical and thus the operator $D_o(x-y)$ in position space vanishes exponentially with increasing distances $|x-y|$. One assumption of the Nielsen–Ninomiya theorem is not satisfied, since the chiral symmetry is realized differently. The Ginsparg–Wilson relation allows for a very soft breaking of the usual chiral symmetry such that the propagating states are effectively chiral and all physical consequences of chiral symmetry are preserved.

To summarize: The overlap operator by Neuberger and Narayanan is local, shows no fermion doubling and preserves (a deformed) chiral symmetry. However, since the inversion of $D_{\mathrm{w}} D_{\mathrm{w}}^{\dagger}$ in presence of gauge fields is quite time-consuming the overlap operator may not always be the best choice in simulations. In addition, if $m = 0$ there may appear zero-modes for non-vanishing gauge fields. Indeed, Ginsparg–Wilson operators obey an exact Atiyah–Singer index theorem on the lattice and thus there are zero-modes for topologically non-trivial background fields [42].

15.6 Yukawa Models on the Lattice

Yukawa models can be used to describe the strong nuclear force between nucleons mediated by pions. The Yukawa interaction between fermions and scalar or pseudoscalar particles is also used in the Standard Model of particle physics to describe the coupling between the Higgs field and massless quark and lepton fields. Through spontaneous symmetry breaking, these fermions acquire a mass proportional to the vacuum expectation value of the Higgs field. A Yukawa interaction has the form

$$y\bar{\psi}\phi\psi \quad \text{or} \quad \mathrm{i}y\bar{\psi}\gamma_5\phi\psi. \tag{15.91}$$

If the fermions and (pseudo)scalars transform according to a non-trivial representation of some internal symmetry group then the trilinears must be invariant. The full Euclidean action of the Yukawa model (with scalar field) reads

$$S = \int \mathrm{d}^d x\, \mathscr{L}(\phi,\psi), \quad \mathscr{L} = \frac{1}{2}(\nabla\phi)^2 + V(\phi) + \bar{\psi}(\not{\partial} + m)\psi + y\bar{\psi}\phi\psi, \tag{15.92}$$

where the potential V is invariant $V(\Omega\phi) = V(\phi)$. Suppose that the classical potential V has a minimum at a constant field $\phi_0 \neq 0$ which is not invariant under the symmetry transformations. Then the classical vacuum configuration breaks the internal symmetry. Expanding the action about ϕ_0 in powers of $\chi = \phi - \phi_0$ we see that the Yukawa interaction yields a term $y\phi_0\bar{\psi}\psi$, which is just a mass term for the fermions with fermion mass $y\phi_0$. The field χ is known as a Higgs field.

The same spontaneous symmetry breaking occurs in the quantized theory if the scalar field acquires a non-zero vacuum expectation value, similar to a non-zero magnetization in spin models. The lattice formulation enables us to study Yukawa theories at strong Yukawa coupling y. On a lattice the expectation value of an observable is given by

$$\left\langle O(\phi,\psi,\bar{\psi})\right\rangle = \frac{1}{Z}\int \mathscr{D}\phi\mathscr{D}\psi\mathscr{D}\bar{\psi}\, O(\phi,\psi,\bar{\psi})\mathrm{e}^{-S[\phi,\psi,\bar{\psi}]}, \tag{15.93}$$

where S is some lattice version of the continuum action (15.92), e.g.

$$S = \frac{1}{2}\sum_{\langle x,y\rangle}(\phi_x - \phi_y)^2 + \sum_x V(\phi_x) + \sum_{x,y}\bar{\psi}_x D(x-y)\psi_y + y\sum_y \bar{\psi}_x\phi_x\psi_x. \tag{15.94}$$

In the normalizing partition function we can integrate over the fermionic degrees of freedom and obtain the determinant of $D + y\phi$,

$$Z = \int \mathscr{D}\phi\mathscr{D}\psi\mathscr{D}\bar{\psi}\mathrm{e}^{-S[\phi,\psi,\bar{\psi}]} = \int \mathscr{D}\phi\,\det(D+y\phi)\mathrm{e}^{-S_\mathrm{B}(\phi)}, \tag{15.95}$$

where S_B denotes the bosonic part of the action, i.e. the ψ-independent part of S in (15.94). For a real scalar field the operator $D + y\phi$ is γ_5-Hermitian and hence has real determinant. But the sign of the determinant may depend on the scalar field and may give rise to the sign problem, in particular for a strong Yukawa coupling y.

15.6.1 Higgs Sector of Standard Model

The Higgs sector of the Standard Model of particle physics represents a $4d$ Yukawa model. A careful analysis of this sector reveals that it defines a trivial theory. Triviality refers to the behavior of the renormalized quartic coupling constant λ_r of the scalar field in dependence on the cutoff parameter Λ. The cutoff has to be introduced to regularize the theory. In a renormalizable theory the cutoff parameter can be sent to infinity while holding all physical observables constant, making the physical predictions arising from such a theory eventually independent of the previously introduced auxiliary parameter Λ, as desired. In a trivial theory, however, all renormalized coupling constants vanish as function of the cutoff parameter in the limit $\Lambda \to \infty$, leading to a free, non-interacting theory when we try to remove the cutoff. Thus the Higgs sector of the Standard Model can only be considered as an effective theory connected with a non-removable cutoff parameter, which can be interpreted as the maximal scale up to which the underlying effective theory can be trusted. As a consequence the renormalized quartic coupling constant at a given cutoff Λ is bounded from above according to $\lambda_r(\Lambda) \le \lambda_{\mathrm{up},r}(\Lambda)$. This bound translates into an upper bound $m_{\mathrm{up},H}(\Lambda)$ on the Higgs boson mass and this bound decreases with increasing cutoff [43]. This remarkable fact tells us that once the Higgs boson has been discovered and its physical mass m_H measured, it would be possible to infer the scale up to which the Standard Model can be valid at most from the comparison of m_H with its cutoff-dependent upper bound.

Early attempts to simulate the Higgs–Yukawa sector of the Standard Model had problems with removing the fermion doublers from the spectrum while maintaining chiral symmetry. More recently P. GERHOLD AND K. JANSEN employed the overlap construction for the free Dirac operator D to simulate the chirally invariant Higgs–Yukawa model. They obtained reliable upper (and lower) bounds on the Higgs boson mass as a function of the cutoff parameter [44, 45]. For example, they conclude that if the cutoff is at $\Lambda = 1.5$ TeV then the mass must be in the range between 50 GeV and 650 GeV. On the other hand, for a Higgs boson mass of about 125 GeV the Standard Model can be valid up to very large cutoff scales.

15.6.2 Supersymmetric Yukawa Models

Supersymmetry is an important ingredient of modern high energy physics beyond the standard model. Since boson masses are protected by supersymmetry in such theories with chiral fermions, it helps to reduce the hierarchy and fine-tuning problems drastically. However, as low energy physics is manifestly not supersymmetric, this symmetry has to be broken at some energy scale. In the case of supersymmetric field theories, a lattice formulation is hampered by the fact that the supersymmetry algebra closes on the generator of infinitesimal translations which do not exist on a discretized spacetime. A related fact is that lattice derivatives do not satisfy the Leibniz rule implying that supersymmetric actions will in general not be invariant under lattice supersymmetries. In generic lattice formulations there are no discrete remnants of supersymmetry transformations on the lattice; in such theories, supersymmetry in the continuum limit can only be recovered by appropriately fine-tuning the bare couplings of all supersymmetry-breaking counterterms.

Particular simple supersymmetric Yukawa theories—Wess–Zumino models in two dimensions—have been the subject of intensive analytic and numerical investigations [46–49]. The models with two supersymmetries contain one Dirac spinor and two real scalar fields. The simpler models with just one supersymmetry contain one real Majorana spinor field and one real scalar field and have the action

$$S = \int \mathrm{d}^2x \frac{1}{2}\big((\partial_\mu\phi)^2 + \bar\psi D\psi + \mathscr{P}(\phi)^2\big), \quad D = \partial\!\!\!/ + \mathscr{P}'(\phi), \tag{15.96}$$

with superpotential $\mathscr{P}$. It is invariant under the supersymmetry transformations

$$\delta\phi = \bar\varepsilon\psi, \qquad \delta\psi = \big(\partial\!\!\!/\phi - \mathscr{P}(\phi)\big)\varepsilon. \tag{15.97}$$

The constant and anticommuting Majorana spinor ε parametrizes the infinitesimal supersymmetry transformation. For models with even superpotential the bosonic part of the action is invariant under a reflection of the scalar field $\phi \to -\phi$. Since

$$\partial\!\!\!/ + \mathscr{P}'(-\phi) = \partial\!\!\!/ - \mathscr{P}'(\phi) = -\gamma_5\big(\partial\!\!\!/ + \mathscr{P}(\phi)\big)\gamma_5 \tag{15.98}$$

the fermionic determinant $\det(D)$ is also invariant under a reflection of the scalar field. In a series of papers various discretizations of models with one or two supersymmetries have been studied and compared [17, 18, 50]. For the models based on the SLAC derivative (introduced on p. 357) for both bosonic and fermionic fields the fermionic operator is γ_5-hermitian and the internal continuum symmetries are realized on the lattice. When one analyzes supersymmetric Ward identities and the particle spectrum one sees that the models with SLAC derivative are superior to other discretizations and yield accurate results already on moderately sized lattices.

Let us consider the model with one supersymmetry and even superpotential

$$\mathscr{P}(\phi) = \frac{\mu_0^2}{\sqrt{2\lambda}} + \sqrt{\frac{\lambda}{2}}\phi^2 \quad \Longrightarrow \quad V(\phi) \equiv \frac{\mathscr{P}(\phi)^2}{2} = \frac{\mu_0^2}{2}\phi^2 + \frac{\lambda}{4}\phi^4 + \text{const.} \tag{15.99}$$

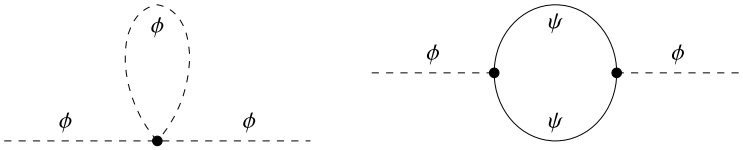

Fig. 15.9 The divergent Feynman diagrams of the Wess–Zumino model in the Z_2 symmetric phase

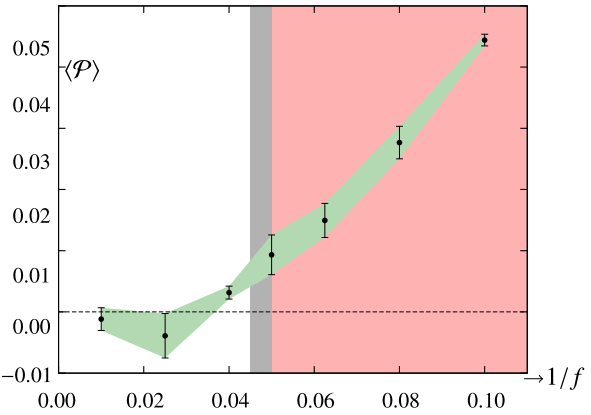

Fig. 15.10 Dimensionless prepotential $\mathscr{P}$ over inverse coupling f^{-1}. The *shaded region* on the right is the Z_2 symmetric phase where SUSY is broken while the *small shaded region* in the *middle* gives the error bound for the Z_2 phase transition

It has vanishing Witten index and hence (at least) two degenerate ground states. One expects that for fixed λ and $\mu_0^2 \ll 0$ the system cannot tunnel between the two ground states so that supersymmetry is unbroken. On the other hand, for $\mu_0^2 > 0$ both ground state energies are lifted above zero and supersymmetry is broken [51, 52]. Two comments should be made at this point. Firstly the analysis of the divergent diagrams in Fig. 15.9 shows that a logarithmic renormalization of the bare mass parameter is necessary to cancel divergent contributions. The renormalization procedure amounts to a normal ordering of interaction terms with respect to a mass parameter in the symmetric phase, for details see [50]. The dimensionless renormalized coupling $f = \lambda/\mu^2$ distinguishes between the Z_2-symmetric phase and broken phase or the phase without supersymmetry and the phase with supersymmetry. Figure 15.10 shows the continuum-extrapolated expectation values of the superpotential. For strong couplings f the expectation value vanishes such that supersymmetry is realized and the Z_2-symmetry is broken. On the other hand, for weak couplings we are in the Z_2-symmetric phase and supersymmetry is dynamically broken. Secondly, the fermionic integral for a theory with Majorana fermions yields the Pfaffian in place of the determinant. Up to a sign the Pfaffian of an antisymmetric matrix is the square root of its determinant. Further properties of the Pfaffian are discussed on p. 379.

15.7 Coupling to Lattice Gauge Fields

Similarly as on p. 351 we consider a collection of Dirac fields with values in $V \otimes \mathbb{C}^{\Delta_f}$. A global symmetry transformation $\psi \to \Omega\psi$ only acts in the vector space V such that the Ω-invariance of the scalar product implies the invariance of the lattice action

$$S_{\mathrm{F}} = \sum_x \bar{\psi}_x (D\psi)_x. \tag{15.100}$$

Replacing lattice derivatives by covariant lattice derivatives one obtains an action which is invariant under (local) gauge transformations $\psi_x \to \Omega(x)\psi_x$. For Wilson fermions with Wilson parameter r the Dirac operator has the form

$$(D_{\mathrm{w}})_{xy} = (m + rd)\delta_{xy} - \frac{1}{2}\sum_{\mu=0}^{d-1}\big((r+\gamma^\mu)U_{y,-\mu}\delta_{x,y-e_\mu} + (r-\gamma^\mu)U_{y,\mu}\delta_{x,y+e_\mu}\big). \tag{15.101}$$

A parametrization introduced by Wilson follows from rescaling

$$\psi \to \frac{1}{\sqrt{m+rd}}\psi, \qquad \bar{\psi} \to \bar{\psi}\frac{1}{\sqrt{m+rd}},$$

and yields the following form for the gauge invariant action:

$$S_{\mathrm{w}} = \sum_x \bar{\psi}_x\psi_x - \kappa\sum_{x,\mu}\big(\bar{\psi}_{x-e_\mu}(r+\gamma^\mu)U_{x,-\mu}\psi_x + \bar{\psi}_{x+e_\mu}(r-\gamma^\mu)U_{x,\mu}\psi_x\big), \tag{15.102}$$

where $\kappa = (2m+2rd)^{-1}$ is called *hopping parameter*. In quantum chromodynamics (QCD) m is a diagonal matrix in flavor space and r is usually chosen flavor independent, mostly $r = 1$. The action for Wilson fermions breaks the chiral symmetry explicitly. Unfortunately, in lattice QCD this leads to a variety of complications. In particular, recovering chiral symmetry in the continuum limit requires unnatural fine-tuning of the bare fermion mass or, equivalently, the hopping parameter.

Gauge theories in particle physics contain both fermions and gauge bosons and one is confronted with lattice path integrals of the form

$$Z = \int \prod_\ell \mathrm{d}U_\ell \prod_x \mathrm{d}\psi_x\,\mathrm{d}\bar{\psi}_x\,\mathrm{e}^{-S_{\mathrm{gauge}}(U)-S_{\mathrm{F}}(\psi,\bar{\psi})} \tag{15.103}$$

$$= \int \prod_\ell \mathrm{d}U_\ell \det\big(D[U]\big)\mathrm{e}^{-S_{\mathrm{gauge}}(U)} \tag{15.104}$$

$$= \int \prod_\ell \mathrm{d}U_\ell \operatorname{sign}(\det D)(\det M)^{1/2}\mathrm{e}^{-S_{\mathrm{gauge}}(U)}, \tag{15.105}$$

where $M = D^\dagger D$ is hermitian and non-negative such that $\det M \geq 0$. For a γ_5-hermitian Dirac operator $\det(D)$ is real and $\operatorname{sign}(\det D) \in \{1, -1\}$. In more general situations and in particular at finite baryon number densities the sign-function can

be a complex phase, leading to the notorious fermion sign problem [53]. Standard Monte Carlo techniques are only applicable if the measure in the path integral is positive. Therefore we assume that either $\det(D)$ has a fixed sign or else simulate with $(\det M)^{1/2} \geq 0$ and treat $\mathrm{sign}(\det D)$ as an insertion into the path integral. In the latter situation where $\det D$ changes sign the reweighing with $\mathrm{sign}(\det D)$ is a delicate issue and, in particular for strong coupling, may fail.

In simulations it is too expensive to calculate the determinant of D or $M = D^\dagger D$ for every gauge field configuration—the computational cost for $\det(M)$ grows with the third power of the lattice volume. Thus one often introduces N_{PF} complex pseudofermion fields [54] and rewrites the partition function as

$$(\det M)^{1/2} = \int \prod_p \mathscr{D}\phi_p^\dagger \mathscr{D}\phi_p \mathrm{e}^{-S_{\mathrm{PF}}}, \quad S_{\mathrm{PF}} = \sum_p \big(\phi_p, M^{-q}\phi_q\big), \tag{15.106}$$

where $q N_{\mathrm{PF}} = 1/2$. The resulting path integral

$$Z = \int \prod_\ell \mathrm{d}U_\ell \, \mathscr{D}\phi \mathscr{D}\phi^* \mathrm{e}^{-S_{\mathrm{w}}(U) - S_{\mathrm{PF}}(U,\phi,\phi^\dagger)} \tag{15.107}$$

can then be estimated with a HMC algorithm with force given by the gradient of the non-local action $S_{\mathrm{gauge}} + S_{\mathrm{PF}}$. In the (rational) HMC dynamics M^{-q} is replaced by a rational approximation according to

$$M^{-q} \approx \alpha_0 + \sum_{r=1}^{N_{\mathrm{R}}} \frac{\alpha_r}{M + \beta_r}, \tag{15.108}$$

where the number of terms N_{R} depends on the required accuracy of the rational approximation and the spectral range of M. The coefficients α and β can be calculated with the Remez algorithm [55]. The force terms in the rHMC dynamics contain the inverse of the matrices $M + \beta_r$ acting on a vector, and this mapping can be approximated with the help of a (multi-mass) conjugate gradient solver. The efficiency of the rHMC algorithm crucially depends on the lowest eigenvalues, i.e. the condition number $\lambda_{\max}/\lambda_{\min}$ of the hermitian operator M used in the rational approximation.

Observables of interest in particle physics are for example hadron masses, decay widths, weak matrix elements or form factors and nowadays these quantities can be estimated by lattice simulations on high performance computer clusters. Although this is a very important field of research in particle physics we refrain from studying this any further but refer the interested reader to the nice textbook of GATTRINGER and C. LANG [4]. Instead we turn to gauge theories under extreme conditions.

15.7.1 Finite Temperature and Density

Finite temperatures are introduced via the boundary conditions in the Euclidean time directions: bosonic fields must be periodic and fermionic fields must be antiperiodic in Euclidean time with period $\beta = 1/k_b T$. The antiperiodic boundary conditions for

fermions originate from the anticommutation relations for fermion field operators. Using this fact and the cyclicity of the trace we see that the thermal Green function for the Euclidean field operator $\hat{\psi}(\tau, \mathbf{x}) = \exp(\tau \hat{H})\hat{\psi}(0, \mathbf{x})\exp(-\tau \hat{H})$ satisfies

$$\begin{aligned} G_\beta(\tau, \mathbf{x}; 0, \mathbf{y}) &= \frac{1}{Z}\operatorname{tr}\left(\mathrm{e}^{-\beta \hat{H}} T \hat{\psi}(\tau, \mathbf{x})\hat{\psi}(0, \mathbf{y})\right) \\ &= -\frac{1}{Z}\operatorname{tr}\left(\mathrm{e}^{-\beta \hat{H}} T \hat{\psi}(\tau, \mathbf{x})\hat{\psi}(\beta, \mathbf{y})\right) = -G_\beta(\tau, \mathbf{x}, \beta, \mathbf{y}), \end{aligned}$$

where T is the time ordering. We conclude that fermion fields must be antiperiodic in Euclidean time inside the path integral, cp. the problem on p. 380.

Dynamical fermions in a fundamental representation of the gauge group break the center symmetry of the pure gauge theory (see the discussion on p. 326) explicitly and this affects the Polyakov loop. In full QCD one finds that the expectation value of the Polyakov loop settles on the real positive axis. In the confined low temperature phase it settles near the origin and in the high-temperature deconfined phase near the trace of the center element $\mathbb{1}$. The Polyakov loop and Wilson loop are no longer true order parameters.

In our theoretical world we may change the mass parameter m entering the Dirac operator. If we let the parameter approach infinity, the quarks decouple and we are in the so-called quenched situation without dynamical quarks. In the quenched approximation the $SU(3)$ theory shows a first-order phase transition from the confined to the deconfined phase. Lowering the quark masses the latent heat decreases and the transition becomes weaker until the transition turns into a crossover. At physical quark masses the confined and deconfined regions in parameter space are analytically connected [56]. The lattice computation now agree on the position of the crossover temperature for physical quark masses ($m_\pi \approx 140$ MeV) at $T_c \approx 170$ MeV [57, 58]. There is clear evidence that the susceptibilities do not diverge.

Finite Baryonic Density

In extreme situations, such as heavy ion collisions or ultra-dense matter in neutron stars, the baryon number density may exceed the density of atomic nuclei. In these extreme situations we must switch to the partition function of the grand canonical ensemble with quark chemical potential μ multiplying the quark number operator $\hat{N}_q$,

$$Z(\beta, \mu) = \operatorname{tr}\left(\mathrm{e}^{-\beta(\hat{H} - \mu \hat{N}_q)}\right). \tag{15.109}$$

Sometimes the baryon number operator $\hat{N}_B = \hat{N}_q/3$ and baryon chemical potential $\mu_B = 3\mu$ are used instead. The quark number density is the zero-component of the conserved Noether vector current $j^\mu = \bar{\psi}\gamma^\mu\psi$ connected to the $U(1)$-invariance of the theory. The corresponding Noether charge

$$\hat{N}_q = \int \mathrm{d}^3 x \hat{\bar{\psi}}\gamma^0\hat{\psi} \tag{15.110}$$

commutes with the Hamiltonian. We can treat the combination $\hat{H} - \mu \hat{N}_q$ as effective Hamiltonian and directly write down the path integral by simply adding

$$-\mu Q = \mu \int \mathrm{d}^d x \, \bar{\psi} \gamma^0 \psi \tag{15.111}$$

to the Euclidean action. Thus at finite temperature and finite chemical potential the fermionic part of the Euclidean continuum action takes the form

$$S_{\mathrm{F}} = \int_0^\beta \mathrm{d}\tau \int \mathrm{d}^{d-1} x \, \bar{\psi} \big(\not{D} + m + \mu \gamma^0 \big) \psi. \tag{15.112}$$

Note that the additional term containing μ is obtained by shifting an Abelian gauge potential according to $A_0 \to A_0 - \mathrm{i}\mu$. This partly explains why the partition function of an Abelian gauge theory in a finite box and subject to periodic boundary conditions in the spatial directions does not depend on the chemical potential [59]. On the lattice one is tempted to add a term $\mu \sum \bar{\psi}_x \gamma^0 \psi_x$ to the lattice action. This simplistic ansatz runs into problems with unphysical divergences of the energy density, though. Closer inspection of the continuum situation clarifies the problem. Determining the Noether current for the lattice action gives the current expressed by nearest-neighbor terms. An easy way to find the correct expression is to recall that the elementary parallel transporter changes under the shift $A_0 \to A_0 - \mathrm{i}\mu$ according to

$$U_{x,\mu} \approx \mathrm{e}^{\mathrm{i} a A_\mu(x)} \to \mathrm{e}^{\mu} U_{x,\mu}. \tag{15.113}$$

Thus the Wilson operator at bare fermion mass m and real chemical potential μ reads

$$\begin{aligned} D_{\mathrm{w},xy}(\mu) &= (m + rd)\delta_{xy} \\ &\quad - \frac{1}{2} \sum_\nu \big((r + \gamma^\nu) \mathrm{e}^{-\mu \delta_{0,\nu}} U_{y,-\nu} \delta_{x,y-e_\nu} + (r - \gamma^\nu) \mathrm{e}^{\mu \delta_{\nu,0}} U_{y,\nu} \delta_{x,y+e_\nu} \big) \end{aligned} \tag{15.114}$$

and similarly for staggered, twisted mass or overlap fermions. The Euclidean action

$$S = S_{\mathrm{gauge}} + \sum_{x,y} \bar{\psi}_x D_{xy}(\mu) \psi_y \tag{15.115}$$

enters the grand partition function for the theory with N_f flavors of Dirac fermions at finite volume, temperature and chemical potential

$$Z(V, T, \mu) = \oint \prod_\ell \mathrm{d}U_\ell \big(\det{}_{\mathrm{ap}} D(\mu) \big)^f \mathrm{e}^{-S_{\mathrm{gauge}}(U)}. \tag{15.116}$$

The index at the determinant indicates that it must be calculated with respect to antiperiodic boundary conditions in the imaginary time direction. Unfortunately the operators $D(\mu)$ have complex determinants for $\mu \neq 0$ and it is impossible to apply stochastic methods directly to estimate the thermodynamic potential or thermal correlation functions at finite baryon density. Dealing with such complex determinants in simulations is one of the most urgent problems in gauge theories at finite densities. Various ways have been suggested to circumvent the problem:

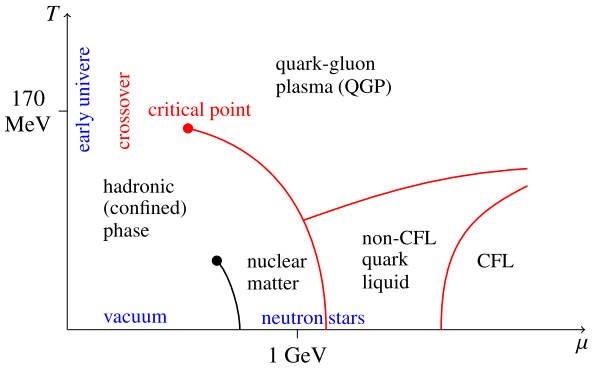

Fig. 15.11 Conjectured form of the phase diagram of QCD at finite temperature and baryon density. At high temperature we expect a deconfined quark–gluon plasma. At low temperatures and low densities we are in the confined hadronic phase. If we increase the density at low temperature then we move from the vacuum sector into the phase with nuclear matter. Increasing the density even further we encounter a quark phase. At ultra-high densities we expect to find a color-flavor-locked (CFL) phase with color-superconducting quark matter. There is a crossover between the confined and deconfined phases at low densities

- One generates ensembles with $\mu = 0$ and treats the μ-dependent part of $\exp(-S)$ as insertion. This reweighing requires the exact evaluation of $\det D$ and works well on small lattices [60].
- One performs a Taylor expansion around $\mu = 0$ where the expansion coefficients are estimated with the ensemble at $\mu = 0$. This works well for small μ [61].
- For imaginary chemical potential the determinant becomes real and one can estimate $Z(V, T, \mathrm{i}\mu)$. The result is analytically continued to real chemical potential. The analytic continuation of an approximation may be a bad approximation to the analytic continuation and indeed the method only works well for small μ [62].

For larger chemical potentials the only results on the phase diagram at finite temperature and finite density are obtained from functional methods or model calculations, that crucially rely on truncations or model building [65, 66]. A different strategy is to investigate QCD-like theories without a sign problem, having as much features in common with QCD as possible. An example of such a theory is two-color QCD with a real determinant at finite density. The phase diagram of the two-flavor model as a function of temperature and net baryon density has been investigated in [63, 64]. Unfortunately the theory has no fermionic baryons and thus cannot support a 'neutron star'. A gauge theory without sign problem and with fermionic baryons is G_2-QCD which can be broken to real-life QCD with a scalar field in the seven-dimensional fundamental representation [67, 68]. All irreducible representation of this exceptional groups can be chosen real and as a consequence the fermionic determinant at finite baryon density is real and non-negative [69, 70]. The theory can be simulated at finite temperature and finite baryon density and the resulting phase diagram looks similar to the expected phase diagram for QCD, depicted in Fig. 15.11.

Listing 15.1 Free fermionic propagator

```
function derinverse;
# inverse of partial + mass for left-derivative,
# antisymmetric derivative and SLAC derivative
# number of lattice sites N must be odd
mass=input("mass = ");
N=51;
x=[0:N-1];
zeroN2=zeros(1,N-2);
zeroN3=zeros(1,N-3);
xshort=1:N-1;
t=pi/N*(-1).^xshort./sin(pi*xshort/N);
# one-dimensional massive Dirac operators
dirac_left=toeplitz([mass+1,-1,zeroN2],[mass+1,zeroN2,-1]);
dirac_ant=toeplitz([mass,-.5,zeroN3,.5],[mass,.5,zeroN3,-.5]);
dirac_slac=toeplitz([0,t],[0,-t])+mass*toeplitz([1,zeroN2,0]);
# propagators of Dirac operators
clf;hold("off");
propagator=inverse(dirac_left);y=propagator(:,1);
plot(x,y,'x',x,y(1)*exp(-mass*x),'-');
legend('left');
propagator=inverse(dirac_ant);y=propagator(:,1);
hilfs=input("antisymmetric derivative: press enter ");
plot(x,y,'o',x,y(1)*exp(-mass*x),'-');
legend('antisymmetric');
propagator=inverse(dirac_slac);y=propagator(:,1);
hilfs=input("slac derivative: press enter ");
plot(x,y,'*',x,y(4)*exp(mass*(3-x)),x,y(5)*exp(mass*(4-x)));
grid ("on");
legend('Slac');
# propagator of squared Slac operator
hilfs=input("slac-Dirac operator squared: press enter ");
clf;hold("off");
dirac_slacsquare=dirac_slac'*dirac_slac;
propagator_slacsquare=inverse(dirac_slacsquare);
y=propagator_slacsquare(:,1);
plot(x,y,'x',x,y(2)*(exp(-mass*(x-1))+exp(mass*(x-N+1))),'-');
legend('Slac squared');
endfunction;
```

15.8 Programs for Chap. 15

The `octave`-program `derinverse` in Listing 15.1 computes the two-point function (15.42) as a function of x. It is normalized to 1 at $x = 1$. One needs to input the mass. The two-point function and the exponential fit $\exp(-mx)$ are plotted.

By using the routine in Listing 15.2, one can plot the vector field of the naive Dirac operator $\tilde{D}_\mu(p)$ in the two-dimensional Brillouin zone.

Listing 15.2 Vector field

```
function vectorfield;
# computes the vector field D_\mu(p) of the
# Dirac operator in momentum space
# number of lattice sites N must be odd
N=input("number of lattice points (10-20)= ");
p=linspace(-pi,pi,N);
[x,y]=meshgrid(p,p);
px=sin(x);
py=sin(y);
quiver(x,y,px,py,linelength=.6);
endfunction;
```

15.9 Problems

15.1 (Pfaffian) Let $\eta_1, \ldots, \eta_{2N}$ be an even number of anticommuting real Grassmann variables, $\{\eta_a, \eta_b\} = 0$. Prove that the Gaussian integral over such variables yields the Pfaffian,

$$\int d\psi_1 \cdots d\psi_{2N}\, \mathrm{e}^{\frac{1}{2}\psi^t M \psi} = \frac{1}{2^N N!} \varepsilon_{a_1 b_1 \ldots a_N b_N} M_{a_1 b_1} \cdots M_{a_N b_N} = \mathrm{Pf}(M). \tag{15.117}$$

By doubling the degrees of freedom prove the important identity

$$\det M = \big(\mathrm{Pf}(M)\big)^2.$$

Transform the Grassmann variables in (15.117) according to $\eta \to R\eta$ and show

$$\mathrm{Pf}\big(R^t M R\big) = \det(R)\, \mathrm{Pf}(M).$$

Prove that for an antisymmetric matrix M of dimensional $2N$ we have

$$\mathrm{Pf}\big(M^t\big) = (-1)^N\, \mathrm{Pf}(M).$$

Show, by using the relation between the Pfaffian and determinant, that

$$\delta \log \det(M) = \mathrm{tr}\big(M^{-1}\delta M\big) \quad \Longrightarrow \quad \delta \log \mathrm{Pf}(M) = \frac{1}{2}\,\mathrm{tr}\big(M^{-1}\delta M\big).$$

Let us assume that the antisymmetric M is a tensor product of a symmetric matrix S and an antisymmetric matrix A. By transforming both matrices into their normal forms prove that

$$\mathrm{Pf}\, M = \mathrm{Pf}(S \otimes A) = (\det S)^{\dim A} \cdot (\mathrm{Pf}\, A)^{\dim S}.$$

15.2 (Staggered fermions) Prove the identity (15.66) which was used to diagonalize the naive Wilson operator to obtain the operator for staggered fermions.

15.3 (Supersymmetric actions) Show that the action (15.96) is left invariant by the supersymmetry transformation (15.97), which contains a constant and anticommuting Majorana parameter ε.

15.4 (Fermions at finite temperature) We have seen that in the path integral for fermions at finite temperature T one integrates over anticommuting fields which are antiperiodic in Euclidean time, $\psi(\tau+\beta_T,\mathbf{x})=-\psi(\tau,\mathbf{x})$. First show that formally the path integral for free fermions with $\mathscr{L}_\mathrm{F}=\bar\psi(\not\partial+m)\psi$ can be rewritten as

$$\begin{aligned}Z_\beta &= \oint \mathscr{D}\psi\mathscr{D}\bar\psi \mathrm{e}^{-S_\mathrm{F}} \propto \det{}_{\mathrm{ap}}(\not\partial+m) = \det{}_{\mathrm{ap}}^{1/2}\big[\big(-\Delta+m^2\big)\mathbb{1}_4\big]\\ &= \det{}_{\mathrm{ap}}^{2}\big(-\Delta+m^2\big),\end{aligned}$$

where the determinants are calculated on the space of antiperiodic functions. You may exploit that $\not\partial+m$ is γ_5-hermitian. Now calculate $\det_{\mathrm{ap}}(-\Delta+m^2)$ on this space (for example, with the zeta-function regularization used in Sect. 5.2 to calculate the determinant with respect to periodic boundary conditions) and show that the resulting free energy density is that for free fermions in a box.

Appendix: The SLAC Derivative

We introduce the SLAC derivative on a one-dimensional periodic lattice with equidistant sampling points

$$x_k = x_0 + k, \quad k = 1,\dots,N. \tag{15.118}$$

The set of lattice functions $x_k \to \psi_k \in \mathbb{C}$, equipped with the scalar product

$$(\phi,\psi) = \sum_{k=1}^{N} \bar\phi_k \psi_k, \tag{15.119}$$

define a Hilbert space. If ψ is normalized to one we may interpret $|\psi_k|^2$ as the probability of finding the particle described by the wave function ψ at site x_k. Then the expectation value of the position operator is given by

$$\langle\hat x\rangle_\psi = \langle\bar\psi|\hat x|\psi\rangle = \sum x_k|\psi_k|^2 \equiv \sum_{kk'} \bar\psi_k x_{kk'}\psi_{k'}. \tag{15.120}$$

As expected, the position operator $\hat x$ is diagonal in real space such that its matrix elements vanish if $k\neq k'$. To introduce the SLAC derivative we switch to momentum space with wave functions $\tilde\psi(p_\ell)\equiv\tilde\psi_\ell$ given by

$$\tilde\psi_\ell = \frac{1}{\sqrt{N}}\sum_{k=1}^{N} \mathrm{e}^{-\mathrm{i}p_\ell x_k}\psi_k, \quad \ell = 1,\dots,N. \tag{15.121}$$

The inverse Fourier transformation reads

$$\psi_k = \frac{1}{\sqrt{N}}\sum_{\ell=1}^{N} \mathrm{e}^{\mathrm{i}p_\ell x_k}\tilde\psi_\ell, \quad k = 1,\dots,N. \tag{15.122}$$

We choose the $\{p_\ell\}$ symmetric with respect to the origin,

$$p_\ell = \frac{2\pi}{N}\left(\ell - \frac{N+1}{2}\right), \tag{15.123}$$

and with this choice the number of sites must be odd to obtain periodic wave functions and it must be even to obtain antiperiodic wave functions.

Now we seek a lattice momentum operator $\hat{p}$ which is diagonal in momentum space and has eigenvalues p_ℓ. This means that below the cutoff it has exactly the same eigenvalues as the continuum operator on the interval. Similarly as in the continuum we interpret $|\tilde{\psi}_\ell|^2$ as probability for finding the eigenvalue p_ℓ of $\hat{p}$. Then the mean value of $f(\hat{p})$ is

$$\begin{aligned}\big\langle f(\hat{p})\big\rangle_\psi &= \sum_\ell f(p_\ell)|\tilde{\psi}_\ell|^2 = \frac{1}{N}\sum_\ell \sum_{kk'} \mathrm{e}^{\mathrm{i}p_\ell(x_k - x_{k'})} f(p_\ell)\bar{\psi}_k\psi_{k'} \\ &= \sum_{kk'} \bar{\psi}_k f(p)_{kk'}\psi_{k'}, \quad f(p)_{kk'} = \frac{1}{N}\sum_\ell \mathrm{e}^{\mathrm{i}p_\ell(x_k - x_{k'})} f(p_\ell).\end{aligned} \tag{15.124}$$

Of course the operator $f(\hat{p})$ is non-diagonal in position space and to find its matrix elements $f(p)_{kk'}$ we define the generating function

$$Z(x) = \frac{1}{N}\sum_{\ell=1}^{N} \mathrm{e}^{\mathrm{i}Np_\ell x} = \frac{\sin(\pi N x)}{N\sin(\pi x)}. \tag{15.125}$$

The matrix elements are obtained by differentiation,

$$f(p)_{kk'} = f\left(\frac{1}{\mathrm{i}N}\frac{\mathrm{d}}{\mathrm{d}x}\right) Z(x)\Big|_{x=t_{kk'}}, \quad t_{kk'} = \frac{k-k'}{N}. \tag{15.126}$$

In particular we find

$$p_{kk} = 0, \quad p_{k\neq k'} = \frac{\pi}{\mathrm{i}N}(-)^{k-k'}\frac{1}{\sin(\pi t_{kk'})}, \tag{15.127}$$

and these matrix elements define the SLAC derivative $\partial_{\mathrm{slac}} = \mathrm{i}\hat{p}$ in position space.

References

1. J. Smit, *Introduction to Quantum Field Theories on a Lattice* (Cambridge University Press, Cambridge, 2002)
2. I. Montvay, G. Münster, *Quantum Fields on a Lattice* (Cambridge University Press, Cambridge, 1994)
3. H.J. Rothe, *Lattice Gauge Theories: An Introduction* (World Scientific, Singapore, 2012)
4. C. Gattringer, C. Lang, *Quantum Chromodynamics on the Lattice*. Springer Lect. Notes Phys., vol. 788 (2010)
5. G. Roepstorff, *Path Integral Approach to Quantum Physics* (Springer, Berlin, 1996)
6. E. Seiler, *Gauge Theories as a Problem of Constructive Quantum Field Theory and Statistical Mechanics* (Springer, Berlin, 1982)

7. V. Mitrjushkin, G. Schierholz (eds.), *Lattice Fermions and Structure of the Vacuum* (Kluwer Academic, Dordrecht, 2000)
8. S. Chandrasekharan, U.-J. Wiese, An introduction to chiral symmetry on the lattice. Prog. Part. Nucl. Phys. **53**, 373 (2004)
9. A. Berezin, *The Method of Second Quantization* (Academic Press, New York, 1966)
10. C. Itzykson, J.M. Drouffe, *Statistical Field Theory I* (Cambridge University Press, Cambridge, 1989)
11. K. Wilson, in *New Phenomena in Subnuclear Physics* (Plenum, New York, 1977)
12. L. Susskind, Lattice fermions. Phys. Rev. D **16**, 3031 (1977)
13. S.D. Drell, M. Weinstein, S. Yankielowicz, Variational approach to strong coupling field theory. 1. ϕ^4 theory. Phys. Rev. D **14**, 487 (1976)
14. S.D. Drell, M. Weinstein, S. Yankielowicz, Strong coupling field theories: 2. Fermions and gauge fields on a lattice. Phys. Rev. D **14**, 1627 (1976)
15. A. Kirchberg, D. Laenge, A. Wipf, From the dirac operator to Wess–Zumino models on spatial lattices. Ann. Phys. **316**, 357 (2005)
16. J. Förster, A. Saenz, U. Wolff, Matrix algorithm for solving Schrödinger equations with position-dependent mass or complex optical potentials. Phys. Rev. E **86**, 016701 (2012)
17. G. Bergner, T. Kaestner, S. Uhlmann, A. Wipf, Low-dimensional supersymmetric lattice models. Ann. Phys. **323**, 946 (2008)
18. T. Kaestner, G. Bergner, S. Uhlmann, A. Wipf, C. Wozar, Two-dimensional Wess–Zumino models at intermediate couplings. Phys. Rev. D **78**, 095001 (2008)
19. L.H. Karsten, J. Smit, The vacuum polarization with SLAC lattice fermions. Phys. Lett. B **85**, 100 (1979)
20. M. Creutz, Chiral anomalies and rooted staggered fermions. Phys. Lett. B **649**, 230 (2007)
21. A. Kronfeld, Lattice gauge theory with staggered fermions: how, where, and why (not), in *PoS LAT2007*, (2007), p. 016. arXiv:0711.0699v2
22. H. Nielsen, M. Ninomiya, Absence of neutrinos on a lattice (I). Proof by homotopy theory. Nucl. Phys. B **185**, 20 (1981)
23. H. Nielsen, M. Ninomiya, Absence of neutrinos on a lattice. 2. Intuitive topological proof. Nucl. Phys. B **193**, 173 (1981)
24. L.H. Karsten, J. Smit, Lattice fermions: species doubling, chiral invariance and the triangle anomaly. Nucl. Phys. B **183**, 103 (1981)
25. D. Friedan, A proof of the Nielsen Ninomiya theorem. Commun. Math. Phys. **85**, 481 (1982)
26. P.H. Ginsparg, K.G. Wilson, A remnant of chiral symmetry on the lattice. Phys. Rev. D **25**, 2649 (1982)
27. M. Lüscher, Exact chiral symmetry on the lattice and the Ginsparg–Wilson relation. Phys. Lett. B **428**, 342 (1998)
28. D. Kaplan, A method for simulating chiral fermions on the lattice. Phys. Lett. B **288**, 342 (1992)
29. Y. Shamir, Chiral fermion from lattice boundaries. Nucl. Phys. B **406**, 90 (1993)
30. V. Furman, Y. Shamir, Axial symmetries in lattice QCD with Kaplan fermions. Nucl. Phys. B **439**, 54 (1995)
31. S.A. Frolov, A.A. Slavnov, An invariant regularization of the standard model. Phys. Lett. B **309**, 344 (1993)
32. R. Narayanan, H. Neuberger, Infinitely many regulator fields for chiral fermions. Phys. Lett. B **302**, 62 (1993)
33. R. Narayanan, H. Neuberger, Chiral determinants as an overlap of two Vacua. Nucl. Phys. B **412**, 574 (1994)
34. P. Hasenfratz, Lattice QCD without tuning, mixing and current renormalization. Nucl. Phys. B **525**, 401 (1998)
35. P. Hasenfratz, Prospects for perfect actions. Nucl. Phys. B, Proc. Suppl. **63**, 53 (1998)
36. P. Hasenfratz, S. Hauswirth, T. Jorg, F. Niedermayer, K. Holland, Testing the fixed point QCD action and the construction of chiral currents. Nucl. Phys. B **643**, 280 (2002)

37. C. Gattringer, I. Hip, New approximate solutions of the Ginsparg–Wilson equation: tests in 2D. Phys. Lett. B **480**, 112 (2000)
38. C. Gattringer, A new approach to Ginsparg–Wilson fermions. Phys. Rev. D **63**, 114501 (2001)
39. C. Gattringer et al., Quenched spectroscopy with fixed point and chirally improved fermions. Nucl. Phys. B **677**, 3 (2004)
40. H. Neuberger, Exactly massless quarks on the lattice. Phys. Lett. B **417**, 141 (1998)
41. H. Neuberger, More about exactly massless quarks on the lattice. Phys. Lett. B **427**, 353 (1998)
42. P. Hasenfratz, V. Laliena, F. Niedermayer, The index theorem in QCD with a finite cutoff. Phys. Lett. **427**, 125 (1998)
43. N. Cabibbo, L. Maiani, G. Parisi, R. Petronzio, Bounds on the Fermions and Higgs boson masses in grand unified theories. Nucl. Phys. B **158**, 295 (1979)
44. P. Gerhold, K. Jansen, Upper Higgs boson mass bounds from a chirally invariant lattice Higgs–Yukawa model. J. High Energy Phys. **1004**, 094 (2010)
45. P. Gerhold, Upper and lower Higgs boson mass bounds from a chirally invariant lattice Higgs–Yukawa model. arXiv:1002.2569v1 [hep-lat]
46. S. Elitzur, E. Rabinovici, A. Schwimmer, Supersymmetric models on the lattice. Phys. Lett. B **119**, 165 (1982)
47. M. Beccaria, C. Rampino, World-line path integral study of supersymmetry breaking in the Wess–Zumino model. Phys. Rev. D **67**, 127701 (2003)
48. S. Catterall, S. Karamov, Exact lattice supersymmetry: the two-dimensional $\mathscr{N} = 2$ Wess–Zumino model. Phys. Rev. D **65**, 094501 (2002)
49. S. Catterall, S. Karamov, A lattice study of the two-dimensional Wess–Zumino model. Phys. Rev. D **68**, 014503 (2003)
50. C. Wozar, A. Wipf, Supersymmetry breaking in low dimensional models. Ann. Phys. **327**, 774 (2012)
51. J. Bartels, J.B. Bronzan, Supersymmetry on a lattice. Phys. Rev. D **28**, 818 (1983)
52. F. Synatschke, G. Gies, A. Wipf, Phase diagram and fixed-point structure of two dimensional $N = 1$ Wess–Zumino models. Phys. Rev. **80**, 085007 (2009)
53. M. Troyer, U.J. Wiese, Computational complexity and fundamental limitations to fermionic quantum Monte Carlo simulations. Phys. Rev. Lett. **94**, 170201 (2005)
54. D.H. Weingarten, D.N. Petcher, Monte Carlo integration for lattice gauge theories with fermions. Phys. Lett. B **99**, 333 (1981)
55. W. Frazer, A survey of methods of computing minimax and near-minimax polynomial approximations for functions of a single independent variable. J. ACM **12**, 295 (1965)
56. F. Brown et al., On the existence of a phase transition for QCD with three light quarks. Phys. Rev. Lett. **65**, 2491 (1990)
57. Y. Aoki, G. Endrődi, Z. Fodor, S. Katz, K. Szabó, The order of the quantum chromodynamics transition predicted by the standard model of particle physics. Nature **443**, 675 (2006)
58. A. Bazavov et al., Equation of state and QCD transition at finite temperature. Phys. Rev. D **80**, 014504 (2009)
59. I. Sachs, A. Wipf, Generalized Thirring models. Ann. Phys. **249**, 380 (1996)
60. Z. Fodor, S.D. Katz, Lattice determination of the critical point of QCD at finite T and μ. J. High Energy Phys. **0203**, 014 (2002)
61. C.R. Allton et al., The QCD thermal phase transition in the presence of a small chemical potential. Phys. Rev. D **66**, 074507 (2002)
62. Ph. de Forcrand, O. Philipsen, The QCD phase diagram for small densities from imaginary chemical potential. Nucl. Phys. B **642**, 290 (2002)
63. J.B. Kogut, M.A. Stephanov, D. Toublan, J.J.M. Verbaarschot, A. Zhitnitsky, QCD-like theories at finite baryon density. Nucl. Phys. B **582**, 477 (2000)
64. S. Hands, S. Kim, J.I. Skullerud, A quarkyonic phase in dense two color matter? Phys. Rev. D **81**, 091502 (2010)
65. R.D. Pisarski, Quark gluon plasma as a condensate of $SU(3)$ Wilson lines. Phys. Rev. D **62**, 111501 (2000)

66. T.K. Herbst, J.M. Pawlowski, B.J. Schaefer, The phase structure of the Polyakov–quark-meson model beyond mean field. Phys. Lett. B **696**, 58 (2011)
67. K. Holland, P. Minkowski, M. Pepe, U.J. Wiese, Exceptional confinement in $G(2)$ gauge theory. Nucl. Phys. B **668**, 207 (2003)
68. B. Wellegehausen, C. Wozar, A. Wipf, Phase diagram of the lattice $G(2)$ Higgs model. Phys. Rev. D **83**, 114502 (2011)
69. A. Maas, L. von Smekal, B. Wellegehausen, A. Wipf, The phase diagram of a gauge theory with fermionic baryons. arXiv:1203.5653 [hep-lat]
70. B. Wellegehausen, Phase diagrams of exceptional and supersymmetric lattice gauge theories. Ph.D.-thesis, Jena (2012)

Index

A. Wipf, *Statistical Approach to Quantum Field Theory*, Lecture Notes in Physics 864,
DOI 10.1007/978-3-642-33105-3, © Springer-Verlag Berlin Heidelberg 2013